Univerza
v Ljubljani

Fakulteta za
gradbeništvo in
geodezijo

PODIPLOMSKI ŠTUDIJ
GRADBENIŠTVA

DOKTORSKI ŠTUDIJ

Kandidatka:

META KRŽAN, univ. dipl. inž. grad.

EKSPERIMENTALNE IN NUMERIČNE PREISKAVE ZA DOLOČITEV KONTROLIRANEGA ODZIVA VEČSLOJNE KAMNITE ZIDOVINE

Doktorska disertacija štev.: 247

PERFORMANCE BASED EXPERIMENTAL AND NUMERICAL ASSESSMENT OF MULTI-LEAF STONE MASONRY WALLS

Doctoral thesis No.: 247

Komisija za doktorski študij je na 29. seji, 13. junija 2012, po pooblastilu 30. seje Senata Univerze v Ljubljani z dne 20. januarja 2009, dala soglasje k temi doktorske disertacije.

Za mentorja je bil imenovan doc. dr. Vlatko Bosiljkov.

Ljubljana, 21. december 2015

Univerza
v Ljubljani

Fakulteta za
gradbeništvo in
geodezijo

Komisijo za oceno ustreznosti teme doktorske disertacije v sestavi:

- doc. dr. Vlatko Bosiljkov,
- prof. dr. Roko Žarnić,
- prof. dr. Boštjan Brank,
- izr. prof. dr. Vojko Kilar, UL FA,

je imenoval Senat Fakultete za gradbeništvo in geodezijo na 30. redni seji, dne 25. aprila 2012.

Poročevalce za oceno doktorske disertacije v sestavi:

- izr. prof. dr. Mark Masia, University of Newcastle,
- prof. dr. Sergio Lagomarsino, University of Genoa,
- izr. prof. dr. Matjaž Dolšek,
- prof. dr. Boštjan Brank

je imenoval Senat Fakultete za gradbeništvo in geodezijo na 22. redni seji, dne 23. septembra 2015.

Komisijo za zagovor doktorske disertacije v sestavi:

- prof. dr. Matjaž Mikoš, dekan UL FGG, predsednik,
- izr. prof. dr. Vlatko Bosiljkov, mentor,
- izr. prof. dr. Mark Masia, University of Newcastle
- prof. dr. Sergio Lagomarsino, University of Genoa,
- izr. prof. dr. Matjaž Dolšek,
- prof. dr. Boštjan Brank,

je imenoval Senat Fakultete za gradbeništvo in geodezijo na 24. redni seji, dne 9. decembra 2015.

University
of Ljubljana

Faculty
of Civil and Geodetic Engineering

IZJAVE

Podpisana Meta Kržan izjavljam, da sem avtorica doktorskega dela z naslovom " Eksperimentalne in numerične preiskave za določitev kontroliranega odziva večslojne kamnite zidovine " (*eng.* " Performance based experimental and numerical assessment of multi-leaf stone masonry walls ").

Izjavljam, da je elektronska različica v vsem enaka tiskani različici.

STATEMENTS

I, the undersigned Meta Kržan, hereby declare that I am the author of the PhD thesis entitled " Performance based experimental and numerical assessment of multi-leaf stone masonry walls " (*slo.* " Eksperimentalne in numerične preiskave za določitev kontroliranega odziva večslojne kamnite zidovine ").

I declare that the digital version of the thesis is identical to the printed one.

Ljubljana, december 2015

(Podpis / Signature)

POPRAVKI / ERRATA

Stran z napako ***Page***	**Vrstica z napako** ***Line***	**Namesto** ***Error***	**Naj bo** ***Correction***

BLANK PAGE

»Ta stran je namenoma prazna.«

BIBLIOGRAPHIC-DOCUMENTALISTIC INFORMATION

UDC:	**550.34.016:519.876.5:66.017:(043)**
Author:	**Meta Kržan**
Supervisor:	**assoc. prof. Vlatko Bosiljkov, Ph.D.**
Title:	**Performance based experimental and numerical assessment of multi-leaf stone masonry walls**
Document Type:	**Doctoral Dissertation**
Notes:	**304 p., 133 tab., 214 fig., 147 eq.**
Keywords:	**multi-leaf stone masonry, historic masonry, seismic behaviour, compression tests, in-plane shear tests, drift limits, plaster damage, grouting, NSM, glass cord, transversal connecting of the wall**

Abstract

In the thesis, the behaviour of three-leaf stone masonry walls under compression loading and in-plane shear loading is studied. An extensive experimental campaign was conducted on 18 walls, accompanied by tests on masonry constituents (mortar and stone). The type of the tested masonry is typical for older representative buildings, which often present important cultural heritage assets. Influence of morphology, level of pre-compression and boundary conditions on various characteristics of the walls behaviour was systematically studied. Besides the strength, the greatest emphasis was on the analysis of the displacement capacity and damage of the walls at characteristic stages of their response. Due to various boundary conditions, different failure mechanisms developed; rocking, mixed and diagonal shear. Leaf separation and the out-of-plane mechanism of the wall was not critical as expected. It developed more evidently in the post-peak phase of the tests for specimens with higher pre-compression. The presence of connecting stones had no influence neither on the obtained shear strength nor on the displacement capacity of the walls. The experimental results were compared to results of analytical models for prediction of shear resistance. For the tested type of masonry, shear strength can be adequately estimated with existing models for the failure mechanisms that developed in the tests. Drift capacity of the walls was however significantly higher than drift capacity allowed in the code provisions (EN 1998-3 in FEMA 306).

In heritage buildings also various artistic assets in the form of painted walls are often present. Lime plaster was applied to the walls in order to study its performance during cyclic shear loading. Reference drift values for walls at 4 different characteristic plaster damage states were determined. They can be used for performance based seismic assessment of historic buildings.

The second part of the thesis deals with strengthening of the damaged three-leaf stone masonry walls. For monumental buildings there are usually strict demands upon the use of materials compatible to existing materials, reversibility, etc., therefore a new strengthening system was developed. Walls were retrofitted along the cracks with lime-cement grout, additionally strengthened with near surface mounted (NSM) glass cords and transversally connected; 10 walls were strengthened with various combinations of measures and re-tested. Grouting successfully retrofitted the walls, while NSM glass cords increased the displacement capacity and, in one case, also shear resistance substantially.

Finally, the results of tests of the un-strengthened walls (drifts) were adopted for the numerical analysis of the seismic performance of an actual building (mansion Vipolže). Nonlinear static analyses using equivalent frame model were conducted. The influence of the assumed drift limits on the seismic resistance was analysed. The increase of seismic performance with increasing drift limits of walls is evident and it would be reasonable to further study the prospect of increasing the drift limits in the code provisions for types of masonry, which are more ductile (historical masonry).

BLANK PAGE

»Ta stran je namenoma prazna.«

BIBLIOGRAFSKO-DOKUMENTACIJSKA STRAN

UDK:	**550.34.016:519.876.5:66.017:(043)**
Avtor:	**Meta Kržan**
Mentor:	**izr. prof. dr. Vlatko Bosiljkov**
Naslov:	**Eksperimentalne in numerične preiskave za določitev kontroliranega odziva večslojne kamnite zidovine**
Tip dokumenta:	**Dokt. Dis.**
Obseg in oprema:	**304 str., 133 pregl., 214 sl., 147 en.**
Ključne besede:	**večslojni kamniti zidovi, historični zidovi, potresno obnašanje, tlačne preiskave, strižne preiskave v ravnini, mejni zasuki, poškodbe ometov, injektiranje, urjevanje v fugah, steklena vrvica, prečno povezovanje zidov**

Izvleček

V sklopu naloge je bilo študirano obnašanje troslojnih kamnitih zidov, in sicer obnašanje pri tlačnih obremenitvah in pri strižnih obremenitvah v ravnini zidov. Izvedene so bile obsežne eksperimentalne preiskave; tlačni in strižni testi skupaj 18 zidov ter spremljajoče preiskave konstituentov (malte in kamna). Preskušani kamniti zidovi so značilni predvsem za reprezentativne starejše objekte, ki pogosto predstavljajo pomemben del naše kulturne dediščine. Za testiran tip zidov je bil sistematično analiziran vpliv morfologije zidov (sestave po prerezu), različnih nivojev pred-obremenitev ter robnih pogojev vpetja na različne karakteristike obnašanja zidov. Poleg nosilnosti je bil poudarek na analizi pomikov ter poškodovanosti zidov v karakterističnih stanjih obnašanja. V odvisnosti od robnih pogojev je pri strižnih testih prišlo do različnih porušnih mehanizmov zidov; upogibnega, mešanega in diagonalnega strižnega, pri čemer v nasprotju s pričakovanji izven-ravninski mehanizem ni bil merodajen. Do slednjega je prišlo bolj opazno pri višjih pred-obremenitvah zidov v fazi mehčanja zidov. Za testirani tip zidov povezovalni kamni preko prereza zidu niso prispevali ne k večji nosilnosti ne k večjim mejnim pomikom. Eksperimentalni rezultati nosilnosti in mejnih zasukov so bili primerjani z analitičnimi modeli. Strižno nosilnost se zadovoljivo oceni z obstoječimi modeli za porušitve, do katerih je pri testih dejansko prišlo. Doseženi mejni pomiki zidov so bili pri testih veliko večji, kot so dovoljeni mejni pomiki v standardih (EN 1998-3 in FEMA 306).

Ker je pri objektih kulturne dediščine poleg same konstrukcije pogosto v interesu ščititi tudi različne poslikave, je bil na zidove nanesen apneni omet, ki je služil študiju obnašanja umetnostih elementov zidov. Določene so bile vrednosti mejnih zasukov zidov za 4 stanja poškodb ometov, ki so uporabne za oceno potresne odpornosti objektov s stališča poškodovanosti ometov.

Drugi del naloge obravnava utrjevanje poškodovanih troslojnih kamnitih zidov. Ker je navadno pri utrjevanju historične zidove zahtevana uporaba kompatibilnih materialov, reverzibilnost ukrepov, itd., je bil v sklopu naloge razvit nov sistem utrjevanja. Poškodovani zidovi so bili injektirani s cementno-apneno injekcijsko mešanico in dodatno utrjeni s stekleno vrvico, s podaljšano apneno malto vgrajeno v horizontalne maltne spojnice, ter z vrvico tudi prečno povezani. Skupaj je bilo z različnimi kombinacijami ukrepov utrjenih in dodatno testiranih 10 zidov. Injektiranje se je izkazalo kot primeren sanacijski ukrep, vrvice v spojnicah pa so povečale duktilnost zidov ter v določenem primeru tudi nosilnost.

Rezultati testov neutrjenih zidov so bili aplicirani na dejanski objekt. Na primeru Vile Vipolže je bil numerično analiziran vpliv predpostavke mejnih pomikov zidov na potresno obnašanje objekta, računano z nelinearno statično analizo konstrukcije na modelu z ekvivalentnimi okvirji. Glede na rezultate (nezanemarljivo povečanje odpornosti v primeru povečanja pomikov) bi bilo za bolj duktilno zidovino, kot je navadno zgodovinska, smiselno dodatno preučiti smotrnost povečanja mejnih vrednosti zasukov v predpisih.

BLANK PAGE

»Ta stran je namenoma prazna.«

ACKNOWLEDGEMENT

The work and partially the strengthening of damaged walls was funded through the Ministry of Science and Technology of the Republic of Slovenia through "Young researchers" financing scheme. Experimental campaign of un-strengthened walls was performed within the project PERPETUATE (www.perpetuate.eu), funded by the European Commission in the 7th Framework Programme (FP7/2007-2013), under grant agreement n° 244229.

Due to extensive experimental campaign various individuals contributed to specific parts (preliminary studies, specimen construction and preparation, help during experiments or analysis of results) of presented work. The work of Janez Korpič, Luka Kurnjek, Damjan Špeglič, Katarina Kodelja, Alja Arrigler and Luka Božič for bachelor thesis is acknowledged. Franci Čepon lead the experiments and was involved in all stages of experimental campaigns. Mortar composition for construction as well as for plasters was designed by assos. prof. dr. Violeta Bokan Bosiljkov, who also helped to design mortar for NSM the cords. Photogrametric measurments were conducted after instructions of Vid Peterman (Modri Planet d.o.o.), who provided the results for further analysis. The pull out tests were done by ZRMK, GrindoSonic tests were conducted with the help of Petra Štukovnik. Boštjan Jursinovič and Alen Lešnik helped set up (some of) the tests and helped during and after experiments. Assoc. prof. dr. Mark Masia provided some recommentdations on the details and number of reinforcement for NSM. The strengthening of the specimens was conducted by GRAS d.o.o., MAPEI d.o.o. supplied the material for strengthening of one wall, which was applied according to their recommendations.

BLANK PAGE

»Ta stran je namenoma prazna.«

ZAHVALA

Zahvalila bi se mentorju izr. prof. dr. Vlatku Bosiljkov za vso pomoč pri nalogi ter tudi za dragoceno možnost sodelovanja na različnih projektih. Zahvala gre tudi prof. dr. Roku Žarniću za predstavljeno področje dela in vabilo na katedro ter prof. Violeti Bokan Bosiljkov za vso pomoč in podporo. Franciju Čeponu iskreno hvala za pomoč pri izvedbi eksperimentalega dela. Za vse lepe besede in pomoč se zahvaljujem tudi dr. Barbari Vodopivec.

I would like to express my warm gratitude to prof. dr. Mark Masia. The experience, recommendations and discussions on NSM strenghtening were of great value.

Kind appreciation also to prof. dr. Sergio Lagomarsino, dr. Serena Cattari and dr. Chiara Calderini for valuable collaboration on the PERPETUATE project and specially to Serena for kindly answering many questions regarding Tremuri over the years.

K uspešnemu izboru ukrepov za utrditev zidov so s pogovori in izkušnjami prispevali dr. Mojmir Uranjek, dr. Samo Gostič, g. Andraž Nedog, g. Dino Berginc in g. Iztok Leskovar. Za podane informacije in pomoč se vsem lepo zahvaljujem.

Za prijazno pomoč pri iskanju primernega objekta za analizo ter informacije o Vili Vipolže bi se zahvalila g. Milošu Ekarju, ge. Ernesti Drole in g. Mitji Mozetiču iz ZVKDS. Za omogočen vpogled v obstoječo dokumentacijo in prijaznost bi se zahvalila ge. Iris Motnik Šernek z Ministrstva za kulturo.

Ani Naglič, Janezu Korpiču, Luki Kurnjeku, Alji Arrigler, Nini Milikič in Luki Božiču se zahvaljujem za narejeno delo, predvsem pa tudi za super družbo v pisarni, v laboratoriju…
Zelo sem vesela, da sem vas spoznala.

Hvala prijateljem in družini, ki ste mi stali ob strani!

David, Petra in Patricia, hvala vam za dobro vzdušje v pisarni, na KPMK in drugje, za vse lepe trenutke ter da ste (pre)večkrat prenašali mojo slabo voljo (za slednje, predvsem David, hvala).
Tebi Petra gre posebna zahvala tudi za sproščujoče popoldneve, večer(j)e in animacijo Jake.

Simona, hvala ti za vso podporo.

Ajka, za pozitivne besede in vso radodarno pomoč se vam lepo zahvaljujem.

Mami in oči (Andreja in Borut), Matevž in Tina ter Ani, Drago in Mateja, hvala vam za vso podporo in pomoč.

Franciju,
ker nesebično, pogosto
preko meni razumnih meja, vedno pomagaš,
da zmoreš in tudi kdaj si oči in mami hkrati,
za vso podporo (takšno in drugačno) in razumevanje.
Hvala ti za vse!

Jaki in Valu!
Ker dajeta smisel.
Vsemu.

BLANK PAGE

»Ta stran je namenoma prazna.«

TABLE OF CONTENTS

BLANK PAGE

»Ta stran je namenoma prazna.«

INDEX OF FIGURES

SEZNAM SLIK

BLANK PAGE

»Ta stran je namenoma prazna.«

INDEX OF TABLES

BLANK PAGE

»Ta stran je namenoma prazna.«

SEZNAM PREGLEDNIC

BLANK PAGE

»Ta stran je namenoma prazna.«

LIST OF ACRONIMS AND ABBREVIATIONS / SEZNAM AKRONIMOV IN OKRAJŠAV

A1	Damage level corresponding to drift at which the first detachment of the plaster was observed
A2	Damage level corresponding to drift at which the first structural crack on the plaster occurred
A3	Damage level corresponding to drift at which plaster was largely detached from the wall but still repairable
A4	Damage level corresponding to drifts at which plaster collapsed
AA	Artistic Asset
AFRP	Aramid Fibre Reinforced Polymer
apn.-cem.	apneno - cementna
BFRP	Basalt Fibre Reinforced Polymer
c.o.v.	Coefficient of variation
CF	Confidence Factor
CFRP	Carbon Fibre Reinforced Polymer
Coeff.	Coefficient
"CP"	Collapse Prevention
DL	Damage level
"DL"	Damage Limitation
DS	Damage state
EB	Externally bonded
EC	Eurocode
Eq.	Equation
"FC"	First Cracking
FF	Fully favourable
"FO"	Fully Operational
FRP	Fibre Reinforced Polymer
GFRP	Glass Fibre Reinforced Polymer
ICOMOS	International Council on Monuments and Sites
"IO"	Immediate Occupancy
KL3	Full knowledge level
LS	Limit state
"LS"	Life Safety
LVDT	Linear variable differential transformer
max.	Maximum
min.	Minimum
"NC"	Near Collapse
NDT	Non destructive testing
NF	Non favourable
No.	Number
NSM	Near surface mounted or near surface mounting
PA FRP	Polyvinyl-alcohol Fibre Reinforced Polymer
PBA	Performance based assessment
PBD	Performance based design
PF	Partially favourable
PGA	Peak ground acceleration
PL	Performance level
PLi	Performance level related to i-th damage level considering structural damage
PLi,AA	Performance level related to i-th damage level considering artistic asset damage
PVC	Polyvinyl chloride
RC	Reinforced Concrete
RILEM	Réunion Internationale des Laboratoires et Experts des Matériaux, systèmes de construction et ouvrages (eng. International Union of Laboratories and Experts in Construction Materials, Systems and Structures)
"SD"	Significant Damage
SE	Structural elements
SEM	Structural Elements Models
SFRY	Socialist Federal Republic of Yugoslavia
SME	Small or medium enterprise
SRG	Steel reinforced grout
SRP	Steel reinforced polymer
st.dev.	Standard deviation
TRM	Textile Reinforced Mortar
UBC	Unified Building Code
ULS	Ultimate limit state
URM	Un-Reinforced Masonry

BLANK PAGE

»Ta stran je namenoma prazna.«

LIST OF SYMBOLS / SEZNAM SIMBOLOV

A_{hyst}	the area within one hysteresis cycle
A_b	bond area between the masonry and paste
A_f	the cross-section area of FRP shear strengthening (in the direction parallel to shear force)
$A_{f,bar}$	area of one FRP rectangular or cicrular bar
A_n	area of FRP net mortared/grouted section
A_w	gross cross-section area of the wall
$A_{w,n}$	net cross-section area of the wall
C_{cr}	experimentally obtained reduction coefficient
C_d	nominal shear strength coefficient
C_E	environmental reduction factor C_E appropriate fibre type and exposure condition. The reduction factor
CF	confidence factor
D	the depth of the groove
E_1	the modulus of elasticity for the exterior multi-leaf masonry layer
E_2	the modulus of elasticity for the interior multi-leaf masonry layer
E_b	modulus of elasticity of the unit
E_{DIS}	dissipated energy
$E_{DIS,i}$	dissipated energy for i-th loading cycle
E_f	FRP modulus of elasticity
$E_{f,\theta}$	modulus of elasticity parallel to the tensile diagonal
E_h	elasticity modulus of the homogeneous system, made of FRP and layer of regularization
$E_{ID,el}$	the total elastic energy absorption of the equivalent elastic-perfectly plastic model
E_{INP}	input energy
$E_{INP,i}$	input energy of the i-th cycle
E_M	modulus of elasticity of the masonry
E_m	modulus of elasticity of the mortar
E_N	normalized cumulative energy dissipation
$E_{N,modified}$	modified normalized cumulative energy dissipation
E_r	elasticity modulus of the regularization layer
F	lateral force induced at shear testing
F_b	base shear capacity
F_{cr}	force at first shear crack
$F_{cr,x}$	force at first flexural crack
F_{dmax}	resistance obtained at maximum displacement
$F_{dmax,i}$	maximum force attained for the i-th loading cycle
F_{id}	idealized force
$F^k_{max,i}$	maximum shear resistance of the k-th positive loading direction part of loading of the i-th amplitude displacements cycle
$F^k_{min,i}$	maximum absolute shear resistance of the k-th negative loading direction part of loading of the i-th amplitude displacements cycle
F_{max}	maximum in-plane shear resistance of the wall
$F_{max,i}$	maximum shear resistance of the i-th amplitude displacements cycle
G	shear modulus
$G_{1.5mm}$	shear modulus determined for displacement 1.5 mm
G_j	shear modulus of joint
G_M	shear modulus of the masonry
H	horizontal force
K	stiffness
K^+	secant stiffness at the cycle maximum displacement
$K_{1.5mm}$	stiffness determined for displacement 1.5 mm
K_{ef}	effective stiffness of the wall/pier
K_i^+ , K_i^-	stiffness determined for maximum ($^+$) and minimum ($^-$) displacement of the i-th amplitude displacement cycle
L_i	effective bond length of the i-th bar intersecting the diagonal crack
Lt	the sum of the bonded lengths of all the rods crossed by the crack
M_u	ultimate moment
N	vertical force transferred to external leaves
N_f	additional vertical compression (strength or load) due to FRP reinforcement
P	vertical force the multi-leaf wall is subjected to
P_d	maximum force at diagonal test
T^*	the elastic period of the idealized bi-linear system
T_L	return period
T_{LR}	reference return period
V	volume

V_b	bond controlled FRP contribution to shear resistance
V_f	the FRP nominal shear strength contribution
V_m	URM wall nominal shear strength contribution
V_{Rd}	design value of shear resistance
V_{Rd} *(net)*	design value of shear resistance considering net cross-section area of the multi-leaf wall
$V_{Rd,d}$	design value of shear resistance considering diagonal cracking
$V_{Rd,dj}$	design value of shear resistance considering diagonal cracking through joints
$V_{Rd,du}$	design value of shear resistance considering diagonal cracking through units
$V_{Rd,f}$	design shear capacity contribution of the FRP reinforcement
$V_{Rd,m}$	design shear capacity contribution of the URM wall
$V_{Rd,r}$	design value of shear resistance considering rocking
$V_{Rd,s}$	design value of shear resistance considering sliding
V_s	steel nominal shear strength contribution
V_t	rupture controlled FRP contribution to shear resistance
a	the width of the prism
a_b	smallest rectangular FRP bar dimension
a_g	design ground acceleration on type A ground
$a_{g,PLi}$	maximum ground acceleration the building can sustain for the evaluated i-th performance level
b	shear distribution factor
b_b	largest rectangular FRP bar dimension
b_d	the width of the bond distribution area
b_f	the width of the FRP reinforcement
$b_{f,ef}$	the effective width of the FRP reinforcement
c	coefficient of cohesion
c_1	experimentally determined coefficient in FRP fracture energy calculation
d	displacement
d	the distance between the compression side of the masonry and the centroid of FRP flexural strengthening
d	displacement
d_1	width of a prism sample
d_2	height of a prism sample
$d_{2/3Fmax}$	displacement where shear force reaches two thirds of the maximal shear resistance
d_b	FRP bar diameter
d_{cr}	displacement at which first crack is attained
$d_{cr,AA}$	displacement of the wall at which first crack on the artistic asset (plaster) is attained
$d_{cr,x}$	displacement of the wall at which first flexural crack is attained
$d_{DS,Ai}$	displacement of the wall at which the i-th damage state of the artistic asset (plaster) is acheved
d_e	elastic displacement of an idealized bi-linear curve
d_{Fmax}	displacement at which maximum resistance is reached
d_{max}	maximum lateral displacement of the evaluated response
$d_{max,AA}$	displacement of the wall at which the artistic asset (plaster) collapses
$d_{max,i}$	maximum displacement attained for the i-th loading cycle
d_u	ultimate displacement of an idealized bilinear curve
d_u^*	reduced ultimate displacement of an idealized bilinear curve
d_u^*	ultimate displacement of an idealized bilinear curve reduced to displacement where the resistance is not lower than F_{id}
d_v	the effective masonry depth
$d_{\zeta min,i}$	displacement corresponding to attainment of minimal values of equivalent damping coefficient
f_0	strength for determining the compressive strength of internal leaf of multi-leaf masonry dependent from mortar compressive strength
f_{bc}	compressive strength of the unit
$f_{bc,n}$	normalised compressive strength of the unit
f_{bm}	average compressive strength of masonry blocks
f_{bt}	tensile strength of the unit
f_{bt}	tensile strength od the unit
f_{btm}	average tensile strength of masonry blocks
f_{bx}	flexural tensile strength of the unit
f_c	compressive strength of concrete
f_{cc}	compressive strength of the core
f_{cst}	splitting tensile strength of the core
f_{fd}	design tensile strength of FRP reinforcement
f_{fdd}	design FRP debonding strength
f_{fe}	FRP effective stress
f_{fu}	FRP ultimate tensile strength
f_{jx}	bond strength of mortar-unit junction determined with Bond Wrench test

f_{Mc}	compressive strength of the masonry
f_{mc}	compressive strength of the mortar
$f_{Mc,k}$	characteristic compressive strength of the masonry
$f_{Mc,x}$	compressive strength of the masonry parallel to the joints
f_{Mc}^{e}	compressive strength of the masonry external leaf
f_{Mc}^{i}	compressive strength of the masonry internal leaf
f_{mf}	flexural tensile strength of the mortar
f_{mk}	masonry characteristic compressive strength
f_{Mt}	diagonal tensile strength of the masonry
$f_{Mt,m}$	masonry average tensile strength
f_{St}	splitting tensile strength
f_t	tensile strength of concrete
f_{tu}^{*}	ultimate tensile strength of the FRP material as reported from the manufacturer
f_{v0}	initial shear strength of the masonry
f_{vk}	characteristic shear strength of masonry
$f_{vk,lim}$	the limit value of characteristic shear strength of masonry
f_{vk0}	characteristic initial shear strength of the masonry
g_M	material safety factor
h	depth of the hole
h_0	distance between the section where the flexural capacity is obtained and the contra-flexure point
h_b	masonry unit (block) height
h_j	height of the mortar joint
h_w	height of wall/pier
k	volume proportion of mortar in the masonry
k	compression strength reduction factor which takes into account filled or unfilled head joints
k'	coefficient dependant of the applied restraint conditions of the element
k_1, k_2, k_3	coefficients dependent of the type of the masonry units
k_b	geometrical corrective factor in FRP fracture energy calculation
k_G	corrective slip factor in FRP fracture energy calculation
l	length of the transfer area in multi-leaf walls
l	length of a prism sample
l	debonded length of the FRP reinforcement
l_b	masonry unit (block) length
l_b	length of the FRP bonded area
l_e	effective FRP bond length
l_f	length of the FRP reinforcement
l_{fc}	the distance between the compression side of the masonry and the centroid of FRP flexural strengthening
l_w	length of wall/pier
l_{wc}	length of the compressed part of the wall/pier
m	mass
n	number of plies of FRP laminates or number of circular and rectangular FRP bars, or both
n_i	porosity of the core stones in multi-leaf masonry
n_s	the number of the strengthened sides of the wall
p_f	the centre-to-centre spacing of FRP reinforcement measured orthogonally to the direction of the shear force
p_{fv}	the total transferred force per unit FRP width for EB FRP or per FRP bar for NSM
q^{*}	equivalent behaviour factor
r	radius of the hole
r	FRP reinforcement efficiency factor
r_b	the number (integer) of rods in the bond controlled region
$r_{b'}$	calculated number of rods in the bond controlled region
r_t	the number of rods in the rupture controlled region
s	thickness of the intermediate layer of multi-leaf masonry
s_f	the centre-to-centre spacing of FRP reinforcement measured orthogonally to the direction of the shear force
s_u	FRP slip interface corresponding to full debonding
t	time
t_1	thickness of external masonry leaf
t_2	thickness of the internal masonry leaf (infill)
t_f	FRP thickness
t_h	thickness of the homogeneous system, made of FRP and layer of regularization
t_m	the thickness of the mortar joints
t_r	thickness of the regularization layer
t_w	thickness of the wall/pier
u_{desno}	displacement of the right plaster edge
u_{levo}	displacement of the left plaster edge
u_{spodaj}	displacement of the bottom plaster edge

u_{zgoraj}	displacement of the upper plaster edge
w	effective width of the FRP sheet in carrying tension
x	the distance of the neutral axis from the extreme compression fibre
x_{min}	the minimum distance between the neutral axis and the extreme compression fibre of the section
α	parameter describing stiffness degradation
α	inclination of the FRP strengthening
α_{POZ}, α_{NEG}, α_{AVE}	parameter describing stiffness degradation evaluated for positive, negative and average cycle characteristic behaviour
β	parameter describing stiffness degradation
β_{POZ}, β_{NEG}, β_{AVE}	parameter describing stiffness degradation evaluated for positive, negative and average cycle characteristic behaviour
γ	shear strain
γ_1	importance/use coefficient
γ_f	partial material factor for FRP in case of FRP rupture
$\gamma_{f,d}$	partial material factor for FRP in case of FRP debonding
Γ_{Fk}	the characteristic specific fracture energy of the FRP strengthened masonry
γ_m	partial material factor
γ_{Rd}	partial factor for resistance models
δ_1	deflection capacity of the unreinforced masonry wall
ΔF_{rel}	Force decrease
δ_{Rd}	design displacement of the FRP strengthened wall
$\delta_{Rd,1}$	displacement of the FRP strengthened wall at the top cross section
$\delta_{Rd,2}$	maximum horizontal displacement compatible with design strain of FRP
$\Delta\varepsilon$	strain difference
$\Delta\sigma$	stress difference
ε	strain
ε_1	FRP warp strain
ε_1	the strain in the FRP ε_1 for a masonry wall deflection of δ_1
ε_2	FRP weft strain
ε_{fd}	FRP ultimate strain
ε_{fdd}	maximum design FRP debonding strain
ε_{fe}	FRP effective strain
ε_{fk}	characteristic FRP failure strain
$\varepsilon_{frp,e}$	the effective FRP strain
$\varepsilon_{frp,u}$	FRP ultimate tensile strain
ε_{fu}	FRP design rupture strain
ζ_1	coefficient for determining elastic modulus of external leaves of multi-leaf masonry depending from the type of masonry
ζ_2	coefficient for determining elastic modulus of internal leaves multi-leaf masonry depending from the type of masonry
η	coefficient used for determining drift limits, which considers boundary conditions
η	coefficient considering boundary conditions
η_a	Environmental conversion coefficient
θ_f	the angle between the wrap of FRP sheet and horizontal base line
θ	drift
θ_{cr}	drift at which first shear crack is obtained
θ_{DL}	drift capacity for the Damage Limitation damage limit state
θ_e	drift capacity corresponding to elastic displacement
θ^e	correction coefficient for external leaf compressive strength calculation
θ_{Fmax}	drift at which maximum resistance is obtained
θ^i	correction coefficients for internal leaf compressive strength calculation
θ_{LS}	drift capacity of the evaluated Limit State
$\theta_{LS,mean}$	mean values of drift capacity for the evaluated Limit State
θ_{max}	maximum drift capacity
θ_{max}	drift capacity corresponding to maximum displacement obtained
θ_{NC}	drift capacity for the Near Collapse damage limit state
θ_{SD}	drift capacity for the Significant Damage damage limit state
θ_u	ultimate drift capacity
θ_u^*	ultimate drift capacity, corresponding to reduced displacement d_u^*
θ_u^*	ultimate drift capacity corresponding to displacement d_u^*
κ_{frp}	coefficient accounting for FRP observed mechanism of failure
κ_v	FRP bond reduction coefficient
μ	coefficient of friction
μ^*	ductility corresponding to displacement d_u^*
ν_M	Poisson's ratio for masonry
ξ	equivalent viscous damping coefficient
ξ_f	coefficient correlative to the area reinforcement rate of FRP
ξ_s	ξ for horizontal FRP reinforcement

ξ_x	ξ for diagonal FRP reinforcement
ρ	density
ρ	area reinforcement rate of FRP
ρ_h	FRP laminates area fraction
ρ_s	horizontal FRP effect coefficient
ρ_x	inclined FRP effect coefficient
σ	stress
σ_0	average compression stress due to vertical loading
σ_1	normal stresses for external masonry leaf
σ_2	normal stresses for internal masonry leaf
σ_a	vertical stress at 1/3 compressive strength of the sample
σ_b	starting reference stress value
σ_d	average vertical stress of the compressed part of the wall
σ_{LS}	biased standard deviation for the evaluated Limit State
σ_{max}	maximal stress obtained
σ_x	load on the masonry parallel to the joints
τ	(limit) shear stress of masonry
τ_0^*	
τ_b	FRP average bond stress
τ_{Fmax}	average shear stress over the whole cross section of the wall at the attained maximum resistance of the wall
τ_j	shear stress at the interface between the joint and the leaf
τ_{M0}	average shear resistance of masonry at diagonal failure
ϕ	interlocking parameter considering the texture of masonry
χ_e	coefficient which describes the bed-joint thickness and the volume of included mortar
χ_i	coefficient taking into account the size of units and presence of voids in the internal (core) layer of multi-leaf masonry
ψ	corrective factor in dependence from boundary conditions
ω	exciting frequency of the system

BLANK PAGE

»Ta stran je namenoma prazna.«

1 INTRODUCTION

1.1 Motivation

Masonry is the oldest construction form in the history of mankind, widespread over the entire world. Old historic masonry buildings of various types constructed in different eras present a significant world architectural heritage themselves, whereas their attributes (such as decorated plasters, stuccos, statues, hanging elements, etc…) can also be of great importance (Figure 1.1). The aspect of heritage is not important only from a historical and cultural point of view, but often plays an important social (e.g. religious) and economical role (e.g. tourism). Since there is a reasoned tendency upon the preservation and further use of such buildings, there should be as much knowledge and as many techniques as possible available for their assessment, conservation and providing their safe use. Assessing the state of an existing building is however a very difficult task, as is the determination of (appropriate) intervention measures.

Figure 1.1: Danse Macabre fresco (left, http://commons.wikimedia.org/wiki/File:Danse_macabre_hrastovlje.JPG) in the Holy Trinity Church in Hrastovlje, Slovenia (right, http://www.publishwall.si/lelj/photos/photo/23345)
Slika 1.1: Freska mrtvaškega plesa (levo, http://commons.wikimedia.org/wiki/File:Danse_macabre_hrastovlje.JPG) v cerkvi svete Trojice, Hrastovlje, Slovenija (desno, http://www.publishwall.si/lelj/photos/photo/23345)

Masonry itself can be found in countless variations; it is constructed from various materials (various block material, binder), differently shaped, layed and connected in-plane and transversally. Buildings, constructed from two or three-leaf masonry, present a significant part of the European as well as Slovenian architectural heritage. The multi-leaf composition presents an additional parameter that contributes to their specific response when subjected to loading and makes it even more complex. Historic masonry characteristics are also defined by the state of conservation, ageing and degradation of the materials. The behaviour of masonry also depends of its integration in the building, i.e. its position, structural role and details of construction. Geometry characteristics, stress state (the loads to

which masonry elements are subjected) and boundary conditions have significant influence on the behaviour. In dependence of all these mentioned parameters, different damage and failure mechanisms of masonry structural elements are obtained. They influence the strength and displacement capacity of the elements. In many cases however the damage and failure mechanism and the capacity are not easily predicted.

In order to obtain an accurate assessment of a structure's resistance under various types of loads, one would need to adequately know the structure, its materials and their mechanical characteristics, one should use appropriate analysis methods and should have available appropriate numerical tools together with all the input data enabling the calculation. Each of the stated above however presents a challenge of its own. In fact, the complexity of ancient masonry buildings, often subjected to many transformations during their life-time, would require a detailed investigation of almost all structural elements, since it is difficult to extend the data acquired in one single point to other parts of the building. In some cases the diagnostic activity may be very intrusive, not compatible with the conservation policy of the asset of interest and therefore not feasible. This brings out the need for diagnosis of the state by means of less invasive NDT (non-destructive testing) techniques and the need for their development. Considering all this collected data, appropriate method for the analysis should be chosen for the assessment.

Different analysis methods are more efficient for various types of structures where similar behaviour is obtained during specific loading [1]. Models of the structure however require quantitative input data for its resistance assessment. Material and/or structural element mechanical properties have to be provided. These can be obtained again through in-situ investigations; in most cases however comprehensive investigation campaigns with a sufficient statistical sample are again not compatible with conservation aims and thus not possible. Not to mention that one has to have in mind the overall cost of the investigation, assessment and the adopted retrofitting/strengthening/rehabilitation measures of the building. For design purposes, whenever possible, the mechanical properties may be obtained by considering the results from in-situ or laboratory tests of similar walls (or other structural element in question), while keeping in mind the decay phenomena [2]. Thus, the availability of reference datasets of parameters gained through experiments to be adopted in models is of fundamental importance for the effective seismic assessment. In some countries or regions, characteristics of different masonry textures and morphologies in a form of tables with reference values to be adopted in design are provided within the national code provisions (e.g. in Italy [3]). This is however not the case in Slovenia. Experimental tests are besides of obtaining proper material characteristic also important in order to enable establishment of proper models for behaviour of various structural elements.

In the last decades severe damage and even collapse of multi-leaf masonry structures during or following an earthquake have occurred. A sudden and unexpected collapse of the famous Noto Cathedral in 1996 happened six years after earthquake due to creep, induced by the long term subjection to compressive stresses (due to dead load) and the weakened masonry characteristics of severely damaged pillars, which were the result of the recent and previous earthquake events. Severe damage was found also in the Santissimo Crocifisso in Noto and Santissima Annunziata Church in Ispica [4]. On the other hand in the recent earthquake events in Italy as the result of poor masonry connectivity also numerous out-of-plane collapses of the external leaves of historic masonry buildings

occurred. The events revealed the lack of understanding of the behaviour of multi-leaf masonry and the need for their more detailed studies.

Figure 1.2: Ruins of the Noto Cathedral after 1996 collapse [5] (left), out-of-plane failure mechanism due to poor connection of the structural elements (middle, http://db.nzsee.org.nz/Seminars/2014/Lagomarsino_Wellington_2014-2-20.pdf) and out-of-plane collapse of masonry wall due to poor connection of the masonry [6] (right) in L'Aquila, Abruzzo, Italy
Slika 1.2: Ruševine katedrale v Notu po porušitvi leta 1996 [5] (levo), izven-ravninska porušitev zidov zaradi slabe povezanosti konstrukcijskih elementov (na sredini, http://db.nzsee.org.nz/Seminars/2014/Lagomarsino_Wellington_2014-2-20.pdf) in izven-ravninska porušitev večslojnega zidu zaradi slabe povezanosti zidovine [6] (desno), L'Aquila, Abruzzo, Italija

For most historic buildings, earthquakes present a large and specific problem, as many of the buildings were not designed for lateral loads that can be induced during earthquakes. Also the recent earthquakes close to Slovenia (in Italy; Umbria-Marche 1997; Molise 2002; L'Aquila 2009; Emilia-Romagna 2012; Turkey 2011, Algeria 2003,…) and the very recent and most devastating ones around the world (Sichuan province in China 2008; Haiti and Chile 2010; Tōhoku in Japan and Christchurch in New Zealand 2011) proved high vulnerability of existing buildings in case of earthquakes, resulting not only in severe damage and collapses of structures, but also in many human casualties.

Through these and other seismic events also some very important heritage was lost. In Figure 1.3, the ruins of Port-au-Prince Cathedral in Haiti and the remains of mural at the Holy Trinity Cathedral in Port-au-Prince, which were destroyed in 2010 earthquake, are presented. The earthquake destroyed or buried much of Haiti's cultural heritage.

Figure 1.3: Ruins of the Port-au-Prince Cathedral in Haiti after 2010 earthquake (left, photo from haitian-truth.org, http://blogs.nd.edu/classicalarch/2012/04/14/design-competition-for-a-new-cathedral-in-port-au-prince-haiti/), the remains of mural at the Holy Trinity Cathedral in Port-au-Prince (right, Thony Belizaire/AFP/Getty Images, http://www.wqxr.org/#!/story/60698-art-conservators-resurrect-haitian-masterpieces/)
Slika 1.3: Ruševine Port-au-Prince-ške katedrale po potresu na Haiti-ju leta 2010 (levo, foto haitian-truth.org, http://blogs.nd.edu/classicalarch/2012/04/14/design-competition-for-a-new-cathedral-in-port-au-prince-haiti/), ostanki stenskih poslikav v Katedrali sv. Trojice v Port-au-Prince-u (desno, Thony Belizaire/AFP/Getty Images, http://www.wqxr.org/#!/story/60698-art-conservators-resurrect-haitian-masterpieces/)

The loss of an iconic building and artefacts can itself result in a social trauma [7]. A cultural trauma emerged after the 1997 Umbria-Marche (Italy) earthquake, where the Basilica of St Francis of Assisi was damaged and the majestic aquamarine ceiling painted with frescoes of Giotto and Cimabue collapsed [7]. The collapse itself and the damage are presented in Figure 1.4.

Figure 1.4: Collapse of the St Francis of Assisi Basilica ceiling during 1997 Umbria-Marche earthquakes (left, http://projecthistoryitalia.altervista.org/26-settembre-1997-terremoto-nelle-marche-e-in-umbria/), destroyed Cimabue fresco vault ceiling in the Assisi Basilica (right, http://it.wikipedia.org/wiki/File:Volta_Cimabue.jpg)
Slika 1.4: Porušitev stropa Bazilike sv. Frančiška Asiškega v Assisi-ju med potresom v Umbria-Marche regiji leta 1997 (levo, http://projecthistoryitalia.altervista.org/26-settembre-1997-terremoto-nelle-marche-e-in-umbria/), uničen obok s freskami Cimabue-ja v Asiški Baziliki (desno, http://it.wikipedia.org/wiki/File:Volta_Cimabue.jpg)

In order to evaluate what are the critical (seismic) loads and the damage for certain limit states not just for the building as a whole unit, but also for its individual structural and non-structural components, performance based assessment (PBA) analyses are carried out. The major shift from the traditional force-based ("strength") design to performance based design (PBD) engineering was made in the last two, three decades [8] evolving to the stage, where it was incorporated in the design code provisions (e.g. NEHRP Recommended Provisions [9]). PBD is displacement oriented, compared to the "strength" design. It considers the structural elements' in-elastic behaviour, their ductility, load re-distribution in the structure, etc. It however still faces many challenges; compared to the new structure design involving mainly concrete and steel structure design, PBA of existing masonry buildings has fallen behind. Due to masonry intrinsic heterogeneity and complexity, there is still a need for work concerning the determination of various in-elastic behaviour models and characteristic limit states with actual displacement capacity values for various structural elements (spandrels, floors,…). The performance assessment of artistic assets is practically still in its early stages [10]; it requires the identification of main damage mechanisms, the definition of proper limit states and, finally, the development of suitable modelling strategies and to evaluate their vulnerability.

Following the assessment of the seismic resistance of the building, the design of strengthening measures is performed, sometimes being rather just the design of retrofitting interventions to minimize the damage due to deterioration or damage induced by some certain events (such as earthquakes). A large variety of retrofitting/strengthening methods and techniques are available nowadays. Some are appropriate for certain application depending of the structural element and its damage, whereas also of the construction material. For heritage building, interventions should be executed considering conservation requirements upon reversibility, minimization of the intervention and compatibility with the original materials, etc. [11]. In the past, due to lack of awareness of the fundamental differences between the modern construction and the traditional building technology some repair measures proved

unsuitable for historic structures. Some modern measures are not just inefficient but have also induced additional damage. One of such examples is the introducing of too stiff materials and structural elements. Use of Portland cement for (re)pointing of old stone (or brick) lime mortar masonry caused leaching of salts and consequent chemical corrosion in the material and water collecting at the joints caused mechanical deterioration due to freeze–thaw action. "For masonry construction, lime mortar separating the stones or bricks is softer than the structural material and allows the building to move and settle differentially without cracking. Lime mortar is also more breathable than these materials, so the majority of evaporation is through the joints." [12]. Inappropriate in practice was also the use of cement for rendering (causing delamination) and for grouting of lime mortar masonry (causing earlier cracking damage under induced loading and changing the load distribution reflecting in significant alternation of the structural behaviour). Development of strengthening methods applicable for historic structures is still in need.

Figure 1.5: Spalling as a result of cement mortars used for pointing (left, http://www.periodliving.co.uk/renovation/expert-advice/exterior-wall-maintenance), delaminating cement render over granite and clay mortared walls on a part of the 16th century manor in St Jean du Doight, Bretagna, France (right, https://jontybarrett.wordpress.com/vernacular/traditional-building-methods/)
Slika 1.5: Propadanje kamna zaradi prefugiranja s cementno malto (levo, http://www.periodliving.co.uk/renovation/expert-advice/exterior-wall-maintenance), odstopanje cementnega ometa na granitnem in opečnem zidu na delu dvorca iz 16. stoletja v St Jean du Doight, Bretanja, Francija (desno, https://jontybarrett.wordpress.com/vernacular/traditional-building-methods/)

In order to contribute to solving some of the issues presented above and to contribute to conservation and safety of masonry cultural heritage, PERPETUATE project (**PER**formance-based a**P**proach to **E**arthquake pro**T**ection of c**U**ltur**A**l heri**T**age in **E**uropean and Mediterranean countries) was funded by the European Commission within the 7th Framework Programme. The project involved 11 partners (universities, research institutes and SMEs from Europe and Algiers) and was led by University of Genoa. University of Ljubljana (Faculty of Civil and Geodetic Engineering) was one of the collaborating partners. The main objectives of the project were (www.perpetuate.eu):

- Development of European Guidelines for the evaluation and mitigation of seismic risk to cultural heritage assets.
- To face the problem of both architectonic assets (historic buildings; macro elements) and artistic assets (frescos, stucco-works, statues, pinnacles, battlements, banisters, balconies …) specifically focused on masonry structures.

- To consider two different scales of assessment: a) assessment of a single cultural heritage asset (hazard analysis; soil foundation and interaction problems; investigations for the building knowledge; seismic analysis; structural health monitoring and strengthening intervention) and b) assessment at the territorial scale including simplified vulnerability and risk analysis and policy issues for seismic risk mitigation.

Some of the work performed within this thesis was performed within the scope of the PERPETUATE project.

1.2 Objectives

Through the studies performed and presented within the thesis we primarily aimed to study the behaviour of three-leaf stone walls, comparing it to the more established and studied behaviour of single leaf walls. The more specific questions were what are their damage mechanisms and strength capacity under compressive load; when is the out-of-plane mechanism of the wall triggered if subjected to in-plane lateral loading and what is the influence of transversal through stones and the testing conditions. Through experimental test and evaluation of the results we wanted to establish, how accurate are the models for multi-leaf walls for obtaining compressive strength and stiffness parameters and how accurate the shear response in terms of strength and displacement capacity is assessed through various models and code provisions. Concerning response of walls subjected to lateral (shear) loading, we focused merely on the loads induced in-plane (behaviour under out-of-plane loading was not studied).

Since during in-plane shear tests the out-of-plane mechanism was due to characteristics of the investigated masonry not as developed as expected, rather less attention than planned was devoted to this mechanism and its analysis. The evaluation of the test results had therefore further focused solely on the in-plane shear behaviour characteristics and on the determination of performance limit states for the investigated type of masonry. We have to emphasize also, that the outcomes apply only for wall structural elements and that no correlation to behaviour of other elements, such as spandrels, was done within the thesis.

Besides the limit states of the walls, the aim was to study and obtain the limit states for plaster behaviour, since, as mentioned, such tests and values had not been performed and provided up to the time of testing. We believed these values would present valuable information for performance assessment of historic buildings containing valuable murals of interest.

For the damaged walls, the goal was to apply retrofitting and strengthening measures which would meet all our requirements regarding suitability for historic masonry (i.e. compatible materials, preserving exposed masonry texture) and to evaluate their efficiency. However, these requirements led to extensive studies of the materials and systems available and finally to initially not planned development of own strengthening “system”. Because the thesis focuses on the performance assessment of the walls, the aim was to verify the existing design recommendations upon how to evaluate the applied retrofitting and strengthening techniques’ contribution or to provide some additional ones.

When planning the thesis work it was presumed, as already mentioned, that the out-of-plane mechanism would be more developed and would determine the in-plane lateral strength capacity. With this in mind, it was planned to perform a numerical parametric analysis of three-leaf masonry walls varying their texture, morphology, dimensions etc. in order to obtain strength and displacement capacity of various type of multi-leaf masonry. As the mechanism was not obtained as expected, numerical model for such out-of-plane behaviour could not be verified.

Therefore instead of the intended parametric study, a numerical performance assessment of a historic cultural heritage building was performed with the intention of applying the results and conclusions obtained through tests to an actual building and to show what difference these values, if applied, present for the assessment results compared to values provided in the code provisions. For the performance assessment also artistic asset in the building was considered for determining performance levels. Through this performance assessment therefore also the results of plasteres were applied.

BLANK PAGE

»Ta stran je namenoma prazna.«

2 LITERATURE OVERVIEW

In the following Chapter an insight on the existing knowledge on the problems dealt with in the thesis is provided. It is assumed, that the reader already has some basic knowledge on the behaviour of masonry and masonry structures under various loading. Since in the thesis various issues were addressed, the presented literature overview is quite miscellaneous. Some topics are presented very shortly, whereas the ones concerning the scientific contribution of the work are presented more thoroughly. All this existing knowledge, presented to a certain level, was needed in order to, first, define the issues of concern and goals, further to plan experimental tests (specimen design and construction, the execution of the tests themselves) and finally to analyse and evaluate the results. In general the overview can be divided into four main subsections:

1. characterization of masonry and plaster (Section 2.1),
2. behaviour of the walls subjected to in-plane lateral loads (Section 2.3) with a more detail review on the behaviour and the existing studies of multi-leaf masonry (Section 2.4),
3. strengthening interventions with focus on those appropriate for improving the behaviour of historic masonry walls and FRP strengthening (Sections 2.5) and
4. performance based assessment of historic masonry structures (Section 2.2).

2.1 Characterization of the masonry walls and plasters

Masonry is a composite, heterogeneous structural material assembled of units and mortar. Units may be either of natural (stone) or artificial source (bricks), laid in courses or randomly distributed, possibly composed in multiple leaves, often with infill material between the leaves. Properties of the masonry components (units, mortar, infill), their volume ratio and bond properties determine the properties of the composite assemblage.

2.1.1 Classification of masonry

There is no universal classification of different masonry typologies. They all represent the state of development and technical achievements of a particular culture in a certain area and time. Regarding

old Greek and Roman masonry found in the Mediterranean basin, some general classification can be found in Marcus Vitruvius [13] and Davies and Jokiniemi [14].

In a broader aspect regarding the type of the unit used to build masonry, a more general division of historical masonry can be made on stone, brick, adobe and rubble masonry [15], [16].

By considering the technology of the production of masonry courses and the level of dressing of stone units, further division can be made for stone rubble masonry to: uncoursed random rubble; coursed random rubble; uncoursed squared rubble; coursed squared rubble; built to regular courses masonry; polygonal rubble; flint rubble and dry (mortarless) rubble masonry. Ashlar masonry can be further classified as fine, roughly tooled, rocked or quarry faced, chamfered, block in course or solely ashlar facing masonry.

Apart from the type of unit and mortar, two main characteristics of stone masonry, that determine its behaviour under different types of in- and out-of-plane loading, are its texture and morphology.

For composite (multi-leaf) masonry cross sections, the apparent texture does not necessarily dictate the overall behaviour of masonry and determine the mechanical characteristics of built masonry. Thus for composite cross sections, where the thickness of outer leaves is negligible in comparison to the gross section, the apparent texture is not of significance for the determination of the behaviour of the masonry. In respect to the morphology of historical masonry three distinguishing typologies of morphology (Figure 2.1) are according to Binda et al [17] identified as:

- **Single-leaf**: stone elements are bound together using mortar, stone elements may be characterized by irregular or regular shapes and the mortar joints are normally thick and horizontally or sub-horizontally inclined. Otherwise, stone units can be regular, staggered and placed on horizontal courses.
- **Double-leaf**: two different layers can be identified on the cross section. Nevertheless, this typology can be differentiated in two further sections: attached leaves, which are completely separated by a vertical joint formed from mortar or voids; interlocked leaves, where stones of subsequent courses of opposite layers are slightly overlapped.
- **Three-leaf**: two load-bearing external leaves with higher thickness and an internal core comprised of stone fragments, normally in incoherent form and without any bound element. In some cases, a transverse connection is provided by irregularly disposed, through-the-thickness elements.

Single-leaf Double-leaf Three-leaf

Figure 2.1. Classification of the masonry with respect to the wall sections (morphology) [18]
Slika 2.1: Razdelitev zidovine glede na prečni prerez (glede na morfologijo) [18]

Depending on the technology of coursing and dressing of the units, the textures of masonry are according to Binda et al [18] further classified as "non" (NF), "partially" (PF) or "fully favourable" (FF) in respect of various loading conditions. For multi-leaf masonry, the level of connection between the leaves determines the monolithic response of masonry and according to the RELUIS methodology of assessment of historical masonry [18,19] masonry can be classified as presented in Figure 2.2.

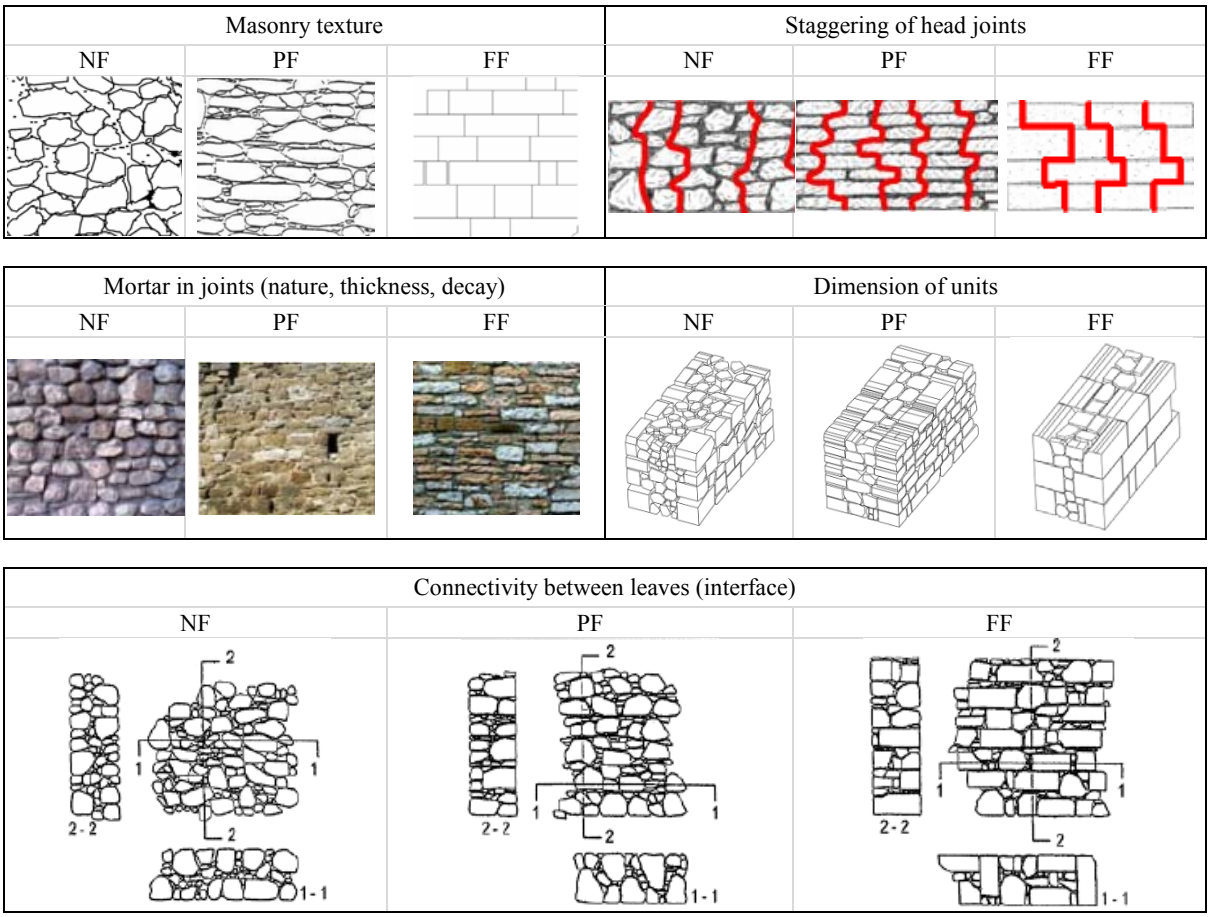

Figure 2.2. Classification of the masonry following visual inspection according to the RELUIS methodology for the assessment of the quality of built masonry (adapted from [16,18-21])
Slika 2.2: Klasifikacija zidovine za določitev ocene kvalitete zidovine z vizualnim pregledom po RELUIS metodologiji (povzeto po [16,18-21])

Following the above mentioned review, visual identification of the masonry can be based on three main parameters: texture, morphology and characteristics of the constituents; further criteria that characterize each of them are presented in Table 2.1 (after [18]).

Moreover, in Borri [20] and Borri and De Maria [22], a procedure to classify historical masonry based on the assignment of a Masonry Quality Index is proposed.

Preglednica 2.1: Klasifikacija glavnih meril za identifikacijo tipa zidovine (povzeto po [18])

Table 2.1: Classification of the main criteria for the identification of the type of masonry (adapted from [18])

Texture	Morphology	Characterization of the constituents:	
- Structural role - Type of masonry - Banded horizontal courses - Banded different types of masonry - Presence of wedges - Horizontally coursed layers - Staggering of perpend joints - Length of plane of the weakness	- Typology - Type of section - Thickness of the section - Presence of wedges - Distribution of voids - Size of the voids - Banded different types of masonry - Presence of headers/cross stones - Length of plane of the weakness	Units: - Type of unit - Source - Workmanship - Conservation - Regularity of the units - Size of the units	Mortar: - Function - Colour of mortar - Colour of the aggregate - Type of the aggregate - Consistency - Shape of the aggregate - Quality of mortar / condition / bond strength

Finally, it should not be forgotten that the conservation state of the masonry should always be regarded with respect to the decay of the material over time. While some of the manifestation of the decay are solely related to aesthetics (surface changes – change of colour, sedimentation, transformation etc.) others relate to physico-chemical parameters and changes (disintegration, layering, crushing, loose material etc.) which may significantly influence the mechanical properties of the constituents and consequently of the masonry [18,23].

2.1.2 Mechanical properties of masonry at a scale of a single constituent, small assemblages and walls

In this Section, a list of mechanical parameters commonly used to characterize the behaviour of masonry at different scales - that of a single constituent, small assemblage and wall – is presented together with reference values found from the literature survey.

2.1.2.1 Units

Only stone unit's characteristics are described hereafter, as our focus were stone masonry walls. For clay and adobe units a more detail overview similar to the one provided can be found in [24].

For the Mediterranean region, the most common types of units (depending on their source) are: sandstone, limestone, travertine, limestone, clay and mud-bricks. The source or the origin of the stone unit may be defined as "local excavation, gravel or quarry". In this regard, even for the same region of origin, multiple options are also possible resulting in significant differences in properties of the rocks [25].

The type of stone unit may also be defined depending on the workmanship or processing of the stone prior to laying; dressed or rough. In this regard, according to Peulić [26] six types are distinguished (see Figure 2.3).

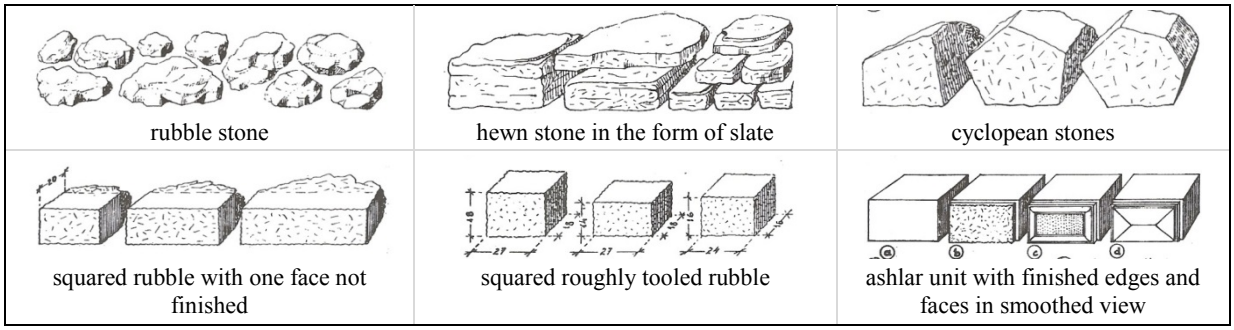

Figure 2.3: Classification of the units depending on the workmanship [26]
Slika 2.3: Klasifikacija gradnikov glede na obdelanost [26]

The characterization of the components of the masonry is performed either on-site or on samples taken from the site and later examined in a laboratory. The most common properties of interest for the characterization of masonry units are porosity, density, water absorption, hardness, thermal expansion, compressive and tensile strength and modulus of elasticity. For the evaluation of structural performance, depending on their geological origin, some of the characteristic values for stone units are presented in Table 2.2 (summarized after [27,28]).

Preglednica 2.2: Mehanske karakteristike različnih kamnin (povzeto po [27,28])

Table 2.2: Mechanical properties of various rocks (adopted from [27,28])

Type of stone *	Density [kg/dm^3]	Compressive strength - f_{bc} [MPa]	Flexural strength - f_{bx} [MPa]	Normal modulus of elasticity - E_b [GPa]	Porosity [%]
Volcanic/Magmatite rocks					
Basalt	2.74-3.20	160-400	15-25	50-100	0.7-29
Diabase	2.80-2.90	180-250	15-25	-	-
Basalt	2.20-2.45	80-150	8-12	-	-
Granite	2.55-2.80	80-300	10-30	35-80	0.1-2.0
Tuff	-	5-40	1-4	4-10	20-50
Sedimentary rocks					
Greywacke	2.58-2.73	15-300	13-25	-	-
Limestone, Dolomite	2.65-2.85	80-180	6-15	15-80	0.1-35
Limestone, soft	1.70-2.60	20-90	5-8	5-20	0.1-35
Travertine	2.40-2.50	20-60	4-10	-	-
Quartz sandstone	2.00-2.65	30-180	3-15	-	-
Sandstone, siliceous	2.60-2.65	120-200	12-20	10-70	1-29
Metamorphic rocks					
Gneiss	2.65-3.00	16-280	13-25	25-80	0.5-4.0
Marble	2.65-2.85	80-180	6-15	15-80	0.4-2.0
Serpentinite	2.60-2.75	140-250	25-35	-	-
Slate	2.60-2.80	-	-	-	-
Quartzite	2.60-2.65	-	-	-	-

* for some rocks depending from their components and state of degradation significantly lower values can be obtained, e.g. for sandstones lower bound may be down to 6 MPa.

2.1.2.2 Mortar

Mortar is used to provide uniform bedding for the units, to level the courses and to fill the gaps in the masonry. The first mortars consisted of clay or clay-straw mixtures. The basic mortar components were also mixed with some other admixtures composed of natural substances, such as blood, egg, fig juice, pig grease, manure, etc. [29]. The Greeks and Romans mixed putty lime and water with sand and crushed stones, producing the earliest type of concrete. Later the Romans mixed putty lime with pozzolana (a volcanic ash) and produced pozzolanic mortars and concrete. When the pozzolana was not available, they also mixed putty lime with crushed and powdered bricks to obtain hydraulic mortars (capable of hardening under the water). They used this material not only in Rome but wherever hydraulic mortars were needed [30]. In the eighteenth century, hydraulic lime was introduced, followed by Portland cement in the early nineteenth century. Combining Portland cement with sand, lime and water a much stronger mortar than previously possible was produced. As a result, both hard and soft mortars were available, depending on the proportions of cement and lime.

Similar to stone, the properties of the mortar used in masonry are quite variable. In addition, the weathering characteristics of mortars, especially of the early mortars, depend very much on local exposure conditions and the thickness of the joints; the properties of historic mortars may vary considerably depending on the position of the samples within the masonry assemblage. Due to the decay process, surface samples may have deteriorated and are apart from the repointing aspect, less useful for the structural characterization of built up masonry. In the following table (Table 2.3) results of tests of various researchers [28,31-34] made on historical mortars are presented, where f_{mc} is the compressive strength and E_m the modulus of elasticity of mortar.

Preglednica 2.3: Mehanske karakteristike malt glede na vrsto veziva

Table 2.3: Mechanical properties of the mortars depending on the binder type

Binder	Soil	Lime	Hydraulic lime	Roman cement	Portland cement
f_{mc} [MPa]	0.5-3	0.5-3	2-10	5-20	10-50
E_m [GPa]	< 1	1-5	5-15	-	20-30

2.1.2.3 Joints

Together with the mortar and the unit, the bonding of these components is the third constitutive element of the masonry. The bond strength of the mortar - unit interface f_{jx} depends on the surface absorption properties of the unit (porosity, initial rate of absorption, etc.) as well as on the properties of the mortar itself. The bond strength of a weak mortar (f_{mc} = 1-3 MPa) measured using a bond wrench test was found to range from 0.01 to 0.13 MPa. However, for mortars with high pozzolanic content, values up to 0.6 MPa may be achievable [35].

2.1.2.4 Infill/Core

The masonry infill may have a good bond, but it is often made up of rubble material of irregular shape and sizes with or without mortar. The most important characteristics are the cohesion, inner friction

and the grade of anisotropy of the material. Infill can be classified by the quantitative stone-mortar relationship and by a parameter for stratification (Figure 2.4).

Figure 2.4: Loose infill material classified with respect to the percentage of fine particles, the size and shape of the coarse material and the type of stratification [36].
Slika 2.4: Nasut material v notranjosti, klasificiran glede na delež finih delcev, velikosti in oblike samega materiala ter tipa urejenosti [36]

Significant for the interaction of the leaves is the contact surface between the inner and the outer shells. According to Sabha and Neuwald-Burg [36] five different types of contact surface may be distinguished. Rock mechanical models may be suitable for their description.

Whether the reaction of the multi-leaf structural element will be monolithic or the load will be transferred solely on the outer leaves depends not only on the type of infill and the contact surface, but on the presence of transverse units (or other tying elements) across the thickness of the wall.

2.1.3 Masonry assemblages and walls

From the above, it may be concluded that the characteristic mechanical properties of masonry depend on numerous combinations of a range of parameters with a wide variety of data. The applicable rules and principles for the determination of the mechanical parameters to be considered in the seismic design of contemporary masonry are only partly applicable to the assessment of historical masonry [24]. In this Section, mechanical parameters that define the behaviour of a masonry assemblage (compressive strength f_{Mc}, initial shear strength f_{v0}, coefficient of friction μ, modulus of elasticity E_M, shear modulus G_M) or those that are commonly introduced to interpret the response of structural walls (diagonal tensile strength f_{Mt}) are presented and discussed.

2.1.3.1 Compressive strength

Unlike brick masonry, where f_{Mc} can be assessed from the strength properties of brick and mortar (Eq. 2.1), this is not the case for stone masonry (unless considering ashlar masonry or regularly dimensioned stone masonry with regular thickness of the joints). Due to the lack of adequate testing equipment, the first design guidelines for the assessment of stone masonry compressive strength made by Baker (from [30]), where f_{Mc} ranged from 1/20 to 1/10 f_{bc}, were unsafe. Since the mortar joints represent planes of weakness within the masonry assemblage, their thickness, elastic properties and volume proportion significantly influence the compressive behaviour of a masonry assemblage. The thinner the mortar joints in relation to the height of the masonry unit, the stronger the masonry will be.

At the same time, however, enough mortar must be used to ensure even bedding with preventing the stones laying on each other and providing a uniform stress distribution between the stones. The smaller the amount of mortar, the more the compressive strength of the masonry depends on the type of unit used.

In the literature there are several theoretical models for the determination of f_{Mc} (summarized in Bosiljkov 1996), however all of them are applicable solely to brick masonry or single-wythe ashlar masonry with regular joints. Most of them consider also the unit/mortar aspect ratio and its influence on the resulting f_{Mc}. This may be of particular importance for masonry with very thick mortar joints.

For regular contemporary stone masonry, according to the EC6 provisions [37], if no test data are available, the characteristic compressive strength of stone masonry $f_{Mc,k}$ may be calculated from the normalized compressive strength of the unit $f_{bc,n}$ and of mortar f_{mc} using Eq. 2.1:

$$f_{Mc,k} = K f_{bc,n}^{0.7} f_{mc}^{0.3}, \qquad \textbf{2.1}$$

where coefficient K is equal to 0.45 for stone ashlar masonry and 0.60 for brickwork masonry.

2.1.3.2 Load transfer and compressive strength of a multi-leaf wall system

Very few models for load distribution and compressive strength calculation can be found in the literature.

According to Binda et al [38] the load transfer between layers under compression load considering strong interface can be calculated according to Eq. 2.2 - 2.4, where parameters in the expressions refer to parameters presented in Figure 2.5 (left) if not stated in the text (some of the parameters will further on present other, commonly represented parameters).

$$F_1 = K_1 \frac{K_2 ea + K_3 (a+b)(e+b)}{K_2 \left(K_1 a^2 + K_3 b^2\right) + K_1 K_3 (a+b)^2} P, \qquad \textbf{2.2}$$

$$F_2 = K_2 \frac{K_1 a (a-e) + K_3 b (e+b)}{K_2 \left(K_1 a^2 + K_3 b^2\right) + K_1 K_3 (a+b)^2} P \qquad \textbf{2.3}$$

$$F_3 = K_3 \frac{K_1 (a+b)(a-e) + K_2 eb}{K_2 \left(K_1 a^2 + K_3 b^2\right) + K_1 K_3 (a+b)^2} P \qquad \textbf{2.4}$$

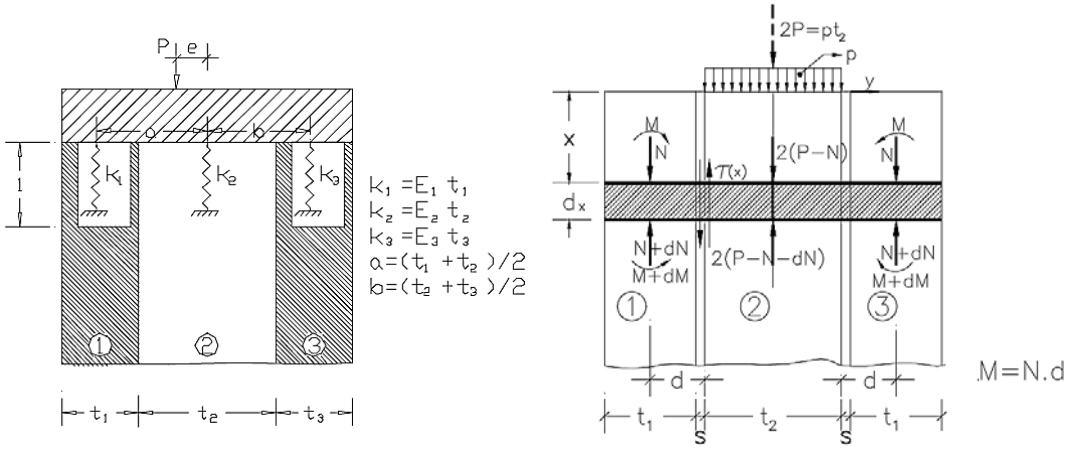

Figure 2.5: Load distribution on leaves with strong (left) and weak (right) interface [38]
Slika 2.5: Porazdelitev obtežbe na sloje pri močni (levo) in šibki (desno) povezanosti slojev [38]

For weak interface (Figure 2.5, right), the force N, which is transferred to the external leaves if a vertical force $2P$ is applied to the composite section, is provided as:

$$N = \frac{1+\tanh(\alpha l)\sinh(\alpha x)-\cosh(\alpha x)}{1+2\left(1+3s/t_1+3s^2/t_1^2\right)E_2t_2/E_1t_1}P, \quad \textbf{2.5}$$

$$\alpha = \sqrt{\frac{G_j}{E_1t_1s}\left(1+\frac{12d^2}{t_1^2}+\frac{2E_1t_1}{E_2t_2}\right)} \quad \textbf{2.6}$$

$$\alpha = s+0.5t_1 \quad \textbf{2.7}$$

where t_1 is the thickness of external leaf, t_2 the thickness of the internal (infill) leaf, s the thickness of the intermediate layer, E_1 and E_2 the elasticity moduli for the exterior and the interior layer, l the length of the transfer area and G_j the shear modulus of the weak joint.

Depending on the cross section, the shear stress τ_j at the interface between the joint and the leaf is expressed by Eq. 2.8 and normal stresses for external σ_1 and internal σ_2 leaf by Eq. 2.9 and Eq. 2.10.

$$\tau_j(x) = dN/dx, \quad \textbf{2.8}$$

$$\sigma_1(x) = \frac{N}{t_1}+\frac{M}{s} = \frac{N}{t_1^2}\left(t_1+6d\right) \quad \textbf{2.9}$$

$$\sigma_2(x) = \frac{2\left(P-N\right)}{t_2} \quad \textbf{2.10}$$

Egermann [39] proposed based on Binda et al [38] "spring" model and the results of the tests performed, the following simplified model for estimation of compressive strength (Eq. 2.11):

$$f_{Mc} = 2\frac{t_1}{2t_1+t_2}\theta^e f_{Mc}^e + \frac{t_2}{2t_1+t_2}\theta^i f_{Mc}^i \quad \textbf{2.11}$$

Parameters θ^e and θ^i present correction coefficients for external f_{Mc}^e and internal f_{Mc}^i leaf compressive strength. Coefficient θ^e depends on the bending stiffness of the external leaf, the boundary conditions and the bending moments and is smaller than 1.0 because the f_{Mc}^e is due to horizontal loading through the yielding infill never reached. Coefficient θ^i presents the ratio between the component stress at failure and the uniaxial compressive strength for the infill; since the lateral deformations of the infill are hindered by the outer leaves and the vertical loading induces triaxial compressive stress state, θ^i is larger than one and it depends on the stratification of the infill.

Binda et al [40] provided a solution considering different hypothesis of the external load supports:

- the external load is completely supported by the stiffer elements i.e. the outer-leaves (Eq. 2.12),
- the external load is supported by each leaf according to its cross-section area ratio (Eq. 2.13),
- the external load is supported by each leaf according to its area ratio and adjusted by a correction factor (Eq. 2.11).

$$f_{Mc} = 2\frac{t_1}{2t_1 + t_2} f_{Mc}^e , \qquad \textbf{2.12}$$

$$f_{Mc} = 2\frac{t_1}{2t_1 + t_2} f_{Mc}^e + \frac{t_2}{2t_1 + t_2} f_{Mc}^i \qquad \textbf{2.13}$$

For three-leaf masonry with keyed collar joints and ashlar masonry in the outer leaves, the authors proposed for correction factors θ^e and θ^i values of 0.7 and 1.3, respectively.

Greek authors Tassios and Chronopoulos [41,42], determined f_{Mc} of a multi-leaf historic masonry (Eq. 2.14) based on the compressive strength of units and mortar, thickness of the joints, shape of the units, type of masonry (stone or brick), where external leaf strength estimation f_{Mc}^e may also serve for evaluation of f_{Mc} of a single-leaf masonry (Eq. 2.15).

$$f_{Mc} = \left(2\lambda_e \delta f_{Mc}^e + \lambda_i f_{Mc}^i\right) / \left(1 + 2\delta\right), \qquad \textbf{2.14}$$

$$f_{Mc}^e = \frac{\frac{2}{3}\sqrt{f_{bc}} + k_1 f_{mc} - k_2}{\xi_e} \qquad \textbf{2.15}$$

$$\xi_e = \frac{1}{1 + 3.5(k - k_0)}$$

$$f_{Mc}{}^i = f_0 e^{(-10 n_i)} \xi_i \qquad \textbf{2.16}$$

$$\delta = t_1 / t_2 \qquad \textbf{2.17}$$

$$\lambda_e = 1 - \left[\frac{0.018}{f_{Mc}^e}\left(\frac{h_w}{t_2}\right)^2 h_w{}^{2/3}\right] : \left[\frac{0.31\left(h_w / t_2\right)^3}{E_1} + \frac{t_2}{E_2}\right] \approx 1 - 0.06\varsigma_e t_1 h_w^{-4/3} \qquad \textbf{2.18}$$

t_1, h_w in [mm]

$$E_1 = \varsigma_1 f_{Mc}^e \qquad \textbf{2.19}$$

$$E_2 = \varsigma_2 f_{Mc}^i \qquad \textbf{2.20}$$

Where k_0, k_1 and k_2 are coefficients dependent of the type and shape of the units; 0.3, 0.6 and 2.5 for rubble stones, 0.2, 0.3 and 0.5 for cut stones, 1.0, 0.2 and 0.0 for ashlar stone blocks, whereas 0.3, 1.0 and 0.0 for bricks; k represents the proportion of mortar in the masonry by volume, ξ_e describes the bed-joint thickness and the volume of the included mortar. For evaluation of elastic moduli of external and internal leaves, ζ_1 and ζ_2 are defined as ζ_1 equal to 500 for rubble, 1000 for cut and 1500 for ashlar masonry, whereas ζ_2 equal to 2000; λ_i is equal to 1, f_0 depends on the f_{mc} and is 35 MPa for f_{mc}~10 MPa, 20 MPa for f_{mc}~4 MPa and 10 MPa for f_{mc}~1 MPa, n_i is the porosity of the core stones, ξ_i is equal to 1.0 if the filling is made of larger or medium-sized blocks where gaps are filled with mortar, otherwise 0.0. Some anomalies of results in dependence from specific parameters, such as height of the wall, are described in [43].

2.1.3.3 *Modulus of elasticity*

The modulus of elasticity E_M may be determined either through laboratory or in-situ testing (Figure 2.6) and is usually determined as the secant modulus (at 1/3 f_{Mc}). This is mainly to allow the closure of the mortar-unit junctions in the early stages of loading that result in a flattened stress-strain diagram. In the absence of experimental values, EC6 prescribes that the E_M is determined as 1000 f_{Mc}. In the literature this ratio (E_M/f_{Mc}) may range between 500 and 1000, with a lower bound range down to 80-140 f_{Mc} [23,35].

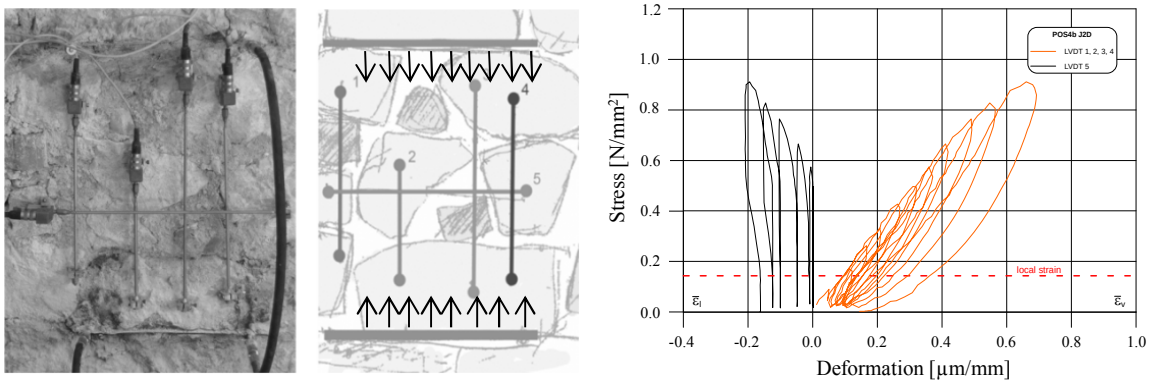

Figure 2.6. Determination of the mechanical properties of the masonry assemblage in compression through in-situ tests; elastic modulus obtained by double flat-jack [44]
Slika 2.6: Določitev mehanskih karakteristik tlačne zidovine z in-situ testi; elastični modul, določen z metodo z dvojno jekleno blazino [44]

Egermann [39] proposes the elasticity modulus of multi-leaf walls to be calculated as (Eq. 2.11):

$$E_M = \frac{2t_1}{t_w} E_1 + \frac{t_2}{t_w} E_2 \qquad \textbf{2.21}$$

2.1.3.4 *Shear modulus*

A simple design assumption of Poisson's ratio ν_M equal to 0.25 and assumption of isotropic material result in equation for the shear modulus $G_M = 0.4\ E_M$. This ratio is also presented in almost all national masonry building codes, including EC6. By considering the orthotropic nature of masonry, through the application of homogenization procedures, the adoption of lower ratios could also be justified, such as

$G_M = E_M/3$; this latter ratio is assumed for the reference values proposed in MIT 2009 [3] and also supported by the results of some experimental campaigns (e.g. those illustrated in Magenes et al 2010 [45] related to the response of undressed double-leaf stone masonry walls).

Shear modulus determined according to these ratios relates to the uncracked or intact masonry. For seismic design purposes, it should be reduced to a value of 5-25% of E_M [46-48]. According to EN 1998-3: 2005 (further in the text referred as EC8-3) [49].

2.1.3.5 Initial shear strength and coefficient of friction

Due to the randomness of masonry and its various texture and morphologies it is rather hard to determine the shear strength of masonry in terms of the characteristics of the unit-mortar junction. Various experimental test set-ups to determine the shear strength properties of unit-mortar junction exist [19,50,51], however most of the methods are designed for units with regular dimensions. One aspect they all have in common is that they are dealing with small (prism sized) masonry specimens and the results of the testing are presented in terms of an initial shear strength or cohesion f_{v0} and a coefficient of friction μ (from an interpretation based on Coulomb-type criteria). In the case of assemblages which are not perfectly regular, the use of these methods is usually not feasible; as an alternative, in order to obtain a "mean" evaluation of such parameters the possibility of using the diagonal compression test (Figure 2.7-b) has been discussed in Calderini et al [52].

For stone masonry, typically f_{v0} ranges from 0.10 for joints of normal thickness, up to 0.30 MPa for thin bed-joints. In the literature there are limited sources regarding the values for f_{v0} and μ for historical masonry (summarized in [35]). For different types of stone masonry, values for μ and f_{v0} are expected in the range of 0.0-0.58 MPa for f_{v0} and 0.29-0.74 for μ, while for brick masonry in the range of 0.08-1.45 MPa and 0.56-0.90, respectively. For the purpose of masonry design, some authors recommend for old masonry with weak mortars design values for f_{v0} in the range of 0.05-0.1 MPa, while for μ values 0.3 for irregular coursed stone masonry and 0.2 for rubble masonry [53].

2.1.3.6 Diagonal tensile strength

For uncoursed stone masonry, where the application of shear strength criteria based on the use of the cohesion and friction coefficient is meaningless, the only criterion at the moment for the evaluation of the lateral resistance of these types of masonry is by considering the principal tensile stresses of the masonry while treating masonry as elastic homogeneous and isotropic material [54]. There is no harmonized test method for the determination of the tensile strength f_{Mt} of masonry. Some of the common ways of testing large masonry elements to simulate seismic effects are presented in Figure 2.7.

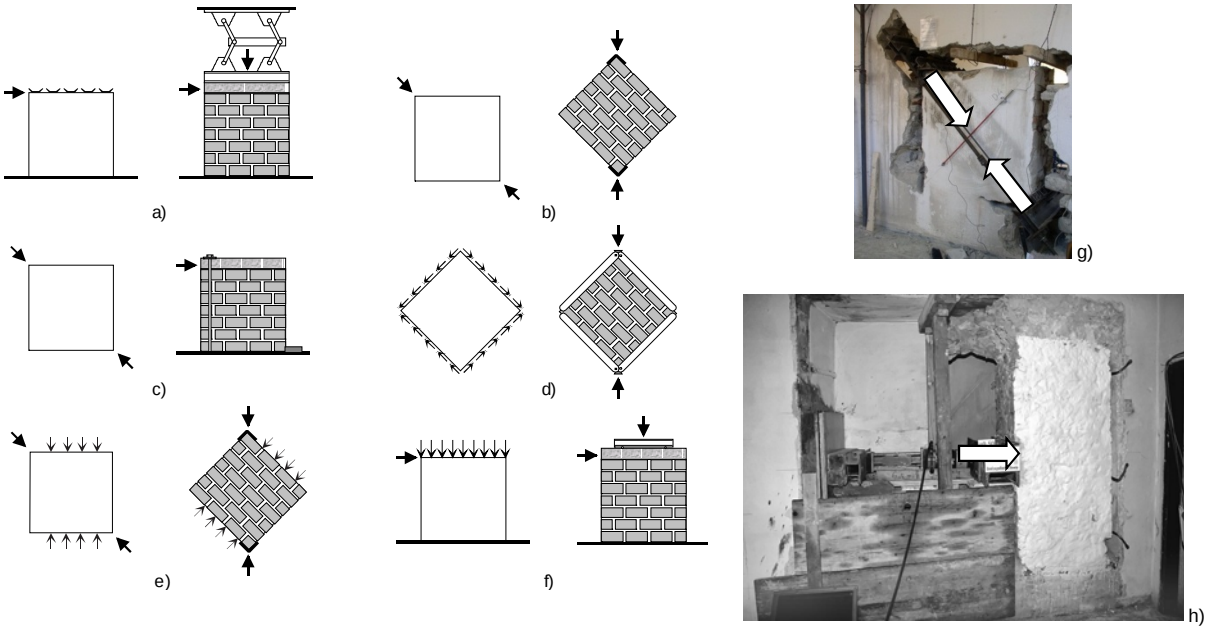

Figure 2.7. Different test methods for the determination of shear/tensile strength of masonry, where methods a) – f) refer to laboratory tests, while g) and h) refer to in-situ test conditions [51,55-57].
Slika 2.7: Različni testi za določitev strižne/natezne trdnosti zidovine, kjer a)-h) prikazujejo laboratorijske teste, g) in h) pa in-situ conditions [51,55-57].

Depending on the type of test, the f_{Mt} can be determined from diagonal tests according to Eq. 2.22 or from the results of shear tests according to Eq. 2.23.

$$f_{Mt} = \frac{0.50\,P_d}{l_w t_w}, \qquad \textbf{2.22}$$

$$f_{Mt} = \sqrt{\left(\frac{\sigma_0}{2}\right)^2 + \left(b\,\tau_{Fmax}\right)^2} - \frac{\sigma_0}{2}, \qquad \textbf{2.23}$$

In Eq. 2.22, P_d is the maximum force at diagonal test, l_w the length of the wall, t_w the thickness of the wall. The adoption of the coefficient 0.5, instead of 0.707 as suggested in some codes (e.g. in ASTM E 519-02 [58]) agrees from a theoretical point of view and is supported by experimental results as discussed in Brignola et al [59] and Calderini et al [52]. In Eq. 2.23, σ_0 is the average compression stress due to vertical loading, τ_{Fmax} the average shear stress over the whole cross section of the wall at the attained maximum resistance of the wall F_{max} and b the shear distribution factor, depending on the wall aspect ratio; $b = h_w/l_w$ for $1 \leq h_w/l_w \leq 1.5$, for $h_w/l_w > 1.5$ limited to 1.5 and for squat walls where $h_w/l_w < 1.0$ equal to 1.0. The h_w presents the height of the wall.

Values for f_{Mt} may vary significantly depending on the type of the tested masonry as well as on the applied boundary testing conditions. In general they may vary between 5-10% of f_{Mc} [46]. In the Italian code provisions NTC08 [60], average shear resistance of masonry τ_{M0} at diagonal failure is introduced and it is defined as $f_{Mt}/1.5$.

2.1.4 Brief classification of plaster, murals and their damage

Plaster serves primarily as a cover skin to protect structural elements (walls, columns, facades…). It is constructed from mortar, which is a mixture of sand grains, a binder (lime, cement, etc.) and water, the same as mortar for constructing masonry, i.e. connecting rocks or bricks.

The properties of mortar mainly depend on the properties of the binder. RILEM established a classification of mortars as a function of its technical application and as a function of the nature of the binder [29], both are provided in Table 2.4. Most of the mortars in the historical heritage have been found to be constituted by lime, lime and pozzolana or portland cement binders.

Preglednica 2.4: RILEM klasifikacija malt (povzeto po [29])

Table 2.4: RILEM classification of mortar (adopted from [29])

RILEM classification of mortar:		
According to its technical application:		According to the nature of the binder:

Mortar for:
- plasters
- application of facings:
  - pavements/floors
  - walls
  - other architectural elements
- decoration:
  - layered
  - reliefs
	Masonry mortar for:
	- bedding
	- pointing
	- sealing
	- stiletto work repairs
		Mortars based on:
		- lime
		- lime and pozzolanic materials
		- hydraulic binders
		- gypsum
		- clay binders
		- organic binders
		- more than one binder

The plasters are however not only vital for the conservation of the "monument" by providing protection against exposure to various agents, but also serve as decorative elements, as already mentioned sometimes of irreplaceable historic or artistic value. Painting, applied directly on a wall, ceiling or other permanent surface of an architectural element is called a mural. In the history of mural paintings many techniques have been used (see [61]); together with a very short description they are summarized in Table 2.5:

Preglednica 2.5: Vrste zgodoviskih tehnik zidnih poslikav

Table 2.5: Historical mural painting techniques

Technique	**Description**
Encaustic painting	A painting technique in which pigments are mixed with hot, liquid beeswax and resin. After all of the colours have been applied to the painting surface, a heating element is passed over them until the individual brush or spatula marks fuse into a uniform film.
Tempera painting	In tempera technique, the pigments are bound in an albuminous medium such as egg yolk or egg white diluted in water
Buon fresco ("true" fresco)	Pigments mixed with water are painted on a thin layer of wet, fresh, lime mortar (plaster). They are then absorbed by the wet plaster; after a number of hours, the plaster dries and reacts with the air. This chemical reaction fixes the pigment particles in the plaster.
Mezzo-fresco	Is painted on nearly-dry plaster, and was defined by the sixteenth-century author Ignazio Pozzo. In mezzo-fresco the pigment only penetrates slightly into the plaster.
Fresco-secco	The painting is done on dry ("secco" in Italian) plaster. The pigments thus require a binding medium, such as egg (tempera), glue or oil to attach the pigment to the wall
Marouflage	A procedure for attaching a painted canvas permanently to a wall (or other permanent element) by means of white lead in oil spread both over the plaster or other surface and the back of the canvas

2.1.4.1 (Mechanical) damage of the plasters

The mortar's heterogeneous composition and its high porosity mainly affect its durability by exposing it to external agents attacks, making the plaster susceptible to instability of materials and damage, finally allowing the initiation of deterioration of materials it is suppose to be protecting. Characterization of mortars, its durability, methods of conservation are thoroughly discussed by Palomo et al [29].

Besides the long-term deterioration, plasters, and consequently artistic assets, are endangered by the mechanical damage, induced through various loads that the structure and the plasters are subjected to. Seismic damage of artistic assets is often related to small damage levels of the load bearing structure itself.

Literature on the mechanical interaction between plaster, stuccos or stone coverings and supporting walls is very scarce. Most of the papers are focused on new renders and not on historic ones and in most of cases the problems of shrinkage and weathering are faced rather than the mechanical behaviour. The behaviour of renders is usually seen as independent from that of supporting walls and the interactions are disregarded [10].

Some research works found in the literature regarding the description of mechanical interactions between structural elements and covering plasters are based on simple mechanical models based on the theory of elasticity [62,63]. The models proposed provide solely indications on the role of the plaster stiffness on the mechanical response of the wall-plaster system. This is an important point, since it confirms the importance of increasing the displacement capability of assets. However these research works also highlight the difficulty of modelling wall-covering interactions within the elastic theory.

For this reason, the use of other modelling techniques based on theory of bonding and fracture mechanics has been investigated. Fracture mechanics has devoted very low attention to this problem, however, conceptually similar problems relating to plaster mechanics also, can be considered. Reference can be made to fracture mechanics of multi-layered media [64-66], and to buckling-driven delamination in thin layers due to in-plane compressive stresses [67,68]. Especially the latter problem could be related to that of detachment of plaster from wall supports.

2.2 Performance-based seismic assessment (PBA) of historical buildings

Performance assessment is a process used to determine the performance capability of the evaluated structure. Structural analysis is conducted in order to predict the building response to earthquake hazards, assess the likely amount of damage and determine the probable consequences of that damage. Seismic performance can be expressed in terms of potential casualties, repair and replacement costs, repair time, etc. [69]. International standards for seismic assessment of existing buildings (EC8, ASCE/SEI 41-13 [70]) demand different Performance Levels (PLs) to be fulfilled in the case of occurrence of the determined earthquake hazard levels (defined by the annual probability of exceedance λ or the return period T_R). For the evaluation of PLs referring to structural collapse of existing buildings, nonlinear static (pushover) analysis is commonly performed and the evaluation of

the seismic demand is conducted either by the Capacity Spectrum Method (as originally proposed by Freeman et al [71]) or the N2 Method (as originally proposed by Fajfar [72]), according to the reduction of acceleration and displacement spectra by the overdamped or inelastic approach [73]. PERPETUATE methodology [1] provides guidelines for the assessment of historical masonry structures, where safety and conservation requirements are proposed by considering distinct sets of PLs, related to use and safety of people, conservation of the building and of the artistic assets if they are present (Figure 2.8).

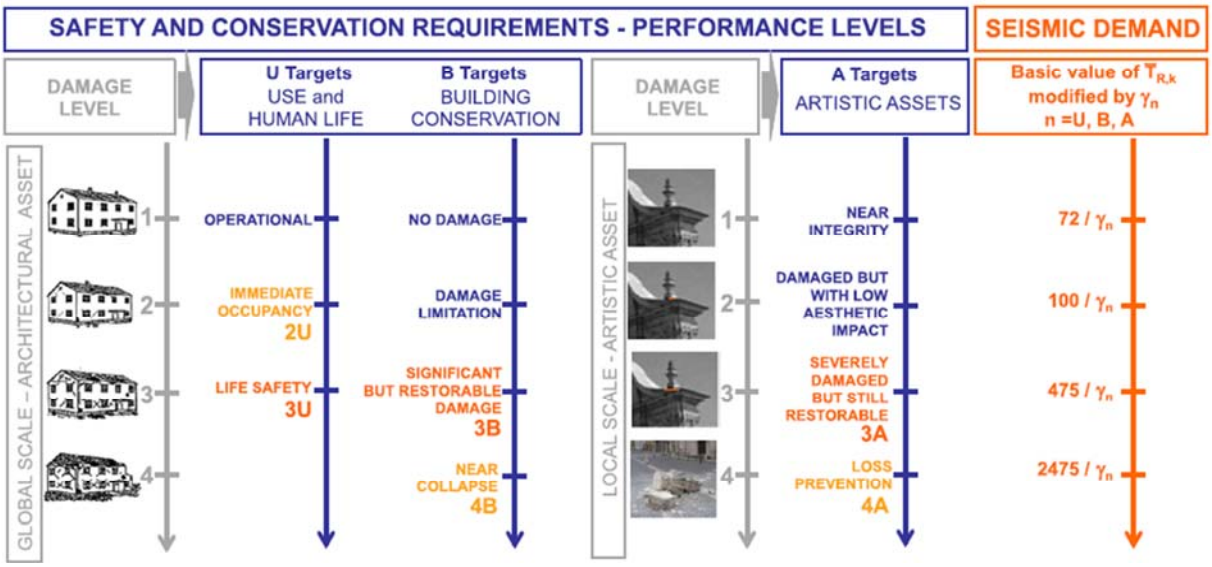

Figure 2.8. PERPETUATE performance levels, corresponding damage levels and related target return periods (for each target, the primary and secondary PLs are marked in orange and light orange) [1]
Slika 2.8: PERPETUATE mejna stanja obnašanja, ki sovpadajo s poškodovanostjo in predvidenimi povratnimi dobami (za vsak kriterij so označena primarna in sedundarna mejna stanja z oranžno in svetlo oranžno) [1]

2.2.1 Modelling strategies for a reliable seismic assessment of masonry structures and behaviour of structural elements

Modelling strategies for a reliable seismic assessment can be chosen with regard to specific types of historical architectonic assets, as various types exhibit different predominant seismic behaviour (e.g. with a prevailing in-plane or out-of-plane response). This issue was addressed in [1] by analysing the use of different modelling strategies, classified according to Calderini et al [74], as a function of six classes of architectonic assets (from A to F, as illustrated in [75]), grouped together considering both the building morphology (architectural shape, proportions) and the technology (type of masonry, nature of horizontal diaphragms, effectiveness of wall-to-wall and floor-to-walls connections).

Concerning the modelling strategies, according to the classification and review of the State-of-the-Art on models presented in [74], they may be classified as follows:

- Continuous Constitutive Law Models, that is finite element modelling with phenomenological or micromechanical homogenized constitutive laws,
- Structural Elements Models (SEM), that is equivalent frame modelling by discretization in terms of piers/spandrels and other nonlinear elements,

- Discrete Interface Models, that is discrete modelling of blocks and interfaces,
- Macro-Block Models, based on the use of theorem of limit analysis.

It is evident that such modelling strategies require a different effort in collecting all the necessary mechanical parameters for a reliable seismic assessment and that consequently also computational cost differs significantly.

For seismic assessment of the structure both nonlinear static and nonlinear dynamic analyses may be used. For architectural assets of class A (i.e. assets which are characterized with a box behaviour such as palaces, castles, religious houses, etc.), the pushover analysis can in most cases be carried out using the SEM modelling approach [1]. A relatively limited number of degrees of freedom even for complex assets and sufficiently representative model of the structure results in acceptable computational efforts as well as in adequate seismic response results.

2.3 In-plane response of walls

Focusing the attention only to the in-plane response and SEM models, primary structural subsystems of masonry assemblage that determine the response of the structure due to seismic motions are piers[1] and spandrels (with lintels), defined by geometry of the openings. Their in-plane stiffness, strength and lateral load-displacement relationships determine the seismic performance of the structure.

Since the focus of our studies was the behaviour of walls, other structural elements were not studied and only the behaviour of walls is presented hereafter. The term wall used in the text hereafter relates to both wall and pier structural elements.

Predicting the response of stone masonry walls when subjected to in-plane lateral loading is a rather difficult task, due to many already mentioned material and structural parameters influencing the behaviour. Parameters needed for the seismic assessment and full performance analysis of masonry structural elements are [46]:

- (global) forces,
- (global) displacements (drifts),
- deformations,
- behaviour characteristics (mode of failure, shape of hysteresis, cracking patterns, ductility capacity, energy absorption, damage evolution etc.).

2.3.1 Characteristic behaviour of masonry walls

2.3.1.1 Failure mechanisms and wall configuration in a building

The parameter which determines the performance of the wall in terms of all of the above stated parameters, is the developed mechanism. It primarily depends on the walls geometry, on their boundary conditions and on the level of pre-compression (vertical load) and then on the mechanical characteristics of the masonry constituents (units, mortar and their junction) and the properties of the

[1] Piers refer to the part of the wall between the opening

masonry assemblage (in terms of its texture and morphology) [76]. Masonry damage and failure mechanisms are [76-79]:

- rocking - horizontal cracks ("opening") at the top and bottom of the pier due to tension in the bed-joints resulting in overturning of the wall (and simultaneous toe crushing),
- toe-crushing – flexural mechanism where the principal compressive strength of masonry is exceeded and crushing of the compressed corners occurs;
- sliding – horizontal cracks along bed-joint (either straight of staircase like) develop; it occurs when the horizontal forces are larger than the shear strength of the bed-joint provided by the initial shear strength and friction;
- diagonal tension – the principal tensile stress exceeds the tensile strength of the masonry and diagonal cracks (diagonal through both units and mortar or staircase through mortar bed and head joints) are formed.

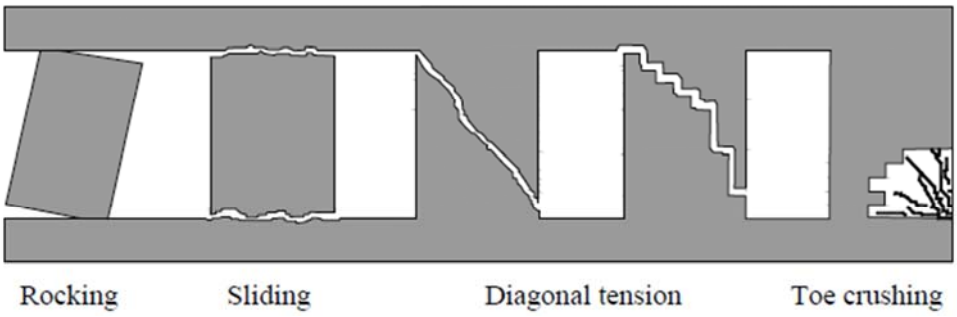

Figure 2.9: Failure mechanisms of masonry piers subjected to in-plane lateral load [80]
Slika 2.9: Porušni mehanizmi zidanih zidov, obremenjenih s horizontalno silo v ravnimi [80]

Regarding the behaviour of walls as a part of a building structural system, three configurations can be distinguished. If walls are connected with floors, which are flexible in the orthogonal direction (even if they are rigid in their plane), they do not transfer the moments resulting from the bending of the wall and they can be treated as cantilever walls (Figure 2.10 left). When piers are weaker than the spandrels, walls are coupled with pier hinging and the damage tends to initiate at the piers (Figure 2.10 middle). In such case the piers will usually fail at the lowest floor. If spandrels are weaker than the piers, coupled walls with spandrel hinging will occur, spandrels behaving as coupling beams, connecting the walls and transferring bending moments (Figure 2.10 right). This is, due to distribution of damage and energy dissipation over the entire structure, the most favourable configuration [46,81].

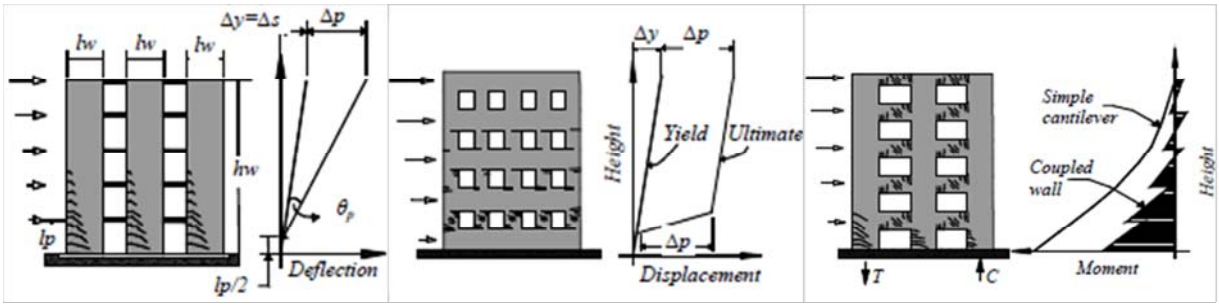

Figure 2.10: In-plane structural wall configurations: cantilever walls connected by flexible floors (left); coupled walls with pier hinging (middle); coupled walls with spandrel hinging (right) ([82], adapted from [81])
Slika 2.10: Obnašanje zidov v ravnini: konzolni zidovi, povezani s podajnimi ploščami (levo); povezani zidovi, kjer so slopovi kritični elementi (na sredini); povezani zidovi, kjer so prekladni elementi kritični (desno) ([82], povzeto po [81])

2.3.2 Experimental shear tests of masonry walls

Numerous experimental tests ([78,83-93], etc.) enabled more in-depth understanding of the masonry behaviour and led to establishment of various analytical models for predicting the shear behaviour of walls.

Due to many of the influencing parameters, complex response and especially the more recent PBD (PBA) superseding the traditional force-based design, the behaviour is still studied and there is a need for future research as well. Particularly studies on the behaviour of masonry structural elements in terms of displacement capacity and damage analysis are needed.

There is no harmonized test method for the determination of the performance and shear resistance of masonry elements under seismic loading. Some of the common ways of testing large masonry elements (in the case of walls) are already presented in Figure 2.7. None of them simulate real conditions, but they have all been chosen because they reproduce static or kinematic boundary conditions which can easily be interpreted and reproduced. According to Tomaževič et al [94] the cyclic character of simulating seismic loads in tests is necessary to obtain reliable data regarding strength and stiffness degradation and deterioration and energy dissipation capacity of masonry walls. In the paper a cyclic testing procedure, where load is imposed through controlled increasing of lateral displacements (stepwise increasing of lateral displacement amplitudes in predefined blocks and repeated three times for each amplitude peak), is evaluated and established as adequate to obtain the mentioned data regarding the behaviour of masonry walls during seismic loading.

2.3.2.1 Characteristic damage states

The most significant information of the walls' in-plane behaviour obtained through testing are the results in terms of lateral load – lateral displacement diagrams, also called hysteretic responses of the walls (Figure 2.11). These hysteresis together with crack recognition define some characteristic limit states in the walls response; points of characteristic displacements (or drifts) and corresponding forces are:

- $d_{cr,x}$, $F_{cr,x}$ - the displacement at which the first flexural crack is attained and the corresponding resistance,

- d_{cr}, F_{cr} - the displacement at which the first shear damage occurs (either by shear cracking or toe crushing) and the corresponding resistance,
- d_{Fmax}, F_{max} - the displacement at which maximum resistance is reached and the maximum resistance,
- d_{max}, F_{dmax} - the maximum displacement attained and the corresponding resistance.

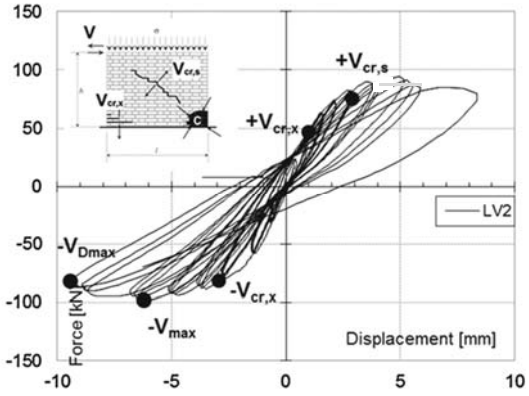

Figure 2.11. Hysteresis loops with characteristic limit state points for walls failed in shear [55]
Slika 2.11: Histerezno obnašanje s karakterističnimi mejnimi stanji zidov pri strižnih obrementivah v ravnini [55]

At this point it can also be mentioned, that limit states d_{cr}, d_{Fmax} and d_{max}, that correspond to progressing damage levels reached in the wall, are in the test results found in literature often referred to as ”FC” (“First Cracking”), ”SD” and ”NC” limit states or as ”FO”, ”LS” and ”CP”. These notations follow the order of performance limit states adopted either in EC8-3 (“Damage Limitation” - ”DL”, “Significant Damage” - ”SD”, “Near Collapse” - ”NC”) or in FEMA 306 [95] (“Fully Operational” - ”FO”, “Immediate Occupancy” - ”IO”, “Life Safety” - ”LS” and “Collapse Prevention” - ”CP”).

Authors Petry and Beyer [96] defined two sets of limit states which are based on the occurrence of obtained characteristic damage; LS-F describe the limit states attained at flexural mechanism, whereas LS-S the limit states attained at shear mechanism. The described limit states were obtained for modern unreinforced clay brick masonry, though. A correlation between the limit states and the lateral load – displacement response is also provided and summarized in Table 2.6.

Preglednica 2.6: Značilna mejna stanja, opažena pri upogibnem (LS-F) in strižnem (LS-S) obnašanju [96]

Table 2.6: Characteristic limit states observed for flexural (LS-F) and shear (LS-S) behaviour [96]

Limit state		Local crack pattern	Influence on global response
Flexural mechanism	LS-F1	First appearance of a crack in a bed-joint	First reduction of stiffness
	LS-F2	Visible separation of the unloaded zone from the compression zone	/
	LS-F3	Appearance of vertical splitting cracks in compressed corner	Peak load is typically attained shortly afterwards
	LS-F4	Loss of part of the toe region due to crushing	Significant loss of the lateral resistance
	LS-F5	Crushing of entire compression zone	Axial load failure
Shear mechanism	LS-S1	First appearance of diagonal stair step cracks in mortar joints	Preceded by a first reduction of stiffness
	LS-S2	First appearance of vertical and inclined cracks through bricks along the diagonals	/
	LS-S3	Deformations start concentrating in one diagonal crack	Peak load is typically attained shortly afterwards
	LS-S4	Shearing off of the corners of the bricks	Significant loss of the lateral resistance
	LS-S5	Crushing of bricks along the diagonal crack	Axial load failure

2.3.2.2 The influence of failure mode on wall performance

Through tests it was established, that there are many parameters which determine the behaviour of the masonry. The failure mechanism which develops influences the resistance capacity as well as the drift limits. Besides mechanical characteristics of the wall and its constituents, level of pre-compression and the internal stress state determine the failure mode.

Wall rocking mechanism (Figure 2.12) is a desirable mode because the lateral force - deflection relation has a very large amount of deformation capacity. Large lateral displacements are obtained with little damage. Since the material remains in the elastic state, rocking mechanism is not high on energy dissipation. In terms of lateral load – displacement dependence, the response is nonlinear, though.

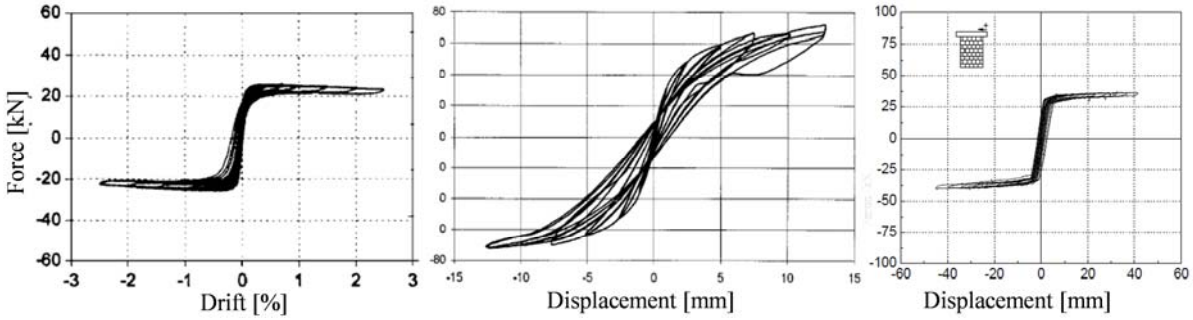

Figure 2.12: Flexural failure force - displacement diagrams for brick (left and middle) and stone (right) unreinforced masonry walls [76,97,98]
Slika 2.12: Diagrami sila - pomik za upogibni mehanizem opečnih (levo in na sredini) in kamnitih (desno) zidov[76,97,98]

Bed-joint sliding (Figure 2.13) is also a desirable mechanism in terms of displacement capacity. The amount of nonlinear displacement capacity can be very large after formation of bed-joint cracks. After the formation of the bed-joint cracks, the frictional forces continue to resist the horizontal forces, provided that the vertical compressive stress is present. Due to its inelastic deformations, sliding can through hysteresis loops dissipate large amounts of energy.

Very often more than one damage mechanism is recognized during loading of the wall. In case the response is characterized by various damage and failure mechanisms, the type of failure is described as mixed.

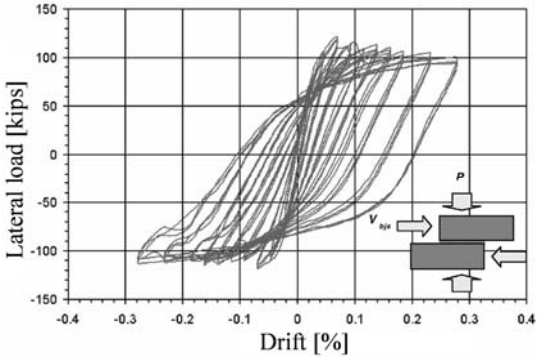

Figure 2.13: Force - deflection diagram for sliding mechanism [99]
Slika 2.13: Diagram sila - rotacija za zdrsni porušni mehanizem zidu [99]

Diagonal shear mechanisms (Figure 2.14) prove a much more brittle behaviour. Depending on the type of failure (through mortar or through units), different post-peak deformations are observed. By failure through unit, there is mainly no post-peak load bearing capacity, on the contrary with failure through mortar, residual displacements can be quite large and after the strength peak a staircase-like hysteresis envelope can be observed. If post-peak deformations occur, then this kind of failure also dissipates a lot of energy.

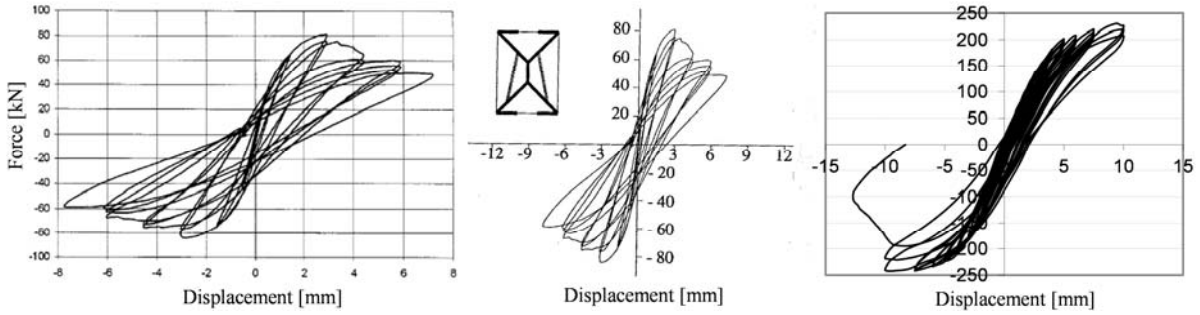

Figure 2.14: Diagonal shear failure force - displacement diagrams [76,100,101]
Slika 2.14: Diagram sila - pomik za diagonalni strižni porušni mehanizem zidu [76,100,101]

In order to quantify the displacement capacity for seismic performance a specific distortion must be assigned to a given performance level and prior that a damage level has to be related to a specific performance level. The researchers are nowadays expressing their results in terms of performance indices ([55,98], etc.), however, the large majority of past experimental research reported mainly on strength results. Regarding the displacement capacity, only the ductility capacity, that is the ratio between ultimate and elastic displacement of an idealized bilinear curve d_u and d_e (parameters described in the following), is usually stated in the literature.

Because of the large number of parameters determining the deformation behaviour of the masonry, the maximum and minimum drift values of brick and stone masonry at different failure mechanisms found in the literature are hereafter summarized for pier/wall type of structural element and for the type of masonry. In Table 2.7, the experimental work of Anthoine et al [100], Abrams et al [97], Gouveia et al [102], Tomaževič [103], Vasconcelos et al [104], Bosiljkov et al [105], Rota et al [106] and Augenti et al [107] was considered. Note that the limit states presented relate to both piers and walls and may strongly be influenced by the slenderness and the stiffness of the tested specimens, the applied boundary conditions and the loading procedure during the testing. Values obtained in the laboratory and in-situ are also provided separately.

The dependence of drift limits also on the compressive state has been recently discussed and verified through some experimental tests on modern masonry in Tomaževič et al [108] and Petry and Beyer [109]; however, the reliability of this assumption in the case of historic masonry still has to be verified.

Preglednica 2.7: Mejne vrednosti zasukov za različna mejna stanja pri različnih porušnih mehanizmih, zbrana iz rezultatov testov, najdenih v literaturi [97,100,102-107]

Table 2.7: Limit drift values for different failure mechanisms for walls derived through testing campaigns and literature survey [97,100,102-107]

Type of failure	Type of test	d_{Fmax} Min. [%]	d_{Fmax} Max. [%]	d_{max} Min. [%]	d_{max} Max. [%]
		Brick masonry (type F masonry)			
Shear	Laboratory	0.70	0.92	0.83	1.21
	In-situ	0.44	0.51	0.89	1.38
Sliding	Laboratory	0.90	-	1.80	-
Rocking	Laboratory	0.25	1.80	0.55	2.90
		Stone masonry (A-E types of masonry)			
Shear	Laboratory	0.51	2.00	0.30*	2.32
	In-situ	0.23	0.58	0.82	1.10
Rocking	Laboratory	0.76	4.64**	0.60*	4.65**
Mix	Laboratory	0.67	1.99	1.00	2.97

* only "NC" state reported
** the ultimate displacement was for this test not achieved (drop of resistance was not obtained)

2.3.2.3 Bi-linear idealization of hysteretic envelopes

For the purpose of seismic design and comparison of the results, the hysteretic behaviour gained through experimental tests is usually presented in the form of envelopes of hysteresis loops for the obtained responses of the walls and further idealised either through bi-linear or multi-linear curves. Most common is bi-linear idealisation, where various slightly different definitions of characteristic limit states taken into account for the idealised curves and procedures for determining the curve can be found in the literature (see Figures 2.15 - 2.17).

The determination of the bi-linear curve is most often based on assumption, that the deformation energy of the actual response and the energy of the bi-linear curve are the same, which means that the areas under the actual and the idealized force - displacement diagrams are equal.

Besides this condition, two others are needed to define the curve. Idealised ultimate displacement d_u is usually determined as the displacement, where 20% drop of maximum resistance F_{max} is attained. However there are some inconsistencies in the literature; in some cases d_u is actually determined as the point, where idealised curve intersects the descending branch of the experimental envelope (to avoid confusion, this displacement shall be further in the text referred as d_u^*); it is also most often not clear, whether the equal energy assumption is fulfilled up to displacement d_u^* or to displacement d_u, where 20% drop of maximum resistance is attained. Tomaževič in [79] assumed the input energy equal up to displacement d_{max}, which could be even higher than d_u.

Besides ultimate displacement d_u, idealised force F_{id} and effective stiffness K_{ef} are to be determined. Usually K_{ef} is presumed (by considering various criteria) and F_{id} calculated post festum. Among the most common criteria for determining effective stiffness K_{ef} are either stiffness obtained at formation of first (significant) shear crack (d_{cr} and F_{cr}) which significantly changes the stiffness of the wall [46,79] (Figure 2.15) or at first damage, which changes the slope of the envelope (elastic stiffness)

[55,98] (Figure 2.16). Stiffness is often determined as the secant stiffness at certain point of response, defined as percentage of F_{max} or F_{id}; 75% F_{id} according to Magenes and Calvi [76] (Figure 2.17 left), 2/3F_{max} according to Bosiljkov and Tomaževič [101] and Čeru [110] (Figure 2.15 right), etc. These criteria seem more appropriate especially in the case if response is characterized by flexural behaviour.

For theoretical calculation of the resistance at elastic limit F_{cr}, Tomaževič [46] introduces experimentally obtained reduction coefficient C_{cr}, which is the ratio between F_{cr} and F_{max}. This ratio varies according to the author from 0.6-0.8, consequently a value of 0.7 is recommended.

Tomaževič [46] also defines coefficient C_{sd} called strength degradation factor as the ratio between F_{dmax} and F_{max}. It is used to evaluate resistance at ultimate displacement and is experimentally evaluated. According to the author (and data available at that time), the values vary from 0.4 to 0.8; the walls however exhibit severe deterioration before collapse, thus it is recommended that no more than 20% of degradation is tolerated for practical calculations.

In Abdel-Halim et al [111] for instance, equal energy assumption is not satisfied but instead idealised the force is determined as percentage of F_{max} (Figure 2.17 right).

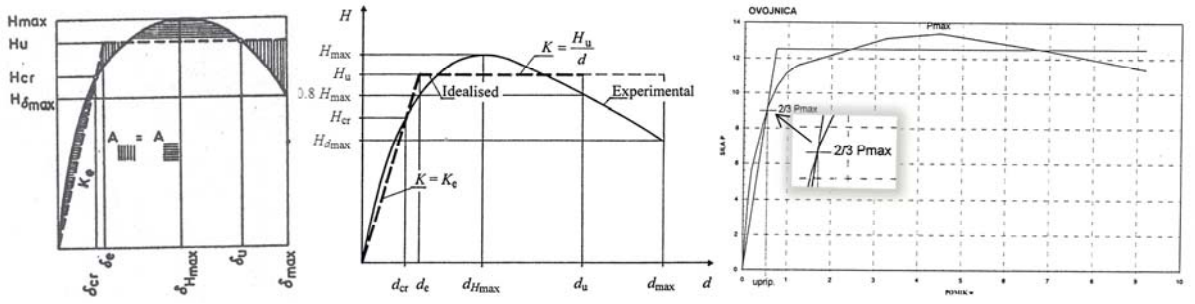

Figure 2.15: Bi-linear idealisation of the hysteresis envelope according to Tomaževič (left) [79] and (middle) [46], and Čeru (right) [110]
Slika 2.15: Bi-linearna idealizacija histerezne ovojnice po Tomaževiču (levo) [79] in (na sredini) [46] ter Čeruju (desno)[110]

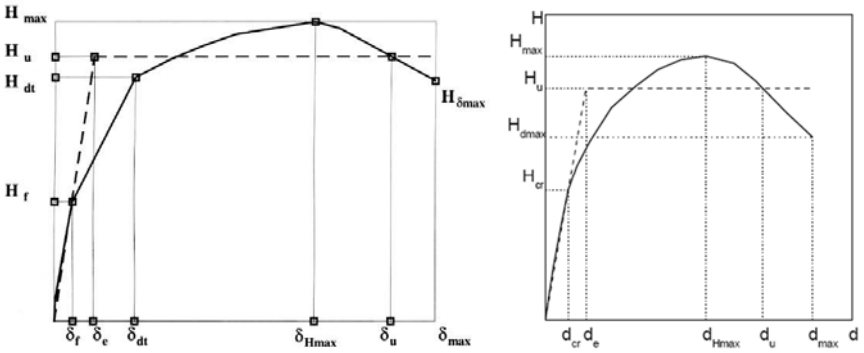

Figure 2.16: Bi-linear idealisation of hysteresis envelope according to Bosiljkov (left) [55] and Vasconcelos (right) [98]
Slika 2.16: Bi-linearna idealizacija histerezne ovojnice po Bosiljkovu (levo) [55] in Vasconcelos (desno) [98]

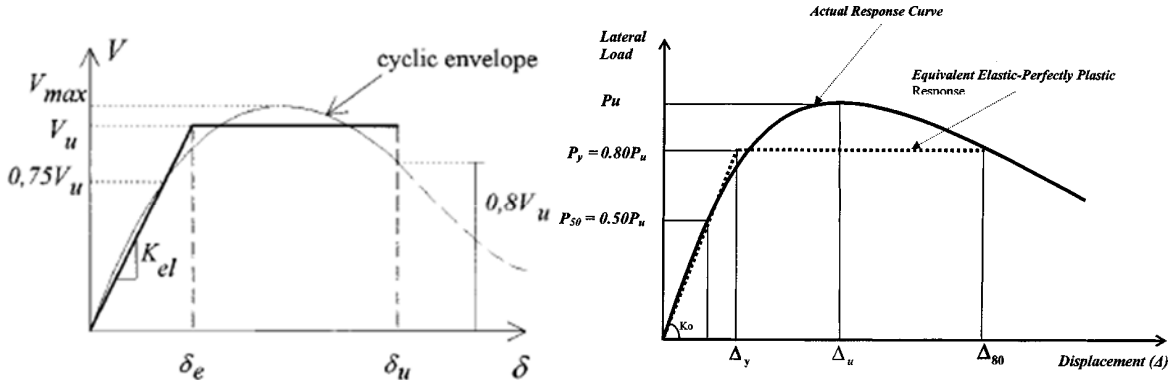

Figure 2.17: Bi-linear idealisation of the hysteresis envelope according to Magenes and Calvi (left) [76] and Abdel-Halim et al (right) [111]
Slika 2.17: Bi-linearna idealizacija histerezne ovojnice po Magenes-u in Calvi-ju (levo) [76] in Abdel-Halim-u s sod. (desno)[111]

A tri-linear idealisation, which is very rarely used, is presented in Figure 2.18 [46]. K_{ef} is defined by the same value of K_{ef} as in the case of bi-linear idealisation, however the maximum resistance is used without any reduction. Regarding theoretical value of resistance at elastic crack limit, Tomaževič [46] recommends the value to be calculated either by using adequate mathematical models or by considering an experimentally obtained values, that is as reduced values of maximum force attained. As mentioned, the author proposes the calculation of resistance at cracking limit as $0.7 \cdot F_{max}$ (in Figure 2.18 denoted as H_{max}).

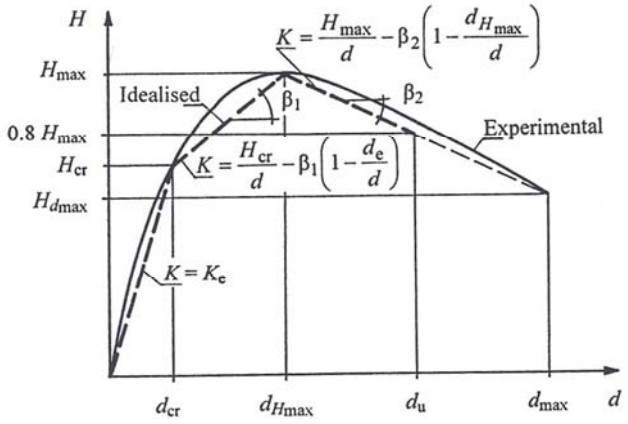

Figure 2.18: Tri-linear idealisation of the hysteresis envelope (from [46])
Slika 2.18: Tri-linearna idealizacija histerezne ovojnice po (iz [46])

2.3.2.4 Energy dissipation and equivalent viscous damping

2.3.2.4.1 Energy dissipation

The behaviour of various types of masonry under different boundary conditions differs also in the amount of dissipated energy during seismic loading. Different behaviour in terms of energy dissipation can be seen from hysteretic responses on force - displacement diagrams, The energy, dissipated at each loading cycle $E_{DIS,i}$ is calculated as the area within one complete hysteretic cycle (Eq. 2.24) and is obtained by numerically integrating the force - displacement loop (Figure 2.19), where H is the resisting force and $d(d)$ differential increment of displacement d.

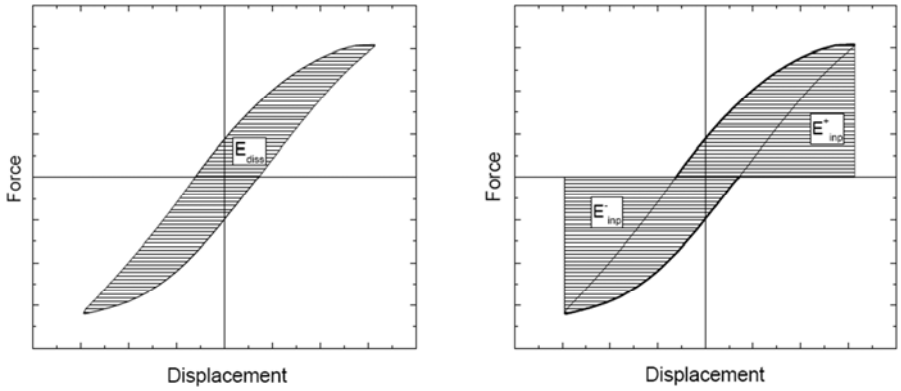

Figure 2.19: Dissipated energy (left) and input energy (right) in one loading cycle [98]
Slika 2.19: Disipirana energija (levo) in vnesena energija (desno) v enem ciklu obremenjevanja [98]

Input energy E_{INP} is defined as the work of the actuator, needed to deform the wall up to a certain displacement. For a certain i cycle, $E_{INP,i}$ is calculated as the sum of areas under the positive and negative part of the hysteresis loop as presented in Figure 2.19. For one cycle, $E_{INP,i}$ can numerically be calculated according to Eq. 2.26. For the purpose of comparing the response of walls in both directions of loading, i.e. positive and negative, both $E_{DIS,i}$ and $E_{INP,i}$ are divided into positive (+) part where $H > 0$ and negative part (-), where $H < 0$ (Eq. 2.28 and 2.29).

$$E_{DIS,i} = \int_{(H=0)_{i-1}}^{(H=0)_i} dE_{DIS} \qquad \textbf{2.24}$$

$$dE_{DIS} = H \cdot d(d) \qquad \textbf{2.25}$$

$$E_{INP,i} = \int_{(H=0)_{i-1}}^{(H=0)_i} dE_{INP} \qquad \textbf{2.26}$$

$$dE_{INP} = H \cdot d(d) \ , \ dE_{INP} = \begin{cases} 0, & H \cdot d(d) < 0 \\ H \cdot d(d), & H \cdot d(d) > 0 \end{cases} \qquad \textbf{2.27}$$

$$E_{DIS,i} = E_{DIS,i}^{+} + E_{DIS,i}^{-} \qquad \textbf{2.28}$$

$$E_{INP,i} = E_{INP,i}^{+} + E_{INP,i}^{-} \qquad \textbf{2.29}$$

Shing [112] proposes a normalized cumulative energy dissipation E_N parameter as a more objective measure of the inelastic performance of the walls. It is defined as in Eq. 2.30, where n is the number of cycles corresponding to displacement to which the idealisation is made and $E_{ID,el}$ the total elastic energy absorption of the equivalent elastic-perfectly plastic model (Eq. 2.31).

$$E_N = \frac{1}{E_{ID,el}} \sum_{i=1}^{n} E_{DIS,i} \ , \qquad \textbf{2.30}$$

$$E_{ID,el} = 0.5 \cdot K_{ef} \cdot d_e^{\,2} = 0.5 \cdot F_{id} \cdot d_e \ , \qquad \textbf{2.31}$$

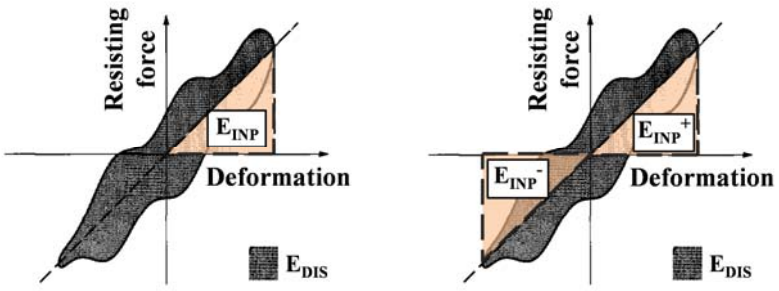

Figure 2.20: Energy dissipated in one cycle and input energy evaluated from the experiment needed for calculation of equivalent viscous damping coefficient according to Eq. 2.34 (left, [113]) and Eq. 2.35 (right)
Slika 2.20: Disipirana energija v enem ciklu obremenjevanja in vnesena energija, potrebna za izračun koeficienta ekvivalentnega dušenja po En. 2.34 (left, [113]) in En. 2.35 (desno)

By Jacobsen [114] the initial work was analysed using the secant stiffness at the maximum displacement $d_{max,i}$ of the analysed hysteretic cycle K^+, rather than the initial stiffness. Dissipated energy E_{DIS} is calculated as the area within one complete hysteretic cycle A_{hyst}. Input energy in case of formulation according to Eq. 2.26 and Eq. 2.27 refers to input energy of the positive amplitude displacement direction as also presented in Figure 2.20 (left) and can be calculated according to the definition in Eq. 2.32, where $F_{dmax,i}$ corresponds to the force attained at maximum displacement $d_{max,i}$ of the loading cycle.

$$E_{INP} = \frac{1}{2} K^+ \cdot {d_{max,i}}^2 = \frac{1}{2} F_{dmax,i} \cdot d_{max,i} \qquad \textbf{2.32}$$

2.3.2.4.2 Equivalent viscous damping

As another indicator of energy dissipation the equivalent viscous damping coefficient ξ is commonly used. Equivalent viscous damping coefficient ξ, which represents the hysteretic damping, was defined by Jacobsen [114] who equated the energy absorbed in a hysteretic cycle to a given displacement of an actual structure and an equivalent viscous system of the substitute structure. It is defined according to Eq. 2.33 on the basis of energy, dissipated in one cycle E_{DIS}, and input energy E_{INP} of the corresponding cycle, also commonly called stored or elastic strain energy (according to Jacobsen calculated considering Eq. 2.32).

$$\xi = \frac{1}{4\pi} \frac{\omega_n}{\omega} \frac{E_{DIS}}{E_{INP}}, \qquad \textbf{2.33}$$

$$\xi = \frac{1}{4\pi} \frac{E_{DIS}}{E_{INP}}, \qquad \textbf{2.34}$$

$$\xi = \frac{1}{2\pi} \frac{E_{DIS}}{E_{INP}} = \frac{1}{2\pi} \frac{E_{DIS}}{({E_{INP}}^+ + {E_{INP}}^-)}, \qquad \textbf{2.35}$$

In Eq. 2.33, ω is the exciting frequency of the system and ω_n the natural frequency of the system. The experiment leading to force - displacement curve and hence E_{DIS} should be conducted at $\omega = \omega_n$, where the response of the system is most sensitive to damping, therefore Eq. 2.33 can be rewritten to

Eq. 2.34. The damping ratio ξ determined from the test would not be correct at any other exciting frequency different to $\omega = \omega_n$, but would be a satisfactory approximation [113].

Some authors [76,101], however, when evaluating experimental results with the hysteretic response tend to take into account the E_{INP} in both directions of loading; positive and negative (Figure 2.20 right). Equivalent viscous damping is therefore in this case rewritten to Eq. 2.35.

2.3.3 Limit states – analytical formulation

2.3.3.1 Strength criteria

Different models are being used and found in the literature to describe different failure mechanisms and to determine limit shear stress τ under bi-axial in-plane loading; Sinha and Hendry [115], Turnšek and Čačović [54], Yokel and Fattal [116], Hegemeir et al [117], Hamid and Drysdale [87,118], Mann and Muller [119], Page [86], Samarasinghe and Hendry [84,85], Ganz and Thürlimann [88,120], Drysdale and Hamid [121], Dhanasekar et al [89], Ganz [90,91], Daou and Hobbs [122], Dialer [123], Andreaus [124], Seim [125] all propose one or more limit strength criteria depending on the failure mechanism. Many other authors tried to produce a material model, independent from the failure mechanism, most often based on soil strength criteria.

However many of these models need various and numerous masonry constituents' mechanical characteristics often difficult to obtain, therefore only some of them are used for the design purposes. In [55,76] and [126] a review of the most common strength criteria proposed in the literature is illustrated, together with the theoretical principles which they are based on and some recommendations on their use as a function of different masonry types. In the following however a brief description and formulation of well-known criteria proposed by Turnšek and Čačović [54], Mann and Müller [119] and Ganz and Thürlimann [127], which are the basis for many national design provisions, are provided. The model of Turnšek and Čačović [54] has been incorporated since the mid 70's into the Italian and former Yugoslavian codes for the seismic design of masonry structures [128], whereas Mann and Müller's model [119] has been built into German Masonry codes [129] and Ganz and Thürlimann's [127] into Swiss ones [130].

Turnšek and Čačović

The model considers diagonal cracking where the masonry wall is considered as an elastic, homogeneous and isotropic structural material. Maximum principal stress acting in the centre of the wall is assumed as the reference stress and by using the theory of elasticity the maximum shear stress τ is expressed as a function of the diagonal tensile strength of the masonry f_{Mt}, the level of pre-compression σ_0 and the geometry of the element (Eq. 2.36).

$$\tau = \frac{f_{Mt}}{b}\sqrt{1+\frac{\sigma_0}{f_{Mt}}} \ , \ , \qquad \textbf{2.36}$$

The major advantage of this model is that it depends solely on one mechanical parameter of masonry, i.e. f_{Mt}.

Mann and Müller

Models proposed (Table 2.8) treat masonry as a composite material, therefore the failures depend on the characteristics of the wall's components. They are based on two hypotheses; bricks are much stiffer than mortar and the contribution of head joints is negligible. Models are based on a phenomenological approach and have been calibrated with the results of other authors derived through the monotonic testing of masonry specimens. They are designed for masonry bond with the units half overlapping.

In sliding mechanism, where the joint is critical, model assumes τ in the centre of the wall as the reference stress. It compares it with limit strength obtained through Mohr – Coulomb criteria, considering cohesion c, μ and the level of pre-compression in the compressed part of the cross section, where l_b and h_b stand for the length and the height of the unit. Additional model predicts failure through units. Diagonal cracking occurs when tensile (diagonal) strength of the unit f_{bt} is exceeded. Reference stress is the maximum principal stress in the unit again at the centre of the wall. Value 2.3 takes into account the actual shear stress in the unit and it depends on the brick's geometry. Mann and Müller also predicted compressive failure of the unit. Cracking occurs, when the stress in more loaded part of the unit exceeds masonry compressive strength.

Preglednica 2.8: Mann and Müller-jevi modeli za oceno mejne strižne odpornosti zidov [111]

Table 2.8: Masonry ultimate shear strength criteria proposed by Mann and Müller [111]

Failure criteria	Analytical model	
Sliding failure (Coulomb – friction):	$\tau = \overline{c} + \overline{\mu}\,\sigma_d$	**2.37**
	$\overline{c} = f_{v0} \cdot \left(1 + \mu \cdot 2l_b / h_b\right)^{-1}$,	**2.38**
	$\overline{\mu} = \mu \cdot \left(1 + \mu \cdot 2l_b / h_b\right)^{-1}$	**2.39**
Splitting (diagonal) tensile failure of the unit:	$\tau = \frac{f_{bt}}{2.3}\sqrt{1 + \frac{\sigma_d}{f_{bt}}}$	**2.40**
Compressive failure of the masonry:	$\tau = \left(f_{Mc} - \sigma_0\right)\frac{l_b}{2h_b}$	**2.41**

The major advantage of this model is that it predicts the failure mode of the bi-axially loaded masonry solely from the results of relatively simple tests on the constituents and from the f_{Mc}. The model has been proved effective in predicting shear strength of monotonically loaded specimens, but does on the other hand not consider the influence of deformation characteristics of the mortar.

Ganz and Thürlimann

The model is based on characteristics, which treat masonry on a macroscopic level, but define the failure with regard to the failure of constituents. The characteristics are compressive strength of the masonry parallel to bed-joints $f_{Mc,x}$, cohesion c and μ. The later two Ganz obtained from bi-axial masonry tests. Considering these parameters they proposed criteria of failure presented in Table 2.9, where σ_x presents the load in the masonry in the direction parallel to the joints.

Preglednica 2.9: Ganz and Thürlimann-ovi modeli za oceno mejne strižne odpornosti zidov [119]

Table 2.9: Masonry ultimate shear strength criteria proposed by Ganz and Thürlimann [119]

Failure criteria	Analytical model	
Tensile failure of the masonry:	$\tau = \sqrt{\sigma_x \sigma_0}$	**2.42**
Compressive failure of the unit:	$\tau = \sqrt{\left(\sigma_x + f_{Mc,x}\right)\left(\sigma_0 + f_{Mc}\right)}$	**2.43**
Shear failure of the unit:	$\tau = \sqrt{\sigma_0 \left(\sigma_0 + f_{Mc}\right)}$	**2.44**
Tensile failure of the unit:	$\tau = \sqrt{\sigma_x \left(\sigma_x + 2c \tan\left(\pi/4 + \mu/2\right)\right)}$	**2.45**
Sliding failure along the bed-joints:	$\tau = \sqrt{\sigma_x \left(\sigma_x + 2c \tan\left(\pi/4 + \mu/2\right)\right)}$	**2.46**
Sliding failure along the bed-joints:	$\tau = c + \sigma_x \mu$	**2.47**

National code provisions

As mentioned, they are mainly based on the presented models; while some are introducing only slight modifications, others try to consider additional parameters.

Since the masonry is a composite material and at a wall scale the stress distribution is rather complex, the most common strength criteria adopted in the codes are based on the choice of a masonry reference stress (either shear, normal or principal stress) and of a reference point or section on which it should be calculated (e.g. the end section or the central transversal cross section). Then, considering the type of masonry and its realistic failure modes, the design shear resistance V_{Rd} is defined as

$$V_{Rd} = \min\left(V_{Rd,\mathrm{s}}, V_{Rd,r}, V_{Rd,\mathrm{d}}\right), \qquad \textbf{2.48}$$

where $V_{Rd,s}$ indicates the value resulting from the strength criterion adopted to interpret the sliding, $V_{Rd,r}$ the rocking and $V_{Rd,d}$ the diagonal cracking shear response, respectively. Table 2.10 summarizes the most common criteria applicable also for historical masonry together with the mechanical parameters needed for their application in the codes. For the shear response, in general the criterion (b) is adopted in the case of irregular textured masonry, while criteria (c) and (d) apply in the case of texture with regular or pseudo-horizontal layers. In some cases, criterion (e) is adopted by neglecting the contribution of cohesion. Parameter ψ is the correction coefficient dependant from boundary conditions; equal to 1 for cantilever and to 2 for both fixed ends walls; φ the interlocking parameter considering the texture of the masonry, l_{wc} the length of the compressed part of the wall and σ_d the average vertical stress of the compressed part of the wall.

Preglednica 2.10: Najpogostejši kriteriji v predpisih za strižno odpornost zidov za različne porušne mehanizme z navedenimi potrebnimi mehanskimi karakteristikami ter nacionalnimi predpisi, v katerih so uporabljeni

Table 2.10: The most common strength criteria for various failure modes proposed in the code provisions for masonry pier with the mechanical parameters which they are based on and code provisions where they are used

Parameter required	Failure mode	Criterion	Analytical model		Codes
f_{Mc}	Rocking/bending	(a)	$V_{Rd,r} = \psi \frac{\sigma_0 \, t_w \, l_w^2}{2h_w}\left(1-\frac{\sigma_0}{f_{Mc}}\right)$	2.49	NTC2008, EC8-3, FEMA 306
f_{Mt}	Shear (diagonal cracking)	(b)	$V_{Rd,\mathrm{d}} = l_w t_w \frac{f_{Mt}}{b}\sqrt{\left(1+\frac{\sigma_0}{f_{Mt}}\right)}$	2.50	NTC2008, FEMA 306
f_{v0} , μ , φ	Shear (diagonal cracking - joints)	(c)*	$V_{Rd,dj} = \frac{l_{wc} \, t_w}{b}\left(\frac{f_{v0}}{1+\mu\varphi}+\frac{\mu}{1+\mu\varphi}\sigma_d\right)$	2.51	DIN 1053-100
f_{bt}	Shear (diagonal cracking - units)	(d)*,**	$V_{Rd,du} = l_w t_w \frac{f_{bt}}{b}\sqrt{\left(1+\frac{\sigma_d}{f_{bt}}\right)}$	2.52	DIN 1053-100
f_{v0} , μ	Shear (sliding)	(e)	$V_{Rd,s} = l_{wc} \, t_w \left(f_{v0}+\mu\sigma_0\right)$	2.53	NTC2008, EC8-3, FEMA 306

* in the original proposal of Mann and Muller *b* was assumed equal to 1; the introduction of *b* is proposed in Lagomarsino et al [131]

** this failure criterion is usually assumed conventionally by codes through a limitation imposed to the value provided by criterion (e). This limitation in most cases is computed as a function of f_{bt}.

For modern masonry, in [132] a review of various code provisions (Australian (AS 3700-2001 [133]), British (BS 5628:2005 [134]), Canadian (CSA S304.1-04 [135]), German (DIN 1053-1000), European (EC6 [37] and EC8-3 [49]), American (2008 MSJC [136]), New Zealand (NZS 4230:2004 [137]) and Swiss (SIA 266 [138])) was presented together with material safety factors and resistance reduction factors. Their values also differ, which additionally influences the final result for V_{Rd} obtained by specific provision. It has to be noted that codes for modern masonry are not always applicable for historic masonry.

2.3.3.2 Stiffness determination

After determining the lateral load bearing capacity of the wall, the initial slope of the idealised envelope can be calculated considering the effective stiffness K_{ef}. Considering the beam theory, the effective stiffness can be calculated according to Eq. 2.54:

$$K_{ef} = \frac{G_M A_w}{1.2h_w\left(1+k'\frac{G_M}{E_M}\left(\frac{h_w}{l_w}\right)^2\right)}, \qquad \textbf{2.54}$$

where A_w is the gross cross-section area of the wall and *k'* a coefficient which describes the applied restraint conditions of the element; 0.83 for both ends fixed and 3.33 for single fixed walls. In [47] the reliability of this approach is discussed and supported also by the comparison with experimental results.

Depending of the code, either cracked or uncracked stiffness characteristics (E_M, G_M) should be considered for calculation of K_{ef}. EC8-3 prescribes the use of cracked stiffness characteristics; if no

other data is available, ½ of the initial stiffness should be considered. In FEMA 306 the bi-linear curve is defined with the initial uncracked stiffness.

For masonry assemblages with multi-leaf morphology, where the two outer leaves are made from coarser stones laid in the form of rubble or ashlar units, and the infill is made from rubble and is weaker (which is usually the case), the calculation of stiffness may be done considering the bond or interface between the infill and the leaves [38]. Note that for some old Roman masonry, where the inner core is made from pozzolanic concrete, the outer leaves are weaker than the inner core. For this type of masonry mechanical parameters should be determined solely on the properties of the inner core.

2.3.3.3 Displacement capacity and performance limit states

In the code provisions force-deflection (displacement) curves are provided usually within models for non-linear seismic analysis through characteristic inter-story drift limitations. Hereafter the term drift θ is always used for rotation, calculated as the average rotation of the entire wall according to Eq. 2.55, where d presents the lateral displacement of the wall.

$$\theta = \frac{d}{h_w}, \qquad \textbf{2.55}$$

Apart from EC8-3 and NTC08, all the other code provisions are based on the experimentally gained results on contemporary masonry. From code provisions it is not for all limit states clear, what the degree of damage is for the certain performance level expected.

According to EC8-3, where the drift capacity of masonry walls is defined in dependent on the failure mode and the aspect ratio, limit state "SD" corresponds to a drift capacity of 0.4% (h_w/l_w) for shear and 0.8% (h_0/l_w) for a flexural failure, where h_0 is the distance between the section where the flexural capacity is attained and the contra-flexure point; respectively. The "NC" drift capacity is defined as 4/3 of the "SD" drift capacity. "DL" is not specifically defined in terms of drift capacity but is defined through maximum resistance; according to this definition it can be positioned at first reach of the limit strength (d_e), which is also in accordance with definition of "DL" performance limit state on the structure's capacity curve (Figure 2.21). Criteria for limit drift values according to EC8-3 are provided in the following table (Table 2.11).

Preglednica 2.11: Mejne vrednosti zasukov po EC8-3 [45]

Table 2.11: Limiting values for drifts according to EC8-3 [45]

Performance level	Masonry walls	
	Elements under normal force and bending (*flexural behaviour*)	Elements under shear force (*shear behaviour)*
"DL"	"Reaching of the maximum strength" – d_e of the predicted curve	
"SD"	In terms of drift limits: 0.008 h_0/l_w (for primary elements) 0.012 h_0/l_w (for secondary elements)	In terms of drift limits: 0.004 h_w/l_w (for primary elements) 0.006 h_w/l_w (for secondary elements)
"NC"	In terms of drift limits: 0.0107 h_0/l_w (for primary elements) 0.016 h_0/l_w (for secondary elements)	In terms of drift limits: 0.0053 h_w/l_w (for primary elements) 0.008 h_w/l_w (for secondary elements)

The described approach of idealisation may underestimate the rotation capacity of structural elements following the propagation of crack patterns. Therefore, additionally to the idealised resistance envelope for structural walls, an extension of the curve for partition walls was introduced in FEMA 273 [99]. Also EC8-3 distinguishes between the response of "primary" and "secondary" walls as it for later determines higher displacement capacity for "SD" and "NC".

FEMA 306 requirements are oriented more towards contemporary masonry with regular texture and morphology and they are provided in Table 2.12. For "moderate damage" limit state (LS), the basic requirements are similar to that stipulated in EC8-3, as the drift is defined as 3/4 of the "CP" drift capacity. The drift capacity specified for the "heavy damage" "CP" limit state for rocking is defined as 0.8% h_w/l_w. For the sliding failure along the joints (stair stepped cracks), FEMA specifies 0.4% and for walls failing due to tension (diagonal cracking) no drift capacities but only ductility capacities are specified. Unlike EC8-3, FEMA defines also a mixed type of failure for walls. For mixed modes considering solely flexural cracking and toe crushing, a drift capacity of 0.3% is prescribed, while for toe crushing, flexural cracking and bed-joint sliding a drift capacity of 1.2% is provided. For the flexural cracking and toe crushing (for mixed mode) a drift capacity of 0.9% is specified for "extreme damage" limit state. For the "IO" performance level, minor cracking of the masonry is allowed and the drift limit is for all failure modes assumed as 0.1%.

Preglednica 2.12: Mejne vrednosti zasukov po standardu FEMA 306 [95]

Table 2.12: Limiting values for drifts according to FEMA 306 [95]

					Acceptable criteria			
					Primary		Secondary	
Behaviour mode	c^* [%]	d^* [%]	e^* [%]	"IO" [%]	"LS" [%]	"CP" [%]	"LS" [%]	"CP" [%]
Bed-joint sliding	0.6	0.4	0.8	0.1	0.3	0.4	0.6	0.8
Rocking	0.6	$0.4\frac{h_0}{l_w}$	$0.8\frac{h_0}{l_w}$	0.1	$0.3\frac{h_0}{l_w}$	$0.4\frac{h_0}{l_w}$	$0.6\frac{h_0}{l_w}$	$0.8\frac{h_0}{l_w}$

* parameters c, d and e refer to performance level presented in Figure 2.21

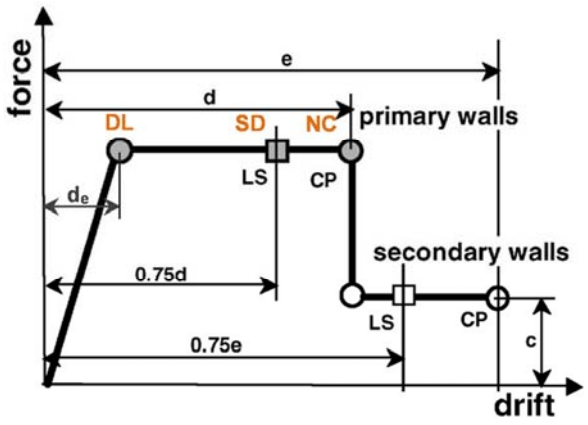

Figure 2.21: Bi-linear curve determined in FEMA 306 with added designations of performance limit states in EC8-3 (adapted from [99])

Slika 2.21: Bi-linearna krivulja, določena po predpisu FEMA 306, z dodanimi oznakami mejnih stanj po EC8-3 (privzeto iz [99])

For wall elements that are considered to be primary (as major lateral-force-resisting structural elements) the assumed force-deflection relation is bi-linear with an ultimate deformation capacity given by the term *d* (see Figure 2.21). If the wall element is considered as a secondary element supporting gravity, but not lateral loads, then up to 40% strength decrease is permitted. In such case, much larger ultimate deflections can be considered (parameter *e*, see Figure 2.21).

Some national codes (SIA D0237) do not define drift capacity in respect of the failure mode but as the function of applied axial stresses and boundary conditions. Ultimate drift capacity θ_u is in SIA D0237 [139] determined by Eq. 2.56, where coefficient η is equal to 0.4 and 0.8 for fixed-ends and cantilever boundary conditions, respectively.

$$\theta_u = \frac{4}{3}\eta\left(1-\sigma_0 / f_{Mc}\right), \qquad \textbf{2.56}$$

2.4 Multi-leaf (stone) masonry walls

Unlike for single-leaf masonry, not many experimental investigations of multi-leaf masonry were conducted until now. Even so, the researchers mainly tried to study the behaviour through compression tests and only scarce number of studies of behaviour under shear loading can be found. Most of the research was also focused on the strengthening techniques for improving the behaviour of multi-leaf masonry (especially grouting), while neglecting the fundamental research on the behaviour of multi-leaf masonry depending from its texture and morphology.

2.4.1 Compression tests

Studies of the load-carrying capacity of grouted stone-masonry walls were conducted by Terčelj et al [140] in 1981. Tomaževič et al [141] studied the possibilities of improving the behaviour of multi-leaf masonry by means of grouting through compression tests of grouted and un-grouted two-leaf rubble stone masonry walls, typical for the Slovenian region. Grouting improved the behaviour of masonry by connecting the leaves to a point that a solid wall response was obtained.

Egermann [39] and Binda et al [40] have established, that the ultimate compressive strength depends on compressive strength of each leaf, their thickness, their connection and boundary conditions of the loading (distribution of the compressive stresses). Compressive strength of the external leaves is usually for a rank higher than the compressive strength of the internal leaf (core) and due to the higher stiffness of the external leaves, more load is transferred to them. Due to incompatible deformation characteristics of the leaves, the connection at their interface fails and the outer layers are subjected to horizontal out-of-plane deformations due to the out-of-plane lateral loading induced by the inner layer (through lateral deformations).

Compressive and/or diagonal compressive tests were also performed by Vintzileou and Tassios [142], Modena [143,144], Toumbakari [145], Valluzzi et al [146], Vintzieou and Miltiadou-Fezans [147], Galasco et al [148]. They were mainly interested in efficiency of specific strengthening techniques

made through comparisons with the results gained on un-strengthened masonry. Various types of grout mixtures were developed, tested and compared. It was established, that the most important effect of grouting is not the increase of the masonry compressive strength, but ensuring a good connection between the leaves. The use of cement-based grouts [141,142] has advanced to the development and use of grouts, more compatible to original historic masonry materials, such as lime-pozzolana-cement-based ones [145] and lime-based grouts [146,147]. Lime-based grouts have proved not to significantly change the stiffness characteristics of the masonry, while still ensuring the sufficient connections between the leaves preventing the out-of-plane deformations.

Vignoli [143] applied grouting and jacketing to masonry walls, mainly of two accosted leaves with irregular stones and cobblestones, in-situ in various sites in Tuscany region. Through the use of flat-jack tests he established a considerable increase of strength and stiffness characteristics for both of the used strengthening techniques.

Valluzzi et al [146] also studied the efficiency of repointing and transversal tying of walls by means of steel ties. Among the various strengthening techniques tested, grout injection proved to be the most efficient, as it besides strength increase also improved the connection between the leaves resulting in a more ductile response and failure of the walls. The best effect was found for a combination of strengthening measures, grouting being one of them.

The influence of existence of the transversal connections was studied already by Toumbakari and Van Gemert [149]. Instead of steel ties Oliveira et al [150] introduced the use of GFRP (»Glass Fibre Reinforced Polymer«) ties. The presence of transversal connections limited the out-of-plane behaviour and leaf separation in the masonry.

2.4.2 Shear tests

For multi-leaf masonry, only some studies on the behaviour under shear loading can be found and in majority their focus is on the studying of specific strengthening techniques. Efficiency of grouting with different grouts was studied through diagonal tests in [142,143,145,147,151]. In Slovenia shear tests under compressive loading were performed in laboratory on walls built for the investigation of the types of historic masonry in SFRY [141,152]. Walls were strengthened with cement grout injections and the comparison of tests results of un-strengthened and strengthened walls showed, that grouting in most cases contributes to higher shear resistance, but also to reduction of maximum displacement capacity. Drei and Fontana [153] studied the influence of different material properties and geometrical characteristics of the walls on the response of multi-leaf walls using numerical modelling, which was based on experimental tests [154]. They have stated that large stress concentrations can occur at the junction of the external and the inner leaf. These concentrations are dependent on the leaves' relative thickness and on the geometry of the shear keys (indentation). The load transfer issue in a composite masonry was addressed also in [40]. It was established from shear tests on small samples that the shear failure in wallettes with straight collar joints occurred due to vertical cracks that arose in the interfaces of leaves, while for wallettes with keyed collar joint, the failure occurred mainly due to development of inclined cracks in the inner core.

Only recently the results of an extensive experimental campaign for the assessment of the in-plane behaviour of three-leaf stone masonry walls, conducted by Silva et al [6], were published. At shear tests on 16 walls with a controlled large percentage of voids in the core without any transversal connection between the leaves, constructed to represent a typical widespread masonry type in Portugal, the geometry aspect ratio (length : height equal to 1:1, 2:3) and the pre-compression level were altered. Some of the walls were tested un-strengthened (black curves in Figure 2.22 right), whereas others were grouted prior testing (red curves).

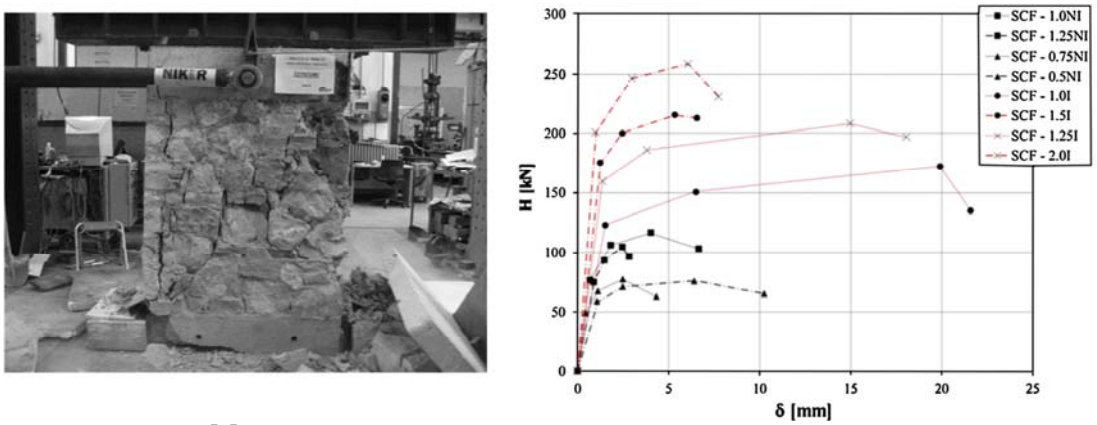

Figure 2.22: Silva et al [6]: crack pattern of the full scale un-grouted wall after shear test (left), comparison of the obtained results for full scale walls (right)
Slika 2.22: Silva et al [6]: poškodovanost neinjektiranega nepomanjšanega zidu po strižnem testu (levo), primerjava rezultatov strižnih testov nepomanjšanih zidov (desno)

Again the positive effect of grouting was confirmed; non-injected walls underwent leaf separation at lower displacements and specimens ultimately failed due to buckling of the external leaves. The grouted specimens on the other hand showed extensive transversal cracking after reaching maximum resistance with cracking of the inner core and no significant leaf separation.

Corradi et al [57,155] presented an extensive in-situ campaign by applying various strengthening techniques (systematic grouting, GFRP and CFRP strips, GFRP mesh used together with GFRP anchors) on a two-leaf wall. Strengthening by means of installing GFRP mesh by hydraulic lime mortar proved less efficient due to poor mortar-masonry bond characteristics. In-situ tests of un-strengthened and with various types of grouts strengthened walls were performed by Uranjek et al [156] in Slovenia, in Posočje region. Results proved an adequate effect of cement-lime grouts (curves LC1 and LC2 in Figure 2.24 right) for shear strengthening compared to the response of the un-strengthened wall.

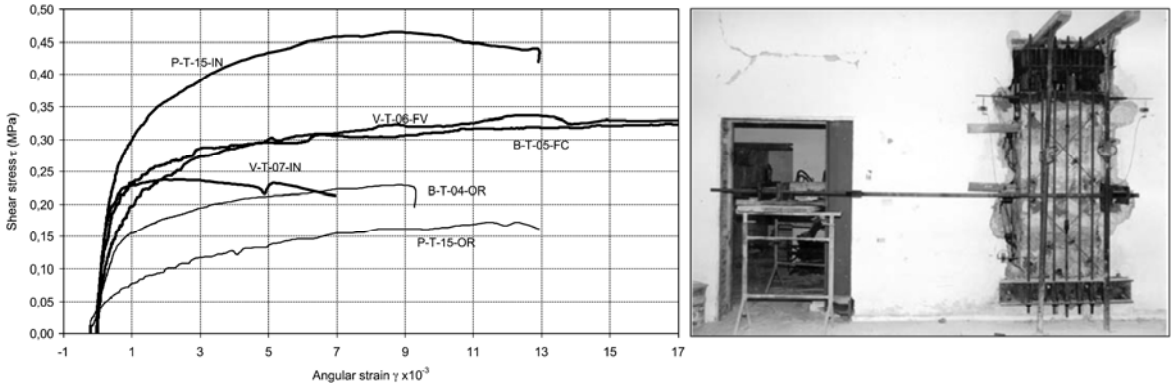

Figure 2.23: Corradi et al [157]: comparison of the results obtained for walls in various buildings (left), test setup for in-situ shear test (right)
Slika 2.23: Corradi et al [157]: primerjava rezultatov strižnih testov zidov v različnih objektih (levo), postavitev in-situ strižnega testa (desno)

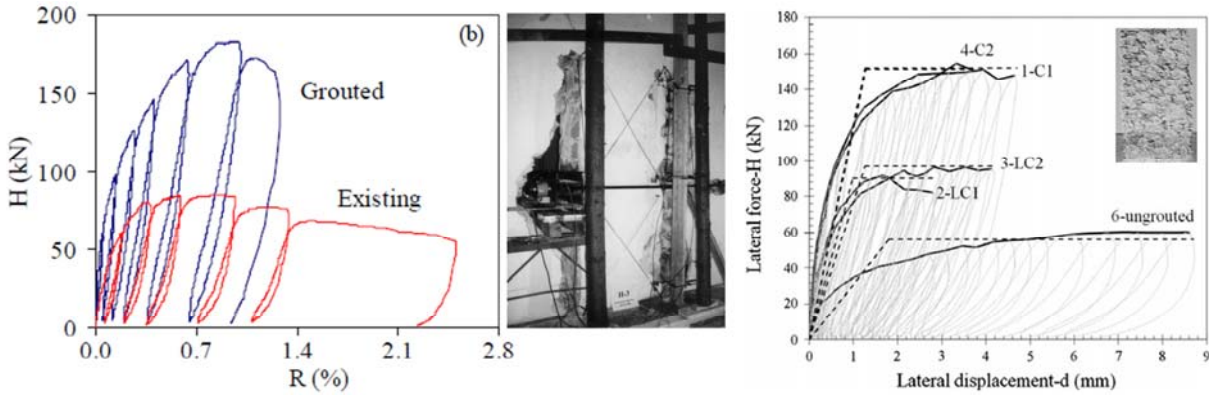

Figure 2.24: Tomaževič et al [158]: comparison of the results of shear tests for grouted and un-grouted wall (left) with test setup (in the middle), Uranjek et al [156]: comparison of the results of shear tests of walls grouted with various grout mixtures and of un-grouted walls (right)
Slika 2.24: Tomaževič et al [158]: primerjava rezultatov strižnih testov injektiranega in neinjektiranega zidu (levo) ter postavitev testa (na sredini), Uranjek et al [156]: primerjava rezultatov strižnih testov z različnimi injekcijskimi mešanicami injektiranih zidov in neinjektiranega zidu (desno)

2.4.3 Multi-leaf stone masonry building shaking table tests

The behaviour of multi-leaf stone masonry building under dynamic loading was studied through shaking table tests performed by Mazzon et al [159,160]. Results of tests on two-storey building models, the first of them strengthened only in the second stage of the research while the second already strengthened prior to testing, proved a positive effect of grouting. The maximal ground acceleration increased by 30% in the first case and by 50% in the second case compared to the un-strengthened structure, significantly reducing the out-of-plane failure of the outer leaves, but not changing the period and shape modes.

2.5 Strengthening of (three-leaf stone) masonry walls

2.5.1 Retrofitting and strengthening of historic masonry buildings

Choosing the proper intervention for repair (retrofitting) or strengthening of masonry building can be a difficult issue, especially if the building presents a cultural heritage asset. In such case the intervention has to be chosen and executed in accordance with the recognized conservation principles (the Venice Charter [161], the ICOMOS Recommendations – for architectural heritage [11],etc.). Though sometimes not possible, aspects such as reversibility, respect of the original conception through minimal intervention, non-intrusiveness and non-obtrusiveness, endurance of the intervention and compatibility of the materials should be considered.

Various retrofitting and strengthening techniques are in use, some traditional, while others more modern, then again some widespread while others uncommon and specific for the problem trying to be solved. Thorough and critical review on existing techniques was provided through reports of the recently finished European projects NIKER [162] and PERPETUATE [163]. In [162] measures are divided considering the compatibility of the intervention; whether they are traditional or modern and further on the basis of issue they are trying to solve. In Table 2.13, a summary of interventions for retrofitting and strengthening of masonry structures based on [162,164] is provided, in which also more detail descriptions for each intervention can be found. Of course the improvement of the masonry quality or the strengthening of individual structural elements results in the change (if designed properly in improvement) of global structural behaviour.

Preglednica 2.13: Metode sanacij in utrjevanj za izboljšanje obnašanja zidanih stavb (adapted from [162,164])

Table 2.13: Repair and strengthening techniques for improving structural behaviour of masonry buildings (povzeto po [162,164])

Improvement of masonry quality and local equilibrium problems	
Strengthening of masonry walls: - Grout injection - Jacketing by RC plaster - Structural repointing (Deep repointing) - Bed-joint reinforced repointing, NSM (near surface mounting) - Anti-expulsion tie-rods or other anchors - Insertion of artificial headers - FRP (Fibre Reinforced Polymer) / SRP (Steel reinforced polymer) / SRG (Steel reinforced grout) / TRM (Textile Reinforced Mortar) application - Confinement for columns and pillars - Others	Local repair of cracks or of decayed portions: - Local dismantling and reconstruction (“scuci-cuci”) - Grout injection of cracks - Bed-joint reinforced Repointing - FRP/SRP/SRG/TRM application - Crack stitching and anchoring - Others Stability improvement: - Enlargement - Buttresses - Strutting - Suspension - Reducing the loads - Pre-stressing

Continues…

…continuation of Table 2.13

Improvement of the global structural behaviour		

Improvement of sub-assemblage connections:
- between the walls:
  - Tie beams
  - Tie-rods
  - Hysteretic dissipation anchors
- between the wall and floor/roof
 	
Structural interventions related to the foundations:
- Soil stabilization (Micro-paling, Jet-grouting, Wooden-pile driving)
- Strengthening of the foundations
 	
Other
- Independent steel or concrete frame
- Introducing of a structural element
- Seismic isolation
	Improvement of wooden floors:
	- The use of wood:
	  - Orthogonal or diagonal planking
	  - Timber flange connected by dowels to main beams
	
	- The use of a reinforced concrete cooperating slab
	  - The Turrini - Piazza (1983) method
	  - The Alessi, Lamborghini, Raffagli (1989) system
	  - The Tampone (1992) system
	
	- The use of steel elements
	  - Metallic plates
	  - Metallic diagonals
	
	- The use FRP materials
		Optimization of vault and arch performance
		- Direct interventions (applied to vaults or arches):
		  - Local dismantling and reconstruction (“scuci-cuci”)
		  - Grout injection of the cracks
		  - Structural repointing (Deep repointing)
		  - Bed-joint reinforced repointing
		  - FRP/SRP/SRG/TRM application
		  - Use of extrados RC jacketing
		  - Reducing the loads from extrados infilling
		  - Extrados stiffening
		
		- Indirect interventions
		  - Insertion of tie-rods and confinement
		  - Buttresses

2.5.2 Techniques for repair and strengthening of (multi-leaf stone) masonry walls

Interventions for improving the mechanical characteristics and response of the walls are listed in Table 2.13. Not all of them meet all the requirements of the basic conservation principals, but are nevertheless necessary. Especially grouting presents the most efficient repair and strengthening technique for multi-leaf walls, since it would be rather hard to attain a monolithic response of more damaged (whether by decay or structural damage) walls by some other means. Grouting is a non-reversible intervention, but if proper grout is chosen, the measure more or less meets all the other conservation requirements. Interventions applicable for historic masonry walls and some most important research work regarding them are shortly presented hereafter.

2.5.2.1 Grouting

Research and the development of grout mixture are already described within Section 2.4. It has to be emphasized, that a careful approach of planning the intervention is strongly recommended, since not all types of walls are injectable and additional damage can be induced through grouting. In order the grouting to be efficient, morphology of the wall has to be suitable, proper grout mixture has to be chosen and the grouting has to be well executed. Recommendations upon the appropriateness of masonry, the choice of grout and execution can be found in [165-167].

2.5.2.2 Structural repointing

Structural repointing is an intervention where mortar in joints is replaced by a better quality mortar up to a certain depth of masonry. It is used in all types of masonry, actually for two main reasons.

Firstly, a significant increase of the mechanical characteristics can be obtained, if the repointing is conducted in a rather large masonry surface area. This is usually the case in slender masonry elements. The efficiency is again dependent on multiple aspects; appropriate masonry (poor mortar and relatively good units), proper mortar choice (compatible materials, stronger than original, but not too stiff), careful execution (adequate depth of stripping, wetting the surface, not making many voids when re-filling, possible repositioning of wedges, if removed during preparation, etc.). Vintzileou and Miltiadou-Fezans [168] have established that masonry compressive strength can be decreased if masonry joints are not fully filled. The authors applied deep repointing to brick masonry wallettes (Figure 2.25 left).

Secondly, application of repointing is actually a part of the preparation process before grouting; it is applied in order to prevent leakage of the grout and to additionally confine the injected material (Figure 2.25 middle and right). Corradi et al [169] have provided detailed information on deep repointing of multi-leaf stone masonry. Compression, diagonal compression and shear tests on repointed specimens confirmed not only the increase of shear strength, but also significant increase of shear stiffness of multi-leaf masonry.

Figure 2.25: Deep repointing of brick (left, adapted from [168]) and of stone masonry (middle and right) [170]
Slika 2.25: Prefugiranje opečne (levo, prilagojena [168]) in kamnite zidovine (na sredini in desno) [170]

2.5.2.3 Bed-joint reinforced repointing, NSM reinforcement

When reinforcement is inserted in the previously partially cleared out mortar bed-joint and then repointed, the intervention can be referred to as bed-joint reinforced repointing or as near surface mounted (NSM) reinforcement (Figure 2.26), even though the term NSM was primarily used, if the reinforcement was installed in a groove cut into the surface of the wall (can be either horizontal or vertical). In any case, for NSM, various reinforcement materials (stainless steel, FRP, etc.) can be installed in various directions with various type of mortar (lime- or cement-based) or other binder.

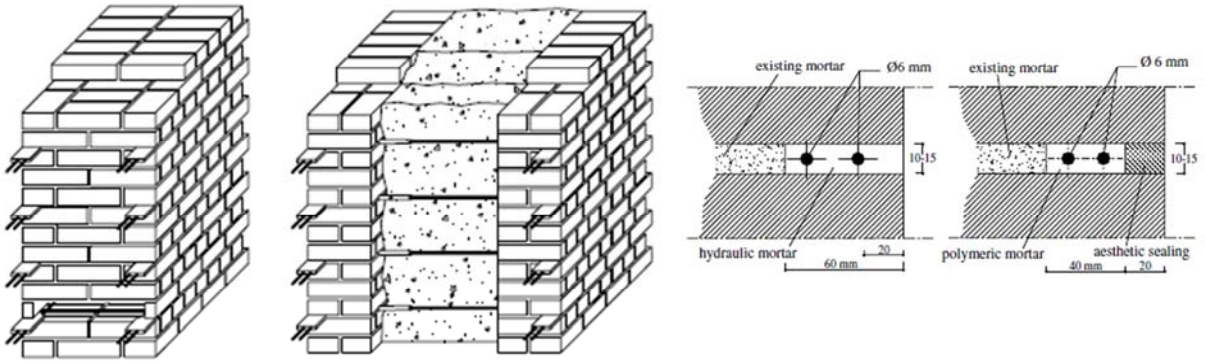

Figure 2.26: NSM of single-leaf, three-leaf masonry, details of reinforced mortar joint after repointing by mortar and resin (from left to right, from [171])
Slika 2.26: NSM eno- in troslojne zidovine, detajla maltne spojnice z ojačitvijo po prefugiranju z malto in polimernim vezivom (iz leve proti desni, iz [171])

In order for the technique to be effective, much attention must again be paid to the choice of the mortar (to prevent undesired chemical reactions), the choice of reinforcement (material characteristics, shape, flexibility), detailing (confining or anchoring of the reinforcement (if applied), bond characteristics, etc.) and execution (sufficient depth, thorough removing of existing mortar, clean surface, etc.), positioning and number of reinforcement (one/both sides of the wall, vertical or horizontal, every joint or just some, etc.). All the above choices largely affect the final characteristics of the behaviour of strengthened wall under loading.

Initially, experimental studies focused on use of steel bars for reinforcement [171-174]. Following the modern use and development of polymer composites for construction [175] and FRP techniques already in use for strengthening of concrete [176], studies involving FRP NSM reinforcement for masonry arose [177-191]. Studies of NSM of FRPs were however few compared to the number of studies of externally bonded (EB) FRPs used for strengthening of masonry. Short review on the FRP strengthening of masonry and the design models are provided in the following Section.

Through the mentioned studies it was established, that NSM of various types of reinforcement can (but not necessarily [171,190]) contribute to the increase of masonry resistance for both vertical and lateral load, but even more important it can contribute to the improvement of the deformation and displacement capacity through reducing the dilatancy of the wall and crack propagation. A more stable behaviour after achieving the strength peak is also recognized [179,183]. It was shown in shear tests performed by Petersen et al [188] as well as in diagonal tests by Mahmood and Ingham [189], that the vertical reinforcement can be very effective for restraining sliding.

Symmetrically positioned reinforcement on both sides of the wall contributes to more stable and ductile behaviour [183], whereas for one side NSM tilting in the direction of the strengthened face is reported [179,188,189]. According to Turco et al [186] applying the FRPs either in every or in every second bed-joint plays no significant role, neither does the choice of embedding material (for aesthetic and economic reasons encourages the use of cementious paste rather than epoxy). Valluzzi et al [171] on the other hand recommend the use of lime-based mortars instead of cement or polymeric products for historic masonry in order to avoid incompatibility of materials.

2.5.3 Fibre Reinforced Polymer (FRP) strengthening

The use of FRPs for strengthening techniques presents a good solution due to their specific characteristics compared to the traditional materials: high strength-to-weight ratio (consequently low influence on the global mass of the structure), fast and easy application to an existing structure (with minimum impact on the buildings functions and size), good corrosion resistance, etc. Various strengthening systems (many of them commercial) can be found, varying in the type and shape of the FRP used, installation, positioning and details of the application. For masonry as already mentioned EB and NSM FRPs are in use as well as structural repointing, jacketing with FRP reinforced renders, pre-stressing and transversal tying. The most widespread is the application of EB FRPs and also most research studies can be found for this type of strengthening. State-of-the-art review with over 60 references of experimental studies performed up to year 2005 is provided in [192], whereas in [189,193-208] studies performed after 2005 are presented.

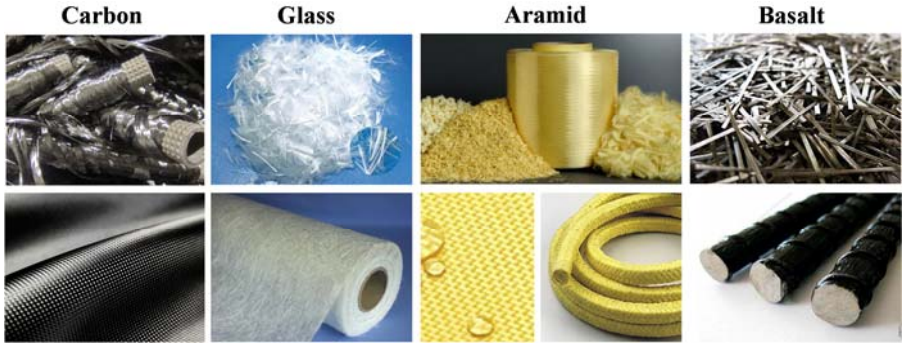

Figure 2.27: Carbon fibre tow (http://www.rockwestcomposites.com/products/10015-d) and fabric (http://www.sailingscuttlebutt.com/2013/10/17/addressing-environmental-impact-carbon-fiber/), glass fibres (http://image.made-in-china.com/4f0j00BvraECiGRWzQ/Glassfiber.jpg) and mat (http://shop.hp-textiles.com/shop/product_info.php/language/en/info/p98_hp-mp300e---textile-glass-mat.html/), aramid fibres and filament (upper photo) and fabric (http://kevlar-fiber.com/), braided aramid (http://www.directindustry.com/prod/aw-chesterton-company/aramid-braided-packing-17469-526554.html aramid), basalt fibres (http://www.technobasalt.com/i/products/439_241/GLY57W8x.jpg) and rods (http://www.directindustry.com/prod/technobasalt-invest-llc/basalt-fiber-reinforced-polymer-bar-65468-1007959.html)

Slika 2.27: Karbonske niti in tkanina, steklena vlakna in blago, aramidna vlakna in niti zgoraj, spodaj tkanina in vrv, bazaltna vlakna ter palice

FRPs include various type of high strength fibres embedded in a resin matrix. Carbon (CFRP) and glass (GFRP) fibres are most often used, but also applications of aramid (AFRP), polyvinyl-alcohol (PA FRP) and recently basalt (BFRP) fibres were conducted. Materials vary significantly in strength but even more important in their stiffness (Figure 2.28).

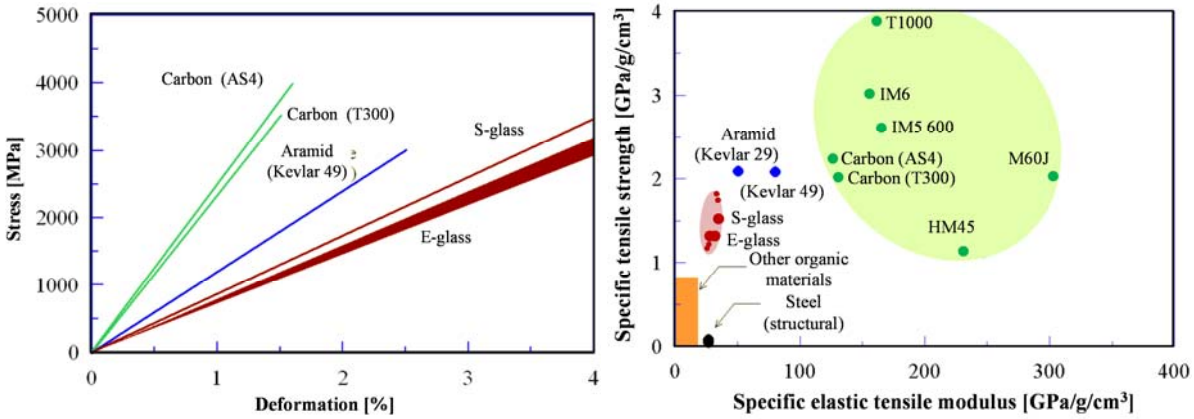

Figure 2.28: Stress - strain diagram (left) and the comparison of specific tensile strengths and elastic moduli of reinforcement material (right) [209]

Slika 2.28: Diagram napetost - deformacija (levo) in primerjava specifičnih nateznih trdnosti in elastičnih modulov različnih ojačitvenih materialov (desno) [209]

For building construction applications, FRPs with epoxy or polyester resin matrices are most commonly used. Since FRPs are heterogeneous and anisotropic, they can be supplied in various forms; unidirectional yarns and rovings or strips and more directional mats, sheets or fabrics. If only fibres (in any form) are supplied, they are further installed with a wet lay-up system (impregnated with resin on site and then installed). However pre-cured systems prepared for direct installation or pre-preg systems, where the fibres are pre-impregnated with resin and partially polymerized, are available.

Through many mentioned studies, a lot of important conclusions were made regarding various aspects of strengthening, only some of them mentioned hereafter. Detail instructions upon design and execution of FRP strengthening considering knowledge gathered in numerous research studies is provided in CNR-DT 200/2004, an Italian guide for the design and construction of EB FRP systems for strengthening existing structures [209].

Less stiff material appeared to be more effective (i.e. GFRP performs better than CFRP) in terms of strength and stiffness increase as well as in decreasing vulnerability to debonding [196,210]. The authors also recommend symmetrical installation on both sides of the walls. Main failure mechanism is in the most cases the result of the loss of the cohesion between the reinforcement and the wall, caused by debonding of the FRP interface, delamination of the superficial part of the masonry (peeling) or FRP rupture. If the later two occur, failure is brittle. ElGawady et al [211] recommend the adhesive to be selected for its strain capacity rather than its strength. If a premature failure of the FRP is avoided through control of the debonding length and possible usage of anchorages, the failure mechanism can be ductile. In NSM a higher strain is developed in the FRP before debonding occurs compared to EB. In case of strengthening with fabrics, due to the evolution of horizontal cracks at the edges of walls and rotation of walls at higher levels of lateral loading, Lutman et al [204,205] and Tomaževič et al [204,205] recognize the need for anchoring of the fabric to surrounding masonry.

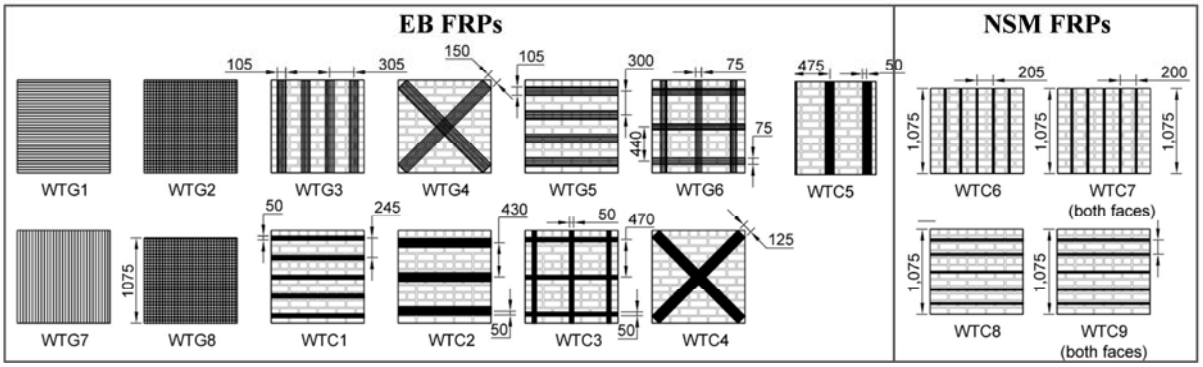

Figure 2.29: Investigation on various EB and NSM FRP layouts performed by Mahmood et al [189]
Slika 2.29: Preiskave različnih razporeditev EB in NSM FRP ojačitev Mahmood-a in Ingham-a [189]

Regarding positioning of the FRPs (Figure 2.29), according to some authors [210] diagonal arrangement proved better in terms of strength increase, whereas the grid configuration performed better in terms of less brittle behaviour due to enabling the spreading of the cracks. However, through extensive investigation on various positioning of FRPs on (historic) brick masonry, Jarc Simonič et al [207] report the grid scheme to be more efficient in terms of strength and ductility compared to the diagonal one. They also report a significant effect of confinement by horizontal FRP strips. Mahmood and Ingham [189] establish that horizontal layout of the FRP does not mitigate the sliding deformations of the un-reinforced masonry (URM) in case it is built with weak mortar. For the mitigation of the sliding deformations, vertical or/and diagonal arrangement suffice.

The fact, whether the masonry has been damaged prior the intervention, does not affect the efficiency of EB FRP strengthening [207], unless the softening of the masonry has already occurred [199].

The use of FRP has some disadvantages [211], though: the binding resins are flammable and in fire result in toxic vapours, the long-term reliability of the materials is largely unproven, FRPs are impermeable to moisture transport.

In CNR-DT 200/2004, special attention is made to environment effects (alkaline environment, moisture, extreme temperatures and thermal cycles, freeze-thaw, ultraviolet radiations) long-term effects (creep and relaxation, fatigue, impact loading, vandalism, fire) and finally to execution (inspection, storage, preparation, tools, positioning with regard to expansion and contraction, molding and sealants, fasteners and their layout, adhesives).

2.5.4 Design recommendations and assessment of in-plane shear FRP strengthening contribution

FRP strengthening can be applied to increase flexural or in-plane shear resistance, thus analytical design models differ in accordance with this intention. Compared to research focused on establishing the effectiveness of strengthening with FRPs, rather few researchers have focused on the development of appropriate design models for resistance of shear capacity of FRP strengthened URM walls [179,183,211-219]. They were prevailingly designed for EB FRPs, except [179,183], where NSM FRPs are modelled. The models can mainly be divided into two categories; strain-based models

([212,213,220]) and truss analogy models ([209,211,214-216,219]). Code provisions CNR-DT 200/2004 [209], its revised version CNR-DT 200 R1/2013 [221] and ACI 440.7R-10 [220] provide guidelines for design of FRP strengthening.

According to Zhuge [222], Mahmood and Ingham [223] and Jarc Simonič et al [207] none of the models consistently predict the FRP shear contribution satisfactory. Hereafter, first the code provision design guidelines are presented, as they comprehensively address the various types of FRP strengthening and accompanying issues. The models, which can be applied also in case of NSM strengthening, are presented afterwards.

2.5.4.1 Code provisions design guidelines

2.5.4.1.1 CNR-DT 200/2004 [209]

The design shear capacity of the strengthened wall V_{Rd} is according to Eq. 2.57 assessed as a sum of the URM wall resistance $V_{Rd,m}$ and the FRP contributions $V_{Rd,f}$ considering failure of the compressed strut of the truss up to the limit (Eq. 2.58). $V_{Rd,m}$ is determined as $V_{Rd,s}$ according to Eq. 2.53.

$$V_{Rd} = \min\left(V_{Rd,m} + V_{rd,f},\ 0.3 \cdot f_{Mc,x} \cdot t_w \cdot l_{fc}\right), \quad \textbf{2.57}$$

$$V_{Rd,f} = \frac{1}{\gamma_{Rd}} \frac{0.6 \cdot l_{fc} \cdot A_f \cdot f_{fd}}{s_f}, \quad \textbf{2.58}$$

$$\varepsilon_{fd} = \min\left(\eta_a \frac{\varepsilon_{fk}}{\gamma_f}, \varepsilon_{fdd}\right), \quad \textbf{2.59}$$

Where γ_{Rd} is the partial factor for resistance models to be assumed for ultimate limit state (ULS) for various response mechanism according to Table 2.14, l_{fc} the distance between the compression side of the masonry and the centroid of FRP flexural strengthening, A_f the cross-section area of the FRP shear reinforcement in the direction parallel to the shear force (FRP width b_f × FRP thickness t_f, see Figure 2.30), s_f the centre-to-centre spacing of the FRP reinforcement measured orthogonally to the direction of the shear force (see Figure 2.32), f_{fd} is the design strength of the FRP reinforcement, defined as the lesser between FRP tensile failure strength f_{fu} and the design FRP debonding strength f_{fdd}. $f_{Mc,x}$ is the design compressive strength of the masonry parallel to the mortar joints.

Preglednica 2.14: Parcialni faktorji γ_{Rd}, odvisni od mehanizma nosilnosti [209]

Table 2.14: Partial factors for resistance models γ_{Rd} dependant from the developed mechanism [209]

Resistance model	γ_{Rd}
Bending / Combined bending and axial load	1.00
Shear / Torsion	1.20
Confinement	1.10

Design FRP ultimate strain ε_{fd} is determined as the maximum strain allowed to the FRP system according to Eq. 2.59, where ε_{fk} presents the FRP characteristic strain at failure and ε_{fdd} the maximum FRP strain once the FRP debonding takes place, calculated according to Eq. 2.64. Environmental

conversion coefficient η_a depending upon fibre/resin type and exposure conditions and the partial factor γ_m, provided as a function of the FRP failure mode - equal to γ_f in case of FRP rupture and $\gamma_{f,d}$ in case of FRP debonding, all provided in the code and summarized in Tables 2.14 and 2.16. For η_a, values may be increased by 10% (not exceeding 1.00) whenever protective coatings tested for their efficiency and properly maintained are used (Table 2.16).

Preglednica 2.15: Parcialni faktorji γ_m za FRP materiale in produkte, odvisni od porušnega mehanizma [209]
Table 2.15: Partial factors γ_m for FRP materials and products dependent from the failure mode [209]

Failure mode	Partial factor	Type-A application *	Type-B application **
FRP rupture	γ_f	1.10	1.25
FRP debonding	$\gamma_{f,d}$	1.20	1.50

* Strengthening systems certified according to the requirements in [209] (each component as well as the final product)

** Strengthening systems certified according to the requirements in [209] (each component only)

Preglednica 2.16: Okoljski konverzijski faktorji η_a za različne pogoje izpostavljenosti FRP utrditev [209]

Table 2.16: Environmental conversion coefficient η_a for different exposure conditions of FRP strengthening [209]

Exposure conditions	Type of fibre/resin	η_a
Internal	Glass/Epoxy	0.75
	Aramid/Epoxy	0.85
	Carbon/Epoxy	0.95
External	Glass/Epoxy	0.65
	Aramid/Epoxy	0.75
	Carbon/Epoxy	0.85
Aggressive environment	Glass/Epoxy	0.50
	Aramid/Epoxy	0.70
	Carbon/Epoxy	0.85

Bond strength at ultimate limit state

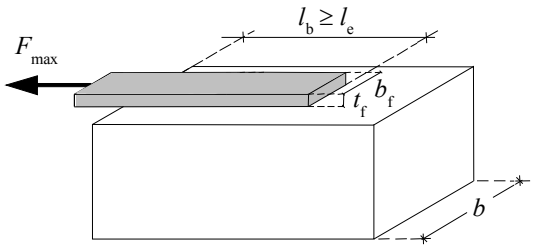

Figure 2.30: Maximum force transferred between the FRP and the masonry [209]
Slika 2.30: Maksimalna sila med FRP in zidovino [209]

The ultimate value of the force transferred from the FRP reinforcement to the support prior to FRP debonding depends on the length l_b of the bonded area (Figure 2.30). Length l_b increases up to a maximum effective length l_e (Eq. 2.60), which is the optimal bond length and corresponds to the minimal bond length able to carry the maximum anchorage force. Further increase of the bonded area does not increase the force that it is possible to transfer. In Eq. 2.60 $f_{Mt,m}$ is the masonry average tensile strength and may be taken as $0.10\,f_{Mc}$, if no other data is available. E_f is the FRP modulus of elasticity.

$$l_e = \sqrt{\frac{E_f t_f}{2 \cdot f_{Mt,m}}} \qquad \text{[length in mm]} \qquad \textbf{2.60}$$

If $l_b \geq l_e$:

$$f_{fdd} = \frac{1}{\gamma_{f,d} \cdot \sqrt{\gamma_M}} \sqrt{\frac{2E_f \cdot \Gamma_{Fk}}{t_f}}, \qquad \textbf{2.61}$$

$$\Gamma_{Fk} = c_1 \sqrt{f_{mk} \cdot f_{Mt,m}} \quad \text{[in MPa]} \qquad \textbf{2.62}$$

If $l_b < l_e$:

$$f_{fdd,red} = f_{fdd} \frac{l_b}{l_e}\left(2 - \frac{l_b}{l_e}\right), \qquad \textbf{2.63}$$

$$\varepsilon_{fdd} = \frac{f_{fdd}}{E_f}, \qquad \textbf{2.64}$$

When debonding involves the first masonry layers (if tensile strength of the adhesive used to install the FRP is larger than that of the masonry substrate) and $l_b \geq l_e$, the f_{fdd} is expressed according to Eq. 2.61. Parameter Γ_{Fk} is the characteristic specific fracture energy of the FRP strengthened masonry; if debonding involves the first masonry layers, it is calculated according to Eq. 2.62, where c_1 is an experimentally determined coefficient, for which 0.015 may be adopted, if no experimental data is available.

If $l_b < l_e$, the l_b is reduced according to Eq. 2.63. If debonding mechanism between FRP and masonry occurs by rupture of a portion of the masonry unit, it is assumed that each masonry unit concur for more than 80% of its length and l_b is determined considering this limitation.

2.5.4.1.2 CNR-DT 200 R1 2013 (revised) [221]

The revised version of the CNR DT 200 document includes formulas and parameters which have been calibrated once more, as the database of the conducted tests and knowledge have expanded, involving also new application systems and techniques. Among the important updates are the revision of coefficients for the calculation of the fracture energy, update of the l_e for EB reinforcements, additions of a clause concerning the verification of FRP reinforcement bonded to primer regularization layers and of a model for shear design of walls with cross diagonal reinforcement [224].

In the revised version values for γ_m are defined differently; for ULS $\gamma_m = \gamma_f$ is equal to 1.10. Only when debonding is critical, the values of γ_m defined as $\gamma_{f,d}$ can be chosen by the designer in a range between 1.20 to 1.50, depending on the higher or lower probability of failure due to debonding.

URM walls and FRP contributions are according to revised version defined as in Eq. 2.65 and 2.66, where x is the distance of the neutral axis from the extreme compression fibre (Figure 2.31 left).

$$V_{Rd,m} = \frac{1}{\gamma_{Rd}} x \cdot t_w \cdot f_{vd}, \qquad \textbf{2.65}$$

$$V_{Rd,f} = \frac{1}{\gamma_{Rd}} 0.6 \cdot l_{fc} \cdot \left(E_f \varepsilon_{fd} \right) \cdot 2 \cdot t_f \frac{b_f}{s_f}, \qquad \textbf{2.66}$$

Shear design of walls with cross diagonal reinforcement

Masonry contribution is calculated according to Eq. 2.67, whereas the entire shear capacity considering also FRP strengthening under an angle θ_f (Figure 2.31 left) and neglecting the contribution of the FRP under compression is then determined according to Eq. 2.68, where the expression $\delta_{Rd} / h_w \left(\sin\theta_f \cos^2\theta_f \cdot E_f A_f \right)$ is the horizontal component of the FRP corresponding to a displacement δ_{Rd}, calculated as the minimum value of displacement at the top of the wall $\delta_{Rd,1}$ (Eq. 2.70) and maximum horizontal displacement $\delta_{Rd,2}$ compatible with design strain of FRP (Eq. 2.71). In Eq. 2.67 x_{min} is the minimum distance between the neutral axis and the extreme compression fibre of the section

$$V_{Rd,m} = x_{\min} \cdot t_w \cdot f_{vd}, \qquad \textbf{2.67}$$

$$V_{Rd} = \frac{\delta_{Rd}}{h_w} \left(\frac{V_{Rd,m}}{0.005} + \sin\theta_f \cos^2\theta_f \cdot E_f A_f \right), \qquad \textbf{2.68}$$

$$\frac{\delta_{Rd}}{h_w} = \frac{1}{h_w} \min\left(\delta_{Rd,1}, \delta_{Rd,2} \right) = \min\left(0.005, \frac{f_{fdd}}{E_f \sin\theta_f \cos\theta_f} \right), \qquad \textbf{2.69}$$

$$\delta_{Rd,1} = 0.005 \cdot h_w, \qquad \textbf{2.70}$$

$$\delta_{Rd,2} = \frac{\Delta D_{fdd}}{\cos\theta_f} = \varepsilon_{fdd} \frac{h_w}{\sin\theta_f \cos\theta_f} = \frac{f_{fdd} h_w}{E_f \sin\theta_f \cos\theta_f}, \qquad \textbf{2.71}$$

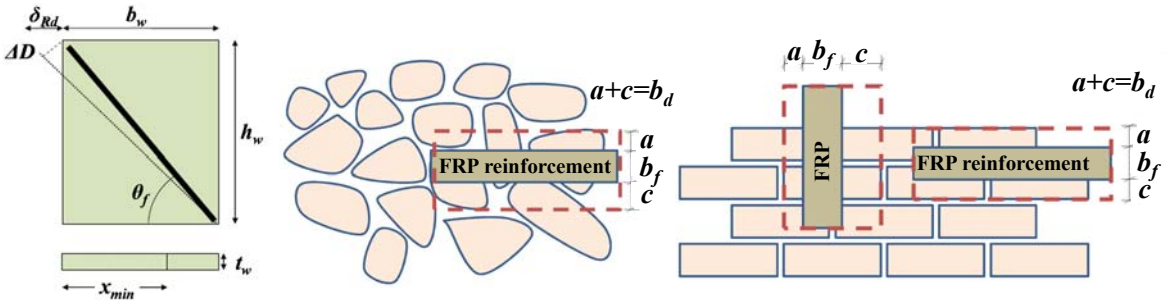

Figure 2.31: Wall strengthened with FRP included by an angle θ_f (left), bond strength distribution for irregular shaped stones (middle) and regular shaped stones (right) [221]
Slika 2.31: Zid, utrjen s pod kotom θ_f nagnjenimi FRP lamelami (levo), vplivno območje za trdnost stika pri nepravilnih (sredina) in pravilnih (desno) gradnikih [221]

Bond strength at ultimate limit state

$$l_e = \min\left(\frac{1}{\gamma_{Rd} f_{bd}} \sqrt{\frac{\pi^2 E_f t_f \Gamma_{Fd}}{2}}, 150 \text{ mm} \right) \qquad \textbf{2.72}$$

$$f_{bd} = \frac{2\Gamma_{Fd}}{s_u}, \tag{2.73}$$

$$\Gamma_{Fd} = \frac{k_b k_G}{CF}\sqrt{f_{bm} f_{btm}}, \tag{2.74}$$

$$k_b = \sqrt{\frac{3 - b_f / b_{f,ef}}{1 + b_f / b_{f,ef}}}, \tag{2.75}$$

$$k_G = \begin{cases} 0.031 \text{ mm} & \ldots\text{for clay brick masonry} \\ 0.048 \text{ mm} & \ldots\text{for tuff stone masonry} \\ 0.012 \text{ mm} & \ldots\text{for Calcarenite and Lecce stone masonry} \end{cases} \tag{2.76}$$

$$f_{fdd} = \frac{1}{\gamma_{f,d}}\sqrt{\frac{2E_f \cdot \Gamma_{Fk}}{t_f}}, \tag{2.77}$$

In the above revised formulas, γ_{Rd} is a corrective coefficient equal to 1.5 for tuff and porous stones and 1.25 for Calcarenite masonry and Lecce stones, s_u the slip interface corresponding to full debonding, if experimental data is not available, values 0.4 mm for tuff and perforated stones and 0.3 mm for Calcarenite masonry and Lecce stones are provided. k_b is a geometrical corrective factor; if no experimental data available k_b is computed according to Eq. 2.75, where $b_{f,ef}$ and b_f are the effective width and the width of the strengthened FRP element; b can be computed as a sum of b_f and the width of the bond distribution area b_d (see Figure 2.31 middle and right). In the case of masonry with irregular shaped stones, b_d is considered equal to the average diameter of the stones, and in the case of regular shaped stones equal to the support block dimension in the perpendicular direction of the FRP principal axis. Coefficient k_G is a corrective slip factor, dependant on the type of masonry. For pre-cured systems, the values of k_G shall be reduced to 40%. *CF* is the confidence factor (>1) which should be considered for the structure to be reinforced and f_{bm} and f_{btm} are the mean compressive and tensile strength of masonry blocks. In absence of experimental evidences, the f_{btm} can be computed as $0.10 f_{bm}$.

The above equations are considered valid when using low viscosity epoxy resin in order to ensure the penetration through the pores present in the masonry block; high viscosity epoxy and low porosity supports shall be used with care.

FRP reinforcement bonded to regularization layer

When FRP systems are applied in intermediate epoxy layer due to irregularity on the masonry surface, debonding strength shall be evaluated at the interface between the layer of regularization and the masonry, provided that the simultaneous curing of the epoxy resin on the mortar and the FRP resin is ensured. The thickness t_h and the modulus of elasticity of the homogeneous system E_h, made of FRP and layer of regularization, shall be calculated as follows (Eq. 2.78):

$$t_h = t_f + t_r, \quad E_h = \frac{E_f t_f + E_r t_r}{t_h}, \tag{2.78}$$

where t_r and E_r are the thickness and the modulus of elasticity of the regularization layer; t_r can be estimated knowing the volume of material applied to the masonry surface and assuming the layer

equivalent to a cylindrical solid. Bonding strength capacity shall be computed by using Eq. 2.72-2.77 and Eq. 2.66, where b_f equal to ($b_f + 2t_r$) should be used.

2.5.4.1.3 ACI 440.7R-10 [220]

This guide discusses the most commonly used application layouts of FRP for shear strengthening; a typical FRP strengthening scheme performed either with wet layup (Figure 2.32 left) or NSM systems (Figure 2.32 right). Other layouts, including fibres placed diagonally are not covered in the scope of the guide.

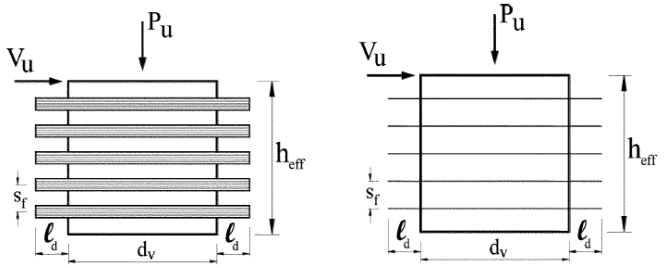

Figure 2.32: EB (left) and NSM (right) FRP strengthening of shear controlled walls [220]
Slika 2.32: Strižno utrjevanje zidov s površinskim lepljenjem FRP (levo) in z namestitvijo FRP utrditev v utore pod površino zidov (desno) [220]

The nominal shear strength of the FRP-strengthened $V_{n,s}$ (Eq. 2.79) wall can be computed by adding the FRP contribution V_f (Eq. 2.82) to the nominal strength of the URM wall V_m (Eq. 2.80), additionally limited by the nominal lateral strength corresponding to toe crushing V_{tc} of the wall. For obtaining V_m, the nominal lateral strength corresponding to joint sliding V_{bjs}, the nominal lateral strength corresponding to diagonal tension V_{dt} and the nominal lateral strength corresponding to toe crushing V_{tc} should be considered (Eq. 2.80). The design lateral strength is obtained according to Eq. 2.81, where the strength reduction factor ϕ is equal to 0.8 for shear-controlled failure modes and to 0.6 for flexure-controlled failure mode (specified in ACI 530 [225]).

$$V_{n,s} = \min\left(V_m + V_f,\ V_{tc}\right), \tag{2.79}$$

$$V_m = \min\left(V_{bjs}, V_{dt}, V_{tc}\right), \tag{2.80}$$

$$\phi V_n \geq V_u, \tag{2.81}$$

$$V_f = \begin{cases} p_{fv} b_f \dfrac{d_v}{s_f} & \text{…for surface mounted FRP systems} \\ p_{fv} \dfrac{d_v}{s_f} & \text{…for NSM FRP systems} \end{cases} \tag{2.82}$$

$$d_v = \min\left(h_w, l_w\right), \tag{2.83}$$

$$f_{fu} = C_E f_{fu}^{*}, \tag{2.84}$$

$$\varepsilon_{fu} = C_E \varepsilon_{fu}^{*} \tag{2.85}$$

$$E_f = \frac{f_{fu}}{\varepsilon_{fu}}, \tag{2.86}$$

Coefficient p_{fv} is computed according to Eq. 2.91, d_v is the effective masonry depth (Eq. 2.83). Design tensile strength f_{fu} (Eq. 2.84) and rupture strain ε_{fu} (Eq. 2.85) are reduced by the environmental reduction factor C_E given in Table 2.17 for the appropriate fibre type and exposure condition. Parameter C_E reflects the use of a protective coating, if the coating has been shown through testing to decrease the effects of environmental exposure and is properly maintained throughout the lifetime of the FRP system; C_E should never be larger than the values provided in Table 2.17 for the interior exposure conditions. f_{fu}^* is the ultimate tensile strength of the FRP material as reported by the manufacturer.

Preglednica 2.17: Okoljski redukcijski koeficient C_E za različne pogoje izpostavljenosti FRP utrditev [220]

Table 2.17: Environmental reduction factor C_E for different exposure conditions of FRP strengthening [220]

Exposure conditions	Fibre type	C_E
Interior exposure (for example partitions)	Carbon	0.95
	Glass	0.75
	Aramid	0.85
Exterior exposure (including internal side of exterior walls)	Carbon	0.85
	Glass	0.65
	Aramid	0.75
Aggressive environment (basement walls)	Carbon	0.85
	Glass	0.50
	Aramid	0.70

Strain and strength limit to prevent debonding

To prevent debonding, a limitation depends on the strain level developed in the FRP laminate. The maximum strain and corresponding stress, that FRP systems can attain before debonding from the masonry substrate occurs, are defined as effective strain ε_{fe} and effective stress f_{fe}. For shear-controlled failure modes they are determined according to Eq. 2.87 and 2.88:

$$\varepsilon_{fe} = \kappa_v \varepsilon_{fu}^* \le C_E \varepsilon_{fu}^*, \quad \textbf{2.87}$$

$$f_{fe} = E_f \varepsilon_{fe} \quad \textbf{2.88}$$

$$\kappa_v = \begin{cases} 0.40 & \text{...for } \omega_f \le 0.20 \\ 0.64 - 1.2\omega_f & \text{...for } 0.20 < \omega_f \le 0.45 \\ 0.10 & \text{...for } \omega_f > 0.45 \end{cases} \quad \textbf{2.89}$$

$$\omega_f = \frac{1}{85} \frac{A_f E_f}{A_n \sqrt{f_m'}}, \quad \textbf{2.90}$$

$$p_{fv} = \begin{cases} nt_f f_{fe} \le 260 \text{ N/mm} & \text{…for surface mounted FRP systems} \\ A_{f,bar} f_{fe} \le 44.5 \text{ N/ba} & \text{…for NSM FRP systems} \end{cases} \quad \textbf{2.91}$$

The bond reduction coefficient for shear-controlled failure modes κ_v (Eq. 2.89) depends on the FRP reinforcement index ω_f, defined as in Eq. 2.90. For shear-controlled failure modes κ_v was calibrated based on experimental data in [178,179,210,211,215,226-230]. Eq. 2.89 is applicable only when the force per unit width (or per bar for NSM systems), that the FRP system transfers to the masonry substrate, satisfies the limitation in Eq. 2.91. The A_n is the area of net mortared/grouted section and $A_{f,bar}$ the area of a single rectangular or circular bar.

Detailing

The code also provides some limited guidance for detailing of EB and NSM FRP systems and design of anchorages.

Regarding debonding of FRPs, for NSM systems, the minimum depth of the grooves D should be at least $1.5d_b$ (d_b being the FRP bar diameter) when an epoxy-based paste is used to embed the bar (according to [231,232]). When a rectangular bar with a large aspect ratio is used, D is suggested to be higher than ($3.0a_b \times 1.5b_b$), where a_b is the smallest bar dimension and b_b the largest. The minimum clear groove spacing for NSM FRP bars should be greater than twice the depth of the NSM groove. Furthermore, a clear edge distance of four times the depth of the NSM groove should be provided to minimize the edge effects, which could accelerate debonding failure [232]. Turco et al [233] assessed the use of cementitious grouts to embed FRP bars; a square groove with a least dimension of $2.5d_b$ could be adequate, however due to limited experimental data, there are no recommendation in the code for D in case of cementitious grouts. For EB FRP systems the weakest link in the masonry-FRP interface is the masonry. The quality and the tensile strength of the substrate limit the overall effectiveness of the bonded FRP system and the debonding of a properly installed FRP laminate can result from a lack of bonded area. Therefore the code recommends proper development length; l_e is adopted from CNR-DT 200/2004 (Eq. 2.60).

The l_e for NSM FRP systems should be provided by the manufacturer and certified by testing independent of the manufacturer. Spacing limits of reinforcements are also recommended; the maximum clear reinforcement spacing for externally bonded strips (or s_f for NSM bars) should be 400 mm. Determination of the FRP reinforcement anchorages to minimize the potential of premature debonding is recommended in the code, but not summarized herein.

2.5.4.2 Models for EB FRP strengthening

2.5.4.2.1 Triantafillou [212]

According to the author, the design of FRP-strengthened members in the case of concrete and masonry can be treated on the basis of the classical truss analogy and by accounting for an effective FRP strain ε_{fe}, which depends on the product of the FRP elastic modulus and the FRP area fraction.

The model stands for a wall, reinforced with horizontal epoxy-bonded FRP laminates on both sides of the wall. Area fraction ρ_h is defined as the total cross-section area of horizontally placed FRP divided by the corresponding area of the wall; as $2t_f/t_w$ for FRP attached over entire area of the wall or as ($2t_f/t_w \times b_f/s_f$) for FRP applied to the wall in the form of strips (see various EB FRP strengthening

layouts in Figure 2.29). Strain $\varepsilon_{M,u}$ is the masonry ultimate compressive strain and $f_{Mc,k}$ characteristic compressive strength.

The model for the design of reinforced masonry subjected to in-plane shear force V_{Rd} is according to Eq. 2.57 based on the assumption that the total shear capacity is determined as the sum of the contribution of $V_{Rd,m}$ and the contribution of shear reinforcement $V_{Rd,f}$, where for masonry walls with several layers of reinforcement, l_{wc} can be taken approximately equal to $0.8l_{\mathrm{w}}$, as suggested by [81] and $V_{Rd,m}$ is proposed to be calculated in accordance to EC6. f_{vko} is according to the author between 0.1 and 0.3 MPa (the lower limit applies in the absence of experimental data), depending on the type of masonry units and the mortar strength; $f_{vk,lim}$ the limiting value of f_{vk}, which is in the range of 1.0±1.7 MPa, depending on the type of masonry units and the mortar strength; f_b, the normalized compressive strength of masonry units (the mean compressive strength of masonry units corrected by the size factor (between 0.65±1.55)). If strengthening was applied without a wholesome retrofitting; that is in the case of damaged masonry walls, the value of f_{vk} should be according to the author taken lower than that which is proposed. Such a reduction should depend on the degree of damage, and can only be estimated on a case by case basis.

The model for assessing the $V_{Rd,f}$ neglects the contribution of the vertical FRP reinforcements, which mainly provide a dowel action effect. The author justifies this by the high flexibility of the laminates in combination with their local debonding in the vicinity of shear cracks. Adopting the classical truss analogy, $V_{Rd,f}$ associated with the action of horizontal FRP laminates is proposed as in Eq. 2.92, where r is a reinforcement efficiency factor, depending on the exact FRP failure mechanism (FRP debonding or tensile fracture). ε_{fe} is calculated according to Eq. 2.93 and it depends on the area of the FRP-masonry bonded interfaces, that is on the FRP "development" length l_e, defined as that necessary to reach FRP tensile fracture before debonding. Apart from the bond conditions, the l_e depends (almost proportionally) on the FRP axial rigidity, expressed by the product $\rho_h E_f$; ε_{fe} is expected to decrease as $\rho_h E_f$ increases. The implication of this argument is that as the FRP laminates or fabrics become stiffer and thicker, debonding dominates over tensile fracture and the ε_{fe} is reduced.

$$V_{Rd,f} = \rho_h E_f \left(r \frac{\varepsilon_{fu}}{\gamma_f} \right) t_w \cdot 0.9d = \frac{0.7}{\gamma_f} \rho_h E_f \varepsilon_{fe} l_w t_w , \qquad \textbf{2.92}$$

$$\varepsilon_{fe} = \begin{cases} 0.0119 - 0.0205\left(\rho_f E_f\right) + 0.0104\left(\rho_f E_f\right)^2 & \text{...if } 0 \le \rho_f E_f \le 1 \text{ GPa} \\ -0.00065\left(\rho_f E_f\right) + 0.00245 & \text{...if } \rho_f E_f > 1 \text{ GPa} \end{cases} \qquad \textbf{2.93}$$

2.5.4.2.2 Triantafillou and Antonopoulos [213]

The corrected Triantafillou [212] model deals with a more accurate assessment of ε_{fe} for concrete elements in shear, strengthened with FRPs. But as in the 1998 model for masonry the same ε_{fe} was assumed for both masonry and concrete elements, the new values may correspond for masonry also.

A key element of the corrected model is the calculation of ε_{fe}, which is taken as the minimum of three values: maximum strain to control crack opening, strain corresponding to premature shear failure due to FRP and strain corresponding to shear failure combined or followed by FRP tensile fracture. The last two strains were through many experimental results shown to depend on the axial rigidity divided

by shear (tensile) strength of concrete $\rho_h E_f/f_t$ (decreasing functions as this quantity increases). The author introduces in the model the tensile strength of concrete f_t and expresses it in dependence of its compressive strength f_c ($f_t = f_c^{2/3}$).

Furthermore, it was established through experiments that the $V_{Rd,f}$ is typically controlled by the first two of the above strains and, for a given concrete strength, it increases linearly with $\rho_h E_f$ until this product reaches a limiting value beyond which debonding prevails and the gain in shear capacity is small unless the FRP is fully wrapped or properly anchored through the use of mechanical anchoring devices. Depending on the type of FRP material, formulas presented in Eq. 2.94 are proposed for the assessment of premature shear failure due to debonding and shear failure combined or followed by an FRP fracture.

$$\varepsilon_{fe} = \begin{cases} 0.17\left(\dfrac{f_c^{2/3}}{E_f \rho_h}\right)^{0.30} \varepsilon_{fu} & \text{…fully wrapped CFRP} \\ 0.048\left(\dfrac{f_c^{2/3}}{E_f \rho_h}\right)^{0.47} \varepsilon_{fu} & \text{…fully wrapped AFRP} \\ \min\left[0.65\left(\dfrac{f_c^{2/3}}{E_f \rho_h}\right)^{0.56} \times 10^{-3}, 0.17\left(\dfrac{f_c^{2/3}}{E_f \rho_h}\right)^{0.30} \varepsilon_{fu}\right] & \text{…side or U-shaped CFRP} \end{cases} \quad \textbf{2.94}$$

For fully wrapped FRPs shear failure mechanism combined or followed by an FRP fracture is predicted, whereas for not fully wrapped or properly anchored FRPs, also premature shear failure due to debonding is considered (first value in the third expression in Eq. 2.94). The ε_{fe} for this type of failure is presented only for CFRP strengthening and should, according to the author, be used with caution for other types of FRPs.

2.5.4.2.3 Nanni et al [214]

The authors present design recommendations for flexural and shear strengthening of URM walls with FRP composites in the form of laminates and bars. The proposed design protocols follow the procedure of existing building codes for traditional materials. In design for shear strengthening, the following three assumptions are adopted: inclination angle of shear cracks is constant and equal to 45°; effective strength, presumed as half of the ultimate, is reached in all reinforcement intersected by the diagonal crack; compression-shear transfer decreases due to load reversal. It is presumed that the FRP reinforcement sustains all the shear demand.

To estimate the shear strength of a masonry wall strengthened with FRP reinforcement, the sum of $V_{Rd,m}$ and the $V_{Rd,f}$ are considered (Eq. 2.95), with no limiting values. The $V_{Rd,m}$ is in the paper not evaluated, but the proposed $V_{Rd,f}$ depends on the tensile stresses developed in the reinforcement (Eq. 2.96). Coefficient κ_{frp} is equal to 0.5 and accounts for the observed mechanism of failure by assuming a limiting value of effective stress in the FRP reinforcement as half of the f_{fu}.

$$V_{Rd} = V_{Rd,m} + V_{Rd,f}\,, \quad \textbf{2.95}$$

$$V_{Rd,\mathrm{f}} = \kappa_{frp}\left(\frac{A_f}{s_f}\right) f_{fu} t_w, \qquad \textbf{2.96}$$

2.5.4.2.4 Wang et al [217]

Wang et al presented a simplified design formula for brick masonry walls reinforced by FRP, where again the nominal shear resistance of a masonry wall is estimated according to Eq. 2.95. The V_m is calculated according to Eq. 2.97, model based on f_{v0} and a statistical coefficient (value 2.10). Resistance V_f is composed of horizontal FRP contribution (index *s*) and contribution of FRP installed with θ_f inclination (index *x*) (Eq. 2.98). Both ρ_s and ρ_x are effect coefficients; when the reinforcement is horizontal, ρ_s = 1.0 and ρ_x = 0.0, whereas when diagonal, vice versa. Coefficient ξ_f is correlated to the area reinforcement rate of FRP ρ and according to the tests also to reinforcement mode; for horizontal and for diagonal sheet ξ_s (Eq. 2.99) and ξ_x (Eq. 2.100) are defined, respectively. For mixed reinforcement mode, values of ξ_f are due to insufficient experimental data not provided.

$$V_m = \left(\frac{f_{v0}}{1.2}\sqrt{1 + 2.1\frac{\sigma_0}{f_{v0}}}\right) A_w \qquad \textbf{2.97}$$

$$V_f = \xi_f E_f \varepsilon_u \left[\delta_s n_s A_{fs} + \delta_x n_x A_{fx}\left(\cos\theta_f + 0.2\sin\theta_f\right)\right] \qquad \textbf{2.98}$$

$$\xi_s = -0.245 \cdot \ln(\rho) - 0.128 \qquad \textbf{2.99}$$

$$\xi_x = -0.411 \cdot \ln(\rho) - 0.107 \qquad \textbf{2.100}$$

.

2.5.4.3 Models for NSM FRP strengthening

2.5.4.3.1 Tumilian [179]

The nominal shear strength of a masonry wall $V_{n,s}$ can be estimated as the sum of V_m, steel shear reinforcement V_s and V_f (Eq. 2.101). The calculation of V_m is not specifically stated, however for the example of calculation in the paper, 1997 UBC [234] is used (Eq. 2.102); C_d is the nominal shear strength coefficient, according to UBC estimated as 1.2. V_f depends on the shear contribution of reinforcing rods developing their full tensile capacity and rods being debonded. Thus, two areas can be identified in a masonry wall; bond controlled region and rupture controlled region (Figure 2.33 left). In calculation, assumptions of constant (45°) inclination angle of the shear cracks and constant distribution of bond stresses along the FRP rods at ultimate state are considered. The ultimate bond strength is assumed to be reached in all of the rods intersected by the crack at ultimate state. The spacing between the rods is limited by the layer height.

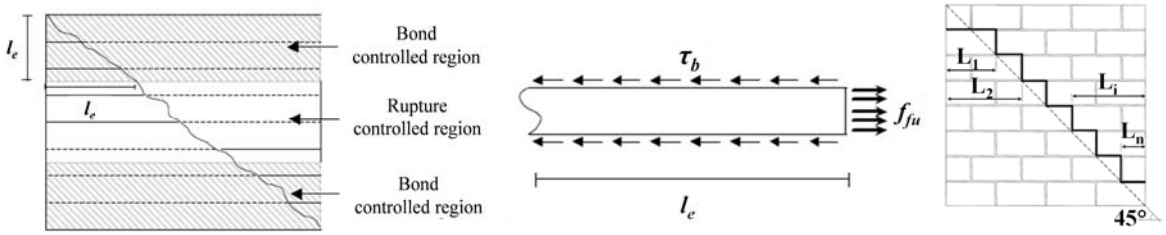

Figure 2.33: Controlling areas to calculate V_f (left), the effective length l_e (middle), both from [179] and the effective bond length L_i predicted for each bar according to Li et al (right)[183])
Slika 2.33: Kontrolna območja za izračun V_f (levo) in efektivna dolžina l_e (na sredini), obe iz [179] in efektivna dolžina stika L_i za posamezno ojačitev po Li et al (desno) [183]

The bond behaviour is dependent on the type of the rod, thereby, the assumption of constant bond stresses at ultimate limit state may not be adequate. In this case, the value of the average bond strength would depend on the bonded length and could be computed from the local bond stress–slip relationship for the given type of FRP rod. The l_e is defined as the length at which the rod breaks, and can be derived from Figure 2.33 (middle) by equilibrating the force due to the bonding stress τ_b to the force generated by the tensile stresses in the rod. The l_e is then expressed as in Eq. 2.103, where f_{fu} is the ultimate tensile strength of the rod and τ_b the assumed average bond stress, predicted as the bond stresses estimated by De Lorenzis [235], reduced in half (1.551 MPa). The reason for this is that in tests neither debonding nor breaking of the GFRP rods were observed. For the same reason, also the strength developed in the GFRP rods is assumed to be half of the f_{fu}^*. f_{fu}^* should also be reduced by C_E provided in ACI 440 [220].

Finally, the V_f (Eq. 2.105) is estimated as contribution of resistance in bond controlled region V_b (Eq. 2.106) and contribution of resistance in rupture controlled region V_t (Eq. 2.110), where n_s is the number of the strengthened sides of the wall (1 or 2) and L_t the sum of the bonded lengths of all the rods crossed by the crack, calculated in the most unfavourable crack position (minimum total length). The number of rods r_b in the bond controlled region is calculated according to Eq. 2.108 and is rounded to the inferior integer. The number of the remaining rods is the number of rods in the rupture controlled region r_t (Eq. 2.111).

$$V_{n,s} = V_m + V_s + V_f , \quad \textbf{2.101}$$

$$V_m = C_d A_w \sqrt{f'_m} , \quad \textbf{2.102}$$

$$l_e = \frac{d_b f_{fu}}{4\ \tau_b} , \quad \textbf{2.103}$$

$$f_{fu} = C_E \cdot 0.5 f_u^* , \quad \textbf{2.104}$$

$$V_f = V_b + V_t , \quad \textbf{2.105}$$

$$V_b = n_s \pi\ d_b \tau_b L_t , \quad \textbf{2.106}$$

$$L_t = r_b\ s , \quad \textbf{2.107}$$

$$r_b' = \frac{l_e}{s} , \quad \textbf{2.108}$$

$$r_b = 2\ r_b' \quad \textbf{2.109}$$

$$V_t = n_s r_t \; A_{f,bar} \, f_{fu} \,, \tag{2.110}$$

$$r_t = n - r_b \,, \tag{2.111}$$

2.5.4.3.2 Li [183]

The nominal shear strength is estimated according to Eq. 2.95. For determining V_m, all possible failure modes are considered; $V_{Rd,ts}$ (Eq. 2.53), $V_{Rd,dj}$ (Eq. 2.51), where stress distribution in block is revised according to Crisafulli et al [236], thus the f_{v0}^{*} and μ^{*} are defined according to Eq. 2.112 and 2.113; $V_{Rd,du}$ (Eq. 2.52) with b equal to 2.3 (see Eq. 2.40) and $V_{Rd,r}$ (Eq. 2.49).

$$f_{v0}^{\;*} = \frac{f_{v0}}{1 + 1.5\mu\left(h_b / l_b\right)} \tag{2.112}$$

$$\mu^{*} = \frac{\mu}{1 + 1.5\mu\left(h_b / l_b\right)} \tag{2.113}$$

For V_f, the resistance is limited by bond failure between adhesive and masonry, where the bond stress between the adhesive and masonry is assumed to be uniform along the effective length of the bar l_e (Eq. 2.114), where t_m is the thickness of the mortar joints; D is usually $1.5d_b$, A_f is the bond area between the masonry and the adhesive. To calculate the resistance of FRP reinforcement related to the bond controlled shear failure, a shear crack with a constant inclination angle of 45° is assumed. Each bar intersected by the crack is divided into two parts at the two sides of the crack as in Figure 2.33 right.

It is also assumed that at ultimate limit state the ultimate bond stress is reached in all of the bars intersected by the cracks and the V_f is computed as the sum of the forces resisted by the bars. The force carried by each FRP bar is calculated as the product of the average bond strength and the surface area of the bond between adhesive and masonry according to the effective bond length of the bar, which is the shortest part of the bar intersected by the diagonal crack L_i (Eq. 2.115).

$$l_e = \frac{f_{fu} A_f}{\left(2D + t_m\right)\tau_b}, \tag{2.114}$$

$$V_f = \sum_{i=1}^{n} A_i f_i = \tau_b \left(2D + t_m\right) \sum_{i=1}^{n} L_i \;, \quad L_i \le l_e \tag{2.115}$$

BLANK PAGE

»Ta stran je namenoma prazna.«

3 EXPERIMENTAL TESTS OF THREE-LEAF STONE MASONRY WALLS

For the experimental evaluation of the behaviour of three-leaf stone masonry walls altogether 18 stone masonry walls intended for compression and in-plane shear tests were built in the structural laboratory. The experiments on walls were performed from February to June, 2012 in Laboratory of Faculty of Civil and Geodetic Engineering and Geodesy, University of Ljubljana. This Chapter covers detailed overview of the executed experimental investigations and their evaluation. First, details upon choices and execution of the specimen construction are presented; alongside to construction of the specimens and tests performed on walls also tests on the specimens' constituents were performed, they are presented in a separate Section. Description of the compression tests with the analysis and evaluation of the results is presented prior to description of the shear tests of walls and the corresponding detailed analysis of the results and performance evaluation. Afterwards the behaviour of plaster attached to walls under in-plane shear loading of walls is presented. At the end of some Sections of this Chapter (compression tests; in-plane shear tests on walls with the analysis of the results), a summary with discussion upon the relevant results and important conclusions is provided.

Connected wall - refers to the wall specimens, which had header stones present (type of morphology)
Unconnected wall - refers to the wall specimens, which had no header stones (type of morphology)
Characteristic displacement – a displacement which corresponds to certain (characteristic) limit state (of either hysteresis envelope or bi-linear curve)
Characteristic amplitude displacements cycles - hysteresis test cycles with amplitude displacements at which a certain characteristic limit state was obtained

3.1 Characteristics and construction of the specimens

The specimens were built specifically for this campaign and were designed to study the behaviour of multi-leaf stone masonry walls and the influence of presence of stones, which are connecting the outer leaves. Therefore half of the specimens had header stones going through the whole depth of the specimens, and the other half had no such connecting stones. Limestone for construction was brought from Bosnia and Herzegovina, but from the same formation as the mountains in Slovenia, which

means it can also be representative for Slovenian built material. As the tests were intended to determine the characteristics of old multi-leaf stone masonry walls, trained masons built the specimens using lime mortar and traditional constructions techniques. External leaves were constructed from regular coursed squared ashlar roughly tooled limestone, while the internal core was filled with stone rubble and lime mortar. The type of masonry build presents better quality masonry and is often characteristic for historic representative buildings. The aim of tests was to determine the performance of multi-leaf stone walls with different morphologies and their characteristic limit states. However, unlike other researchers, for the first time, we also applied lime plaster on one side of the specimens to study the performance of plaster; as already explained a non-structural element potentially carrying a valuable artistic asset such as frescoes or mosaics in a cultural heritage building. In order for the plaster to represent mechanical characteristics of historic plaster, two layers of plaster were applied (coarse and fine lime plaster) according to specifications of professional company from Italy specialized in historic plaster preservation.

Significant attention was given to proper choice of mortar composition and preparation. For the aggregate, only gravel was used. Traditionally produced lime putty was used for the mortar composition. In order to accelerate the maturation process, up to 20% (volume ratio) of tuff was added to the binder. With this addition, we were still able to produce mortar, representative for historic mortar, since the aim was not to exceed 2 MPa of mortar compressive strength. Different compositions of mortars for construction of walls and application of coarse and fine plasters were used; they are presented in detail in mortar descriptions (Section 3.2.3).

Two wallettes (one of each morphology) of dimensions 100/40/100 cm ($l_w/t_w/h_w$) were built for compression tests and 16 walls of dimensions 100/40/150 cm for shear tests. Later 2 of the 16 walls were additionally tested in compression.

3.1.1 Construction of three-leaf masonry walls

Reinforced concrete foundation

To be able to move and set the wall specimen in the testing position, reinforced concrete foundation blocks at the top and at the bottom of the specimen were built. The construction and details of concrete foundation were designed through graduation thesis work by Janez Korpič [43]. The built-in steel bars which served for transportation and fixing the specimen into testing setup had to be positioned with the highest possible precision in order not to have problems in positioning the specimens in the appropriate testing position. Concrete of strength class C30/37 composed of aggregate size < 32 mm was built in the cast with a help of a vibration needle.

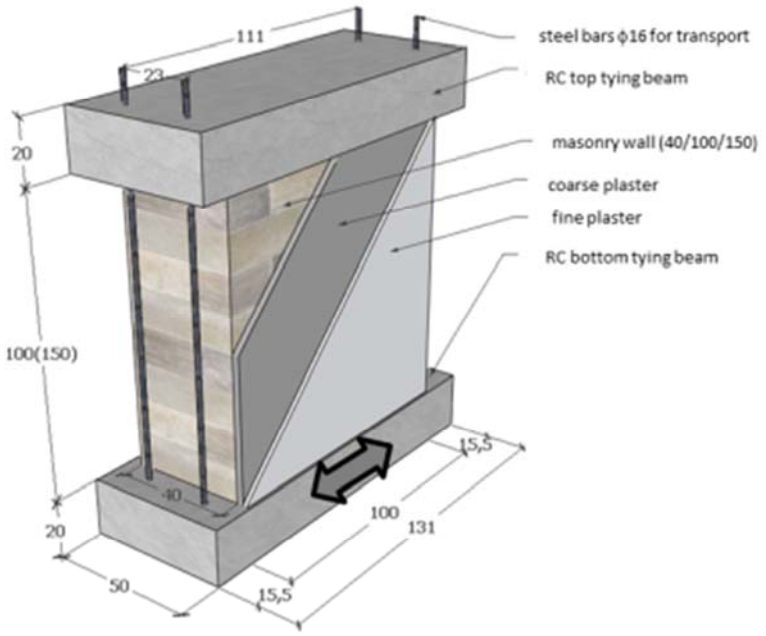

Figure 3.1: Wall specimen with concrete foundation blocks and steel bars for transport [43]
Slika 3.1: Kamniti zid z betonskima temeljema in jeklenimi palicami za transport [43]

Masonry wall

After construction of foundation blocks, trained masons, specialized in stone construction, gradually built the masonry walls and wallettes. Each day only a couple of rows were built as subsequent construction is necessary for the quality of masonry. Too fast construction could due to soft mortar result in undesired out-of-plane deformations or settlements. As already mentioned, accompanying the construction, mortar consistency was measured and samples for mortar compression and flexural tests were prepared.

Two types of three-leaf masonry were constructed; one with connecting stone blocks in every other stone row (in Slovenian "vezniška zidarska zveza") and another type without these through stones present ("smerniška zidarska zveza"). Composition of all mortars was designed by prof. dr. Violeta Bokan-Bosiljkov. Volume ratio of lime putty : tuff : aggregate was 1:0.2:4. Thickness of the horizontal bed-joints was in average 1.5 cm.

Preglednica 3.1: Sestava malte v volumskih deležih sestavin

Table 3.1: Volume composition of mortar compounds

	Lime putty (binder) [unit of *V*]	Aggregate 0/4 mm [unit of *V*]	Tuff (mineral additive) [unit of *V*]	Added water/ lime putty
Construction mortar	1	4	0.20	0.39

Size of stones varied in length, width and the least in height. Due to desired texture of the wall with straight horizontal bed-joints the dimensions of the stones (especially the height) had to be approximately similar. Average size of stones was approximately 20/15/11 cm (length/width/height), and of through stones 40/15/11 cm. Average thickness of the outer leaves was 15 cm, while 10 cm of

the inner core. These dimensions give ratio of 0.75 for thickness of the outer leaf compared to the core. The core was filled with stone rubble and lime mortar. It has to be noted, that the core was filled without many voids which is a rather rare case in existing multi-leaf walls of structures in Slovenia.

Construction of the concrete foundation

Mortar consistency control during construction

Cross section with connecting header stones

Cross section with no connecting stones

Masons building the specimens

Built specimens waiting for the upper concrete block

Figure 3.2: Construction of the specimens
Slika 3.2: Izgradnja preskušancev

Application of coarse plaster

After the masonry has dried for one month, coarse plaster was applied (Figure 3.4 left). Composition of mortar is presented in the Table 3.2; gravel aggregate of size 0-4 mm was used in volume ratio 3:1

to lime putty and 0.1 volume unit of tuff was added to the mixture. Again experienced masons from a construction company, of which primary practice involves work on protected cultural heritage buildings, casted the plasters. The thickness of the coarse plaster varied due to different shapes of stones from 1 cm to 3.5 cm, with predominant thickness of 2 cm.

Preglednica 3.2: Sestava grobega ometa v volumskih deležih

Table 3.2: Volume composition of coarse plaster compounds

	Lime putty (binder) [unit of *V*]	Aggregate 0/4 [unit of *V*]	Tuff (mineral additive) [unit of *V*]	Added water/ lime putty
Coarse plaster	1	3	0.1	0.41

Reinforced concrete tie beam on top

When coarse plaster was dry enough, reinforced concrete tie beams were constructed. Their purpose was to provide uniform distribution of the vertical load applied and to fix the wall specimen into the testing setup. It also served for transporting the specimen; the wall had been connected (pre-stressed) from foundation block to the upper one by 4 steel bars. The casting (Figure 3.3) had to be done with extra care, otherwise the holes for fixing the specimen to the test setup would not be positioned properly and fixing would not be possible. For the same reason also the lower and top plane of concrete foundation block and upper lintel had to be parallel.

Figure 3.3: Cast with steel reinforcement for the upper concrete block [43]
Slika 3.3: Opaž z armaturo za zgornji betonski blok [43]

Application of fine plaster

Finally, 42 days after the application of coarse plaster, a layer of fine plaster was applied over it. Again the plasters were applied by professionals from the specialised construction company in two stages; first the render was applied, then after partial drying it was finely scraped (Figure 3.4 right). Lime putty was mixed with sand in 1:2 volume ratio; composition is presented in Table 3.3.

Preglednica 3.3: Sestava finega ometa v volumskih deležih

Table 3.3: Volume composition of fine plaster compounds

	Lime putty (binder) [unit of *V*]	Aggregate 0/4 [unit of *V*]	Tuff (mineral additive) [unit of *V*]	Added water/ lime putty
Fine plaster	1	2	/	0.12

Figure 3.4: Application of the coarse (left two photos) and fine (right two photos) plaster [43]
Slika 3.4: Nanos grobega (levi dve sliki) in finega (desni dve) ometa [43]

Both wall and wallette specimens are presented in Figure 3.5, where the different morphology of the specimens and the different plaster layers are clear (last photo in Figure 3.5 shows the result of the plaster mortar pull out test).

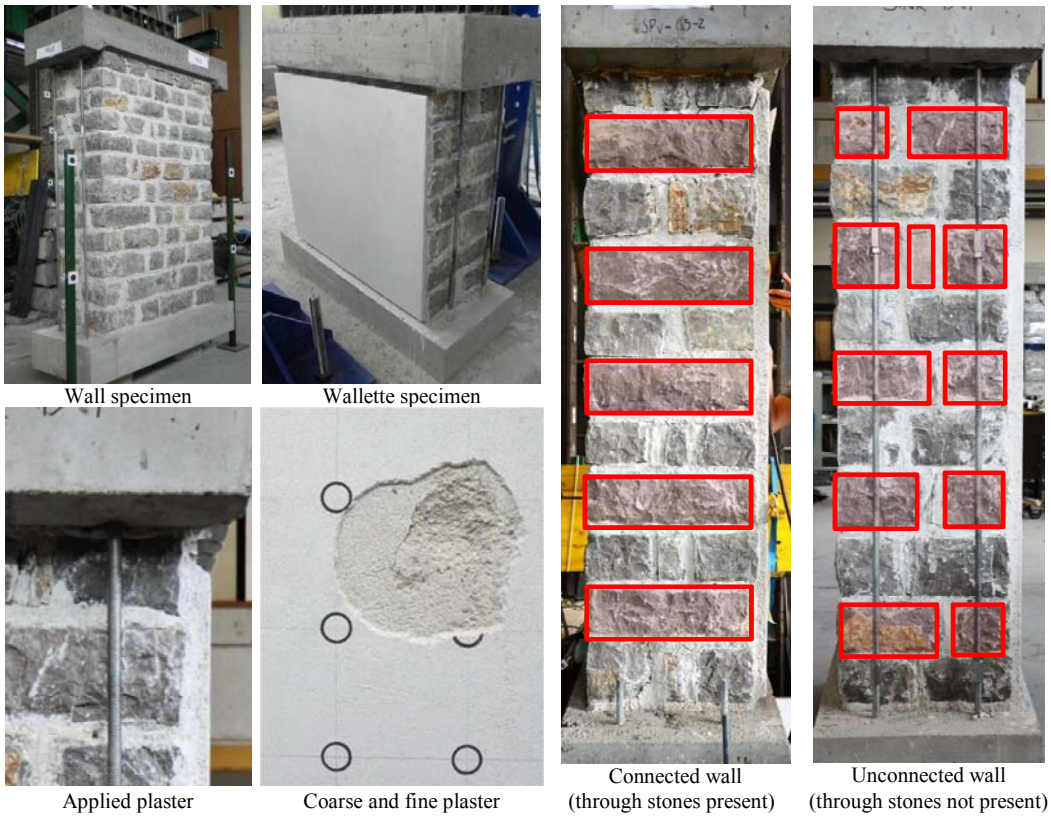

Figure 3.5: Different wall specimens; side view and the applied lime plaster - coarse and fine layer
Slika 3.5: Zid za preskušanje s pogledom od strani na povezani in nepovezani zid ter zidek z nanesenim in suhim apnenim ometom; viden grobi in fini apneni omet (z leve proti desni)

3.2 Tests of building materials and masonry constituents

3.2.1 Tests of mortars during construction

During construction of the walls and the application of plasters, for each mortar mixer the compounds' weight, mortar consistency and bulk density (including pores and inter-particle void volume) of fresh mortar were measured (results presented in Table 3.4). Necessary water added for achieving the wanted workability was measured, whereas lime putty already contained water (mass ratio 1:1). Consistency tests were performed according to SIST 1015-3 [237] by flow table, where the diameter of the spread mortar was measured. Bulk density was calculated according to SIST 1053-6 [238] with the formula in Eq. 3.1, where m is the mass of the mortar in fresh state and V its volume (volume of the standardized container).

$$\rho = m / \mathrm{V} \qquad 3.1$$

Preglednica 3.4: Čas gradnje in rezultati meritev konsistence in specifične teže za uporabljene malte

Table 3.4: Time of construction and results of consistency measurements and bulk density for used mortars

Type of mortar	Time of construction	Diameter of spread mortar [mm]	Bulk density [kg/dm^3]
Construction of walls	14.-24.11.2011	116	2.16
Coarse plaster	11.-12.1.2012	145	2.08
Fine plaster	22.-23.2.2012	143	1.92

Figure 3.6: Mortar consistency test by flow table
Slika 3.6: Preskus maltne konsistence na udarni mizici

3.2.2 Compression and flexural strength of lime mortar for wall

Mortar compressive and flexural strength tests were performed according to standard EN 1015-11 [239]. Compressive strength f_{mc} was determined according to Eq. 3.2, where F is the maximum force attained and A the contact area, calculated as a^2 (a the width), of the sample (prism). Flexural tensile strength f_{mf} was tested with three-point bending test (Figure 3.7) and calculated according to Eq. 3.3, where l, d_1 and d_2 are the length, the width and the height of the prism.

$$f_{mc} = \frac{F}{A} \qquad \textbf{3.2}$$

$$f_{mf} = \frac{3F \cdot l}{2d_1 \cdot d_2^2} \qquad \textbf{3.3}$$

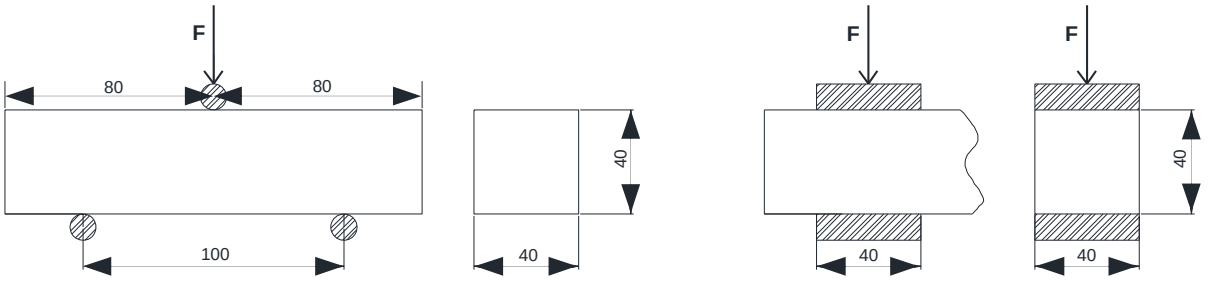

Figure 3.7: Three-point bending (left) and compressive (right) test
Slika 3.7: Tri-točkovni upogibni preizkus maltne prizme (levo) in tlačni preizkus (desno)

Tests were performed on 28, 90 and 120 days old samples. At each age, 3 prisms were tested (resulting in 3 flexural tests and 6 compression tests). Average compressive strength of mortar f_{mc} was after 28 days 1.00 MPa and average flexural strength f_{mf} 0.30 MPa. Average f_{mc} of mortar was after 90 days 2.15 MPa and average f_{mf} 0.64 MPa. At 120 days age however the f_{mc} slightly decreased to 1.88 MPa with coefficient of variation (c.o.v., here and hereafter calculated considering standard deviation of the entire population, not sample) equal to 5.9%. Average f_{mf} after 120 days also decreased to 0.61 MPa (c.o.v. 11.5%).

3.2.3 Compressive and flexural strength of lime mortar for coarse and fine plaster

Compression and flexural tests were performed also on mortar used for coarse plaster of the walls at 28 and 56 days of age and for mortar used for fine plaster at 28 days. Tests were conducted on 3 mortar prisms at each age. On the basis of sonic wave impulse test with instrument GrindoSonic, which allows determination of elastic properties of the material's dynamic elasticity modulus was also determined. Average dynamic modulus of elasticity was determined according to procedure used in [240] on 365 days old samples.

For coarse plaster a decrease of average strength occurred and is most likely the result of low number of tests and high standard deviation of the results. The average f_{mc} of coarse mortar was after 28 days 1.16 MPa (c.o.v. 3.36%) and the average f_{mf} 0.37 MPa (c.o.v. 21.8%). After 365 days, the corresponding strengths were 3.05 MPa (c.o.v. 5.2%) and 1.07 MPa (c.o.v. 5.7%), respectively. The dynamic modulus of elasticity determined with ultrasound (GrindoSonic) was 2927 MPa (c.o.v. 45.9%). The significant strength increase was the result of added tuff and consequent pozzolanic reaction, which is a long-term process and provokes phase changes.

The average f_{mc} of fine mortar was after 28 days 1.79 MPa (c.o.v. 6.13%), the average flexural strength 0.52 MPa (c.o.v. 6.44%) and the dynamic modulus of elasticity 2226 MPa (c.o.v. 2.4%).

3.2.4 Results of core tests

Compressive and splitting tensile strengths f_{cc} and f_{cst} of the core were determined on cylinder specimens of 150 mm diameter and 300 mm length. Cylinders were filled with mortar used for construction and with stone rubble, similar to the core in the walls. They were prepared at the same time as the walls were built but the tests were performed approximately 1 year later, following the accomplishment of shear tests on the walls.

Figure 3.8: Compressive (left) and splitting tensile strength (right) test of the cylinder core sample
Slika 3.8: Tlačni (levo) in cepilni (desno) preizkus valjastega vzorca jedra

Prior strength tests (Figure 3.8), also density 2.05 kg/dm^3 of the samples was determined. Average compressive strength of 0.90 MPa (c.o.v. 23.6%) was determined on 3 samples according to Eq. 3.2 with A in this case being the circular contact area. Splitting tensile strength was calculated according to Eq. 3.4 provided in SIST EN 12390-6:2001 [241], determined from maximum splitting force F. Average value 0.16 MPa with c.o.v. of 52.5% was determined on 3 test results.

$$f_{cst} = \frac{2F}{\pi l d} \qquad 3.4$$

We were not able to perform tests to determine the elastic modulus, as the core specimens were very fragile and disintegrated almost immediately when subjected to loading (mounting of strain-gauges was unfeasible).

3.2.5 Tests on stone

Average density of stone blocks was 2.65 kg/dm^3. Compression tests were performed on 6 cubes of 7/7/7 cm after taking their measurements and weighing them. The obtained f_{bc} ranged from 107.9 to 219.9 MPa, average being 171.5 MPa with c.o.v. of 24.1%.

Flexural tests were performed on 3 prisms of 4/4/16 cm (Figure 3.9 left). The flexural strength f_{bf} ranged from 19.9 to 28.4 MPa, average f_{bf} being 24.2 MPa with c.o.v. of 17.4%.

Suction of stone was done on three cubes of dimensions 7/7/7 cm, that were dried until constant mass and then sunk in the water until final saturation. Water suction was between 0.172% and 0.185% with average of 0.176%.

Figure 3.9: Three-point bending test of stone sample (left), "Bond wrench" test and mortar stone junction failure.
Slika 3.9: Tri-točkovni upogibni test vzorca kamna (levo), "Bond wrench" test in porušitev stika malte in kamna

3.2.6 Mortar – stone junction tests

Bond wrench tests on 3 samples were performed to determine bond strength f_{jx} of stone-mortar joints (Figure 3.9 middle). Samples to determine the strength were taken from the wall, after the wall has been tested in compression. Average flexural tensile strength was 0.03 MPa with c.o.v. of 26.6%. The failure occurred in the mortar stone junction. Such low strength could be the result of the fact that the samples were in partly damaged state.

3.3 Compression tests on walls

3.3.1 Test set-up description

At first it was planned that two wallettes with different morphology (one with and one without through stones) would be tested in compression. The first one was tested in the hydraulic jack of 5000 kN capacity. During the test it was observed that with this test set-up (Figure 3.10, left two) uniform distribution of compressive stresses within the specimen will not be achieved, so the test was stopped and a second set-up was prepared (Figure 3.10, right). For this set-up, hydraulic jack with capacity of only 2500 kN was used and the uniform load distribution was achieved. Despite numerous cracking within the masonry assemblage, the maximum capacity of the wallettes was not obtained because of the insufficient jack capacity. Therefore it was decided that besides wallettes, an additional two walls (again one of each morphology type) would be tested in compression. Due to more slender specimens, this time the maximum compression capacity was obtained. The results of compression tests served also for determining the level of pre-compression for the shear tests.

Figure 3.10: Test setup for the first test in the 5000 kN hydraulic jack (left two) and the following with 2500 kN capacity (right)
Slika 3.10: Postavitev testa za prvi tlačni preskus s hidravličnim batom kapacitete 5000 kN (levi dve sliki) ter za naslednje z batom kapacitete 2500 kN (desna)

3.3.2 Measuring positions and loading protocol

For the compression tests the load was increased with constant rate. The loading rate in different tests varied from 0.25 kN/s to 1.0 kN/s. To measure the vertical and horizontal deformations of the wall during the experiment, 12 linear variable differential transformers (LVDTs) were attached to the wall. Their position is presented in Figure 3.11.

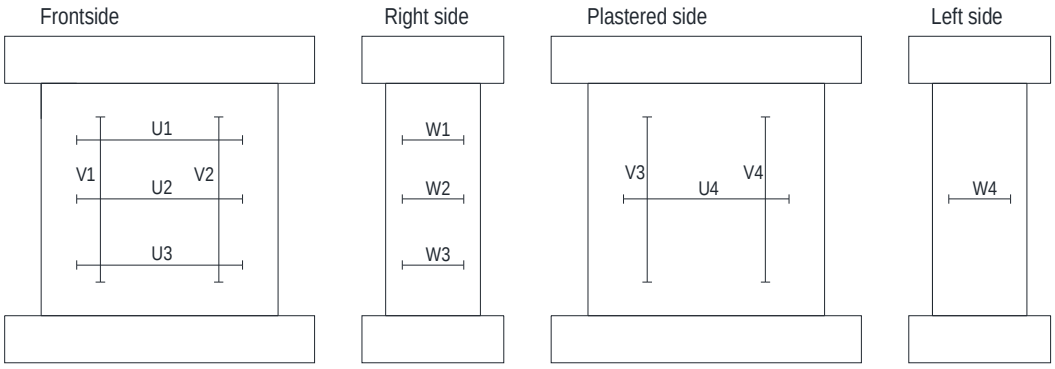

Figure 3.11: Position of the measuring devices for the compression tests
Slika 3.11: Postavitev merilnih mest pri tlačnem preizkusu

3.3.3 Test results

3.3.3.1 Wallette with no header stones (TN-1, TN-2)

For the first test set-up, the damage pattern obtained after the test is presented in Figure 3.12 (left two), whereas in Figure 3.13 the crack pattern evolution on the wall and on the plaster in dependence from the actuator force is presented.

Figure 3.12: Damage on the wallette without through stones due to non-uniform load distribution under hydraulic jack of 5000 kN capacity after the 1st test (TN-1, left two) and after the 2nd test under 2500 kN jack (TN-2, right two)
Slika 3.12: Poškodbe na nepovezanem zidku zaradi neenakomerne porazdelitve sil pri 1. testu s 5000 kN batom (TN-1, levi dve sliki) ter po 2. testu z 2500 kN batom (TN-2, desni dve)

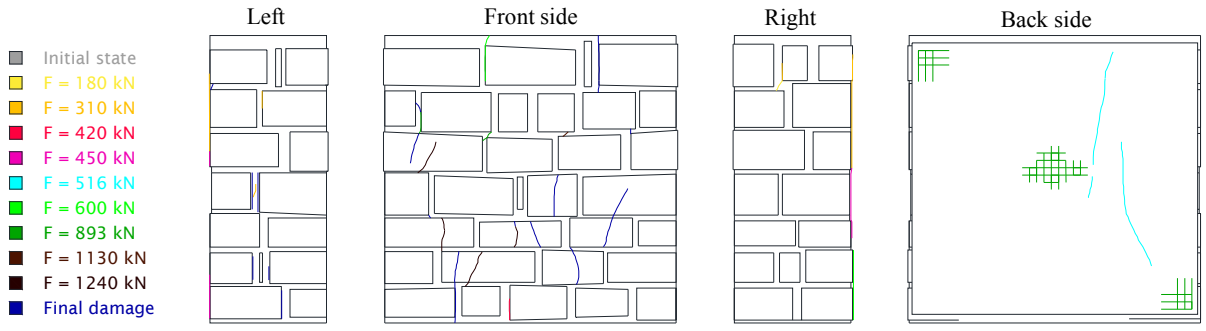

Figure 3.13: Crack pattern development on the wallette without header stones and on the plaster at the 1st test (TN-1)
Slika 3.13: Razvoj poškodb na nepovezanem zidku in ometu pri 1. testu (TN-1)

For the test under a different test setup (2500 kN jack), the load was applied with constant force increase of 0.83 kN/s. Maximum compressive stress 7.34 MPa was obtained for the wall. The damage of the wallette after the test is presented in Figure 3.12 (right two) and crack pattern evolution in Figure 3.14. Stress-strain relations for LVDTs are presented in Figure 3.15. Since the test was repeated and the wallette already damaged, some of the LVDTs were removed for the second test.

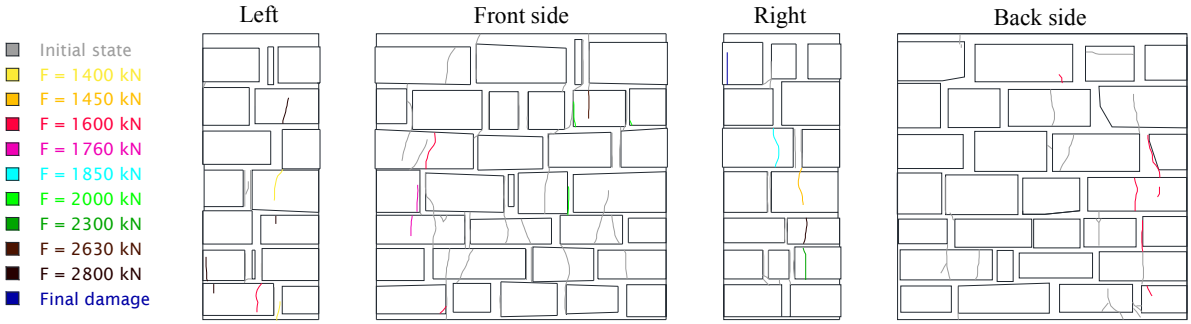

Figure 3.14: Crack pattern development on the wallette without header stones at the 2nd test (TN-2)
Slika 3.14: Razvoj poškodb na nepovezanem zidku pri 2. testu (TN-2)

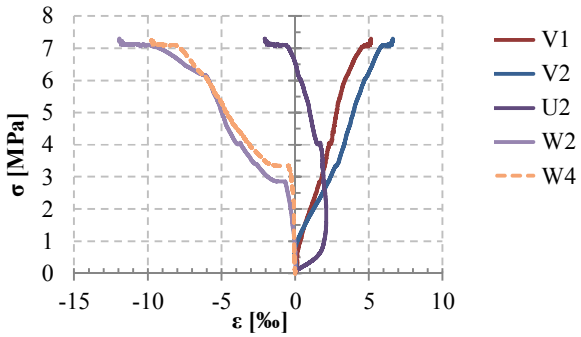

Figure 3.15: Stress - strain diagram for various LVDTs for compression test of wallette without header stones TN-2
Slika 3.15: Diagram napetost - deformacija za induktivne merilnike pri tlačnem testu nepovezanega zidka TN-2

The results of LVDTs W2 and W4, which measured the transversal displacements on the sides, showed, that cracks occurred at approximately 3.0 MPa of vertical loading. Afterwards the leaves began to separate evidently.

3.3.3.2 Wallette with header stones (TP-1)

For the test of the wallette with header stones, again the failure was not attained at test with the 2nd test setup (2500 kN jack). Maximum stress attained was 7.28 MPa. During the test the loading rate was in average 0.44 kN/s. Damage pattern after and during the test are presented in Figures 3.16 and 3.17, while the stress - strain relations for LVDTs in Figure 3.18.

Figure 3.16: Damage of the wallette with header stones after test TP-1
Slika 3.16: Poškodbe na povezanem zidku po testu TP-1

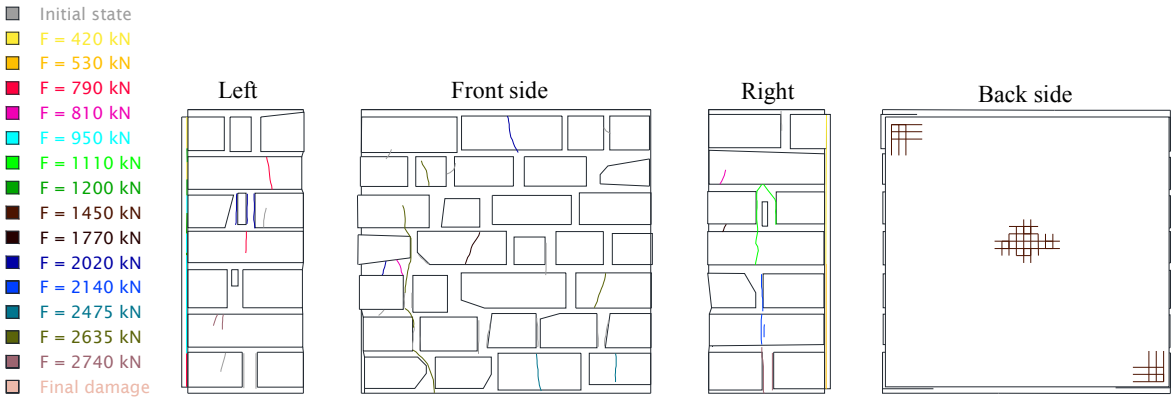

Figure 3.17: Crack pattern development on the wallette with header stones and on the plaster at test TP-1
Slika 3.17: Razvoj poškodb na povezanem zidku in ometu pri testu TP-1

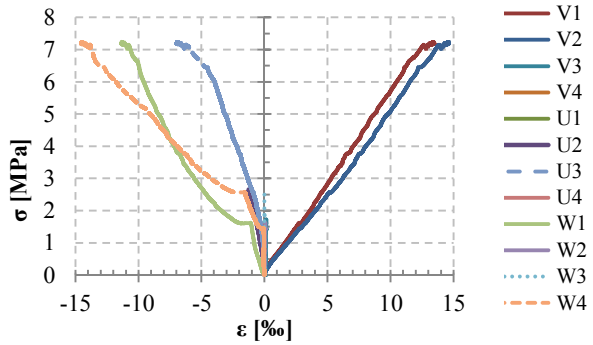

Figure 3.18: Stress - strain diagram for various LVDTs for compression test of wallette with header stones TP – 1
Slika 3.18: Diagram napetost - deformacija za različne induktivne merilnike pri tlačnem testu povezanega zidka TP-1

Comparing the results, for wallette with header stones (TP-1), the leaves began to separate a bit earlier than at test TN-2 (wallette without header stones), which was not expected. Comparing strains at stresses approaching to σ_{max}, one can assume that the wallette with header stones was closer to failure than the wallette without header stones.

3.3.3.3 Wall without through stones (TN-visoki)

In compression tests of both connected and unconnected walls compressive strength of masonry f_{Mc} and the softening were obtained. For the test of wall without through stones f_{Mc} of 6.10 MPa was obtained. Average velocity of loading during the test was 0.91 kN/s. Crack pattern after and during the test can be seen in Figure 3.19 and Figure 3.20, respectively. The leaves separated and a crack thicker than 1 mm evolved between them. One side of the wall was obviously more damaged. The stress-strain diagrams are presented in Figure 3.21.

Figure 3.19: Damage of the wall without through stones after test TN-visoki
Slika 3.19: Poškodbe na nepovezanem zidu po testu TN-visoki

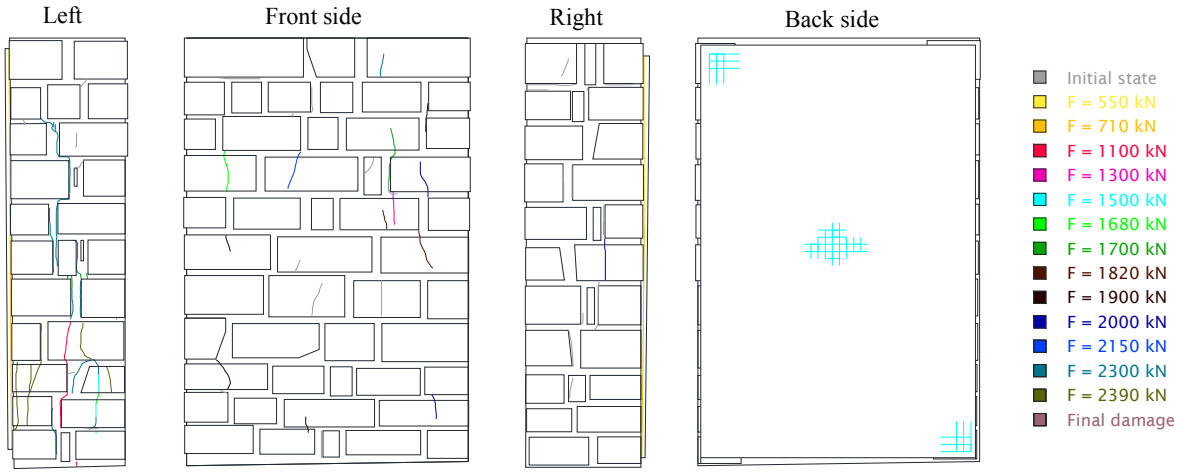

Figure 3.20: Crack pattern development on the wall without through stones and on the plaster at test TN-visoki
Slika 3.20: Razvoj poškodb na nepovezanem zidu in ometu pri testu TN-visoki

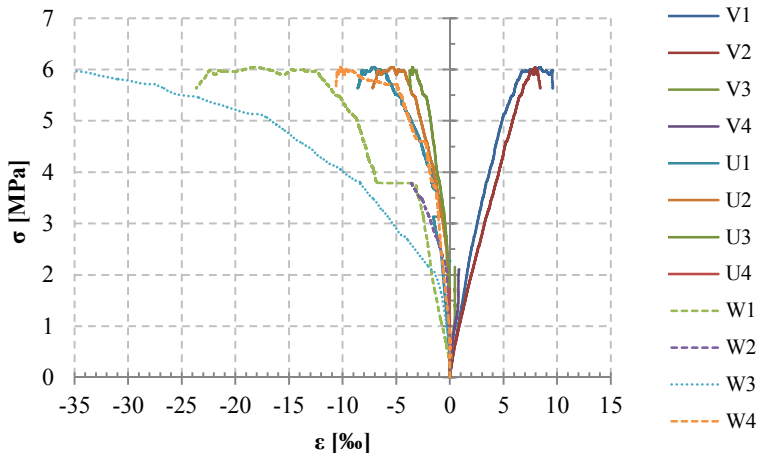

Figure 3.21: Stress - strain diagram for various LVDTs for compression test of wall without through stones TN-visoki
Slika 3.21: Diagram napetost - deformacija za induktivne merilnike pri tlačnem testu nepovezanega zidu TN-visoki

3.3.3.4 Wall with through stones (TP-visoki)

In the test of the wall with through stones compressive strength f_{Mc} 6.00 MPa was attained. Force increase during the test was 0.90 kN/s. Cracks wider than in the test of the wall with no through stones occurred. The first through stone cracked at stress 2.85 MPa, which is less than half of the compressive strength. The stress-strain diagrams for LVDT's are presented in Figure 3.24.

Figure 3.22: Damage of the wall with through stones after test TP-visoki
Slika 3.22: Poškodbe na povezanem zidu po testu TP-visoki

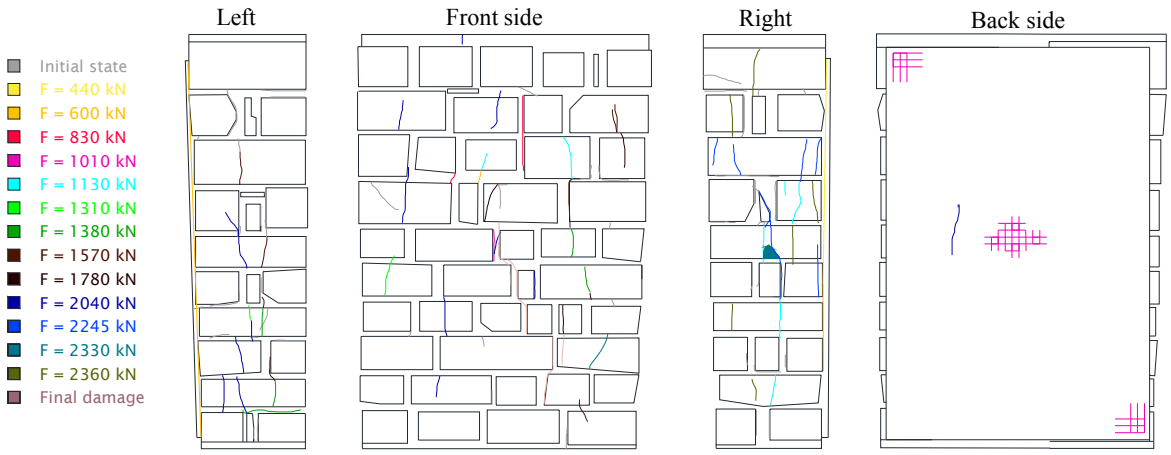

Figure 3.23: Crack pattern development on the wall with through stones and on the plaster at test TP-visoki
Slika 3.23: Razvoj poškodb na povezanem zidu in ometu pri testu TP-

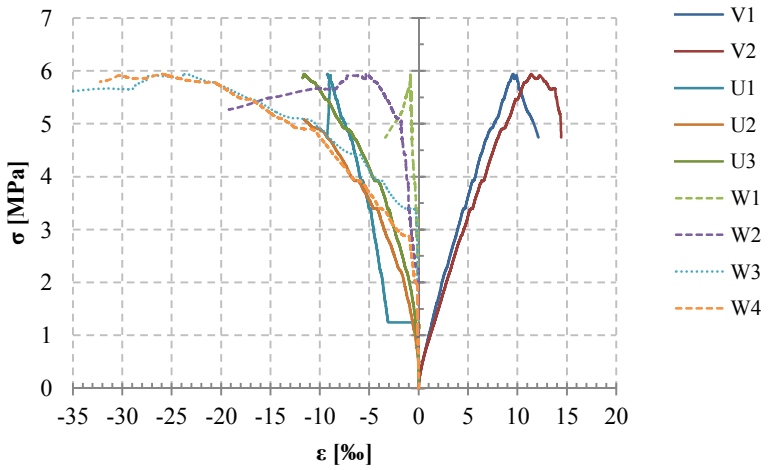

Figure 3.24: Stress - strain diagram for various LVDTs for compression test of the wall with through stones TP-visoki
Slika 3.24: Diagram napetost - deformacija za induktivne merilnike pri tlačnem testu povezanega zidu TP-visoki

3.3.4 Analysis of the results

3.3.4.1 Strength comparison

In tests of walls average compressive strength f_{Mc} of 6.05 MPa was obtained. There was no obvious difference in behaviour of the wall with and the wall without through stones. Contrary to predictions, the f_{Mc} of the wall without through stones was even slightly, but not significantly, higher (see Figure 3.25). In Figure 3.25 minimal and maximal values provided by NTC08 code provisions [60] and the design values from Croatia [242] are also presented.

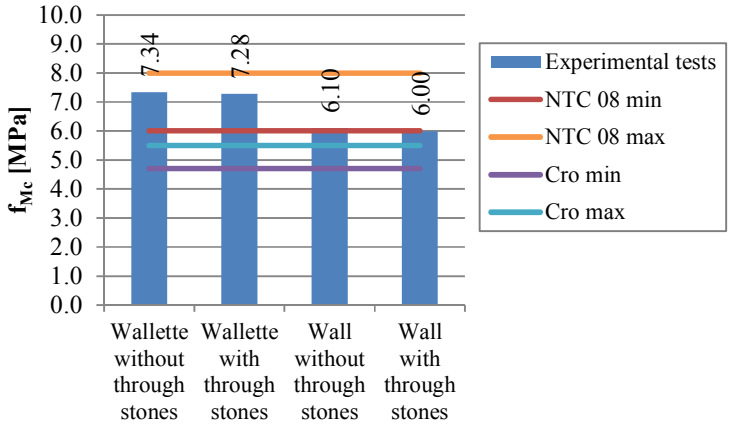

Figure 3.25: Comparison of compressive strengths, obtained at tests on wallettes and walls
Slika 3.25: Primerjava tlačnih trdnosti, dobljenih pri testih zidkov in zidov

3.3.4.2 Stiffness characteristics of the walls

Moduli of elasticity E_M were calculated from the average vertical strains and stresses at 1/3 f_{Mc} (for tests of walls) and at 1/3 σ_{max} (for tests of wallettes) for the cross section at mid height. Obtained values are presented in Figure 3.26. Shear moduli were also calculated after linear elastic theory for homogenous isotropic linear elastic materials, even though this assumption is not accurate for masonry:

$$G_M = \frac{E_M}{2 \cdot (1 + \nu_M)}, \qquad \textbf{3.5}$$

where ν_M were determined as the ratio between average horizontal strain and average vertical strain, where both in-plane (gained from measurements of LVDTs named U) and transversal horizontal (gained from measurements of LVDTs named W) deformations were considered. It has to be noted, that results for Poisson's ratio υ_M differ considerably in dependence of which horizontal deformations are considered for the calculation. In the case of the second test on the wallette without through stones, due to previous testing the evaluation of the ratio was not possible with considering only in-plane deformations of the wall. Also with the high wall with through stones, the results considering these deformations produced unrealistic results; the ratio was greater than 0.70 for all measured positions. The average of all horizontal deformations was therefore considered for the determination of υ_M. The influence of considering different deformations on the calculation of shear modulus is also not negligible; the comparison of two possibilities can be seen in Figure 3.27.

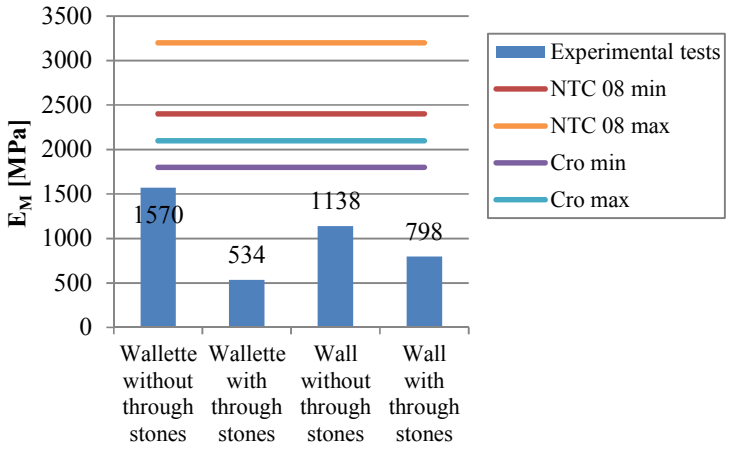

Figure 3.26: Moduli of elasticity obtained from compression tests
Slika 3.26: Moduli elastičnosti, dobljeni iz tlačnih testov

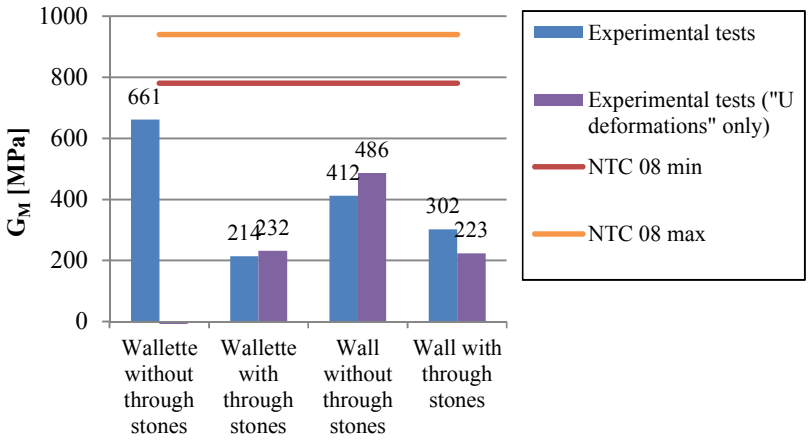

Figure 3.27: Shear moduli obtained from compression tests
Slika 3.27: Strižni moduli, dobljeni iz tlačnih testov

The comparison of results of walls with and without through stones shows, that elastic and shear modulus are significantly lower in case of wall with through stones; E_M for 29.9% and G_M for 26.9%. The difference is even higher in case of wallettes. With initial assumption on homogenous isotropic material and uncertain values of assumed υ_M, the derived values of G_M are unreliable, though. Ratio between shear and elastic modulus calculated at one third of the maximum stress is for all tests between 0.36 and 0.42 which is in accordance with recommendations [37,46].

Preglednica 3.5: Rezultati tlačnih testov zidov

Table 3.5: Results of compression tests on walls

Test		σ_{max} [MPa]	ave. σ_{max} [MPa]	E_M [MPa]	ave. E_M [MPa]	υ_M	G_M [MPa]	ave. G_M [MPa]	G_M/E_M
1	Wallette without through stones	7.34*	7.31	1570	1052	0.187	661	438	0.42
2	Wallette with through stones	7.28*		534		0.265	214		0.40
3	Wall without through stones	6.10	6.05	1138	968	0.226	412	357	0.36
4	Wall with through stones	6.00		798		0.319	302		0.38

* values correspond to the peak stress at severely cracked masonry assemblage

3.3.4.3 Leaf separation analysis

Regarding the leaf separation and crack evolution during the tests, Figure 3.28 presents leaf separation during tests of the high walls for transversal horizontal LVDTs in terms of displacement-stress diagrams, as displacement can directly be related to crack width between the leaves.

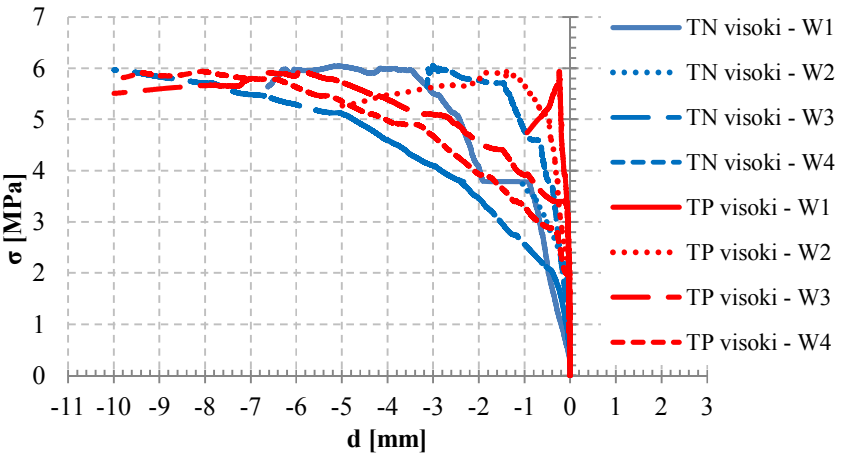

Figure 3.28: Stress – displacement relations for transversal horizontal LVDTs (labelled W) for compression tests of walls
Slika 3.28: Diagrami napetost - pomik za prečne induktivne merilnike (označene z W) pri tlačnih testih

It can be seen that the crack width varied in dependence of position and side of the specimen, where it was measured. For both specimens it is evident, that when comparing measurements on the same side of the specimen, the crack was the widest at the bottom. There was also practically no difference in maximum leaf separation for walls with and without through stones.

3.3.5 Evaluation of compression test results through comparison with literature values and analytical models

To validate the f_{Mc} of the walls obtained in the tests, the values were compared to limit values provided in the literature and values obtained through analytical models. Obtained f_{Mc} were compared to minimum and maximum values provided in NTC08 for the closest type of masonry to tested (Dressed rectangular stone), in PIET 70 [243] for ashlar masonry with h_b < 30 cm and f_{bc} > 100 MPa and to results of tests on ashlar rough tooled, multi-leaf wall from Slovenia [244] and on uncoursed filled with rubble three-leaf wall from Croatia [242] (all presented in Table 3.6). Minimal and maximal values for dressed rectangular stone from NTC08 provisions (6.0 and 8.0 MPa) as well as reference values for the uncoursed three leaves masonry filled with rubble stone from Croatia (4.7 and 5.5 MPa) are presented also in Figure 3.25. These references seem to be the closest to masonry typology of the tested walls. The Italian OPCM provision [245] however provides even lower minimal and maximal values of f_{Mc} for such type of masonry; 3.0 and 4.0 MPa, respectively.

For the purpose of analytical assessment of f_{Mc}, design procedures provided in EC6 (Eq. 2.1) and models for multi-leaf f_{Mc} estimation proposed by Egermann and Binda et al (Eq. 2.11, 2.13) and

Tassios and Chronopoulos (Eq. 2.14 for multi-leaf and Eq. 2.15 for single-leaf) were considered (Table 3.6). For Egermann and Binda et al models, for f_{Mc}^{e} minimum(*) and maximum(**) values according to NTC08 were considered, as among all of the recommendations, in this code the most structured values with regard to the type of masonry are provided. For f_{Mc}^{i}, results of core tests were considered. According to Tassios recommended coefficients for cut stone masonry (+) as well as for ashlar masonry (++) were considered in the analysis.

Preglednica 3.6: Referenčne vrednosti f_{Mc} iz literature ter izračunane po različnih analitičnih modelih

Table 3.6: Literature reference f_{Mc} values and values calculated according to various analytical models

f_{Mc} [MPa]								
Literature values				Analytical models				
NTC08 (Italy)	PIET 70 (Spain and Portugal)	Slovenia [244]	Croatia [242]	EC6	Egermann	Binda	Tassios	Tassios (single-leaf)
6.0 (min)	4.0	1.2 (min)	4.7 (min)	19.9	3.44 (*)	4.73 (*)	2.66 (+)	6.51 (+)
8.0 (max)		1.6 (max)	5.5 (max)		4.49 (**)	6.23 (**)	1.42 (++)	6.75 (++)

As already mentioned, NTC08 recommendations for f_{Mc} seem to be satisfactory. Results calculated according to analytical models vary considerably, though. The EC6 model significantly overestimates f_{Mc} and is not appropriate for historic masonry with low mortar strength. Analytical models for three-leaf masonry however all underestimate the f_{Mc} of the tested walls. This is probably the case due to very good connection of the internal and the external leaves, which prevented the out-of-plane failure of the multi-leaf masonry. Formulation of Tassios and Chronopoulos for estimation of f_{Mc} of single-leaf masonry provides the most accurate estimation and therefore seems to be the most appropriate one. It overestimates f_{Mc} by 7.6% compared to f_{Mc} according to tests of the higher walls, but underestimates it if compared to f_{Mc} of the wallettes.

3.3.6 Summary and discussion of the results of compressive tests

Two wallettes and additionally two walls (one of each morphology type; with and without through stones) were tested in compression, because due to the lower actuator capacity, the maximum resistance of the wallettes was not achieved. In compression tests of wall specimens, the compressive strength of masonry f_{Mc} was obtained and softening occurred. Average f_{Mc} for connected and unconnected wall was 6.05 MPa. There was no obvious difference in behaviour of the wall with and the wall without through stones. Contrary to predictions, the f_{Mc} of the wall without through stones was even slightly higher (6.10 MPa compared to 6.00 MPa). These values correspond well with values provided for dressed rectangular stone in the Italian code provisions NTC08; where minimal and maximal values are 6 MPa and 8 MPa, respectively.

If obtained results are compared to analytically calculated results for f_{Mc}, design models for three-leaf masonry (Egermann, Binda et al and Tassios and Chronopoulos) underestimate the compressive strength. The reason for this probably is, that the formulas were not intended for masonry where the out-of-plane behaviour is not an issue (sufficient connection between the leaves provided by the adequately filled inner core). EC6 highly overestimates f_{Mc} (factor 3.3 f_{Mc} determined through the

experiments). Model by Tassios and Chronopoulos for single-leaf masonry however provides good results (1.08 f_{Mc} of walls). All the models are sensitive to input parameters, therefore for design purposes we recommend always to critically evaluate the calculated results also by comparing them to some reference values in the code provisions or to reference values in the literature for masonry of the same or similar type.

Moduli E_M and G_M obtained in the tests are lower than expected. According to NTC08, values range between 2400 and 3200 MPa for E_M and 780 and 940 MPa for G_M moduli. From the tests on wall, average E_M obtained for both morphology type of walls was 968 MPa, while 357 MPa was the average G_M modulus obtained. It has to be noted, that the G_M moduli were derived through assumption of a homogeneous isotropic material, which is not accurate for masonry. The results of Poisson's ratio υ_M varied considerably in dependence of horizontal deformations of the wall, considered for the calculation. The estimation of G_M moduli from compression tests of stone masonry is therefore unreliable. Comparing the results of the wall with and without through stones, it may be concluded that E_M and G_M are lower in case of the wall with through stones (E_M for 29.9% and G_M for 26.9%). This difference may result from the fact, that connected wall had 10 courses of stone units and thicker mortar bed-joints compared to unconnected wall, which had 11 courses. Ratio between shear and elastic modulus calculated at one third maximum stress is for all tests within expected values; from 0.36 to 0.42.

Leaf separation occurred at a lower load at test of wall without through stone. However once the through stones cracked in the connected walls, leaf separation advanced to the same extent and there was no significant difference in maximum leaf separation values obtained for walls of both morphology type.

3.4 Cyclic in-plane shear tests on walls

3.4.1 Test setup description

Cyclic in-plane shear tests of walls under compression were performed on the testing machine presented in Figure 3.29 and Figure 3.30. The vertical load was applied with concrete weights which acted through a lever on the bottom of the wall. At the top, the wall specimen's RC tie beam was placed under a steel beam, designed especially for this experiment allowing the vertical load to distribute uniformly over the whole cross section.

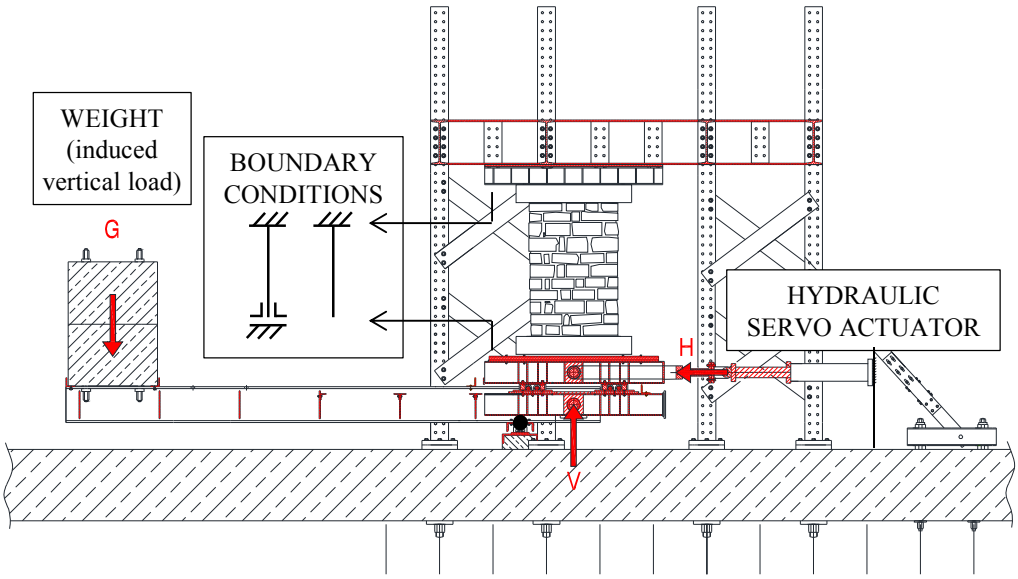

Figure 3.29: Test setup for in-plane shear tests of the walls
Slika 3.29: Postavitev za strižne teste zidov

Figure 3.30: Wall specimen in position for testing
Slika 3.30: Zid v poziciji za testiranje

The test setup allows the maximum vertical load up to 500 kN on the specimens and the servo-hydraulic actuator is capable of inducing horizontal displacements in both directions with the capacity of 250 kN. On the lower edge of the specimen, two types of the boundary conditions were used; in one case the rotation and the horizontal displacement were released, which made the wall a cantilever turned upside down, in the other case the rotation at the bottom was restrained, which made the wall a system with fixed rotations at both ends.

The possibilities of the testing setup therefore allowed us to perform various combinations of loading and boundary conditions. To obtain different failure mechanisms of the walls, two levels of pre-compression and cantilever and fixed-fixed boundary conditions were applied. In Table 3.7, the matrix of performed experimental tests is presented. Except of the specimens, tested as a cantilever under lower level of pre-compression, each combination of pre-compression, boundary conditions and morphology had one repetition. Test on the first wall was repeated, as due to pure rocking mechanism the pre-compression level was increased from 5 to 7.5% of f_{Mc}.

Preglednica 3.7: Kombinacije za strižno testiranje zidov

Table 3.7: Combinations for shear tests of the walls

Test no.	Name	Level of vertical pre-compression [% of f_{Mc}]	Boundary conditions	Connecting through stone
1	SPk-5-1	5	cantilever	YES
1.2	SPk-5-1 (7.5)	7.5	cantilever	YES
2	SNk-7.5-1	7.5	cantilever	NO
3	SNv-7.5-1	7.5	fixed-fixed	NO
4	SPv-7.5-1	7.5	fixed-fixed	YES
5	SNv-7.5-2	7.5	fixed-fixed	NO
6	SPv-7.5-2	7.5	fixed-fixed	YES
7	SPv-15-1	15	fixed-fixed	YES
8	SNv-15-1	15	fixed-fixed	NO
9	SPv-15-2	15	fixed-fixed	YES
10	SNv-15-2	15	fixed-fixed	NO
11	SNk-15-1	15	cantilever	NO
12	SPk-15-1	15	cantilever	YES
13	SPk-15-2	15	cantilever	YES
14	SNk-15-2	15	cantilever	NO

Comment: in the presented table and further on in the thesis in the analysis of the results, red fonts apply to results of tests on walls with through stones (connected walls)

The names for specific walls and shear testing conditions combinations provided in Table 3.7 (for instance "1_SNk-75-1") and used further in the text have the following meaning:

1-14 … means the number of the test,
S … refers to Shear test;
N or P … indicate the morphology of the wall;
- P … indicates wall with through stones (in Slovenian "Povezani") and
- N … wall without through stones (in Slovenian "Nepovezani")

k or v … indicate the boundary conditions;
- k … means that cantilever boundary conditions were applied (in Slovenian "konzola")

- v … fixed-fixed boundary conditions were applied (in Slovenian "vpeto")

5, 7.5 or 15 … indicate the level of pre-compression applied during shear testing;

- 5 … vertical load equal to 5% of f_{Mc}
- 7.5 … vertical load equal to 7.5% of f_{Mc}
- 15 … vertical load equal to 15% of f_{Mc}

1 or 2 … refers to the number of repetition of the test, where the same morphology, boundary conditions and pre-compression levels were applied.

3.4.2 Measuring positions and loading protocol

The displacement increase was controlled at the bottom of the wall through a LVDT attached to the concrete block. To attain displacements of the wall and to control the flexural cracks between the wall and concrete foundation and also possible sliding between the steel element and concrete tie beam (see Figure 3.29), 19 LVDTs were used. The positions of measuring points are presented in Figure 3.31.

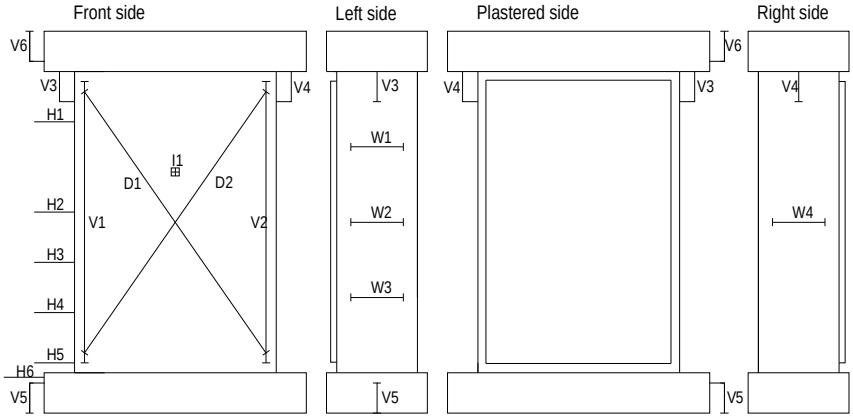

Figure 3.31: Measuring positions at shear test
Slika 3.31: Merilna mesta pri strižnih testih

Due to the risk of damaging the measuring equipment, the instruments were not attached to the plaster. For this reason the displacements of the plaster were measured with close range photogrammetry methods. Signal points were placed and measured with theodolite, on the plaster a grid with a gap of 10x10 cm^2 was drawn with black dots of 2 cm diameter at the intersections. Throughout each test a survey of crack formation and propagation was conducted.

During the test the displacement was imposed with constant velocity within the same blocks of cycles with specific displacement amplitudes (see Table 3.8). Each amplitude peak was repeated three times to get the stiffness and strength degradation and deterioration in the nonlinear range. The typical displacement time history can be seen in Figure 3.32. It changed however in dependence of maximum displacement and failure mechanism obtained (some amplitude displacement cycles were omitted). The tests were conducted up to the displacement, at which 20% drop of shear resistance was attained, or to the displacement, at which it was due to the developed damage estimated, that the increase of displacements would be dangerous.

Preglednica 3.8: Maksimalni amplitudni pomiki in pripadajoče hitrosti obremenjevanja za določene cikle

Table 3.8: Peak amplitude displacements and corresponding velocities of loading for the loading cycles

Peak amplitude displacement [mm]	0.25, 0.5	0.75, 1.0, 1.5, 2.0, 3.0	7.5, 10.0	12.5	15.0, 17.5	20.0, 22.5, 25.0, 27.5, 30.0, 35.0	40.0, 45.0	50.0	60.0
Velocity [mm/s]	0.025	0.04	0.12	0.15	0.20	0.30	0.35	0.40	0.50

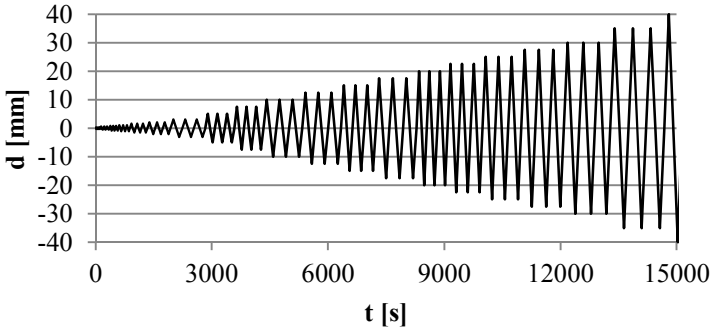

Figure 3.32: Imposed lateral displacement time history for shear tests
Slika 3.32: Protokol obremenjevanja z vsiljevanjem pomikov za strižne teste

3.4.3 Characteristic damage and obtained failure mechanisms

Through various pre-compression levels and boundary conditions applied, various damage and failure mechanisms were obtained. The damage propagation and failure mechanisms obtained during tests are described and supported by the results of LVDTs measurements for each test separately in [246]. Photographs of walls during and after testing together with crack pattern evolution figures are also provided in details. Damage evolution on each wall plaster is described in [246] following damage on the wall in order to make easier parallels with the behaviour of the walls as structural elements. Typical damage obtained in the tests is however presented in Figure 3.33.

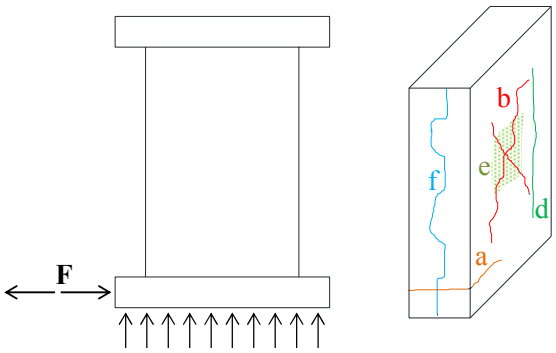

Figure 3.33: Characteristic damage obtained on the walls at shear tests
Slika 3.33: Karakteristične poškodbe zidov pri strižnih testih

The first test (test 1) under cantilever boundary conditions and the lowest pre-compression level (5% f_{Mc}) exhibited pure rocking behaviour with no other damage except flexural "opening" of the

horizontal bed-joint between the first two rows of stones (mechanism "a" in Figure 3.33, Figure 3.34 a). For the same boundary conditions, but 7.5% f_{Mc} pre-compression level (test 1.2 and 2), the response mechanism was still rocking, yet some random very tiny shear cracks through joints were observed at higher displacement amplitudes (35 mm at test 1.2 and 17.5 mm at test 2).

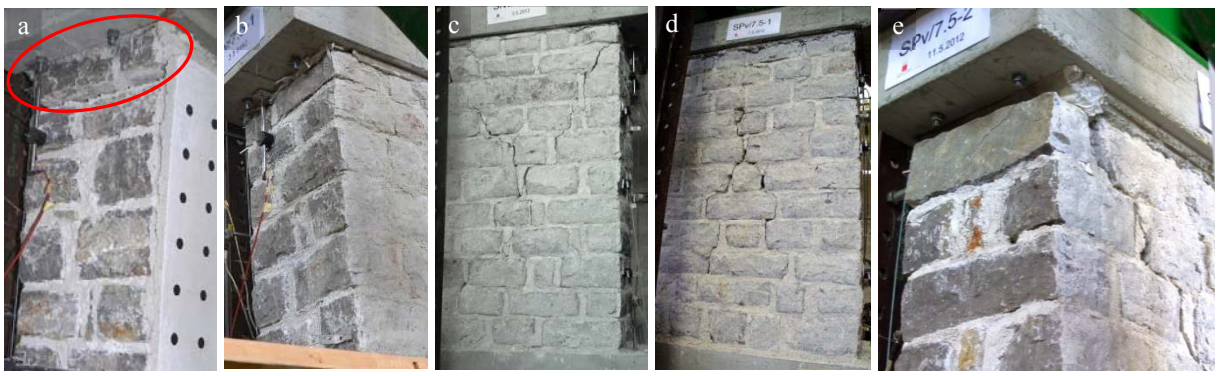

Figure 3.34: a) rocking of the wall with opening of the mortar joint between the first two rows of stone during test 2 - SNk-7.5-1, b) rocking damage during test 3 - SNv-7.5-1, c) diagonal shear damage after test 3 - SNv-7.5-1, crack pattern on the wall d) after test 4 - SPv-7.5-1 and e) after test 6 - SPv-7.5-2
Slika 3.34: a) upogibni mehanizem z odpiranjem maltne spojnice med prvima vrstama kamnitih blokov pri testu 2 - SNk-7.5-1, b) upogibni mehanizem pri testu 3 - SNv-7.5-1, c) strižne poškodbe zidu po testu 3 - SNv-7.5-1, razpoke zidu d) po testu 4 - SPv-7.5-1 in e) po testu 6 - SPv-7.5-2

Restraining the bottom rotation for tests 3-6 resulted in triggering more evident shear behaviour and not so apparent rocking mechanism as in cantilever boundary conditions (Figure 3.34 b-d). They both were detected either at the same amplitude displacement or rocking was detected first. Diagonal shear cracks (mechanism "b" in Figure 3.33) had formed mainly through mortar, though some cracks occurred in the stone as well. At higher displacements, mortar started visibly to crush and fall out from the joints and was in some tests even "pouring" out from the central part of the specimens (mechanism "e" in Figure 3.33). In test 6, crushing of the mortar was observed in the upper corners. During this test at displacement 15 mm the stone at the top right side cracked and later also detached from the concrete block at the top (Figure 3.34 e).

Higher pre-compression level (15% f_{Mc}) enabled the shear mechanism with diagonal cracks going through both mortar joints as well as through stones, to prevail for both types of the applied boundary conditions (Figures 3.35 and 3.36). At higher loads, in the centre of the specimen and also at the top corners, the mortar was crushing and vertical cracks (which passed mainly through mortar) formed a kind of vertical columns on one or both sides of the specimens (tests 9, 10, 14, see mechanism "d" in Figure 3.33). In some tests, (part of) these columns started "buckling" to the side of the wall (Figure 3.36 d). In some tests performed under higher pre-compression level, at the last (post-peak) phases of tests, the mortar was "pouring" out at the centre of the wall and also at the top corners; for instance in test 8 the centre stone was noticeably being pushed out while in test 12 a part of stone even fell off. For cantilever boundary conditions rocking mechanism was observed simultaneously (tests 11, 12) or before shear damage; in tests 13 and 14 diagonal mechanism at the beginning formed only in the negative direction of loading. On the contrary, for fixed-fixed boundary conditions, rocking damage was recognized later in the test.

Figure 3.35: Crack pattern on the walls after test 8 - SNv-15-1 (a, b) and test 10 - SNv-15-2 (c, d)
Slika 3.35: Poškodovanost zidov po testu 8 - SNv-15-1 (a, b) in testu 10 - SNv-15-2 (c, d)

Figure 3.36: Crack pattern on the walls after test 12 - SPk-15-1 (a, b) and 14 - SNk-15-2 (c, d)
Slika 3.36: Poškodovanost zidov po testu 12 - SPk-15-1 (a, b) in testu 14 - SNk-15-2 (c, d)

The obtainment of different damage and failure mechanisms was supported also by results of LVDT measurements. Their comparison for some of the walls, tested under certain boundary conditions in dependence from induced lateral displacement can be made from Figure 3.37 (diagonal LVDTs D1, D2), Figure 3.38 (top vertical LVDTs V3, V4) and further on from Figure 3.40 (middle side horizontal LVDTs W2, W4), respectively.

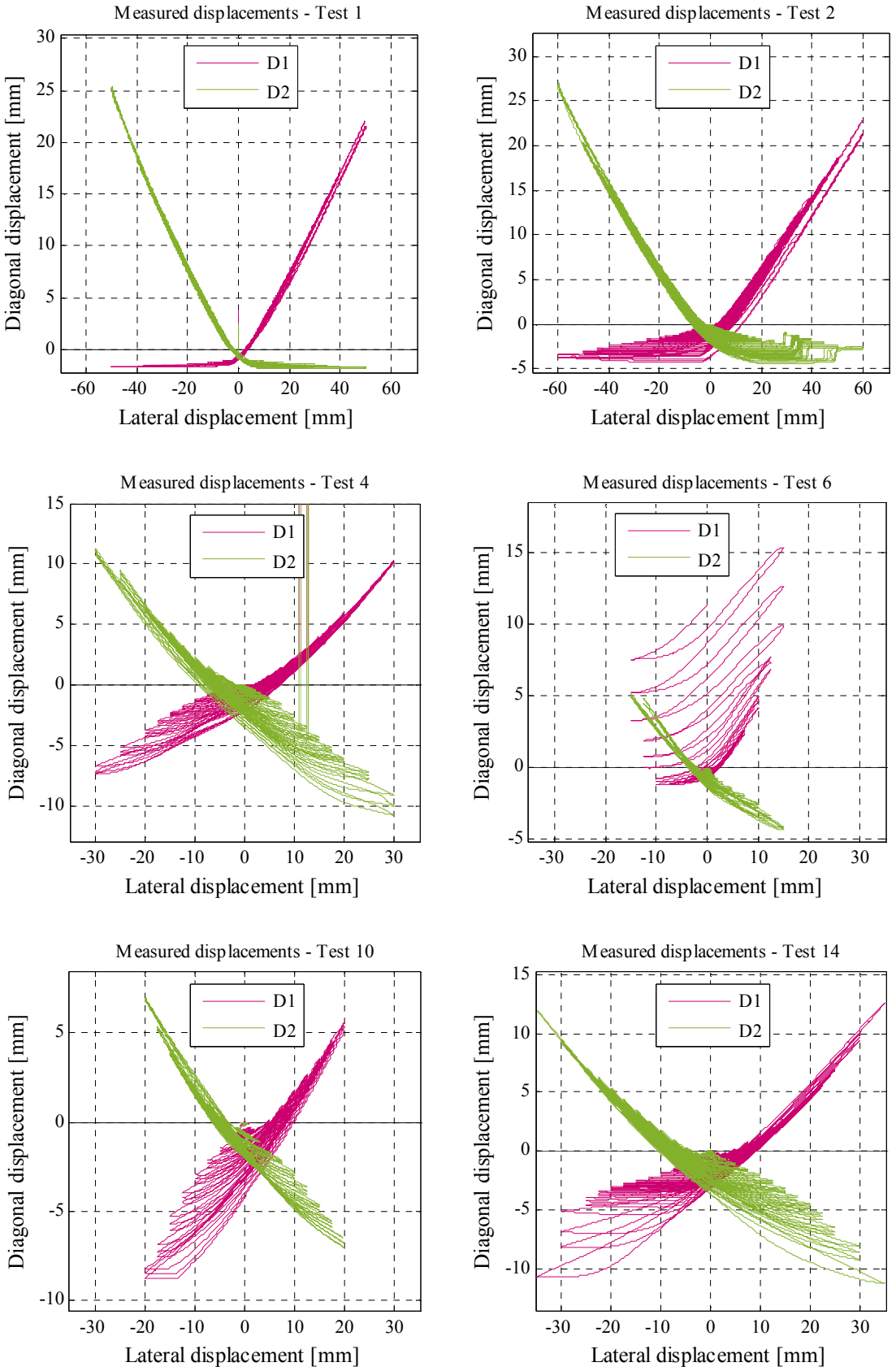

Figure 3.37: Measurements of LVDTs D1, D2 in dependence of walls' lateral displacement for tests 1, 2, 4, 6, 10, 14
Slika 3.37: Meritve LVDT-jev D1, D2 v odvisnosti od horizontalnega pomika zidu za teste 1, 2, 4, 6, 10 in 14

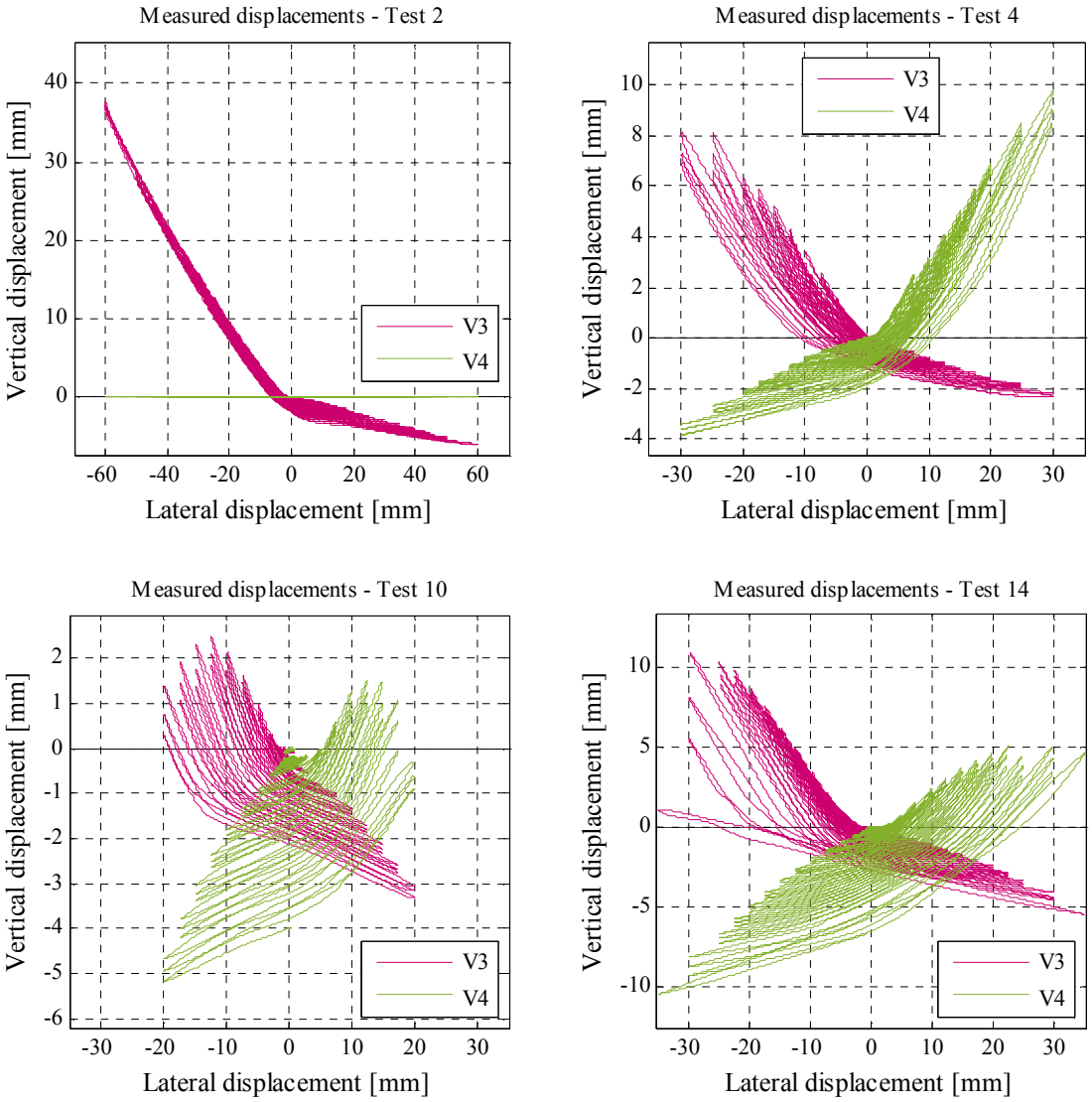

Figure 3.38: Measurements of LVDTs V3, V4 in dependence of walls' lateral displacement for tests 2, 4, 10 and 14
Slika 3.38: Meritve LVDT-jev V3, V4 v odvisnosti od horizontalnega pomika zidu za teste 2, 4, 10 in 14

Regarding the out-of-plane deformations and leaf separation (mechanism "f" in Figure 3.33), leaf separation proved problematic with the occurrence of shear mechanism; more apparent leaf separation occurred in tests 8, 10, 12, 13 and 14. In these tests, the measurements of the LVDTs exceeded 3.0 mm in at least one measuring position. Leaf separation after the test is for some of them presented in Figure 3.39, whereas results of the LVDT measurements for the typical responses can be compared in Figure 3.40. In Table 3.9 maximum values of LVDT measurements indicating leaf separation (W1-W4) and out-of-plane displacements (I1, I2) are presented.

With cantilever boundary conditions leaf separation was more apparent, whether the header stones were present or not. For fixed-fixed boundary conditions though, the through stones limited the separation in the post-peak phase of the test (see values of tests 7 and 9 compared to tests 8 and 10). For tests 1, 1.2, 4, 6 and 7, no vertical crack along the side of the specimen indicating separation of the leaves was observed.

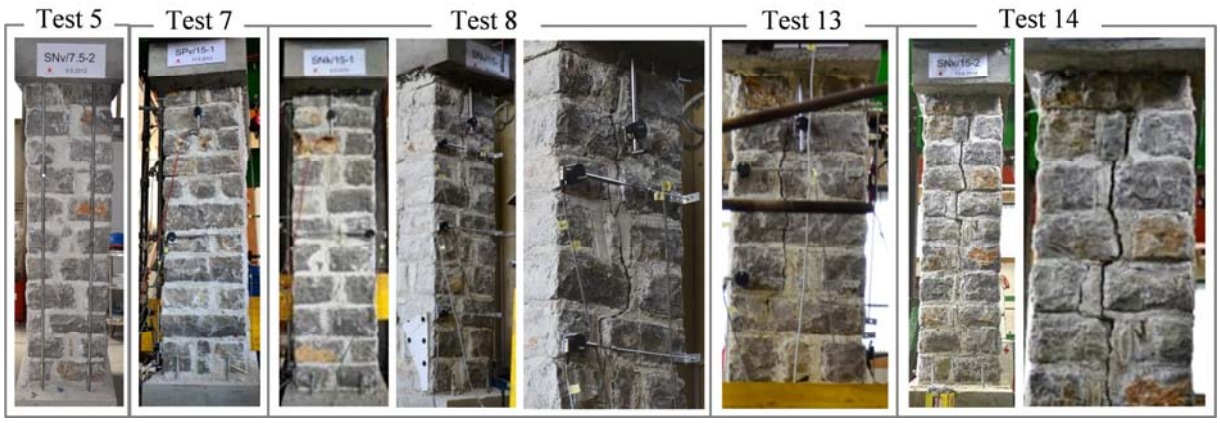

Figure 3.39: Crack indicating the leaf separation (if present) for some of the tests
Slika 3.39: Razpoka, ki nakazuje razslojevanje zidu (če prisotna), za nekatere teste

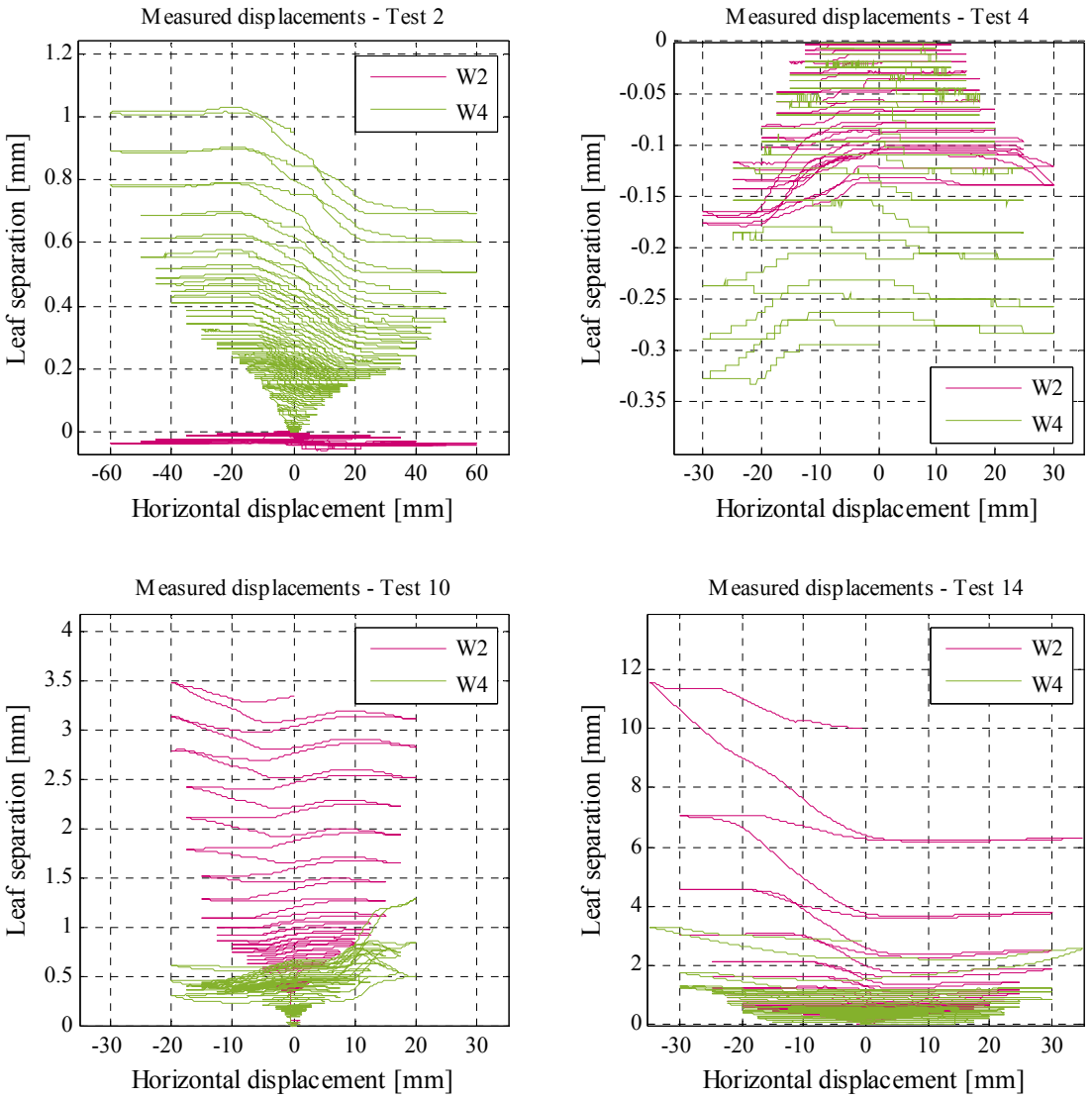

Figure 3.40: Measurements of LVDTs W2, W4 in dependence of the walls' lateral displacement for tests 2, 4, 10, 14
Slika 3.40: Meritve LVDT-jev W2, W4 v odvisnosti od horizontalnega pomika zidu za teste 2, 4, 10 and 14

Preglednica 3.9: Maksimalne vrednosti meritev induktivnih merilcev, ki kažejo ločevanje slojev zidov (W1-W4) in izven-ravninske pomike zidov (I1, I2,)

Table 3.9: Maximum values of LVDT measurements indicating leaf separation (W1-W4) and out-of-plane displacements (I1, I2)

Test no.	Name	W1 [mm]	W2 [mm]	W3 [mm]	W4 [mm]	I1 [mm]	I2 [mm]
1	1-SPk-5-1	0.25	1.06	0.29	0.00	23.07	0.42
1.2	1.2-SPk-7.5-1	0.13	0.02	0.00	0.01	0.01	-0.01
2	2-SNk-7.5-1	0.65	0.00	0.56	1.03	13.01	-0.69
3	3-SNv-7.5-1	0.00	0.97	1.15	0.21	1.15	-1.20
4	4-SPv-7.5-1	0.01	0.00	0.31	0.00	2.76	-0.98
5	5-SNv-7.5-2	0.61	0.29	0.17	0.01	0.75	-8.44
6	6-SPv-7.5-2	0.14	0.04	0.03	0.03	0.31	-1.83
7	7-SPv-15-1	0.14	0.00	0.05	0.02	1.03	-0.78
8	8-SNv-15-1	7.76	8.59	2.45	0.72	0.01	-9.09
9	9-SPv-15-2	0.88	0.00	0.17	0.01	0.88	-5.67
10	10-SNv-15-2	3.19	3.48	2.04	1.28	0.08	-6.07
11	11-SNk-15-1	1.17	0.19	0.22	0.43	1.33	-2.28
12	12-SPk-15-1	2.34	4.11	1.32	0.00	0.60	-3.93
13	13-SPk-15-2	8.94	4.15	0.00	0.88	0.25	-6.27
14	14-SNk-15-2	16.01	11.57	4.28	3.32	5.32	-5.16

Clear influence of internal stresses gained through various pre-compression level and boundary conditions on obtained mechanism is indeed apparent. Low pre-compression level (5 and 7.5%) and cantilever boundary condition provoked rocking mechanism. Restraining the rotations at the bottom enabled shear mechanism to partially develop, whereas high pre-compression level induced shear behaviour with some toe crushing and formation of vertical columns. In Table 3.10 damage and failure mechanism for each test are summarized.

Preglednica 3.10: Porušni mehanizmi, dobljeni pri strižnih testih zidov

Table 3.10: Failure mechanisms obtained at shear tests of walls

Test no.	Name	Damage mechanism	Failure mechanism	Leaf separation
1	SPk-5-1	Rocking	Rocking	/
1.2	SPk-5-1 (7.5)	Rocking	Rocking	/
2	SNk-7.5-1	Rocking, mortar crushing at corners	Rocking	Minor*
3	SNv-7.5-1	Rocking, shear, mortar crushing in the corners and in the middle	Mixed	Minor*
4	SPv-7.5-1	Rocking, Shear, mortar crushing in the middle	Mixed	/
5	SNv-7.5-2	Rocking, Shear, mortar crushing in the middle	Mixed	Minor*
6	SPv-7.5-2	Shear, rocking	Mixed	/

Continues…

…continuation of Table 3.10

7	SPv-15-1	Shear, mortar crushing in the middle and at corners, vertical column formation on one side	Shear	/
8	SNv-15-1	Shear, toe crushing, crushing of mortar in the middle	Shear	Major**
9	SPv-15-2	Shear, mortar crushing in the middle and at corners, vertical column formation on the sides	Shear	Minor*
10	SNv-15-2	Shear, toe crushing, vertical column formation on the sides	Shear	Major**
11	SNk-15-1	Shear, mortar and stone crushing in the middle, mortar crushing at corners, vertical column formation on one side	Shear	Minor*
12	SPk-15-1	Shear, mortar and stone crushing in the middle, mortar crushing at corners, vertical column formation on one side	Shear	Major**
13	SPk-15-2	Shear, mortar crushing in the middle and at corners, vertical column formation on one side	Shear	Major**
14	SNk-15-2	Rocking, shear, mortar crushing in the middle and at corners, vertical column formation on both sides	Shear	Major**

* Minor - at least one of W1-W4 LVDT measurements over 0.5 mm

** Major - at least one of W1-W4 LVDT measurements over 3 mm

3.4.4 Hysteretic response of the walls

The most significant results concerning the response of the walls as structural elements (characteristic displacements and resistances) are summarized hereafter. In Figures 3.41 and 3.42, lateral force - displacement (bottom LVDT H6) diagrams for all 15 tests obtained are presented. Values of displacement and forces obtained at characteristic limit states of the response obtained in both directions of loading are summarized in Table 3.11, whereas average values for both directions in Table 3.12. Within the thesis of Luka Kurnjek [247], algorithms for automatic evaluation of the test results were written for Matlab computing environment. They served as a basic code and with some improvements enabled a detail analyses and comparisons of the test results.

First shear crack displacements d_{cr} refer to cycles, where shear cracks were first visually observed during testing. The reason for this is that it was in most cases not possible to attain some specific point, where the damage occurred, from the LVDTs' measurements, as most of them showed changes from the very beginning of the test (this can most probably be attributed to "soft" mortar characteristics). From the same reason also points, where rocking damage occurred, are not provided.

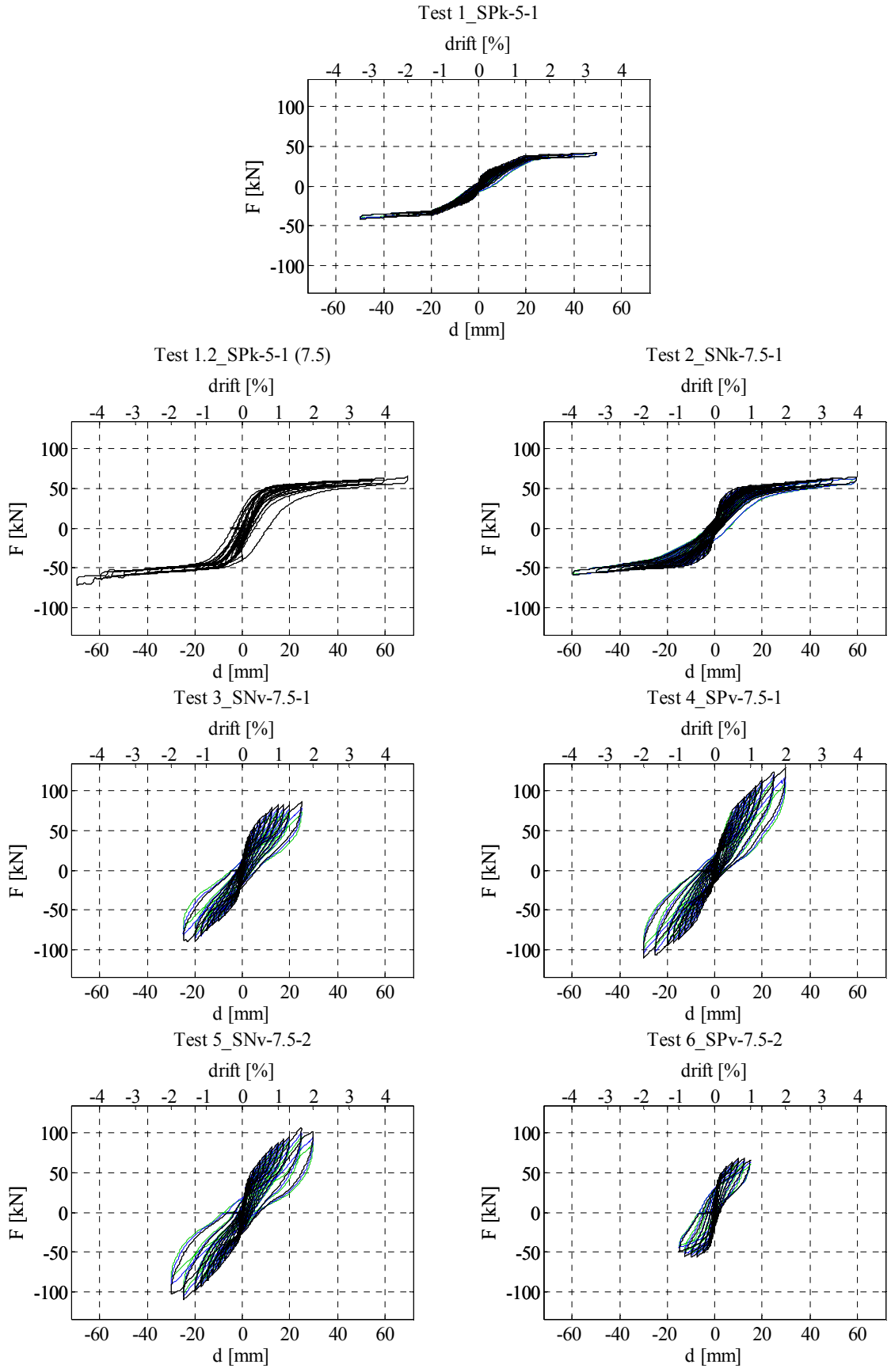

Figure 3.41: Hysteretic lateral load - lateral displacement diagrams obtained for tests with lower pre-compression level; tests 1-2 cantilever and tests 3-6 fixed-fixed boundary conditions

Slika 3.41: Diagrami histereznega odziva horizontalna sila - horizontalni pomik za teste z nižjim nivojem vertikalnih obremenitev; testi 1-2 konzolno in testi 3-6 obojestransko vpeti robni pogoji

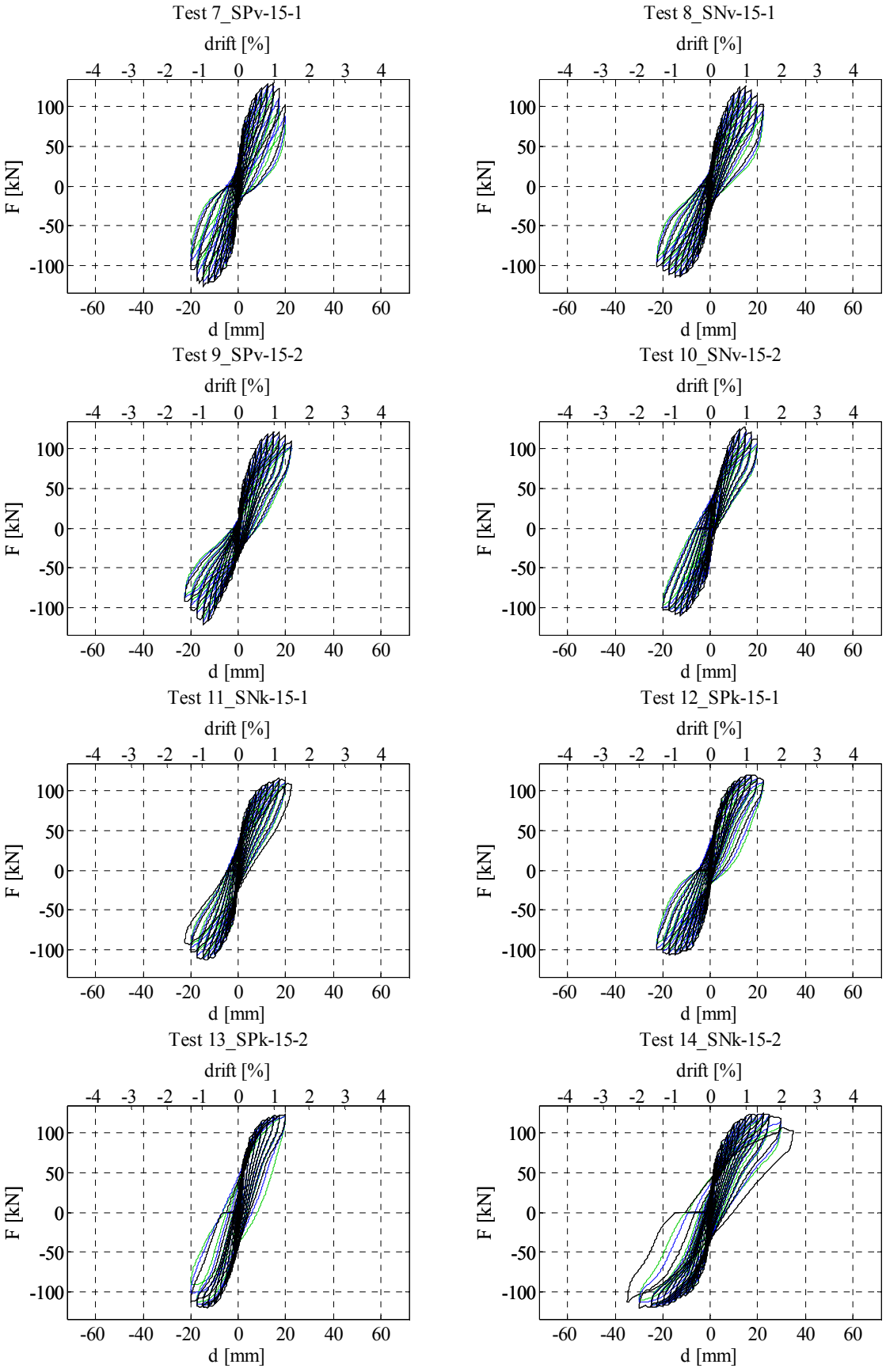

Figure 3.42: Hysteretic lateral load - lateral displacement diagrams obtained for tests with higher pre-compression level; tests 7-10 fixed-fixed and tests 11-14 cantilever boundary conditions

Slika 3.42: Diagrami histereznega odziva horizontalna sila - horizontalni pomik za teste z višjim nivojem vertikalnih obremenitev; testi 7-10 obojestransko in testi 11-14 konzolno vpeti robni pogoji

Preglednica 3.11: Vrednosti pomikov in sil v karakterističnih točkah diagramov sila - pomik za obe smeri testov

Table 3.11: Values of displacements and forces in characteristic points of force - displacement diagrams obtained in tests for both directions

Test	First shear crack				Maximum force				Maximum displacement			
	d_{cr}^{+} [mm]	d_{cr}^{-} [mm]	F_{cr}^{+} [kN]	F_{cr}^{-} [kN]	d_{Fmax}^{+} [mm]	d_{Fmax}^{-} [mm]	F_{max}^{+} [kN]	F_{max}^{-} [kN]	d_{max}^{+} [mm]	d_{max}^{-} [mm]	F_{dmax}^{+} [mm]	F_{dmax}^{-} [mm]
1-SPk-5-1	0.00	0.00	0.0	0.0	49.6	-49.6	41.9	-42.3	49.8	-49.8	40.8	-41.5
1.2-SPk-7.5-1	34.76	-34.64	58.8	-56.6	69.6	-69.5	65.0	-72.1	69.8	-69.7	63.4	-68.8
2-SNk-7.5-1	17.35	-17.40	53.7	-50.2	56.7	-59.5	63.9	-59.7	59.8	-59.8	62.3	-58.4
3-SNv-7.5-1	7.46	-7.42	64.9	-57.5	24.9	-19.8	85.8	-90.6	24.9	-24.8	72.4	-73.7
4-SPv-7.5-1	7.46	-7.43	65.5	-56.3	29.8	-29.7	128.9	-110.9	29.9	-29.8	108.4	-95.0
5-SNv-7.5-2	9.95	-9.92	74.7	-71.4	24.7	-24.7	107.2	-110.8	29.9	-29.9	86.2	-80.4
6-SPv-7.5-2	7.46	-7.44	63.8	-56.7	9.9	-9.9	68.0	-55.8	14.9	-15.0	59.3	-42.2
7-SPv-15-1	2.98	-2.98	80.4	-82.3	14.8	-14.9	130.3	-128.1	19.9	-19.9	76.5	-87.3
8-SNv-15-1	4.97	-4.96	84.2	-87.1	14.9	-14.8	126.7	-115.7	22.4	-22.4	89.1	-91.5
9-SPv-15-2	1.98	-1.98	52.3	-52.7	17.4	-14.8	121.8	-122.4	22.4	-22.4	102.4	-84.8
10-SNv-15-2	3.00	-2.96	52.0	-69.9	14.5	-12.4	128.3	-110.5	19.9	-19.9	104.6	-97.1
11-SNk-15-1	2.98	-2.98	65.4	-71.2	17.0	-13.0	115.8	-113.3	22.4	-22.4	107.0	-90.2
12-SPk-15-1	2.98	-2.98	67.3	-64.4	15.2	-15.3	120.6	-107.4	22.4	-22.4	109.8	-91.9
13-SPk-15-2	2.98	-2.97	71.0	-73.3	19.8	-12.7	124.0	-121.1	19.9	-19.9	120.5	-88.9
14-SNk-15-2	4.97	-4.97	84.6	-84.4	22.3	-29.7	125.5	-121.9	34.9	-34.8	102.3	-113.7

Preglednica 3.12: Povprečne vrednosti karakterističnih točk diagramov sila - pomik obeh smeri obremenjevanja

Table 3.12: Average values of characteristic points of force - displacement diagrams for both directions of loading

Test No.	Name	First shear crack		Maximum force		Maximum displacement	
		d_{cr} [mm]	F_{cr} [kN]	d_{Fmax} [mm]	F_{max} [kN]	d_{max} [mm]	F_{dmax} [mm]
1	1-SPk-5-1	0.00	0.0	49.6	42.1	49.8	41.2
1.2	1.2-SPk-7.5-1	34.70	57.7	69.5	68.5	69.7	66.1
2	2-SNk-7.5-1	17.37	51.9	58.1	61.8	59.8	60.3
3	3-SNv-7.5-1	7.44	61.2	22.3	88.2	24.9	73.0
4	4-SPv-7.5-1	7.45	60.9	29.7	119.9	29.9	101.7
5	5-SNv-7.5-2	9.93	73.0	24.7	109.0	29.9	83.3
6	6-SPv-7.5-2	7.45	60.2	9.9	61.9	14.9	50.8
7	7-SPv-15-1	2.98	81.4	14.8	129.2	19.9	81.9
8	8-SNv-15-1	4.96	85.7	14.9	121.2	22.4	90.3
9	9-SPv-15-2	1.98	52.5	16.1	122.1	22.4	93.6
10	10-SNv-15-2	2.98	60.9	13.4	119.4	19.9	100.8
11	11-SNk-15-1	2.98	68.3	15.0	114.5	22.4	98.6
12	12-SPk-15-1	2.98	65.8	15.2	114.0	22.4	100.9
13	13-SPk-15-2	2.98	72.2	16.2	122.5	19.9	104.7
14	14-SNk-15-2	4.97	84.5	26.0	123.7	34.9	108.0

From comparison of the obtained hysteretic response, the influence of boundary condition and pre-compression level on the behaviour is evident (the influence of boundary conditions at higher pre-compression level is less evident though). With regard to obtained failure mechanism the obtained maximum resistances and ultimate displacement capacities of the walls differ. Average values for the characteristic limit states are for the tests with the same pre-compression level and boundary conditions presented in Table 3.14, and for the tests with the same prevailing failure mechanism in Table 3.15. With rocking mechanism, lower resistance was obtained whereas displacements were

significantly higher as in comparison to other prevailing mechanisms. In case of mixed mechanism the resistance had increased but the displacement capacity was greatly reduced. This capacity is comparable with capacity obtained with shear mechanism, but still slightly higher if test 6 is excluded from the comparison. The different response in terms of maximum resistance and maximum displacement capacity for test 6 (compared to other three tests with the same boundary conditions and pre-compression level applied, i.e. tests 3-5) is the consequence of greater bed-joint thickness h_j of the masonry in this wall. Instead of typical 11 or even 12 rows of stone as in other wall specimens, this wall was constructed of only 10. With respect to fewer rows of stone, the thickness of horizontal mortar joints was greater (h_j of 2-3 cm instead of 1.5-2.5 cm or for walls for test 8 and 10, which had 12 courses, 1-2 cm) and this apparently weakened the wall; it reduced the resistance by 48.3% and ultimate displacement capacity by 49.9% compared to the second specimen with the same morphology, tested under the same conditions (test 4).

By considering the influence of boundary conditions and also comparing the mean values in all characteristic states (Table 3.14), cantilever boundary conditions in most cases performed better in comparison to fixed-fixed boundary conditions in terms of their displacement capacity. This effect was expected, even though the influence of the effective height of the specimens or shear span length (moment contra flexure points) on the displacement capacity was not as evident as anticipated. Since rocking mechanism was only obtained with cantilever boundary conditions, the comparison with recommendations provided by the EC8-3 and FEMA provisions (to consider effective height instead of height to calculate drift limits; see Section **2.3.3.3**) is not possible.

Regarding the influence of morphology, the presence of header stones proved to significantly contribute neither to higher resistance, nor to higher displacement capacity at in-plane shear loading. Results for walls with the same morphology are summarized in Table 3.13, where the average values for test repetitions are provided. As wall no. 6 had different masonry thickness of joints, values of the other wall tested under the same boundary conditions and pre-compression level are also provided in the table (row “without test no. 6”). In fact, since test 6 cannot be directly compared to other tests, in the thesis (if not stated differently), the average results for the lower pre-compression level and fixed-fixed boundary conditions and for tests where mixed mechanism was obtained do not include results of test 6. Header stones proved higher resistance only in case of higher pre-compression level and fixed-fixed boundary conditions, where the resistance was for 4.4% higher. If test 6 is not considered, also at lower pre-compression level and fixed-fixed boundary conditions header stones contributed to 21.6% higher resistance. With higher pre-compression level and cantilever boundary conditions, slightly lower average resistance was obtained for walls with header stones; the difference between both is however within 1%. Maximum resistance obtained in tests 1.2 and 2, where rocking mechanism occurred, cannot be compared, as ultimate displacement and softening were not obtained in the tests (tests were stopped because there was a risk of damaging the LVDT through which the tests were controlled). The higher resistance of the wall with header stones (test 1.2) obtained can be attributed to higher displacement obtained with this test. Regarding the relation of displacement capacity vs. the presence of header stones, higher ultimate displacement capacity was obtained only by lower pre-compression level and fixed-fixed boundary, otherwise either lower average displacement capacity was obtained (higher pre-compression level and cantilever boundary conditions), or the same (higher pre-compression level and fixed-fixed boundary conditions).

As there is no obvious difference related to presence of header stones with respect to maximum strength or displacement capacity, further in the test evaluation, their average values depending from the level of pre-compression and boundary conditions applied or/and for prevailing failure mechanism obtained will be stated.

From the hysteresis diagrams and values of maximum lateral forces obtained in both direction of loading, it can also be concluded, that the response of the walls was quite symmetrical. In 6 tests (1, 7, 9, 11, 13 and 14) the difference between maximum force obtained in negative and in positive direction of loading was below 3%. In 5 tests (tests 1.2, 4, 6, 10 and 12) this difference exceeds 10% with the highest difference 17.9% in test 6.

Preglednica 3.13: Povprečne vrednosti karakterističnih točk diagramov sila - pomik testov glede na morfologijo, nivo vertikalnih obremenitev ter robne pogoje

Table 3.13: Mean values of force - displacement response characteristic values for tests considering the morphology, pre-compression level and boundary conditions

Limit state	First shear crack				Maximum force				Maximum force			
	d_{cr} [mm]		F_{cr} [kN]		d_{Fmax} [mm]		F_{max} [kN]		d_{max} [mm]		F_{dmax} [kN]	
Header stones present:	Yes	No	Yes	No	Yes	No	Yes	No	Yes	No	Yes	No
7.5% f_{Mc}, cantilever	34.7	17.4	57.7	51.9	69.5	58.1	68.5	61.8	69.7	59.8	66.1	60.3
7.5% f_{Mc}, fixed-fixed	7.45	8.69	60.9	67.1	29.7	23.5	119.9	98.6	29.9	27.4	101.7	78.1
15% f_{Mc}, fixed-fixed	2.48	3.97	66.9	73.3	15.5	14.1	125.7	120.3	21.1	21.1	87.7	95.6
15% f_{Mc}, cantilever	2.98	3.97	69.0	76.4	15.7	20.5	118.2	119.1	21.1	28.6	102.8	103.3

Preglednica 3.14: Povprečne vrednosti karakterističnih točk diagramov sila - pomik testov glede na nivo vertikalnih obremenitev ter robne pogoje

Table 3.14: Mean values of characteristic points of force - displacement response for tests with the same pre-compression level and boundary conditions

Limit state	First shear crack				Maximum force				Maximum force			
Pre-compression level, Boundary conditions	d_{cr} [mm]	c.o.v.	F_{cr} [mm]	c.o.v.	d_{Fmax} [mm]	c.o.v.	F_{max} [kN]	c.o.v.	d_{max} [mm]	c.o.v.	F_{dmax} [kN]	c.o.v.
7.5% f_{Mc}, cantilever	26.0	33.3	54.8	5.3	63.8	9.0	65.2	5.1	64.8	7.7	63.2	4.6
7.5% f_{Mc}, fixed-fixed	8.27	14.2	65.0	8.7	25.6	12.1	105.7	12.4	28.2	8.3	86.0	13.8
15% f_{Mc}, fixed-fixed	3.23	33.5	70.1	19.7	14.8	6.3	123.0	3.0	21.1	5.9	91.7	7.4
15% f_{Mc}, cantilever	3.48	24.8	72.7	9.9	18.1	25.3	118.7	3.8	24.9	23.5	103.0	3.5

Preglednica 3.15: Povprečne vrednosti karakterističnih točk diagramov sila - pomik po testih glede na dobljeni porušni mehanizem

Table 3.15: Mean values of characteristic points of force - displacement response for tests with the same prevailing failure mechanism

Limit state	First shear crack				Maximum force				Maximum force			
Prevailing failure mechanism	d_{cr} [mm]	c.o.v.	F_{dcr} [mm]	c.o.v.	d_{Fmax} [mm]	c.o.v.	F_{max} [kN]	c.o.v.	d_{max} [mm]	c.o.v.	F_{dmax} [kN]	c.o.v.
Rocking	26.0	33.3	54.8	5.3	59.1	13.8	57.5	19.5	59.8	13.6	56.3	19.8
Mixed	8.27	14.2	65.0	8.7	25.6	12.1	105.7	12.4	28.2	8.3	86.0	13.8
Shear	3.35	29.4	71.4	15.5	16.5	22.5	120.8	3.8	23.0	20.1	97.3	8.1

3.4.4.1 Test results idealization and analysis

In the analysis of our test results, bi-linear idealization of the hysteresis envelope was used. Experimental envelopes were defined as skeleton curves, where also force decreases within the same displacement amplitude cycles were considered. Envelopes for tests are presented in Figures 3.43 and 3.44. Bi- linear idealization was done for each direction of loading separately.

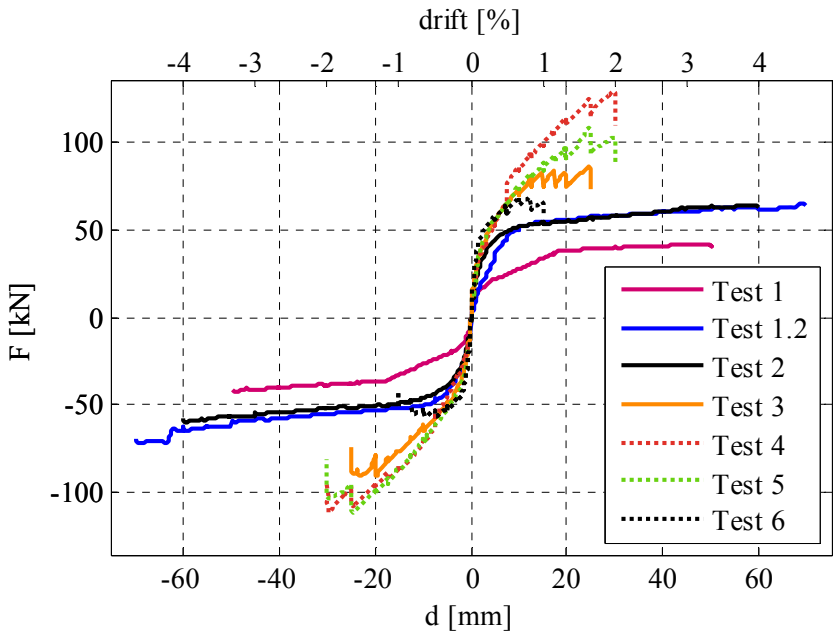

Figure 3.43: Hysteretic envelopes of lateral load - lateral displacement responses for tests 1-6
Slika 3.43: Histerezne ovojnice odziva horizontalna sila - horizontalni pomik za teste 1-6

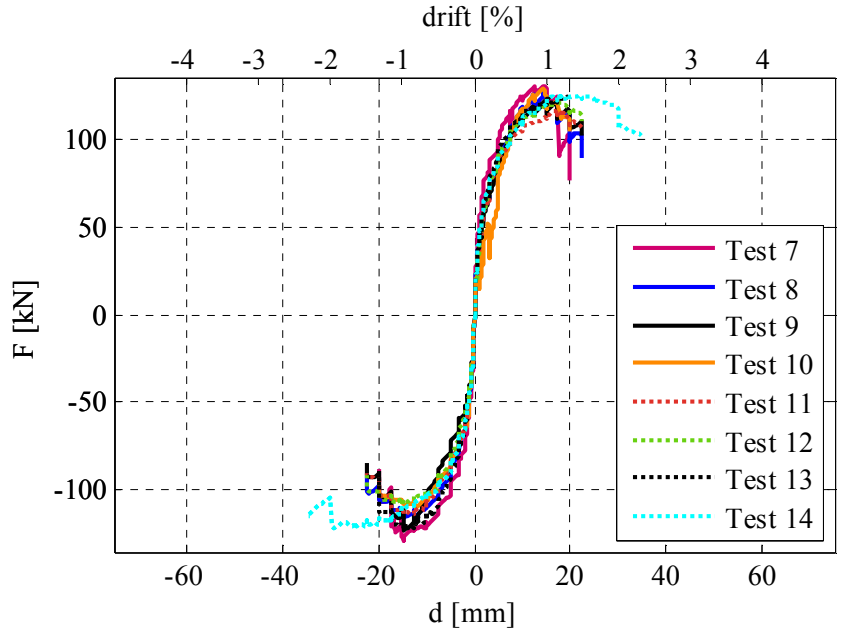

Figure 3.44: Hysteretic envelopes of lateral load - lateral displacement responses for tests 7-14
Slika 3.44: Histerezne ovojnice odziva horizontalna sila - horizontalni pomik za teste 7-14

For the idealization of curves, criteria of equal energy input of the idealized and experimental response was assumed, ultimate displacement was limited to displacement d_u, at which the shear resistance decreases to 80% of maximum resistance obtained, and K_{ef} was initially presumed according to two different criteria (Eq. 3.6 and Eq. 3.7):

$$K_{ef} = \frac{2/3 \cdot F_{\max}}{d_{2/3 \cdot F_{\max}}}, \qquad \textbf{3.6}$$

$$K_{ef} = \frac{F_{cr}}{d_{cr}} \qquad \textbf{3.7}$$

where displacement $d_{2/3Fmax}$ is defined as the displacement, where the resistance reaches two thirds of the maximum resistance obtained (2/3 F_{max}), d_{cr} the displacement, where first shear crack was observed, and F_{cr} the corresponding lateral force. Idealisation of the hysteresis envelope with K_{ef} determined at 2/3 F_{max} is presented in Figure 3.45.

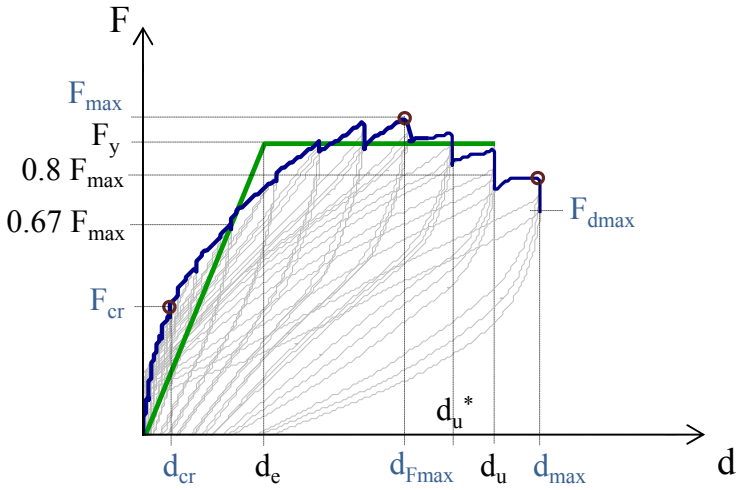

Figure 3.45: Bi-linear idealisation of the hysteresis envelope according to criterion "2/3 F_{max}"
Slika 3.45: Bi-linearna idealizacija histerezne ovojnice po kriteriju "2/3 F_{max}"

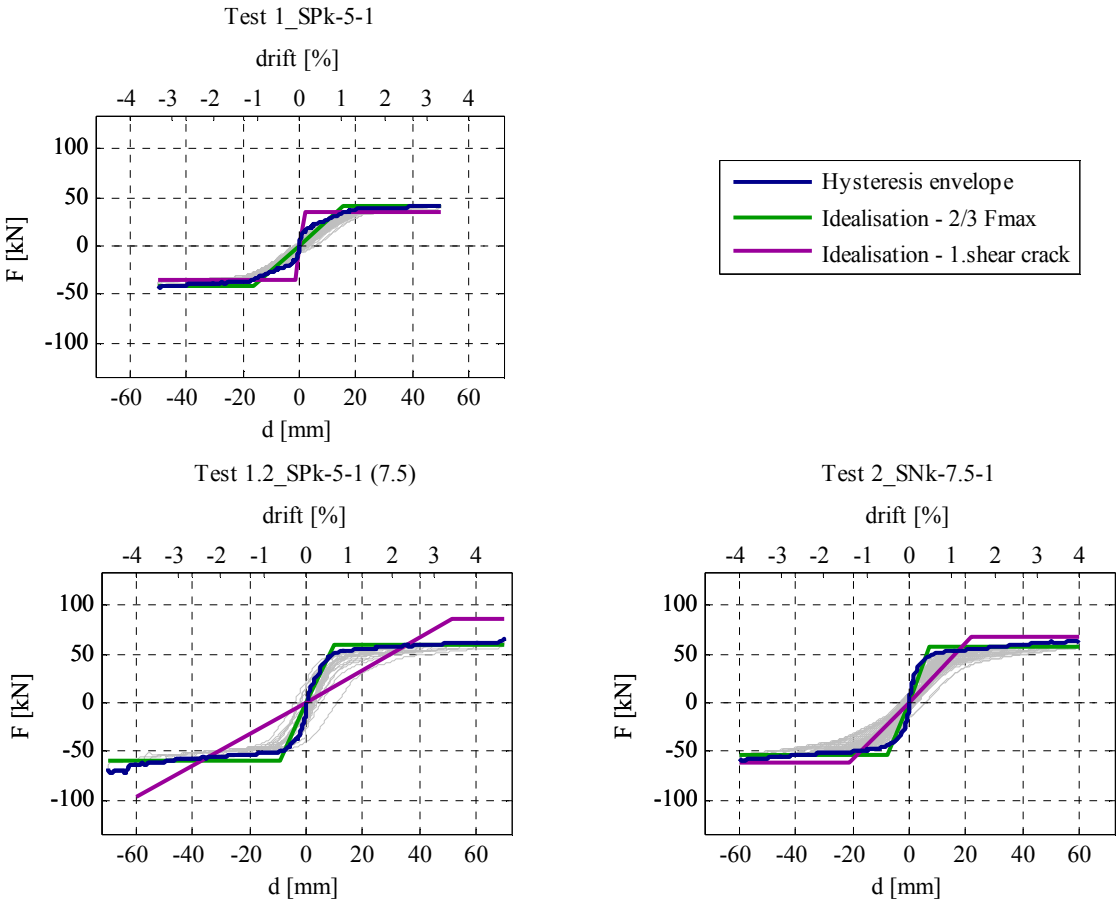

Figure 3.46: Hysteresis envelopes and bi-linear curves obtained according to two criteria for tests 1-2
Slika 3.46: Histerezne ovojnice in bi-linearna idealizacija po dveh kriterijih za teste 1-2

From the idealised curves in Figure 3.46 it is apparent, that due to the prevailing rocking mechanism in some combinations of pre-compression level and boundary conditions, the criterion for determining K_{ef} at d_{cr} is not appropriate, as not only that it cannot produce representative curves but for some cases the calculation of the idealised curve is not feasible (see Test 1.2 in Figure 3.46). Therefore in the following analysis only the results gained considering the 1st criterion (K_{ef} determined at 2/3 F_{max}) are evaluated and presented (Figures 3.47 and 3.48).

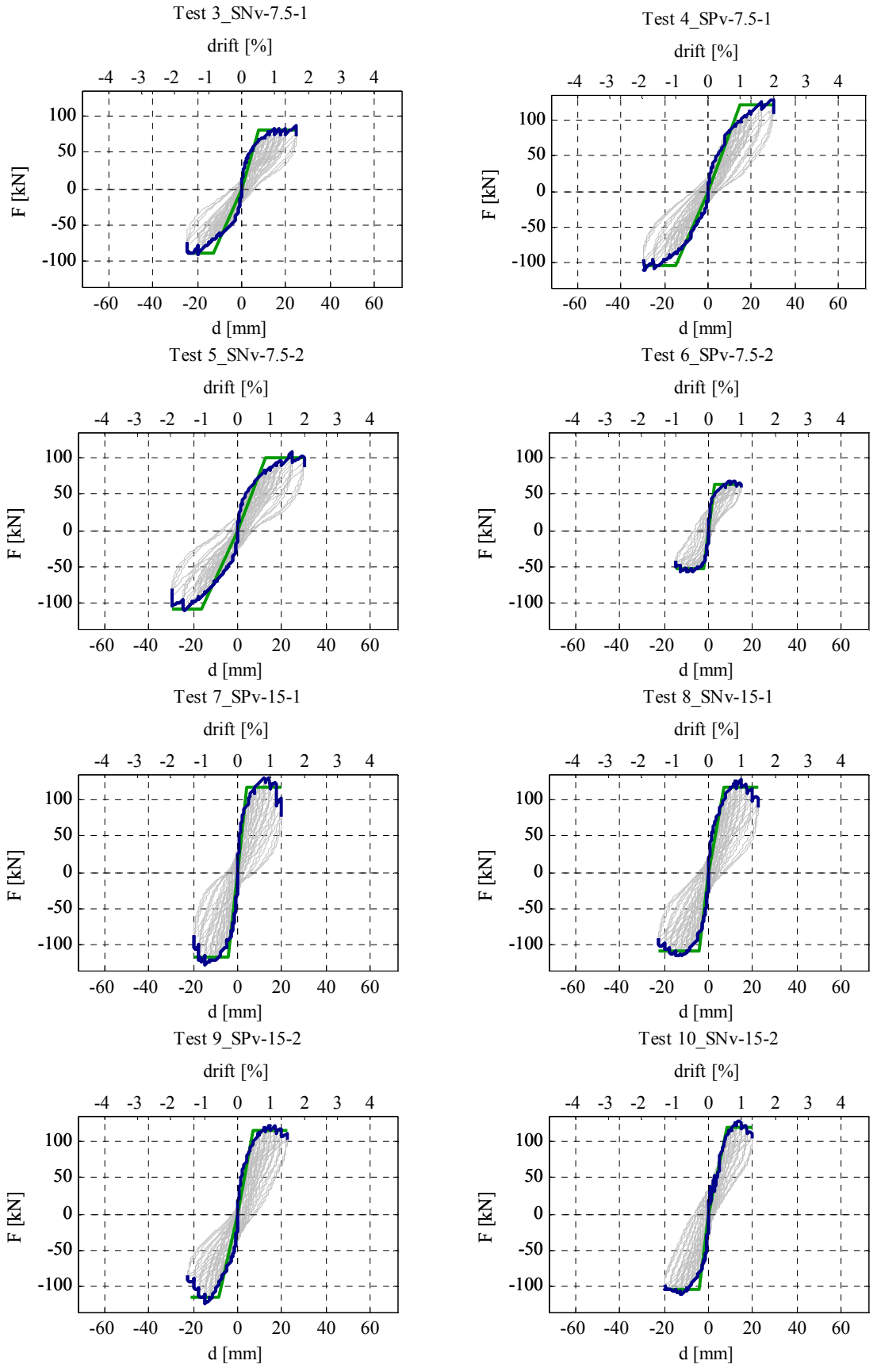

Figure 3.47: Hysteresis envelopes and bi-linear curves obtained according to criteria K_{ef}= K_{ef} (2/3 F_{max}) for tests 3-10
Slika 3.47: Histerezne ovojnice in bi-linearna idealizacija po kriteriju K_{ef} = K_{ef} (2/3 F_{max}) za teste 3-10

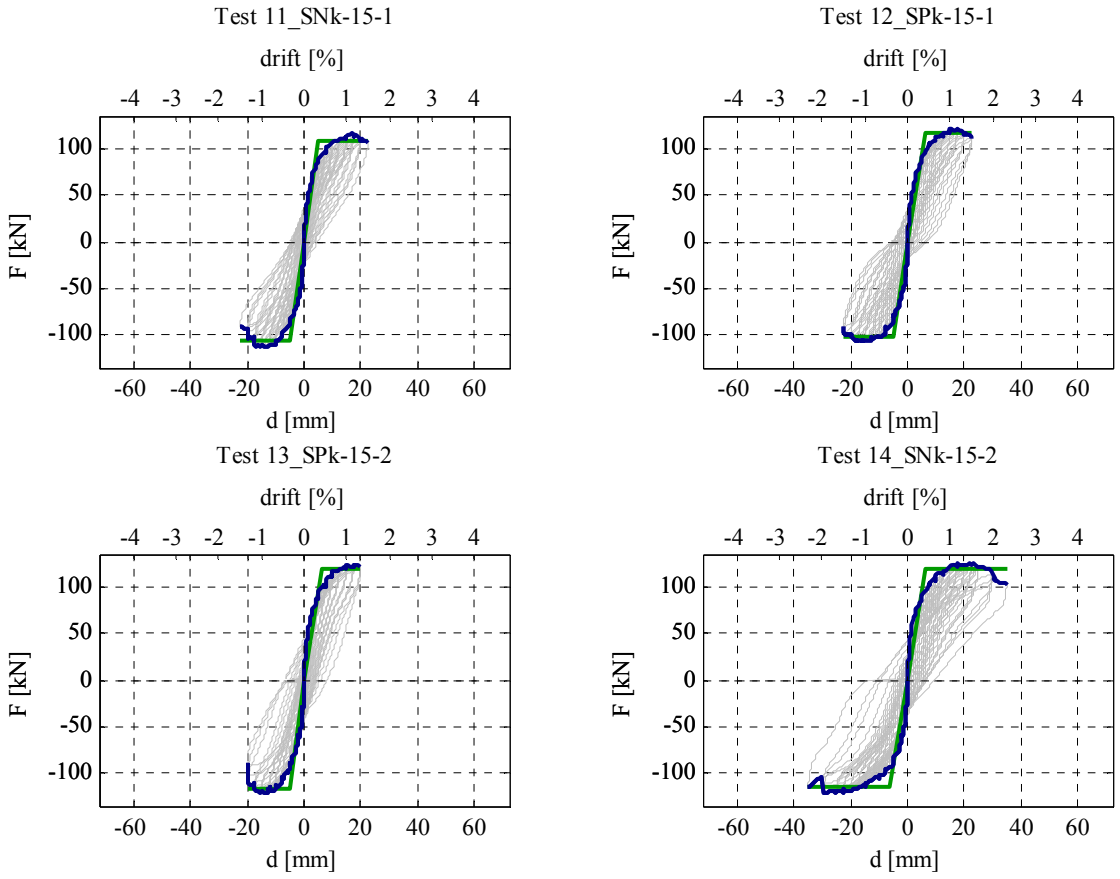

Figure 3.48: Hysteresis envelopes and bi-linear curves obtained according to criteria $K_{ef} = K_{ef}$ (2/3 F_{max}) for tests 11-14
Slika 3.48: Histerezne ovojnice in bi-linearna idealizacija po kriteriju $K_{ef} = K_{ef}$ (2/3 F_{max}) za teste 11-14

From the idealized curves (effective stiffness K_{ef} and idealized resistance F_{id}), idealized elastic displacement d_e was obtained (Eq. 3.8). One of the most common indicators of the non-linear behaviour when subjected to lateral loading is the ductility coefficient μ, which is a characteristic of the idealised curve; i.e. the ratio between the ultimate lateral displacement d_u and the idealized elastic displacement d_e (Eq. 3.9). With regard to displacement d_u^* (see Figure 3.45), also corresponding ductility μ^* was for the purpose of comparison calculated according to Eq. 3.10.

$$d_e = \frac{F_{id}}{K_{ef}}, \qquad \textbf{3.8}$$

$$\mu = \frac{d_u}{d_e} \qquad \textbf{3.9}$$

$$\mu^* = \frac{d_u^*}{d_e} \qquad \textbf{3.10}$$

Characteristic values of calculated bi-linearly idealised curves are for both loading directions (indices + and – representing positive and negative direction) summarized in Table 3.16.

Preglednica 3.16: Vrednosti v karakterističnih točkah bi-linearno idealiziranih diagramov sila - pomik za obe smeri obremenjevanja

Table 3.16: Values of bi-linearly idealised force - displacement diagrams in characteristic points for each directions of loading

Test	F_{id}^{+} [kN]	F_{id}^{-} [kN]	d_e^{+} [mm]	d_e^{-} [mm]	K_{ef}^{+} [kN/mm]	K_{ef}^{-} [kN/mm]	d_u^{+} [mm]	d_u^{-} [mm]	μ^{+}	μ^{-}
1-SPk-5-1	41.0	-40.6	15.75	-16.30	2.6	2.5	49.8	-49.8	3.17	3.06
1.2-SPk-7.5-1	59.3	-59.8	9.97	-9.31	5.9	6.4	69.8	-69.7	7.00	7.49
2-SNk-7.5-1	58.5	-53.6	6.80	-7.57	8.6	7.1	59.8	-59.8	8.79	7.90
3-SNv-7.5-1	79.9	-89.1	7.67	-12.83	10.4	6.9	24.9	-24.8	3.25	1.94
4-SPv-7.5-1	120.6	-103.2	14.92	-14.84	8.1	7.0	29.9	-29.8	2.00	2.01
5-SNv-7.5-2	99.5	-108.8	12.74	-16.19	7.8	6.7	29.9	-29.8	2.34	1.84
6-SPv-7.5-2	62.5	-52.4	2.81	-1.97	22.3	26.6	14.9	-14.9	5.32	7.58
7-SPv-15-1	117.5	-116.0	4.32	-3.92	27.2	29.6	19.9	-19.9	4.61	5.08
8-SNv-15-1	117.6	-107.2	6.77	-4.32	17.4	24.8	22.4	-22.4	3.31	5.18
9-SPv-15-2	114.8	-115.3	6.68	-8.55	17.2	13.5	22.4	-21.3	3.35	2.48
10-SNv-15-2	118.7	-102.9	8.24	-4.05	14.4	25.4	19.9	-19.9	2.41	4.91
11-SNk-15-1	108.6	-105.6	5.09	-4.71	21.3	22.4	22.4	-22.4	4.40	4.75
12-SPk-15-1	116.0	-102.6	6.06	-4.81	19.1	21.3	22.4	-22.4	3.69	4.66
13-SPk-15-2	119.5	-116.3	6.02	-5.02	19.8	23.2	19.9	-19.9	3.30	3.97
14-SNk-15-2	118.0	-114.5	6.58	-6.24	17.9	18.4	34.9	-34.8	5.30	5.59

For the purpose of comparison, in Table 3.17 besides the average values for both directions also displacement of the intersection of the idealised curve with the envelope (d_u^{*}) and corresponding ductility coefficient (μ^{*}) are presented.

Preglednica 3.17: Povprečne vrednosti karakterističnih točk bi-linearnih idealiziranih diagramov sila - pomik obeh smeri obremenjevanja

Table 3.17: Average values of bi-linearly idealised force - displacement diagrams in characteristic points of both directions

Test	F_{id} [kN]	d_e [mm]	K_{ef} [kN/mm]	d_u [mm]	μ	d_u^{*} [mm]	μ^{*}
1-SPk-5-1	40.8	16.02	2.55	49.8	3.11	/	/
1.2-SPk-7.5-1	59.5	9.64	6.18	69.7	7.24	/	/
2-SNk-7.5-1	56.1	7.18	7.85	59.8	8.35	/	/
3-SNv-7.5-1	84.5	10.25	8.68	24.9	2.59	22.4	2.40
4-SPv-7.5-1	111.9	14.88	7.52	29.9	2.01	29.9	2.01
5-SNv-7.5-2	104.2	14.46	7.27	29.9	2.09	24.9	1.74
6-SPv-7.5-2	57.4	2.39	24.4	14.9	6.45	11.2	4.75
7-SPv-15-1	116.7	4.12	28.4	19.9	4.85	14.9	3.63
8-SNv-15-1	112.4	5.55	21.1	22.4	4.24	16.2	3.12
9-SPv-15-2	115.0	7.61	15.3	21.8	2.92	16.2	2.18
10-SNv-15-2	110.8	6.15	19.9	19.9	3.66	16.2	3.05
11-SNk-15-1	107.1	4.90	21.9	22.4	4.58	18.7	3.80
12-SPk-15-1	109.3	5.44	20.2	22.4	4.17	19.9	3.71
13-SPk-15-2	117.9	5.52	21.5	19.9	3.64	17.4	1.74
14-SNk-15-2	116.3	6.41	18.1	34.9	5.44	29.8	4.66

Values d_u^* and μ^* could not be calculated for tests 1-2 because the force decrease was in these tests not obtained. In Tables 3.18 and 3.19, average values obtained for walls with the same pre-compression level and boundary condition and the developed failure mechanism are presented.

Preglednica 3.18: Povprečne vrednosti karakterističnih točk bi-linearno idealiziranih diagramov sila - pomik (s c.o.v.) glede na nivo vertikalnih obremenitev ter robne pogoje

Table 3.18: Average values of bi-linearly idealised force - displacement diagrams characteristic points with c.o.v. for the same pre-compression level and boundary condition applied

Pre-compression level, Boundary conditions	F_{id} [kN]	c.o.v. [%]	d_e [mm]	c.o.v. [%]	K_{ef} [kN/mm]	c.o.v. [%]	d_u [mm]	c.o.v. [%]	μ	c.o.v. [%]
7.5% f_{Mc}, cantilever	57.8	3.0	8.4	14.6	7.0	11.8	64.8	7.7	7.80	7.1
7.5% f_{Mc}, fixed-fixed	100.2	11.5	13.2	15.8	7.8	7.9	28.2	8.3	2.23	11.6
15% f_{Mc}, fixed-fixed	113.7	2.0	5.9	21.4	21.2	22.1	21.0	5.3	3.92	18.2
15% f_{Mc}, cantilever	112.6	4.0	5.6	9.7	20.4	7.1	24.9	23.5	4.46	14.8

Preglednica 3.19: Povprečne vrednosti karakterističnih točk bi-linearnih idealiziranih diagramov sila - pomik s c.o.v. glede na dobljeni porušni mehanizem

Table 3.19: Average values of bi-linearly idealised force - displacement diagrams characteristic points with c.o.v. for the same prevailing failure mechanism obtained

Prevailing failure mechanism	F_{id} [kN]	c.o.v. [%]	d_e [mm]	c.o.v. [%]	K_{ef} [kN/mm]	c.o.v. [%]	d_u [mm]	c.o.v. [%]	μ	c.o.v. [%]
Rocking	52.1	15.6	10.9	34.0	5.53	40.0	59.8	13.6	6.23	36.1
Mixed	100.2	11.5	13.2	15.8	7.82	7.9	28.2	8.3	2.23	11.6
Shear	113.2	3.2	5.7	17.1	20.81	16.8	22.9	20.2	4.19	17.6

Also from Tables 3.18 and 3.19, the influence of both testing conditions and failure mechanisms obtained during the testing is clear. The same comments as for F_{max} and d_{max} (discussed earlier) apply also for F_{id} and d_u. Regarding the evaluation of the effective stiffness K_{ef} of the wall; K_{ef} was higher in case of applied fixed-fixed boundary than in case of cantilever boundary conditions. Stiffness increase due to higher pre-compression level is also apparent.

In theory, boundary conditions should influence the stiffness, the level of the vertical load however not. It can be concluded that the attained K_{ef} were highly dependent of the developed damage mechanism and that determining the stiffness of masonry elements analytically according to Eq. 2.54 by also considering boundary conditions is questionable in case of historic masonry.

Comparing the ductility μ of the walls, it can be seen that cantilever boundary conditions produce higher μ (as do ultimate displacements); by 138% in case of lower pre-compression level and by 13.8% in case of higher pre-compression level. Even more obvious is the difference of μ obtained for the same prevailing failure mechanisms. Rocking in average exhibits by 48.9% higher μ than obtained with shear failure and by 179% higher than obtained with mixed mechanism. In average more than 2-times higher elastic displacements obtained with mixed mechanism compared to shear mechanism, result from lower effective stiffness and are the main reason for such low μ in case of mixed mechanism. In terms of μ, mixed mechanism has proved to be the less favourable.

3.4.5 Performance evaluation of walls as structural elements

3.4.5.1 Performance in terms of lateral drifts

Following the performance limit states evaluation, the results for all walls in terms of drifts θ are for both directions of the walls' loading as well as for their average values presented in Table 3.20 and in Figure 3.49. Average results considering different testing conditions and failure modes are summarized in Tables 3.21 and 3.22. Drifts θ are for all walls, regardless the boundary conditions applied, calculated as average rotations of the entire specimens according to Eq. 2.55.

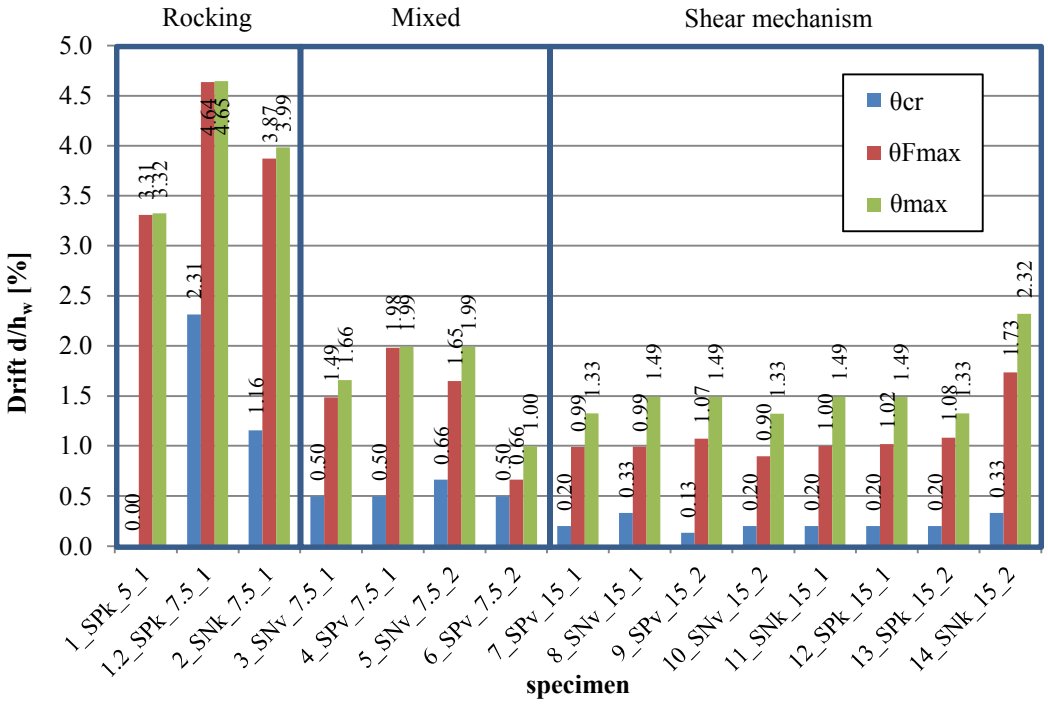

Figure 3.49: Average drifts d/h_w for both directions in characteristic performance limit states for each test
Slika 3.49: Povprečni zasuki d/h_w obeh smeri obremenjevanja v karakterističnih točkah odziva za posamezne teste

Preglednica 3.20: Zasuki v karakterističnih točkah histereznih ovojnic v obeh smereh obremenjevanja

Table 3.20: Drifts at characteristic limit states of hysteretic envelopes for both directions of loading

Limit state	First shear crack			Maximum force			Maximal displacement		
Test	Θ_{cr}^{+} [%]	Θ_{cr}^{-} [%]	Θ_{cr} (av.) [%]	Θ_{Fmax}^{+} [%]	Θ_{Fmax}^{-} [%]	Θ_{Fmax} (av.) [%]	Θ_{max}^{+} [%]	Θ_{max}^{-} [%]	Θ_{max} (av.) [%]
1-SPk-5-1	0.00	0.00	0.00	3.31	-3.31	3.31	3.32	-3.32	3.32
1.2-SPk-7.5-1	2.32	-2.31	2.31	4.64	-4.63	4.64	4.65	-4.65	4.65
2-SNk-7.5-1	1.16	-1.16	1.16	3.78	-3.97	3.87	3.99	-3.99	3.99
3-SNv-7.5-1	0.50	-0.49	0.50	1.66	-1.32	1.49	1.66	-1.66	1.66
4-SPv-7.5-1	0.50	-0.50	0.50	1.99	-1.98	1.98	1.99	-1.99	1.99
5-SNv-7.5-2	0.66	-0.66	0.66	1.65	-1.65	1.65	1.99	-1.99	1.99
6-SPv-7.5-2	0.50	-0.50	0.50	0.66	-0.66	0.66	1.00	-1.00	1.00
7-SPv-15-1	0.20	-0.20	0.20	0.99	-0.99	0.99	1.33	-1.33	1.33
8-SNv-15-1	0.33	-0.33	0.33	0.99	-0.99	0.99	1.49	-1.49	1.49
9-SPv-15-2	0.13	-0.13	0.13	1.16	-0.99	1.07	1.49	-1.49	1.49
10-SNv-15-2	0.20	-0.20	0.20	0.97	-0.82	0.90	1.33	-1.32	1.33

Continues…

…continuation of Table 3.20

11-SNk-15-1	0.20	-0.20	0.20	1.13	-0.87	1.00	1.49	-1.49	1.49
12-SPk-15-1	0.20	-0.20	0.20	1.01	-1.02	1.02	1.49	-1.49	1.49
13-SPk-15-2	0.20	-0.20	0.20	1.32	-0.84	1.08	1.33	-1.33	1.33
14-SNk-15-2	0.33	-0.33	0.33	1.49	-1.98	1.73	2.32	-2.32	2.32

Different maximum displacement capacity obtained during tests and its dependence on the failure mechanism was already partly discussed and commented within the hysteretic response evaluation. There was however no comment on the values of other performance limit states obtained (d_{cr} and d_{Fmax}) and evaluation of characteristic displacements (or drifts) of bi-linear curves. Their comparisons to characteristic limit states of hysteretic envelopes, their comparisons in dependence of testing conditions applied and failure mechanism obtained, and finally, comparison to recommendations of drift limits provided in various code provisions are provided hereafter. In Tables 3.21 and 3.22 therefore also average drifts for characteristic limit states on the bi-linear curves calculated for the same testing conditions and failure mechanisms obtained are presented, respectively.

Since in the EC8-3 and FEMA code provisions the limit states of bi-linear diagrams are provided, results of tests in terms of drifts at displacements d_e and d_u or d_u^* are compared. In Table 3.23 drift limits according to EC8-3 and FEMA recommendations for obtained mechanisms, with regard to slenderness of the tested walls and boundary conditions applied, are provided.

Preglednica 3.21: Povprečni zasuki s c.o.v. v karakterističnih točkah histereznih ovojnic in bi-linearno idealiziranih krivulj za teste z enakim nivojem vertikalnih obremenitev in robnimi pogoji

Table 3.21: Average drifts with c.o.v. at characteristic limit states of hysteretic envelopes and of bi-linearly idealised curves for tests with the same pre-compression level and boundary conditions applied

	Hysteresis envelopes					
Limit state	First shear crack		Maximum force		Maximum displacement	
Pre-compression level, Boundary conditions	Θ_{cr} [%]	c.o.v. [%]	Θ_{Fmax} [%]	c.o.v. [%]	Θ_{max} [%]	c.o.v. [%]
7.5% f_{Mc}, cantilever	1.74	33.3	4.25	9.0	4.32	7.7
7.5% f_{Mc}, fixed-fixed	0.55	14.2	1.71	12.1	1.88	8.3
15% f_{Mc}, fixed-fixed	0.22	33.5	0.99	6.3	1.41	5.9
15% f_{Mc}, cantilever	0.23	24.8	1.21	25.3	1.66	23.5
	Bi-linearly idealised curves					
Limit state	Elastic displacement		Ultimate displacement		Ultimate displacement*	
Pre-compression level, Boundary conditions	Θ_e [%]	c.o.v. [%]	Θ_u [%]	c.o.v. [%]	Θ_u^* [%]	c.o.v. [%]
7.5% f_{Mc}, cantilever	0.56	14.6	4.32	7.7	/	/
7.5% f_{Mc}, fixed-fixed	0.88	15.8	1.88	8.3	1.71	12.1
15% f_{Mc}, fixed-fixed	0.39	21.4	1.40	5.3	1.06	3.4
15% f_{Mc}, cantilever	0.37	9.7	1.66	23.5	1.43	22.9

*Drift corresponding to displacement d_u^*

Preglednica 3.22: Povprečni zasuki s c.o.v. v karakterističnih točkah histereznih ovojnic in bi-linearno idealiziranih krivulj za teste z enakim porušitvenim mehanizmom

Table 3.22: Average drifts and c.o.v. at characteristic limit states of hysteretic envelopes and of bi-linearly idealised curves for the tests with the same prevailing failure mechanism obtained

	Hysteresis envelopes					
Limit state	First shear crack		Maximum force		Maximum displacement	
Prevailing failure mechanism	Θ_{cr} [%]	c.o.v. [%]	Θ_{Fmax} [%]	c.o.v. [%]	Θ_{max} [%]	c.o.v. [%]
Rocking	1.74	33.3	3.94	12.8	3.99	12.5
Mixed	0.55	14.2	1.71	12.1	1.88	8.3
Shear	0.22	29.4	1.10	22.5	1.53	20.1
	Bi-linearly idealised curves					
Limit state	Elastic displacement		Ultimate displacement		Ultimate displacement*	
Prevailing failure mechanism	Θ_e [%]	c.o.v. [%]	Θ_u [%]	c.o.v. [%]	Θ_u^* [%]	c.o.v. [%]
Rocking	0.73	34.0	3.99	13.6	/	/
Mixed	0.88	15.8	1.88	8.3	1.71	12.1
Shear	0.38	17.1	1.53	20.2	1.24	24.0

*Drift corresponding to displacement d_u^*

Preglednica 3.23: Priporočene vrednosti zasukov po EC8-3 in FEMA predpisih glede na vitkost testiranih zidov in robne pogoje testov

Table 3.23: Recommended drift limits according to EC8-3 and FEMA code provisions considering specific slenderness of the tested walls and boundary conditions applied

		Drift limits [%]					
Code	Prevailing failure mechanism	Rocking			Shear		
EC8-3	Limit state	DL	SD	NC	DL	SD	NC
	Drift	/*	0.8 h_0/l_w	4/3 θ_{SD}	/*	0.4	4/3 θ_{SD}
	Cantilever	/*	1.20	1.60	/*	0.4	0.53
	Fixed-fixed	/*	0.60	0.80	/*		
FEMA	Limit state	IO	LS	CP	IO	LS	CP
	Drift	0.1	0.3 h_0/l_w	0.4 h_0/l_w	/**	/**	/**
	Cantilever	0.1	0.45	0.60	/**	/**	/**
	Fixed-fixed		0.225	0.30	/**	/**	/**

*drift limits are determined analytically from stiffness and resistance of the wall

**shear mechanism is according to FEMA in general considered as a brittle mechanism and is consequently force-controlled

Drift values provided in Table 3.23 for obtained rocking mechanism for walls of slenderness and boundary condition (cantilever) as in our tests, are for drifts at collapse ("NC" or "CP") 1.60% according to EC8-3 and 0.60% according to FEMA. These values are exceeded significantly in our tests; drifts are 149% higher than those recommended by EC8-3 and 564% than those by FEMA. Regarding drifts at elastic displacement of the bi-linear curve, which can be compared to "IO" drift limit equal to 0.1% provided in FEMA, average drift obtained at tests is by 630% higher.

In case of shear mechanism, drift limits are only provided according to EC8-3; for limit state at collapse (NC) 0.53% is provided. This value is exceeded no matter to which limit state it is compared; d_{max} or d_u^*; d_{max} is higher by 188% and d_u^* by 133%, respectively.

In the following, characteristic displacement (or drift) limit states of both hysteretic envelopes as well as of idealised bi-linear curves are analysed relatively to each other. Tables 3.24 - 3.26 various ratios

for each test and average values for tests with the same testing conditions and failure mechanism obtained are presented for drift limit states of hysteretic envelopes, whereas in Tables 3.27 - 3.29 for drift limit states of both bi-linear curves and hysteretic envelopes.

Preglednica 3.24: Razmerja med posameznimi pomiki (oz. zasuki) v karakterističnih točkah histereznih ovojnic

Table 3.24: Ratios between displacements (or drifts) in various characteristic limit states of hysteretic envelopes

Test	d_{cr}/d_{Fmax}	d_{Fmax}/d_{max}	d_{cr}/d_{max}
1-SPk-5-1	0.000	0.995	0.000
1.2-SPk-7.5-1	0.499	0.997	0.498
2-SNk-7.5-1	0.299	0.972	0.291
3-SNv-7.5-1	0.333	0.897	0.299
4-SPv-7.5-1	0.250	0.996	0.249
5-SNv-7.5-2	0.401	0.829	0.333
6-SPv-7.5-2	0.750	0.664	0.498
7-SPv-15-1	0.201	0.745	0.150
8-SNv-15-1	0.334	0.664	0.222
9-SPv-15-2	0.123	0.718	0.089
10-SNv-15-2	0.222	0.676	0.150
11-SNk-15-1	0.199	0.668	0.133
12-SPk-15-1	0.196	0.681	0.133
13-SPk-15-2	0.183	0.816	0.150
14-SNk-15-2	0.191	0.747	0.143

Preglednica 3.25: Povprečne vrednosti razmerij med pomiki v karakterističnih točkah histereznih ovojnic za teste z enakimi vertikalnimi obremenitvami in robnimi pogoji

Table 3.25: Average values of ratios between displacements in various characteristic limit states of hysteretic envelopes for tests with the same pre-compression level and boundary conditions applied

Pre-compression level, Boundary conditions	d_{cr}/d_{Fmax}	d_{Fmax}/d_{max}	d_{cr}/d_{max}
7.5% f_{Mc}, cantilever	0.399	0.984	0.394
7.5% f_{Mc}, fixed-fixed	0.328	0.907	0.294
15% f_{Mc}, fixed-fixed	0.220	0.701	0.152
15% f_{Mc}, cantilever	0.192	0.728	0.140

Preglednica 3.26: Povprečne vrednosti razmerij med pomiki v karakterističnih točkah histereznih ovojnic za teste z enakim porušnim mehanizmom

Table 3.26: Average values of ratios between displacements in various characteristic limit states of hysteretic envelopes for tests where the same prevailing failure mechanism was obtained

Prevailing failure mechanism	d_{cr}/d_{Fmax}	d_{Fmax}/d_{max}	d_{cr}/d_{max}
Rocking	0.399	0.988	0.394
Mixed	0.328	0.907	0.294
Shear	0.206	0.714	0.146

The occurrence of the first shear cracks is as expected evidently dependent from the obtained mechanism; it occurs first in walls where shear mechanism is activated and last, if at all, if rocking

mechanism is the prevailing mode. Also limit state d_{Fmax} occurs in our tests at an earlier stage relatively to the occurrence of d_{max} in case of shear mechanism (at 71.4% d_{max}) than in case of mixed (at 90.7% d_{max}) and rocking mechanism (at 98.8% d_{max}). This raises the question, whether ”SD” or ”LS” limit states, defined in provisions, are referred to this state; and if so; would it be more appropriate to determine these limit states with regard to failure mechanism obtained. For both EC8-3 and FEMA the drift at limit state of ”SD” or ”LS” is provided as 3/4 of drift at collapse (“NC” or ”CP”). Nevertheless, this value seems to correspond to obtainment of maximum force in case of shear mechanism, as according to our tests this value is 0.714. For other failure modes the value in provisions, if it indeed corresponds to drift at F_{max}, is conservative compared to our test results. On the other hand, another point regarding the actual response possibly corresponding to limit state ”SD” or ”LS” could be the consideration of the displacement/drift d_u^*. It’s consideration would make sense looking from the designers point of view, as up to this point, the actual resistance of the response is always higher or equal to the one supposed (f_{Mt} of the walls is calculated from resistance of idealised bi-linear curve and if diagonal cracking occurred in the wall, this calculated resistance would be, compared to the actual response, ensured up to d_u^*).

Preglednica 3.27: Razmerja med posameznimi pomiki karakterističnih točk histereznih ovojnic in bi-linearno idealiziranih krivulj za posamezne teste

Table 3.27: Ratios between displacements in various characteristic limit states of both hysteretic envelope and idealised bi-linear curve for each test

Test	d_{Fmax}/d_u	d_{Fmax}/d_u^*	d_u/d_{max}	d_u^*/d_{max}	d_u^*/d_u	μ/μ^*
1-SPk-5-1	1.00	0.99	1.000	/	/	/
1.2-SPk-7.5-1	1.00	/	1.000	/	/	/
2-SNk-7.5-1	0.97	/	1.000	/	/	/
3-SNv-7.5-1	0.90	1.00	1.000	0.900	0.900	1.081
4-SPv-7.5-1	1.00	1.00	1.000	1.000	1.000	1.000
5-SNv-7.5-2	0.83	0.99	1.000	0.833	0.833	1.200
6-SPv-7.5-2	0.66	0.88	1.000	0.751	0.751	1.358
7-SPv-15-1	0.75	0.99	1.000	0.750	0.750	1.334
8-SNv-15-1	0.66	0.92	1.000	0.723	0.723	1.360
9-SPv-15-2	0.74	0.99	0.975	0.722	0.740	1.342
10-SNv-15-2	0.68	0.83	1.000	0.813	0.813	1.198
11-SNk-15-1	0.67	0.80	1.000	0.833	0.833	1.203
12-SPk-15-1	0.68	0.77	1.000	0.888	0.888	1.126
13-SPk-15-2	0.82	0.93	1.000	0.874	0.875	1.048
14-SNk-15-2	0.75	0.87	1.000	0.856	0.856	1.168

Preglednica 3.28: Povprečne vrednosti razmerij med pomiki karakterističnih točk histereznih ovojnic in bi-linearih idealizacij za teste z enakim nivojem vertikalnih obremenitev ter robnimi pogoji

Table 3.28: Average values of ratios between displacements in various characteristic limit states of both hysteretic envelopes and idealised bi-linear curves for tests with the same pre-compression level and boundary conditions

Pre-compression level, Boundary conditions	d_{Fmax}/d_u	d_{Fmax}/d_u^*	d_u/d_{max}	d_u^*/d_{max}	d_u^*/d_u	μ/μ^*
7.5% f_{Mc}, cantilever	0.98	/	1.000	/	/	/
7.5% f_{Mc}, fixed-fixed	0.91	1.00	1.000	0.911	0.911	1.094
15% f_{Mc}, fixed-fixed	0.71	0.93	0.994	0.752	0.757	1.309
15% f_{Mc}, cantilever	0.73	0.84	1.000	0.863	0.863	1.136

Preglednica 3.29: Povprečne vrednosti razmerij med pomiki karakterističnih točk histereznih ovojnic in bi-linearih idealizacij za teste z enakim porušnim mehanizmom

Table 3.29: Average values of ratios between displacements in various characteristic limit states of both hysteretic envelopes and idealised bi-linear curves for tests where the same prevailing failure mechanism was obtained

Prevailing failure mechanism	d_{Fmax}/d_u	d_{Fmax}/d_u^*	d_u/d_{max}	d_u^*/d_{max}	d_u^*/d_u	μ/μ^*
Rocking	0.99	/	/	/	/	/
Mixed	0.91	1.00	1.000	0.911	0.911	1.094
Shear	0.71	0.89	0.997	0.807	0.810	1.222

From relative comparison of displacements d_u^* and d_u (Table 3.27), ratios from 0.723 to 1.000 were obtained. Ratio 1.000 was attained at rocking mechanism and is due to the deficient idealisation not relevant, 1.00 was also attained at test 4. This value indicates that a drop of the lateral force was obtained at the same displacement. Average value for shear mechanism of this ratio is 0.81, which is greater than 0.75 as in provisions (in case it is presumed that the limit state "SD" relates to state at d_u^*) and therefore on the safe side. Only for two tests the ratio is lower than 0.75, whereas if d_{Fmax} is compared to d_{max}, the ratio is lower than 0.75 in 8 tests, of which 7 at higher pre-compression level.

According to the results, the difference between d_u^* and d_u is relatively the largest when shear mechanism is attained. It is also noticeably higher for fixed-fixed boundary conditions compared to cantilever (by 24.3% compared to 13.7% for higher pre-compression level, respectively). With regard to these differences also the ductility coefficients for both limit states do not differ inconsiderably; from 0 to 36%. Regarding this observation, a more specific and precise description of the damage state or of the actual (not idealized) capacity of the walls, that is within the code provisions related to "NC" and "CP" limit states, is lacking.

3.4.5.2 Performance in terms of shear resistance

Shear resistance (lateral forces) at characteristic limit states was already provided within Section 3.4.4 and idealised shear resistance within Section **2.3.2.3**. In the following, the ratios between shear resistances at characteristic limit states of hysteretic response as well as of bi-linear curves are presented; in Table 3.30 for each test separately and in Tables 3.31 and 3.32 the average results for the same testing conditions and failure modes obtained.

Preglednica 3.30: Razmerja med posameznimi strižnimi silami v karakterističnih točkah histereznih ovojnic in bi-linearno idealiziranih krivulj za posamezne teste

Table 3.30: Ratios between shear resistances in various characteristic limit states of hysteretic envelopes and idealised bi-linear curves for each test

Test	F_{cr}/F_{max}	F_{dmax}/F_{max}	F_{id}/F_{max}	F_{dmax}/F_{id}
1-SPk-5-1	0.000	0.977	0.970	1.008
1.2-SPk-7.5-1	0.842	0.964	0.869	1.110
2-SNk-7.5-1	0.840	0.975	0.907	1.076
3-SNv-7.5-1	0.694	0.828	0.958	0.864
4-SPv-7.5-1	0.508	0.848	0.934	0.908
5-SNv-7.5-2	0.670	0.764	0.956	0.799
6-SPv-7.5-2	0.972	0.820	0.927	0.884

Continues…

…continuation of Table 3.30

7-SPv-15-1	0.630	0.634	0.903	0.701
8-SNv-15-1	0.707	0.745	0.927	0.803
9-SPv-15-2	0.430	0.766	0.942	0.814
10-SNv-15-2	0.511	0.845	0.928	0.910
11-SNk-15-1	0.596	0.861	0.935	0.921
12-SPk-15-1	0.578	0.885	0.959	0.923
13-SPk-15-2	0.589	0.854	0.962	0.888
14-SNk-15-2	0.783	0.873	0.940	0.929

Preglednica 3.31: Povprečne vrednosti razmerij med strižnimi silami v karakterističnih točkah histereznih ovojnic in bi-linearih idealizacij za teste z enakim nivojem vertikalnih obremenitev ter robnimi pogoji

Table 3.31: Average values of ratios between shear resistances in various characteristic limit states of both hysteretic envelopes and idealised bi-linear curves for tests with the same pre-compression level and boundary conditions

Pre-compression level, Boundary conditions	F_{cr}/F_{max}	F_{dmax}/F_{max}	F_{id}/F_{max}	F_{dmax}/F_{id}
7.5% f_{Mc}, cantilever	0.841	0.970	0.888	1.093
7.5% f_{Mc}, fixed-fixed	0.624	0.813	0.949	0.857
15% f_{Mc}, fixed-fixed	0.569	0.748	0.925	0.807
15% f_{Mc}, cantilever	0.635	0.868	0.949	0.915

Preglednica 3.32: Povprečne vrednosti razmerij med strižnimi silami v karakterističnih točkah histereznih ovojnic in bi-linearih idealizacij za teste z enakim porušnim mehanizmom

Table 3.32: Average values of ratios between shear resistances in various characteristic limit states of both hysteretic envelopes and idealised bi-linear curves for tests where the same prevailing failure mechanism was obtained

Prevailing failure mechanism	F_{cr}/F_{max}	F_{dmax}/F_{max}	F_{id}/F_{max}	F_{dmax}/F_{id}
Rocking	0.841	0.972	0.915	1.065
Mixed	0.624	0.813	0.949	0.857
Shear	0.602	0.808	0.937	0.861

Shear resistance at first shear crack F_{cr} ranged from 43.0% to 97.2% of maximum resistance F_{max}, where the later was obtained for test 6. With changing the failure mechanism from rocking to shear, F_{cr} relatively decreased (compared to F_{max}) and was according to tests in average 60.2% F_{max} for shear mechanism. This confirms the choice of calculating effective stiffness at 2/3 of F_{max} for calculation of bi-linear curve in case the shear mechanism develops.

Analysing the post-peak resistance F_{dmax} of the walls tested, the results show up to 36.6% decrease (obtained at test 7) compared to F_{max} obtained. This drop refers to 3rd cycles of loading. Strength degradation through increasing of amplitude displacements and cycle repetitions will be more thoroughly discussed within Section 3.4.7. Again the highest drop was obtained where shear mechanism developed (in average 19.2%), whereas at rocking mechanism this decrease was only minor (2.8%). Higher decrease was proved for fixed-fixed compared to cantilever boundary conditions. The value of C_{sd} by Tomaževič 0.4-0.8 [46] (see Section **2.3.2.3**) seems reasonable and so does the limitation to 0.8 F_{max} for idealisation, as deterioration progressed extensively within the repetitions of loading cycles.

Another question of interest is the value of idealised resistance F_{id} compared to F_{max} and F_{dmax}. According to the tests, the F_{id} is at least 90.3% F_{max}, if tests, where rocking mechanism occurred, are not considered, since F_{max} was not achieved. The difference is also similar for all tests except for those where rocking mechanism occurred. Similarly also F_{dmax} compared to F_{id} is in average close for mixed and shear mechanism (85.7% if test 6 is not considered vs. 86.1%). The difference is slightly bigger in dependence from the boundary condition (by higher pre-compression level); 80.7% for fixed-fixed vs. 91.5% for cantilever boundary conditions. In the worst case the difference is lower for 29.9% (test 7).

If a linear static procedure is used for the design of a building or an assessment of an existing one, the deformation capacity of the elements can be taken into account by multiplying the resistance with the ductility coefficient. Ductility coefficient higher than 1.0, is according to FEMA allowed for displacement-controlled components, of which strength is governed either by rocking or by bed-joint sliding. Shear and toe compression mechanisms are believed to be brittle and if none more accurate information is available, such elements are force controlled and ductility should be equal 1.0. The tests performed demonstrated a ductile behaviour also in the case of shear mechanism. In Table 3.33 equivalent elastic resistance for tests, calculated as $F_{id} \cdot \mu$, both obtained from tests, and their average results for the same testing conditions and failure mechanism obtained, are presented. Ductility corresponding to both d_u as well as to d_u^* are considered.

Preglednica 3.33: Ekvivalentne elastične nosilnosti za teste in povprečne vrednosti za teste z enakimi pogoji preskušanja ter enakimi dobljenimi porušnimi mehanizmi

Table 3.33: Equivalent elastic resistances for the tests and average values for the same testing conditions and failure mechanism obtained

Test	Equivalent elastic resistance $F_{id} \cdot \mu$ [kN]	Average $F_{id} \cdot \mu$ Pre-compression level, Boundary conditions [kN]	Average $F_{id} \cdot \mu$ Prevailing failure mechanism [kN]	Equivalent elastic resistance $F_{id} \cdot \mu^*$ [kN]	Average $F_{id} \cdot \mu^*$ Pre-compression level, Boundary conditions [kN]	Average $F_{id} \cdot \mu^*$ Prevailing failure mechanism [kN]
1-SPk-5-1	127	/		/	/	
1.2-SPk-7.5-1	431	450	342	/	/	/
2-SNk-7.5-1	468			/		
3-SNv-7.5-1	219			203		
4-SPv-7.5-1	225	258 (221)	258 (221)	225	220 (203)	220 (203)
5-SNv-7.5-2	218			182		
6-SPv-7.5-2	370			273		
7-SPv-15-1	566			424		
8-SNv-15-1	477	446		351	341	
9-SPv-15-2	336			250		
10-SNv-15-2	406		474	338		391
11-SNk-15-1	490			407	441	
12-SPk-15-1	456	502		405		
13-SPk-15-2	429			409		
14-SNk-15-2	633			542		

If both F_{id} and μ are considered in evaluating of the tests performed, for the tests performed, shear mechanism is without a doubt the most favourable mechanism (474 kN in average), rocking exhibited 342 kN (27.8% less) and the least favourable mechanism is mixed, where in average only 221 kN was obtained (53.3% less as by shear). It has to be noted though, that with rocking mechanism ultimate

displacements were not achieved. Comparing the effect of boundary condition, walls tested under cantilever boundary condition performed overall better as those under fixed-fixed if they are exposed to the same pre-compression level.

3.4.5.3 Mechanical properties of masonry

Tensile strength of masonry f_{Mt} was calculated as an indicator for shear strength of masonry from idealized shear resistance F_{id}, gained from idealized force - displacement curves. It was calculated according to Turnšek and Čačovič as the critical value of principal stress in the centre of the pier, by which the diagonal shear failure occurs (Eq. 3.11)

$$f_{Mt} = -0.5 \cdot \sigma_0 + \sqrt{(0.5 \cdot \sigma_0)^2 + (b \cdot \tau)^2}\,, \qquad \textbf{3.11}$$

For our case, b = 1.5 was assumed, as the walls had aspect ratio equal to 1.5. The average f_{Mt}, calculated from average F_{id} for both directions of loading, is for all tests presented in Table 3.34 and in Figure 3.50, where the results are compared with values recommended for such type of masonry according to Italian code provisions NTC08. Minimum and maximum values according to NTC08 are for such type of masonry 0.135 and 0.18 MPa, respectively.

Preglednica 3.34: Natezne trdnosti f_{Mt} in strižni moduli G_M, izračunani po različnih metodah, za vse izvedene teste

Table 3.34: Tensile strength f_{Mt} and shear moduli G_M, obtained with different methods, for all performed tests

Test	f_{Mt} [MPa]	G_M [MPa]	$K_{1.5\ mm}$ [kN/mm]	$^{**}G_{1.5\ mm}$ [MPa]	$^{***}G_{1.5\ mm}$ [MPa]
1-SPk-5-1	0.064*	13.0	9.4	74.8	35.4
1.2-SPk-7.5-1	0.092*	38.8	0.0	0.0	0.0
2-SNk-7.5-1	0.083*	55.5	16.1	277.2	60.5
3-SNv-7.5-1	0.164	43.6	20.4	119.9	76.6
4-SPv-7.5-1	0.251	37.0	18.7	106.9	70.0
5-SNv-7.5-2	0.226	35.7	21.5	128.5	80.7
6-SPv-7.5-2	0.087	153.0	26.4	170.1	98.9
7-SPv-15-1	0.172	189.5	40.5	339.2	151.8
8-SNv-15-1	0.162	126.7	33.8	247.8	126.7
9-SPv-15-2	0.168	84.0	30.3	208.2	113.4
10-SNv-15-2	0.158	119.4	25.8	164.3	96.6
11-SNk-15-1	0.148	4105	33.0	-291.8	123.6
12-SPk-15-1	0.154	2442	31.4	-322.8	117.8
13-SPk-15-2	0.175	1346	34.4	-268.9	129.2
14-SNk-15-2	0.171	484	34.9	-263.6	130.7

*values obtained are not representative, as rocking mechanism occurred in these tests

**calculated according to Eq. 3.12 (considering both flexural and shear component)

***calculated according to Eq. 3.13 (shear stress τ to shear strain γ ratio)

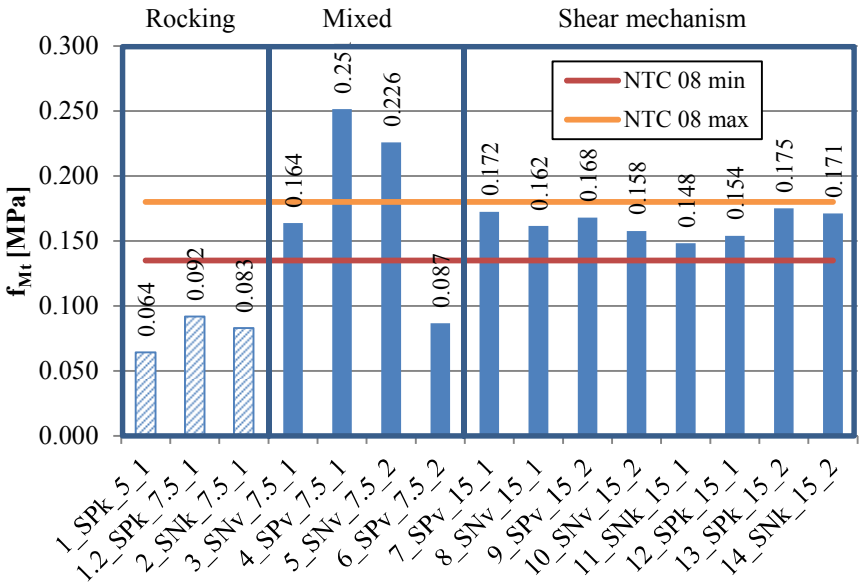

Figure 3.50: Tensile strength of tested walls
Slika 3.50: Natezna trdnost testiranih zidov

The highest f_{Mt} are exhibited in tests with low pre-compression level and fixed-fixed boundary conditions (tests where mixed failure mechanism occurred). This can be confirmed from the average results for the same pre-compression level and boundary conditions (Table 3.35) and for the same prevailing failure mechanism (Table 3.36). Walls, where mixed failure mechanism occurred, exhibited by 30.7% higher tensile strength than walls where shear mechanism occurred. The walls at tests with fixed-fixed boundary conditions and lower pre-compression level, which exhibited mixed behaviour, finally failed due to diagonal shear mechanism. The calculation of tensile strength from these tests results seems therefore not questionable. The higher tensile strength is possibly the result of the influence of the pre-compression level on the tensile strength value.

Preglednica 3.35: Natezne trdnosti f_{Mt} in strižni moduli G_M, izračunani po različnih metodah, za teste z enakimi nivoji vertikalnih obremenitev ter robnimi pogoji

Table 3.35: Average tensile strength f_{Mt} and shear moduli G_M, obtained with various methods, for tests with the same pre-compression level and boundary conditions applied

Pre-compression level, Boundary conditions	f_{Mt} [MPa]	c.o.v.	G_M [MPa]	c.o.v.	$K_{1.5mm}$ [kN/mm]	c.o.v.	$^{*}G_{1.5mm}$ [MPa]	c.o.v.	$^{**}G_{1.5mm}$ [MPa]	c.o.v.
7.5% f_{Mc}, cantilever	0.087	5.1	47.2	17.7	16.1	/	277	/	122	/
7.5% f_{Mc}, fixed-fixed	0.214	17.2	38.8	8.9	20.2	5.8	118	7.5	76	20.7
15% f_{Mc}, fixed-fixed	0.165	3.4	129.9	29.3	26.8	31.3	240	26.9	122	26.0
15% f_{Mc}, cantilever	0.162	7.0	2094	64.6	33.4	4.0	-287	-8.1	125	19.1

*calculated according to Eq. 3.12 (considering stiffness and E_M modulus)

**calculated according to Eq. 3.13 (shear stress τ to shear strain γ ratio)

Preglednica 3.36: Natezne trdnosti f_{Mt} in strižni moduli G_M, izračunani po različnih metodah, za teste z enakimi porušnimi mehanizmi

Table 3.36: Average tensile strength f_{Mt} and shear moduli G_M, obtained with various methods, for tests with the same prevailing failure mechanism

Pre-compression level, Boundary conditions	f_{Mt} [MPa]	c.o.v.	G_M [MPa]	c.o.v.	$K_{1.5mm}$ [kN/mm]	c.o.v.	$^{*}G_{1.5mm}$ [MPa]	c.o.v.	$^{**}G_{1.5mm}$ [MPa]	c.o.v.
Rocking	0.080	14.4	35.8	48.9	24.3	33.8	-10.8	-2669	91.3	1.0
Mixed	0.214	17.2	38.8	8.9	20.2	5.8	118.4	7.5	75.8	20.7
Shear	0.163	5.5	1112	123.3	33.0	12.0	-23.5	-5.4	123.7	12.0

*calculated according to Eq. 3.12 (considering stiffness and E_M modulus)

**calculated according to Eq. 3.13 (shear stress τ to shear strain γ ratio)

From K_{ef} and elastic modulus E_M, obtained in compression tests, G_M was calculated according to Eq. 3.12, derived from Eq. 2.54, where ψ is a factor taking into account boundary conditions; for cantilever $\psi = 4$ and for fixed-fixed $\psi = 1$.

$$G_M = \frac{K_{ef}}{\frac{l_w \cdot h_w}{1.2 \cdot h_w} - \frac{\psi \cdot K_{ef}}{1.2 \cdot E_M}\left(\frac{h_w}{l_w}\right)^2}, \qquad \textbf{3.12}$$

The average results of K_{ef} attained according to criteria $2/3F_{max}$ of both directions of loading are presented in Figure 3.51 and in Table 3.34 as well are the results for the calculated shear modulus G_M. Shear moduli in dependence of induced vertical load are presented in Figure 3.52.

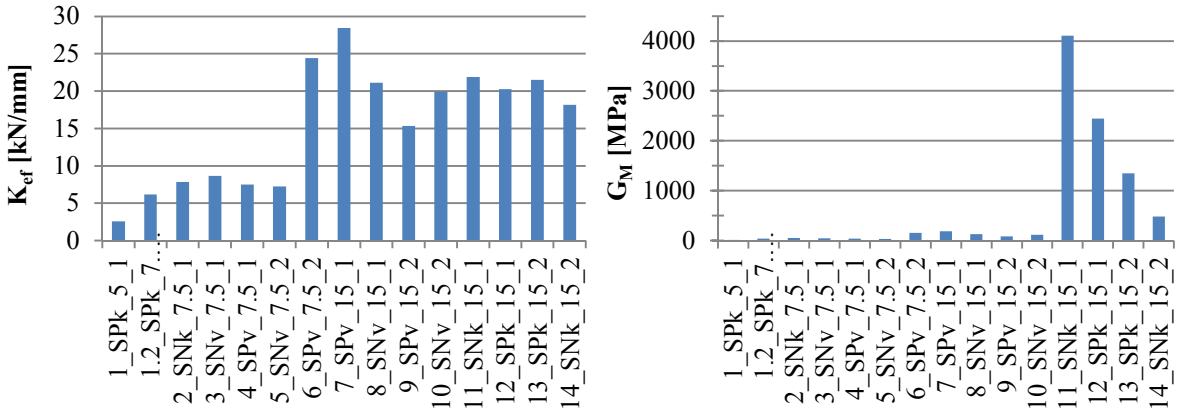

Figure 3.51: Average K_{ef} of both directions considering criteria 2/3 F_{max} and G_M moduli, calculated from K_{ef} and E_M moduli, for tested walls

Slika 3.51: Povprečne vrednosti K_{ef} obeh smeri obremenjevanja, določenih po kriteriju 2/3 F_{max}, ter G_M moduli, izračunani iz K_{ef} in E_M modulov, za testirane zidove

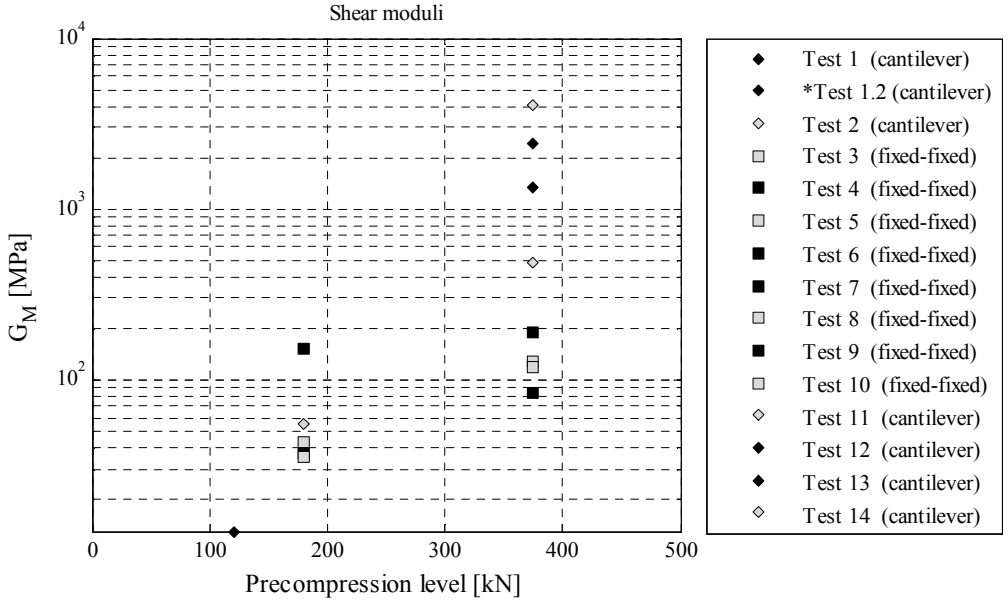

Figure 3.52: Shear moduli, calculated from effective stiffness in dependence of pre-compression load
Slika 3.52: Strižni moduli, izračunani iz efektivne togosti, v odvisnosti od nivoja predkompresije

The results for shear modulus G_M calculated according to Eq. 3.12 are in some cases unrealistic. Because the different boundary conditions applied for the test proved not to influence the effective stiffness, from hystereses average stiffnesses K for both directions at the 1st cycles of amplitude displacements d = 1.5, 3 and 5 mm (labelled $K_{1.5\ mm}$, $K_{3\ mm}$ and $K_{5\ mm}$) were evaluated (Figure 3.53 left). From these stiffnesses shear modulus was calculated according to Eq. 3.12 as well as the ratio of shear stress τ to the shear strain γ (Eq. 3.13):

$$G_M = \frac{\tau}{\gamma} = \frac{F \cdot h_w}{A_w \cdot d}, \qquad \textbf{3.13}$$

Where F is the lateral force attained during evaluated point of testing, and d the corresponding lateral displacement. Obtained values of G_M modulus $G_{1.5\ mm}$, $G_{3\ mm}$ and $G_{5\ mm}$ are presented in Figure 3.53 right and are calculated for amplitude displacement d = 1.5 mm also in Tables 3.34, 3.35 and 3.36.

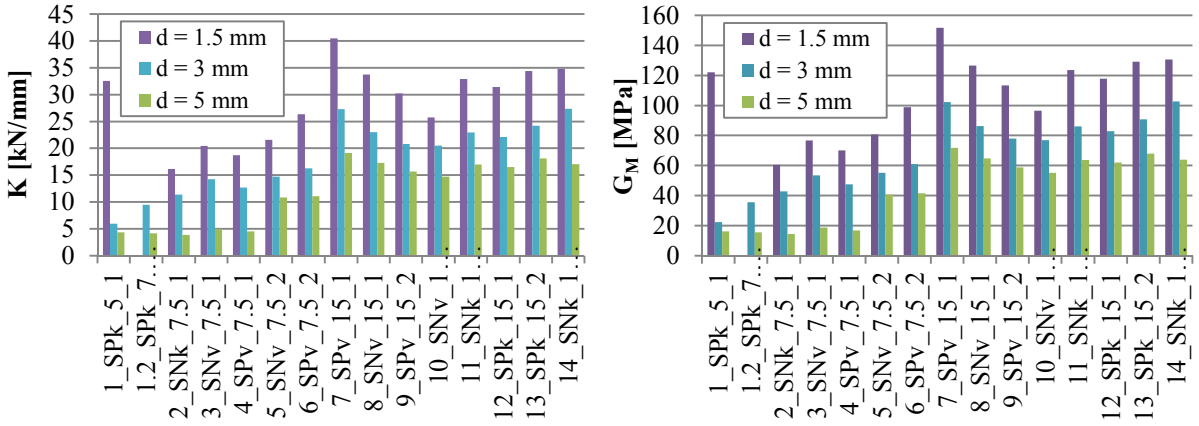

Figure 3.53: Average stiffness K_{ef} and modulus G_M, calculated according to Eq. 3.13, of both directions for the 1st cycles of amplitude displacements d = 1.5, 3 and 5 mm of the tested walls
Slika 3.53: Povprečne vrednosti K_{ef} in modulov G_M, izračunanih po En. 3.13, obeh smeri obremenjevanja za prve cikle amplitudnih pomikov d = 1.5, 3 in 5 mm testiranih zidov

As already mentioned, G_M modulus calculated from K_{ef} according to Eq. 3.12 results in unrealistically low or high values. Similar happens if it is calculated from the initial elastic stiffness $K_{1.5\,mm}$. The reason for this is that Eq. 3.12 in general produces unrealistic results for masonry with low E_M modulus. This was established in [47], where determination of the G_M modulus and its problems are discussed. More stable results are gained with calculation from experimental tests results as the ratio of shear stress to shear strain (Eq. 3.13) for the elastic state ($G_{1.5\,mm}$) or just before shear cracking. However even with this approach obtained values of G_M are significantly lower than the values obtained from compressive tests (Table 3.5 in Section 3.3.4.2).

3.4.6 Energy dissipation evaluation

3.4.6.1 Energy dissipation parameters

In [246], for each test dissipated energy E_{DIS} at each cycle of certain amplitude displacement is presented, together with dissipated energy of "half" cycles, that is in positive and negative direction. Values of "half" cycles are multiplied by 2, in order to compare them with E_{DIS} of the entire cycle. Besides E_{DIS} also the ratio of dissipated and input energy E_{DIS}/E_{INP} is presented, again for each cycle and "half" cycles at certain displacement amplitude. At both diagrams the values for all cycle repetitions and both positive and negative "half" cycles are plotted at positive values of amplitude displacements of 1st cycles. In Figure 3.54 dissipated energy E_{DIS} and in Figure 3.55 dissipated vs. input energy ratios E_{DIS}/E_{INP} at 1st cycles of each amplitude displacement for all tests are presented.

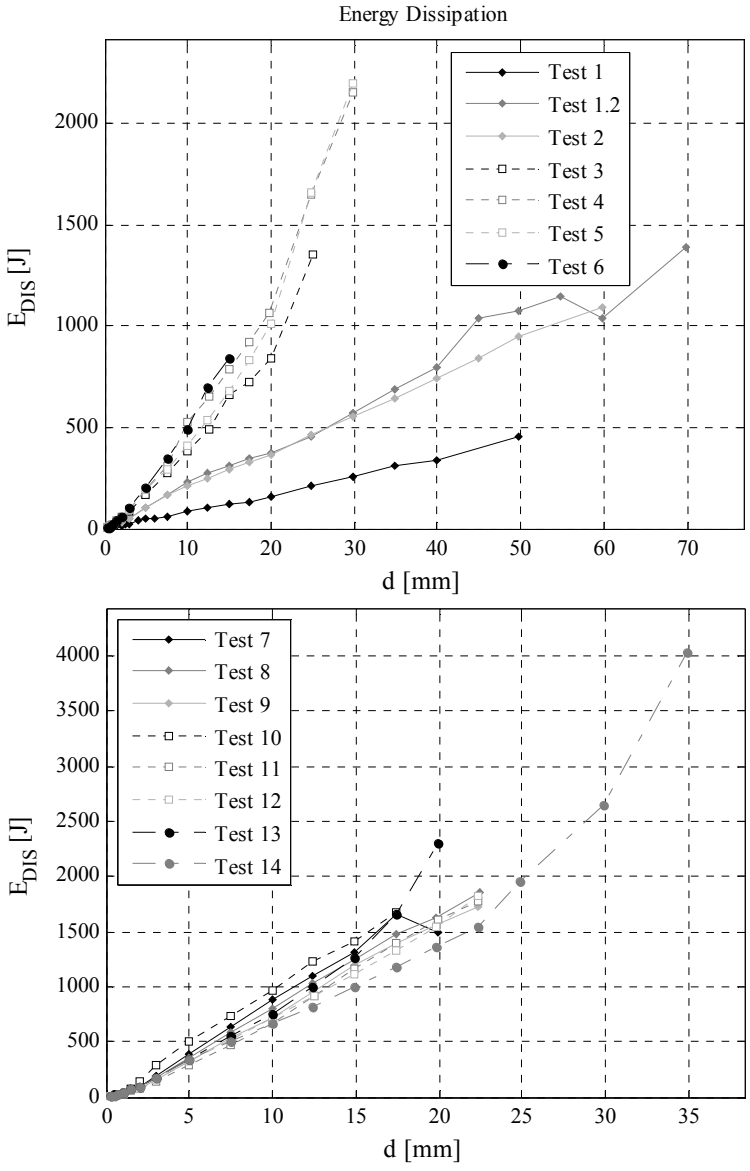

Figure 3.54: Dissipated energy at 1st cycles of each amplitude displacement for tests 1-6 and tests 7-14
Slika 3.54: Disipirana energija v 1. ciklih posameznih amplitudnih pomikov za teste 1-6 in teste 7-14

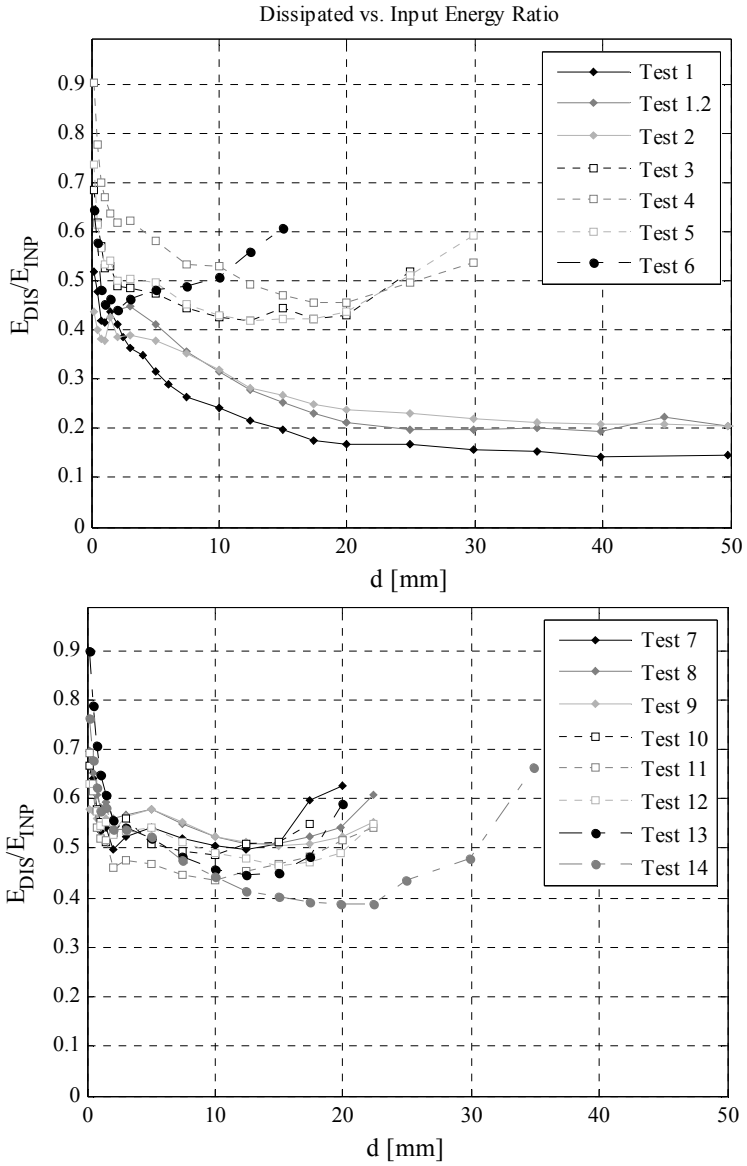

Figure 3.55: Dissipated and input energy ratio at 1st cycles of each amplitude displacement for tests 1-6 and 7-14
Slika 3.55: Razmerje disipirane in vnesene energije v 1. ciklih posameznih amplitudnih pomikov za teste 1-6 in 7-14

The difference in energy dissipation between test results of walls with different pre-compression levels and boundary conditions and consequently different failure mechanisms obtained is apparent (Figures 3.54 and 3.55). Dissipated energy in test 1, where characteristic flexural mechanism occurred is noticeably lower than for tests 1.2 and 2 where slight shear damage was present. Dissipated energy for tests 3-14 was comparable and significantly higher as in tests 1-2. Also the ratios E_{DIS}/E_{INP} are in different range for tests 1-2 and 3-14. It can be observed that dissipated energy's evolution is approximately linearly proportional to lateral displacements up to a certain level regardless the failure mechanism observed. In some tests from some point forward (in test 2 from displacement 40 mm, in tests 4 and 5 from 20 mm, in tests 7 and 13 from 17.5 mm and in test 14 from 22.5 mm) higher increase is evident, which can be attributed to the more significant damage developed during this phase of testing. Due to its definition, the overall dissipated energy increases with displacements, thus a more objective indicator of the dissipated energy could be the ratio between dissipated and input energy E_{DIS}/E_{INP}. If amplitude displacements up to first 2 mm are not considered, in all tests except 1,

1.2, 13 and 14, two phase increase in dissipation is observed. An exception is test 6, where this ratio is increasing during entire test. Otherwise after displacement 5 mm or lower, a decrease in dissipation is observed in most of the tests. In tests 7-14 the ratio increases again after displacement where maximum lateral force was attained in one direction or one cycle earlier. Ratio E_{DIS}/E_{INP} in dependence of displacement, normalized to displacement d_{Fmax} (where d_{Fmax} is the displacement in direction of loading, where F_{max} was attained first), is presented in Figure 3.56 and Figure 3.57. In tests 3-6, however, the ratio starts to increase even earlier; approximately at displacement, which coincides with the elastic displacement. Ratio E_{DIS}/E_{INP} in dependence of displacement, normalized to elastic displacement d_e, is for tests 1-6 presented in Figure 3.58.

The results show that the energy dissipation is closely related to prevailing failure mechanism and that it is relatively the highest compared to input energy at lower displacements where the initial damage on the specimens occurs. In the case of failure mechanisms, which are large in dissipation, the dissipation progressively increases in the post-peak phase.

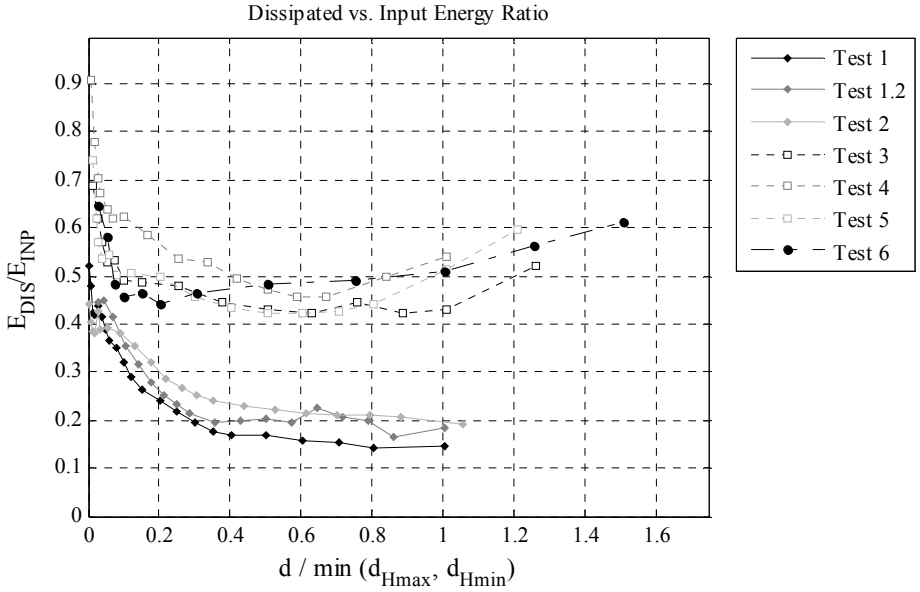

Figure 3.56: Dissipated and input energy ratio at 1st cycles of each amplitude displacement in dependence of amplitude displacements normalized to displacement d_{Fmax} for tests 1-6
Slika 3.56: Razmerje disipirane in vnesene energije v 1. ciklih posameznih amplitudnih pomikov v odvisnosti od pomikov, normaliziranih na d_{Fmax}, za teste 1-6

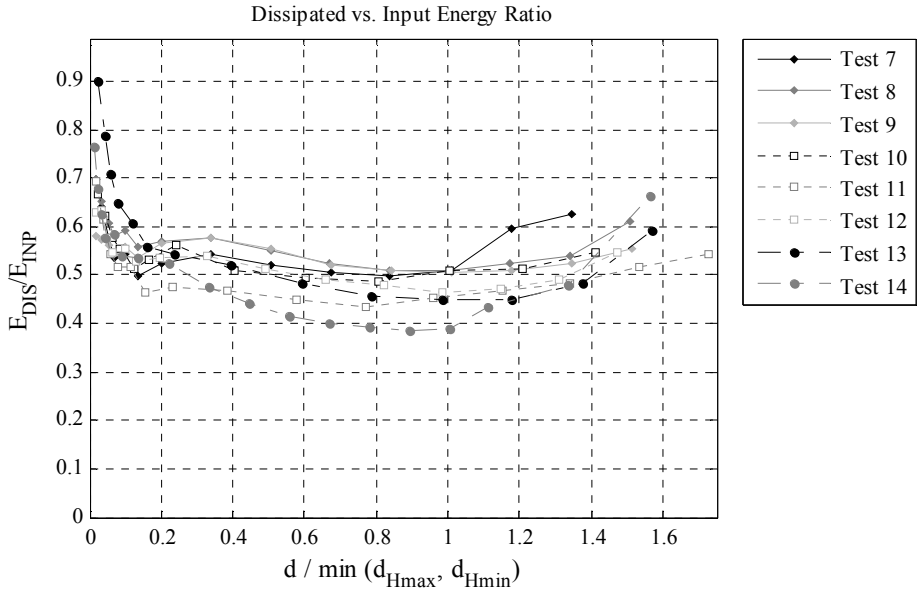

Figure 3.57: Dissipated and input energy ratio at 1st cycles of each amplitude displacement in dependence of amplitude displacements normalized to displacement d_{Fmax} for tests 7- 14

Slika 3.57: Razmerje disipirane in vnesene energije v 1. ciklih posameznih amplitudnih pomikov v odvisnosti od pomikov, normaliziranih na d_{Fmax}, za teste 7-14

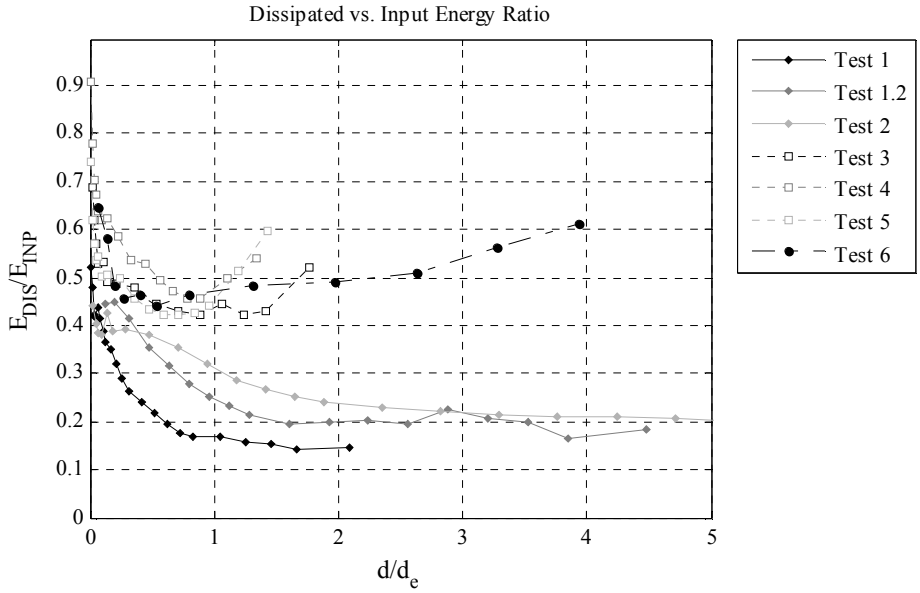

Figure 3.58: Dissipated and input energy ratio at 1st cycles of each amplitude displacement in dependence of amplitude displacements normalized to elastic displacement for tests 1-6

Slika 3.58: Razmerje disipirane in vnesene energije v 1. ciklih posameznih amplitudnih pomikov, v odvisnosti od pomikov, normaliziranih na d_e, za teste 1-6

The results for dissipated energy E_{DIS}, input energy E_{INP} and their ratio E_{DIS}/E_{INP} in characteristic limit states (d_{cr}, d_e, d_{Fmax} and d_{max}) are summarized in Table 3.37. The results are presented for the 1st cycles of the characteristic displacements.

Evaluating the results in Table 3.37, there seems to be no rule regarding energy dissipation concerning connected and unconnected specimens at any of the characteristic limit states.

In Table 3.38 mean values of E_{DIS}/E_{INP} ratio are presented for the same boundary conditions and pre-compression levels. At d_{cr} and d_e, the ratio increases from lower pre-compression level to higher and from cantilever to fixed-fixed boundary conditions. At d_{Fmax} and d_{max} however a significant difference is obtained depending from the failure mechanism achieved (flexural compared to shear), where for the shear mechanism the values are close. For d_{Fmax} average E_{DIS}/E_{INP} value for shear mechanism is 0.504 (c.o.v. 9.0%) compared to 0.187 (c.o.v. 2.2%) for flexural, whereas for d_{max} 0.579 (c.o.v. 7.1%) for shear and the same as for d_{Fmax} for flexural mechanism was obtained.

It should be emphasised, that if the developed flexural mechanism would also involve toe-crushing, the dissipated energy would most probably be significantly larger.

Comparing the dissipated energy for positive and negative directions of loading, there seems to be no rule regarding in which direction a larger amount of energy is dissipated; similar is with relative dissipation (compared to input energy). One of the observations is, that if E_{DIS} is higher in positive direction of the loading, the same is not necessary for E_{DIS}/E_{INP}. The opposite is true for tests 4, 5, 6, 8, 9, 10, 12 and 14. This is the result of strength and stiffness changes in dependence from direction and repetitions of loading. Comparing the cycle repetitions, no rule is observed for the dissipated energy itself, but for E_{DIS}/E_{INP}, in most of the tests after obtaining F_{max}, the 3rd cycles exhibit relatively the largest energy dissipation (tests 1, 2, 3, 8, 9, 10, 12, 13, 14 and except of the very last amplitude displacement cycle also tests 4, 5 and 6). In most of these tests also relatively higher energy dissipation is obtained in the 2nd cycles than in the 1st ones. Before the obtainment of maximum shear resistance, relatively the most energy is dissipated in the 1st cycles.

Preglednica 3.37: Disipirana in vnesena energija za 1. cikle karakterističnih amplitudnih pomikov testov

Table 3.37: Dissipated and input energy for the 1st cycles of characteristic limit states attained at tests

Test no.	Name	d_{cr}			d_e			d_{Fmax}			d_{max}		
		E_{DIS} [J]	E_{INP} [J]	E_{DIS}/E_{INP}	E_{DIS} [J]	E_{INP} [J]	E_{DIS}/E_{INP}	E_{DIS} [J]	E_{INP} [J]	E_{DIS}/E_{INP}	E_{DIS} [J]	E_{INP} [J]	E_{DIS}/E_{INP}
1	1-SPk-5-1	0	0	0.000	120	613	0.196	456	3131	0.146	456	3131	0.146
1.2	1.2-SPk-7.5-1	688	3418	0.201	227	716	0.317	1384	7569	0.183	1384	7569	0.183
2	2-SNk-7.5-1	329	1308	0.251	167	469	0.355	1089	5701	0.191	1089	5701	0.191
3	3-SNv-7.5-1	272	612	0.445	272	612	0.445	1351	2599	0.520	1351	2599	0.520
4	4-SPv-7.5-1	310	578	0.536	785	1663	0.472	2151	3998	0.538	2151	3998	0.538
5	5-SNv-7.5-2	409	946	0.433	533	1265	0.421	1660	3224	0.515	2197	3695	0.595
6	6-SPv-7.5-2	342	695	0.492	100	214	0.465	494	968	0.510	839	1376	0.610
7	7-SPv-15-1	182	347	0.524	388	714	0.543	1306	2573	0.508	1496	2391	0.626
8	8-SNv-15-1	356	615	0.579	356	615	0.579	1250	2460	0.508	1849	3034	0.609
9	9-SPv-15-2	79	148	0.534	321	555	0.578	1392	2739	0.508	1726	3110	0.555
10	10-SNv-15-2	293	523	0.561	733	1482	0.494	1407	2737	0.514	1677	3058	0.549
11	11-SNk-15-1	139	291	0.477	284	605	0.470	1393	2879	0.484	1764	3250	0.543
12	12-SPk-15-1	149	280	0.534	316	585	0.540	1117	2400	0.465	1819	3315	0.549
13	13-SPk-15-2	169	312	0.542	339	652	0.519	2297	3883	0.592	2297	3883	0.592
14	14-SNk-15-2	331	630	0.525	331	630	0.525	1544	3986	0.387	4031	6076	0.663

Preglednica 3.38: Povprečne vrednosti razmerij disipirane in vnesene energije za 1. cikle karakterističnih pomikov s c.o.v. za teste z enakimi nivoji vertikalnih obremenitev ter robnimi pogoji

Table 3.38: Mean values of dissipated to input energy ratios with c.o.v. in 1st cycles of characteristic limit states for the same pre-compression level and boundary conditions for the 1st cycles

	d_{cr}		d_e		d_{Fmax}		d_{max}	
Pre-compression level, Boundary conditions	E_{DIS}/E_{INP} mean	c.o.v. [%]	E_{DIS}/E_{INP} mean	c.o.v. [%]	E_{DIS}/E_{INP} mean	c.o.v. [%]	E_{DIS}/E_{INP} mean	c.o.v. [%]
7.5% f_{Mc}, cantilever	0.226	11.1	0.336	5.6	0.187	2.2	0.187	2.2
7.5% f_{Mc}, fixed-fixed	0.471	9.8	0.446	4.7	0.524	1.9	0.551	5.8
15% f_{Mc}, fixed-fixed	0.549	3.9	0.549	6.3	0.509	0.5	0.585	5.7
15% f_{Mc}, cantilever	0.519	4.9	0.514	5.1	0.482	15.1	0.587	8.2

In order to obtain a clear difference in behaviour of the tested walls in terms of their energy dissipation, also cumulative values of dissipated, input energy and their ratio has been evaluated. They are summarized for all tests at d_{max} in Table 3.39. Two values for cumulative ratio E_{DIS}/E_{INP} were calculated; one is the ratio between cumulative dissipated energy and cumulative input energy ($cumE_{DIS}/cumE_{INP}$) whereas the second is the cumulative value of E_{DIS}/E_{INP} ratio in the test ($cum(E_{DIS}/E_{INP})$). With the second one the intention was to take into account also the maximum displacement reached as with higher displacements, the number of cycles increases and consequently $cum(E_{DIS}/E_{INP})$ is higher than with lower displacements. This also explains why cum(E_{DIS}/E_{INP}) for test 1.2 is lower as in test 1. The reason for this is that in the test protocol displacement amplitudes lower than 2 mm were omitted. In case of comparing $cumE_{DIS}/cumE_{INP}$ attained at d_{max} of connected and unconnected walls, for the same boundary conditions and imposed vertical load, in all cases with exception of test 8, connected walls dissipated more energy than unconnected. This can be explained by the fact, that additional energy was required to break the connecting stones. In Table 3.40 mean values for the same level of imposed vertical load and the same boundary conditions are summarized. With comparison of $cumE_{DIS}/cumE_{INP}$ it is evident, that energy dissipation increases from low pre-compression level and cantilever boundary conditions to fixed-fixed boundary conditions, and then to high pre-compression level (again from cantilever boundary conditions to fixed-fixed boundary conditions). Value of $cum(E_{DIS}/E_{INP})$ at d_{max} exhibits lower difference considering the obtained failure mechanisms due to already mentioned reasons. Here the results for higher pre-compression level and fixed-fixed boundary conditions exhibit lower value as at cantilever conditions. One of the reasons for this lies within test 14 (high pre-compression level, cantilever), where due to higher displacement reached, the number of the cycles was higher; $cum(E_{DIS}/E_{INP})$ at d_{max} can be seen in Figure 3.59.

Preglednica 3.39: Kumulativno disipirana in vnesena energija ter njihova razmerja za 1. cikle maksimalnih pomikov, pomikih na meji elastičnosti in celotna vnesena energija idealiziranega odziva, normalizirana disipirana energija (po Shing-u [112]) in modificirana normalizirana disipirana energija za teste z enakimi nivoji vertikalnih obremenitev ter robnimi pogoji

Table 3.39: Cumulative dissipated and input energy for the 1st cycles and their ratio at maximum amplitude displacement cycles, elastic strain and entire input energy of idealized response, normalized dissipated energy (after Shing [112]) and modified normalized dissipated energy

Test no.	Name	*cum* E_{DIS} [J]	*cum* E_{INP} [J]	*cum* E_{DIS} /*cum* E_{INP}	*cum* (E_{DIS}/E_{INP}) [J]	$E_{ID,el}$ [J]	E_{ID} [J]	E_N (Shing) [J]	E_N modified [J]
1	1-SPk-5-1	2451	14328	0.171	6.44	327	1708	7.5	1.44
1.2	1.2-SPk-7.5-1	10070	49247	0.204	4.72	346	3897	29.1	2.58
2	2-SNk-7.5-1	7112	31867	0.223	6.39	201	3150	35.3	2.26

Continues…

…continuation of Table 3.39

3	3-SNv-7.5-1	5080	11138	0.456	7.51	433	1670	11.7	3.04
4	4-SPv-7.5-1	8490	16893	0.503	9.51	832	2509	10.2	3.38
5	5-SNv-7.5-2	8029	16439	0.488	8.22	752	2356	10.7	3.41
6	6-SPv-7.5-2	2813	5211	0.540	6.19	69	790	41.0	3.56
7	7-SPv-15-1	7878	14399	0.547	7.82	242	2083	32.6	3.78
8	8-SNv-15-1	9356	17210	0.544	8.60	311	2204	30.1	4.25
9	9-SPv-15-2	8751	16584	0.528	8.17	472	2128	18.6	4.11
10	10-SNv-15-2	7080	13689	0.517	7.09	341	1862	20.8	3.80
11	11-SNk-15-1	8587	17582	0.488	7.64	308	2146	27.9	4.00
12	12-SPk-15-1	8639	17323	0.499	8.00	297	2149	29.1	4.02
13	13-SPk-15-2	8276	16484	0.502	8.19	325	2019	25.5	4.10
14	14-SNk-15-2	16451	34991	0.470	9.31	457	3710	36.0	4.43

Preglednica 3.40: Povprečne vrednosti kumulativno disipirane in vnesene energije ter njihova razmerja s c.o.v. za 1. cikle maksimalnih pomikov za teste z enakimi nivoji vertikalnih obremenitev ter robnimi pogoji

Table 3.40: Mean values of cumulative dissipated and input energy for the 1st cycles and their ratio with c.o.v. at maximum amplitude displacement for the same testing conditions

Pre-compression level, Boundary conditions	*cum* E_{DIS}		*cum* E_{INP}		*cum* E_{DIS} / *cum* E_{INP}		*cum* (E_{DIS}/E_{INP})	
	mean [J]	c.o.v. [%]	mean [J]	c.o.v. [%]	mean	c.o.v. [%]	mean	c.o.v. [%]
7.5% f_{Mc}, cantilever	8591	17.2	40557	21.4	0.214	4.4	5.56	15.0
7.5% f_{Mc}, fixed-fixed	7200	21.0	14823	17.6	0.482	4.1	8.41	9.8
15% f_{Mc}, fixed-fixed	8266	10.4	15471	9.5	0.534	2.3	7.92	7.0
15% f_{Mc}, cantilever	10488	32.8	21595	35.9	0.490	2.5	8.28	7.5

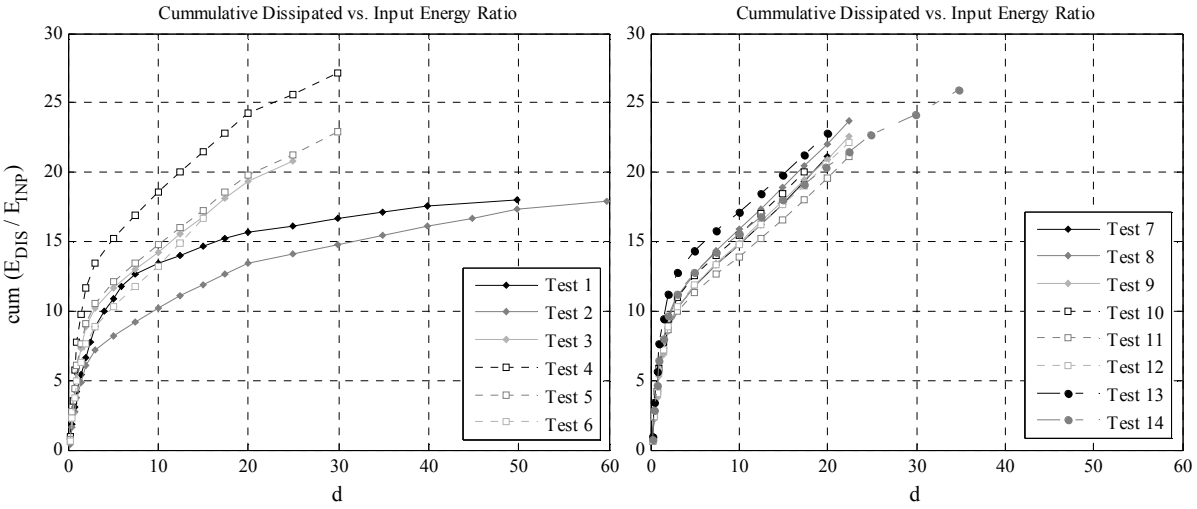

*test 1.2 excluded, as the loading protocol involved only one cycle and started at higher displacement amplitude than at other tests

Figure 3.59: Cumulative ratio cum(E_{DIS}/E_{INP}) at 1st cycles of amplitudes displacement for tests 1-6 and tests 7-14
Slika 3.59: Kumulativno razmerje cum(E_{DIS}/E_{INP}) v 1. ciklih amplitudnih pomikov za teste 1-6 in teste 7-14

As mentioned, by comparing $cumE_{DIS}/cumE_{INP}$ at the end of the tests, it is clear, that dissipated energy is dependant from the type of damage and developed failure mechanism. In Figure 3.60 ratios of $cumE_{DIS}/cumE_{INP}$ at d_{max} are presented for tests in dependence from vertical load imposed. The

diagram confirms that not the pre-compression level or the boundary condition itself, but the failure mechanism which they induce, influences on the amount of the dissipated energy. In Figure 3.60, diamonds refer to tests with cantilever and squares to fixed-fixed boundary conditions, whereas black marks to walls with connecting stones and grey ones to walls without them.

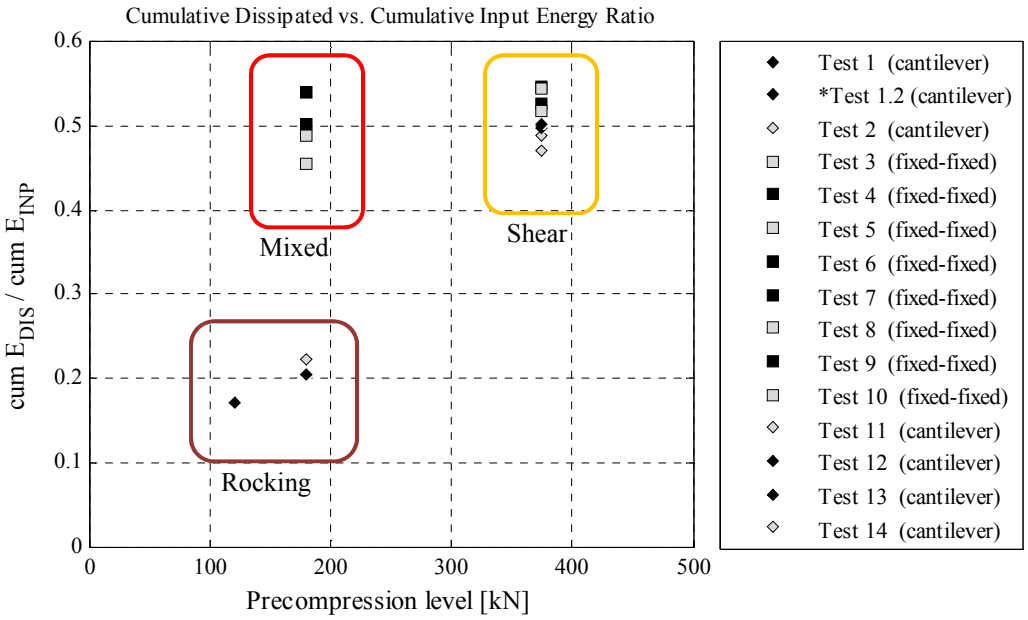

*the loading protocol in test 1.2 involved only one cycle and started at higher displacement amplitude than other tests

Figure 3.60: Ratio of cumulative dissipated to cumulative input energy in dependence of pre-compression load
Slika 3.60: Razmerje kumulativne disipirane in kumulativno vnesene energije v odvisnosti od nivoja predkompresije

In order to evaluate energy dissipation, additional measures for energy evaluation were considered. Values of normalized cumulative energy dissipation E_N at maximum displacements together with elastic $E_{ID,el}$ and total energy absorption of the equivalent elastic-perfectly plastic model E_{ID} (considered up to d_u) are presented in Table 3.39, whereas mean values for tests with the same pre-compression level and boundary condition in Table 3.41.

Preglednica 3.41: Povprečne vrednosti elastične in celotne vnesene energije idealiziranega odziva ($E_{ID,el}$ in E_{ID}), normalizirane disipirane energije E_N (Shing)in modificirane normalizirane disipirane energije $E_{N,\,modified}$ za teste z enakimi nivoji vertikalnih obremenitev ter robnimi pogoji

Table 3.41: Mean values of the elastic strain energy and the entire input energy of the idealized response ($E_{ID,el}$ and E_{ID}), normalized dissipated energy E_N (Shing) and modified normalized dissipated energy $E_{N,\,modified}$

Pre-compression level, Boundary conditions	$E_{ID,el}$		E_{ID}		E_N (Shing)		$E_{N,\,modified}$	
	mean [J]	c.o.v. [%]	mean [J]	c.o.v. [%]	mean	c.o.v. [%]	mean	c.o.v. [%]
7.5% f_{Mc}, cantilever	274	26.5	3524	10.6	32.2	9.7	2.42	6.7
7.5% f_{Mc}, fixed-fixed	672	25.6	2178	16.7	10.9	5.7	3.28	5.1
15% f_{Mc}, fixed-fixed	341	24.4	2069	6.1	25.5	23.3	3.99	5.0
15% f_{Mc}, cantilever	347	18.6	2506	27.8	29.6	13.2	4.14	4.2

Evaluating the results in both tables, walls in test 6 and then in tests 14 and 2 had the highest E_N. The reason for this is either very low $E_{ID,el}$, as in test 6 (which is also seen in Figure 3.61), either a very high d_{max}, which resulted in higher values of cumulative dissipated energy as in test 14 and 2.

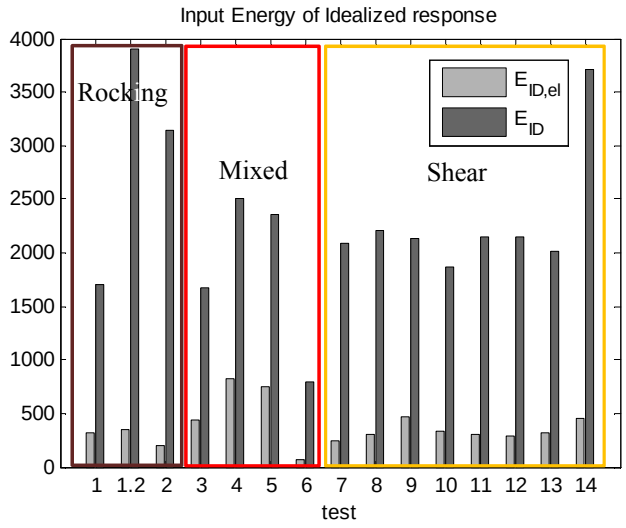

Figure 3.61: Input energy of the idealized response (of the elastic part $E_{ID,el}$ and the entire response E_{ID})
Slika 3.61: Vnesena energija idealiziranega odziva (elastičnega $E_{ID,el}$ in celotnega odziva E_{ID})

Since the E_N does not differ between hysteretic responses with higher and lower maximum displacement, a modification of E_N calculation is proposed (referred as $E_{N,modified}$). Instead of using $E_{ID,el}$, total energy E_{ID} of the equivalent bi-linear model is considered (Eq. 3.14)

$$E_{N,modified} = \frac{1}{E_{ID}} \sum_{i=1}^{n} E_i \,, \qquad \textbf{3.14}$$

With this modification with using also the inelastic part of the input energy, a difference obtained at d_{max} is obvious. The results of $E_{N,modified}$ are for all tests also summarized in Table 3.40 and mean values for the same pre-compression level and boundary condition in Table 3.41. $E_{N,modified}$ shows similar results as E_{DIS}/E_{INP} or ($cumE_{DIS}/cumE_{INP}$) showing different behaviour in accordance to hysteretic response typical for certain pre-compression level and boundary conditions and corresponding failure mechanism.

3.4.6.2 Equivalent viscous damping coefficient

For the determination of the equivalent viscous damping coefficient ξ of the performed tests, energy input in both directions was considered and therefore the calculation was done according to Eq. 2.35 (see Section 2.3.2.4.2), where for E_{INP} evaluation according to Eq. 2.32 both maximum and minimum amplitude displacements $d_{max,i}^{+}$ and $d_{max,i}^{-}$ and corresponding forces $F_{dmax,i}^{+}$ and $F_{dmax,i}^{-}$ of analysed *i*th cycle were considered.

The calculated ξ are presented in Figure 3.62, where they are compared only for 1st hysteretic cycles corresponding to certain amplitude displacements and presented at corresponding amplitude displacement values in positive direction.

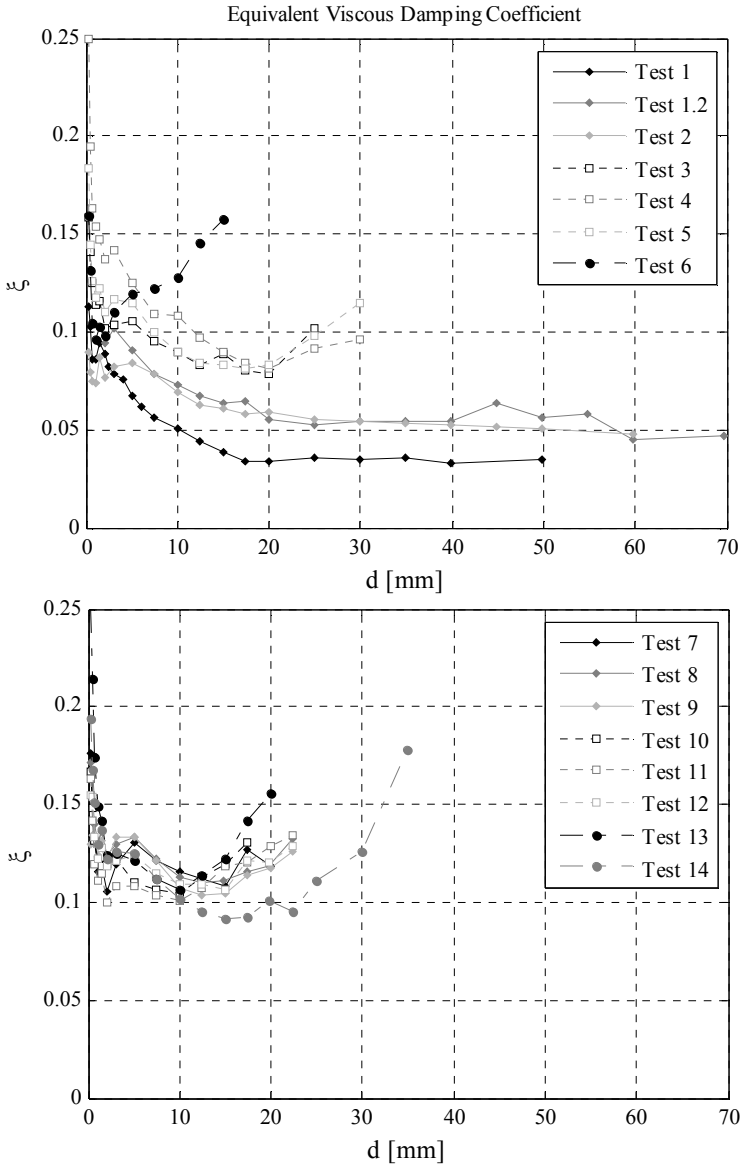

Figure 3.62: Comparison of the equivalent viscous damping coefficient ξ for the 1st cycles of amplitude displacements for tests 1-6 and tests 7-14
Slika 3.62: Primerjava koeficientov ξ za 1.cikle amplitudnih pomikov za teste 1-6 in 7-14

In accordance with all the previous observations, from Figure 3.62 a difference can be seen between ξ obtained in dependence of failure mechanism; for flexural mechanism significantly lower ξ was obtained. In most of the tests, in cycles with amplitude displacements up to approximately 1.0 - 1.5 mm, ξ is relatively high, in tests 4, 10 and 13 it even exceeds 0.2. Then ξ is gradually decreasing up to certain displacement and afterwards starts to increase in most cases, where the flexural mechanism is not prevalent. Again, the increase of ξ is different for test 6, that is test of wall with thicker mortar joints than in other walls; the increase starts earlier and it reaches higher values compared to tests on walls with the same level of pre-compression and boundary conditions (tests 3-5). One of the reasons

for this is, that flexural behaviour was accompanied with some toe crushing. For each test, ξ is presented separately in Figure 3.63 and Figure 3.64, where results for all three cycles at certain amplitude displacements are presented also for the purpose of comparison of values within cycle repetitions. It has to be noted that where values of ξ are zero, in reality the cycle was not executed (referring to 2nd and 3rd cycle at maximum amplitude displacement).

Regarding the already mentioned point, where the increasing starts, in test 3 and then in all tests 7-13, the turning point occurred in the amplitude displacement cycle, where the F_{max} was obtained in one direction or one amplitude displacement cycle before.

Minimum values of ξ achieved during the tests are similar for the same level of pre-compression and boundary condition and can be found in Table 3.42 together with corresponding amplitude displacements $d_{\xi min,i}$.

Preglednica 3.42: Minimalne vrednosti ξ, dosežene med testi, in pripadujoči amplitudni pomiki $d_{\xi min,i}$

Table 3.42: Minimum values of ξ achieved during the tests and corresponding amplitude displacements $d_{\xi mini}$

Test no.	Name	Failure mechanism	1st cycle		All cycles	
			ξ	$d_{\xi min,i}$	ξ	$d_{\xi min,i}$
1	1-SPk-5-1	Rocking	0.034	39.9	0.030	17.4
1.2	1.2-SPk-7.5-1		0.045	59.8	0.045	59.8
2	2-SNk-7.5-1		0.048	59.8	0.048	59.8
3	3-SNv-7.5-1	Mixed	0.078	20.0	0.077	20.0
4	4-SPv-7.5-1		0.082	19.9	0.077	19.9
5	5-SNv-7.5-2		0.081	17.4	0.079	17.4
6	6-SPv-7.5-2		0.096	1.0	0.076	1.0
7	7-SPv-15-1	Shear	0.106	2.0	0.086	2.0
8	8-SNv-15-1		0.110	12.4	0.099	12.4
9	9-SPv-15-2		0.104	12.4	0.094	12.4
10	10-SNv-15-2		0.105	10.0	0.098	7.5
11	11-SNk-15-1		0.100	2.0	0.085	2.0
12	12-SPk-15-1		0.106	14.9	0.094	5.0
13	13-SPk-15-2		0.107	10.0	0.096	10.0
14	14-SNk-15-2		0.092	14.9	0.085	14.9

Not only the values but also their increasing/decreasing in dependence of increasing displacements are influenced by the failure mechanism. With rocking and mixed failure mode, minimum values of ξ are proved to occur at earlier displacements.

In Table 3.43, the values of equivalent viscous damping coefficient in characteristic points of hysteretic response are presented for all tests, whereas in Table 3.44 average values with c.o.v. for the same morphology types, boundary and pre-compression conditions, i.e. for test repetitions, are summarized. Furthermore in Table 3.45, the average values for the same boundary conditions and pre-compression level for both morphology types are evaluated.

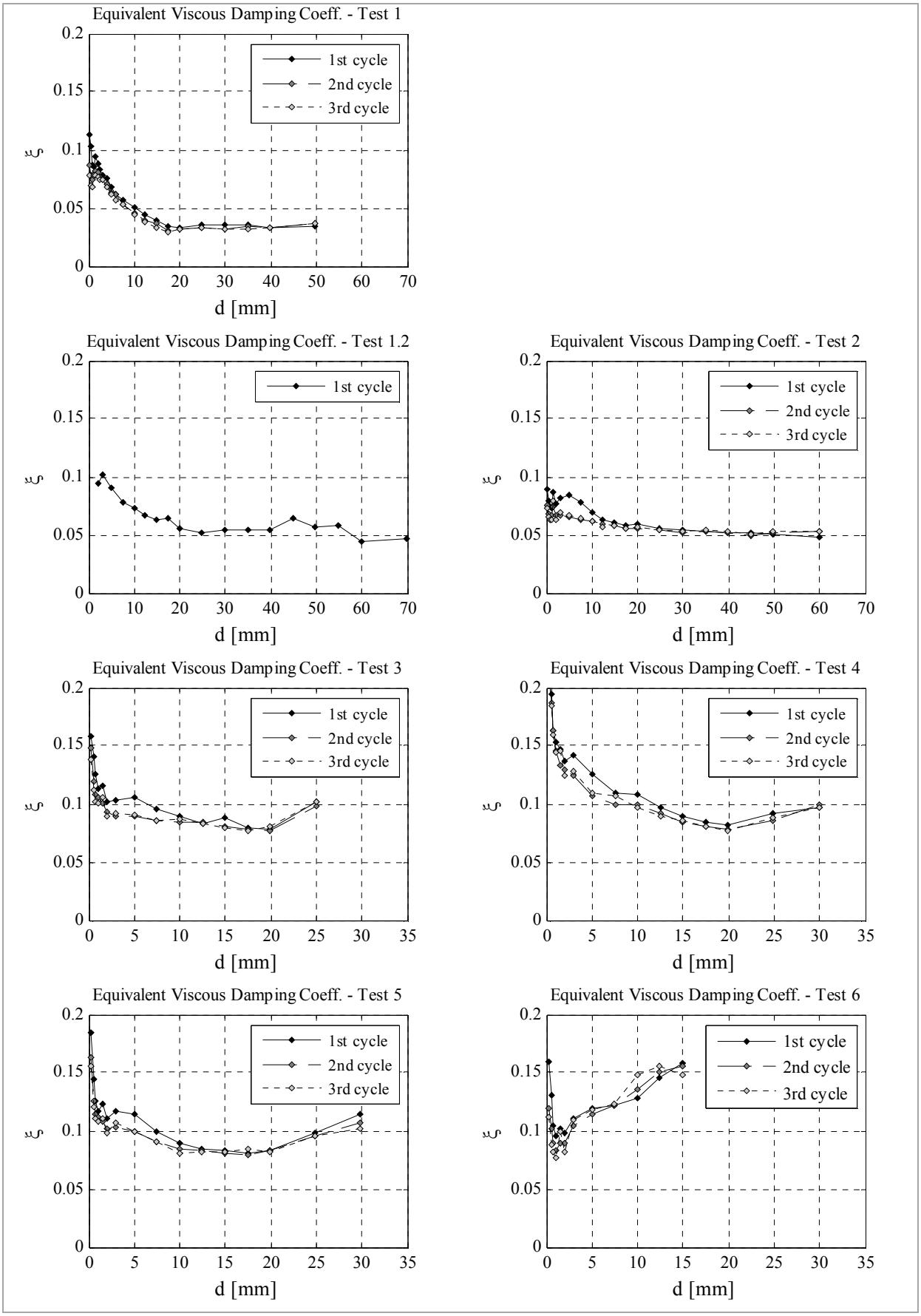

Figure 3.63: Equivalent viscous damping coefficients ξ evaluated for all the three cycles for tests 1-6
Slika 3.63: Koeficienti ekvivalentnega viskoznega dušenja ξ za vse tri cikle amplitudnih pomikov testov 1-6

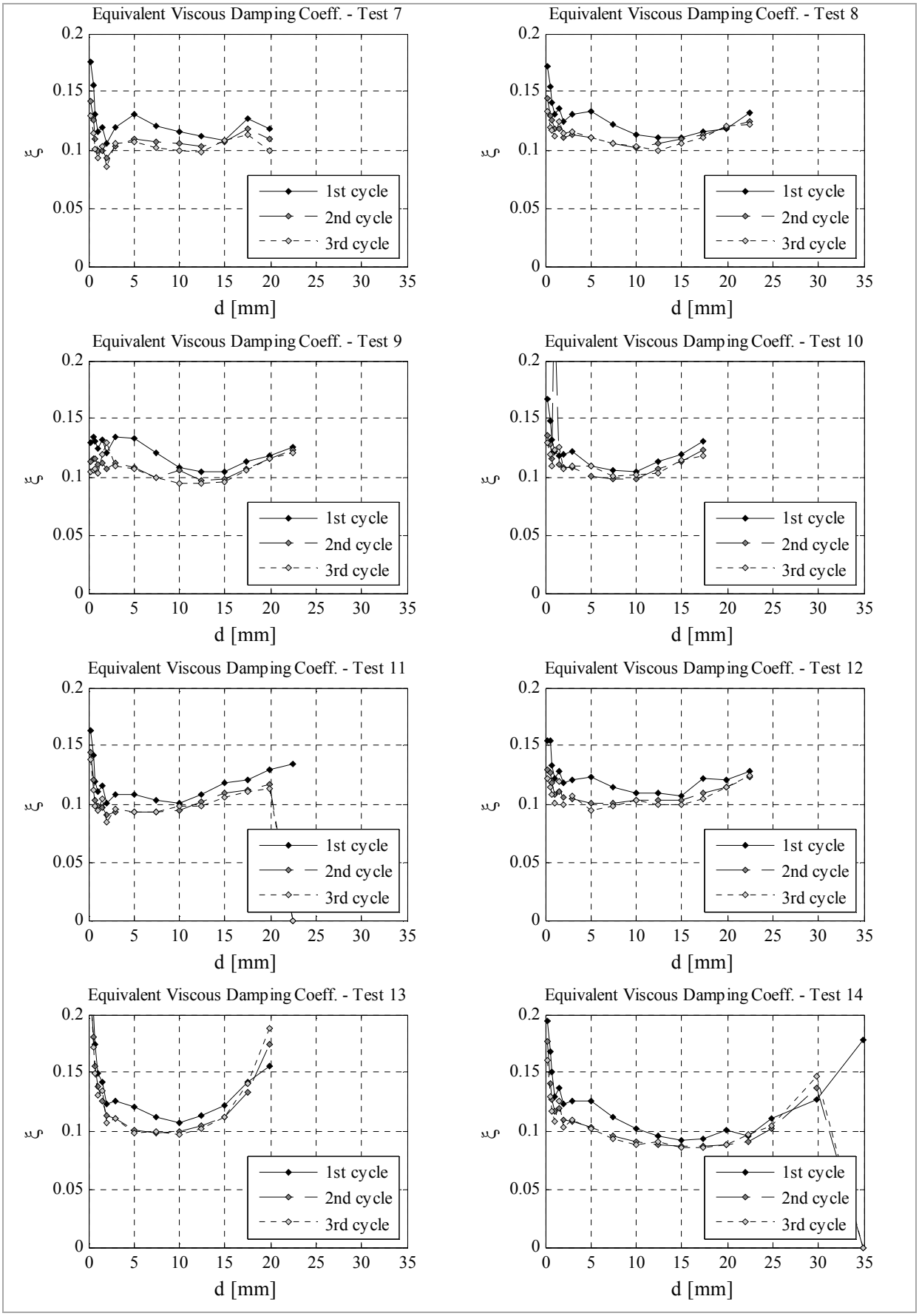

Figure 3.64: Equivalent viscous damping coefficients ξ evaluated for all the three cycles for test 7-14
Slika 3.64: Koeficienti ekvivalentnega viskoznega dušenja ξ za vse tri cikle amplitudnih pomikov testov 7-14

Preglednica 3.43: Vrednosti ξ za cikle karakterističnih mejnih stanj testov

Table 3.43: Values of ξ for characteristic limit state cycles of the tests

Test no.	Name	ξ at cycle			
		d_{cr}	d_e	d_{Fmax}	d_{max}
1	1-SPk-5-1	/	0.039	0.035	0.035
1.2	1.2-SPk-7.5-1	0.055	0.073	0.047	0.047
2	2-SNk-7.5-1	0.058	0.078	0.048	0.048
3	3-SNv-7.5-1	0.095	0.095	0.101	0.101
4	4-SPv-7.5-1	0.109	0.090	0.096	0.096
5	5-SNv-7.5-2	0.090	0.085	0.098	0.115
6	6-SPv-7.5-2	0.122	0.110	0.128	0.158
7	7-SPv-15-1	0.119	0.131	0.108	0.118
8	8-SNv-15-1	0.133	0.133	0.111	0.132
9	9-SPv-15-2	0.121	0.134	0.114	0.126
10	10-SNv-15-2	0.123	0.106	0.120	0.130
11	11-SNk-15-1	0.108	0.108	0.120	0.134
12	12-SPk-15-1	0.121	0.124	0.106	0.129
13	13-SPk-15-2	0.125	0.121	0.156	0.156
14	14-SNk-15-2	0.125	0.125	0.095	0.178

Preglednica 3.44: Povprečne vrednosti ξ za cikle karakterističnih mejnih stanj ponovljenih testov

Table 3.44:Average values of ξ for characteristic limit state cycles for test repetitions

Pre-compr. level	Boundary condition	Morphology	Characteristic limit state							
			d_{cr}		d_e		d_{Fmax}		d_{max}	
			ξ mean	c.o.v. [%]	ξ mean	c.o.v. [%]	ξ mean	c.o.v. [%]	ξ mean	c.o.v. [%]
5	cantilever	Connected	/	/	0.039	/	0.035	/	0.035	/
7.5	cantilever	Connected	0.055	/	0.073	/	0.047	/	0.047	/
		Unconnected	0.058	/	0.078	/	0.048	/	0.048	/
	fixed-fixed	Connected	0.116	5.4	0.100	10.2	0.112	14.0	0.127	24.1
		Unconnected	0.093	2.7	0.090	5.8	0.100	1.7	0.108	6.1
15	cantilever	Connected	0.120	0.7	0.132	1.0	0.111	2.3	0.122	3.0
		Unconnected	0.128	4.1	0.120	11.3	0.115	3.7	0.131	0.8
	fixed-fixed	Connected	0.123	1.6	0.122	1.1	0.131	18.9	0.142	9.7
		Unconnected	0.117	7.3	0.117	7.3	0.108	11.6	0.156	14.0

Preglednica 3.45: Povprečne vrednosti ξ za cikle karakterističnih mejnih stanj za teste z enakimi pogoji preskušanja

Table 3.45: Average values of ξ for characteristic limit state cycles for tests with the same testing conditions

Pre-compression level Boundary conditions	Characteristic limit state							
	d_{cr}		d_e		d_{Fmax}		d_{max}	
	ξ mean	c.o.v. [%]	ξ mean	c.o.v. [%]	ξ mean	c.o.v. [%]	ξ mean	c.o.v. [%]
7.5% f_{Mc}, cantilever	0.056	2.8	0.076	3.7	0.047	1.7	0.047	1.7
7.5% f_{Mc}, fixed-fixed	0.098	8.21	0.090	4.54	0.098	2.09	0.104	7.73
15% f_{Mc}, fixed-fixed	0.124	4.3	0.126	9.2	0.113	3.6	0.127	4.3
15% f_{Mc}, cantilever	0.120	5.8	0.119	5.6	0.119	19.2	0.149	13.1

Comparing the ξ for the characteristic limit state cycles for tests with the same boundary conditions and pre-compression level of the unconnected and connected walls, there is no rule, for which type of morphology ξ for the characteristic limit state cycles is greater (Table 3.44). ξ is for all characteristic limit state cycles considerably smaller for the tests 1-2, where flexural mechanism developed; 0.047 in average at d_{max}. If fixed-fixed boundary conditions under the same pre-compression level or both boundary conditions and higher pre-compression level were applied, the lowest value of ξ at d_{Fmax} cycles for tests is 0.106. As expected, for pre-compression level 15% f_{Mc}, values of ξ are for tests at all characteristic limit state displacements higher than for lower pre-compression level, whereas in tests with fixed-fixed boundary conditions for higher pre-compression level ξ are at d_{Fmax} and d_{max} smaller compared to cantilever conditions – not as one would expect having in mind energy dissipation indicators analysed within the previous subsection. The reason for this lies within the simplification of the E_{INP} calculation.

3.4.6.2.1 Comparison with values of ξ obtained by other authors

In the literature not many values of ξ can be found for tested masonry elements. Equivalent viscous damping was also evaluated and it's evolution thoroughly described for an in-situ stone masonry test by Costa et al [248]. The tested wall behaviour was characterized by diagonal cracking and shear sliding The authors' observations are: »Even for small drift values as 0.1%, the hysteresis is significant leading to an equivalent hysteretic damping value of 12% mainly explained by permanent deformations developed at the joints already for small displacement levels. It is a considerably high value, which is not usually associated with this type of material (double leaf stone masonry with poor infill). The evolution of hysteretic damping is almost linear with the evolution of drift up to the formation of a complete diagonal crack to the foundation which occurred for the drift cycle of 0.75%. Therefore, it led to significant residual deformations along the wall and an equivalent hysteretic damping level of 26%. The final part of the test (drift of 1.0 and 1.25%) shows a constant hysteretic damping level close to 25% as a result of the severe damage observed and permanent deformations of the wall.«

Compared to results of Costa et al, values obtained in our tests (for shear response 0.131) are lower and can be compared only to the lowest value of ξ (0.12) and not to higher values obtained towards the end of the test (0.26).

3.4.7 Strength degradation

Due to repetitions of cycles at the same amplitude displacements, it was possible to analyse stiffness and strength changes at repetitions. In [246], plots of strength decrease (in percentage) for each loading repetition, both in positive and in negative direction are presented in dependence of amplitude displacement of the evaluated cycle repetitions. The decrease ΔF_{rel} of the kth cycle of loading is calculated as the difference of the maximum resistance at 1st positive cycle of loading $F^{1}_{max,i}$ and either maximal force $F^{1}_{max,i}$ or absolute value of minimal force obtained $F^{1}_{min,i}$ (in dependence to direction of loading), normalized to the $F^{1}_{max,i}$ (Eq 3.15). Negative values therefore present an increase of absolute minimal or maximal force relative to force attained at 1st cycle.

$$\Delta F_{rel} = \begin{cases} \dfrac{F^{1}_{\max,i} - F^{k}_{\max,i}}{F^{1}_{\max,i}}, & \text{if } F > 0 \\ \dfrac{F^{1}_{\max,i} - abs(F^{k}_{\min,i})}{F^{1}_{\max,i}}, & \text{if } F < 0 \end{cases} \qquad \textbf{3.15}$$

The average strength decrease at the 2nd cycle (left) and 3rd cycle (right) of loading is for each test presented in dependence of positive amplitude displacement, normalized to minimal of absolute displacements where maximal and minimal force were attained (labelled as d_{max}). Values of strength decrease for each "half" cycle at characteristic limit states d_{cr}, d_{Fmax} and d_{max} for all tests are presented in Tables 3.46-3.48. "Half" cycle refers to loading and unloading the wall in one direction, whereas the other "half" cycle to loading and unloading the wall in the other direction.

Preglednica 3.46: Padanje nosilnosti za posamezno smer obremenjevanja ter ponovitve ciklov pri amplitudnih pomikih, kjer so bile zaznane prve strižne razpoke

Table 3.46: Strength decrease in each loading direction and cycle repetitions at amplitude displacements where the first shear cracks were observed

Test no.	Name	ΔF_{rel} at displacement d_{cr} [%]				
		1st neg	2nd pos	2nd neg	3rd pos	3rd neg
1	1-SPk-5-1	/	/	/	/	/
1.2	1.2-SPk-7.5-1	3.7	/	/	/	/
2	2-SNk-7.5-1	6.6	0.0	6.5	-0.1	6.6
3	3-SNv-7.5-1	11.3	0.7	12.2	0.9	12.8
4	4-SPv-7.5-1	14.0	0.6	6.5	-16.7	6.3
5	5-SNv-7.5-2	4.4	1.3	5.5	2.5	5.8
6	6-SPv-7.5-2	11.2	2.4	13.8	3.7	15.8
7	7-SPv-15-1	-2.4	-3.1	-5.1	-5.0	-6.8
8	8-SNv-15-1	-3.3	-1.1	-5.3	-2.3	-6.1
9	9-SPv-15-2	-0.8	-1.0	-2.3	-1.4	-4.4
10	10-SNv-15-2	-33.2	-13.2	-34.5	-19.2	-34.2
11	11-SNk-15-1	-8.9	-2.8	-11.5	-4.5	-13.4
12	12-SPk-15-1	4.2	-2.9	2.9	-4.4	1.4
13	13-SPk-15-2	-3.2	-2.9	-4.6	-4.6	-5.7
14	14-SNk-15-2	0.2	-2.4	-2.2	-4.3	-3.7

Preglednica 3.47: Padanje nosilnosti za posamezno smer obremenjevanja ter ponovitve ciklov pri amplitudnih pomikih, kjer so bile dosežene maksimalne nosilnosti

Table 3.47: Strength decrease in loading direction and cycle repetitions at amplitude displacements, where maximum resistances were obtained

Test no.	Name	ΔF_{rel} at displacement d_{max} [%]				
		1st neg	2nd poz	2nd neg	3rd poz	3rd neg
1	1-SPk-5-1	-1.0	1.8	-0.9	1.9	-1.0
1.2	1.2-SPk-7.5-1	-10.9	/	/	/	/
2	2-SNk-7.5-1	6.6	2.1	6.6	1.8	6.6
3	3-SNv-7.5-1	-5.4	8.1	-5.6	15.1	-0.8
4	4-SPv-7.5-1	13.9	8.7	18.4	14.2	23.1
5	5-SNv-7.5-2	-3.4	6.0	-0.5	10.2	3.6
6	6-SPv-7.5-2	16.6	3.9	20.0	6.5	22.4
7	7-SPv-15-1	1.7	2.9	4.7	7.6	9.2
8	8-SNv-15-1	8.7	3.9	11.8	6.3	13.2
9	9-SPv-15-2	5.0	3.3	1.2	6.7	3.8
10	10-SNv-15-2	12.7	3.6	17.5	7.5	18.1
11	11-SNk-15-1	3.3	0.6	-2.5	1.7	-2.8
12	12-SPk-15-1	9.2	-0.9	9.5	-1.3	10.1
13	13-SPk-15-2	8.5	1.1	0.9	0.9	1.1
14	14-SNk-15-2	4.6	-0.4	6.4	1.4	8.7

Preglednica 3.48: Padanje nosilnosti za posamezno smer obremenjevanja in ponovitve ciklov pri maksimalnih amplitudnih pomikih

Table 3.48: Strength decrease in loading direction and cycle repetitions at maximum amplitude displacements

Test no.	Name	ΔF_{rel} at displacement d_{Fmax} [%]				
		1st neg	2nd poz	2nd neg	3rd poz	3rd neg
1	1-SPk-5-1	-1.0	1.8	-0.9	1.9	0.0
1.2	1.2-SPk-7.5-1	-10.9	/	/	/	/
2	2-SNk-7.5-1	6.6	2.1	6.6	1.8	6.6
3	3-SNv-7.5-1	-5.4	8.1	3.5	15.1	0.0
4	4-SPv-7.5-1	13.9	8.7	18.4	14.2	23.1
5	5-SNv-7.5-2	-1.0	7.0	10.5	14.6	19.2
6	6-SPv-7.5-2	24.0	3.8	31.7	8.1	34.8
7	7-SPv-15-1	-3.5	14.3	6.3	24.7	14.3
8	8-SNv-15-1	1.9	7.1	6.5	13.2	11.1
9	9-SPv-15-2	15.3	4.4	19.5	6.2	0.0
10	10-SNv-15-2	7.8	4.0	10.0	6.0	12.4
11	11-SNk-15-1	10.3	/	/	/	/
12	12-SPk-15-1	13.5	3.3	15.3	5.3	19.6
13	13-SPk-15-2	8.5	1.1	17.4	0.9	25.7
14	14-SNk-15-2	0.1	0.0	6.4	0.0	8.7

Average values of strength decrease for each cycle are presented (Figures 3.65, 3.66; Tables 3.49, 3.5, 3.51). They are for *i*-th amplitude displacement determined as the difference between average maximum force of 1st cycle and *k*th cycle (2nd or 3rd), normalized to average maximum force of the 1st cycle (Eq. 3.16).

$$\Delta F_{rel} = \begin{cases} (F^1_{\max,i} - F^1_{\min,i}) - (F^k_{\max,i} - F^k_{\min,i}) \\ (F^1_{\max,i} - F^1_{\min,i}) \end{cases} \quad \textbf{3.16}$$

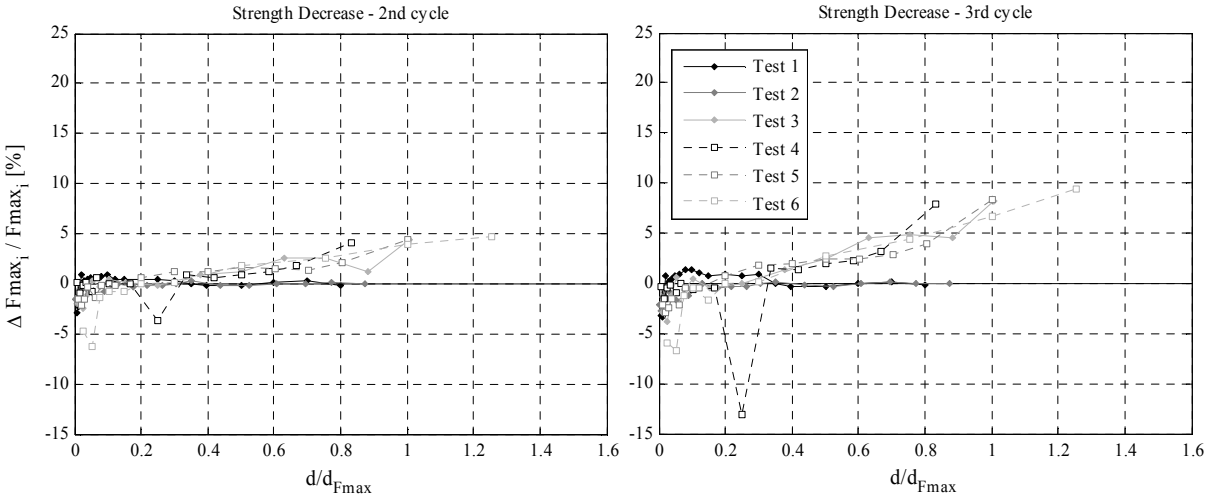

Figure 3.65: Average strength decrease in 2nd (left) and 3rd (right) cycles at amplitude displacements for tests 1-6
Slika 3.65: Povprečno padanje nosilnosti v 2. (levo) in 3. ciklih (desno) v amplitudnih pomikih za teste 1-6

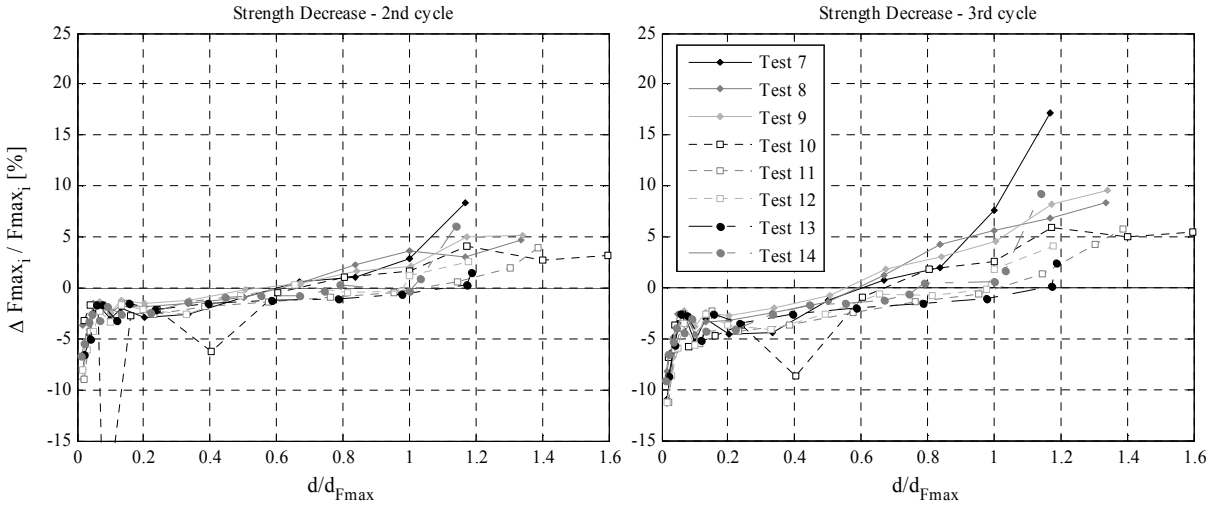

Figure 3.66: Average strength decrease in 2nd (left) and 3rd (right) cycles at amplitude displacements for tests 7-14
Slika 3.66: Povprečno padanje nosilnosti v 2. (levo) in 3. ciklih (desno) v amplitudnih pomikih za teste 7-14

Preglednica 3.49: Povprečno padanje nosilnosti pri ponovitvah ciklov pri karakterističnih pomikih

Table 3.49: Average strength decrease in cycle repetitions for tests at characteristic limit states

Test no.	Name	Mean ΔF_{rel} at d_{cr} [%]		Mean ΔF_{rel} at d_{Fmax} [%]		Mean ΔF_{rel} at d_{max} [%]	
		2nd cycle	3rd cycle	2nd cycle	3rd cycle	2nd cycle	3rd cycle
1	1-SPk-5-1	0.000	0.000	0.974	0.938	0.974	2.363
1.2	1.2-SPk-7.5-1	0.000	0.000	0.000	0.000	0.000	0.000
2	2-SNk-7.5-1	-0.048	-0.010	1.076	0.906	1.076	0.906

Continues…

…continuation of Table 3.49

3	3-SNv-7.5-1	0.833	1.291	8.297	16.169	8.297	17.382
4	4-SPv-7.5-1	-3.685	-13.146	7.094	12.599	7.094	12.599
5	5-SNv-7.5-2	1.246	1.986	4.355	8.416	9.215	17.326
6	6-SPv-7.5-2	2.632	4.392	3.972	6.700	6.513	10.718
7	7-SPv-15-1	-2.864	-4.596	2.945	7.573	11.830	20.837
8	8-SNv-15-1	-1.483	-2.516	3.692	5.652	5.940	11.309
9	9-SPv-15-2	-1.277	-2.516	4.966	8.238	4.681	-1.639
10	10-SNv-15-2	-6.272	-8.696	2.772	4.975	3.221	5.474
11	11-SNk-15-1	-2.593	-4.321	1.985	4.202	/	/
12	12-SPk-15-1	-2.134	-3.706	-0.262	-0.187	2.727	6.052
13	13-SPk-15-2	-2.106	-3.477	5.162	9.393	5.162	9.393
14	14-SNk-15-2	-2.408	-4.124	-0.254	0.638	/	/

From the results in Table 3.49 it can be seen, that in tests, where shear mechanism occurred, despite the noticed cracks (at d_{cr}) strength decrease with cycle repetitions did not occur, whereas it occurred in tests where mixed mechanism was obtained (except for test 4). If strength increase occurred (for mixed or shear failure mechanism), it increased with cycle repetition. Similarly the strength degradation increased with cycle repetition at d_{Fmax} and d_{max} for all tests except at d_{max} of test 10 and d_{Fmax} of test 12 and 14.

Preglednica 3.50: Povprečno padanje nosilnosti v ponovitvah ciklov karakterističnih pomikov za teste z enakimi pogoji preskušanja

Table 3.50: Average strength decrease in cycle repetitions for tests with the same testing conditions

Pre-compression level, Boundary conditions	Mean ΔF_{rel} at d_{cr} [%]		Mean ΔF_{rel} at d_{Fmax} [%]		Mean ΔF_{rel} at d_{max} [%]	
	2nd cycle	3rd cycle	2nd cycle	3rd cycle	2nd cycle	3rd cycle
7.5% f_{Mc}, cantilever	-0.05	-0.01	1.08	0.91	1.08	0.91
7.5% f_{Mc}, fixed-fixed	-0.54	-3.29	6.58	12.39	8.20	15.77
15% f_{Mc}, fixed-fixed	-2.97	-4.58	3.59	6.61	6.42	9.00
15% f_{Mc}, cantilever	-2.31	-3.91	1.66	3.51	3.94	7.72

Preglednica 3.51: Povprečno padanje nosilnosti v ponovitvah ciklov karakterističnih pomikov za teste z enakim porušnim mehanizmom

Table 3.51: Average strength decrease in cycle repetitions for tests with the same prevailing failure mechanism

Failure mechanism	Mean ΔF_{rel} at d_{cr} [%]		Mean ΔF_{rel} at d_{Fmax} [%]		Mean ΔF_{rel} at d_{max} [%]	
	2nd cycle	3rd cycle	2nd cycle	3rd cycle	2nd cycle	3rd cycle
flexural	/	/	0.97	0.94	1.02	1.63
mixed	-0.05	-0.01	1.08	0.91	1.08	0.91
shear	-1.68	-3.29	3.73	7.03	6.47	10.95

According to Table 3.51, in average the highest decrease is obtained in tests where shear mechanism prevailed. Also fixed-fixed boundary conditions (Table 3.50) provoke higher strength decrease at maximum displacements than cantilever boundary conditions.

3.4.8 Stiffness degradation

For each loading cycle *i*, stiffness was evaluated at maximum and at minimal force and corresponding displacements in positive (K_i^+) and negative (K_i^-) direction of loading (Eq. 3.17, 3.18 and Figure 3.67).

$$K_i^+ = \frac{F_{\max,i}}{d_{F\max,i}} \quad \textbf{3.17}$$

$$K_i^- = \frac{F_{\min,i}}{d_{F\min,i}} \quad \textbf{3.18}$$

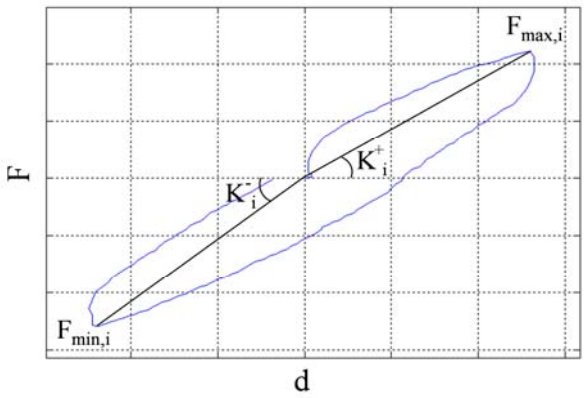

Figure 3.67: Stiffness definition for both directions of loading of a loading cycle
Slika 3.67: Definicija togosti za obe smeri obremenjevanja posameznega cikla obremenjevanja

Stiffness degradation for 1st cycles of all tests is presented in [246]. Both K_i^+ and K_i^- are, for the purpose of comparisons, normalized to effective stiffness K_{ef} for each direction and presented in dependence of corresponding displacements normalized to average displacement at which the maximum and (absolute) minimum force were first attained. In addition to normalized K_i^+ and K_i^-, also average secant stiffness K_i is presented. It was calculated as the slope between the points of the maximum and minimum force of the evaluated cycle (Eq. 3.19).

$$K_i = \frac{F_{\max,i} - F_{\min,i}}{d_{F\max,i} - d_{F\min,i}} \quad \textbf{3.19}$$

In Figure 3.68 a comparison of the stiffness degradation is presented; average stiffness values obtained for the 1st cycles, normalized to average K_{ef}, in dependence from displacements, normalized to the displacement (absolute value), where the maximum resistance was obtained first.

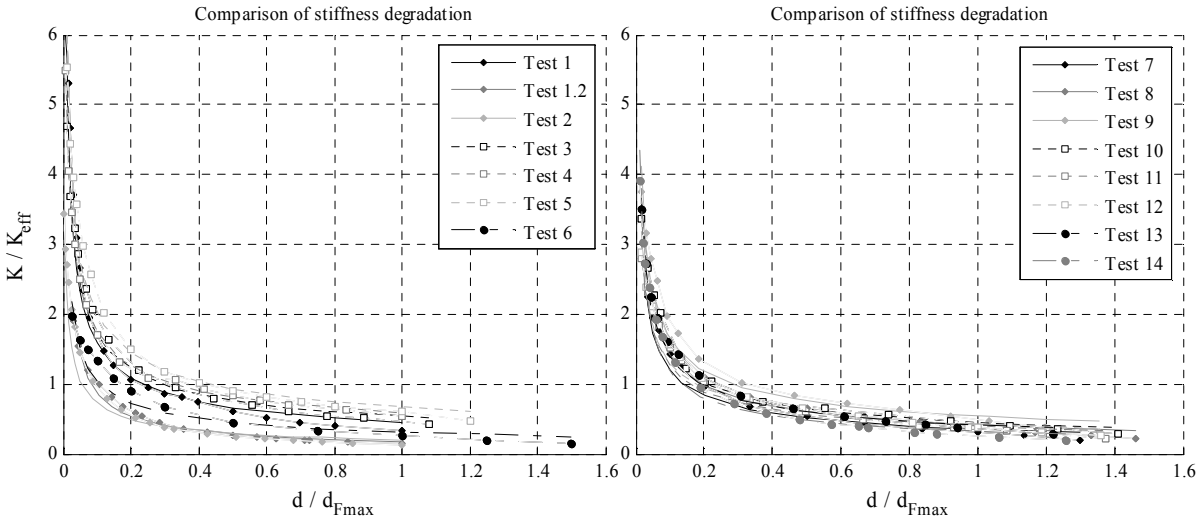

Figure 3.68: Stiffness degradation at 1st cycles of amplitude displacements for tests 1-6 and tests 7-14
Slika 3.68: Padanje togosti za 1. cikle amplitudnih pomikov za teste 1-6 in teste 7-14

From the above it can be seen, that the stiffness falls below the effective in the displacement range of 0.1 to 0.45 d_{Fmax}. Tests 7-14 display more similar stiffness degradation, whereas bigger differences were obtained for tests 1-6, where also rocking and mixed failure mechanisms occurred instead of prevailing shear mechanism.

It can be seen that the shape of the stiffness degradation is similar for all tests. In [94]a simple exponential function is proposed to correlate the stiffness and the deformation of the tested walls (Eq. 3.20):

$$\frac{K}{K_{ef}} = \alpha \left(\frac{d}{d_{F\max}} \right)^{\beta} \qquad \textbf{3.20}$$

Where α and β present the parameters of the stiffness degradation; β the rate and occurrence of the degradation, where with lower values of β, stiffness changes faster and sooner, but it involves lower drop toward its limiting point, whereas α indicates the values of the lower bound (it directly indicates the relative stiffness attained at displacement d_{Fmax}). The values of α and β were calculated separately for K_i^+/K_{ef}^+ (α_{POZ} and β_{POZ}), K_i^-/K_{ef}^- (α_{NEG} and β_{NEG}) and K_i/K_{ef} (α_{AVE} and β_{AVE}). They are presented in Table 3.52.

Preglednica 3.52: Parametri padanja togosti testov, izračunani za pozitivno in negativno smer obremenjevanja ter za njihove povprečne vrednosti

Table 3.52: Stiffness degradation parameters for tests calculated for positive and negative direction of loading and for their average values

Test	Name	Failure mechanism	α_{POZ}	α_{NEG}	α_{AVE}	β_{POZ}	β_{NEG}	β_{AVE}
1	1-SPk-5-1		0.457	0.433	0.449	-0.530	-0.580	0.550
1.2	1.2-SPk-7.5-1	Rocking	0.204	0.161	0.180	-0.590	-0.750	-0.680
2	2-SNk-7.5-1		0.204	0.200	0.202	-0.520	-0.580	-0.550

Continues…

…continuation of Table 3.52

3	3-SNv-7.5-1	Mixed	0.426	0.720	0.538	-0.520	-0.470	-0.500
4	4-SPv-7.5-1		0.600	0.576	0.588	-0.450	-0.490	-0.470
5	5-SNv-7.5-2		0.653	0.689	0.665	-0.430	-0.520	-0.480
6	6-SPv-7.5-2		0.370	0.256	0.310	-0.490	-0.580	-0.530
7	7-SPv-15-1	Shear	0.380	0.324	0.351	-0.490	-0.570	-0.530
8	8-SNv-15-1		0.521	0.334	0.412	-0.480	-0.580	-0.530
9	9-SPv-15-2		0.502	0.586	0.536	-0.420	-0.560	-0.490
10	10-SNv-15-2		0.581	0.369	0.448	-0.480	-0.560	-0.520
11	11-SNk-15-1		0.400	0.405	0.397	-0.440	-0.550	-0.500
12	12-SPk-15-1		0.487	0.371	0.423	-0.420	-0.550	-0.490
13	13-SPk-15-2		0.433	0.431	0.418	-0.460	-0.570	-0.520
14	14-SNk-15-2		0.382	0.275	0.323	-0.500	-0.610	-0.560

In all tests except test 3, β obtained for negative direction of loading exceeded β for positive, which means that stiffness degradation occurred faster in negative direction of loading. No other rule can be obtained regarding this parameter. The average values for both directions range from -0.47 to -0.68. Regarding α obtained for tests, if test 6 is excluded from comparisons, noticeably larger values of α were obtained for tests where mixed behaviour occurred (average values from 0.538 to 0.665), which is again the consequence of smaller K_{ef} values. In tests 1.2 and 2 the lowest values were obtained; 0.18 and 0.20 for average values of both directions. For the shear mechanism, α ranged from 0.323 to 0.536 (average of both directions). According to Tomaževič [46] these parameters depend on the lateral load history and compressive stresses; the author recommends values of α = 0.3 and β = -0.85 for determining K in the case pre-compression load does not exceed 20% of f_{Mc} and if other experimental data is not available. These values define degradation, which is in comparison to our results on the safe side.

3.4.9 Evaluation of shear test results through comparison with analytical models

Considering the strength criteria provided in Table 2.10 (Section 2.3.3.1), the design shear resistance V_{Rd} was evaluated with respect to different boundary conditions and level of pre-compression, considering only mean values for the mechanical properties and not any materials safety coefficients; results are presented in Table 3.53. Ratios of calculated V_{Rd} (according to various criteria) and F_{id} obtained in the test are for each test presented in Figure 3.70, whereas the average of the ratio for tests with the same testing conditions in Table 3.54.

Criterion for evaluating the resistance in the case of diagonal cracking through joints produced in all cases the lowest results. For the calculation of the results, average unit length equal to 20 cm was considered, (despite the units varying in length); even if smaller length is considered, the results are still the most critical. Though cracking through joints indeed occurred in the experimental tests, the estimated $V_{Rd,dj}$ are significantly smaller than resistances obtained in the tests except for test 6. One of the conclusions therefore could be that the diagonal joint criterion underestimates the resistance in case of weak, ductile mortars if the mortar thickness is not excessively thick. Results for $V_{Rd,dj}$ are less conservative, if value 1.0 is considered for b, as opposed to value 1.5 (results for both assumptions are presented in Table 3.53 and Figure 3.70)

For the calculation of $V_{Rd,d}$ (i.e. diagonal cracking resistance), f_{Mt} of 0.18 MPa according to NTC08 code provisions was considered. Upper bound value was chosen due to controlled good quality of masonry. Diagonal cracking model produced the most accurate results for tests, where diagonal shear mechanism has indeed occurred. The results were moderately non-conservative for higher pre-compression level (not higher than 10% in any test except test 6), as the presumed f_{Mt} of the masonry was higher than the actual obtained from the tests. It has to be noted, that for fixed-fixed boundary conditions and higher pre-compression level, results indicate rocking failure prior to diagonal cracking failure of the wall ($V_{Rd,r}$ and $V_{Rd,d}$ are 0.939 F_{id} and 1.064 F_{id}, respectively)

At this point, we can conclude, that if diagonal cracking and rocking occur, criteria a) and b) in Table 2.10 adequately determine the design resistance; provided that the tensile strength is properly estimated. This is not the case only in already mentioned test 6, where all the criteria except diagonal cracking through joint highly overestimate the resistance.

Preglednica 3.53: Po modelih za različne porušne mehanizme analitično izračunane mejne horizontalne sile (v odvisnosti od različnih nivojev predkompresije in robnih pogojev)

Table 3.53: Analytically calculated shear resistances considering models for various failure mechanisms (in dependence of pre-compression level and boundary conditions)

Pre-compression level, Boundary conditions	$V_{Rd,r}$ [kN]	$V_{Rd,d}$ [kN]	$V_{Rd,dj}$ [kN] (b=1.5)	(b=1.0)	$V_{Rd,du}$ [kN]	$V_{Rd,s}$ [kN]	Prevailing mechanism obtained in the tests
7.5% f_{Mc}, cantilever	55.5	89.8	31.6	33.7	6659	60.0	rocking
7.5% f_{Mc}, fixed-fixed	111.1	89.8	36.9	43.3	6549	119.9	mixed; shear failure
15% f_{Mc}, cantilever	105.6	119.6	55.7	81.6	6538	124.9	shear
15% f_{Mc}, fixed-fixed	211.3	119.6	59.8	86.2	6495	249.5	shear

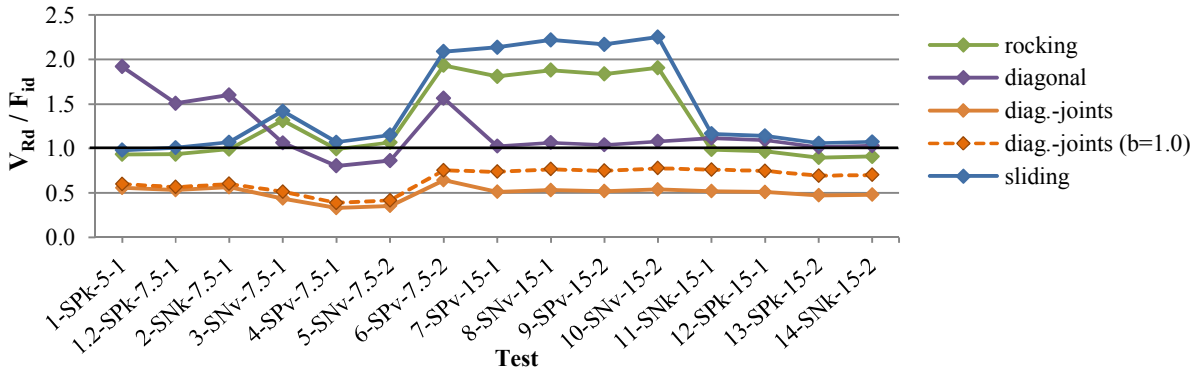

Figure 3.69: Ratio between analytically calculated shear resistances for various failure mechanisms and from tests idealized shear resistance for each test

Slika 3.69: Razmerja med analitično izračunanimi mejnimi horizontalnimi silami za različne porušne mehanizme z iz testa idealizirano maksimalnimo strižno silo za posamezni test

Preglednica 3.54: Povprečne vrednosti razmerij analitično izračunanih mejnih horizontalnih sil za različne porušne mehanizme z idealiziranimi maksimalnimi silami, dobljenimi po testih

Table 3.54: Average ratios of analytically calculated shear resistances for various failure mechanisms and idealized resistances obtained through tests

Pre-compression level, Boundary conditions	$V_{Rd,r} / F_{id}$		$V_{Rd,d} / F_{id}$		$V_{Rd,dj}^{*} / F_{id}$		$V_{Rd,du} / F_{id}$		$V_{Rd,s} / F_{id}$	
	(A_w)	$(A_{w,n})$	(A_w)	$(A_{w,n})$	(A_w)	$(A_{w,n})$	(A_w)	$(A_{w,n})$	(A_w)	$(A_{w,n})$
7.5% f_{Mc}, cantilever	0.96	0.94	1.56	1.30	0.58	0.68	115.3	85.7	1.04	1.04
7.5% f_{Mc}, fixed-fixed (all)	1.33	1.29	1.07	0.90	0.52	0.56	78.2	58.5	1.43	1.43
without test no.6	1.12	1.09	0.91	0.76	0.44	0.48	66.3	49.6	1.21	1.21
Samo test št. 6	1.93	1.88	1.56	1.30	0.75	0.82	114.0	85.2	2.09	2.09
15% f_{Mc}, konzolno	1.86	1.74	1.05	0.89	0.76	0.71	57.1	43.5	2.19	2.19
15% f_{Mc}, vpeti	0.939	0.88	1.064	0.90	0.73	0.66	58.1	44.3	1.11	1.11

* $V_{Rd,dj}$ is calculated considering b=1.0

Results provided in Table 3.54 and in Figure 3.70 also show the adequacy of V_{Rd} estimation considering entire wall cross section A_w as oppose to considering net cross section $A_{w,n}$, where only external leaves are considered. For three-leaf masonry, where the inner core is without larger voids and the thickness of the external leaves is not less than 75% of the entire thickness ($2t_l \geq 75\%\ t_w$), the contribution of inner core should not be treated separately for the estimation of lateral resistance.

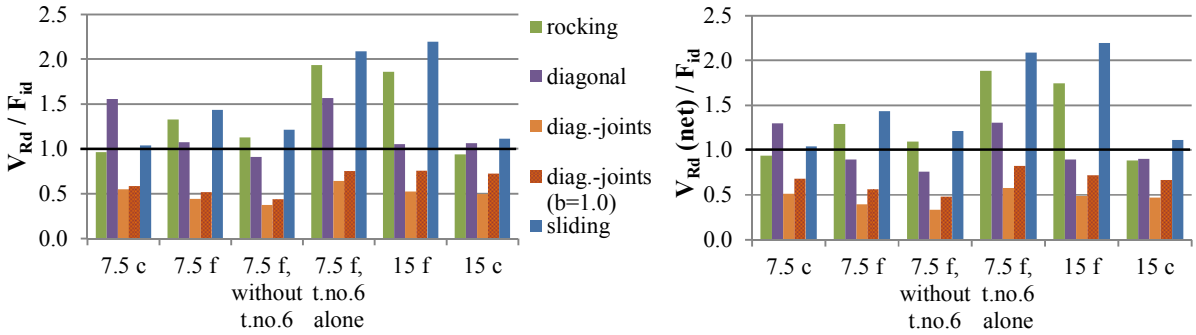

Figure 3.70: Average ratios between analytically calculated shear resistances for various failure mechanisms, considering gross (left) and net (right) cross section and idealized resistances obtained through tests

Slika 3.70: Povprečne vrednosti razmerij med analitično izračunanimi mejnimi horizontalnimi silami za različne porušne mehanizme z upoštevanjem celega (levo) in neto (desno) prečnega prereza zidu z idealiziranimi maksimalnimi silami, dobljenimi po testih

3.4.10 Summary and discussion of the results

Within the experimental studies, altogether 15 in-plane cyclic shear tests were performed on 14 walls. In order to study the behaviour in case of different failure mechanisms, the testing conditions were varied. Besides the different morphology of the specimens (with or without through stones), different pre-compression load ((5), 7.5 and 15% of f_{Mc}) and boundary conditions (cantilever or fixed-fixed) were applied.

With varying testing conditions indeed various failure mechanisms of the walls were attained. Lower pre-compression ((5), 7.5% f_{Mc}) and cantilever boundary conditions provoked rocking, where the joint between the first and the second row of stones due to flexure opened. Restraining the rotations at the bottom enabled diagonal shear mechanism to partially develop; this failure mechanism was classified as mixed. High pre-compression level (15% f_{Mc}) induced diagonal shear behaviour with some toe crushing and formation of vertical columns along the edges in both cases of boundary conditions.

Out-of-plane deformations were not as problematic issue as expected; leaf separation occurred with the development of shear mechanism, however it significantly progressed only in the post-peak phase of the test. Leaf separation was more apparent with cantilever boundary conditions, with header stones present or not, as oppose to fixed-fixed boundary conditions, where through stones, if present, limited the separation of the leaves. Similar conclusion as from compressive tests can therefore be drawn also from shear tests; besides the mentioned effect of limiting the post-peak leaf separation, the presence of header stones did not have any influence on the response of the tested type of masonry (external leaves thickness more than 75% of t_w, inner core sufficiently filled and connected, not too many voids present).

The type of the formed mechanism had the greatest effect on the strength and displacement capacity of the walls. In dependence of the developed damage and failure mechanism also other characteristic parameters of in-plane shear hysteretic response of walls (i.e. stiffness and shear modulus, energy dissipation, strength and stiffness degradation) differed.

With rocking mechanism, as expected, the resistance was the lowest (average F_{max} equal to 57.5 kN), but the displacement capacity was the highest (59.8 mm). Mixed failure obtained through fixed boundary conditions increased the resistance (F_{max} 105.7 kN), but decreased the displacement capacity significantly (28.2 mm). Resistance was the highest for shear failure (F_{max} 120.8 kN), but since the developed mechanism was diagonal (and not sliding), the displacement capacity additionally decreased (23.0 mm). It however has to be emphasized, that even for shear failure, brittle failure did not occur; the walls exhibited a considerable post-peak displacement capacity; in average d_{max} was equal to 1.40 d_{Fmax}. Rocking mechanism exhibited very ductile behaviour with slight strength decrease, (in average 2.8%), but on the other hand mixed failure led to more brittle failure (in average d_{max} equal to 1.10 d_{Fmax}). Post-peak resistance decrease (at the same amplitude) was the highest at shear mechanism (in average 19.8%), but differed significantly with respect to boundary conditions applied; in average 35.2% for fixed-fixed whereas 13.2% for cantilever boundary conditions.

In order to compare our results to values from the literature and code provisions, the hysteresis envelopes were idealized to bi-linear curves. The procedure for bi-linear idealization is not specifically determined therefore some disagreements with the results of some authors may occur. One of the

problematic and in the literature not consistently determined parameters is the ultimate displacement d_u; for the tests, it was assessed according to both wide used variations; as the displacement at 20% of maximum resistance drop (or d_{max} if this drop is not achieved) and as displacement where the same determined curve intersects the hysteretic envelope (referred as d_u^*).

Idealized resistance F_{id} obtained was used to determine tensile strength of the walls f_{Mt}. For walls tested under higher pre-compression level average f_{Mt} equal to 0.164 MPa was evaluated whereas for tests with lower pre-compression level and fixed-fixed boundary conditions, where mixed failure mechanism occurred, corresponding average f_{Mt} is 0.182 MPa.

Comparing the ultimate displacement capacity (d_u), the specimens that failed due to rocking exhibited average drifts equal to 3.99%, specimens at which mixed failure occurred 1.88% (average value without test 6) and for shear mechanism equal to 1.53%. The obtained ultimate displacement capacities are significantly higher than those recommended in the code provisions; for our walls for rocking 1.60% and 0.80% for cantilever and fixed boundary conditions according to EC8-3 (NC limit) whereas 0.60% and 0.30% according to FEMA (CP limit); for shear the ultimate drift capacity is 0.53% according to EC8-3. The values of drifts obtained in our tests as well as some other studies on historic masonry walls (of which the main characteristic compared to modern is a more ductile mortar) indicate, that displacement capacity of such masonry can be significantly underestimated. One of the possibilities for solving this issue would be to provide drift limits in correspondence to the type of masonry.

Regarding the evaluation of other performance limit states of the tested walls, the first shear cracks (d_{cr}) were obtained at average drift of 0.22% for shear mechanism, whereas at 0.55% for mixed mechanism. Drift limit in case of mixed mechanism seem to be increased for similar value for both d_{cr} (for 0.33%) and d_{max} (for 0.35%) limit states compared to drift limits in the case of shear mechanism. Maximum resistance is reached at average drift of 3.94% for rocking mechanism, 1.71% for mixed and 1.10% for shear mechanism. Drifts corresponding to elastic displacement d_e were 0.73% for rocking, 0.88% for mixed and 0.38% for shear mechanism. Corresponding ductility coefficients (considering d_u) were 6.23, 2.23 and 4.19 for rocking, mixed and shear mechanism, respectively. Regarding ductility, cantilever boundary conditions produce higher μ ratios. For our tests, in average more than 2-times higher elastic displacements were obtained with mixed mechanism compared to shear, which result from lower effective stiffnesses. In terms of μ, mixed mechanism therefore proved to be the less favourable.

The effective stiffness K_{ef} depends considerably from the idealization criteria and as the hysteretic responses differ due to various failure mechanisms obtained, the G_M modulus calculated from K_{ef} produced in some cases unrealistic results; for higher pre-compression level and cantilever boundary conditions average G_M was equal to 2094 MPa, while for fixed-fixed boundary conditions to 129.9 MPa. More stable was the estimation of G_M directly from the hystereses; however for the initial phases of the test with no or very slight damage (i.e at displacement d = 1.5 mm) obtained values for shear moduli are significantly lower (average G_M in case of shear mechanism equal to 123.7 MPa) than the values obtained from compressive tests (357 MPa). In NTC08, the recommended values for G_M of dressed rectangular stone masonry are 780 MPa (minimum) and 940 MPa (maximum).

For evaluating the dissipation of energy, various parameters were analysed; input and dissipated energy, their ratios at characteristic amplitude displacement cycles as well as on the global scale (their cumulative values). Also input energy of the bi-linear idealized response, normalized cumulative energy dissipation according to Shing, as well as the within the thesis proposed modified normalized cumulative energy dissipation were assessed. The results show that energy dissipation is closely related to prevailing damage mechanism and that it is relatively (compared to input energy) the highest at lower displacements, when initial damage on the specimens occurs, and after the peak resistance when the major damage occurs. For rocking, the dissipated energy compared to the input energy (E_{DIS}/E_{INP}) is the lowest throughout the tests (compared to mixed and shear mechanism); at maximum resistance E_{DIS}/E_{INP} was 0.187, whereas 0.521 and 0.496 were obtained for mixed and for shear mechanism. Similar values were obtained for cumulative ratio $cumE_{DIS}/cumE_{INP}$; 0.214, 0.497 and 0.512 for rocking, mixed and shear mechanism, respectively.

Also the analysis of equivalent viscous damping coefficients ξ provided the same conclusions upon energy dissipation; average value for flexural response at d_{max} was 0.035, for mixed 0.047 and for shear 0.131. Except for the comparison of energy dissipation of connected and unconnected walls, the evaluation through ξ did not provide the same conclusions as the comparison of E_{DIS}/E_{INP} ratio; that is that the connected walls dissipate relatively higher amount of energy than the unconnected. The reason for this lies within the simplification of the calculation of the input energy in the evaluation of ξ according to Jacobsen [114].

It can be concluded that, with respect to energy dissipation (diagonal) shear failure seems to be more favourable compared to rocking behaviour.

At this point it should be mentioned, that for additional evaluation of the results, equivalent elastic resistance ($F_{id}\cdot\mu$) was analysed; 342, 258 and 474 kN were obtained for rocking, mixed and shear failure mechanism. This also indicates the shear mechanism not necessarily being the worst possible.

Analytical models for evaluation of shear resistance estimate the resistance sufficiently for both rocking (V_{Rd} = 0.96 F_{id}) and diagonal shear mechanism (V_{Rd} = 1.02 F_{id}), which we obtained in the tests. The problem however is, that other strength criterion (i.e. diagonal joint failure mechanism) provided more critical results for all cases. The criterion obviously underestimates the resistance in case of weak, ductile mortars in case the mortar thickness is not excessively thick (as in test 6).

It has to be mentioned, that for test 6, significantly lower shear resistance and displacement capacities were obtained (f_{Mt} 0.087 MPa, 1.00% drift) which was the consequence of thicker horizontal mortar joints. All masonry specimens had 11 or 12 courses of stone units (mainly of joint thickness 1.0-2.5 cm), while specimen no.6 had only 10 (resulting in joint thickness 2-3 cm). As most models in the codes do not consider horizontal thickness parameter as influential (except perhaps as dry or thin bed-joints), this influence should be investigated and incorporated in models or some other additional recommendations within code provisions.

3.5 Performance evaluation of the plaster attached to the wall

Within this Section, the plaster damage during the lateral loading of the wall is evaluated and conclusions upon the damage limit states with recommendations for the performance based assessment of existing building carrying plaster with preservation interest, are provided. Results provided hereafter are primarily based on the visual inspection of the plaster during shear loading. Throughout the test, the plaster damage was monitored; a detailed inspection of the plaster surface at each amplitude displacement, the crack development and propagation in sense of both extending (over the plaster surface) and widening were documented. With inspection of the plaster's left and right edge, its detachment was monitored.

During shear tests, 4 specimens were in two different amplitude displacement load cycles monitored also by ground penetrating radar in echo mode and active infrared thermography. This was, in fact, the work of Patricia Cotič within her PhD studies and Damjan Špeglič within his Bachelor thesis work. The results are therefore in detail presented in [249] and [250]. The aim of the measurements was to study the effectiveness of different NDT techniques for the evaluation of gradual plaster damage propagation resulting from the induced shear load. Because the procedures are time consuming and a single shear test would have lasted a few days if these NDT were executed at every amplitude displacement, they were applied rather as a study method and not as a monitoring system for the plaster behaviour during the entire test. Apart from the plaster delamination, NDT enabled to visualize the masonry's typical structure (texture and morphology with the type of connection between leaves) and to study both surface and subsurface crack propagation. It was shown that NDT can help determine the PLs for plasters attached to the wall.

3.5.1 Plaster behaviour

The behaviour of the plaster proved highly dependent on the behaviour (damage and failure mechanism) of the wall. Damage of the plaster during each test is provided in [246] together with structural damage of the walls, as in such way a more clear comparison with the behaviour and the damage of the wall itself can be made. Some typical damage of the plaster is presented in Figure 3.71.

For lower pre-compression level and cantilever boundary conditions, where rocking response of the wall developed, the plaster did not collapse during the tests, despite being significantly detached at sides. Some tiny cracks on the plaster occurred though (Figure 3.73). During these tests, the vertical crack at the side edge indicating plaster detachment usually started to form at the top (damage "a" in Figure 3.71) and it propagated with increasing displacements over entire height (damage "e", Figure 3.71). Afterward, the crack's widened (Figure 3.72).

For walls with shear mechanism, shear cracks formed at lower displacements (damage "b" and "c" in Figure 3.71) and sometimes prevented either the plaster detachment over entire height or the widening of the crack between the wall and the plaster at side (Figure 3.74). In some tests, the plaster collapsed subsequently with increasing displacements (Figure 3.75), whereas in most cases the collapse of the entire plaster was immediate (Figure 3.76).

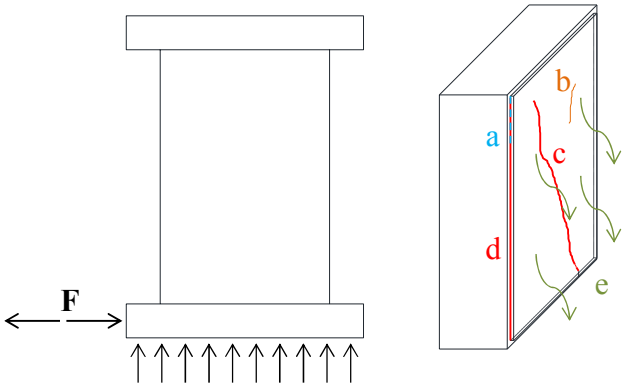

Figure 3.71: Characteristic damage obtained on the plaster at shear tests of walls
Slika 3.71: Karakteristične poškodbe ometov pri strižnih testih zidov

Figure 3.72: Increasing of the plaster's detachment with increasing amplitude displacements at test 8 - SNv-15-1
Slika 3.72: Povečevanje odstopanja ometa s povečevanjem amplitud pomikov pri testu 8 - SNv-15-1

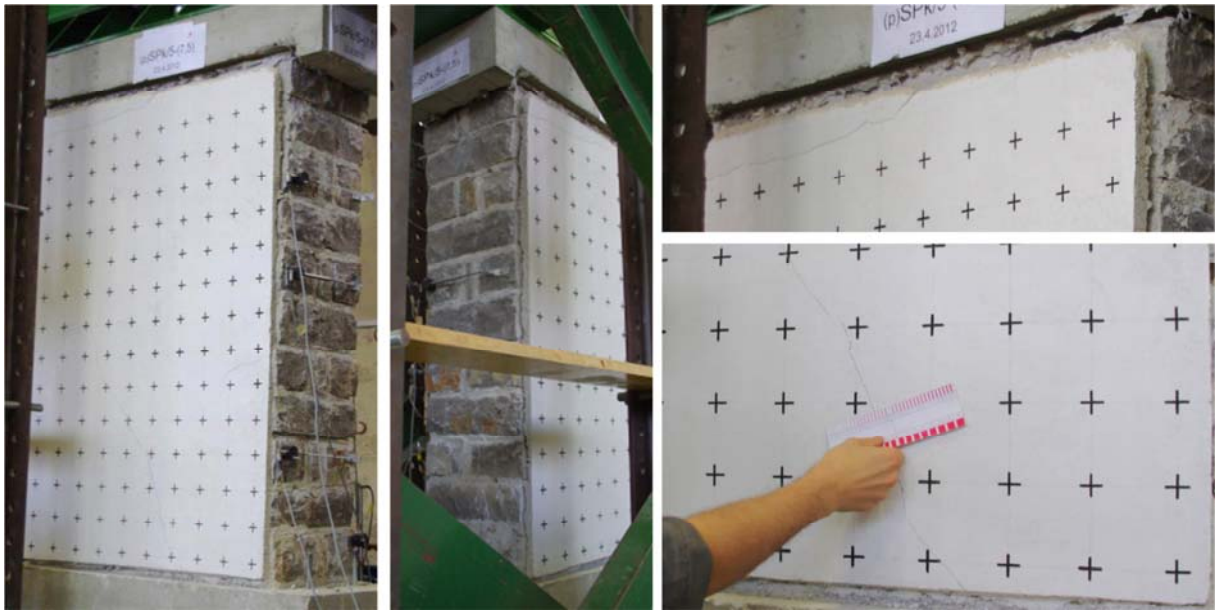

Figure 3.73: Detachment of the plaster and horizontal and diagonal crack on the plaster at test 1.2 - SPk-5-1 (7.5)
Slika 3.73: Odstopanje ometa in horizontalna ter diagonalna razpoka na ometu pri testu 1.2 - SPk-5-1 (7.5)

Figure 3.74: Detachment and collapse of the plaster at test 12 - SPk-15-1 (left two) and 14 - SNk-15-2 (right three)
Slika 3.74: Odstopanje in porušitev ometa pri testu 12 - SPk-15-1 (levi dve sliki) in testu 14 - SNk-15-2 (desne tri)

Figure 3.75: Detachment of the plaster prior its collapse and its subsequent collapse at test 8 - SNv-15-1
Slika 3.75: Odstopanje ometa pred porušitvijo in postopna porušitev pri testu 8 - SNv-15-1

Figure 3.76: Top view of progress of the plaster's collapse at test 14 - SNk-15-2 (photo Željko Stevanić for UL FGG)
Slika 3.76: Pogled od zgoraj na potek porušitve ometa pri testu 14 - SNk-15-2 (foto Željko Stevanić za UL FGG)

3.5.2 Plaster performance limit states

Through damage evaluation, 4 characteristic damage states DS of the plaster were determined:

- DS A1 - first detachment of the plaster;
- DS A2 - first visible crack on the plaster ($d_{cr,AA}$);
- DS A3 - plaster largely detached but still repairable;
- DS A4 - collapse of the plaster ($d_{max,AA}$).

Damage states were labelled with DS A1 – DS A4 in accordance with PERPETUATE methodology and are presented in Figure 3.77. DS A3 was determined as the state, where on (at least) one side edge of the plaster, a detachment over the entire height of the wall was obtained, whereas DS A4 as the state, where the plaster collapsed (either partial or full collapse).

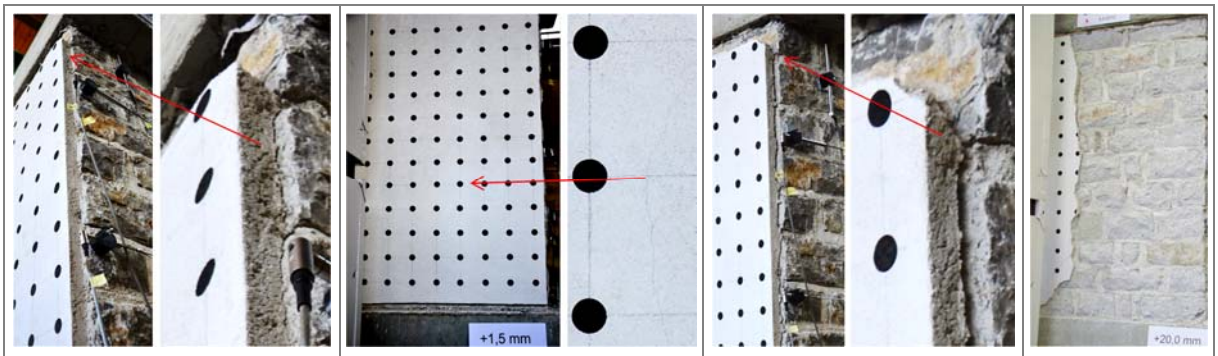

DS A1: first detachment of the plaster	DS A1: first visible crack on the plaster ($d_{cr,AA}$)	DS A3: plaster largely detached but still repairable	DS A4: collapse of the plaster ($d_{max,AA}$)

Figure 3.77. Characteristic damage states of the plaster attached to the wall
Slika 3.77: Karakteristične poškodbe ometa na zidu

The data collected during the tests is presented in Table 3.55 and Figure 3.78, where amplitude displacements and corresponding drifts of the walls, where the four characteristic plaster limit states were obtained, are provided.

Preglednica 3.55: Amplitudni pomiki in pripadajoči zasuki zidov za karakteristična stanja poškodb ometa

Table 3.55: Amplitude displacements and corresponding drifts of the walls in characteristic damage states of the plaster

		Amplitude displacements [mm]				Corresponding drifts [%]			
Test	Name	DS A1	DS A2 ($d_{cr,AA}$)	DS A3	DS A4 ($d_{max,AA}$)	DS A1	DS A2 ($d_{cr,AA}$)	DS A3	DS A4 ($d_{max,AA}$)
1	1-SPk-5-1	6.0	/	/	/	0.40	/	/	/
1.2	1.2-SPk-7.5-1	/	35.0	55.0	/	/	2.33	3.67	/
2	2-SNk-7.5-1	5.0	15.0	60.0	/	0.33	1.00	4.00	/
3	3-SNv-7.5-1	2.0	3.0	12.5	17.5	0.13	0.20	0.83	1.17
4	4-SPv-7.5-1	3.0	7.5	17.0	17.5	0.20	0.50	1.13	1.17
5	5-SNv-7.5-2	2.0	10.0	17.5	20.0	0.13	0.67	1.17	1.33
6	6-SPv-7.5-2	2.0	2.0	10.0	12.5	0.13	0.13	0.67	0.83
7	7-SPv-15-1	1.0	1.0	5.0	10.0	0.07	0.07	0.33	0.67
8	8-SNv-15-1	1.0	1.5	2.0	12.5	0.07	0.10	0.13	0.83
9	9-SPv-15-2	1.5	1.5	7.5	10.0	0.10	0.10	0.50	0.67
10	10-SNv-15-2	1.0	1.0	7.5	12.5	0.07	0.07	0.50	0.83
11	11-SNk-15-1	1.0	1.0	5.0	12.5	0.07	0.07	0.33	0.83
12	12-SPk-15-1	0.8	0.8	7.5	12.0	0.05	0.05	0.67	0.80
13	13-SPk-15-2	1.0	1.5	3.0	10.0	0.07	0.10	0.20	0.67
14	14-SNk-15-2	1.5	0.8	10.0	15.0	0.10	0.05	0.67	1.00

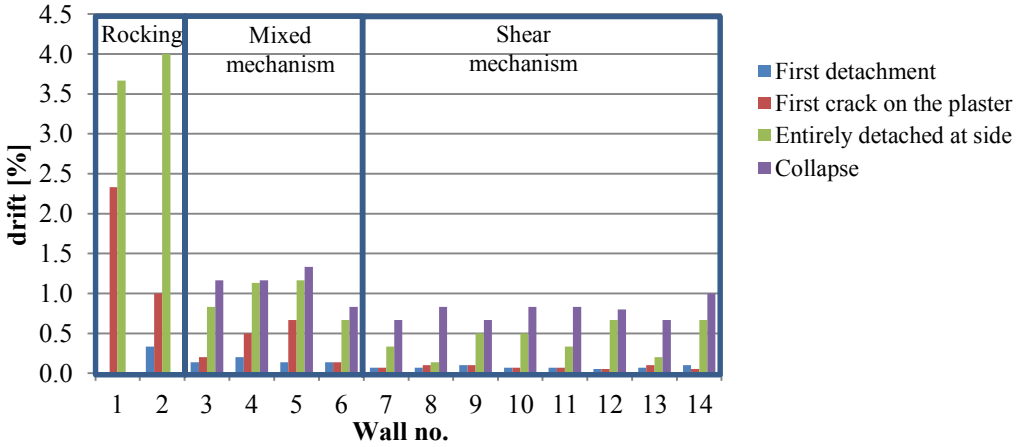

Figure 3.78: Drift values of walls for characteristic plaster performance points
Slika 3.78: Zasuki zidov pri karakterističnih točkah obnašanja ometa

For specimens which exhibited rocking behaviour, the plaster did not collapse, but was however severely detached. For mixed type of failure, drift values for DS A3-A4 states are significantly higher in comparison to the drift limits for the specimens that failed in shear. Average values of drifts at certain characteristic performance points are for the same failure mechanism provided in Table 3.56.

Preglednica 3.56: Povprečne vrednosti amplitudnih pomikov in pripadajoči zasuki zidov za karakteristična stanja poškodb ometov za zidove z enakim porušnim mehanizmom zidov

Table 3.56: Average values of amplitude displacements and corresponding drifts of walls in characteristic damage states of the plaster for walls with the same (wall) failure mechanisms

Prevailing failure mechanism	Drifts [%]							
	DS A1	c.o.v.	DS A2 ($d_{cr,AA}$)	c.o.v.	DS A3	c.o.v.	DS A4 ($d_{max,AA}$)	c.o.v.
Rocking	0.37	0.09	1.67	0.40	3.83	0.04	/	/
Mixed (with test 6)	0.15	0.19	0.38	0.58	0.95	0.22	1.13	0.16
Shear	0.07	0.23	0.08	0.27	0.42	0.45	0.79	0.14

Regarding characteristic damage states before the collapse, DS A2 is in case of rocking mechanism again very high (1.0-2.33%), if attained at all (at test 1, no shear cracks were obtained). Average drift values 0.08% with 0.02% st. dev. and 0.05% minimum drift were obtained for DS A2 in case of shear mechanism. This value is significantly higher, if mixed mechanism was attained (0.38% with 0.22 st. dev. and 0.13% minimum drift). Also DS A3 drifts are the smallest for shear mechanism (average 0.42% with 0.19% st. dev. and minimum 0.13%), followed by mixed (average 0.95% with 0.21% st. dev. and minimum 0.67%) and then by rocking (average drift 3.83%) mechanism. There is however an obvious difference between shear and mixed failure (see Figure 3.78); DS A3 is for mixed failure obtained at larger drift but relatively closer to the plaster's collapse (DS A4), whereas in shear mechanism relatively higher amount of the drift capacity prior collapse remains after achieving DS A3. Comparison of various plaster limit state drifts is for each test presented in Table 3.57 and the average values for the same failure mechanism in Table 3.57.

Preglednica 3.57: Primerjava pomikov (ali zasukov) različnih mejnih stanj ometov in karakterističnih pomikov zidov

Table 3.57: Comparison of various plaster limit state displacements (drifts) to characteristic displacements of the wall

Test	Name	$d_{DS,A2}/d_{cr}$	$d_{DS,A2}/d_e$	$d_{DS,A2}/d_{DS,A4}$	$d_{DS,A4}/d_{DS,A3}$	$d_{DS,A3}/d_e$	$d_{DS,A4}/d_e$	$d_{DS,A4}/d_u$
1	1-SPk-5-1	1.00	/	/		/	/	0.40
1.2	1.2-SPk-7.5-1	/	3.63	/		5.71	/	/
2	2-SNk-7.5-1	0.86	2.09	/		8.35	/	/
3	3-SNv-7.5-1	0.40	0.29	0.17	1.40	1.22	1.71	0.70
4	4-SPv-7.5-1	1.00	0.50	0.43	1.03	1.14	1.18	0.59
5	5-SNv-7.5-2	1.00	0.69	0.50	1.14	1.21	1.38	0.67
6	6-SPv-7.5-2	0.27	0.84	0.16	1.25	4.18	5.23	0.84
7	7-SPv-15-1	0.34	0.24	0.10	2.00	1.21	2.43	0.50
8	8-SNv-15-1	0.30	0.27	0.12	6.25	0.36	2.25	0.56
9	9-SPv-15-2	0.76	0.20	0.15	1.33	0.98	1.31	0.46
10	10-SNv-15-2	0.34	0.16	0.08	1.67	1.22	2.03	0.63
11	11-SNk-15-1	0.34	0.20	0.08	2.50	1.02	2.55	0.56
12	12-SPk-15-1	0.25	0.14	0.06	1.60	1.38	2.21	0.54
13	13-SPk-15-2	0.50	0.27	0.15	3.33	0.54	1.81	0.50
14	14-SNk-15-2	0.15	0.12	0.05	1.50	1.56	2.34	0.43

Preglednica 3.58: Povprečne vrednosti razmerij pomikov pri različnih mejnih stanjih ometa in karakterističnih pomikov zidov za teste z enakim porušnim mehanizmom (s k.v.)

Table 3.58: Average ratio values of various plaster and wall characteristic limit states displacements for the same failure mechanism (with c.o.v.)

Prevailing failure mechanism	$d_{DS,A2}/d_{cr}$ (c.o.v.)	$d_{DS,A2}/d_e$ (c.o.v.)	$d_{DS,A2}/d_{DS,A4}$ (c.o.v.)	$d_{DS,A4}/d_{DS,A3}$ (c.o.v.)	$d_{DS,A3}/d_e$ (c.o.v.)	$d_{DS,A4}/d_e$ (c.o.v.)	$d_{DS,A4}/d_u$ (c.o.v.)
Rocking	0.94	2.86	/	/	7.03	/	/
	(0.078)	(0.270)	/	/	(0.188)	/	/
Mixed	0.81	0.50	0.37	0.85	1.19	1.42	0.65
	(0.353)	(0.328)	(0.385)	(0.124)	(0.029)	(0.154)	(0.076)
Mixed (with test 6)	0.67	0.58	0.32	0.84	1.94	2.37	0.70
	(0.505)	(0.351)	(0.481)	(0.113)	(0.669)	(0.699)	(0.129)
Shear	0.37	0.20	0.10	2.00	1.04	2.12	0.52
	(0.274)	(0.359)	(0.375)	(0.368)	(0.176)	(0.173)	(0.274)

Comparing the performance of the plaster and of the wall, it may be concluded that the damage was much more apparent on the plaster than on the wall. In most cases it was visually confirmed at earlier stage of loading compared to the damage visually observed on the wall. The structural cracks on the wall refer to the un-plastered leaf, since on the plastered leaf they could not be monitored. It is not necessary, that the occurrence of cracks on the plastered leaf coincided with their occurrence. The results, presented in Table 3.57, are however based on the presumption that they did.

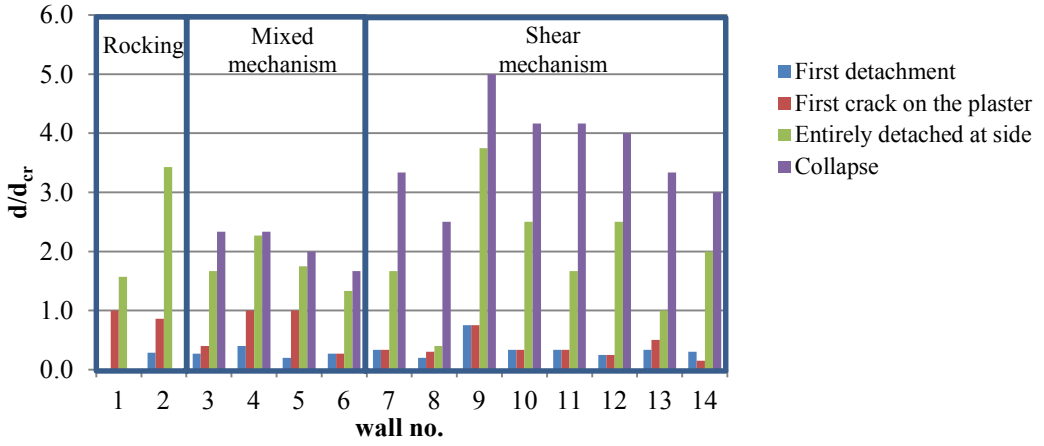

Figure 3.79: Displacements of the wall at plaster performance limits relative to amplitude displacement of the first shear crack on the wall (d_{cr})

Slika 3.79: Pomiki zidov pri mejnih stanjih ometa relativno na amplitudne pomike zidov pri njihovi 1. strižni razpoki (d_{cr})

For artistic asset damage prevention, the most important limit state is DS A2, where the first crack is obtained. Compared to drifts, where first structural crack was obtained θ_{cr}, in all cases, where shear mechanism was obtained, DS A2 was significantly lower than θ_{cr}; in average slightly over 1/3 of θ_{cr}, but in some cases as low as 15% of θ_{cr}. For mixed mechanism the ratio $d_{DS,A2}/d_{cr}$ was higher; between 27-100%. In two cases the drifts at which the cracks appear on the wall and on the plaster coincide (see Figure 3.79).

For rocking (and mixed mechanism in the first stage of rocking) due to low bond strength of the wall and of the plaster, their junction failed, whereas for shear mechanism (i.e. diagonal failure), the cracks formed due to reached tensile strength of the plaster. Consequently, for mixed mechanism, DS A2 is achieved later compared to θ_{cr}, because the formation of cracks is delayed due to initial rocking mechanism of the wall. Considering the results, rocking positively contributes to drift capacity of the plaster, whether it is the prevailing or just partial damage mechanism. If results for mixed and shear mechanism are compared, average drift capacity after attaining DS A2 prior collapse ($\theta_{DS,A4}$ - $\theta_{DS,A2}$) is very similar; for shear mechanism 0.71%, whereas for mixed 0.75%. This implies that the drift capacity after achieving DS A2 is the same, regardless the size of the drift, where the DS A2 itself occurs.

Regarding the recommendations for the designer, who is assessing the performance of an existing heritage building and is interested in the performance limit states of a wall with an artistic asset, one possibility on how to determine the critical DS of AA would be, to consider absolute drift limits for AA. For this however, the database of the results for different variations of masonry and structural elements, artistic assets, etc. does not exist. Results obtained through our studies provide such drift limits, however they could only be used if the limit displacement of the walls as structural elements would be increased, compared to the values provided in the codes. For example, for DS A4 we obtained minimum value of 0.67% drift, but according to the codes, 0.4% drift is the ”NC” limit for the wall itself, therefore also this value would have to be increased. This is probably an unsafe procedure.

Therefore a better option would be to determine the limit performance states of plaster considering the predicted response of the walls, which is usually a bi-linear curve, since nonlinear analysis is usually performed. As the reference drift for the further estimation we propose the elastic drift of the wall (a value, which does not exist in reality). In Figure 3.80, drifts of plaster damage states relatively to the drifts of walls at d_e are presented, whereas results are also provided in Tables 3.57 and 3.58.

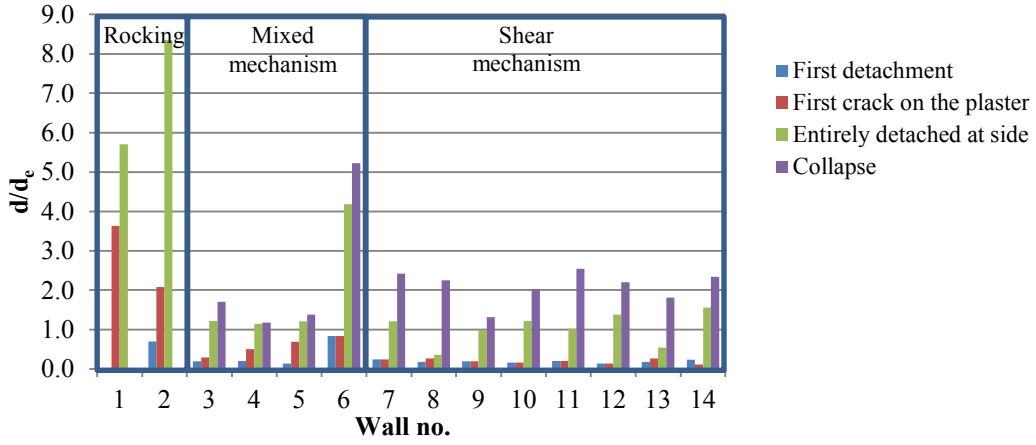

Figure 3.80: Displacements of the wall at plaster performance points relative to elastic displacements of the walls d_e
Slika 3.80: Pomiki zidov pri mejnih stanjih ometa relativno na elastične pomike zidov d_e

In Table 3.59 drift limits for performance limit states θ_{LS}, where limit states are in accordance with the EC code provisions named ”DL”, ”SD” and ”NC”, are proposed for rocking and for shear mechanism.

Drift limit state "DL" corresponds to DS A2, "SD" to DS A3 and "NC" to DS A4. The provided values are calculated as approximate 95% confidence interval (CI) of the test results obtained (approximate due to rounding of the values obtained for 95% CI according to Eq. 3.21).

$$95\%\ \text{CI:}\quad \theta_{LS} = \theta_{LS,mean} - 1.959964 \cdot \sigma_{LS}, \qquad \textbf{3.21}$$

Where θ_{LS} is the proposed drift for certain LS (limit state), $\theta_{LS,mean}$ the average value of the test results and σ_{LS} the (biased) standard deviation.

Preglednica 3.59: Predlog za oceno pomikov za mejna stanja ometov glede na predvideni upogibni ali strižni mehanizem obnašanja zidov, podan v odvisnosti od elastičnega pomika bi-linearne krivulje d_e

Table 3.59: Proposal for plaster performance limit states estimation relative to elastic displacement of the bi-linear curve d_e with regard to predicted response of the wall for shear and rocking failure mechanism

	Performance limit state		
Failure mechanism	θ_{DL}	θ_{SD}	θ_{NC}
Rocking	1.3 d_e	4 d_e	/
Shear	0.1 d_e	0.3 d_e	1.3 d_e

3.5.3 Photogrammetry measurements and results

To confirm the visually determined behaviour of the plaster, at $d_{max,i}$ in both loading directions in each 3rd cycle of every amplitude displacement loading step, a close range photogrammetry, which provided accurate displacements of the signalized points on the plaster, was performed for all tests except for test 1.2. The instructions for data acquisition, the digital image processing and the analysis of the collected data using "bundle adjustment" was done by a professional company, specialised in surveying measurements based on data acquisition and photogrammetric processing. Prior to the tests, black dots, which served as the mentioned signalized points, were painted on the plaster at raster 100 mm x 100 mm. Control points and their 3D position were provided (total station). At each "measuring step", six shots of the plaster (together with control points) were taken from different angles with camera NIKON D7000 (resolution of 4928x3264 pixels). Image position of signalized points on the plaster and of control points were with 1 pixel accuracy obtained by normalized cross-correlation, whereas the following "adaptive least squares image matching" algorithm provided 0.1 pixel accuracy. Bundle adjustment of image measurements of control points, their 3D position and the image measurements of signalized points provided the results for camera positions at certain measurements with camera intrinsic parameters: focal length, radial distortion parameters and, results of our interest, 3D positions of the signalized points on the plaster. The final accuracy of the method was estimated on 0.3 mm.

Unfortunately, the accurate plaster detachment measurements (relative to the wall) could not be obtained from the results of the plaster out-of-plane displacements, because the wall consisted of two outer leaves, each having its own deformations. Even if the displacements of the un-plastered side of wall were measured by photogrammetry, the accurate detachment over the entire surface could not directly be obtained, but only deduced from mechanical measurements on the edges. Nevertheless, the absolute out-of-plane displacements indicating plaster detachment are for all walls presented in Figures 3.81 - 3.84. Surface plots present the out-of-plane displacements at last lateral displacement amplitude before the plaster's collapse, whereas displacements on the edge of the plaster u_{levo} (left),

u_{desno} (right), u_{zgoraj} (upper) in u_{spodaj} (bottom) are provided for 1st measured amplitude displacements, prior which characteristic damage on the plaster and on the wall was obtained.

In Table 3.60 maximum and minimum values of displacements on the left and right edge of the plasters, measured by photogrammetry, are presented.

Preglednica 3.60: Maksimalne in minimalne vrednosti s fotogrametrijo izmerjenih pomikov na levem in desnem robu ometa za posamezne teste

Table 3.60: Maximum and minimum values of displacements on the left and right edge of the plasters, measured by photogrammetry

	Leaf separation	left edge*		right edge	
	Test	*u* (minimum) [mm]	*u* (maximum) [mm]	*u* (minimum) [mm]	*u* (maximum) [mm]
1	1-SPk-5-1	-3.4	1.7	-1.9	9.8
2	2-SNk-7.5-1	-1.1	20.4	-2.3	18.5
3	3-SNv-7.5-1	-1.4	5.9	-0.8	7.8
4	4-SPv-7.5-1	-1	28.5	-0.7	20.1
5	5-SNv-7.5-2	-0.7	10.8	-0.3	15.3
6	6-SPv-7.5-2	-0.6	14.5	-0.1	17.4
7	7-SPv-15-1	-5.2	1.9	-8.3	0.8
8	8-SNv-15-1	-33.7	1.1	-36.6	0.8
9	9-SPv-15-2	-6.8	4.6	-6.6	4.4
10	10-SNv-15-2	-12.8	2.2	-12.1	10.5
11	11-SNk-15-1	-6.5	8.1	-9.4	0.8
12	12-SPk-15-1	-6.5	8.1	-9.4	0.8
13	13-SPk-15-2	-3.7	0.5	-4.4	0
14	14-SNk-15-2	-5.4	2.4	-7.9	1.8

*Left edge does not refer to the left edge but to the measured displacements of the leftest vertical line of signalized points

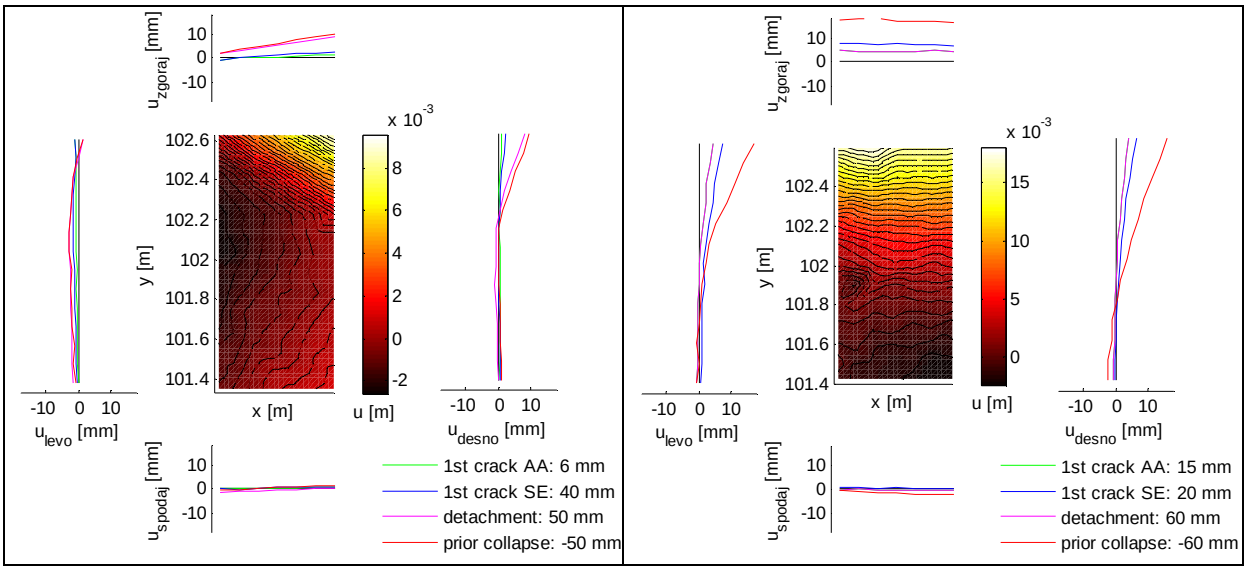

Figure 3.81: Photogrammetry results for tests 1 and 2; out-of-plane displacements of the plaster prior to its collapse and displacements of the plaster edges in characteristic damage states

Slika 3.81: Rezultati fotogrametrije za testa 1 in 2; izven-ravninski pomiki ometa pred porušitvijo in pomiki robov ometa v karakterističnih mejnih stanjih

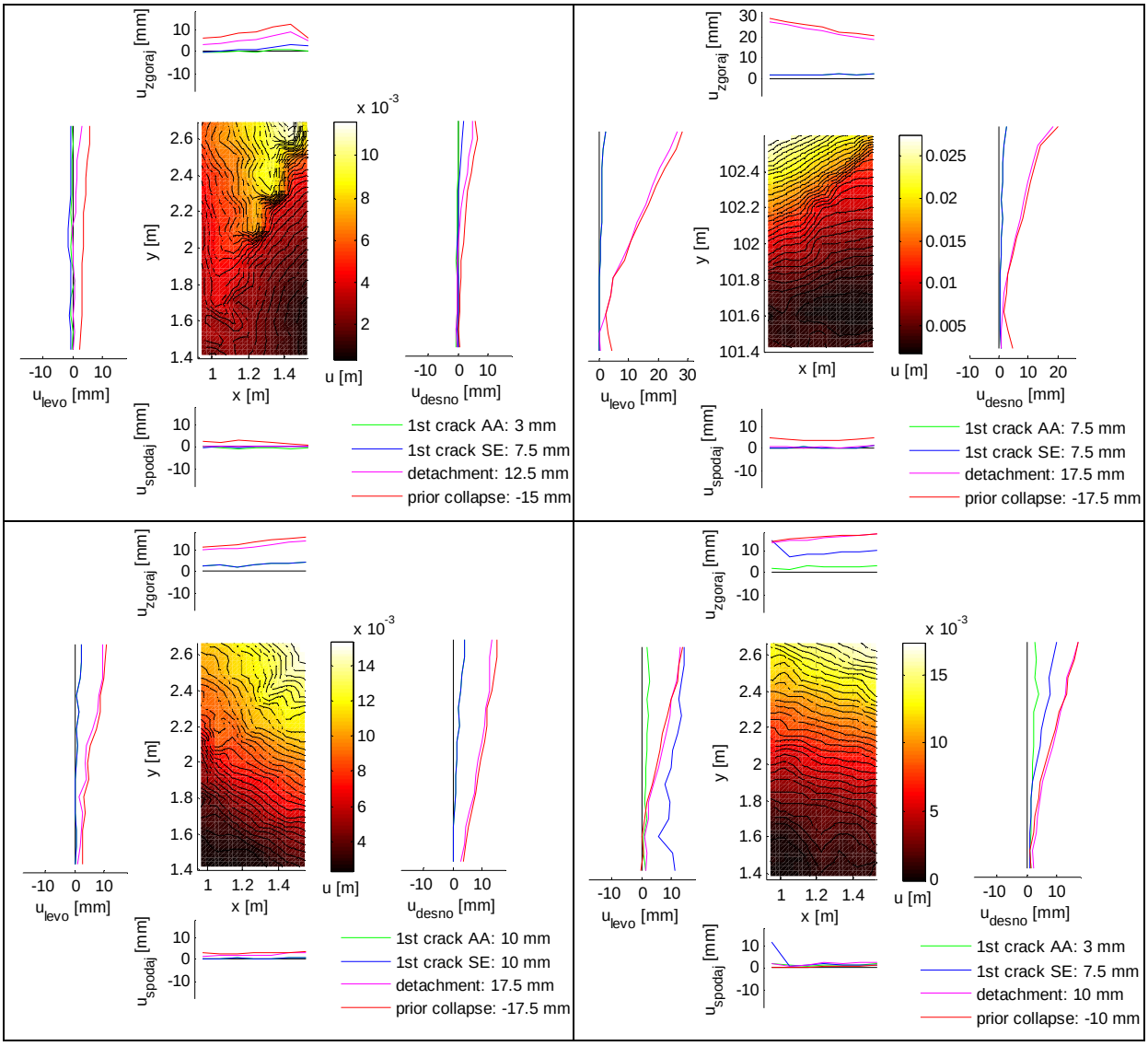

Figure 3.82: Photogrammetry results for tests 3-6; out-of-plane displacements of the plaster prior to its collapse and displacements of the plaster edges in characteristic damage states

Slika 3.82: Rezultati fotogrametrije za teste 3-6; izven-ravninski pomiki ometa pred porušitvijo in pomiki robov ometa v karakterističnih mejnih stanjih

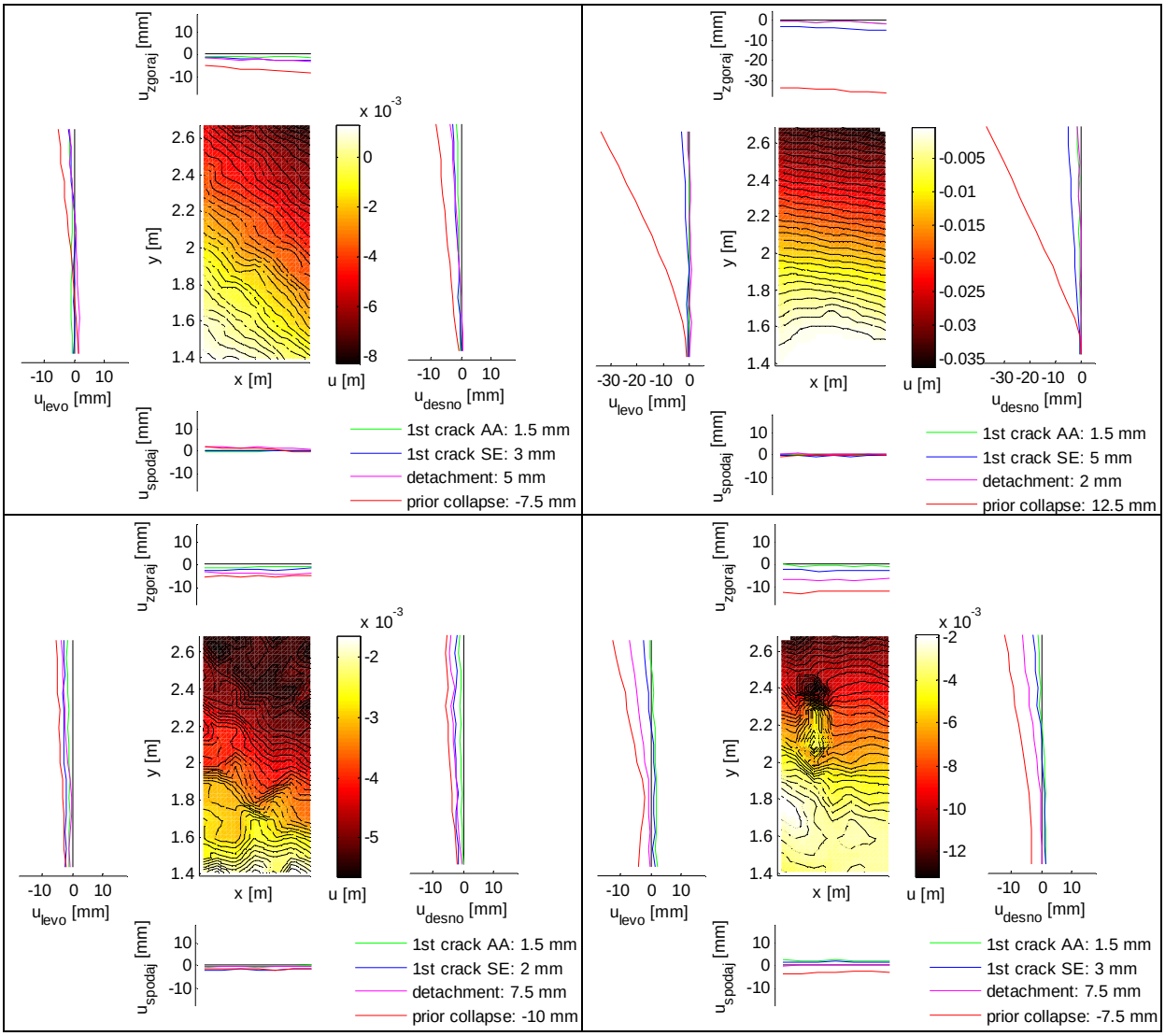

Figure 3.83: Photogrammetry results for tests 7-10; out-of-plane displacements of the plaster prior to its collapse and displacements of the plaster edges in characteristic damage states

Slika 3.83: Rezultati fotogrametrije za teste 7-10; izven-ravninski pomiki ometa pred porušitvijo in pomiki robov ometa v karakterističnih mejnih stanjih

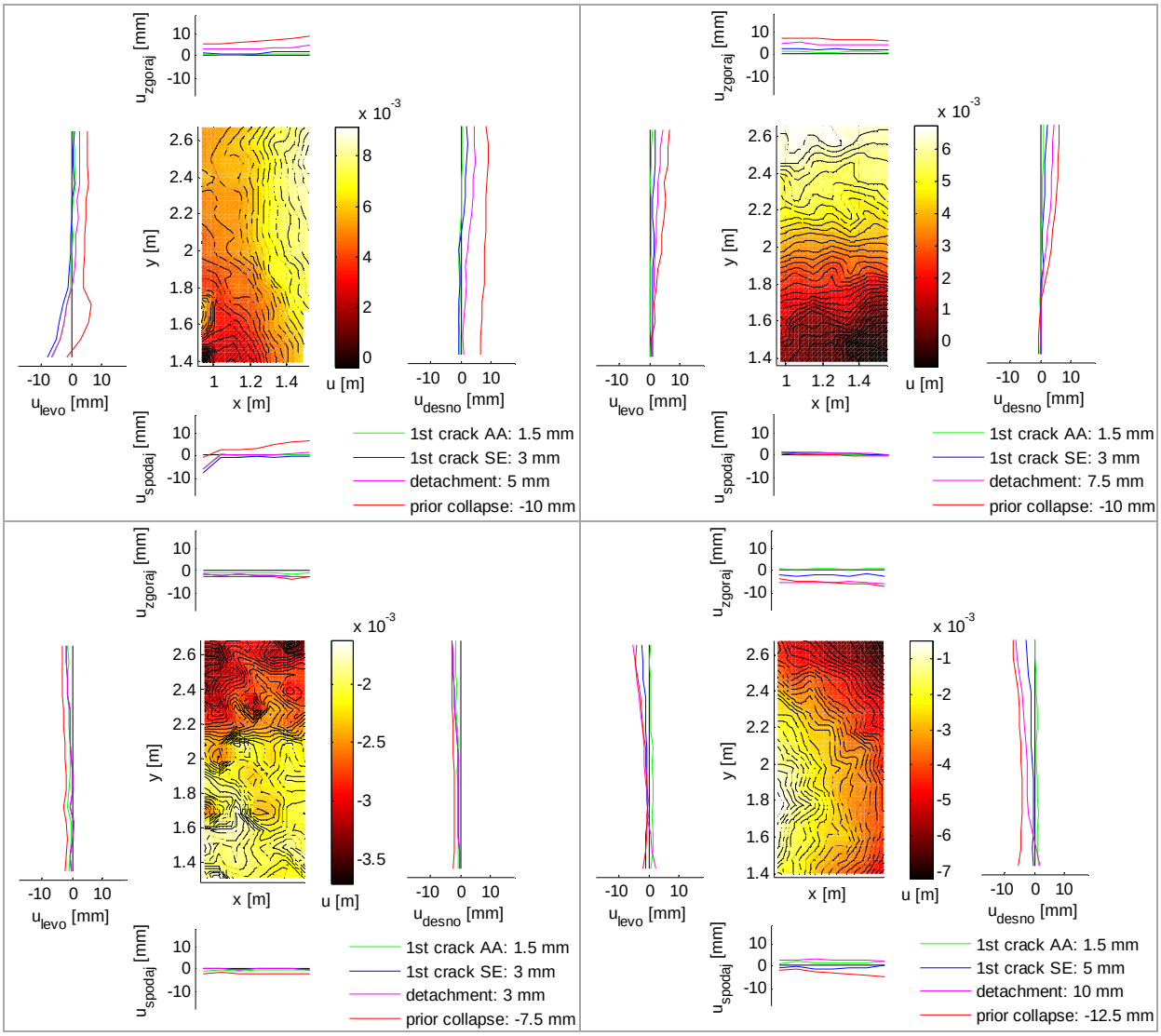

Figure 3.84: Photogrammetry results for tests 11-14; out-of-plane displacements of the plaster prior to its collapse and displacements of the plaster edges in characteristic damage states

Slika 3.84: Rezultati fotogrametrije za testa 11-14; izven-ravninski pomiki ometa pred porušitvijo in pomiki robov ometa v karakterističnih mejnih stanjih

BLANK PAGE

»Ta stran je namenoma prazna.«

4 RETROFITTING AND STRENGTHENING OF THE DAMAGED WALLS WITH CHARACTERIZATION OF THE MATERIALS

After the performed experimental campaign, which was described in the previous Chapter, 16 significantly damaged walls remained. All of them had a similar extent of damage and were still able to carry vertical load. It was decided to take the opportunity and to make use of these walls once more; to retrofit, strengthen and test them again. An innovative solution appropriate for strengthening of historic masonry was developed and through various variations of the strengthening applied, its efficiency was studied. In the presented Chapter the retrofitting and within the thesis developed strengthening measures and the used materials are thoroughly described and argumented.

Un-damaged walls – refers to walls tested for the first part of experimental campaign (prior tests un-damaged and un-strengthened, after tests these walls are referred to as **damaged walls**)
Strengthening – the term is used for both retrofitting and strengthening measures, when referring to the part of the campaign, where the specimens were either retrofitted or retrofitted and additionally strengthened
Strengthened walls - refers to walls, to which a retrofitting or strengthening measure was applied

4.1 Selection of materials and techniques for strengthening

Various parameters affected the choice of the strengthening techniques and the materials. Our choice was determined by the fundamental requirements we wanted the interventions to fulfil, whereas to some point also by the range of products available on the market in Slovenia. As strengthening should be appropriate for historic buildings of high value, we wanted three major requirements to be met:

- materials should be compatible with the existing materials of the building;
- the intervention should be reversible;
- the intervention should not affect the existing texture and appearance of masonry.

The walls were severely damaged from the preceding tests (see Section 0), thus a conventional measure for retrofitting and strengthening of masonry walls, grouting, was a necessary measure. Except reversibility, grouting meets the above mentioned requirements.

For additional strengthening, the intention was to use flexible FRPs. With regard to the third requirement, “Near Surface Mounting” (NSM) of the reinforcements to the joints was chosen, as with sheets or strips in various dispositions installed on the face of the walls (externally bonded) the visual perception of the masonry’s texture would be disturbed, if not destroyed. Our aim was to test the

efficiency of various positions and amount of FRP as well as the possibilities of controlling the failure mechanism of the tested walls and increasing their strength and displacement capacity.

Multi-leaf walls are, as already mentioned, characterized also by their out-of-plane deformations and leaf separations when subjected to in-plane lateral force. Also the tests performed within this thesis work on un-damaged walls have shown significant leaf separation under specific boundary conditions in the post-peak behaviour of the walls (see Section 3.4.3). To prevent leaf separation and to enable a more uniform behaviour of multi-leaf walls under seismic loading, transversal connections of the leaves are in practice usually provided. In this experimental campaign, transversal connections were applied for some combinations of strengthening. They were executed with the same cords as used for NSM.

4.1.1 Grout

Considering the damage pattern, the only option for grouting was line crack grouting, as the morphology of the walls did not allow systematic grouting. A lot of effort was put into choosing the proper grout mixture. The idea was to use one without cement additions. Three different types of mixtures based on lime putty, hydraulic lime and hydrated lime with different additives (tuff, aggregate, water – water/binder ratio, type and amount of plastificators, etc.) were varied in composition and tested. Also commercial grout, supposably (according to producers specifications) without any content of cement, was tested. Experimental investigations and results for different options are thoroughly presented in the thesis of Alja Arrigler [251]. However at the time of research, none of the grout options proved to satisfy all of the demands yet. In favour of maintaining the efficiency of grouting to re-connect the damaged wall, a commercial cement-lime grout was chosen for the retrofitting. Results presented by Uranjek [252] confirm the sufficiency of the use of such grouts for restoring the walls strength and displacement capacity. Additional advantage of such grouts is their minor contribution to increasing stiffness characteristics of the walls, which was a desired feature. In this way, the contribution of other strengthening measures would be more evident and their effect could be studied more precisely.

4.1.2 NSM strengthening

It was decided to imbed the strengthening elements into horizontal mortar joints. Due to geometrical characteristics of the walls (height to length ratio 1.5) it made more sense to position reinforcements horizontally rather than vertically. With inserting the cords into horizontal mortar joints, the visual appearance is less altered and cutting into joints is easier than cutting through stones.

4.1.2.1 Glass cords

Various types of FRP materials are nowadays used. Carbon and glass fibres are mostly used, but recently also some other types of fibres emerged also for structural application. Due to material compatibility issues, our first choice were basalt fibres (to prevent potential alkali-silica reaction [253]). But we were limited by the capacity of the actuator, so we had to use glass fibres instead

(Basalt fibre elements could only be supplied in diameter of 10 mm). Glass fibres were preferred to carbon fibres because they are less stiff and we had assumed they would enable higher ultimate lateral displacements of strengthened walls during seismic loading. We find the form of fibres in cords/strings to have many advantages compared to rods; besides the easier transport due to less space needed for the same length as pre-prepared rods, their impregnation on the spot allows them to be bendable and therefore formed into desired shape. This would allow strengthening by means of NSM of cords in the joints also in the case of irregular masonry or masonry with not completely regular courses. For these types of masonry strengthening with rods (pre-cured reinforcements) is not feasible. In such cases the reinforcement could be less effective due to various directions (between the stones) of its layout.

Before the final selection of the type, amount and position of fibres installed in the wall, the contribution of the FRP strengthening to final resistance had to be assessed. Optimization of the amount and position of the glass fibre cords in the walls was conducted according to ACI code provision recommendations [254] (see Section 4.3).

4.1.2.2 Mortar for installation

The primary concern, when choosing mortar for mounting the cords, was the quality of mortar - cord and cord - wall junction to ensure the transfer of the load to the cords. Typically epoxy based binders are used to install FRP products. The strength characteristics of the bond are in such case not an issue. We however estimated, that the use of such stiff binder was not necessary and presumed that a weaker bond would be sufficient. Despite the common practice, epoxy mortar was used only in case of one wall, while for the others cement-lime mortar was used. This is a traditional material and is more compatible with existing materials. Lime addition in mortar provides a more ductile behaviour and longer workability of the mortar. The comparison of properties of the connection in case of various binders used for installing the cords to the joints was made within the thesis work of Luka Božič [255].

4.1.2.3 Anchoring of the strings

No anchoring was provided for the cords except in strengthening combination for test 8. It was assumed, that the bond to the wall and the mortar along the cord would be sufficient to provide the load transfer.

4.1.3 Transversal connections

For the walls, selected to be transversally connected, the connecting was provided with the same type of glass cords as used for NSM. They were built-in at five evenly spaced positions on the wall. The amount of connection was 3.33 connections per m^2, which is similar to number of ties in Valluzzi et al [146]. They were positioned at horizontal joints, mainly because their installation would be easier compared to drilling through the stones. For wall 8, the cords were anchored by spreading the fibres in various directions and attaching them to the wall with mortar according to the recommendation of the producer. For other walls this was omitted, as when the connections were installed (pulled through the

hole), the sand used for coating of the cord and the impregnation resin formed a plug. It was decided on the spot, that this plug should be a sufficient anchor when hardened.

4.1.4 Strengthening combinations

The combinations of retrofitting/strengthening measures were conducted in such a way, that the efficiency of a single measure could easily be distinguished. Unfortunately we were partially limited by the number of walls. Combinations of retrofitting and strengthening measures for different walls are presented in Table 4.1. The names of strengthening measures for the specimens, used in the table and further in the text, are used as following:

First letter and number relate to the type and number of the test:
T*i* … compression test, where *i* presents the number of the test,
S*i* … shear test, where *i* presents the number of the test,

Next labels refer to the type of retrofitting/strengthening performed and the presence of header stones:
I … indicates, whether the wall was grouted,
S … indicates the application of NSM:
- 1 … application of cords on one side of the wall and
- 2 … application on both sides of the wall,
- - … application of NSM in every second joint and
- e … the use of epoxy mortar instead of cement-lime for NSM of cords;

P … indicates walls, which were transversally connected,
(n) or (p) … explain the presence of header stones in the wall:
- n … wall without header stones and
- p … wall with header stones.

Because all of the walls were retrofitted by line grouting along the cracks, we wanted to evaluate the strength and displacement capacity as well as stiffness properties after the grouting itself. Three walls were therefore only grouted. Two were tested in shear; S1 - I (n) was less damaged after prior tests, whereas damage on S2 – I (p) was more severe. With S2 – I (p) we wanted to establish, to what extent a more damaged wall can be retrofitted by grout mixture, compatible to historic masonry. One wall was in addition to grouting transversally connected in order to evaluate the effect of ties (S7 - I.P (n)).One only grouted wall was tested in compression (T1 – I (n)).

One wall was tested in compression without being retrofitted and strengthened in order to establish residual compressive strength of wall, damaged in the preceding shear test ((T3 – (n)).

As the main goal was to assess the effect of NSM of cords on the seismic resistance of stone masonry, we had predicted that the most efficient strengthening method would be NSM of cords in every horizontal mortar joint and transversally connecting the leaves. On such walls we performed three shear tests (S4, S5 and S8 varied in the testing boundary conditions and strengthening materials) and one compression test (T2 – I.S2.P (n)).

Preglednica 4.1: Kombinacije utrditev zidov

Table 4.1: Retrofitting and strengthening combinations

Retro-fitting scheme / Test no.	and name	Previous test	Header stones	Grouted	NSM	NSM sides of the wall	NSM no. of joints on one side	NSM mortar	Trans. connect.
Walls for shear tests									
S1	I (n)	2-SNk-7.5-1	NO	YES	NO	/	/	/	NO
S2	I (p)	13-SPk-15-2	YES	YES	NO	/	/	/	NO
S3	I.S1 (p)	1.2-SPk-5-7.5	YES	YES	YES	1	10	Cement-lime	NO
S4	I.S2 (p)	4-SPv-7.5-1	YES	YES	YES	2	10	Cement-lime	NO
S5	I.S2.P (p)	9-SPv-15-2	YES	YES	YES	2	10	Cement-lime	YES
S6	I.S2-.P (n)	10-SNv-15-2	NO	YES	YES	2	6	Cement-lime	YES
S7	I.P (n)	14-SNk-15-2	NO	YES	NO	/	/	/	YES
S8	I.S2e.P (n)	11-SNk-15-1	NO	YES	YES	2	10	Epoxy	YES
Walls for compression tests									
T1	I (n)	3-SNv-7.5-1	NO	YES	NO	/	/	/	NO
T2	I.S2.P (n)	5-SNv-7.5-2	NO	YES	YES	2	10	Cement-lime	YES
T3	(n)	8-SNv-15-1	NO	NO	NO	/	/	/	NO
Figure of strengthening schemes with glass cords									

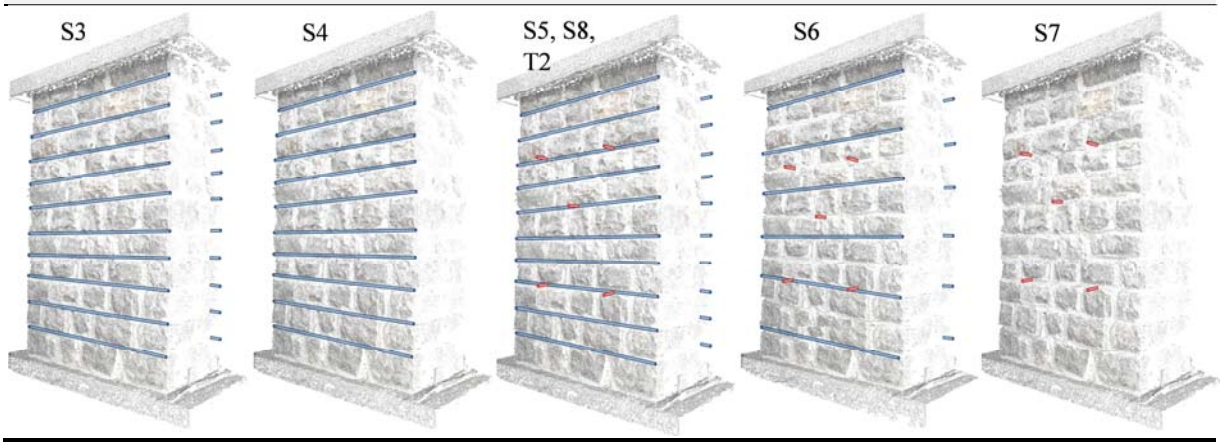

To evaluate the influence of boundary conditions and to possibly attain different failure mechanism for similar interventions, 4 walls were tested under cantilever (tests S1-S4) and 4 under fixed-fixed boundary conditions (tests S5-S8).

To investigate the performance of NSM strengthened walls in case of absence of the transversal connections; two walls were strengthened by NSM, but not connected (S3 - I.S1 (p) and S4 - I.S2 (p)). These two walls were tested under the same boundary condition (cantilever).

Because the developed strengthening interventions were primarily designed for historic structures, one of the questions was the efficiency of application of NSM on only one side of the wall. Conservation requirements limit or prohibit interventions due to valuable artistic assets preservation in many buildings. Sometimes the possibility of strengthening on both sides is limited due to some other reason (for instance accessibility). Therefore for test S3 - I.S1 (p), NSM of cords was applied on one side of the wall only (the other side still contained plaster).

Another question aimed to be answered was also the efficiency of NSM strengthening, where not every, but perhaps only every second or third, horizontal joint would be strengthened. One testing scheme therefore involved embedment of cords on both side of the walls but only into every second horizontal joint (S6 - I.S2-.P (n)).

Another strengthening variation was using epoxy mortar instead of cement-lime one for installing the cords into the wall. With one of the walls our intention was to test the influence of type of mortar (adhesive, binder) for installation. The recommendations of supplier of the cords were considered and epoxy mortar was used for installation into joints instead of cement-lime mortar (S8 - I.S2e.P (n)). The epoxy mortar was bonded directly to the stones and it was also used for repointing the emptied grooves. For this test also recommendations of the supplier for anchoring of the cords were applied.

4.2 Materials' characterization

4.2.1 Grout

Due to damage of the walls, grouting along the major cracks was a necessary measure, therefore all of the strengthened and re-tested walls were grouted with cement-lime grout which is commonly used for retrofitting of historical buildings in Slovenia.

The used cement-lime grout mixture was a commercial product. It was prepared according to the suppliers instructions [256]. Dry mixture of cement, lime, mineral and chemical additives was mixed with water/binder mass ratio equal 0.5. Cement : lime mass ratio of the mixture is 78:22. The mineral composition of the grout was analysed by X-ray powder diffraction method within PhD studies of Mojmir Uranjek [252]; the results are presented in Figure 4.1. Minerals alite, belite, brownmillerite, aluminate, portlandite, quartz and calcite were found in the sample.

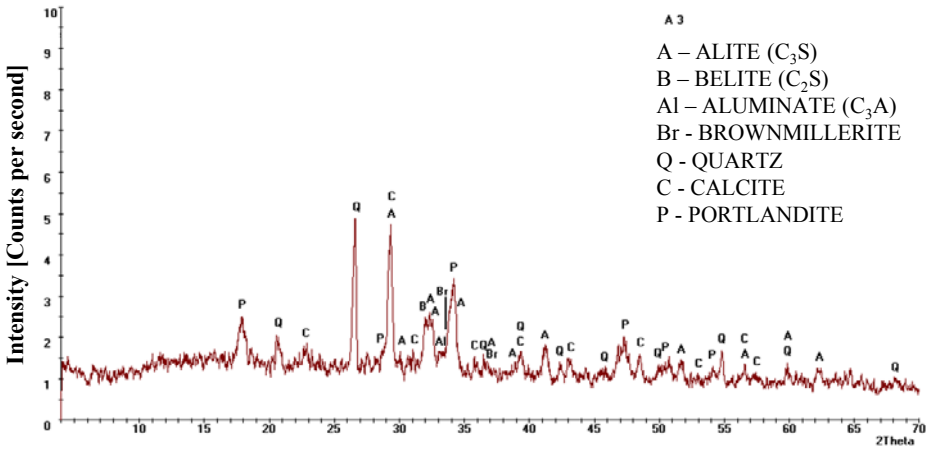

Figure 4.1: X-ray powder diffraction diagram of the grout mixture, after [257]
Slika 4.1: Difraktogram vzorca injekcijske mešanice AC1 [257]

4.2.1.1 Fresh grout

Density of mixture, fluidity and bleeding of grout in fluid state were determined (Table 4.2). Density test, performed according to provision EN 1015-6 [238], provided density of 1626 kg/m^3. Fluidity was assessed with cone method described in SIST EN 445:2008 [258], which is actually a standard for testing grouts for pre-stressed tendons, as there are no standards for testing grouts for masonry grouting (Figure 4.2 right two). According to the standard, measurements should be conducted twice: right after mixing (t = 0) and after 30 minutes (t = 30 min). Mixture meets the demands if 1 l of mixture flows through the cone of the prescribed geometry characteristics in less than 25 s and if time results of both tests do not vary by more than 10%. Fluidity results were not in accordance with requirements of SIST EN 445, as recommended values are 20 (±5) s while our grout flowed through 10 s. Water content was however not changed as already said, this was a commercial grout mixture and it was prepared following instructions from the producer. Regardless the obtained test results, the grout was used for grouting of the walls and it has proved not problematic.

Figure 4.2: Bleeding test (left) and fluidity test (middle and right)
Slika 4.2: Preizkus izločanja vode (levo) in pretočnosti (na sredini in desno)

Bleeding was tested with wick-induced test prescribed by the same standard [258]. Grout of 100 ml volume was poured in the tube of prescribed dimensions, water evaporation was minimised and after 3h the amount of segregated water was registered Figure 4.2 left). Bleeding is expressed as the ratio of after 3 hours segregated water's volume and the volume of mixture poured in the tube. Acceptable bleeding is limited to 2%. Tested lime-cement grout mixture exhibited no water bleeding.

Preglednica 4.2: Rezultati prostorninske mase, pretočnosti in izločanja vode injekcijske mešanice

Table 4.2: Results of density, fluidity and bleeding tests of grout in fluid state

Date of testing	Density [kg/m^3]	Fluidity [s]		Bleeding		
		t = 0	t = 30 min	Volume of grout mixture [ml]	Volume of segregated water [ml]	[%]
22.2.2013	1626	9.78	11.13	99.0	0.0	0.00

4.2.1.2 Hardened grout

The characteristics of grout were tested on standard grout prisms and on cylinders, which simulated the masonry core and were therefore filled with stone rubble and grout. Tests were performed after 22

days of maturing. On cylinders of 150 mm diameter and 300 mm height compressive and splitting tensile strength were determined, whereas on 40/40/160 mm grout prisms flexural tensile strength, compressive strength and density were determined and shrinkage measured.

Cylinders for grout injecting were prepared (Figure 4.3) to simulate the core of the three-leaf walls, which was filled with stone rubble and at which a higher amount of voids was present (than the amount of voids in our walls). In order to simulate such samples, stone rubble of specific grain size distribution was used (according to Uranjek [252]). It was prepared by crushing the same lime stone blocks, which were used for construction of the walls, and sieving them. For the composition, 37% of entire rubble mass consisted of aggregate of the largest fraction used; fraction 45/63 mm; further on 37% of mass presented aggregate of fraction 32/45 mm, 25% aggregate of fraction 16/32 mm and 1% aggregate of fraction 8/16 mm.

Figure 4.3: Crushing of stone blocks first by hydraulic jack, then by drilling and finally with hammer, sieved stone rubble and cylinders before grout injecting
Slika 4.3: Drobljenje kamna najprej z batom, nato z vrtanjem in nazadnje s kladivom, s sejanjem ločene frakcije kamna ter valji, napolnjeni s kamenjem, pred injektiranjem

The actual volume ratio of injected grout was determined by weighing the injected samples and samples prior grouting. Determined average grout volume ratio was 50.0%.

Figure 4.4: Grout injecting of cylinder specimens
Slika 4.4: Injektiranje valjastih vzorcev

4.2.1.2.1 Tests on prisms

Density of hardened grout was determined according to SIST EN 1015-10:2001/A1:2007 [259] and was 1378 kg/m^3 with c.o.v. 2.78%. All throughout the hardening of the samples, shrinkage of grout was monitored. The shrinkage of the used grout mixture was negligible.

Flexural tensile strength f_{mf} was determined according to EN 1015-11 [239] with three-point bending test on 6 samples (Table 4.3). Average f_{mf} equal to 2.10 MPa was determined (c.o.v. 8.02%).

Preglednica 4.3: Povprečni rezultati testov za določanje upogibne natezne trdnosti

Table 4.3: Average results of flexural tensile tests on prisms

No. of samples	F (average) [kN]	Span length [cm]	height d_1 [cm]	width d_2 [cm]	f_{mf} [Mpa]	c.o.v. [%]
6	0.90	10	4.03	4.00	2.10	8.02

Figure 4.5: Flexural (left) and compressive (right) test on the mortar prisms [251]
Slika 4.5: Upogibni (levo) in tlačni (desno) preizkus maltne prizme [251]

Compressive strength of prisms f_{mc} was determined according to EN 1015-11 [239] by mono-axial compressive test performed on samples left from flexural tensile strength tests (both presented in Figure 4.5). Average compressive stress of grout prisms determined was 14.7 MPa (c.o.v. 6.27%, Table 4.4). Average dynamic modulus of elasticity determined with GrindoSonic was 5.86 GPa with c.o.v. equal to 2.6%.

Preglednica 4.4: Rezultati tlačnih testov injekcijske mešanice

Table 4.4: Results of compressive tests on prisms

No. of samples	F (average) [kN]]	width a [cm]	f_{mc} [MPa]	c.o.v. [%]
12	23.8	4.0	14.7	6.27

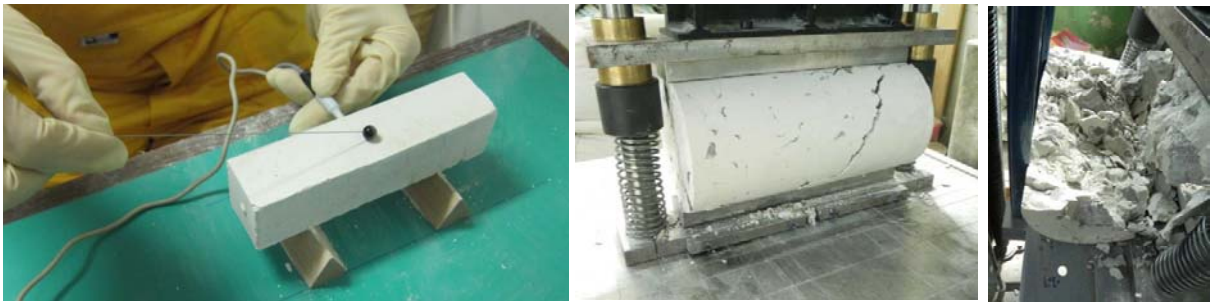

Figure 4.6: GrindoSonic test for the determination of the dynamic modulus of elasticity (left) and splitting tensile strength test and failure of the cylinder (middle and right) [251]
Slika 4.6: Meritev dinamičnega modula elastičnosti z GrindoSonic-om (levo) ter test natezne cepilne trdnosti in porušitev valja (na sredini in desno) [251]

4.2.1.2.2 Tests on cylinders

Splitting tensile test of cylinders f_{cst} was determined according to SIST EN 12390-6:2001 [241]. The test indicates the quality of connection between parts of the wall; stone blocks and binder. By the conducted test of cylinder, injected with investigated grout, the cylinder divided in two and the failure went through grout as well as through stones), but also separation or division of stones not surrounded by grout occurred (Figure 4.6 right). In Table 4.5 results of the test are summarized; average f_{cst} determined was 1.00 MPa.

Preglednica 4.5: Rezultati testov cepilne natezne trdnosti valjastih preizkušancev

Table 4.5: Results of splitting tensile tests on cylinders

No. of samples	F (average) [kN]	Length l [mm]	Diameter d [mm]	f_{cst} [MPa]
2	70.75	300	150	1.00

In compressive tests of grouted cylinders (Figure 4.7), average compressive strength f_{cc} of 7.95 MPa was determined (Table 4.6). With increasing compressive load, progressive material crushing and falling off (of grout and of stones) was present over the entire surface area.

Preglednica 4.6: Rezultati tlačnih testov valjev

Table 4.6: Results of compression tests on cylinders

F (average) [kN]	Length [mm]	Diameter [mm]	f_{cc} [MPa]
140.50	300	150	7.95

Figure 4.7: Failure mechanism of the cylinder during compressive test [251]
Slika 4.7: Porušitveni mehanizem valja pod tlakom [251]

Static elastic modulus E_M was determined according to Yugoslavian standard JUS U.M1.025 [260]. Cylinder was loaded to approximately 0.5 MPa stress (σ_b ; loading was induced by displacement) and afterwards loaded to 1/3 of compressive strength (σ_a) with constant velocity 0.6 ± 0.4 MPa per second and unloaded again to 0.5 MPa. 3 cycles should be performed; however the modulus was calculated at 1/3 of compressive strength test after 5 cycles according to Eq. 4.1, where $\Delta\varepsilon$ corresponds to average strain difference for strains at σ_a and σ_b and is calculated from corresponding contraction of the sample. Average E_M determined from the three measuring positions was 12.4 MPa.

$$E_M = \frac{\Delta\sigma}{\Delta\varepsilon} \quad \textbf{4.1}$$

$$\Delta\sigma = \sigma_a - \sigma_b \quad \textbf{4.2}$$

4.2.2 NSM of glass cords

4.2.2.1 Cord, epoxy impregnation resin and quartz sand

A dry cord made from high-strength, mono-directional glass fibres wrapped in a protective gauze sheet (Figure 4.8) was used for strengthening; for NSM as well as for transversal connecting of walls' leaves. It is a commercially available product which is mostly used for structural connecting of elements and anchoring. The supplier offers a complete system consisting of a range of products for structural strengthening, which was not used in our campaign, though.

Figure 4.8: Dry glass fibre cords [251]
Slika 4.8: Vrvice s steklenimi vlakni [251]

The producer offers the following technical data [261] (Table 4.7):

Preglednica 4.7: Tehnični podatki o vrvici s steklenimi vlakni [261]

Table 4.7: Technical data on the used glass cord [261]

Type of fibre	Type E-glass
Density [g/cm^3]	2.62
Tensile strength [N/mm^2]	2560
Modulus of elasticity [GPa]	80.7
Elongation at breakage [%]	3–4
Equivalent surface area of dry fabric [mm^2] for Φ 6 mm	15.70
and Φ 10 mm	26.79

Prior the cords were build-in, they were impregnated with a super-fluid solvent free epoxy resin made up of two components; A – resin and B – hardener, and coated with quartz sand grain size 1.0-2.0 mm to improve the bond between the cord and the mortar. Technical data provided by the producer for the epoxy impregnation resin [262] is summarized in Table 4.8 and for quartz sand [263] in Table 4.9.

Preglednica 4.8: Tehnični podatki o epoksidni impregnacijski mešanici [262]

Table 4.8: Technical data on the used epoxy impregnation resin mix [262]

Density [g/cm^3]	1.1
Brookfield viscosity [mPa s]	300
Application temperature [°C]	10-30
Tensile strength (ASTM D 638) [N/mm^2]	30
Tensile elongation (ASTM D 638) [%]	1.2
Compressive strength (ASTM C 579) [N/mm^2]	65
Flexural strength (ISO 178) [N/mm^2]	55
Modulus of elasticity under compression (ASTM C 579) [N/mm^2]	2000
Modulus of elasticity in flexion (ISO 178) [N/mm^2]	2500

Preglednica 4.9: Tehnični podatki o kremenovem pesku za posip [263]

Table 4.9: Technical data for quartz sand [263]

Grain size [mm]	1.2 – 2.0
Hardness [Mohs]	7
Bulk density [g/cm^3]	1.37
Moisture	$\leq$ 0.2%
Chemical composition	SiO_2 > 99%

4.2.2.2 Mortar for inserting the cords in the joints

4.2.2.2.1 Cement-lime mortar

A cement-lime mortar was used for NSM of the cords. Cement : lime : aggregate mass ratio 1:1:6 was chosen; regular cement (CEM I), hydrated lime and aggregate of fraction 0/2 mm were used. The appropriate water/binder ratio was determined with a consistency test by means of a spread test according to SIST EN 1015-3 [237]. When inserting the cords; first lower water/binder ratio was used

(0.63); however when the cords were already inserted, it was easier to close the joints with more fluid mortar, so finally 0.77 water/binder ratio was used. Results of spread test are presented in Table 4.10 and Figure 4.9.

Preglednica 4.10: Rezultati razleza v odvisnosti od vodovezivnega razmerja malte

Table 4.10: Results of spread test of the mortar in dependence of water/binder ratio

Test	1	2	3	4	5
Water/binder ratio	0.63	0.67	0.71	0.72	0.77
Spread [mm]	120	135	145	155	180

Figure 4.9: Spread tests of mortar with various water/binder ratios [251]
Slika 4.9: Razlez vzorcev malte z različnimi vodovezivnimi razmerji [251]

Density of the mortar in hardened state was 1811 kg/m^3. Flexural tensile and compressive strength of the mortar f_{mc} and f_{mf} were determined after 28 days on 6 samples; f_{mf} was 2.29 MPa and f_{mc} 9.29 MPa. Results are summarized in Table 4.11.

Preglednica 4.11: Rezultati testov prostorninske mase, upogibne natezne in tlačne trdnosti 28 dni starih prizem iz podaljšane cementne malte

Table 4.11: Average results of density, flexural tensile and compressive strength test on 28 days old cement-lime mortar samples

Date of testing	Density [g/dm^3]	f_{mf} [MPa]	f_{mc} [MPa]
22.4. 2013	1811	2.29	9.29

4.2.2.2.2 Epoxy mortar and epoxy primer

As already mentioned, in one wall (scheme S8, Table 4.1) the cords were built-in using a commercial »system« products. Cords were installed with epoxy mortar instead of cement-lime mortar, whereas prior insertion also a two-component epoxy primer specifically formulated for the mentioned commercial system was applied.

For the installation of cords a two-component, slow-setting, thixotropic epoxy grout, primarily meant as regularization layer for concrete or masonry surfaces before applying the producer's FRP fabrics, was used. Technical information provided by the producer [264] is presented in Table 4.12. The primer used is, according to the producer, a solvent-free epoxy resin based product, made up of two pre-dosed components, which are mixed together prior to use. The primer's technical data [265] is presented in Table 4.13.

Preglednica 4.12: Tehnični podatki za uporabljeno dvokomponentno epoksidno malto [264]

Table 4.12: Technical data on the two-component epoxy grout [264]

Product identity		
Component	A	B
Density [g/cm^3]	1.72	1.55
Brookfield viscosity* [mPa s]	900	600
Application data		
Mix ratio	Part A:Part B = 3:1	
Mix consistency	Thixotropic paste	
Density [g/cm^3]	1.7	
Application temperature [°C]	10-30	
Complete hardening time [days]	7	
Final performance		
Linear shrinkage (EN 12617-1) [%]	0 (at 23°C); 0.03 (at 70°C)	
Compressive modulus of elasticity (EN 13412) [N/mm^2]	6000	
Coefficient of thermal expansion (EN 1770)	46e^{-6} K^{-1}	
Glass transition temperature (EN 12614)	> +40°C	
Durability (EN 13733)	Compressive shear load > tensile strength of concrete; no failure of steel test sample	
Reaction to fire (Euroclass)	C-s1, d0	
Concrete-steel bond strength (EN 1542) [N/mm^2]	> 3 (failure of concrete)	
Concrete-Carboplate bond strength (EN 1542) [N/mm^2]	> 3 (failure of concrete)	
Bonded mortar or concrete		
Bond strength to concrete (EN 12636)	Failure of concrete	
Shear strength (EN 12615) [N/mm^2]	> 10	
Compressive strength (EN 12190) [N/mm^2]	> 70	
Strengthening using bonded plate		
Shear strength (EN 12188) [N/mm^2]	at 50° > 28; at 60° > 25; at 70° > 22	
Bond strength: -pull out (EN 12188) [N/mm^2]	> 18	
-inclined shear strength (EN 12188) [N/mm^2]	at 50° > 58; at 60° > 60; at 70° > 70	

* viscosity measured with a Brookfield Viscometer

Preglednica 4.13: Tehnični podatki proizvajalca za dvokomponentni epoksidni temeljno sprijemni premaz [265]

Table 4.13: Technical data, provided by the producer, on the used two-component epoxy primer [265]

Component	A	B
Density [g/cm^3]	1.2	1.0
Brookfield viscosity* [mPa s]	350	50
Mix ratio	Part A:Part B = 3:1	
Mix consistency	liquid	
Density [g/cm^3]	1.1	
Application temperature [°C]	10-30	
Complete curing time [days]	7	
Adhesion to concrete [N/mm^2]	>3 (after 7 days at 23°C substrate failure)	

* viscosity measured with a Brookfield Viscometer

4.2.2.3 Stone-mortar-cord junction

In order to obtain data for calculation of the FRP contribution to strength of the masonry specimen, tests of stone-mortar-cord junction were performed, since in some design models, bond shear strength is a necessary input parameter. Because of the specific type of strengthening by means of NSM of cord, a special test setup had to be developed in accordance with the testing equipment available. These studies were performed within graduation thesis of Luka Božič [255], where besides the test setup establishment, also a set of stone-mortar-cord junction tests varying mortar (three different types) and stone (limestone and sandstone) was performed. The preparation of the samples and the test setup, which is a sort of a pull-out test, is presented in Figure 4.10. For the test, the glass cord was pulled out from a stone cube, in which a hole was drilled and into this hole the cord was installed by the selected mortar. The cord was mounted with epoxy mortar in a PVC cap and this cap was fixed on the actuator, which pulled the cord from the fixed stone cube.

Figure 4.10: Preparation of the samples for the stone-mortar-cord junction tests: a) with epoxy resin impregnated cord coated with quartz sand and mounted with epoxy mortar in a PVC cap, b) hardening of the cords, c) application of the primer (in case of epoxy mortar), d) installing the cord with selected mortar, e) vertical positioning of the cord, f) hardening of the samples and g) test setup (adopted from [255])

Slika 4.10: Priprava vzorcev za teste stika kamen-malta-vrvica: a) impregnirana in s kremenčevim peskom posuta steklena vrvica, vpeta v PVC čep, b) sušenje vrvic, c) nanos temeljno sprijemnega premaza (v primeru uporabe epoksi malte), d) vgradnja vrvice z izbrano malto, e) vertikalna poravnava vrvice v vzorcu, f) strjevanje vzorcev, g) postavitev testa (povzeto po [255])

Since the preparation of samples required quite some skills in cutting and drilling of stone, among all the tests [255], 5 tests were performed on samples with the glass cord installed to limestone stone by cement-lime mortar and 5 with the glass cord installed by epoxy mortar to limestone stone surface primed with epoxy primer. In the performed tests, three types of failure occurred (Figure 4.11); failure of mortar (type A), stone-mortar junction failure (type A) and failure of the cord (at the spot, where the cord was mounted in the PVC cap, type C).

A - mortar failure B - stone-mortar junction failure C - failure of the cord

Figure 4.11: Type of failure [255]
Slika 4.11: Tip porušitve vzorca [255]

In Table 4.14 results of the pull-out tests in terms of maximum forces F_{max}, types of failure and calculated bond strengths τ_b are presented for both cement-lime mortar (labelled CL) and epoxy mortar (labelled E) samples. τ_b is calculated according to the following equation (Eq. 2.26):

$$\tau_b = F_{\max} / A_{circ}, \quad \textbf{4.3}$$

$$A_{circ} = \pi r^2 + 2\pi rh \quad \textbf{4.4}$$

A_{circ} is the circumference area of the drilled hole and was therefore calculated according to Eq. 4.4, where r is the radius and h the depth of the hole.

Preglednica 4.14: Rezultati izvlečnih testov za določitev trdnosti stika kamen-malta-vrvica

Table 4.14: Results of the pull-out tests for determination of the stone-mortar-cord junction strength

Name	F_{max} [kN]	Type of failure*	τ_b [MPa]	τ_b (average: 5 samples) [MPa]
CL 1	0.98	A	0.248	0.23 (c.o.v. 0.280)
CL 2	0.61	A	0.163	
CL 3	1.10	A	0.265	
CL 4	0.57	50% A; 50% B	0.156	
CL 5	1.20	70% A; 30% B	0.328	
E 1	6.43	C	1.750	≥ 2.31 (c.o.v. 0.262)
E 2	12.49	C	3.340	
E 3	6.89	C	1.940	
E 4	9.76	C	2.657	
E 5	7.32	C	1.863	

* notation corresponds to the types of failure presented in Figure 4.11

As expected, the results showed that the bond strengths of both chosen mortars are in different categories; in average 0.23 MPa for cement-lime mortar, whereas more than 10-times higher for epoxy mortar. It has to be noted, that with epoxy mortar the failure at the stone-mortar-cord junction was actually not achieved, as due to the test setup the cord always failed at the spot where it was mounted to the PVC cap. From the tests we can therefore only establish, that the bond strength of epoxy mortar is higher than the highest result obtained (3.34 MPa).

4.3 Optimization of the cross section and the position of the glass cords

To determine the contribution of the cords inserted into the walls to the final lateral resistance V_f of the walls ACI code provisions (ACI 440.7R 2010) [254] were used. The contribution was also assessed according to CNR-DT 200 REV. 2013 provision, but because the contributions evaluated were lower than those according to ACI, ACI was used in order to be on the conservative side in respect of the actuator. Tests of un-strengthened walls proved maximum lateral resistance of approximately 130 kN. As in shear tests the maximum lateral force had to be limited to the actuator capacity 250 kN, maximum desired shear resistance contribution due to FRP strengthening was limited to 100 kN.

Calculations were performed for various diameters of glass cords d_b in various layouts. In Table 4.15 the results for 6 mm and 10 mm diameter cords, which were available at the time, are presented. The $A_{f,cord}$ is the equivalent surface area of the fibres in the cord. In the schemes, the number of strengthened joints, the number of cords per joints and the spacing distance between the cords s_f were varied.

Preglednica 4.15: Prispevek FRP utrditev V_f k strižni nosilnosti zidu za različna premera in postavitve vrvic

Table 4.15: Increase in lateral resistance of walls due to FRP reinforcement V_f for various cord diameters and their positions

	Scheme 1*	Scheme 2*	Scheme 3*	Scheme 1*	Scheme 2*	Scheme 3*
d_b [mm]	6	6	6	10	10	10
No. of strengthened joints	10	10	6	10	10	6
No. of cords per joint	1	2	2	1	2	2
$A_{f,cord}$ [mm^2]	16.3	16.3	16.3	27.6	27.6	27.6
s_f [mm]	136	136	250	136	136	250
V_f [kN]	123.0	146.5	133.5	156.2	103.8	131.6

*Scheme 1 – cord in each horizontal joint on one side only (Test 3),
Scheme 2 – cord in each horizontal joint on both sides (Test 4, 5, 8),
Scheme 3 – cord in every second horizontal joint on both sides (Test 6)

Based on the results, we decided to strengthen the walls with 6 mm diameter cords, even though some inconsistencies in the results appeared (scheme 2* with 10 mm cord resulted in lower additional strength contributions than scheme 2* with 6 mm cords) and that the predicted values of FRP contribution to lateral strength were higher than desired. The issues concerning the results obtained according to ACI are in more detail discussed in [251], whereas for higher values of FRP contribution, according to test results of many researchers, the contribution is lower than estimated analytically (FRP strengthening mainly results in higher ductility). Code provisions also do not take into consideration different position of cords in the wall. Results are according to the codes therefore the same, whether the cords are applied on both sides or on one side only (if two cords were inserted into the joint).

4.4 Execution of strengthening

4.4.1 Grouting

Grouting was executed by an experienced team of professionals. Holes were drilled into the walls and metal tubes inserted at an approximate distance of 50 cm; somewhere tubes were just inserted into existing cracks (Figure 4.12 left). Cracks were closed up by a cement-based binder in order the grout not to leak out during grouting, the wall was pre-wetted prior grouting (Figure 4.12 right) and the grout was injected through the tubes under approximately 2 bars of pressure (manual adjustment).

Figure 4.12: Inserting tubes (left) and pre-wetting the wall (right) (photos Željko Stevanić for UL FGG)
Slika 4.12: Umeščanje cevk v zidove (levo) in vlaženje zidu (desno) (foto Željko Stevanić for UL FGG)

The grouting started from the bottom up. When the grout was injected and all the cracks and voids in the walls were filled with grout, the grout leaked out either from a higher positioned tube (Figure 4.13 left) or from tube on the other side of the wall (Figure 4.13 right).

Figure 4.13: Leakage of the grout from a higher tube (left) and from a tube on the other side of the wall (right) (photos Željko Stevanić for UL FGG)
Slika 4.13: Iztekanje injekcijske mešanice pri injektiranju iz cevke na višjem mestu (levo) in iz cevke na drugi strani zidu (desno) (foto Željko Stevanić for UL FGG)

After the grouting was finished, the tubes were removed. In average approximately 30 l of grout was injected into each wall, which is an acceptable value as the walls did not have many voids in the core and only line crack grouting was executed. If more voids were present in the walls, up to 80 kg of

grout could be inserted per cubic meter of wall according to Bergant and Dolinšek [266] and even up to 150 kg according to Tomaževič and Apih [141].

Figure 4.14: Grouted wall specimens (photo Željko Stevanić for UL FGG)
Slika 4.14: Preizkušanci po linijskem injektiranju (foto Željko Stevanić for UL FGG)

4.4.2 NSM of glass cords

For inserting the cords, first the mortar was removed from the chosen horizontal joints up to 5-6 cm in depth (Figure 4.15 left). Various tools were used and it was a rather time-consuming procedure, especially as the work took place in a laboratory and grinders could not be used in order not to dust the laboratory equipment. After the joints had been emptied, they were cleaned with a vacuum cleaner and sprayed with water (Figure 4.15 middle), in order to assure better bond of the repointing mortar and the stones.

Figure 4.15: Process of emptying horizontal mortar joints: removal of mortar, vacuuming, water cleaning of emptied joints and wall with partially emptied joints
Slika 4.15: Proces praznjenja horizontalnih fug: odstranitev malte, sesanje, čiščenje fug z vodo in zid z delno izpraznjenimi fugami

After the joints had been emptied, approximately 1 cm of the repointing mortar (lower water/binder ratio 0.63) was inserted into the joint prior inserting the cords. Cords approximately 120 cm long were dipped into epoxy resin (Figure 4.16 left), impregnated and rolled into quartz sand (Figure 4.16 right), except in case of wall for test S8, where they were built-in by epoxy mortar. Coating the cords into sand proved to be a good decision not only for better cord-mortar junction characteristics but also due to prevention of the intensive dripping of the resin. The negative results of dripping of the

impregnation resin can be seen in case of wall for test S8, where the resin dripped on the face of the wall (Figure 4.19 right)

Figure 4.16: Impregnating the cord with an epoxy resin (left) and coating the cords in quartz sand (right)
Slika 4.16: Namakanje vrvice v epoksi smolo (levo) in valjanje vrvice v kremenčevem pesku (desno)

When the cords were inserted into the joints, they were manually stretched with approximately 10 cm hanging out on each side (see Figure 4.17). The remaining empty part of the joint was filled (repointed) with mortar with higher water/binder ratio of 0.75. This procedure had to be done fast, to avoid premature hardening of the mortar.

Figure 4.17: Cords placed into the joints with cement-lime mortar, cord placed into the groove with cement-lime mortar (upper) and with epoxy mortar over epoxy primer (bottom), with cement-lime mortar repointed joints and with epoxy mortar repointed joints (from left to right)
Slika 4.17: Vrvice, nameščene v spojnice s podaljšano cementno malto; vrvica, nameščena v izpraznjeno spojnico z apneno-cementno malto (zgoraj) in z epoksidno malto preko temeljnega sprijemnega premaza (spodaj), s podaljšano cementno malto zapolnjene spojnice ter z epoksidno malto zapoljnjene spojnice (od leve proti desni)

In all of the walls except walls for tests S1 and S8, the remaining parts of cords were left hanging out from the wall. In these two walls they were built-in the wall; in case of wall 1 bended and built-in into the joint on the transversal side of the wall and in case of wall 8 the fibres were spread on the upper and lower part of the emptied joint on the transversal side. It has to be mentioned, that for an actual application on the real monuments, the procedure of strengthening should be improved, especially with strengthening of the wall for test S8 (use of epoxy mortar and primer), as already mentioned, the impregnation resin was dripping over the wall, which would in reality not be permissible (if the feature was to be preserved). This could be, as mentioned, avoided by dipping the cords into sand. Also the procedure of repointing with epoxy mortar did not produce the most aesthetic result.

Compared to cement-lime mortar, epoxy mortar leaves on the wall more noticeable marks, which are also harder to remove.

4.4.3 Transversal connecting

The wall was transversally connected with glass cords. Perpendicularly, 5 holes of diameter 20 mm were drilled through the walls (Figure 4.18). For walls for tests S3-S7 and T2, impregnated cords, dipped into quartz sand, were pulled through the depth of the wall. At the end, a sort of plug was created by the quartz sand impregnated with resin that did not pass through the hole. Transversal connecting was done prior application of NSM cords into the horizontal joints. Cords for the transversal connection of the wall for test S 8 were not coated with sand. At both sides of this wall the fibres of the cords were spread on both sides of the emptied horizontal joint and prior repointing fixed with epoxy mortar for the installation of NSM cords.

Figure 4.18: Drilling of the hole, the insertion of the impregnated cord coated in sand and sand "plug", transversal connection with impregnated cord (upper right) and with spread and fixed fibres (test 8 only, bottom right)
Slika 4.18: Vrtanje luknje, povezovanje slojev zidu z impregnirano in s peskom posuto vrvico, peščeni "čep", prečna povezava z impregnirano vrvico (zgoraj desno) in razprostrta in prilepljena vlakna (samo test 8, spodaj desno)

Figure 4.19: Retrofitted and NSM strengthened walls
Slika 4.19: Injektirani in z vrvicami v fugah utrjeni zidovi

4.5 Conclusive remarks

Retrofitting and strengthening measures were executed as planned with some minor adjustments. Commercial cement-lime grout for retrofitting of all walls was easy to work with and in fact there were no problems by grouting the walls along pre-existing cracks. NSM of glass cords, repointing the walls and transversally tying them with compatible materials present a completely new system.

Emptying the horizontal mortar joints was a rather time-consuming process. It could have been accelerated if grind-saw could have been used. When inserting the cords into the joints, coating them with quartz sand proved convenient; it prevented dripping of the impregnation resin and consequently reduced the number of unwanted stains on the walls and not to mention on the workers.

Mortar with higher consistency was used to partially fill the joints prior inserting the cords, whereas lower consistency mortar proved better for repointing of the walls. It could be placed in the joint, and by so, fill it in extent, that the mortar was joined together with the cord as well as with the upper and lower stone surface. It also left less stains on the face of the wall. On the contrary, the use of epoxy mortar for NSM of cords and repointing the walls needed more effort and it still left permanent marks on the wall. The same conclusions apply for transversal connecting of walls.

For connecting the walls, larger holes had to be drilled than planned; cord of 6 mm diameter could barely be pulled through hole of 22 mm diameter, if it was coated with sand. In case the walls would have thinner joints or the connection would be thicker, drilling through stone would be necessary. In case of strong stone and thick walls, this could be a difficult task.

Overall, the strengthening satisfied the primary desire to leave the wall's texture seen and not changed much. If the procedure would be used more common for historical buildings, it could be improved to be less time consuming.

5 EXPERIMENTAL TESTS OF STRENGTHENED WALLS

While in the previous Chapter the retrofitting and strengthening measures are justified and their execution thoroughly described, the following Chapter presents and evaluates the results of compression and shear tests performed on the retrofitted/strengthened walls. The efficiency of various strengthening schemes is evaluated and compared in order to provide some recommendations upon the execution of such NSM strengthening. In the analytical part of this Chapter strength contribution of the NSM glass cords to the total lateral strength, obtained through shear tests, is compared to the theoretical obtained (calculated) ones and conclusions upon the use of various code provisions and models are provided.

Non-retrofitted (damaged) wall – wall, which was damaged in the preceding shear test, but was not retrofitted
Only grouted wall – damaged wall to which no other measures were applied except line grouting
Un-strengthened walls – refer to walls, tested in the preceding experimental campaign (i.e. tests of un-strengthened walls) and their results

5.1 Compression tests on walls

Two compression tests were performed on retrofitted/strengthened wall specimens and additional one on a non-retrofitted wall, which had been damaged in shear tests. The later was conducted in order to obtain residual compression capacity of the damaged masonry and to compare it with the compressive strength of the un-damaged walls and of the damaged walls after the intervention. All the tests were performed on walls without header stones.

The used test setup was the same as in tests of un-strengthened higher wall specimens (see Section 3.3.1). Hydraulic jack of 2500 kN capacity was used and force was during the tests increased with constant velocity; it varied for the three tests from 0.85 to 1.12 kN/s. Deformations were measured with LVDTs, positioned to both sides of the walls (Figure 3.11, Section 3.3.2). For the tests of the damaged non-retrofitted specimen (T3 (n)), only LVDTs named V3, V4, U4 and W2 were applied, as the specimen was severely damaged and its failure was unpredictable. Due to this reason also the installed LVDTs were removed at an early stage of the test.

5.1.1 Test results

5.1.1.1 Wall, retrofitted with lime-cement grout injection (T1 - I(n))

The tested wall was retrofitted by grouting of cracks, caused by previous shear test (Test 3-SNv-7.5-1). Damage patterns after failure are presented in Figure 5.2.

Figure 5.1: Grouted wall with existing damage pattern prior testing (test T1 - I(n))
Slika 5.1: Injektirani zid z obstoječimi razpokami pred testiranjem (test T1 - I(n))

Figure 5.2: Damage pattern after failure attained at test T1 - I(n)
Slika 5.2: Poškodovanost zidu po testu T1 - I(n)

Compressive strength f_{Mc} obtained during the test was 6.55 , which is 8.3% more than the average compressive strength of the un-damaged walls. Stress-strain diagrams for LVDTs are presented in Figure 5.3.

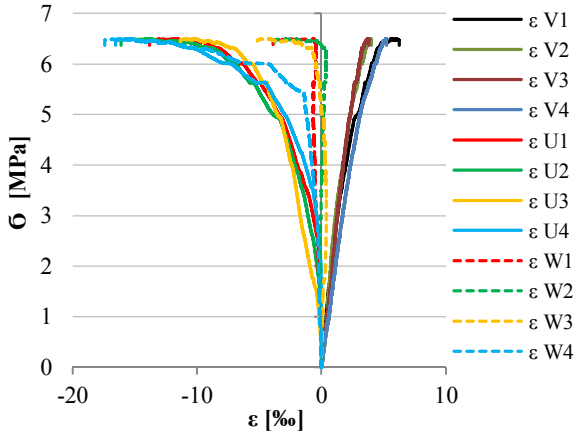

Figure 5.3: Stress - strain diagram for various LVDTs for test T1 - I(n)
Slika 5.3: Diagram napetost - deformacije za različne LVDT-je za test T1 - I(n)-n

Cracks occurred not only where they pre-existed, but also elsewhere on the wall. So it was established, that line crack grouting sufficiently connected the wall. Cracks through stones mainly progressed from pre-existing cracks in vertical mortar joints (grouted and others). They were observed over the entire specimen, many developed during the test, whereas some already existed from prior shear tests and widened. At corners vertical continuous cracks creating "columns" were evident. Vertical cracks observed at sides due to leaf separation, indicated eccentric out-of-plane behaviour (Figure 5.2 right).

5.1.1.2 Wall, retrofitted with lime-cement grout injection and additionally strengthened with NSM of glass cords and transversal tying (T2 – I.S2.P (n))

Besides lime-cement line grouting, the wall was strengthened with glass cords, inserted in every horizontal mortar joint on both sides of the wall, and transversally connected with glass cords (Figure 5.40). Maximum force of 2849 kN was obtained in the actuator, which corresponds to compressive strength 7.18 MPa calculated again for the bottom section of the specimen. The damage pattern after failure is presented in Figure 5.5 and the stress-strain relations for LVDTs in Figure 5.6.

Figure 5.4: Grouted wall, additionally strengthened with NSM and transversally tied with glass cords (T2 – I.S2.P (n)) prior testing (existing damage pattern)
Slika 5.4: Injektirani zid, dodatno utrjen s steklenimi vrvicami v horizontalnih maltnih spojnicah, pred testom z obstoječimi razpokami pred testiranjem (T2 – I.S2.P (n))

Figure 5.5: Damage pattern after failure attained at test T2 – I.S2.P (n)
Slika 5.5: Poškodovanost zidu po testu T2 – I.S2.P (n)

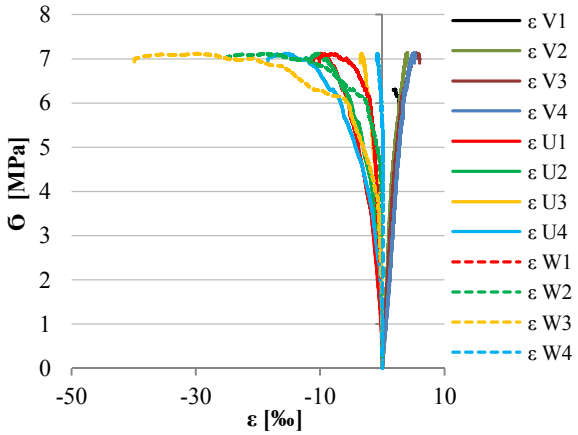

Figure 5.6: Stress - strain diagram for various LVDTs for test T2 – I.S2.P (n)
Slika 5.6: Diagram napetost - deformacije za različne LVDT-je za test T2 – I.S2.P (n)

Compared to the only grouted wall T1, glass cords in horizontal joints proved to limit horizontal (longitudinal – "U") deformations which allowed achieving higher vertical loads. On the surface of the specimen, glass cords were detached from the wall. The failure mainly occurred at the connection between the mortar and the cord (see Figure 5.5). Mounting of cords at the end of the joints only by mortar (not using anchors) proved sufficient, as there were no signs of failure of connection at extents. Out-of-plane deformations were also higher compared to test T1 (maximum 41.1‰ for test T2 compared to maximum 17.4‰ for test T1). Maximum horizontal deformations for both directions (longitudinal and transversal) are for all three tests presented in Table 5.3. Due to transversal ties, which controlled the leaf separation and enabled the achievement of higher resistance, also the post-peak leaf separation was considerable.

Leaf separation was more apparent towards the obtainment of the maximum strength (at vertical load over approximately 80% f_{Mc}). From that point onward, the vertical cracks indicating leaf separation were more obvious on one side of the specimen (LVDTs W1-W3). The highest crack opening was reached at LVDT W3, where also a vertical "column" at the bottom corner had developed.

5.1.1.3 Damaged, non-retrofitted wall (T3-n)

This test was performed on a wall specimen, which had in previous test (Test 8-SNv-15-1) exhibited extensive diagonal cracking through joints as well as through stones (see Figure 3.35). The specimen was severely weakened in the central part of the wall, where some vertical mortar joints were empty and the gaps between the stones were more than 1 cm wide. Also vertical cracks indicating leaf separation on the sides were more than 3 mm wide.

As already mentioned, deformations were measured with only 4 LVDTs and they were detached from the walls at an early stage of the test. Their results (stress-strain diagram) up to approximately one third of the obtained maximum force are presented in Figure 5.9. Maximum actuator force obtained was 1844 kN; it corresponds to vertical stress of 4.66 MPa at the bottom section of the specimen. Damage evolution and damage after failure are presented in Figures 5.7 and 5.8.

Figure 5.7: Damage of the wall obtained after test T3-n
Slika 5.7: Poškodovanost zidu po testu T3-n

Figure 5.8: Leaf separation obtained at test T3-n
Slika 5.8: Razslojevanje slojev zidu pri testu T3-n

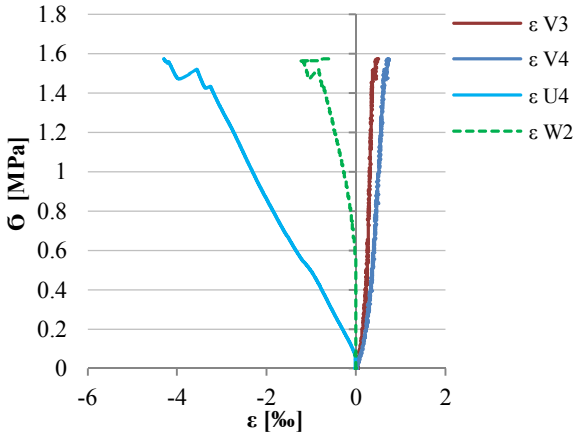

Figure 5.9: Stress - strain diagram of various LVDTs for the early stage of test T3-n
Slika 5.9: Diagram napetost - deformacije za različne LVDT-je za začetni del obremenjevanja pri testu T3-n

During the test, first the existing cracks widened but afterwards also some new cracks evolved. Damage was prevailingly concentrated on the side of the wall, where leaf separation was more evident. Large out-of-plane deformations and cracks in the upper corner are presented in Figure 5.7. Vertical cracks on the other transversal side seemed not to widen or additionally evolve.

5.1.2 Mechanical properties and leaf separation analysis (retrofitting/strengthening efficiency evaluation)

The obtained results for the three compression tests are in Figure 5.10 compared to average compressive strength of un-strengthened walls (considering walls without and with header stones). In the Figure 5.10 also expected values according to Italian code provision NTC08 are presented, if as a reference the average result of un-strengthened walls is considered. In the code a correction coefficient of 1.2 for strength and stiffness characteristics for the case of grouted dressed rectangular stone masonry is provided. The obtained results are summarized in Table 5.1.

Elastic moduli E_M and shear moduli G_M were calculated after the same procedure as for tests of un-strengthened walls. In Figure 5.11 they are compared to expected values of E_M and G_M according to Italian code provision NTC08. Poisson's ratio ν_M and consequently G_M were determined considering both in-plane (gained from measurements of LVDTs named U) and transversal horizontal deformations (gained from measurements of LVDTs named W); the results are provided in Table 5.2. For the test of the damaged wall, E_M and G_M are not stated as the values are unrealistic, because they cannot refer to an un-cracked section (elastic state).

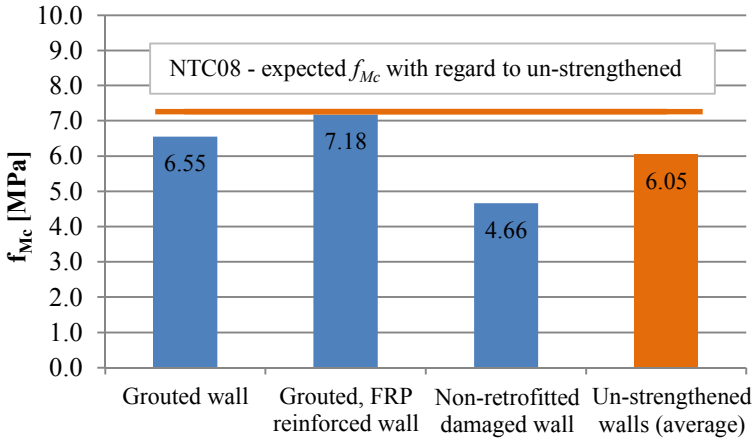

Figure 5.10: Comparison of compressive strength f_{Mc} of retrofitted/strengthened and un-strengthened walls
Slika 5.10: Primerjava tlačnih trdnosti f_{Mc} utrjenih in neutrjenih zidov

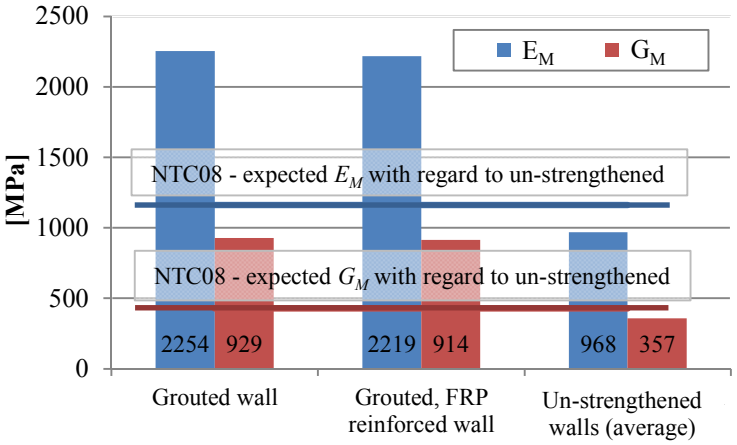

Figure 5.11: Moduli of elasticity E_M and shear moduli G_M of retrofitted/strengthened and un-strengthened walls
Slika 5.11: Moduli elastičnosti E_M in strižni moduli G_M utrjenih in neutrjenih zidov

Preglednica 5.1: Rezultati tlačnih testov (f_{Mc} in E_M)

Table 5.1: Results of compression tests (f_{Mc} and E_M)

	Test	σ_{max} [MPa]	Ratio to un-strengthened	Ratio to damaged	E_M [MPa]	Ratio to un-strengthened
T1	Grouted wall	6.55	1.083	1.40	2254	2.33
T2	Grouted, FRP reinforced wall	7.18	1.187	1.54	2219	2.29
T3	Non-retrofitted wall (damaged)	4.66	0.771			

Preglednica 5.2: Rezultati tlačnih testov (v_M, E_M in G_M/E_M)

Table 5.2: Results of compression tests (v_M, E_M and G_M/E_M)

	Test	considering both "U" and "W" direction deformations				considering only "U" direction deformations			
		v_M	G_M [MPa]	Ratio to un-strengthened	G_M/E_M	v_M	G_M [MPa]	Ratio to un-strengthened	G_M/E_M
T1	Grouted wall	0.214	929	2.60	0.412	0.259	895	2.53	0.397
T2	Grouted, FRP reinforced wall	0.214	914	2.56	0.412	0.452	764	2.15	0.344

The results show that both grouting and NSM with tying provide strength and stiffness characteristics higher than those of original walls. Increase is less significant for strength characteristics; 8.3% for grouted wall and 18.7% for grouted and with glass cords strengthened wall. This amplification is however lower than expected (20% increase according to NTC08). If obtained strength is compared to the compressive strength of the damaged wall (test T3), increase is 40% in the case of the grouted wall. As said, according to NTC08, the expected increase of strength in case of grouting is 20%. If weaker grouts are used, this value is probably conservative in case the grouting is applied to (severely) damaged walls, while otherwise not necessarily. Comparing stiffness characteristics, both E_M and G_M are more than two times higher than those of un-strengthened wall. Comparison shows, that this increase is to be attributed to grouting, as values are even slightly higher for test T1 as for additionally strengthened wall (test T2). Ratios of shear to elastic modulus G_M/E_M for un-cracked section are within expected values; from 0.34 to 0.41.

Leaf separation and crack evolution during the tests were already discussed; in Figure 3.28 leaf separation is compared for the three tests; test of non-strengthened high wall without headers (TN visoki) and retrofitted and strengthened tests T1 and T2. Results for the transversal horizontal LVDTs W1-W4 are presented in terms of stress-displacement diagrams (Figure 5.12), whereas maximal measured horizontal deformations in positions of both front face and transversal side of the walls $\varepsilon_{max,i}$ are summarized in Table 5.3.

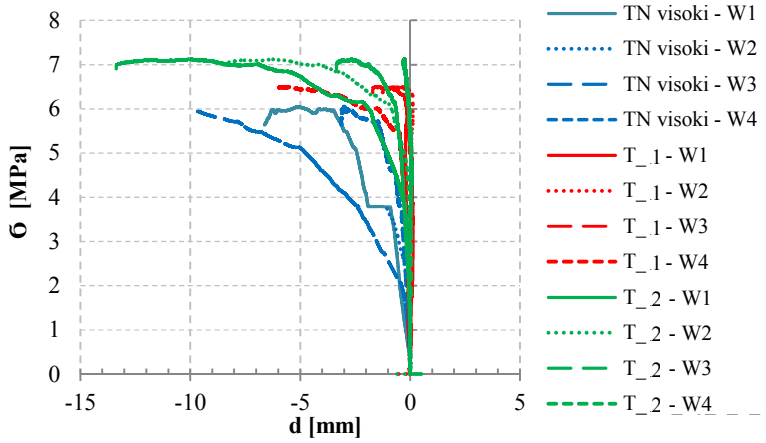

Figure 5.12: Stress - displacement diagram for the transversal horizontal LVDTs (labelled W) for the performed compression tests

Slika 5.12: Diagram napetost - deformacije za prečne horizontalne LVDT-je (označene z W) za izvedene tlačne teste

Preglednica 5.3: Maksimalne deformacije $\varepsilon_{max,i}$ različnih LVDT-jev

Table 5.3: Maximal strains obtained $\varepsilon_{max,i}$ by various LVDT measurements

	Test	$\varepsilon_{max,U1}$	$\varepsilon_{max,U2}$	$\varepsilon_{max,U3}$	$\varepsilon_{max,U4}$	$\varepsilon_{max,W1}$	$\varepsilon_{max,W2}$	$\varepsilon_{max,W3}$	$\varepsilon_{max,W4}$
T1	Grouted wall	-13.8	-16.1	-11.3	-16.5	-4.1	-3.9	-5.6	-17.4
T2	Grouted, FRP reinforced wall	-11.1	-11.5	-3.5	-18.4	-10.1	-26.7	-41.1	-1.2
T3	Non-retrofitted wall (damaged)				-4.4		-1.2		

The grouting sufficiently connected and retrofitted the wall; the final leaf separation is similar compared to the un-strengthened wall and it starts more evidently to increase at higher vertical stresses. Wall strengthened with NSM of glass cords exhibits similar cracking as the grouted wall at its maximum loading, but because the cords in the joints limit the longitudinal horizontal deformations, higher compressive strength is obtained and vertical cracks between the leaves are, due to transversal ties controlling the out-of-plane deformations, allowed to propagate.

5.2 Cyclic in-plane shear tests on walls

5.2.1 Test setup, loading protocol and measuring positions

The same test setup was used as for shear tests of un-strengthened walls (Section 3.4.1). Concerning the testing conditions, the higher pre-compression level (15% f_{Mc} of the un-strengthened walls) was applied and both cantilever and fixed boundary conditions were used. Under cantilever boundary conditions tests S1-S4 were performed in order to prove, whether the shear mechanism could be changed to rocking and to see the effect of strengthening on the leaf separation, which proved to be more problematic in tests of un-strengthened walls for cantilever boundary conditions. Tests S5-S8 were performed under fixed-fixed boundary conditions. To assure the credibility of the results comparison, the testing conditions and the loading protocol for tests remained the same as in the tests of un-strengthened walls (Section 3.4.2). Also positions and number of LVDTs to measure the displacements were not changed (Section 3.4.2) with the exception of adding one new LVDT. LVDT named W5 was installed horizontally at approximate middle height $h_w/2$ of the wall on the back side of the wall to measure the horizontal deformations of the wall and the width of the gap in the centre of the wall. Deformations of the cords were not measured, as due to the flexibility and shape of the cords, strain-gauges could not be installed.

5.2.2 Characteristic damage and obtained failure mechanisms

Through applying various strengthening measures (see Table 4.1), various damage and failure mechanisms were enabled (Table 5.4). It has to be noted, that for all shear tests of un-strengthened walls, tested under the same boundary conditions (cantilever and fixed-fixed) and pre-compression level as applied in tests of strengthened walls, the prevailing failure mechanism was shear.

For the first two walls which were only grouted, the failure mechanism was similar to that of the un-strengthened walls tested under high pre-compression level and cantilever boundary condition (diagonal shear through mortar and stones, crushing and falling off of the mortar in vertical joints in the centre part of the wall, vertical column formation). For the first strengthened wall (test S1 - I(n)), which was not very heavily damaged after the first tests, also rocking damage (bed-joint opening) was detected at an early stage of loading and was soon followed by shear damage already described for un-strengthened walls. No rocking was however detected for the prior grouting more severely damaged wall (test S2 – I(p)). For this wall, the formation of the vertical crack in one of the upper corners resulted in slumping of the outer stone block (Figure 5.13). Leaf separation occurred more apparently only in the post-peak phase of the test.

Figure 5.13: Damage after test S2 – I(p) on the front and transversal sides of the wall
Slika 5.13: Razpokanost zidu na prednji in stranskih straneh zidu po testu S2 – I (p)

Under the same boundary conditions NSM FRP strengthening changed the behaviour of the wall from shear to rocking. For both test specimens S3 – I.S1(p) and S4 - I.S2(p) rocking was the prevailing failure mechanism (Figure 5.14), only that for wall S3 – I.S1(p) at higher displacements also some cracks through mortar over entire wall area indicating diagonal shear mechanism developed. For both tests crushing of mortar in the upper part of the wall was attained with some toe crushing. For wall S4 - I.S2(p), crushing of the mortar at positions of FRP installation could be recognized already at an early stage of the test. For both tests, the crack between the leaves progressed in the last stages of the tests, but was not significant.

Figure 5.14: Rocking and minor shear damage on the wall after test S3 – I.S1(p) and rocking and toe crushing at test S4 - I.S2(p)
Slika 5.14: Upogibne in manjše strižne poškodbe zidu po testu S3 – I.S1(p) ter upogibne poškodbe s porušitvijo pete po testu S4 - I.S2(p)

Fixed-fixed boundary conditions triggered different behaviour for the various strengthening combinations; for test S5 - I.S2.P (p), which can be compared to test S4 - I.S2 (p), after initial rocking behaviour shear mechanism developed at displacement of 15 mm. First, some new cracks parallel to vertical mortar joints over the entire surface area of the wall developed, then they were later followed by some cracks through stones. After 37.5 mm (d_{Fmax}), more apparent damage occurred on the wall; cracks with no principal diagonal direction, widened (Figure 5.15 a, b) and leaf separation became

more evident (Figure 5.16 a, b). At the centre of the walls detachment of the cords from the wall surface area was more visible with each new loading cycle (Figure 5.15 c, d). The cords themselves were not damaged. The crack between the leaves, which developed on one side only, widened significantly with each loading cycle also and was at d_{max} (45 mm) at the upper part of the wall over 3 cm wide, whereas the gap of the crack together with the emptied vertical joint measured in total over 6 cm (Figure 5.16 c). On the wall also toe crushing damage (of stones) was obtained (Figure 5.15 e).

Figure 5.15: Crack pattern on the wall (a, b) with cord detachment (c, d) and toe crushing (e) after test S5 - I.S2.P(p)
Slika 5.15: Razpokanost zidu (a, b) z odstopanjem vrvice (c, d) in zdrobljeno peto (e) po testu S5 - I.S2.P(p)

Figure 5.16: Leaf separation with toe-crushing (a-c) , damage of the transversal connections (d, e) of the wall after test S5 - I.S2.P(p)
Slika 5.16: Razpoka (vrzel) med slojema ter zdrobljena peta (a-c), poškodovanost prečnih povezav (d, e) zidu po testu S5 - I.S2.P(p)

Damage attained at test S6 - I.S2-.P(n) (Figure 5.17) was to some point similar to S5 - I.S2.P(p), however no rocking mechanism was observed at the beginning. Severe toe crushing damage occurred in the last phases of the test though. Wide gaps between the leaves evolved at both sides of the wall.

Figure 5.17: Leaf separation, toe-crushing damage and cord detachment with partially emptied mortar joints after test S6 - I.S2-.P (n)

Slika 5.17: Razpoka med sloji, zdrobljena peta in odstopanje vrvic z deloma izpraznjenimi horizontalnimi spojnicami po končanem testu S6 - I.S2-.P (n)

For wall S8 – I.S2e.P (n), where instead of cement-lime mortar epoxy binder was used to install the cords and to repoint the wall, characteristic rocking mechanism with flexural cracks between the first row of stones and concrete slab developed, while no other damage occurred.

Shear mechanism comparable to mechanism of un-strengthened walls occurred for test S7 - I.P (n); at first rocking mechanism developed, whereas the existing grouted cracks through stones reopened in the next loading cycles. Afterwards other stones cracked too. Crushing and falling out of mortar in the vertical mortar joints at the central area, vertical column formation and leaf separation, more distinct on the side of the wall, occurred.

Preglednica 5.4: Karakteristične poškodbe, prevladujoči porušni mehanizmi ter razslojitev slojev pri strižnih testih utrjenih zidov

Table 5.4: Summary of characteristic damage, obtained failure mechanisms and leaf separation of the retrofitted/strengthened walls, tested in shear

Test no.	Name	Testing boundary conditions	Damage	Failure mechanism	Leaf separation
1	S1 - I (n)	cantilever	Shear, toe crushing	Shear	Moderate, post-peak
2	S2 - I (p)		Shear	Shear	Moderate, post-peak
3	S3 - I.S1 (p)		Rocking, (shear, toe crushing)	Mixed	Significant, post-peak
4	S4 - I.S2 (p)		Rocking, toe crushing	Rocking	minor
5	S5 - I.S2.P (p)	fixed-fixed	Shear, toe crushing	Shear	Significant; moderate prior peak, progressive post-peak
6	S6 - I.S2-.P (n)		Shear, toe crushing	Mixed	Significant; moderate prior peak
7	S7 - I.P (n)		Shear	Shear	Moderate; considerable prior
8	S8 – I.S2e.P (n)		Rocking	Rocking	/

The damage development and propagation description for each performed test is presented, supported by photographs of characteristic damage during and after the test and some LVDT results in [267]. In Table 5.4 the damage and final failure mechanisms obtained at shear tests of retrofitted/strengthened

walls are summarized. In Table 5.5 maximum leaf separations and out-of-plane displacement for strengthened walls gained from LVDT measurements are also provided.

Some significant changes in the behaviour of NSM strengthened walls were for some cases achieved. Wall strengthened by NSM in every joint and tested under cantilever boundary condition (S4) changed its failure mode from shear to rocking. The same occurred for the wall with NSM of cords built-in with epoxy mortar instead of cement-lime one tested under fixed-fixed boundary condition (S8). If NSM was applied with cement-lime mortar (S5), still shear mechanism developed, but this was the only case where the glass cords were evidently activated and, as it will be seen later on, the response of the wall was significantly changed. Besides shear damage of the walls also toe-crushing occurred. Both variations of strengthening (where NSM was not applied in every joint or on both sides of the wall, i.e. S6 and S3), changed the behaviour compared to the behaviour of un-strengthened walls. It can be seen, that every seemingly insignificant variation of either boundary conditions or of strengthening intervention, can reflect in significant change of the walls' response and consequently in their strength and displacement capacity. This will be reaffirmed further on in the analysis of the results.

Preglednica 5.5: Maksimalne širine razpok med sloji, izmerjenih z LVDT-ji W1-W4, ter izven-ravninski pomiki na zadnji strani zidu, izmerjeni z I1 in I2

Table 5.5: Maximum leaf separation measured by LVDTs W1-W4 and out-of-plane displacement of back side (leaf) of the wall measured by I1 and I2

		Maximum LVDT measurements					
Test no.	Name	W1 [mm]	W2 [mm]	W3 [mm]	W4 [mm]	I1 [mm]	I2 [mm]
1	S1 - I (n)	1.08	1.67	0.47	5.93	0.00	-1.12
2	S2 - I (p)	4.34	2.60	0.59	0.63	0.11	-2.00
3	S3 - I.S1 (p)	11.14	5.06	1.35	8.21	10.58	-1.00
4	S4 - I.S2 (p)	1.15	0.08	0.03	1.62	0.79	-2.93
5	S5 - I.S2.P (p)	21.55	22.62	20.10	0.01	1.28	-9.72
6	S6 - I.S2-.P (n)	28.01	28.15	17.92	17.96	0.55	-5.84
7	S7 - I.P (n)	6.47	8.09	3.88	2.15	0.02	-5.61
8	S8 – I.S2e.P (n)	0.51	0.30	0.00	0.04	35.31	-0.10

Walls tested under cantilever boundary conditions (S1-S4) were not transversally connected. For these walls, similar maximum leaf separation was attained for both only grouted walls (S1 and S2), whereas the wall, additionally strengthened with NSM cords only, sustained a greater leaf separation. This can be attributed to limitation of longitudinal horizontal deformations (i.e. cracks) by the glass cords installed in the joints. Walls under fixed-fixed boundary conditions were all transversally connected. Test S7, where besides grouting only transversal tying was applied, proved a moderate increase of the leaf separation compared to only grouted walls (S1 and S2). However, if both ties and NSM (in every joint as for S5 or in every second joint as for test S6) are applied, significantly higher ultimate leaf separation is achieved. If rocking mechanism develops (tests S4 and S8), the presence of transversal connection is irrelevant, since leaf separation is not problematic (for the tested type of masonry).

5.2.3 Hysteretic response

The evaluation of the characteristic hysteretic behaviour is provided in the following Section. Hysteresis diagrams of induced lateral force are presented in dependence from lateral (H6 LVDT) displacement of the wall.

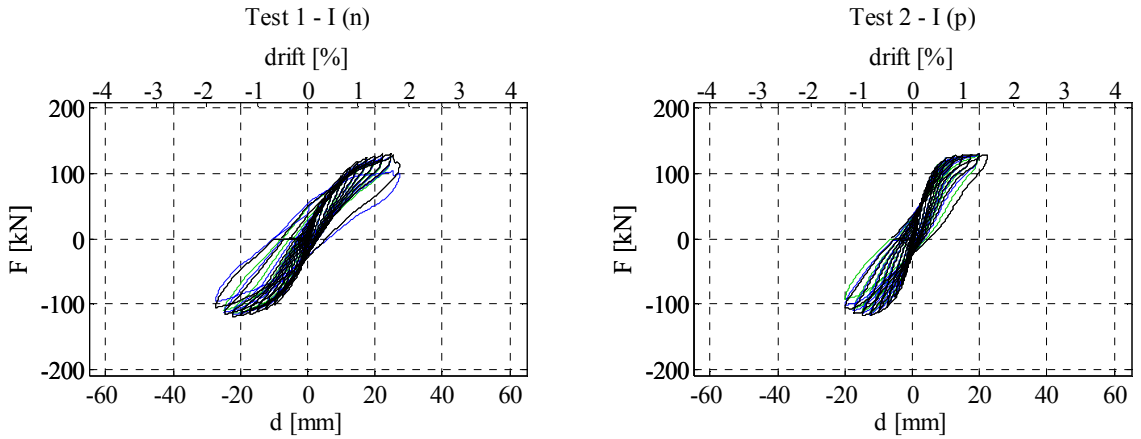

Figure 5.18: Force - displacement diagrams for the tests of only grouted walls; less damaged wall – test S1 - I(n) and more damaged wall – test S2 – I(p)
Slika 5.18: Diagrami sile v odvisnosti od prečnega pomika za samo injektirana zidova; za manj poškodovani zid - test S1 - I(n) in bolj poškodovani zid – test S2 – I(p)

In Figure 5.18 the response of only grouted walls is presented. Compared to average values of maximum forces and displacements attained at tests 7-10 of un-strengthened walls (presented in Table 5.7), where the same boundary conditions and pre-compression level were applied, similar values were obtained, from which it can be concluded, that line crack grouting was sufficient to restore the walls to the original condition. One of the important conclusions is that less strong and less stiff grout injections do not significantly change neither stiffness characteristics of walls, nor strength capacity, which is important when designing repair interventions measures for the building. Using such measures guarantees that the global response of the building remains unchanged (compared to state before the repairs).

The hysteretic behaviour of walls strengthened by glass cords (either by NSM, transversally connecting the leaves or with both measures) is presented in Figure 5.19.

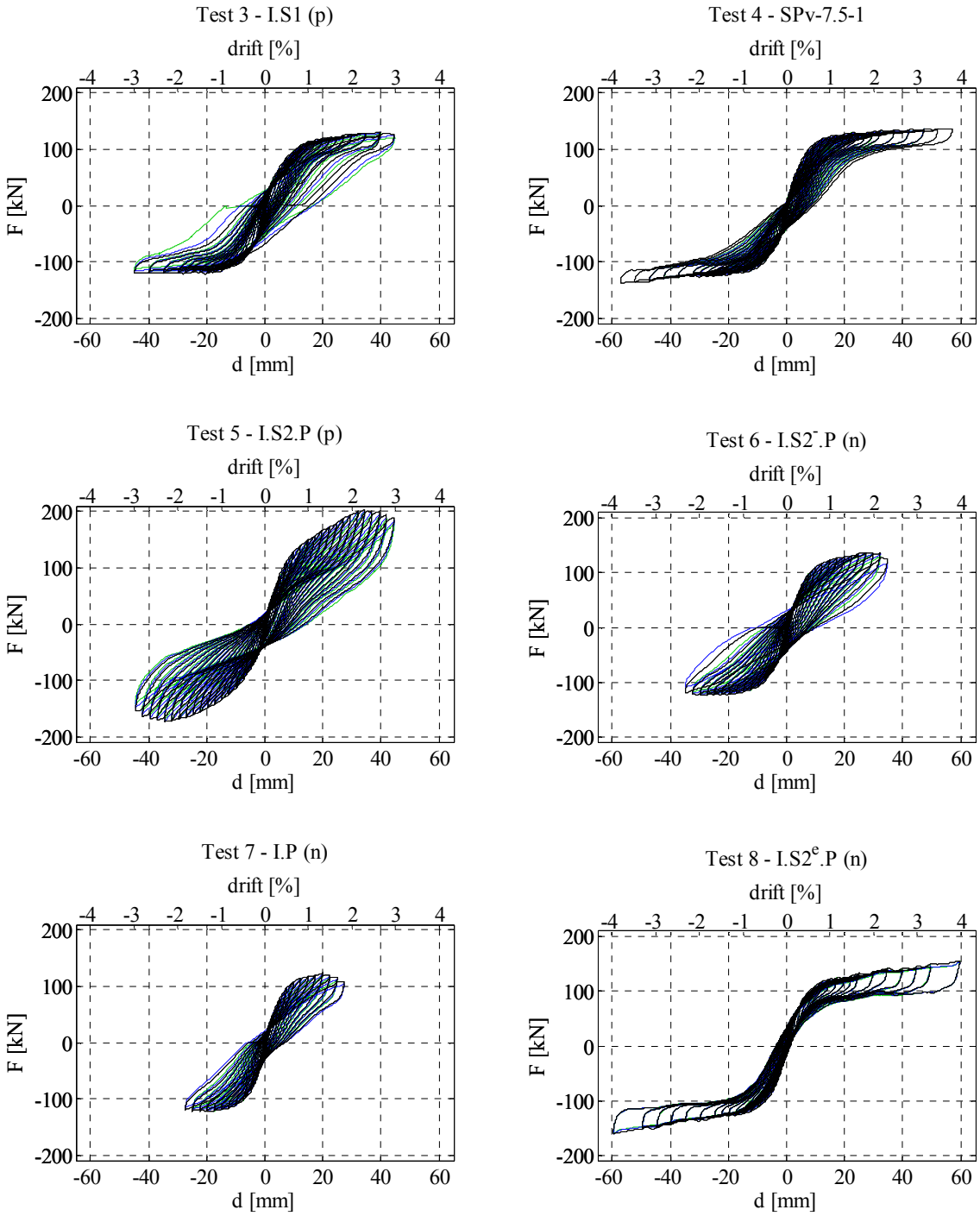

Figure 5.19: Force - displacemet diagrams for tests S3 - S8
Slika 5.19: Diagrami sile v odvisnosti od prečnega pomika za teste S3 - S8

Characteristic values of lateral load - displacement diagrams are presented in Table 5.6, where displacements and corresponding forces at first visual shear cracks d_{cr}, maximum forces reached F_{max} and maximum displacements attained d_{max} for both directions are presented, whereas in Table 5.7 average values for negative and positive direction are provided. For the comparison, in both tables also average values obtained at tests of un-strengthened walls with the same boundary conditions and pre-compression level are presented.

Preglednica 5.6: Vrednosti karakterističnih točk odziva sila - pomik za posamezno smer obremenjevanja utrjenih zidov

Table 5.6: Characteristic values of force - displacement diagrams obtained in both directions

Limit state	First shear crack				Maximum force				Maximum displacement			
Test	d_{cr}^{+} [mm]	d_{cr}^{-} [mm]	F_{cr}^{+} [kN]	F_{cr}^{-} [kN]	d_{Fmax}^{+} [mm]	d_{Fmax}^{-} [mm]	F_{max}^{+} [kN]	F_{max}^{-} [kN]	d_{max}^{+} [mm]	d_{max}^{-} [mm]	F_{dmax}^{+} [mm]	F_{dmax}^{-} [mm]
Strengthened												
S1 - I (n)	7.5	-7.4	80.4	-89.4	24.8	-22.2	129.9	-119.8	27.4	-27.3	99.8	-94.9
S2 - I (p)	3.0	-3.0	61.9	-69.0	19.8	-14.9	129.7	-118.5	22.3	-19.9	126.9	-104.7
S3 - I.S1 (p)	27.2	-25.3	124.8	-120.0	39.6	-20.1	130.8	-121.9	44.7	-44.8	120.5	-112.0
S4 - I.S2 (p)	5.0	-5.0	77.3	-81.6	52.5	-57.0	137.0	-138.1	57.1	-57.1	136.2	-136.5
S5 - I.S2.P (p)	14.8	-14.8	150.0	-135.0	34.2	-34.4	203.5	-173.9	44.5	-44.6	176.1	-140.8
S6 - I.S2-.P (n)	9.9	-9.9	110.0	-106.9	27.6	-27.8	136.8	-124.0	34.7	-34.8	114.6	-108.3
S7 - I.P (n)	12.4	-12.4	115.1	-115.8	19.7	-17.8	123.7	-122.0	27.3	-27.3	103.6	-115.4
S8 - I.S2e.P (n)					59.3	-59.3	154.8	-160.9	59.6	-59.5	153.9	-159.6
Un-strengthened (average)												
11-14 cantilever	3.5	-3.5	72.1	-73.3	18.6	-17.7	121.4	-115.9	24.9	-24.9	109.9	-96.2
7-10 fixed-fixed	3.2	-3.2	67.2	-73.0	15.4	-14.2	126.8	-119.2	21.2	-21.1	93.1	-90.2

Preglednica 5.7: Povprečne karakteristične vrednosti diagram sila – pomik obeh smeri obremenjevanja utrjenih zidov

Table 5.7: Average characteristic values of force - displacement diagrams for both directions

Limit state	First shear crack		Maximum force		Maximum displacement	
Test	d_{cr} [mm]	F_{cr} [kN]	d_{Fmax} [mm]	F_{max} [kN]	d_{max} [mm]	F_{dmax} [mm]
Strengthened						
S1 - I (n)	7.5	84.9	23.5	124.9	27.4	97.3
S2 - I (p)	3.0	65.4	17.3	124.1	21.1	115.8
S3 - I.S1 (p)	26.3	122.4	29.9	126.4	44.8	116.3
S4 - I.S2 (p)	5.0	79.4	54.7	137.5	57.1	136.3
S5 - I.S2.P (p)	14.8	142.5	34.3	188.7	44.5	158.4
S6 - I.S2-.P (n)	9.9	108.5	27.7	130.4	34.8	111.5
S7 - I.P (n)	12.4	115.4	18.8	122.9	27.3	109.5
S8 - I.S2e.P (n)			59.3	157.8	59.6	156.8
Un-strengthened (average)						
11-14 cantilever	3.5	72.7	18.1	118.7	24.9	103.0
7-10 fixed-fixed	3.2	70.1	14.8	123.0	21.1	91.7

If the maximum forces obtained from the tests are compared (Figure 5.20), it is evident that with all strengthening combinations, where the same failure mechanism was obtained as in tests of un-strengthened walls (prevailingly shear mechanism), no major increase in F_{max} was obtained. At test S4, where under the same boundary conditions different failure mechanism was achieved and the wall was beside grouting on both sides also strengthened by glass cords in every horizontal joint, 16% increase of F_{max} was attained (compared to F_{max} achieved at same conditions prior strengthening). If this force is compared to the average F_{max} achieved with rocking mechanism (under different boundary conditions and pre-compression level), which is 64.8 kN, the increase is 112%, and even higher, 144%, for wall test where rocking mechanism was obtained under fixed-fixed boundary conditions (test S8 - NSM by epoxy mortar). NSM cords have therefore enabled higher resistance of walls if rocking mechanism was triggered.

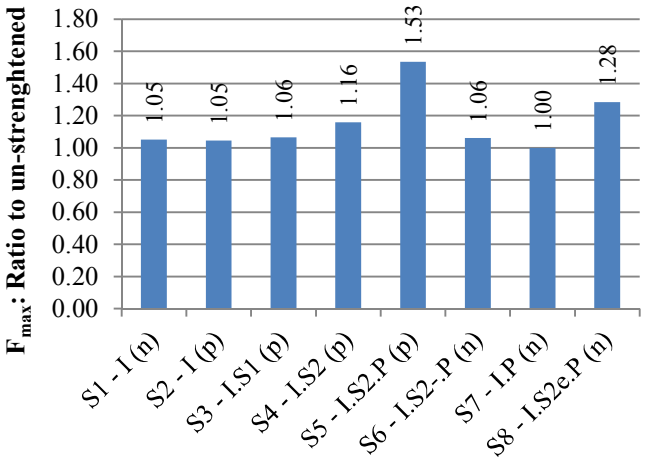

Figure 5.20: Ratio of maximum forces F_{max}, obtained at tests of strengthened walls, and average maximum forces of the un-strengthened walls
Slika 5.20: Razmerje maksimalnih sil F_{max}, dobljenih pri testih utrjenih zidov, in povprečnimi vrednostmi neutrjenih zidov

Maximum displacements achieved were however, regardless the strengthening intervention additional to grouting, higher; from 29 to 282%. Performance of walls in terms of displacement capacity and ductility is in more detail presented in the following Sections.

5.2.4 Bi-linear idealization of hysteretic envelopes

According to the same procedure and following the same assumptions as in Section 3.4.4.1, where results of un-strengthened walls were evaluated, envelopes and idealisation of the hystereses were made for strengthened walls. Hysteresis envelopes and their bi-linear idealisation are presented in Figure 5.21 and compared in Figure 5.22, whereas characteristic values of bi-linear idealized curves are presented in Tables 5.8 and 5.9.

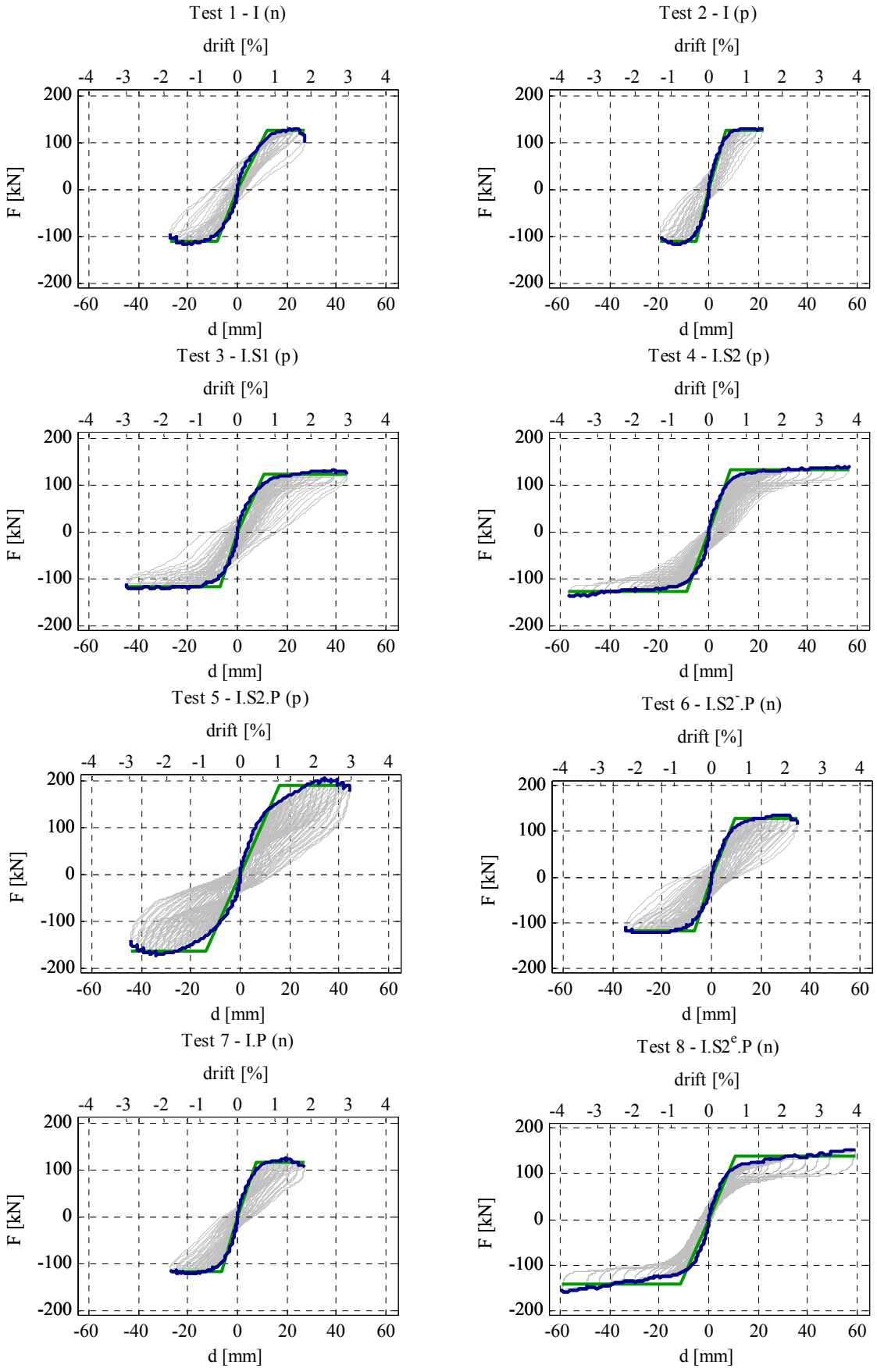

Figure 5.21: Hysteresis envelopes and corresponding bi-linear idealisation curves for each shear test of the strengthened walls

Slika 5.21: Histerezne ovojnice in pripadujoče idealizirane krivulje za posamezne strižne teste utrjenih zidov

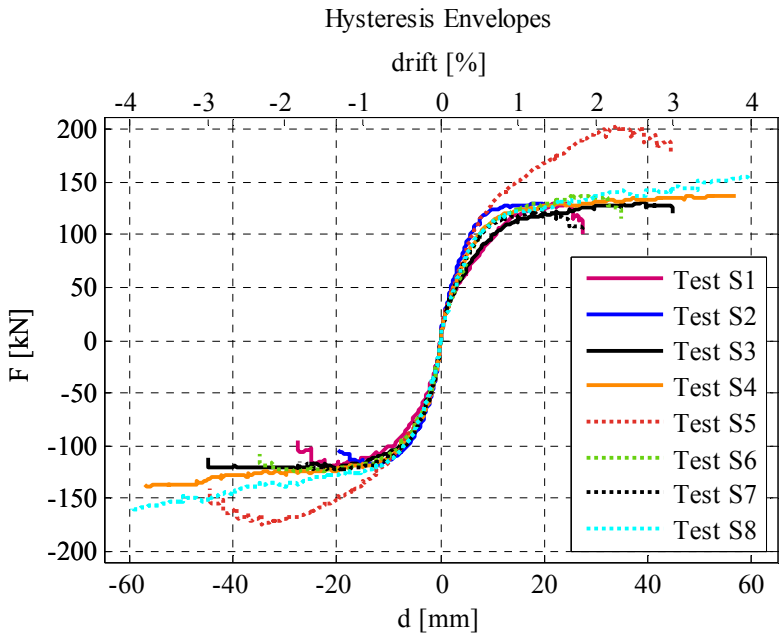

Figure 5.22: Comparison of hysteresis envelopes of all shear tests of strengthened walls
Slika 5.22: Primerjava histereznih ovojnic vseh strižnih testov utrjenih zidov

Preglednica 5.8: Karakteristične vrednosti idealiziranih krivulj za posamezno smer obremenjevanja utrjenih zidov

Table 5.8: Characteristic values of bi-linearly idealised force - displacement diagrams obtained in both directions

Test	F_{id}^{+} [kN]	F_{id}^{-} [kN]	d_e^{+} [mm]	d_e^{-} [mm]	K_{ef}^{+} [kN/mm]	K_{ef}^{-} [kN/mm]	d_u^{+} [mm]	d_u^{-} [mm]	μ^{+}	μ^{-}
Strengthened										
S1 - I (n)	125.4	-113.3	11.9	-8.3	10.5	13.6	27.4	-27.3	2.30	3.28
S2 - I (p)	126.6	-112.5	6.9	-5.3	18.3	21.3	22.3	-19.9	3.23	3.76
S3 - I.S1 (p)	123.1	-118.1	10.7	-7.2	11.5	16.5	44.7	-44.8	4.18	6.26
S4 - I.S2 (p)	130.6	-128.3	9.1	-8.9	14.3	14.4	57.2	-57.1	6.26	6.39
S5 - I.S2.P (p)	189.4	-163.5	15.7	-14.1	12.1	11.6	44.5	-44.6	2.84	3.16
S6 - I.S2-.P (n)	129.4	-119.4	9.6	-7.2	13.4	16.6	34.7	-34.8	3.61	4.84
S7 - I.P (n)	116.0	-118.4	7.8	-6.5	14.8	18.2	27.3	-27.3	3.49	4.19
S8 - I.S2e.P (n)	138.7	-142.0	11.0	-11.2	12.6	12.7	59.6	-59.5	5.41	5.32
Un-strengthened (average)										
11-14 cantilever	115.5	-109.7	5.9	-5.2	19.6	21.3	24.9	-24.9	4.17	4.74
7-10 fixed-fixed	117.1	-110.3	6.5	-5.2	19.0	23.3	21.2	-20.9	3.42	4.41

Preglednica 5.9: Povprečne karakteristične vrednosti idealiziranih krivulj obeh smeri obremenjevanja utrjenih zidov

Table 5.9: Average characteristic values of bi-linearly idealised force - displacement diagrams for both directions

Test	F_{id} [kN]	d_e [mm]	K_{ef} [kN/mm]	d_u [mm]	μ	d_u^{*} [mm]	μ^{*}
Strengthened							
S1 - I (n)	119.3	10.1	12.1	27.4	2.79	25.1	2.56
S2 - I (p)	119.6	6.1	19.8	21.1	3.49	19.9	3.26
S3 - I.S1 (p)	120.6	8.9	14.0	44.8	5.22	44.8	5.22
S4 - I.S2 (p)	129.5	9.0	14.3	57.2	6.33	57.2	6.33

Continues…

…continuation of Table 5.9

S5 - I.S2.P (p)	176.4	14.9	11.8	44.6	3.00	42.0	2.82
S6 - I.S2-.P (n)	124.4	8.4	15.0	34.8	4.22	32.3	3.92
S7 - I.P (n)	117.2	7.2	16.5	27.3	3.84	25.4	3.60
S8 - I.S2e.P (n)	140.4	11.1	12.6	59.6	5.37	59.6	5.36
Un-strengthened (average)							
11-14 cantilever	112.63	5.57	20.44	24.88	4.46	19.3	3.48
7-10 fixed-fixed	113.74	5.86	21.18	21.00	3.92	15.9	3.00

For easier comparison with un-strengthened walls also ratios of characteristic values for tests S1-S8 to average characteristic values of un-strengthened walls are presented in the following table (Table 5.10); and ratios of ductility, effective stiffness K_{ef} and shear modulus G_M are compared in Figure 5.23.

Preglednica 5.10: Razmerje povprečnih vrednosti karakterističnih točk idealiziranih krivulj sila - pomik obeh smeri obremenjevanja utrjenih zidov s povprečnimi rezultati neutrjenih zidov

Table 5.10: Ratio of average characteristic values of idealised force - displacement diagrams for both directions of strengthened and un-strengthened walls

Test	F_{id} ratio	d_e ratio	K_{ef} ratio	d_u ratio	μ ratio	D_u^* ratio	μ^* ratio
Strengthened to Un-strengthened							
S1 - I (n)	1.06	10.1	0.59	1.10	0.63	1.17	0.65
S2 - I (p)	1.06	6.10	0.97	0.85	0.78	0.93	0.83
S3 - I.S1 (p)	1.07	8.93	0.69	1.80	1.17	2.09	1.34
S4 - I.S2 (p)	1.15	9.04	0.70	2.30	1.42	2.67	1.62
S5 - I.S2.P (p)	1.55	14.9	0.56	2.12	0.77	2.65	0.94
S6 - I.S2-.P (n)	1.09	8.41	0.71	1.66	1.08	2.04	1.31
S7 - I.P (n)	1.03	7.17	0.78	1.30	0.98	1.60	1.20
S8 - I.S2e.P (n)	1.23	11.1	0.60	2.84	1.37	3.75	1.79

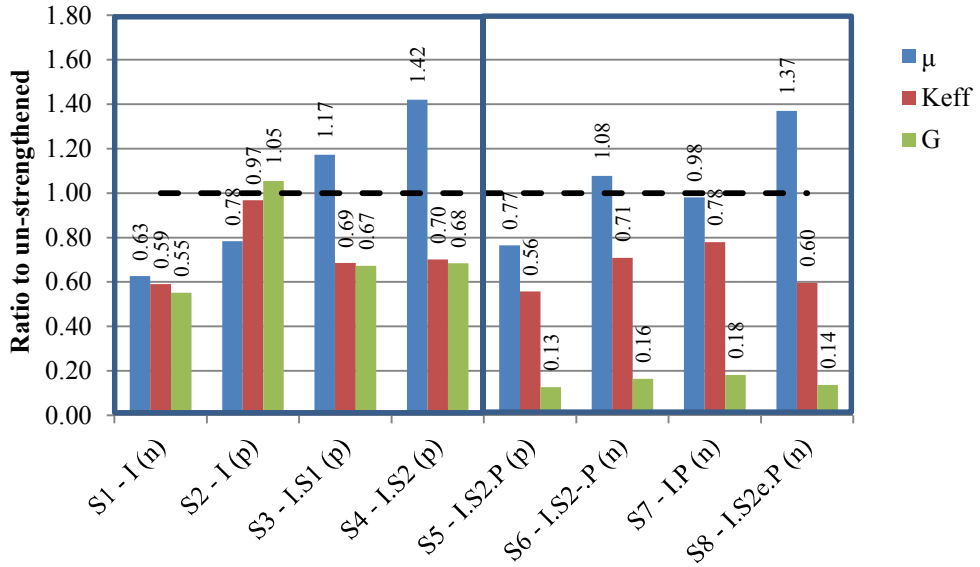

Figure 5.23: Comparison of ductility μ, effective stiffness K_{ef} values and shear moduli G_M of the strengthened walls against the average values of the un-strengthened walls

Slika 5.23: Primerjava duktilnosti μ, efektivnih togosti K_{ef} in strižnih modulov G_M utrjenih zidov s povprečnimi vrednostmi neutrjenih zidov

One of the surprising observations is that ductility coefficient μ is not significantly increased or it is even lower compared to un-strengthened walls, especially with tests where rocking was the prevailing mechanism (test S3, S4 and S8), despite the fact, that the attained d_{max} are more than 2-times higher. The reason for this is that in these tests d_u were not achieved as no significant force drop was obtained. Consequently, also such idealisation is not the most appropriate. Additionally, because the criteria for determining K_{ef} was stiffness at displacement, where 2/3 F_{max} was achieved, K_{ef} is lower and d_e higher, which decreases μ. As it can be seen, d_e are significantly higher; from 6- (test S2) to almost 15-times (test S5). For this reason a better option is to compare lateral displacements or lateral drifts at characteristic limit states.

5.2.5 Performance evaluation

5.2.5.1 Tensile strength and shear modulus

From idealised curves again tensile strength f_{Mt} and G_M modulus were calculated according to the same equations and assumptions adopted for un-strengthened walls presented in Section 3.4.5.3; the results are presented in Table 5.11. Results for f_{Mt} are compared in Figure 5.24 and their ratio to f_{Mt} of the un-strengthened walls in Figure 5.25. Further in Figure 5.24, the results for G_M are presented.

Preglednica 5.11: Natezne trdnosti f_{Mt} in strižni moduli G_M, dobljeni po različnih principih, za teste utrjenih zidov in njihovo razmerje s povprečnimi rezultati testov neutrjenih zidov

Table 5.11: Tensile strength f_{Mt} and shear moduli G_M, obtained according to two criteria, for tests of strengthened walls and their ratio to average values of un-strengthened walls

Test	f_{Mt} [MPa]	ratio to un-strengthened	G_M [MPa]	ratio to un-strengthened	$K_{1.5mm}$ [kN/mm]	$^{*}G_{1.5mm}$ [MPa]	$^{**}G_{1.5mm}$ [MPa]
Strengthened							
S1 - I (n)	0.179	1.019	66.5	0.552	22.6	154.4	84.7
S2 - I (p)	0.180	1.023	126.9	1.054	27.2	210.2	102.1
S3 - I.S1 (p)	0.183	1.037	81.0	0.672	22.9	160.8	86.0
S4 - I.S2 (p)	0.206	1.170	82.4	0.684	23.1	162.9	86.6
S5 - I.S2.P (p)	0.343	2.043	55.7	0.127	25.3	126.4	95.0
S6 - I.S2-.P (n)	0.193	1.149	71.7	0.164	23.3	115.7	87.5
S7 - I.P (n)	0.174	1.037	79.3	0.181	24.8	123.4	93.1
S8 - I.S2e.P (n)	0.236	1.408	59.8	0.137	22.4	110.6	84.1
Un-strengthened (average)							
11-14 cantilever	0.176		120.4		33.4	215.3	94.4
7-10 fixed-fixed	0.168		272.1		32.6	226.2	115.1

* calculated according to Eq. 3.12 (considering stiffness and E_M modulus)

**calculated according to Eq. 3.13 (according to its definition; shear stress τ to shear strain γ ratio)

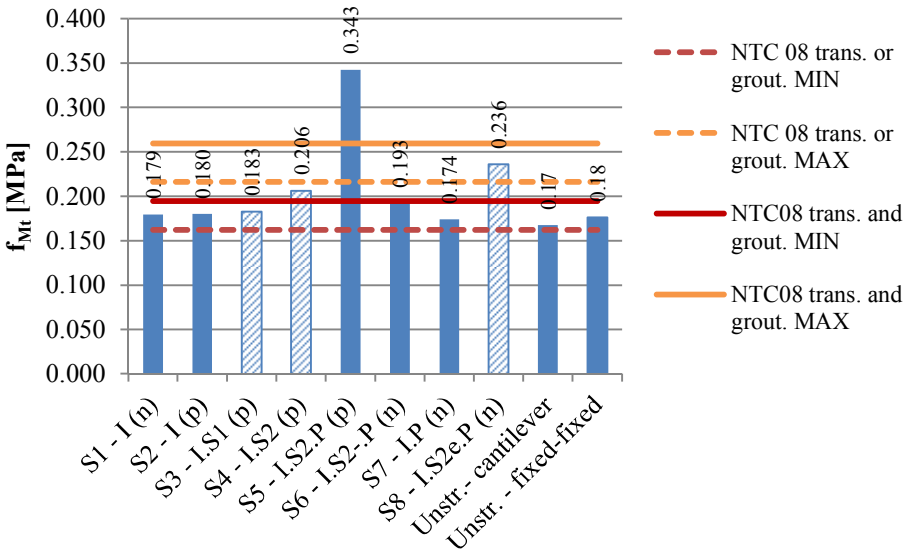

Figure 5.24: Tensile strength f_{Mt} of the strengthened walls calculated from the idealised resistances obtained through bi-linear idealisation compared to values provided in NTC08
Slika 5.24: Natezna trdnost f_{Mt} utrjenih zidov, izračunana za utrjene zidove iz bi-linearno idealiziranih krivulj, primerjana z vrednostmi iz NTC08

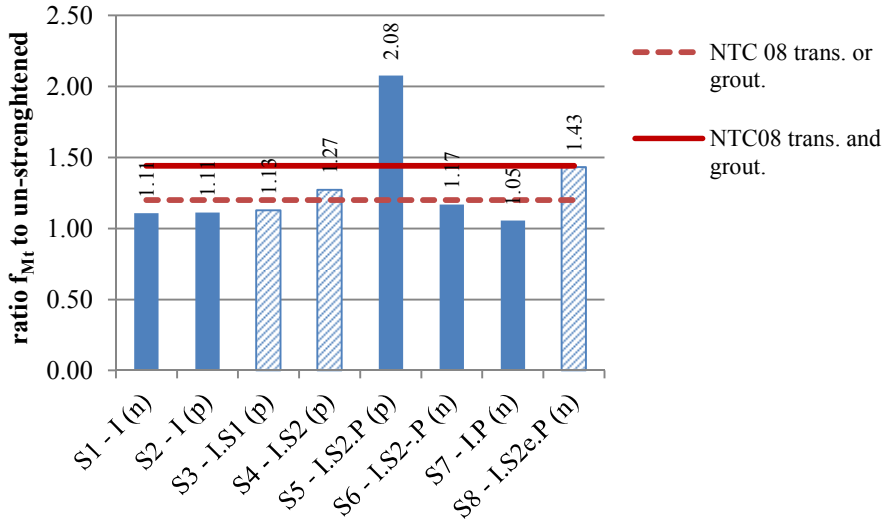

Figure 5.25: Comparison of tensile strength f_{Mt} of strengthened walls against average values of un-strengthened values
Slika 5.25: Primerjava nateznih trdnosti f_{Mt} utrjenih zidov s povprečnimi vrednostmi neutrjenih

Substantial tensile strength f_{Mt} increase was obtained only for test S5, where over 100% increase was obtained. For S5, this strength increase is the result of the significant FRP contribution. It has to be noted that for tests S3, S4 and S8, the f_{Mt} were calculated only indicatively, since rocking mechanism was obtained for these walls. All other measures applied on the walls, including also retrofitting by means of grouting, have enabled the walls to restore the strength of un-strengthened walls.

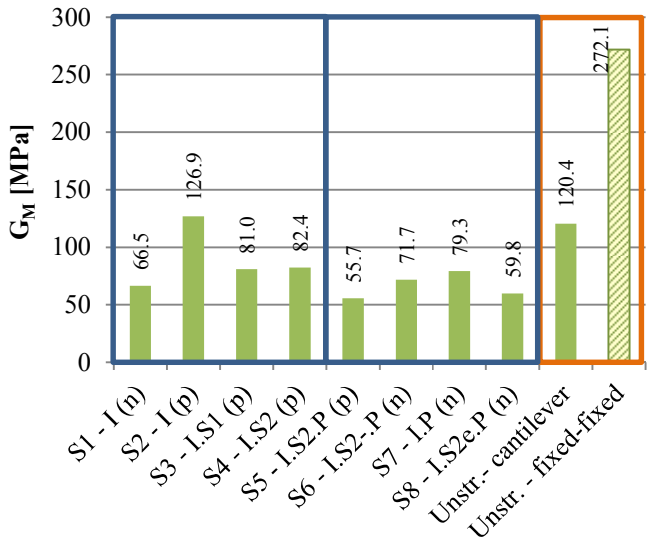

Figure 5.26: Shear moduli G_M of strengthened walls calculated from effective stiffness K_{ef} according to Eq. 3.12
Slika 5.26: Strižni moduli G_M utrjenih zidov, izračunani iz efektivnih togosti K_{ef} po En. 3.12

Shear modulus, calculated according to Eq. 3.12 from K_{ef} and E_M gained from compression tests, are lower than those obtained in tests of un-strengthened walls. Contrary to evaluation of G_M for un-strengthened walls, calculation was due to higher E_M feasible (average value of G_M for un-strengthened walls, tested under higher pre-compression level and fixed-fixed boundary condition was unrealistic). If values are compared to values gained through compression tests, again the difference is very large. Value of 55.7 MPa gained through shear test S5 compared to 914 MPa gained through compression test for the wall with the same strengthening measures (T2) makes up a 16.4 ratio between them. If instead of K_{ef} the actual stiffness of the walls at the beginning of the test (at amplitude displacement 1.5 mm) is considered, according to Eq. 3.12 higher values are obtained, however still significantly lower than through compression test; 126.4 MPa instead of 55.7 MPa. If G_M modulus for the same stress and deformation states (d = 1.5 mm) are calculated from shear tests as the ratio of shear stress to shear strain (Eq. 3.13), lower values are obtained; 95.0 MPa for test S5.

5.2.5.2 Lateral drifts and evaluation of efficiency of the strengthening interventions

As evident from the bi-linear results evaluation, ductility is not necessary the most correct way to represent strengthening efficiency in terms of displacement capacity. In order to be able to make direct comparisons to code provisions recommendations, displacements at attainment of characteristic damage states are presented in terms of drifts (Table 5.12 and Figure 5.27).The results are compared to results of un-strengthened wall in Table 5.13 and in Figure 5.28.

Preglednica 5.12: Rotacije utrjenih zidov v karakterističnih mejnih stanjih

Table 5.12: Drifts of the strengthened walls at characteristic limit states

Limit state	First shear crack			Maximum force			Maximal displacement		
Test	Θ_{cr}^{+} [%]	Θ_{cr}^{-} [%]	Θ_{cr} (av.) [%]	Θ_{Fmax}^{+} [%]	Θ_{Fmax}^{-} [%]	Θ_{Fmax} (av.) [%]	$\Theta_{u,max}^{+}$ [%]	$\Theta_{u,max}^{-}$ [%]	$\Theta_{u,max}$ (av.) [%]
Strengthened									
S1 - I (n)	0.50	-0.49	0.50	1.65	-1.48	1.57	1.83	-1.82	1.82

Continues…

…continuation of Table 5.12

S2 - I (p)	0.20	-0.20	0.20	1.32	-0.99	1.15	1.49	-1.32	1.41
S3 - I.S1 (p)	1.81	-1.69	1.75	2.64	-1.34	1.99	2.98	-2.99	2.98
S4 - I.S2 (p)	0.33	-0.33	0.33	3.50	-3.80	3.65	3.81	-3.81	3.81
S5 - I.S2.P (p)	0.98	-0.99	0.99	2.28	-2.29	2.29	2.96	-2.97	2.97
S6 - I.S2-.P (n)	0.66	-0.66	0.66	1.84	-1.85	1.85	2.32	-2.32	2.32
S7 - I.P (n)	0.82	-0.83	0.82	1.31	-1.19	1.25	1.82	-1.82	1.82
S8 - I.S2e.P (n)	0.00	0.00	0.00	3.96	-3.96	3.96	3.97	-3.97	3.97
Un-strengthened (average)									
11-14 cantilever	0.23	-0.23	0.23	1.24	-1.18	1.21	1.66	-1.66	1.66
7-10 fixed-fixed	0.22	-0.21	0.22	1.03	-0.95	0.99	1.40	-1.41	1.41

Preglednica 5.13: Razmerja mejnih rotacij utrjenih zidov in povprečnih vrednosti neutrjenih zidov

Table 5.13: Ratios of obtained drift limits of the strengthened walls to the average values of the un-strengthened walls

Test	Θ_{cr} ratio	Θ_{Fmax} ratio	Θ_{max} ratio
Strengthened to Un-strengthened			
S1 - I (n)	2.14	1.30	1.10
S2 - I (p)	0.86	0.96	0.85
S3 - I.S1 (p)	7.55	1.65	1.80
S4 - I.S2 (p)	1.43	3.02	2.30
S5 - I.S2.P (p)	4.58	2.32	2.11
S6 - I.S2-.P (n)	3.07	1.87	1.64
S7 - I.P (n)	3.84	1.27	1.29
S8 - I.S2e.P (n)		4.01	2.82

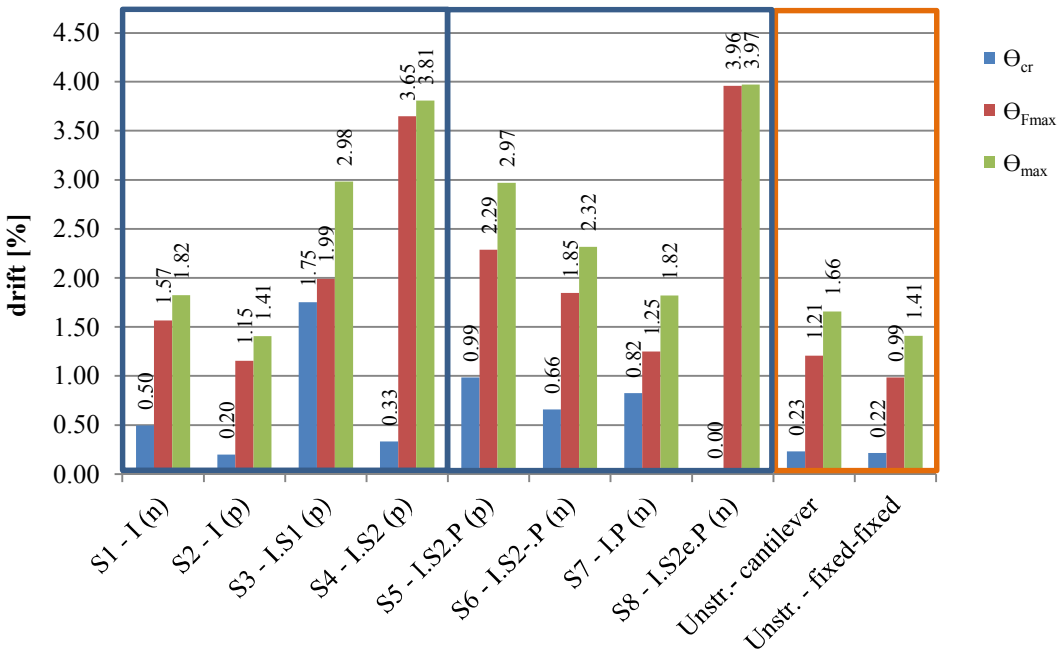

Figure 5.27: Drift limits of strengthened walls and average values of un-strengthened walls
Slika 5.27: Mejne rotacije utrjenih zidov in povprečne vrednosti neutrjenih zidov

The ultimate drift capacities are significantly higher than those expected according to the code provisions (see Section 2.3.3.3). Highest ultimate drift capacity was obtained at tests where rocking mechanism developed (tests S3, S4 and S8), however also at test S5, where shear mechanism occurred and the cords were activated, the ultimate drift limit is almost 3%.

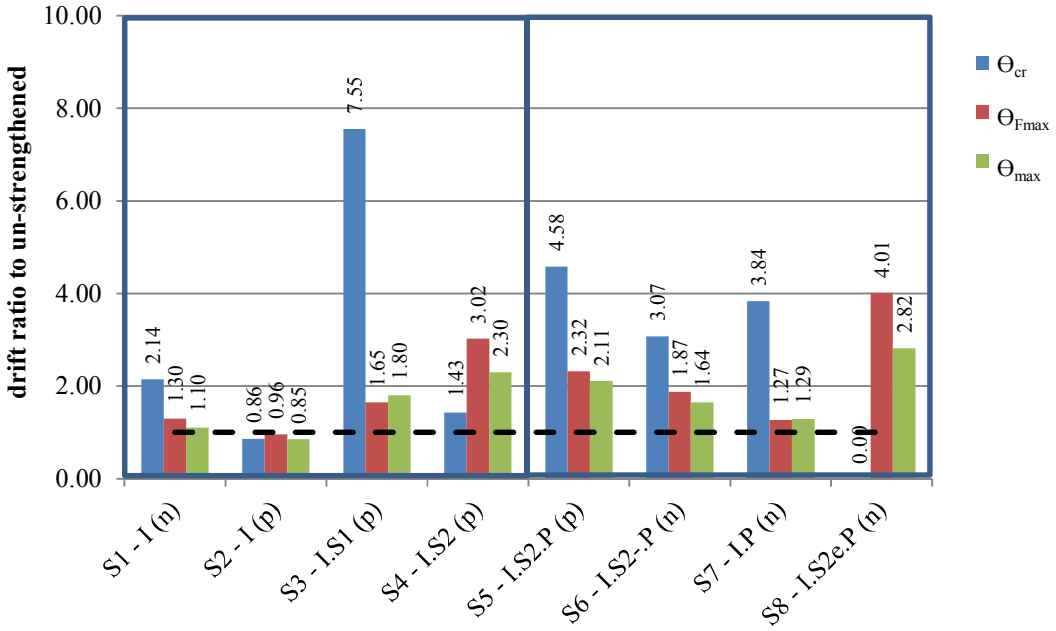

Figure 5.28: Comparison of drift limits of strengthened walls to average values of un-strengthened walls
Slika 5.28: Primerjava mejnih rotacij utrjenih zidov s povprečnimi vrednostmi neutrjenih zidov

Regarding the first shear crack d_{cr} limit state, with all strengthening measures, except for grouting of more damaged wall (test S2), shear cracks occurred at larger displacement. If NSM of glass cords was executed (tests S3-S6, S8) the maximum force was attained at higher displacements; drifts θ_{Fmax} are from 1.65- to 4-times higher. Even though significant increase of F_{max} was obtained only when glass cords were inserted into every horizontal joint, significant ultimate drift capacity increase was obtained regardless the NSM strengthening dispositions. Despite the fact that less favourable mechanism in terms of the ultimate drift capacity - shear – had developed at test S6, the ultimate drift capacity was increased by 64%.

Drift limits corresponding to limit states of bi-linearly idealised curves (elastic displacement d_e, ultimate displacement d_u and reduced ultimate displacement d_u^*), are summarized in Table 5.14.

Preglednica 5.14: Rotacije utrjenih zidov v karakterističnih točkah pomikov idealiziranih krivulj

Table 5.14: Drift limits at characteristic displacements of bi-linear curves of strengthened walls

Limit state	Elastic displacement d_e			Ultimate displacement d_u			Reduced ultimate displacement d_u^*		
Test	Θ_e^+ [%]	Θ_e^- [%]	$\Theta_{e,av.}$ [%]	Θ_u^+ [%]	Θ_u^- [%]	$\Theta_{u,av.}$ [%]	Θ_u^{*+} [%]	Θ_u^{*-} [%]	$\Theta_{u,av.}^*$ [%]
Strengthened									
S1 - I (n)	0.79	-0.56	0.67	1.83	-1.82	1.82	1.70	-1.65	1.67
S2 - I (p)	0.46	-0.35	0.41	1.49	-1.33	1.41	1.49	-1.16	1.32
S3 - I.S1 (p)	0.71	-0.48	0.60	2.98	-2.99	2.98	2.98	-2.99	2.98
S4 - I.S2 (p)	0.61	-0.60	0.60	3.81	-3.81	3.81	3.81	-3.81	3.81

Continues…

…continuation of Table 5.14

S5 - I.S2.P (p)	1.05	-0.94	0.99	2.97	-2.98	2.97	2.80	-2.80	2.80
S6 - I.S2-.P (n)	0.64	-0.48	0.56	2.32	-2.32	2.32	2.15	-2.15	2.15
S7 - I.P (n)	0.52	-0.43	0.48	1.82	-1.82	1.82	1.57	-1.82	1.69
S8 - I.S2e.P (n)	0.73	-0.75	0.74	3.97	-3.97	3.97	3.97	-3.97	3.97
Un-strengthened (average)									
11-14 cantilever	0.40	-0.35	0.37	1.66	-1.66	1.66	1.16	-1.41	1.28
7-10 fixed-fixed	0.43	-0.35	0.39	1.41	-1.39	1.40	1.04	-1.08	1.06

5.2.6 Energy dissipation and equivalent viscous damping

In Figure 5.29 dissipated energy E_{DIS} and in Figure 5.30 dissipated vs. input energy ratios E_{DIS}/E_{INP} at 1st cycles of each amplitude displacement are presented for all tests of strengthened walls.

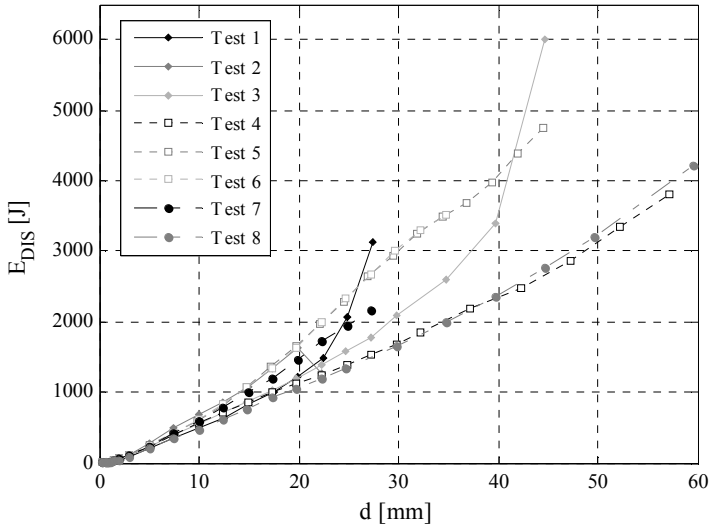

Figure 5.29: Dissipated energy at 1st cycles of amplitude displacements for shear tests of strengthened walls
Slika 5.29: Disipirana energija pri 1. ciklih posameznih amplitud pomika pri strižnih testih utrjenih testov

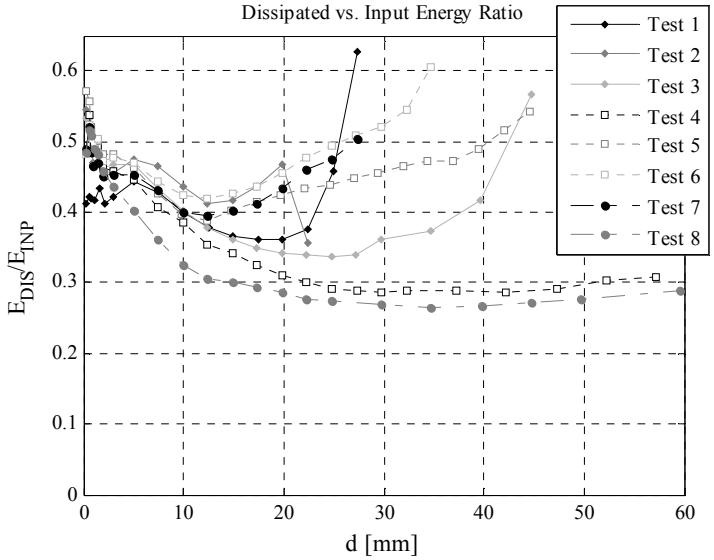

Figure 5.30: Ratio E_{DIS}/E_{INP} at 1st cycles of amplitude displacements for shear tests of strengthened walls
Slika 5.30: Razmerje E_{DIS}/E_{INP} 1. ciklov posameznih amplitud pomikov pri strižnih testih utrjenih testov

Comparing the results of strengthened walls, similar results in dependence of failure mechanism are obtained. Dissipated energy is smaller (absolutely and relatively – compared to input energy) in case of rocking mechanism, which were obtained with test S4 and S8 and partially in test S3. In the later, the dissipation increase is clear in the post-peak part of the response. E_{DIS}/E_{INP} ratio in dependence of amplitude displacement relative to d_{Fmax} (achieved first in either positive or negative direction of loading) is presented in Figure 5.31. In tests S5 and S6, where the walls were strengthened with NSM cords and shear mechanism was obtained, evident increasing of the dissipation started prior reaching the peak resistance. This proves that the cords contribute to higher dissipation of energy not only in the peak and post-peak part of the response but already after d_e is attained. E_{DIS}/E_{INP} ratio in dependence of amplitude displacement relative to d_e is for all tests also presented in Figure 5.31.

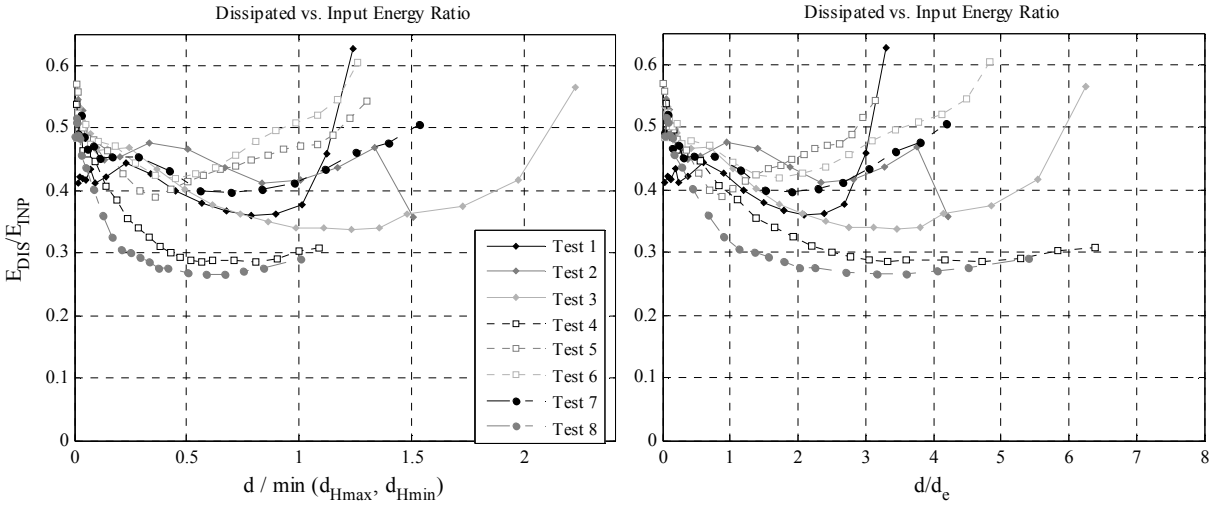

Figure 5.31: Dissipated and input energy ratio E_{DIS}/E_{INP} for tests on strengthened walls at 1st cycles of amplitude displacements, normalized to displacement d_{Fmax} and to elastic displacement d_e
Slika 5.31: Razmerje disipirane in input energije E_{DIS}/E_{INP} utrjenih zidov za 1. cikle posameznih amplitud pomikov, normalizirane na pomike pri maksimalni sili d_{Fmax} ter na pomike na meji elastičnosti d_e

The results for dissipated energy E_{DIS}, input energy E_{INP} and their ratio E_{DIS}/E_{INP} in characteristic limit states are summarized in Table 5.15. They are presented for the 1st cycles at corresponding amplitude displacements together with average results of un-strengthened walls with the same testing conditions.

Preglednica 5.15: Disipirana in vnesena energija za 1. cikle amplitudnih pomikov pri karakterističnih mejnih stanjih testov utrjenih zidov

Table 5.15: Dissipated and input energy for 1st cycles of characteristic limit states attained at tests of un-strengthened walls

Limit state	First shear crack d_{cr}			Maximum force d_{Fmax}			Maximal displacement d_{max}			Elastic displacement d_e		
Test	E_{DIS} [J]	E_{INP} [J]	E_{DIS}/E_{INP}	E_{DIS} [J]	E_{INP} [J]	E_{DIS}/E_{INP}	E_{DIS} [J]	E_{INP} [J]	E_{DIS}/E_{INP}	E_{DIS} [J]	E_{INP} [J]	E_{DIS}/E_{INP}
Strengthened												
S1 - I (n)	348	816	0.427	501	1252	0.400	1478	3930	0.376	3127	4995	0.626
S2 - I (p)	114	252	0.454	495	1063	0.466	1630	3486	0.468	1265	3543	0.357
S3 - I.S1 (p)	1773	5205	0.341	546	1357	0.403	3394	8163	0.416	6008	10623	0.566
S4 - I.S2 (p)	238	533	0.446	570	1481	0.385	3344	11050	0.303	3802	12328	0.308
S5 - I.S2.P (p)	1078	2683	0.402	1078	2683	0.402	3497	7415	0.472	4744	8758	0.542
S6 - I.S2-.P (n)	616	1452	0.424	616	1452	0.424	2680	5271	0.509	3511	5810	0.604
S7 - I.P (n)	786	1985	0.396	424	980	0.433	1472	3384	0.435	2158	4278	0.505
S8 - I.S2e.P (n)	0	0	0	474	1459	0.325	4223	14570	0.290	4223	14570	0.290
Un-strengthened (average)												
11-14 cantilever	197	378	0.519	317	618	0.514	1588	3287	0.482	2478	4131	0.587
7-10 fixed-fixed	228	408	0.549	449	841	0.549	1339	2627	0.509	1687	2898	0.585

Comparing the results the same conclusions as for the un-strengthened walls can be drawn; dissipation is dependent primarily on the obtained failure mechanism. Considerably smaller relative energy dissipation was again obtained for rocking mechanism (tests S4 and S8).

The same as for un-strengthened walls also other energy dissipation parameters are evaluated and summarized in Table 5.16. They again mostly vary in dependence of failure mechanism attained and some in dependence of maximum displacements reached; one of these is cumulative value of E_{DIS}/E_{INP} (*cum* (E_{DIS}/E_{INP}), which is presented in Figure 5.32.

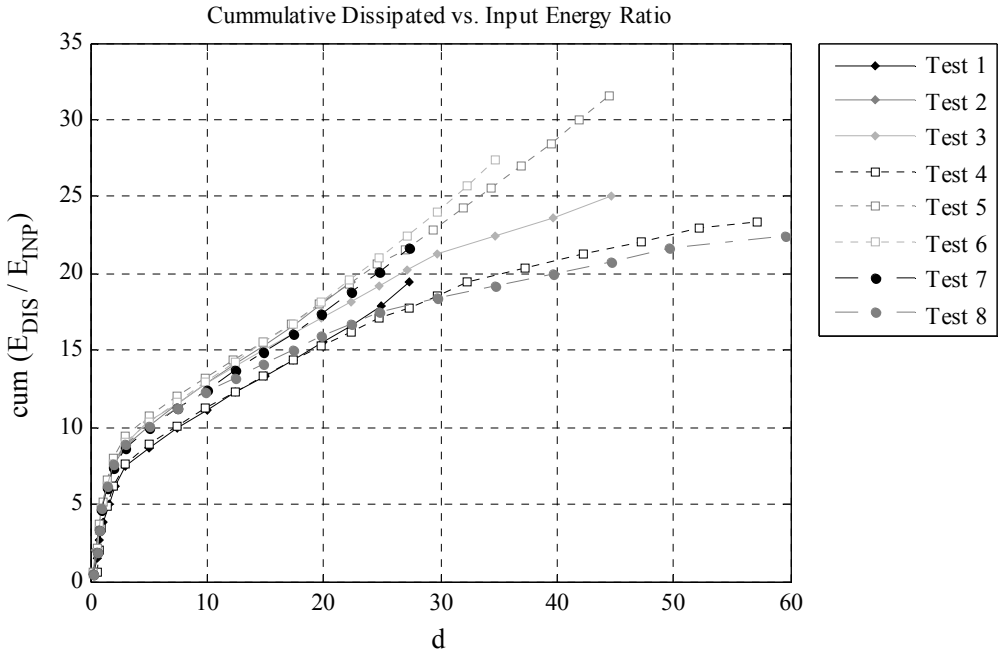

Figure 5.32: Ratio of cumulative dissipated and input energy *cum(E_{DIS}/E_{INP})* for tests of strengthened walls at 1st cycles of displacement amplitudes
Slika 5.32: Razmerje kumulativne disipirane in input energije *cum(E_{DIS}/E_{INP})* utrjenih zidov za 1. cikle posameznih amplitud pomikov

The comparison of cumulative E_{DIS}/E_{INP} ratio confirms the achievement of various failure mechanisms, with tests S4 and S8, where rocking mode developed, the lowest values were obtained at the same amplitude displacement cycles; e.g. at amplitude displacement 30 mm. The highest values were obtained (again at same displacement and overall in the end of the tests) in tests S5 and S6. Only for these two tests (among others tested) the final values present a significant increase of this ratio compared to un-strengthened walls; by 44% in test S5 and by 22% in test S6.

Preglednica 5.16: Kazalci disipacije energije za utrjene zidove

Table 5.16: Energy dissipation parameters for strengthened walls

Name	*cum E_{DIS}*	*cum E_{INP}*	*cum E_{DIS} /cum E_{INP}*	*cum (E_{DIS}/E_{INP})*	$E_{ID,el}$ *INP*	E_{ID}	E_N (Shing)	E_N modified
Strengthened								
S1 - I (n)	11596	26496	0.438	7.13	603	2661	19.2	4.36
S2 - I (p)	7896	18566	0.425	6.88	365	2159	21.6	3.66
S3 - I.S1 (p)	23998	59355	0.404	8.95	538	4861	44.6	4.94
S4 - I.S2 (p)	27499	90674	0.303	8.45	585	6815	47.0	4.03
S5 - I.S2.P (p)	39751	85055	0.467	11.26	1316	6548	30.2	6.07
S6 - I.S2-.P (n)	23215	46387	0.500	9.70	523	3801	44.4	6.11
S7 - I.P (n)	11785	26405	0.446	7.70	420	2782	28.1	4.24
S8 - I.S2e.P (n)	23323	82869	0.281	7.83	780	7582	29.9	3.08
Un-strengthened (average)								
11-14 cantilever	10488	21595	0.490	8.28	347	2506	29.6	4.14
7-10 fixed-fixed	8266	15471	0.534	7.92	341	2069	25.5	3.99

For $cumE_{DIS}/cumE_{INP}$, the values again differ more in dependence of mechanism obtained than of strengthening measure applied; rocking mechanism developed in tests S3, S4, S8 induces the lowest values, which are far lower, than for un-strengthened walls (by 38% in test S4 and by 47% in test S8 compared to average values of un-strengthened walls). Comparing E_N according to Shing, in all cases, where besides grouting additional measures were applied to walls, an increase in dissipation was obtained compared to un-strengthened walls; in tests S3, S4 and S6 by more than 50%. If $E_{N,modified}$ are compared, only tests S5 and S6 prove significant improvement regarding energy dissipation. The lowest values are obtained in tests S2, S4 and S8. In tests S4 and S8 rocking mechanism occurred, whereas in test S2 lower value can be attributed to level of damage on the wall prior strengthening (compared to test S1) and was therefore capable of lesser dissipation through damage development.

In Figure 5.33 obtained equivalent viscous damping coefficients ξ for all tests are presented in dependence of amplitude displacements of cycles, whereas in Table 5.17 minimum values of ξ for all tests on strengthened walls as well as their ratios to un-strengthened walls are provided.

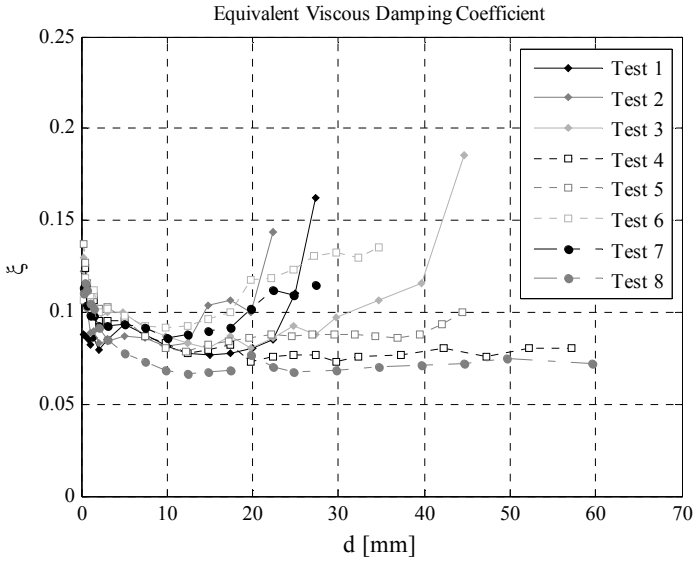

Figure 5.33: Equivalent viscous damping coefficient at 1st cycles of amplitude displacements for strengthened walls
Slika 5.33: Koeficient ekvivalentnega viskoznega dušenja utrjenih zidov za 1. cikle posameznih amplitud pomikov

In tests S1-S3; a significant increase of ξ was obtained for the last few amplitude displacement cycles. For tests S6 and S7 this increase is more uniform and it started at smaller displacements. This can be attributed to strengthening interventions of connecting the walls.

Preglednica 5.17: Minimalne dosežene vrednosti ξ (1. in vseh ciklov strižnih testov) pri utrjenih zidovih s pripadajočimi amplitudnimi pomiki $d_{max,i}$ in njihovo razmerje s povprečnimi rezultati neutrjenih zidov

Table 5.17: Minimum values of ξ (of 1st and of all cycles) achieved during the tests and corresponding amplitude displacements $d_{max,i}$ for tests of strengthened walls and their ratio to average results of un-strengthened walls

Name	1st cycle				All cycles			
	ξ	ξ ratio	$d_{max,i}$ [mm]	$d_{max,i}$ ratio	ξ	ξ ratio	$d_{max,i}$ [mm]	$d_{max,i}$ ratio
Strengthened								
S1 - I (n)	0.077	0.76	15.0	1.43	0.063	0.69	0.33	0.04

Continues…

…continuation of Table 5.17

S2 - I (p)	0.091	0.89	2.01	0.19	0.080	0.89	3.00	0.38
S3 - I.S1 (p)	0.081	0.79	14.9	1.42	0.078	0.86	14.9	1.87
S4 - I.S2 (p)	0.073	0.72	29.8	2.85	0.069	0.77	22.3	2.80
S5 - I.S2.P (p)	0.079	0.74	12.3	1.34	0.073	0.78	9.88	1.15
S6 - I.S2-.P (n)	0.091	0.86	9.92	1.08	0.083	0.88	0.24	0.03
S7 - I.P (n)	0.086	0.81	9.94	1.08	0.082	0.87	3.02	0.35
S8 - I.S2e.P (n)	0.066	0.62	12.4	1.35	0.064	0.68	9.93	1.16
Un-strengthened (average)								
11-14 cantilever	0.101	/	10.5	/	0.090	/	7.97	/
7-10 fixed-fixed	0.106	/	9.21	/	0.094	/	8.59	/

In cases where the strengthening measure changed the mechanism from shear to rocking, consequently minimum value of ξ obtained for the test at maximum displacements decreased significantly compared to un-strengthened walls.

5.2.7 Equivalent elastic strength evaluation

For tests of strengthened walls, equivalent elastic resistances considering μ as well as μ^* are provided in Table 3.33.

Preglednica 5.18: Ekvivalentne elastične nosilnosti utrjenih zidov in povprečni rezultati za neutrjene zidove, testiranih pri enakih robnih pogojih z dobljenim enakim porušnim mehanizmov, in njihovo razmerje

Table 5.18: Equivalent elastic resistances for tests on strengthened walls and average results for the same testing conditions and failure mechanism obtained of un-strengthened walls and their ratios

Test	$F_{id}(\mu)$ [kN]	Strengthened / Un-strengthened	$F_{id}(\mu^*)$ [kN]	Strengthened / Un-strengthened
Strengthened				
S1 - I (n)	274	0.547	255	0.578
S2 - I (p)	386	0.769	386	0.876
S3 - I.S1 (p)	504	1.005	504	1.144
S4 - I.S2 (p)	810	1.615	810	1.839
S5 - I.S2.P (p)	500	1.122	471	1.383
S6 - I.S2-.P (n)	449	1.006	417	1.222
S7 - I.P (n)	409	0.918	352	1.032
S8 - I.S2e.P (n)	760	1.704	760	2.229
Un-strengthened (average)				
11-14 cantilever	502	/	441	/
7-10 fixed-fixed	446	/	341	/

In order to increase the overall performance of the wall utmost, its failure mechanism ought to be changed. It is however difficult to assess, what type of measure should be applied in order to obtain the change. If NSM is applied, it should be conducted in every horizontal mortar joint. If the change of the failure mechanism is the best decision for a wall, implemented in a building (where it perhaps won't be able to reach its full displacement capacity), is questionable. From this point of view it is

better to increase its strength and energy dissipation; if not changing its stiffness is feasible, even better. NSM of (glass) cords presents such a solution, but only if they are indeed activated in a way to adopt the shear load surpass themselves and by so increase the resistance.

5.3 Analytical evaluation of cords' contribution to total lateral resistance

A comparison of the analytical predictions for the contribution of FRP strengthening V_f and the total shear resistance of the strengthened walls V_{Rd} with the experimental results of shear tests on NSM strengthened walls was done. Contributions of the FRP to lateral resistance were computed according to different code provisions (ACI 440.7R 2010, CNR-DT 200/2004 and CNR-DT 200 REV. 2013) and models, described in Section 2.5.4 – those which are suitable for the type of strengthening applied, i.e. NSM to horizontal joints (Triantafillou (1998), Triantafillou et al (2000), Nanni et al (2003), Tumilian (2001), Li (2005), Wang (2006)). Also total estimations of the shear resistance V_{Rd} of NSM strengthened walls, including resistance of URM walls, were analysed according to the models, which provide recommendations for its calculation. Results are provided in Table 5.19 and presented in Figure 5.34. From performed experimental tests the difference between the idealised shear resistances F_{id} of strengthened and un-strengthened walls was considered as the FRP contribution V_f and F_{id} obtained from tests of strengthened walls as V_{Rd}. In the Figure, first columns (labelled as "V_exp") for specific strengthening schemes, present the actual experimental results. It should be noted, that among all models, only Tumilian (2001) and Li (2005) models were developed specifically for NSM strengthening, while others for EB FRP strengthening.

Preglednica 5.19: Po različnih predpisih in modelih izračunani FRP prispevki k strižni nosilnosti V_f ter celotne strižne nosilnosti zidov V_{Rd} za različne sheme utrditev

Table 5.19: FRP contributions V_f and total lateral resistances V_{Rd}, calculated according to various code provisions and models for various strengthening schemes

	Testing scheme									
	S3 - I.S1 (p)		S4 - I.S2 (p)		S5 - I.S2.P (p)		S6 - I.S2-.P (n)		S8 - I.S2e.P (n)	
Analytical model	V_f [kN]	V_{Rd} [kN]	V_f [kN]	V_{Rd} [kN]	V_f [kN]	V_{Rd} [kN]	V_f [kN]	V_{Rd} [kN]	V_f *[kN]*	V_{Rd} *[kN]*
ACI 440.7R 2010	123.0	325.3	146.5	348.8	146.5	464.5	133.5	451.5	146.5	464.5
CNR-DT 200/2004	252.9	454.0	266.8	467.9	266.8	467.9	472.5	600.0	266.8	521.3
CNR-DT 200 REV. 2013	53.1	171.9	37.5	156.3	37.5	156.3	89.1	207.9	37.5	156.3
Triantafillou (1998)	77.4	226.5	148.4	297.4	148.4	297.4	51.3	200.3	148.4	297.4
Triantafillou et al (2000)	23.4	172.5	37.8	186.9	37.8	186.9	38.7	187.8	37.8	186.9
Nanni et al (2003)	153.8	/	307.6	/	307.6	/	167.3	/	307.6	/
Tumilian (2001)	5.9	/	11.8	/	11.8	/	13.0	/	220.7	/
Li* (2005)	75.4	220.4	150.9	295.9	150.9	295.9	82.8	227.8	816.8	961.8
Wang (2006)	328.5	477.2	522.7	671.4	522.7	671.4	373.0	521.7	522.7	671.4

* For the assessment, the actual inclination of cracks (instead of 45° inclination) was assumed for the FRP contribution calculation

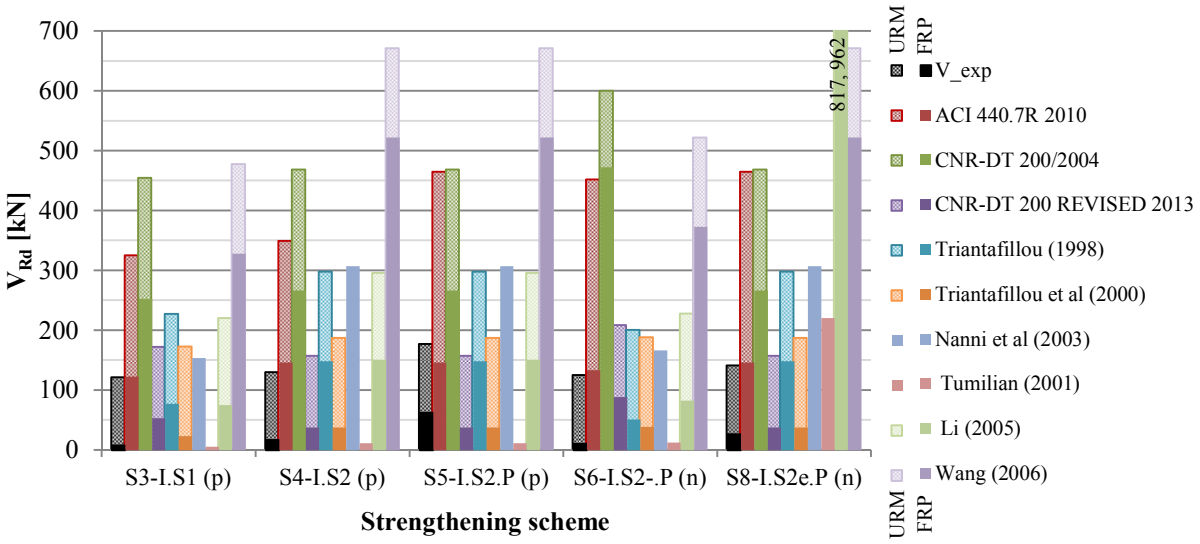

Figure 5.34: FRP and URM contributions to walls' total lateral resistance V_{Rd} obtained through tests and calculated according to various code provisions and models for various strengthening schemes
Slika 5.34: FRP prispevki in prispevki neutrjenih zidov k strižni nosilnosti zidov V_{Rd}, dobljeni iz testov in izračunani po različnih predpisih in modelih, za različne sheme utrditev

Comparison of the results showed, that no model for proper assessment of total shear resistance, which would provide roughly accurate results for various strengthening schemes applied exists. As the results of the URM (Un-Reinforced Masonry) walls' lateral resistance according to various code provisions and models were already discussed (Section 3.4.9), here mainly the results of FRP contribution calculation and the total resistance of strengthened walls will be analysed. Numerical comparison of results obtained through models and through experiments in terms of the FRP contribution V_f as well as the total lateral resistance V_{Rd} is provided in Table 5.20, whereas for easier comparison also presented in Figures 5.35 and 5.36.

Preglednica 5.20: Razmerja FRP prispevkov ter celotnih strižnih nosilnosti zidov, izračunanih po različnih predpisih in modelih, z dobljenimi iz testov za različne sheme utrditev

Table 5.20: Ratio of FRP contributions and total lateral resistances, calculated according to various code provisions and models, to the tests results for various strengthening schemes

	V_f (calculated) / V_f (experimental)					V_{Rd} (calculated) / V_{Rd} (experimental)				
Strengthening scheme / Analytical model	S3-I.S1 (p)	S4-I.S2 (p)	S5-I.S2.P (p)	S6-I.S2-.P (n)	S8-I.S2e.P (n)	S3-I.S1 (p)	S4-I.S2 (p)	S5-I.S2.P (p)	S6-I.S2-.P(n)	S8-I.S2e.P (n)
ACI 440.7R 2010	15.43	8.71	2.34	12.57	5.51	2.70	2.69	2.63	3.63	3.31
CNR-DT 200/2004	31.72	15.86	4.26	44.48	10.03	3.76	3.61	2.65	4.82	3.33
CNR-DT 200 REV. 2013	6.66	2.23	0.60	8.39	1.41	1.43	1.21	0.89	1.67	1.11
Triantafillou (1998)	9.71	8.82	2.37	4.83	5.58	1.88	2.30	1.69	1.61	2.12
Triantafillou et al (2000)	2.94	2.25	0.60	3.64	1.42	1.43	1.44	1.06	1.51	1.33
Nanni et al (2003)	19.29	18.28	4.91	15.75	11.56	/	/	/	/	/
Tumilian (2001)	0.74	0.70	0.19	1.22	8.29	/	/	/	/	/
Li (2005)	9.46	8.97	2.41	7.79	30.69	1.83	2.29	1.68	1.83	6.85
Wang (2006)	41.21	31.06	8.34	35.11	19.64	3.96	5.19	3.81	4.20	4.78

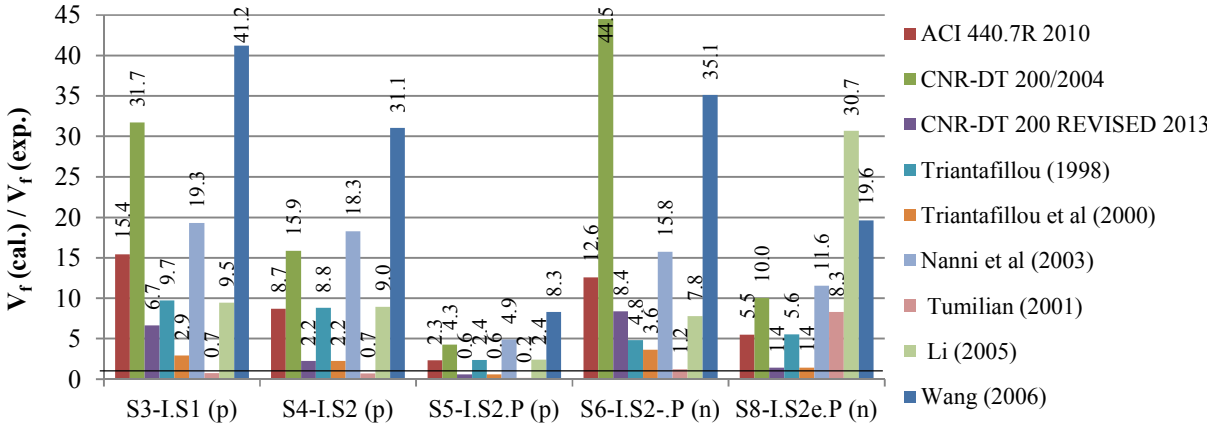

Figure 5.35: Ratio of FRP contributions to walls' lateral resistance, calculated according to various code provisions and models, to tests results for various strengthening schemes
Slika 5.35: Razmerja FRP prispevkov k strižni nosilnosti zidov, izračunanih po različnih predpisih in modelih, z dobljenimi idealiziranimi iz testov za različne sheme utrditev

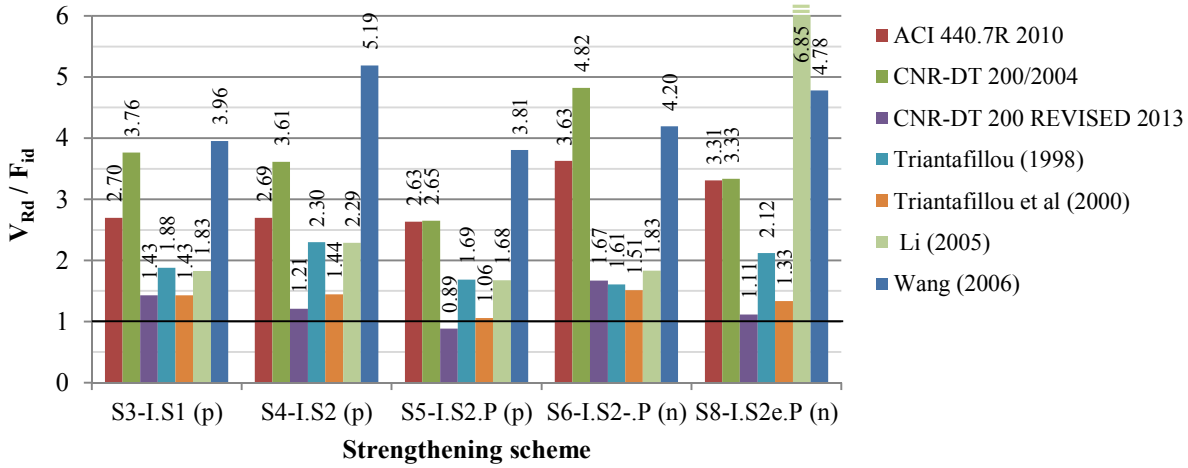

Figure 5.36: Ratio of the total wall lateral resistances, calculated according to various code provisions and models, to the idealized lateral resistances obtained in the tests for various strengthening schemes
Slika 5.36: Razmerja celotnih strižnih nosilnosti zidov, izračunanih po različnih predpisih in modelih, z dobljenimi idealiziranimi iz testov za različne sheme utrditev

It is clear, that some of the models highly overestimate V_{Rd}. ACI 440.7R 2010, CNR-DT 200/2004 and Wang (2006) provide by more than 200%, Wang by almost 400% higher results in all cases. Also models by Triantafillou (1998) and Li (2005) provide V_{Rd} results, which are at least 160% higher than experimental results; Triantafillou (1998) in two cases by more than 200% and Li in case of epoxy mortar strengthening even by 685%.

The main reason for the overestimations is for all the models overestimated value of V_f. For CNR-DT 200/2004 and Wang, values for V_f are extremely high. The estimations are the closest for testing scheme S5 (I.S2.P(p)), but for all the other cases the CNR produces more than 12- and Wang more than 19-times higher results. Also Nanni overestimates V_f by more than 11-times in all cases except for scheme S5. His model as already mentioned, however, does not provide the recommendation for URM contribution; therefore for this model V_{Rd} was not calculated.

ACI in all cases, except scheme S5, overestimates V_f by more than 5-times, but the results are not so excessive as according to CNR-DT 200/2004 and Wang, but more comparable to Triantafillou (1998) and Li, which still overestimate V_f significantly. For schemes, where NSM was applied to every joint, they produce similar results. Higher overestimations of V_{Rd} are in case of ACI in comparison to Triantafillou (1998) and Li, the result of higher overestimations of URM lateral resistance. Results according to revised CNR and revised Triantafillou (2000) models are significantly improved; for schemes where NSM was applied to every joint (schemes S4 - I.S2(p), S5 - I.S2.P(p), S8 - I.S2e.P(n)) the overestimation is at most 225%, but for scheme S5, the V_f is conservatively estimated (60% of the experimentally obtained).

Model by Tumilian is the only one, where V_f are for all tests, where cement-lime mortar was used for NSM, if not underestimated, overestimated only by 22%. All other models overestimate the FRP contribution in all schemes except for strengthening scheme S5.

One of the obvious conclusions therefore is, that all of the models presume, that the available additional strengthening contribution is indeed activated. Therefore some additional recommendations upon the applications of strengthening (details which influence the response) are still missing.

For the calculation of V_f, none of the models takes into account the different internal forces due to applied boundary conditions (S4 vs. S5), even though they according to our results influence the strengthening effect. Total lateral resistance is according to some models also different due to the model used for the calculation of the URM wall contribution.

The amount of reinforcement (comparing results for schemes S3 - I.S1(p) and S4 - I.S2(p)) is according to expectations reflected in all of the models, except in both versions of CNR; the V_f contribution is smaller, if the amount of reinforcement is reduced. In CNR higher V_f is the result due to expression for f_{fdd} calculation, where f_{fdd} is inversely proportional to reinforcement height t_f (see Eq. 2.61 in Section 2.5.4.1.1).

Comparison of the results with different reinforcement spacing distances s_f showed that both versions of CNR, Nanni and also Tumilian model, in case of higher amount of reinforcement, estimate higher V_f for larger spacing (in case of the same amount of reinforcement). Results according to all other models show either lower V_f or the same (in the case of higher amount of reinforcement).

5.4 Summary and discussion of the results

5.4.1 Grouting

Through failure mechanism and strength obtained by compression tests of the grouted and of the non-retrofitted damaged wall it was established, that also less strong and less stiff grout, such as in our case used cement-lime one, reconnects the leaves sufficiently. Grouted wall proved 40% higher compressive strength than the non-retrofitted one and 8% higher than the un-strengthened undamaged

wall. Stiffness characteristics E_M and G_M are more than two times higher than those of un-strengthened walls.

The same was observed at shear tests of grouted walls, where retrofitting restored the walls in a state, comparable to their initial state; strength capacity was for tests S1 and S2 by 11% higher (in terms of f_{Mt}) compared to un-strengthened walls, whereas displacement capacity had for prior retrofitting more damaged wall S2 decreased for 15% compared to un-strengthened wall, however still significantly higher than the values recommended for shear in the code requirements (EC8-3, FEMA).

It has to be noted, that despite restoring the walls strength and displacement capacity, the grouting does not restore the masonry energy dissipation capacity; especially if the wall is severely damaged. This can be confirmed through the results of test S2.

5.4.2 NSM of glass cords with transversal connections

NSM of glass cords and transversal tying of walls have proved to increase the compressive strength by 54.0% compared to the damaged wall and by 18.7% compared to un-damaged wall. Transversal ties allowed the crack/gap between the leaves to increase, but prevented the out-of-plane collapse, whereas the cords in the horizontal mortar joins limited the longitudinal horizontal cracks and deformations of the wall. Providing no anchoring of the cords proved as sufficient, since no failure of cord-wall bond at extents of the cords was obtained. In the central area of the walls surface cords were detached from the joints; mainly the bond between the mortar and the cord failed. The cords themselves were undamaged.

Shear tests on the walls with different variations of strengthening provided some interesting and important conclusions. Each strengthening detail can affect the behaviour under lateral load in a great deal, as can the conditions, to which the wall is subjected (pre-compression, boundary conditions).

Failure mechanism, which develops, influences the most on the strength and displacement capacity of the wall. Strengthening intervention has to be well thought out, as it can change the failure mechanism. This was proven for tests S4 and S8, where shear failure mechanism was changed into rocking due to increase of the shear strength of the wall. In test S4, the wall was strengthened by NSM of glass cords to every joint by cement-lime mortar, whereas in S8 by epoxy mortar. The later wall was tested with fixed-fixed boundary conditions, whereas test S4 with cantilever ones. With fixed-fixed boundary conditions, the NSM of the cords by cement-lime mortar (S5) did not improve the shear resistance of the wall enough to change its failure mechanism from shear to rocking.

However for S5, a different strengthening effect was obtained; through the developed shear mechanism the glass cords were activated in a way to sustain the excessive shear load themselves. Through this load transfer and with NSM and transversal cords limiting and controlling deformations, total shear resistance was significantly increased; by 53% higher if F_{max} and by 55% if F_{id} are compared. For such strengthening and shear mechanism developed also more than a 100% increase of the ultimate drift capacity was attained. Such a strengthening effect on the walls behaviour could be preferable to rocking mechanism, as it significantly increases the resistance but also the displacement

capacity without significantly changing the stiffness characteristics. Also energy dissipation is larger than for rocking mechanism.

If NSM is applied only to one side (S3) or in every second horizontal joint (S6), the strengthening proved neither sufficient to affect the failure mechanism nor to contribute to significant change of resistance. For both tests S3 and S4, F_{max} were increased for 6% compared to average values of un-strengthened walls. Nevertheless, the measure increases the displacement capacity d_{max}; an 80% increase of d_{max} was obtained for S3 and 64% increase for S6.

An explicit conclusion on how the transversal ties contribute to the behaviour cannot be made as in tests, where shear mechanism was obtained; the walls were always transversally connected, whereas their presence was not relevant in case when rocking mechanism was obtained. However, taking into account the compression test and the out-of-plane damage mechanism at shear tests, where they were present, we agree they are necessary.

If the intention of the NSM strengthening is to change the failure mechanism of the three-leaf stone masonry walls of better quality, NSM should be applied in every horizontal joint on both leaves. Anchorage of the cords at their ends proved to be unnecessary, as their bond to the wall in the central area failed; mainly at mortar-cord junction.

One of the main conclusions and contributions of this strengthening campaign is the confirmation, that instead of epoxy based binder also common cement-lime mortar can be used for NSM. As it is less stiff and more ductile compared to epoxy binders, it allowed the activation of the cords. This fact is even more important for historic masonry, which is commonly built with less stiff and more ductile mortar and for which earthquake resistance depends much more on the displacement capacity of the elements as current code provisions allow.

5.4.3 Analytical evaluation of the grouting effect

Regarding numerical evaluation of retrofitting and strengthening measures according to provisions or models; grouting is considered with amplified mechanical (strength and stiffness) characteristics. According to NTC08, the expected amplification of the strength (f_{Mc}, f_{Mt}) as well as stiffness (E_M, G_M) in case of grouting is 20%. The performed tests show, that this value is probably safe also if weaker grouts are used. The walls however have to be injectable; either containing enough voids or being (severely) damaged.

5.4.4 Analytical evaluation of NSM strengthening effect

All of the evaluated models for estimation of FRP strengthening contribution except of model by Nanni provide the estimation of the total resistance as the sum of the resistance of URM masonry V_m and the FRP strengthening contribution to resistance V_f.

CNR-DT 200/2004, Wang (2006) and Nanni (2003) highly overestimate V_{Rd}, due to excessively high estimation of FRP contributions V_f. Also ACI 440.7R 2010, Triantafillou (1998) and Li (2005)

significantly overestimate V_{Rd}; Triantafillou (1998) and Li (2005) through overestimation of V_f resistance, whereas ACI through too high V_m. Results according to revised CNR and Triantafillou (2000) models are significantly improved.

For all models except the Tumilian model (2001) the results for V_f are most accurate for test S5. One of the conclusions therefore is, that all of the models presume, that the available additional strengthening contribution is indeed activated.

For scheme S5, V_f is conservatively estimated by revised CNR and Triantafillou (2000) models (60% of the experimentally obtained one), whereas according to model by Tumilian (2001) V_f is highly underestimated. The Tumilian model underestimates or only slightly overestimates the FRP contribution also in all other cases where NSM was executed by cement-lime mortar. All other models are not so conservative; on the contrary, they highly overestimate V_f for most of the cases.

None of the models considers the different internal forces in dependence of the applied boundary conditions for the calculation of V_f, even though they influence the failure mechanism and consequently the seismic capacity (scheme S4 vs. scheme S5). Tumilian and Li models are the only two models that consider the NSM bond strength.

Following the results of the FRP contribution to the final shear resistance, it can be concluded that estimations according to CNR-DT 200 REV. 2013, Triantafillou (2000), ACI 440.7R 2010 and Tumilian (2001) are close if the shear mechanism and the cords are indeed activated. However for masonry, it is never absolutely certain, which mechanism will be activated. Therefore when numerically estimating the FRP strengthening contribution for masonry, it would be safer to increase the displacement capacity of the strengthened elements. This could be done by increasing either the ductility of the element, or the drift capacity. According to the presented test result, for all cases, where NSM was applied (regardless the strengthening scheme), a 64% (S6) or higher increase of the ultimate drift capacity was obtained. With consideration of test results of other authors (Section 2.5.2.3 and 2.5.3), a coefficient of conservative value of 1.5 could be applied to ultimate drift capacity in the case of FRP strengthening of masonry.

BLANK PAGE

»Ta stran je namenoma prazna.«

6 NUMERICAL APPLICATION OF THE EXPERIMENTAL RESULTS ON THE SEISMIC PERFORMANCE ASSESSMENT OF THE HISTORICAL CASE STUDY

In this Chapter the influence of the experimentally obtained displacement capacity of the walls on the buildings seismic performance is presented. Seismic performance assessment of an actual heritage building is evaluated with adopting various drift limits of the walls for its calculation. The description of the actual building, which served as a case study, together with its model and variation of parameters for the study are described, followed by the analysis of its seismic performance and comparison of results considering different drift limit assumptions. Finally, the seismic performance assessment of the building, where the performance levels were determined considering both structural as well as artistic asset damage, is presented.

6.1 Introduction

For the seismic assessment of an existing building, as already mentioned, large amounts of information regarding the construction details and the built-in materials are needed for accurate evaluation. Within the PERPETUATE project a sensitivity analysis was proposed as a step of the seismic assessment of the structure [1], in order to evaluate to what extent the identified specific parameter actually affects the seismic behaviour of the examined building. These parameters can be related to geometry, mechanical parameters or construction details. On the basis of the results, various confidence factors for specific parameters are determined and plan of in-situ investigation can be made. However it is not common in the analyses to change the assumption on the limit drift capacity of the walls mainly due to two reasons; firstly, the drifts are already prescribed in the codes (changing them would mean not to follow the codes) and secondly, in order to obtain the proper drifts values, one would have to either perform destructive tests or have available a large database (for all the various type and state of masonry).

The results of experimental tests show, that in many cases the drift limit is however significantly higher than assumed in the codes. Thus a comparison of the results of seismic performance assessment of an actual heritage building by considering the drift capacity prescribed in EC and the drift capacity obtained in the performed tests is presented.

The Vipolže mansion (Figure 6.1) was chosen as the case study, because it has similar type of masonry (Figure 6.1 top, middle) as tested; multi-leaf stone masonry with tooled stones in regular courses, leaves connected with transversally laid stones and not many voids. Another reason is that it on some walls possesses paintings (Figure 6.1 top, right), that enable us to explore the potential of the experimentally obtained plaster drift limits for the purpose of the performance assessment considering

artistic asset. Since the goal was to demonstrate the importance of assumptions on displacement capacity of the elements and to apply the through experimental tests obtained results to an actual structure, some characteristics of the building were assumed and some simplifications were made. The assessment of the earthquake performance should therefore serve only indicatively and not be considered as definitive.

6.2 Description of the analysed building with its brief historical information

The renaissance mansion Vipolže is situated in Vipolže, in western part of Slovenia (Goriška Brda). It was built in its current concept in the 16th century under the Thurn counts. The central part of the building is 41 m long and 16.6 m wide with walls positioned slightly in a shape of a parallelogram (Figure 6.2). It has 3-4 storeys; the basement floor is from two sides (longitudinally) under the ground level and does not extend under the entire building. Two lower towers at the north corners of the central part have dimensions 10 m x 11 m and are positioned a bit kite like.

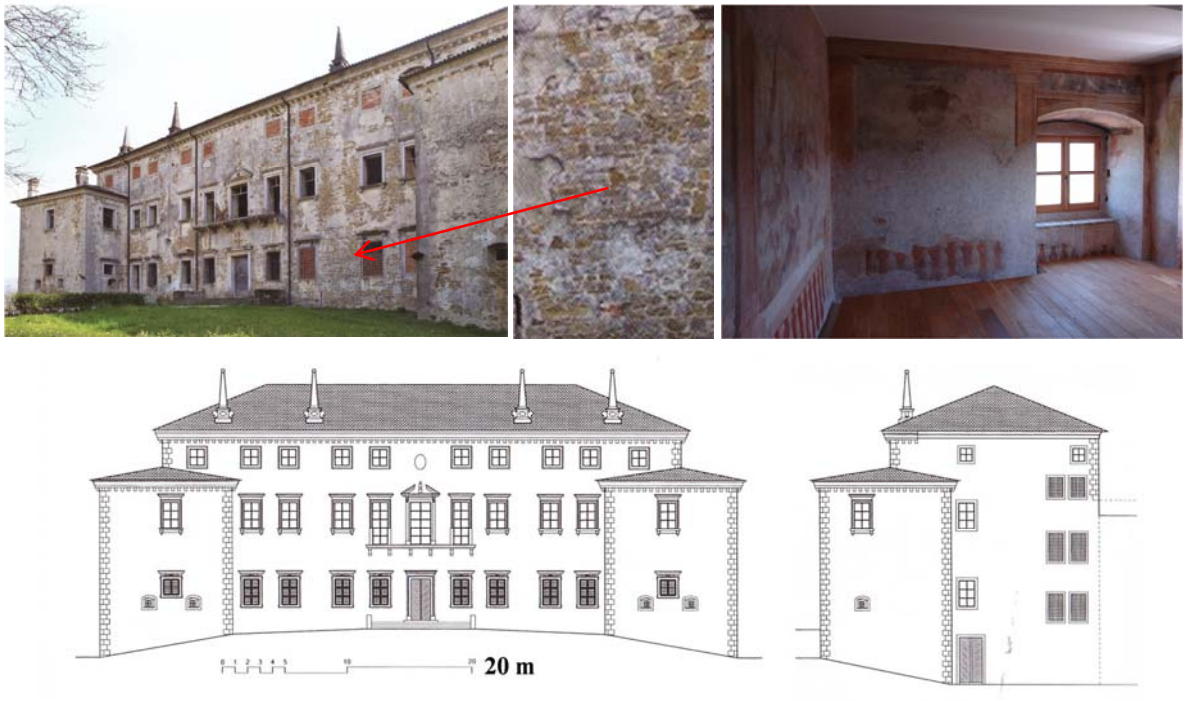

Figure 6.1: North façade of the mansion and masonry texture (top left and middle) [268], frescoes in the top floor (top right), drawings of the mansion's north (bottom left) and west (bottom right) façade [269]
Slika 6.1: Severna fasada vile in tekstura zidovine (zgoraj levo in na sredini) [268] ter freske v zgornjem nadstropju (zgoraj desno), izrisani severna (levo spodaj) in zahodna (spodaj desno) fasada [269]

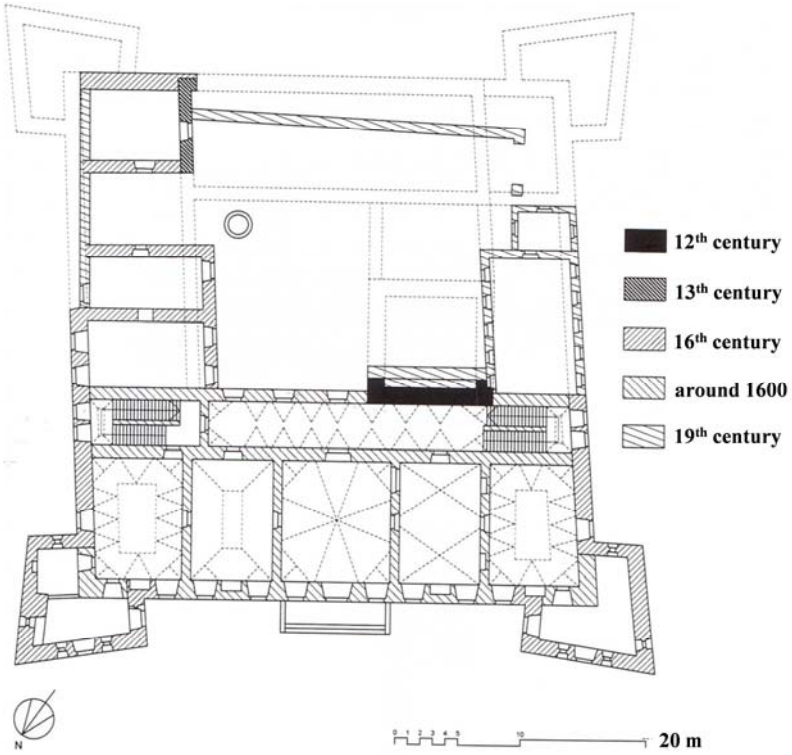

Figure 6.2: Ground floor plan of the mansion with marked construction phases [269]
Slika 6.2: Tloris pritličja vile z označenim stavbnim razvojem [269]

The vertical load bearing structure consists of masonry similar to our within the thesis tested masonry; roughly tooled stone multi-leaf masonry, with inner core substantially connected with mortar and through stones - not at all a typical construction for the region, time and type of the building. In the ground floor the walls are from 82 cm (the inner walls) to 140 cm thick; the thickness of the outer walls decreases in the upper floors. Horizontal structure above the basement level consists of barrel brick masonry vaults, above the ground floor rooms various type of vaults can be found; mixtures of ribbed, cap and squinch vaults, whereas in the hallway (south part of the central part of the building), the vault can be classified as barrel like (on squinches). Higher floor levels have wooden floor systems. Hipped roof is wooden, with the main wooden beams constructed as a modified "Pratt" trusses.

On the walls in the top floor hallway over the eastern staircases, an illusionistic painting in fresco technique is preserved (Figure 6.1 top right). It was probably created in the last third of the 17th century and it can be assumed from the motives, that it is the work of northern masters [269]. It is the only painting in the mansion.

The information of the building construction history is mainly summarised after Sapač [269]. The mansion as such was placed next to the old medieval castle, which was severely damaged in 1510 during the Habsburg and Venetian Republic war and additionally damaged under strong earthquake in East Friuli. The first mention of the early structure at the location dates to 12th century. The building gradually developed to its current state. The oldest part of the current building is the wall to the back yard and dates to third quarter of the 12th century. The existing medieval castle was gradually rebuilt after the mentioned earthquake in 1511 and prevailingly finished until the end of 16th century, when

also the main part of the building was built. To the beginning of the 17th century the castle was shaped into a late renaissance or Mannerist mansion. The damage of the mansion in siege and conquer by the Venice troops after 1616 is unknown (some repair measures were recognized). Only through the rehabilitation and renovation work in the last few years, it was established that the towers were built after that time, because the construction quality and materials of the masonry were very similar to the ones of the main part of the building. The damage of the building after the fire at the end of the 17th century is also unknown. In 1800 the mansion was hit by lightning and probably at that time all the roofs and wooden floors were destroyed. The roof over the main part of the building was rebuilt, but due to the large expenses, the building was from that time forward never fully restored and never again served for representative purposes. In 1806 also the south side part of the structure (medieval) was demolished, whereas the northern-east (medieval) side part was shortened and lowered. From that point onward, also the remaining parts of the building located on the position of the initial medieval castle were not considered as "the mansion" anymore. Slight damage on the roof after 1st World war caused further degradation of the wooden floors over the 1st floor and the top floor. After the war, the roof was repaired and the mansion served as a ware house, barn and a horse stable, which caused the removal of some transversal walls in the 1st floor. In 1948, the mansion was again burned and the cultural heritage protection service prevented its destruction by rebuilding the roof. Only some of the floors were afterward rebuilt for the necessities of the local community. In 1962 a part of the ground floor was rearranged to a restaurant. Already in the 60's, first plans for complete restoration were made, however it was not until recently when a comprehensive rehabilitation and renovation of the building was conducted. Construction phases reconstructed by Sapač are presented in Figure 6.2.

6.3 Seismic resistance analysis

The seismic resistance of the building was assessed according to EC provisions with nonlinear static ("pushover") analysis. Design ground acceleration a_g for 475 years return period for Vipolže (Goriška Brda) for soil type A is 0.20 g. Considering soil factor for ground type B (S = 1.2) and use coefficient γ_I = 1.0 for building of importance class II, the peak ground acceleration (PGA) amounts to 0.24 g. Also for the evaluation of damage limitation performance limit state, for the demand, the return period 95 years was adopted according to EC8-1 [270] and so was the recommendation for calculation of the corresponding a_g by considering importance factor γ_I (Eq. 2.78). Parameters T_{LR} and T_L refer to the reference return period (475 years) and the return period, for which a_g is evaluated.

$$\gamma_I = (T_{LR} / T_L)^{-1/3}, \qquad \textbf{6.1}$$

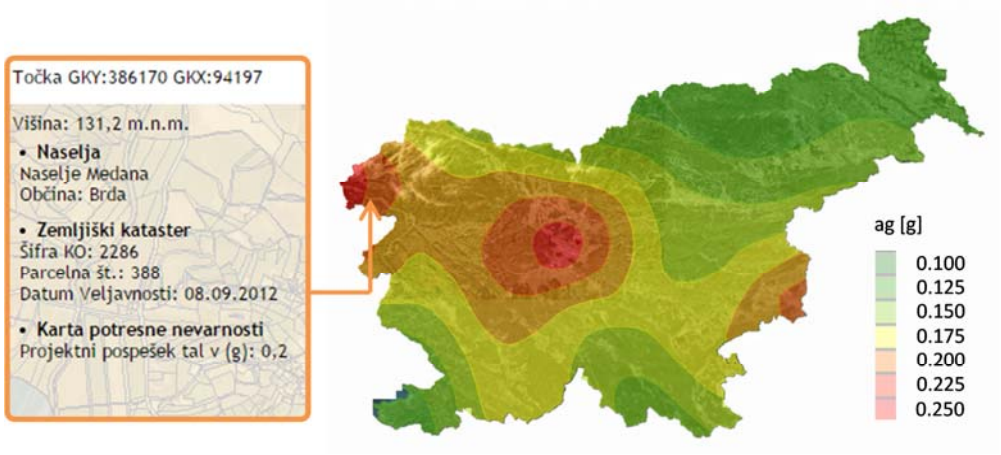

Figure 6.3: Seismic hazard map of Slovenia with reference ground accelerations for return period 475 years and the loacation of the building (http://gis.arso.gov.si/atlasokolja/profile.aspx?id=Atlas_Okolja_AXL@Arso&culture=sl-SI)
Slika 6.3: Karta potresne nevarnosti Slovenije z referenčnimi pospeški tal za povratno dobo 475 let ter lokacijo objekta (http://gis.arso.gov.si/atlasokolja/profile.aspx?id=Atlas_Okolja_AXL@Arso&culture=sl-SI)

For seismic capacity evaluation, variable loads were assigned according to EC1-1 [271] with regard to the current use; for 1st floor, where public events can be held 3.0 kN/m^2, whereas for the 2nd floor 2.0 kN/m^2.

According to EC8-3 confidence factors *CF*, which take into account the knowledge level of the building, have to be considered. As this case study is only illustrative, regardless the actual knowledge of the building, full knowledge level (KL3) was assumed (for such assumption very good knowledge upon structural system, details and materials is necessary). In the analysis, therefore, *CF* equal to 1.0, corresponding to KL3, was considered.

6.3.1 Model of the building in 3Muri and the adopted parameters

Pushover analysis was performed on an equivalent frame model [272] of the building, for which software 3Muri [273] was used. The model of the building was established on the basis of visual inspection of the building and the information obtained from existing documentation (Project for retrofitting and conservation of the Vipolže mansion façade [274]) and literature [269] considering the state prior the recent comprehensive renovation of the building. The knowledge of the building was limited and as already mentioned, some characteristics of the building were assumed and some simplifications for the modelling were made.

For the model, floors above the basement floor were considered; walls in the highest floor (attic) were not modelled but only considered as linear dead load on the walls below. Structural elements were considered as they were at some historical point prior the start of the retrofitting and restoration of the building; over 1st and 2nd floor wooden floors were modelled. In the model low-stiffness wooden floors with shear modulus G = 10 MPa were assumed. They were assumed to be sufficiently connected to the perimeter beams and planks (also assumed for the definition of the floors in 3Muri), which means that the floor's elastic stiffness was presumed in both directions. Over the ground floor storey, vaults of

various types were assumed, for which stiffness calculation was conducted with 3Muri assuming some of the possible built-in types of vaults (cap, barrel).

A 3D numerical model of the mansion is presented in Figure 6.4, whereas in Figure 6.5 the floor plan of walls in the model with front view of transversal and longitudinal walls labelled P1 and P4, where frescoes are located, is presented.

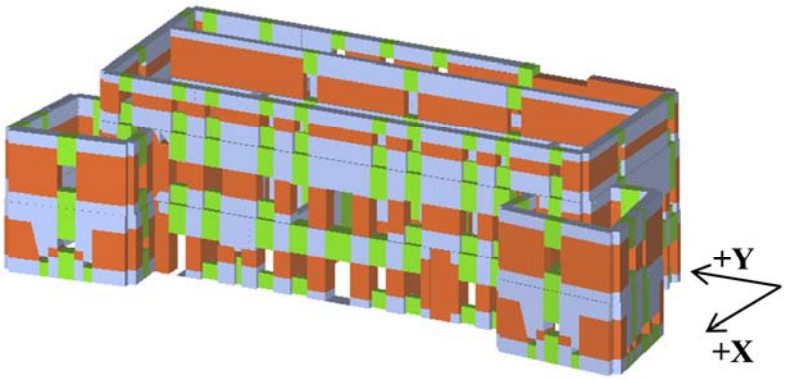

Figure 6.4: Equivalent frame 3D model of the structure in 3muri with coordinate axes for the analysis
Slika 6.4: 3D model z ekvivalentnimi okvirji stavbe v 3Muriju, z označenimi koordinatnimi osmi za analizo

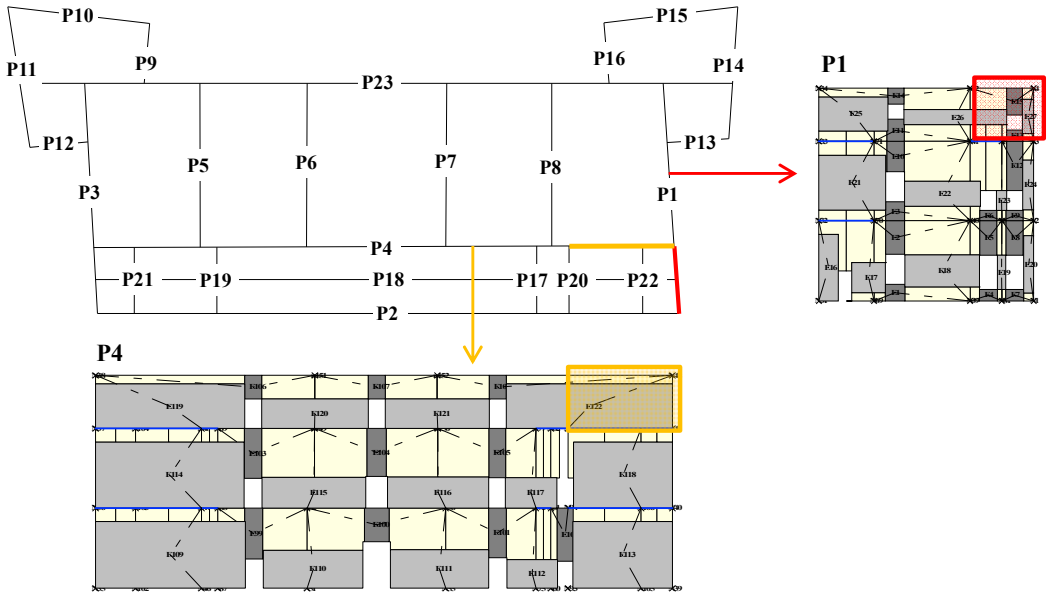

Figure 6.5: Position plan of the walls in the model with marked part of the walls P1 and P4, where frescoes are located
Slika 6.5: Postavitev zidov v tlorisu modela z označenima deloma zidov P1 in P4, kjer se nahajajo freske

The pushover analyses were performed for two perpendicular directions of the building; for north-south, transversal (X) and east-west, longitudinal (Y) direction. Both positive and negative directions for the applied displacement were analysed (adopted coordinate system can be seen in Figure 6.4). In the analysis 5% mass eccentricity was presumed and two possible lateral load patterns were considered; 1st modal mode and uniform lateral load pattern.

The initial basic calculation (model labelled A1: EC) was performed using the material characteristics attained through the tests, whereas displacement capacity of structural elements presumed according to EC8-3 in terms of maximum drifts of elements for shear and bending 0.4% and 0.8%. For the comparative parametrical study the ultimate drift capacities assumed were changed into capacities obtained from the performed tests; to minimum obtained drift values (labelled A2: tests_min) and to average obtained drifts (labelled A3: tests_ave). The material characteristics and the variations of drift limits assumed for the analyses are presented in Table 6.1.

Preglednica 6.1: Mehanske karakteristike zidovine in mejni zasuki elementov, upoštevani v potresni analizi

Table 6.1: Material characteristics of the masonry and the variation of drift capacity in the seismic analysis

Analysis	E_M [MPa]	G_M [MPa]	f_{Mc} [MPa]	f_{Mt} [MPa]	Θ_u (shear) [%]	Θ_u (bending) [%]
A1: EC					0.4	0.8
A2: tests_min	968	357	6.05	0.16	1.33	3.32
A3: tests_ave					1.53	3.99

The criterion for describing the shear response of walls was the Turnšek-Čačović model (use of f_{Mt}) whereas flexural response was considered according to the following equation (Eq. 6.2):

$$M_u = \frac{(\sigma_0 A_w) l_w}{2}\left(1 - \frac{\sigma_0}{0.85 f_{Mc}}\right), \qquad \textbf{6.2}$$

6.3.2 Results of the illustrative numerical analysis with varied drift capacity of walls

Pushover analysis results (shear base capacity F_b in dependence of top floor lateral displacements d, i.e. pushover curves), were idealized to bi-linear curves with criteria of equal input energy, where the ultimate displacement capacity was determined at the point of 20 % of maximum shear resistance decay and the stiffness equal to stiffness at a point, where shear base first reaches 70% of the maximum shear base resistance, according to Italian code provisions OPCM [245].

In Figure 6.6 the obtained pushover curves for the three analyses (A1, A2 and A3) for the most critical cases in transversal (X) and longitudinal (Y) directions (in terms of maximal design ground acceleration $a_{g,\,PLi}$ that the building can sustain for the evaluated performance level) are presented. The intensity measure chosen for the seismic assessment of the building was the design ground acceleration a_g, which is reported as an adequate parameter for this type of building according to Lagomarsino and Cattari [1]. On each pushover curve three damage levels (DLs) for the related performance levels (PLs) are marked (the damage level is assumed to coincide with the corresponding PL). PL2 was considered as the elastic displacement of the idealized pushover curve (corresponding to "DL" in the EC), while PL3 as the displacement equal to 0.75% d_u. For PL4 displacement d_u was considered and it was defined at a global scale at 20% reduction of the obtained maximum shear base capacity. For the definition of PL4, also a limitation according to OPCM of the obtained equivalent behaviour factor q^* to maximum value 3 was considered. PL3 and PL4 coincide with EC performance limit states "SD" and "NC".

The critical cases are not the same for all the evaluated PLs; for the analyses in case of A1: EC, the critical curves for PL2 are other than for PL3 and PL4 (for both directions). In Table 6.2 the critical cases for the analyses for both directions are presented in terms of results of the idealised curve and maximum $a_{g,PLi}$ corresponding to evaluated PLs; $a_{g,PLi}$ corresponding to specific displacements of the bi-linear curve were calculated according to N2 method [72].

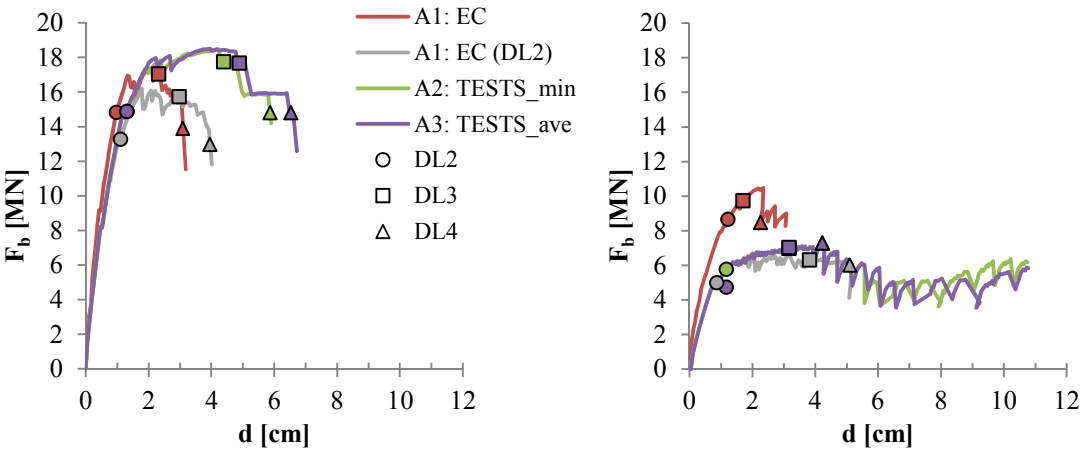

Figure 6.6: Pushover curves for X (left) and Y (right) direction of analyses with marked DLs
Slika 6.6: Potisne krivulje za X (levo) in Y (desno) smer analiz z označenimi stanji poškodovanosti (DL)

Preglednica 6.2: Karakteristične vrednosti idealiziranih potisnih krivulj za obe smeri obremenjevanja ter mejni pospeški tal $a_{g,PLi}$ za različna analizirana mejna stanja, izračunani ob različnih predpostavkah mejnih zasukov zidov

Table 6.2: Characteristic values of the idealized critical pushover curves for both directions and maximum ground accelerations $a_{g,PLi}$ for different PLs obtained with varying drift capacity of the walls

Analysis	Critical case		F_{id} [MN]	d_e [cm]	d_u [cm]	μ	T^* [s]	$a_{g,PL2}$ [g]	$a_{g,PL3}$ [g]	$a_{g,PL4}$ [g]
A1: EC	X	+ Mass	16.6	0.98	3.10	3.16	0.302	0.109	0.200	0.253
A1: EC (PL2)		+ First mode	15.4	1.11	3.96	3.56	0.334	0.101	0.215	0.275
A2: tests_min		+ First mode	17.4	1.31	5.87	4.47	0.342	0.115	0.299	0.344*
A3: tests_ave		+ First mode	17.4	1.31	6.53	4.97	0.342	0.115	0.329	0.345*
A1: EC	Y	+ First mode	10.2	1.23	2.26	1.85	0.423	0.071	0.094	0.122
A1: EC (PL2)		- First mode	6.2	0.86	5.10	5.90	0.457	0.043	0.177	0.128
A2: tests_min		- First mode	6.8	1.17	4.23	3.62	0.505	0.048	0.131	0.144*
A3: tests_ave		- First mode	6.8	1.17	4.23	3.62	0.505	0.048	0.131	0.144*

* values were determined considering limitation of q^*

The results show, that the obtained maximum $a_{g,PL4}$ for the ultimate limit state (PL4) obtained with model of the building considering various drift capacities of the walls do not satisfy the demand according to EC8-1. Transversal (Y) direction of the building proved to be more critical. The reason for this is significantly lower resistance obtained, though also the ductility is smaller (see idealized shear base F_{id} and μ in Table 6.20). In Figure 6.7 deformed shape of the building and in Figure 6.8 the damage and failure of structural elements at PL4 for two outer longitudinal walls (P2 and P23) for the critical X direction analysis (left), and for three transversal walls (P1, P3 and P11) for the critical Y direction (right) analysis results for A2: tests_min are presented. In X direction at first flexural damage on spandrels had developed on the building, which was followed by flexural as well as shear damage on the walls and piers. At PL4, piers at the lowest floor failed in shear. For the Y direction, flexural

damage was attained first on walls (due to lower vertical loads compared to longitudinal walls). It was later followed by damage of spandrels. Only few piers had shear damage.

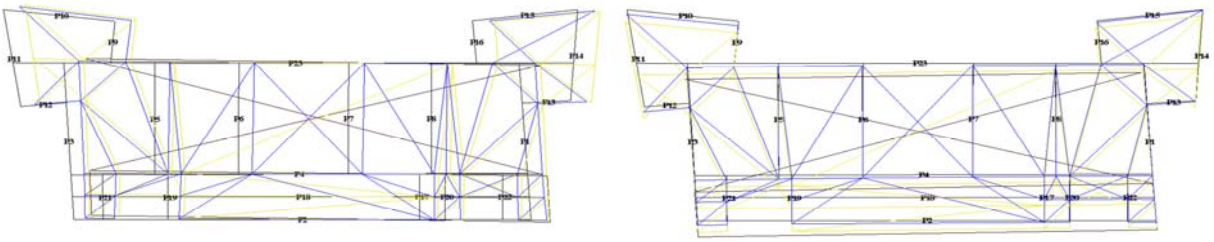

Figure 6.7: Deformed shape of the building at PL4 for critical case in X (left) and Y (right) direction (A2: tests_min)
Slika 6.7: Deformacijski obliki stavbe pri PL4 za kritični primer v X (levo) in Y (desno) smeri (A2: tests_min)

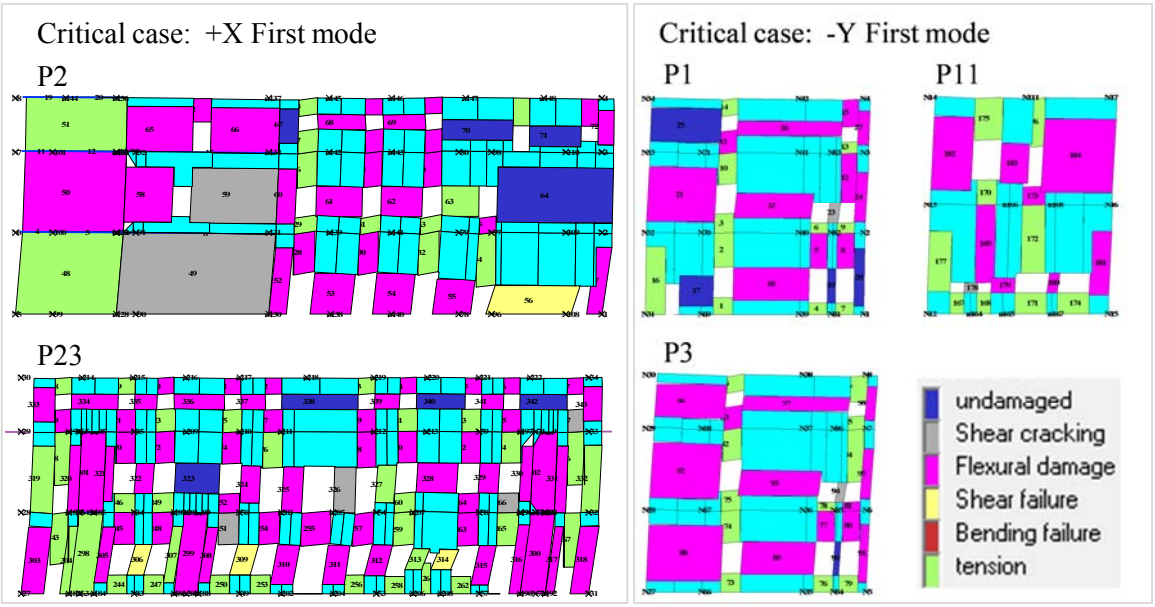

Figure 6.8: Damage and collapse of structural elements of the longitudinal walls P2 and P23 at PL4 of the critical analysis in X direction and of transversal walls P1, P3 and P11 in Y direction obtained for A2: tests_min
Slika 6.8: Poškodbe in porušitev konstrukcijskih elementov vzdolžnih zidov P2 in P23 pri PL4 za kritično analizo v X smeri in prečnih zidov P1, P3 in P11 v Y smeri za A2: tests_min

The influence of the assumed drift capacity is rather clear. If minimum drift capacity of the walls obtained in tests is considered (A2: tests_min) instead of drifts prescribed in EC (A1: EC), $a_{g,PL4}$ significantly increases; by 36.4% in X direction and by 18.1% in Y direction. Additional increase if the average values of drifts obtained in tests are considered (A3: tests_ave) compared to minimum values (A2: tests_min) is neglible. Figure 6.9 and

Figure 6.10 show the values of $a_{g,PLi}$ corresponding to each PL for X and Y direction of the analyses A1-A3, as well as the demand for the target performance levels PL2 and PL4 (0.117 g and 0.20 g). The critical results for PLs for both directions of loading in terms of maximum $a_{g,PLi}$ are presented also in Table 6.3. It is clear that the structure cannot sustain the seismic demand for PL4 nor for PL2.

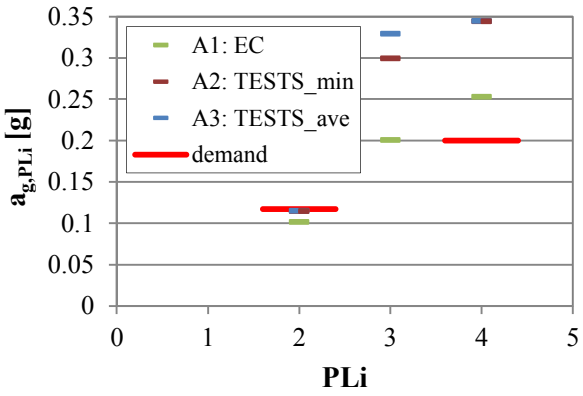

Figure 6.9: Maximum ground acceleration values for the performance levels, obtained with the three different drift capacity assumptions (A1-A3), for X direction of the analyses
Slika 6.9: Vrednosti mejnih pospeškov tal za analizirana mejna stanja, dobljene s tremi različnimi predpostavkami mejnih zasukov (A1-A3), za X smer analiz

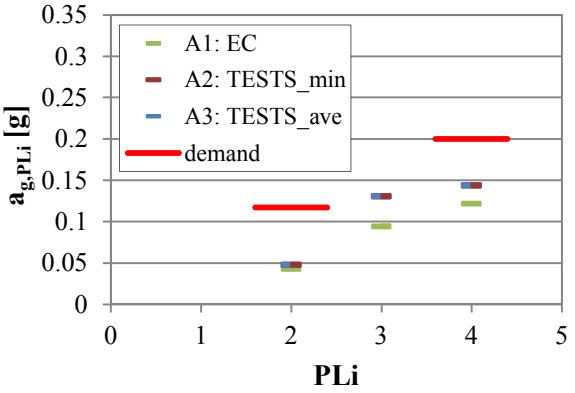

Figure 6.10: Maximum ground acceleration values for the performance levels, obtained with the three different drift capacity assumptions (A1-A3), for Y direction of the analyses
Slika 6.10: Vrednosti mejnih pospeškov tal za analizirana mejna stanja, dobljene s tremi različnimi predpostavkami mejnih zasukov (A1-A3), za Y smer analiz

Preglednica 6.3: Potresne povratne dobe za analizirana mejna stanja, dobljene s tremi različnimi predpostavkami mejnih zasukov (A1-A3), za X in Y smer analiz

Table 6.3: Maximum ground acceleration values for the performance levels, obtained with the three different drift capacity assumptions (A1-A3), for X and Y direction of the analyses

	$a_{g,PLi}$ [g] - X direction			$a_{g,PLi}$ [g] - Y direction		
	PL2	PL3	PL4	PL2	PL3	PL4
A1: EC	0.043	0.094	0.122	0.101	0.200	0.253
A2: tests_min	0.048	0.131	0.144	0.115	0.299	0.344
A3: tests_ave	0.048	0.131	0.144	0.115	0.329	0.345

6.3.3 Performance assessment considering artistic asset preservation

Besides performance assessment of the building considering criteria related to structural damage also a simple assessment of the building's performance considering artistic asset preservation was conducted for A2: tests_min. Frescos are, as already mentioned, located at the top floor, on walls P1 and P4; the

exact position is presented in Figure 6.5. For the analysis the evolution of the damage on the mentioned walls, more exact of the piers, containing the asset, was followed. All analysis cases were checked and not only the critical ones in terms of $a_{g,PLi}$ concerning structural damage. The occurrence and the type of damage mechanism, developed on the critical elements, with corresponding drifts were analysed. The analysed performance levels of artistic asset PL,AA were chosen on the basis of experimental results and the recommendations provided in Table 3.59; the occurrence of first cracks on the plaster (PL1,AA corresponding to "DL" of AA), significant but still repairable damage (PL2,AA corresponding to "SD" of AA) and collapse of the plaster (PL3,AA corresponding to "NC" of AA) were determined at points, where drifts of the critical structural elements achieved values in Table 3.59 defined for the developed mechanism and determined relatively to d_e of the evaluated element. In Figure 6.11 the damage pattern on walls for critical cases for X and Y direction is presented for states, where first pier damage on the part of the wall containing artistic asset was obtained. Since the frescoes are located in the top floor, in both X and Y direction of analysis, the critical element containing fresco was the end pier on the transversal wall (P1) and the damage was flexural. The large wall (P4) was damaged only in some X direction analyses at large displacements of the building.

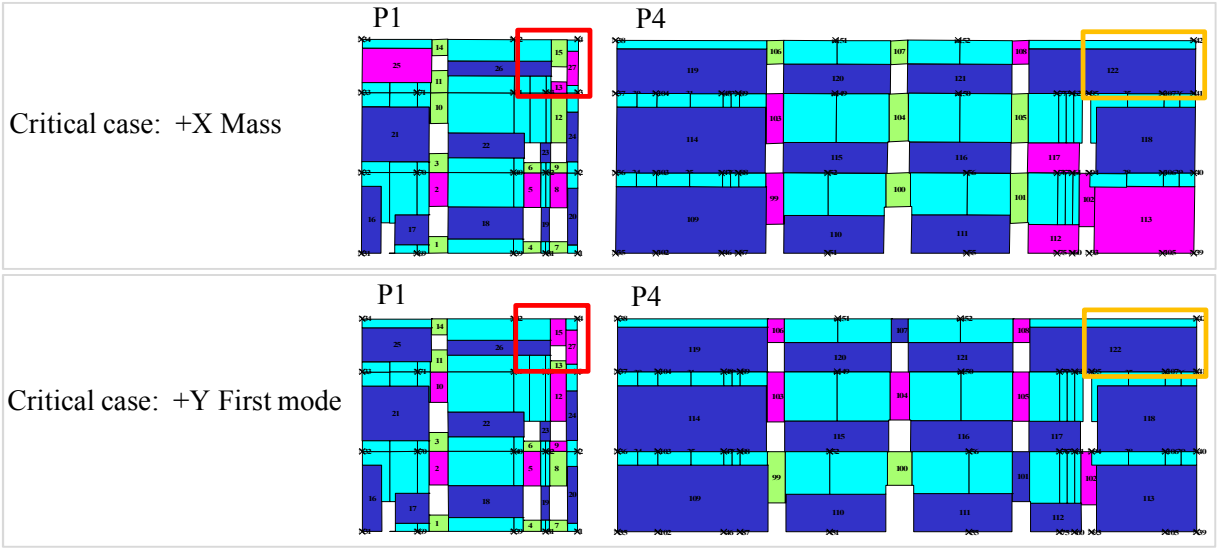

Figure 6.11: First damage of structural elements on parts of walls P1 and P4, where the frescoes are located, for the critical analysis in X direction (upper) and in Y direction (lower) obtained for A2: tests_min
Slika 6.11: Prve poškodbe konstrukcijskih elementov na delih zidov P2 in P23, kjer se nahajajo freske, za kritično analizo v X smeri (zgoraj) in v Y smeri (spodaj) za A2: tests_min

Because the obtained damage mechanism of the pier was flexural, the collapse of the plaster (PL3,AA) was not critical; PL3,AA is connected to collapse of the element and the latter was not achieved prior collapse of the building, PL3,AA coincided with PL4 (considering structural damage). In Figure 6.12 the obtained maximum $a_{g,PLi}$ for the performance limit states concerning artistic assets (PLi,AA) as well as structural damage and safety (PLi) are presented for drift assumptions A2: tests_min.

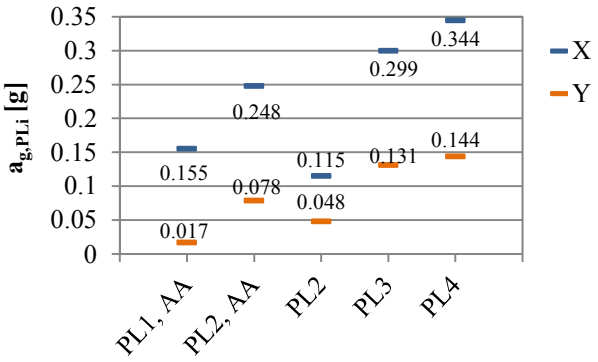

Figure 6.12: Maximum design ground accelerations which the building can sustain considering various performance levels with regard to structural damage (PLi) and to frescoes (PLi,AA) for A2: tests_min
Slika 6.12: Izačunani maksimalni projektni pospeški tal, ki jih stavba prenese, pri upoštevanju različnih mejnih stanj obnašanja glede na konstrukcijske poškodbe (PLi) ter na freske (PLi,AA) za A2: tests_min

Small damage on plaster (PL1,AA) occurs already at very low $a_{g,PL1,AA}$ in Y direction. More interesting is, that due to the location of the building and the consequent "late" occurrence and the type of damage (flexural), more severe damage of the plaster (PL2,AA) is attained relatively at a relatively rather high displacement of the building.

6.4 Summary and discussion of the results

A comparison of the influence of the assumed values for drift capacity of masonry elements on the seismic performance of an actual heritage building was made. Vipolže masion was chosen for the comparison because it is constructed from very similar type of masonry as tested within the thesis. A 3D equivalent model of the building in Tremuri was set up and seismic evaluation according to EC was performed. Pushover analyses were conducted. Material characteristic of the masonry were assumed following our test results, whereas drift capacity limits were varied. In one set of analyses drift limits according to EC codes were assumed and in the other two drift limits obtained in the test (minimum and average values). The increase of drift limit for shear mechanism from 0.4% to 1.33% and for flexural mechanism from 0.8% to 3.32% (from EC values to minimum drift limits obtained in the tests) resulted in 36.4% increase of maximum design ground acceleration $a_{g,PL4}$ that the building can sustain in X direction and in 18.1% increase in Y direction. This increase in both directions is even higher, if the limitation of the equivalent behaviour factor q^* to 3 (according to OPCM) would be omitted; by 53.3% in X direction, whereas by 43.4% in Y direction. If instead of minimum drift values obtained in the tests (A2: tests_min), average values were considered (A3: tests_ave), additional increase of performance was negligible (limitation of q^* considered).

Despite the fact, that drift limits were significantly increased, the increase of performance in terms of maximum $a_{g,PL4}$ is not to be disregarded. An important fact also is, that the ductility has increased for critical cases in X direction by 41.4% whereas in Y direction by 95.9% if minimum test drift limits were considered. It would be reasonable to further study the prospect of increasing the drift limits in the code provisions for types of masonry, which are more ductile (historical masonry).

The performance assessment of Vipolže mansion considering material characteristics and minimum obtained drift limits obtained in the tests, and other assumptions regarding the characteristics of the

structure, show that the building would not sustain a 475 years return period earthquake as demanded by the codes. For performance state "NC" (PL4), $a_{g,PL4}$ in X direction is 0.344 g whereas in Y direction only 0.144 g (475 years return period design a_g is 0.20 g). Also the demand for "DL" performance level (95 years return period design a_g 0.117 g) is not met for X direction (PL2). However the maximum $a_{g,PLi}$ for performance levels considering damage of frescoes are rather high compared to structural performance levels. Three performance states were evaluated: first cracks on the plaster (PL1,AA), significant but still repairable damage (PL2,AA) and collapse of the plaster (PL3,AA). It turned out, that the frescoes would not be destroyed (PL3,AA) prior the collapse of the building. The reason for this is that they are situated on the top floor, where the damage on the walls occurs relatively late and is of flexural type. Values of maximum $a_{g,PL1,AA}$ for first damage on the plaster (PL1,AA) are 0.155 g and 0.017 g for X and Y direction whereas for significant damage (PL2,AA) 0.248 g and 0.078 g, respectively.

BLANK PAGE

»Ta stran je namenoma prazna.«

7 CONCLUSIONS

7.1 Summary and final conclusions

The work performed within the thesis is composed of three experimental parts and one numerical part; 1.) the experimental tests and the analysis of results of (un-strengthened) three-leaf stone masonry walls, 2.) the evaluation of plaster performance during the tests, 3.) the strengthening of the damaged walls and their experimental testing with evaluation of strengthening efficiency and finally 4.) the numerical application of the results to an actual heritage building. A summary of the research work with the most important conclusions is presented in the following text.

Structural behaviour of (un-strengthened) three-leaf stone masonry walls was studied through results of experimental tests on 18 actual walls, built to represent the historical masonry. Altogether, 4 compression tests and 15 cyclic in-plane shear tests were conducted, accompanied with experimental tests on the masonry constituents. The influence of the masonry morphology (some walls had header stones transversally connected leaves, some not) and boundary conditions of testing on the seismic performance was studied by applying different pre-compression level ((5%), 7.5% and 15% f_{Mc}) and boundary conditions (cantilever vs. fixed-fixed).

The experimental results were analysed and various aspects of behaviour were compared for tests with varied boundary conditions and morphology. Quantitative results of mechanical characteristics (such as strength or stiffness parameters) and other parameters (deformation capacity, energy dissipation parameters, etc.) obtained for the tests were not only compared to each other, but also to values provided in the code provisions and literature or provided by analytically obtained results.

The compression tests proved similar behaviour of walls with connected and unconnected leaves. Leaf separation occurred earlier in the tests of unconnected walls, however it occurred as intensively also for the connected walls once the through stones cracked. There was no significant difference in maximum leaf separation values obtained regardless of the morphology type.

The tests provided average compressive strength f_{Mc} 6.05 MPa considering both morphologies of the walls; f_{Mc} of the wall without and the wall with through stones were 6.10 MPa and 6.00 MPa, respectively. The obtained f_{Mc} correspond well to the values provided in the Italian code provisions NTC08 for dressed rectangular stone (minimal and maximal values 6 MPa and 8 MPa). Elastic and shear moduli E_M and G_M obtained from the tests were however lower than expected; average for both morphology 968 MPa and 357 MPa (compared to minimal values 2400 MPa and 780 MPa in NTC08). The results for G_M highly depend on the position of measuring devices for horizontal deformations, considered for the evaluation of the Poisson's ratio and may therefore be unreliable.

Cyclic in-plane shear tests provided deep insight into various features of seismic behaviour of this type of masonry. With varying testing conditions indeed various failure mechanisms of the walls were obtained. Lower pre-compression ((5), 7.5% f_{Mc}) and cantilever boundary conditions provoked rocking, at which the joint between the first two rows of stones opened while the rest of the specimen

was rocking. Restraining the rotations at the bottom enabled diagonal shear mechanism to partially develop (this failure mechanism was referred to as mixed), whereas higher pre-compression level (15% f_{Mc}) induced diagonal shear behaviour with some toe crushing and formation of vertical columns in case of both boundary conditions of restraint.

Leaf separation occurred in the walls with the occurrence of shear mechanism; it significantly progressed only in the post-peak phase of the test though. It was more apparent with cantilever boundary conditions (regardless of the presence of header stones), as opposed to fixed-fixed boundary conditions, where through stones, if present, limited the separation of leaves.

The strength and displacement capacity of the walls depended mainly on the type of the formed mechanism. The developed mechanism was crucial also for other characteristic parameters of obtained hysteretic response of walls, i.e. stiffness and shear modulus, energy dissipation, strength and stiffness degradation. With rocking mechanism the lowest shear resistance but the highest displacement capacity were obtained (average F_{max} and d_{max} equal to 57.5 kN and 59.8 mm). Mixed failure obtained through fixed boundary conditions increased the resistance but decreased the displacement capacity (105.7 kN and 28.2 mm). Shear resistance was the highest for shear failure, but since the developed mechanism was diagonal (and not sliding), the displacement capacity additionally decreased (120.8 kN and 23.0 mm). The tensile strength of the walls f_{Mt}, calculated from bi-linearly idealized shear resistances F_{id} of the walls, obtained for tests, where diagonal shear failure prevailed (tests 7-14) was 0.163 MPa.

The effective stiffness K_{ef} depended considerably on the idealization criteria and as the hysteretic responses differed due to various failure mechanisms obtained, the G_M modulus calculated from K_{ef} and E_M (from compression tests) produced in some cases unrealistic results; for higher pre-compression level and cantilever boundary conditions average G_M was 2094 MPa, while for fixed-fixed boundary conditions 129.9 MPa. More stable was the estimation of G_M directly from the tests (as the ratio of average shear stress to average shear strain); however for the state with no or very slight damage (i.e. at displacement d = 1.5 mm) obtained values for shear moduli were significantly lower (average G_M for tests with shear mechanism 123.7 MPa compared to average G_M obtained from compressive tests 357 MPa).

Average drifts corresponding to ultimate displacement capacity were 3.99%, 1.88% (average value without test 6) and 1.53% for walls with rocking, mixed and shear mechanism, respectively. These obtained drift capacities are significantly higher than those recommended in the code provisions, which are in dependence of the boundary conditions applied for walls of the tested geometry according to EC8-3 (NC state) 1.60% for fixed-fixed and 0.80% for cantilever boundary conditions, whereas according to FEMA (CP state) 0.60% and 0.30%; for shear, the ultimate drift capacity is according to EC8-3 0.53%.

According to test results it was established, that in the case of historic masonry, for which the main characteristic compared to modern is a more ductile mortar, the drift limitations provided in the codes can significantly underestimate their actual drift capacity.

Drifts corresponding also to some other performance levels were evaluated as well; average drifts, where first shear cracks were visually recognised, for tests at which mixed and shear mechanism

developed were 0.55% and 0.22%, respectively. Maximum resistance was reached at average drift of 3.94% for rocking mechanism, 1.71% for mixed and 1.10% for shear mechanism. Ductility coefficients (ratio between ultimate and elastic displacement of the idealized curve) for rocking, mixed and shear mechanism were 6.23, 2.23 and 4.19. Ductility was for tests with mixed mechanism compared to tests with shear mechanism lower due to two-times larger elastic displacements attained for tests with mixed mechanism. Nevertheless, higher ductility was exhibited by all failure mechanisms, also for shear, which is commonly considered as brittle failure.

That the failure in case of shear mechanism was not brittle is also confirmed by the fact, that the walls exhibited a considerable post-peak displacement capacity also for shear mechanism; in average ultimate displacements were 40% higher than displacements where the maximum resistance was obtained (d_{max} = 1.40 d_{Fmax}) and the average post-peak resistance drop was 19.8%. The resistance drop at shear mechanism however differed significantly with respect to boundary conditions applied; in average 35.2% drop was obtained for fixed-fixed boundary conditions whereas 13.2% for cantilever. The mixed failure led to a more brittle failure (in average d_{max} = 1.10 d_{Fmax}). Since at flexural mechanism toe crushing did not occur, the rocking mechanism exhibited very ductile behaviour with very slight strength decrease (in average 2.8%).

Considering energy dissipation, (diagonal) shear failure proved to be more favourable compared to rocking behaviour. Various parameters for evaluating the energy dissipation were analysed; input and dissipated energy, their ratios at characteristic amplitude displacement cycles as well as (their cumulative values) on the global scale. Also other parameters regarding energy dissipation were assessed (input energy of the bi-linear idealized response, normalized cumulative energy dissipation according to Shing [112], modified (modification proposed within the thesis) normalized cumulative energy dissipation and equivalent viscous damping coefficient). The results confirm that the energy dissipation is closely related to prevailing damage pattern and that it is compared to input energy the highest for lower displacements, where initial damage on the specimens occurs, and after the peak resistance, where the major damage occurs. The analysis of equivalent viscous damping coefficients ξ provided average value at d_{max} for flexural response 0.035, for mixed 0.047 and for shear 0.131.

For tests also equivalent elastic resistance ($F_{id}\cdot\mu$) was analysed; 342, 258 and 474 kN were obtained for rocking, mixed and shear failure mechanism, respectively. This also indicates that the shear mechanism is not necessarily the worst possible mechanism.

Evaluation of analytical models for estimation of compressive strength as well as for prediction of maximum shear resistance of (three-leaf) masonry in dependence from failure mechanism was conducted.

Analytical models for the evaluation of three-leaf masonry compressive strength by Egermann [39], Binda et al [40] and Tassios and Chronopoulos [41,42] underestimate f_{Mc} for the type of the tested walls. They were probably not designed for multi-leaf masonry where the out-of-plane behaviour is not problematic (because of sufficient connection between the leaves). On the other hand, the model provided in EC6 highly overestimates f_{Mc} (ratio 3.3 to experimentally obtained f_{Mc}), and is therefore highly inappropriate for historic masonry. Good estimation was provided by model of Tassios and Chronopoulos [41,42] for single-leaf masonry (ratio 1.08 to experimentally obtained f_{Mc}). All the models are sensitive to input parameters, therefore one of the conclusions is, that the calculated results

should always be critically assessed and compared to reference values in the code provisions or to test results of masonry of the same or similar type.

Because the out-of-plane mechanism was not as critical as predicted, the analytical models for evaluation of shear resistance considering models for the actual developed mechanisms estimated the shear resistance sufficiently; for rocking, V_{Rd} (calculated shear resistance) was in average equal to 0.96 F_{id} (idealized shear resistance obtained for the tests) whereas for diagonal shear mechanism diagonal shear mechanism to 1.02 F_{id}. The problem however was that another strength criterion (i.e. diagonal joint failure mechanism model) provided more critical results for all cases. The criterion obviously underestimates the resistance of walls with weak, ductile mortars in case the mortar thickness in the joints is not excessively thick (as in test 6). All the results were calculated considering the entire cross section; for walls of the tested type of masonry (external leaves thickness more than 75% of t_w, inner core sufficiently filled and connected, not too many voids present) the evaluation of the resistance should be made considering the entire cross section and not only the external leaves.

It can also be mentioned, that for test 6, significantly lower results were obtained (f_{Mt} 0.087 MPa, 1.00% ultimate drift) which was the consequence of thicker horizontal mortar joints compared to other walls. As most models in the codes do not consider bed-joint thickness parameter as influential (except perhaps as dry or thin bed-joints), this influence should be investigated and incorporated in models or taken into account through some other additional recommendations.

Performance of artistic assets (plasters), was studied through careful monitoring of the plaster behaviour during compression and shear tests. Besides visual inspection also photogrammetry was used for measuring plaster displacements during loading. The results provided identification of various damage states of plasters with regard to structural behaviour of the wall and the first quantitative values of drift limits for seismic performance assessment of structures with artistic assets (such as frescos) in the world.

When rocking mechanism of the wall developed, the plaster did not collapse during the tests, despite being significantly detached at sides. Some tiny cracks on the plaster occurred though. For the walls with shear mechanism, shear cracks formed at earlier displacements and sometimes prevented the plaster's detachment over the entire height or the widening of the gap between the wall and the plaster at side. In some tests, the plaster collapsed subsequently with increasing displacements, whereas in most cases the collapse of the entire plaster was immediate.

Through damage evaluation, 4 characteristic damage states of the plaster were identified and they were labelled from DS A1 – DS A4. Damage state of artistic asset DS A1 refers to first detachment of the plaster (at plaster edge), DS A2 to first visible crack on the plaster ($d_{cr,AA}$), DS A3 to state, where the plaster is either largely detached either characterized by a significant (thick or long) crack (still repairable) and DS A4 to collapse of the plaster ($d_{max,AA}$).

For artistic asset damage prevention, the most important limit state is DS A2, where the first crack was obtained. Compared to drifts of the wall, where the first structural crack was obtained θ_{cr}, DS A2 was in all cases, where shear mechanism was obtained, significantly lower than θ_{cr}; in average slightly over 1/3 of θ_{cr} (minimum value 15% of θ_{cr}). For mixed mechanism the ratio is higher; between 27-100%; in two cases the drifts at which the cracks appeared on the wall and on the plaster coincide.

Drifts corresponding to artistic asset loss prevention (collapse, DS A4) were for shear mechanism of the wall in average 0.79% and for mixed mechanism 1.13%. As mentioned, with rocking mechanism the plasters did not collapse. These values are higher that the ultimate limit drift of walls provided in the codes.

For the assessment of performance of existing building considering artistic asset, recommendations upon the determination of characteristic performance limit states of plasters on the wall is presented. They should be determined relative to elastic displacements of the evaluated walls. Quantitative drift values, where certain damage states occur, in dependence of mechanism, relative to elastic displacements, are provided.

Retrofitting and strengthening of the damaged walls was conducted and the efficiency of the selected measures evaluated through analysis of **experimental test results of strengthened walls**. For strengthening, a new "system" appropriate for historic masonry was developed; more compatible materials were used and the intervention minimally interferes with the masonry aesthetic appearance. Near Surface Mounting (NSM) of flexible glass cords into horizontal mortar joints by cement-lime mortar was applied, some walls were also transversally connected by the same glass cords. But since most of the walls were severely damaged, they were first retrofitted by line-crack grouting. Extensive investigations were conducted for the proper choice of materials in the case of retrofitting (grout choice) as well as NSM strengthening. Various combinations of strengthening variations were applied in order to test the influence of some specific details. Following the testing procedures and conditions of un-strengthened walls, two retrofitted/strengthened walls and one damaged (after shear testing) wall were tested in compression, while eight strengthened walls were tested in shear. The results were analysed and compared to analytical predictions of FRP strengthening. contributions.

Grouting was done with a commercial cement-lime grout, commonly used in Slovenia for grouting of heritage buildings, because up to that time, own developed grout mixtures without cement still possessed some deficiencies (mostly related to shrinkage).

For **NSM of glass cords**, 6 mm glass cord was impregnated with epoxy resin, dipped into quartz sand (to improve the cord-mortar bond) and still flexible installed into emptied (depth of the grove approximately 5 cm) horizontal joints. For installation in all cases except one, a common (with respect to cement : lime : aggregate ratio) cement-lime mortar was used. The cords were not anchored. The joints were repointed by the same mortar as used for the installation of the cords. For some walls, the cords were installed into every joint on both sides of the wall, whereas also variations, where NSM was applied into every second joint or just on one side (face) of the wall were made. For one specimen the NSM cords were bonded using epoxy mortar.

Transversal connection of the walls was in some combinations provided by glass cords on 5 positions on the wall. Holes were drilled through horizontal mortar joints and impregnated cords, dipped into sand, were inserted into them. Anchoring of the string was provided by the sand "cork", which had formed when pulling the string through the hole, or in one case by spreading and fixing the fibres of the cords on the wall.

Results of experimental tests and comparison of efficiency of different measures provided some important conclusions. For **grouting,** it was established that also less strong and stiff grout (such as in

our case used cement-lime one) reconnects the walls sufficiently. Grouted (along the cracks) wall proved 40% higher compressive strength than the non-retrofitted one and 8% higher than the un-strengthened undamaged wall. Stiffness characteristics E_M and G_M were more than two times higher than those of un-strengthened walls. Tensile strength obtained in shear tests increased for tests S1 (prior retrofitting less damaged wall) and S2 (prior retrofitting more damaged wall) by 11%, whereas displacement capacity for test S2 decreased by 15% compared to un-strengthened wall. The displacement capacity was however still significantly higher than the values recommended for shear mechanism in the code. **NSM of glass cords and transversal tying of the walls** proved to increase the compressive strength by 54.0% compared to the damaged wall and by 18.7% compared to un-damaged wall if the NSM was applied to every joint on both sides. Transversal ties allowed the crack/gap between the leaves to increase, but prevented the out-of-plane collapse, whereas the cords in the horizontal mortar joins limited the longitudinal horizontal cracks and deformations of the wall.

From results of shear tests on the walls with different variations of strengthening, it was established, that each strengthening detail can affect the behaviour under lateral load in a great deal. Also the conditions, to which the wall is subjected to (pre-compression, boundary conditions) influence the result.

Some strengthening interventions have changed the failure mechanism under certain conditions of testing. This happened for tests S4 (NSM of glass cords to every joint by cement-lime mortar) and S8 (NSM of glass cords to every joint by epoxy mortar), where shear failure mechanism has changed to rocking due to increase of the shear strength of the wall. Test S8 was tested under fixed-fixed boundary conditions, whereas test S4 under cantilever ones. For fixed-fixed boundary conditions, the NSM of the cords by cement-lime mortar for test S5 has not strengthened the wall well enough to change its failure mechanism from shear to rocking.

However for S5, the glass cords were, through the developed shear mechanism, activated in a way that additional shear load was transferred to them. With NSM and transversal cords limiting and controlling the in- and out-of-plane deformations, maximum shear resistance was increased by 53%. For such strengthening and shear mechanism developed, also more than a 100% increase of the ultimate drift capacity was attained. Such a strengthening effect on the walls' behaviour is from some points of view preferable to rocking mechanism, as it significantly increases the resistance but also the displacement capacity without significantly changing the stiffness characteristics. Also energy dissipation is significantly larger.

If NSM was applied only to one side of the wall (S3) or in every second horizontal joint (S6), the strengthening proved not sufficient neither in a way to affect the failure mechanism nor to contribute to significant change of resistance. For both tests S3 and S4, F_{max} were increased by 6% compared to average values of un-strengthened walls. Nevertheless, the applied strengthening measures increased the displacement capacity d_{max}; an 80% increase of d_{max} was obtained for S3 and 64% increase for S6.

From the results it can be derived that if it would be desired to change the failure mechanism (of the three-leaf stone masonry walls of better quality), NSM should be applied in every horizontal joint on both leaves.

Through the tests it was confirmed, that the anchorage of the cords at their ends is unnecessary, if their bond-strength is sufficient. In the tests the connection of the cord to the wall in the central part of the wall failed; mainly at mortar-cord junction. The cords did not break.

One of the main conclusions and contributions of this strengthening campaign is the confirmation, that instead of epoxy based binder also common cement-lime mortar can be used for NSM. As it is less stiff and more ductile compared to epoxy binders, it allowed the activation of the cords. This fact is even more important for historic masonry, which is commonly built with less stiff and more ductile mortar and for which earthquake resistance depends on the displacement capacity of the structural elements.

Analytical evaluation of NSM strengthening effect was calculated according to various models and code provisions, which provide the estimation of the total resistance as the sum of the resistance of URM masonry and the FRP strengthening contribution to resistance. Models in CNR-DT 200/2004 [209], Wang [217] and Nanni et al [214] highly overestimate V_{Rd}, due to excessively high estimation of FRP contributions. Also ACI 440.7R 2010 [220], Triantafillou et al [212] and Li [174] significantly overestimate the total resistance; Triantafillou et al and Li through overestimation of FRP contribution, whereas ACI through too high URM masonry resistance. Results according to revised CNR (CNR-DT 200 REV. 2013) [221] and Triantafillou [213,220] models are significantly improved.

For all models except the Tumilian model, the results are the most accurate for test S5. One of the obvious conclusions therefore is, that all of the models presume, that the additional strengthening shear resistance contribution of the FRP is enabled by the shear load transfer to the reinforcements.

Following the experimental results of the FRP contribution to the final shear resistance, it can be concluded that estimations according to revised CNR and Triantafillou models, ACI 440.7R 2010 and Tumilian (2001) are sufficiently accurate if the shear mechanism and the cords are indeed activated. However as shown, it cannot certainly be predicted, what type of mechanism will actually be activated. Therefore when numerically estimating the FRP strengthening contribution, it would be safer to increase the displacement capacity of the strengthened elements rather than to assign additional strength contribution. This could be done by increasing either the ductility or the drift capacity of the element.

Numerical analysis of the influence of the obtained results on the seismic performance assessment of an actual historic structure was conducted. The Vipolže mansion was chosen for the seismic performance assessment because it is built from similar type of masonry as tested in our experimental programme. The intention was not to accurately assess the seismic performance of the building but rather to demonstrate the influence of the experimentally obtained limit drift capacity for the walls on the seismic performance. Therefore for the assessment, the assumptions on the drifts were varied from those prescribed in EC8 to those obtained in the tests; minimum and average values obtained in the tests were assumed. Pushover analysis was performed on a 3D equivalent frame model of the building. Critical results in terms of maximum ground acceleration a_g proved a 36.4% increase of $a_{g,PL4}$ (performance level for displacement d_u - "Near Collapse") for X and 18.1% for Y direction considering the limitation of equivalent behaviour factor q^*, in case of changing the drift limits from EC (0.4% for shear and 0.8% for bending) to drifts obtained in tests (1.33% and 3.32% for shear and bending). Without the limitation for q^* though, the increase was 53.3% in X direction, whereas 43.4%

in Y direction. The ductility of the response (obtained pushover curves) increased for critical cases in X direction by 41.4% while in Y direction by 95.9%.

Despite the fact, that drift limits were significantly increased, the increase of performance in terms of maximum $a_{g,PLi}$ is considerable. One of the conclusions is, that it would be reasonable to study the prospect of increasing the drift limits in the codes for types of masonry which are more ductile, such as historical masonry.

7.2 Original scientific contributions

The presented research work contributes to the improved knowledge of behaviour under compressive and shear loads of not only multi-leaf stone masonry walls, but of historical masonry walls in general as well.

Original contributions of the research work can be summarised as follows:

- 4 compression tests and 15 cyclic shear tests of three-leaf stone masonry walls of two different morphology; systematic variation of pre-compression level and boundary conditions at shear tests;
- conclusions upon the out-of-plane mechanism behaviour under in-plane shear loading for the tested type of masonry;
- evaluation of influence of presence of transversal connections (stone units) in the masonry on the behaviour of three-leaf masonry walls of the tested type;
- performance oriented analysis of the shear test results with emphasis on the evaluation of non-linear lateral force – lateral displacement relationship, i.e. displacement/drift capacity in correspondence with damage obtained, resistance and drifts in characteristic points of hysteretic response, strength degradation, etc.;
- application of plaster on the walls and analysis of the compression and shear tests results with regard to plaster behaviour;
- first (in the world) quantitative drift values of masonry walls related to plaster damage states (absolute drifts and drifts relative to elastic drifts of walls, for the case of rocking and diagonal shear mechanisms of walls), needed for performance assessment of historical structures with respect to artistic asset conservation performance levels;
- design of new strengthening "system" for damaged walls – NSM of glass cords into (horizontal) mortar joints by cement-lime mortar (significant contribution is the use of cement-lime mortar as the binder);
- 2 compression and 8 cyclic shear tests of strengthened walls;
- systematic variations of strengthening measure's details (NSM in every or in every second joint, on one or both sides of the wall) and study of their influence through shear tests.

7.3 Suggestions for future research

Despite the fact, that many experimental studies of masonry walls exist, due to the composite, non-homogenous nature of masonry, a wide range of parameters influence its behaviour. Systematic experimental testing of masonry, representative of various types of historic single- and especially multi-leaf masonry is still needed. Even though most of the tests are preformed and evaluated in a similar manner, some differences in idealisation of results which influence the further comparison were recognized. Therefore a standardization of both testing procedures and evaluation of the obtained results is needed.

Concerning plaster performance assessment, these first steps of research should probably be followed again by systematic experimental testing of walls with plasters, characterized by various stiffness and mechanical characteristics of walls as well as plasters. The performance of plasters through analysis of damage in the case of other damage and failure mechanisms of walls should be studied as well.

The composed strengthening intervention with NSM of glass cords in every horizontal joint by means of cement-lime mortar should be tested under different boundary conditions in order to fully understand, when the certain mechanisms of the response are triggered. It could also be tested, whether the intervention is indeed appropriate also for masonry with less regular courses. Research for adopting different type of adhesive (with no cement addition) for mounting the cords could be conducted. Also the potential alkali-silica reaction should be investigated and prevented. Finally, for the actual use of the intervention, the procedure of application could be optimised (in sense of time consumption (cost) as well as aesthetic outcome).

As seen in the thesis, the (seismic) performance assessment of cultural heritage masonry buildings is complex and wide knowledge is needed in order to define the problems whereas also to solve them. In Slovenia, an efficient and feasible integration of different aspects of professional expertises with interdisciplinary work of various experts should be developed and established.

BLANK PAGE

»Ta stran je namenoma prazna.«

8 RAZŠIRJENI POVZETEK V SLOVENSKEM JEZIKU

V sledečem poglavju je povzeto delo, ki je bilo narejeno v sklopu doktorske disertacije. V uvodu je podan opis problematike, ki je bil motivacija za samo delo, ter glavni cilji. Obravnavana problematika kot tudi podpoglavja se lahko v grobem razdelijo na tri sklope;

- preiskave in analiza rezultatov tlačnih in strižnih (neutrjenih) troslojnih kamnitih zidov ter ometov na zidovih,
- raziskave za določitev sanacijskih in utrditvenih ukrepov, njihova aplikacija na zidove ter preiskave utrjenih zidov,
- numerična študija vpliva dobljenih rezultatov z njihovo aplikacijo na obstoječem objektu kulturne dediščine.

Pregled literature področij ni povzet. V strnjenih zaključkih so podani najpomembnejši rezultati, ugotovitve ter komentarji za razmislek o nadaljnjih študijah.

8.1 Uvod

Motivacija z opisom problematike

Zidani kamniti objekti predstavljajo precejšen del obstoječega fonda starejših objektov, od katerih so mnogi pomembna arhitekturna kulturna dediščina, velikega pomena pa so lahko tudi njihovi kulturno-umetniški sestavni elementi, kot so poslikani ometi, mozaiki, štukature, kipi, itd. (Slika 8.1).

Slika 8.1: Freska mrtvaškega plesa (levo, http://commons.wikimedia.org/wiki/File:Danse_macabre_hrastovlje.JPG) v cerkvi svete Trojice, Hrastovlje, Slovenija (desno, http://www.publishwall.si/lelj/photos/photo/23345)
Figure 8.1: Danse Macabre fresco (left, http://commons.wikimedia.org/wiki/File:Danse_macabre_hrastovlje.JPG) in the Holy Trinity Church in Hrastovlje, Slovenia (right, http://www.publishwall.si/lelj/photos/photo/23345)

Precej zidov historičnih objektov je po prerezu sestavljenih iz več slojev. Pri nas so od romanike naprej značilni troslojni zidovi, kjer sta zunanja sloja sestavljena iz kamna, notranja plast pa je

zapolnjena z apneno malto, pomešano z ostanki kamenja, ter ima več ali manj votlin. Takšni zidovi se razlikujejo glede na uporabljene materiale, način zlaganja ter obliko in obdelavo kamna (tekstura oziroma lice zidu), so pa različni tudi po sestavi po prerezu (morfologija zidu). V nekaterih zidovih kamniti bloki, ki potekajo čez celoten prerez, povezujejo zunanja dva sloja. Obnašanje zidov je že pri enoslojnih zidovih težko napovedati, saj nanj vpliva veliko parametrov, pri večslojnih pa je to še toliko težje. Pri različnih obremenitvah se različni sloji lahko različno obnašajo, prihaja do razslojevanja, itd. V zadnjih desetletjih smo se srečali s hudimi poškodbami, celo s porušitvami, zaradi tlačne preobremenjenosti večslojnih slopov in zidov. Po porušitvi katedrale v Notu leta 1996 v Italiji [275] in hudih poškodbah cerkva Santissimo Crocefisso in Santissimo Annunziata [4] je prišlo do spoznanja, da je konstrukcijsko obnašanje večplastne zidovine precej neraziskano.

Za analizo konstrukcijskega obnašanja stavb tako pri statičnih obremenitvah, kot tudi pri dinamičnih obremenitvah (potres) ter za analizo učinkovitosti sanacije oziroma različnih utrditvenih ukrepov, je ključnega pomena ocena mehanskih karakteristik posameznih zidov ter napoved njihovega obnašanja pri različnih obremenitvah. Napovedovanje obnašanja je zaradi velikega števila (pogosto neznanih) vplivnih parametrov zahtevna naloga. Na obnašanje konstrukcijskih elementov zelo vplivajo tudi parametri, ki niso neposredno vezani na lastnosti materiala, temveč so odvisni od same konstrukcije in obtežb. Na obnašanje tako vplivajo vpetost konstrukcijskih elementov, njihova geometrija ter pripadajoče vertikalne obremenitve. Ker se tudi na področju zaščite kulturne dediščine vedno bolj uveljavlja način ocene stanja oziroma projektiranja konstrukcij s kontroliranim obnašanjem (eng. »Performance based assessment« oziroma »design«), nas pri analizi odziva konstrukcijskih elementov zanima nelinearni odziv sila – pomik, poleg mejnih sil in mejnih pomikov tudi drugi karakteristični pomiki (oziroma sile); pomiki, kjer pride do prvih razpok, pomiki, kjer so dosežene maksimalne sile, ter pomiki, kjer pride do porušitve (ali drugih mejnih stanj) določenih elementov.

Mehanske karakteristike zidovine za analizo odpornosti objekta lahko določimo bodisi po priporočilih iz standardov, bodisi po podatkih iz literature ali z natančnejšimi preiskavami karakterističnih zidov obravnavane konstrukcije. Pri prvih dveh možnostih se za predpostavljene vrednosti v večini primerov odločimo na podlagi vidne strani zidovine. Glede na teksturo zidu, ocenjeno vrsto in kvaliteto gradnikov (kamna oziroma opeke ter veziva) predpostavimo vrednosti tlačne, natezne in strižne trdnosti ter vrednosti elastičnega in strižnega modula. Pri tem navadno ne vemo, kakšna je dejanska sestava zidu po prerezu (morfologija). Pri večslojnih zidovih lahko najdemo različne debeline slojev, za rimski opus sta npr. značilni tanjši zunanji plasti, notranjost pa sestavlja debela plast »rimskega betona«, ki je sestavljen iz apna, pucolanske zemlje, peska ter zdrobljene opeke. Pri zidovih v romaniki je debelina vmesne plasti odvisna od debeline zidu, so pa zunanje plasti glede na notranje relativno debelejše kot v antiki. Tudi zunanji plasti nista vedno enako debeli. Glede na debelino in karakteristike tako srednje plasti, kot zunanjih, se spreminja prevzem obremenitev in celotno obnašanje zidov pri različnih obremenitvah. Karakterizacija zidov zgolj z vidne strani tako prinaša negotovosti, ki se jim brez bolj natančnih preiskav ne moremo izogniti. Z izvedbo bolj ali manj invazivnih (neporušne, delno-porušne ter porušne metode) in obsežnih preiskav dobimo natančnejše podatke za analizo [276], vendar pa te preiskave žal velikokrat niso mogoče, saj so (pre)drage, mnogokrat pa porušnih in delno-porušnih metod ne dopuščajo kulturno-varstveni pogoji.

Tudi napovedovanje obnašanja zidov v smislu ne samo mejnih sil, temveč tudi togosti in duktilnosti oziroma mejnih pomikov in rotacij, je kompleksen problem. Za analizo pri potresni obtežbi nas

zanima predvsem obnašanje zidov pri dvoosnih obremenitvah, in sicer pri kombiniranih vertikalnih in horizontalnih strižnih obremenitvah. Pri zidovih lahko pri strižnih obremenitvah v ravnini zaradi njihove nehomogenosti pride do različnih porušitev [277], in sicer do diagonalne porušitve preko spojnic ali preko kamna oziroma opeke, do zdrsa, do upogibne oziroma tlačne porušitve ter njihovih kombinacij. Pri večslojnih zidovih pa lahko pride tudi do večjih pomikov in porušitve izven ravnine zidu.

Za različne tipe porušitev obstajajo različni analitični modeli za napoved strižnih nosilnosti, ki pa v točno določenih primerih zidov dajejo boljše oziroma slabše napovedi. V posameznih modelih niso vedno upoštevani vsi parametri, ki so karakteristični za obravnavani zid in znatno vplivajo na njegovo obnašanje. Obstaja le nekaj modelov, ki pri izračunu mejnih strižnih sil upoštevajo večplastnost zidov. Mejne sile, izračunane po različnih modelih, med seboj precej odstopajo; nekatere ocene so nerealne, saj pri dejanski porušitvi zidu ne pride do predpostavljenega mehanizma. Tudi standardi za izračun mejnih nosilnosti pri strigu uporabljajo različne modele, ki jih bolj ali manj modificirajo, poleg tega pa jim dodajo tudi svoje varnostne faktorje, s čimer je raztros vseh izračunanih rezultatov še večji.

Ker pa so mejne sile in pomiki posameznega zidu med bistvenimi predpostavkami pri potresni analizi, se temu primerno tudi rezultati potresne odpornosti posameznega objekta z upoštevanjem različnih standardov in modelov za izračun strižne odpornosti med seboj precej razlikujejo.

V praksi ponavadi oceni stanja objekta sledi načrtovanje in izvedba sanacijskih oziroma utrditvenih ukrepov. Na voljo je velika množica različnih ukrepov, katerih primernost je odvisna od konstrukcijskih elementov in poškodb, za katere se uporabljajo, ter tudi od materialov. Za objekte kulturne dediščine naj bi ukrepi zadostili konservatorskim pogojem, med katerimi so med drugim reverzibilnost in minimizacija ukrepov ter uporaba materialov, kompatibilnih z originalnimi. Mnogi sodobni ukrepi, kot npr. uporaba cementnih injekcijskih mas, vgradnja togih betonskih plošč, itd., so se izkazali za neprimerne. Potreba po razvoju in raziskavah ukrepov, primernih za objekte kulturne dediščine, je velika.

Predvideni in tekom dela spremenjeni cilji doktorske naloge

V sklopu doktorske naloge smo se osredotočili na obnašanje večslojnih zidov, in sicer s poudarkom na strižnem obremenjevanju v ravnini, saj je na tem področju poznavanje pomanjkljivo. Narejenih je občutno manjše število eksperimentalnih preiskav kot za enoslojne zidove. V literaturi je kar nekaj eksperimentalnih testov, katerih študija so mehanske karakteristike in obnašanje pri tlačnih obremenitvah, medtem ko strižnih testov v ravnini večslojnih zidovih skorajda ni. Cilj je torej eksperimentalno pokazati, kakšno je obnašanje izbranega tipa troslojnih kamnitih zidov pri strižnih obremenitvah v ravnini zidov, razbrati vpliv posameznih parametrov na obnašanje ter podati vrednosti mejnih sil in predvsem pomikov za upoštevanje takšnih zidov pri analizi konstrukcije. Preiskave obnašanja večslojnih zidov pri izven-ravninskem strižnem obremenjevanju niso bile predvidene. Prav tako se študije nanašajo na obnašanje zidov in ne drugih konstrukcijskih elementov, kot so npr. preklade.

Kot del doktorske naloge ter hkrati evropskega projekta PREPETUATE (PERformance - based aPproach to Earthquake proTection of cUlturAl heriTage in European and Mediterranean countries,

www.perpetuate.eu) je bil cilj izvesti obsežne preiskave troslojnih kamnitih zidov za določanje njihovega obnašanja v primeru potresov.

Ker se, kot že rečeno, na takšnih kamnitih zidovih, ki jih najdemo v reprezentativnih stavbah, kot so gradovi, dvorci, cerkve ipd., na ometih pogosto nahajajo pomembne poslikave, smo pri preiskavah želeli analizirati tudi mejna stanja in poškodbe na ometih, zato so bili zidovi ometani.

Namen je bil tudi preizkusiti obstoječe utrditvene ukrepe ter potrditi njihovo učinkovitost, vendar pa je iskanje primernih rešitev, ki bi zadoščale zahtevam po uporabi primernih materialov ter ohranitve vidne teksture zidov, privedlo do obširnih (tudi eksperimentalnih) raziskav primernih materialov ter končno do razvoja in aplikacije še neuporabljenega načina utrjevanja zidov z namestitvijo steklenih vrvic v horizontalne maltne spojnice z duktilno apneno - cementno malto. S tlačnimi in strižnimi testi različno utrjenih zidov smo želeli prispevali k večjemu razumevanju delovanja ojačitev na tovrstnih zidovih ter preveriti učinkovitost lastne zasnove utrditve.

Načrtovana je bila tudi parametrična numerična študija obnašanja troslojnih zidov, katerih model bi bil verificiran z rezultati testov neutrjenih zidov. Ker pa predvideni odziv ni bil dobljen (izven-ravninske deformacije in razslojevanje zidov ni bilo problematično), študija ni bila več smiselna. Namesto le-te so bili eksperimentalni rezultati testov aplicirani na dejanski objekt kulturne dediščine, zgrajen s podobno zidovino. Narejena je bila numerična analiza potresnega obnašanja glede na različna mejna stanja, pri čemer je bil namen prikazati vpliv predpostavljenih mejnih zasukov zidov na potresno obnašanje ter določiti mejna stanja obnašanja tudi glede na poškodovanost fresk v objektu. S slednjim je bila prikazana uporabnost rezultatov testov zidov z ometi.

V prošnji za odobritev teme doktorske disertacije smo podali naslednje hipoteze, ki naj bi jih preverili s sklopu doktorske naloge:

- Večplastnost zidov pomembno vpliva na obnašanje pri potresnih obremenitvah; pri strižnih obremenitvah v ravnini večplastnih zidov pride tudi do izven-ravninskega porušnega mehanizma.
- Boljše povezave med zunanjima in notranjim slojem znatno izboljšajo celoten odziv; pozneje pride do porušitve izven ravnine.
- Tlačno obnašanje večslojnih zidov se da zadovoljivo napovedati z obstoječimi modeli [278].
- Z ustreznimi sanacijskimi ukrepi je možno zagotoviti povezavo med sloji poškodovanih zidov ter izboljšati odziv pri strižnem obremenjevanju.
- Modeli za oceno strižne nosilnosti zidov obstoječih stavb po EC8-3 [279] ter v praksi uporabljenih starih JUS standardih [128] ne podajajo zanesljivih ocen nosilnosti za večslojne zidove.
- Lahko naredimo analitični model, s katerim zadovoljivo napovemo maksimalne nosilnosti večplastnih zidov pri strižnih obremenitvah v ravnini.

8.2 Eksperimentalne preiskave troslojnih kamnitih zidov

Preiskave neutrjenih troslojnih kamnitih zidov so obsegale tlačne in strižne teste ter spremljajoče preiskave konstituentov zidov (malte in kamna). Testi so bili namenjeni študiju obnašanja kamnitih

večslojnih zidov; poleg maksimalnih nosilnosti predvsem tudi analizi mejnih pomikov ter poškodovanosti v karakterističnih stanjih. S preiskavami je bil sistematično analiziran vpliv morfologije zidov (sestave po prerezu), različnih nivojev tlačnih obremenitev ter robnih pogojev vpetja pri strižnih obremenitvah.

8.2.1 Značilnosti in izgradnja preizkušancev ter rezultati preizkusov konstituentov

Preizkušanci so bili zgrajeni v laboratoriju za namene preiskav obnašanja starih kamnitih večslojnih zidov, zato so jih zgradili izučeni zidarski mojstri, ki so za gradnjo uporabili apneno malto. Zunanji sloji zidov so bili zgrajeni iz pol obdelanih kamnitih blokov iz apnenca, položenih v ravne pravilne vrste. Polovica zidov je bila zgrajena z vezniško zvezo, to je s povezovalnimi kamnitimi bloki, ki so po prerezu v vsaki drugi vrsti potekali čez vse tri sloje. Druga polovica zidov pa je bila zgrajena s smerniško zvezo, to je brez povezovalnih blokov. Debelina maltnih spojnic je bila v povprečju 1.5 cm. Notranji sloj je bil zapolnjen z ostanki kamna od zidave ter apneno malto, vseboval pa je tudi manjši delež votlin. Zaradi hitrejšega vezanja je bilo malti glede na volumen apna dodano 20% vulkanskega pepela, za reprezentativnost historičnih malt pa je bil cilj ne preseči 2 MPa tlačne trdnosti malte. Zidovi so bili z ene strani ometani; nanesena sta bila dva sloja ometa, in sicer grobi ter fini omet. Debelina ometa je glede na različne oblike kamna znašala med 1 in 3.5 cm. Tekom gradnje zidov se je merilo konsistenco malte ter pripravljalo standardne maltne vzorce za preiskave mehanskih karakteristik strjene malte ter valjaste vzorce malte in odpadnega kamenja za simulacijo in preiskave jedra zidu.

Slika 8.2: Gradnja zidov z vezniško zvezo (levo), s smerniško zvezo (na sredini) ter preizkušanci pred izdelavo zgornjih betonskih blokov (desno)
Figure 8.2: Construction of the wall with (left) and without (middle) header stones and the wall specimens prior construction of the upper concrete slab (right)

Vse skupaj je bilo zgrajenih 16 zidov dimenzij 100/40/150 cm ter dva zidka 100/40/100 cm. Zidovi so bili zgoraj in spodaj vpeti v armirano-betonske bloke, ki so služili za vpetje v preizkuševalne naprave, za raznos obtežbe ter za transport po laboratoriju. Konstrukcija in detajli preizkušancev so opisani v [43].

Malta za zidanje je imela po 120 dneh povprečno tlačno trdnost f_{mc} 1.88 MPa s koeficientom variacije (k.v.) 5.9% ter povprečno upogibno trdnost f_{mf} 0.61 MPa (k.v. 11.5%). Malta za grobi omet je po 365 dneh dosegla f_{mc} 3.05 MPa in f_{mf} 1.07 MPa, trdnosti malte za fini omet pa sta po 28 dneh znašali 1.79

MPa in 0.52 MPa. Povprečna tlačna trdnost kamna f_{bc} je znašala 171.5 MPa (k.v. 24.1%), upogibna f_{bf} pa 24.2 MPa (k.v. 17.4%).

Slika 8.3: Morfologija povezanega zidu in nepovezanega zidu, zid za preizkušanje, zidek z ometom ter omet z vidnim grobim in finim slojem (od leve proti desni)
Figure 8.3: Morphology of the wall with and without through stones, the wall specimen, the plastered wallette and lime plaster with coarse and fine layer (from left to right)

Izvedeni so bili tudi tlačni in cepilno natezni preizkusi valjev, ki naj bi simulirali jedro zidu. Po 342 dneh sta tlačna f_{cc} in cepilna natezna f_{cst} trdnost jedra znašali 0.90 MPa (k.v. 23.6%) in 0.16 MPa (k.v. 52.5%). Vzorci so bili krhki in so razpadali že pri majhni obtežbi, zaradi česar ni bilo možno narediti preizkusov za določitev elastičnega modula.

Z "Bond-wrench" testom je bila po tlačnem preizkusu zidu določena upogibna natezna trdnost stika kamen-malta f_{jx}, in sicer 0.03 MPa, pri čemer je prišlo do porušitve na stiku malte in kamna.

8.2.2 Tlačni testi zidov

Najprej sta bila preskušana zidka, eden nepovezan in drugi povezan, ter nato še zidova. Pri zidkih maksimalna nosilnost ni bila dosežena zaradi omejitve opreme (hidravlični bat kapacitete 2500 kN). Hitrost obremenjevanja je bila konstantna, in sicer med 0.25 kN/s in 1.0 kN/s za posamezne teste. Vertikalni in horizontalni pomiki zidov so bili spremljani z 11-imi induktivnimi merilci.

Slika 8.4: Postavitev tlačnega testa (levo) ter poškodovanost povezanega zidu po testu (ostale)
Figure 8.4: Compression test setup (left) and damage of the wall with header stones after the test

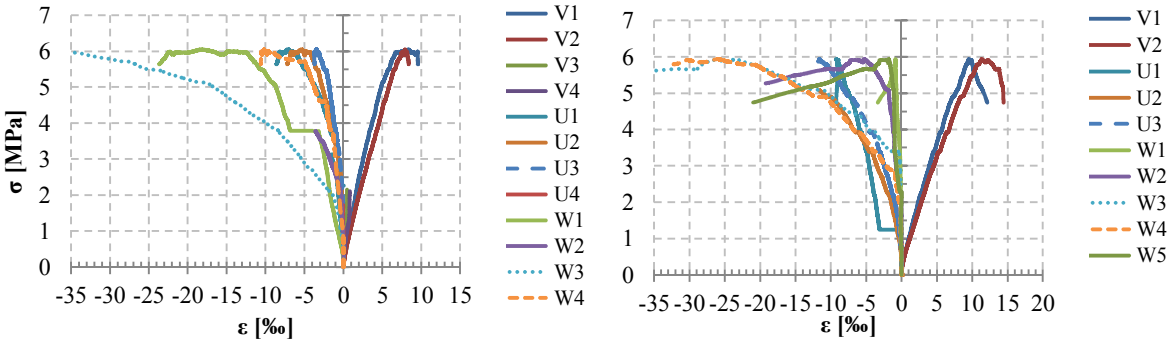

Slika 8.5: Diagram napetost - deformacija za različne induktivne merilce za test nepovezanega zidu (levo) in test povezanega zidu (desno)
Figure 8.5: Stress - strain diagram for various LVDTs for test on wall without (left) and with (right) through stones

Dosežene so bile napetosti 7.34 MPa za nepovezani zidek ter 7.28 MPa za povezani zidek. Pri zidovih pa so tlačne trdnosti bile dosežene, in sicer 6.10 MPa za povezan in 6.00 MPa za nepovezan zid. Na Sliki 8.4 so prikazane poškodbe po porušitvi povezanega zidu, na Sliki 8.5 pa diagrami napetost - deformacija induktivnih merilcev za nepovezani in povezani zid.

V nasprotju s pričakovanji ni bilo skoraj nobene razlike med mejnimi tlačnimi napetostmi povezanega in nepovezanega zidovja. Nasprotno, nepovezano je doseglo še malenkost večjo tlačno trdnost. Tudi pri horizontalnih prečnih deformacijah oziroma razpokami med sloji med obema tipoma zidu ni bilo druge večje razlike, kot da so povezovalni kamni približno do obremenitve 1/3 f_{Mc} omejevali horizontalne prečne deformacije.

Vrednosti elastičnega modula E_M, izračunanega iz povprečnih vertikalnih deformacij in napetosti pri 1/3 f_{Mc} zidov oziroma maksimalnih napetosti zidkov, in strižnega modula G_M, ki je po teoriji elastičnosti za homogene izotropne linearno elastične materiale izračunan iz elastičnega modula in Poisson-ovega količnika, so višje pri nepovezanem zidovju, vendar pri zidovih manj očitno; E_M je za povezani zid 30% manjši v primerjavi s nepovezanim zidom in G_M za 27%. Razmerje strižnega in elastičnega modula je za rezultate vseh preiskav med 0.38 in 0.42.

Table 8.1: Results of compression tests on walls
Preglednica 8.1: Rezultati tlačnih testov zidov

Test		σ_{max} oz. f_{Mc} [MPa]	ave. σ_{max} [MPa]	E_M [MPa]	ave. E_M [MPa]	υ_M	G_M [MPa]	ave. G_M [MPa]	G_M/E_M
1	Nepovezani zidek	7.34*	7.31	1570	1052	0.187	661	438	0.42
2	Povezani zidek	7.28*		534		0.265	214		0.40
3	Nepovezani zid	6.10	6.05	1138	968	0.226	412	357	0.36
4	Povezani zid	6.00		798		0.319	302		0.38

* vrednosti se nanašajo na napetosti pri močno poškodovanem zidu

8.2.3 Strižni testi zidov

Za analizo obnašanja zidov pri potresnih obtežbah je bilo ciklično strižno testiranih 14 zidov. Zidovi dveh različnih morfologij so bili preskušani pri različnih nivojih tlačnih obremenitev ter z različnimi robnimi pogoji vpetja.

8.2.3.1 Opis testov (postavitev, kombinacije testiranj, merjenje, postopek obremenjevanja)

Zid v postavitvi za strižno preizkušanje ter skica postavitve preiskave sta predstavljena na Sliki 8.6. Vertikalna obtežba v obliki bremena se na preizkušanec nanese s spodnje strani preko ročice (betonske kocke na Sliki 8.6). Postavitev je dimenzionirana na maksimalno 500 kN obremenitev, servo-hidravlični bat pa je sposoben zidu vsiljevati pomike v obe smeri s kapaciteto 250 kN. Pomik je bil med testom voden z induktivnim merilcem na spodnjem robu zidu. Pomike se je vsiljevalo iz ravnovesne lege v obe smeri ciklično z naraščanjem amplitud po treh ciklih z enako amplitudo. En cikel predstavlja obremenitev do amplitudnega pomika najprej v eno smer (pozitivne histerezne zanke), vrnitev v ravnovesno lego ter nato obremenitev do amplitudnega pomika v drugo smer in nazaj (negativne histerezne zanke). Pomiki in deformacije zidu, stiki med betonskima temeljema in zidom ter betonskim temeljem in jeklenim profilom zgoraj so bili med testom merjeni z 19 induktivnimi merilci. Testi so se izvajali do pomika, pri katerem je bil dosežen padec sile po dosegu nosilnosti za 20%, oziroma do pomika, za katerega smo ocenili, da je nadaljnje obremenjevanje nevarno (za varnost ljudi in opreme).

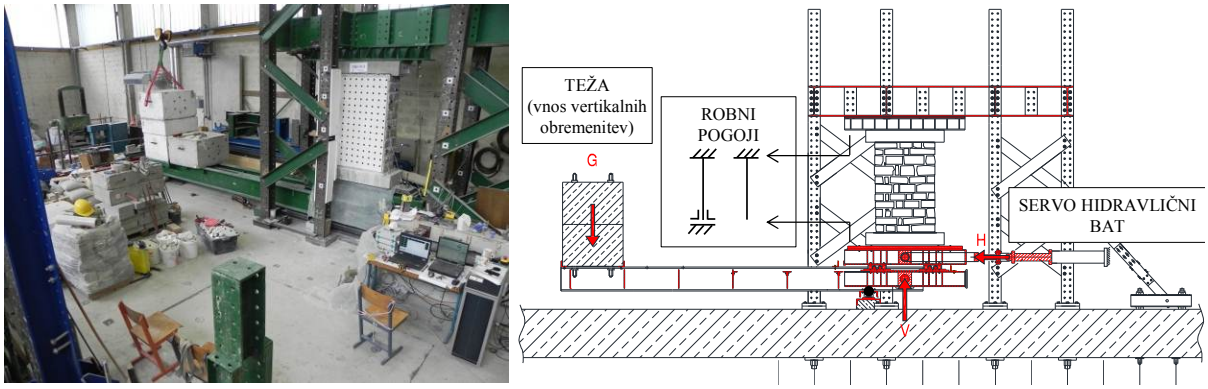

Slika 8.6: Postavitev strižnega testa
Figure 8.6: Shear test setup

Elementi postavitve omogočajo več možnosti vpetja; tako je bil zid v nekaterih primerih vpet na zgornjem robu, medtem ko sta bila horizontalni pomik in rotacija na spodnjem robu sproščena (obrnjena konzola), v drugih primerih pa je bila dodatno preprečena še spodnja rotacija (v Preglednici 8.2 so preizkušanci označeni kot »vpeti«). V Preglednici 8.2 so prikazane kombinacije morfologije, nivoja tlačnih obremenitev ter robnih pogojev za posamezne strižne preizkuse. Preizkus 1.2 se nanaša na ponovno obremenjevanje prvega preizkušanca z drugačnim nivojem tlačnih obremenitev (7.5% tlačne trdnosti zidu namesto 5%). Tlačne obremenitve so bile izbrane tako, da so bili sproženi različni mehanizmi obnašanja in njihove vrednosti primerljive z obremenitvami v realnih objektih.

Table 8.2: Combinations for shear wall testing
Preglednica 8.2: Kombinacije za strižno testiranje zidov

št. testa	Ime	Nivo tlačnih obremenitev [% f_{Mc}]	Robni pogoji	Povezovalni kamni
1	SPk-5-1	5	konzola	DA
1.2	SPk-5-1 (7.5)	7.5	konzola	DA
2	SNk-7.5-1	7.5	konzola	NE

Se nadaljuje…

…nadaljevanje Preglednice 8.2

3	SNv-7.5-1	7.5	vpeto	NE
4	SPv-7.5-1	7.5	vpeto	DA
5	SNv-7.5-2	7.5	vpeto	NE
6	SPv-7.5-2	7.5	vpeto	DA
7	SPv-15-1	15	vpeto	DA
8	SNv-15-1	15	vpeto	NE
9	SPv-15-2	15	vpeto	DA
10	SNv-15-2	15	vpeto	NE
11	SNk-15-1	15	konzola	NE
12	SPk-15-1	15	konzola	DA
13	SPk-15-2	15	konzola	DA
14	SNk-15-2	15	konzola	NE

8.2.3.2 Tipične poškodbe, porušni mehanizmi ter ločevanje slojev

Z izvedenimi kombinacijami robnih pogojev je prišlo do različnih mehanizmov obnašanja zidov (Slika 8.7). Pri nizkih tlačnih obremenitvah in konzolnem vpetju se je sprožil upogibni mehanizem, pri katerem se je »odpirala« spojnica med prvo in drugo vrsto kamnov. Pri vpetih zidovih se je pri nižji tlačni obremenitvi že delno aktiviral strižni mehanizem (dobljeni odziv je v nadaljevanju imenovan »mešan«), pri višjih vertikalnih obremenitvah se je tako pri konzolnih kot tudi vpetih robnih pogojih aktiviral strižni porušni mehanizem. Porušitev je večinoma potekala skozi maltne spojnice, razpokali pa so tudi kamni. Pri večjih pomikih je bilo prisotno drobljenje malte in praznjenje spojnic v sredinskem delu zidov, ponekod tudi v zgornjih vogalih. Vertikalne razpoke skozi spojnice in tudi čez kamne so tvorile (pri nekaterih testih bolj, pri drugih manj) izrazite vertikalne stebre na enem ali obeh robovih zidov.

Slika 8.7: Upogibni mehanizem z odpiranjem maltne spojnice med prvima vrstama kamnitih blokov pri testu 2 - SNk-7.5-1, diagonalne strižne poškodbe zidu po testu 13 - SPk_15_2 ter razpoka med slojema po istem testu, razpoka med slojema zidu po testu 14 - SNk_15_2 (od leve proti desni)

Figure 8.7: Rocking of the wall with opening of the mortar joint between the first two rows of stone at test 2 - SNk-7.5-1, diagonal shear damage after test 13 - SPk_15_2 and crack between the leaves after the same test, leaf separation at test 14 - SNk_15_2 (from left to right)

Pri testih 1, 1.2, 4, 6 in 7 vertikalna razpoka med sloji ob strani zidov ni bila zaznana. Izven-ravninski mehanizem se je opazno aktiviral le pri strižnem mehanizmu in je bil bolj izrazit pri konzolnem vpetju ne glede na prisotnost povezovalnih blokov. Le v primeru vpetih robnih pogojev so povezovalni kamni pri povezanih zidovih, v primerjavi z nepovezanimi zidovi, zmanjšali ločevanje slojev zidov v fazi padanja sile po dosegu maksimalne nosilnosti.

8.2.3.3 Histerezni odziv zidov

Najpomembnejše informacije o obnašanju zidov se dobijo iz analize histereznega diagrama odziva, to je iz diagrama prečne sile v odvisnosti od horizontalnih pomikov. Na Sliki 8.8 so prikazani tipični histerezni diagrami (horizontalna sila - spodnji horizontalni pomik), ki so bili dobljeni za posamezen tip porušnega mehanizma, na Sliki 8.9 pa so primerjane histerezne ovojnice vseh ciklov obremenjevanja za vse teste.

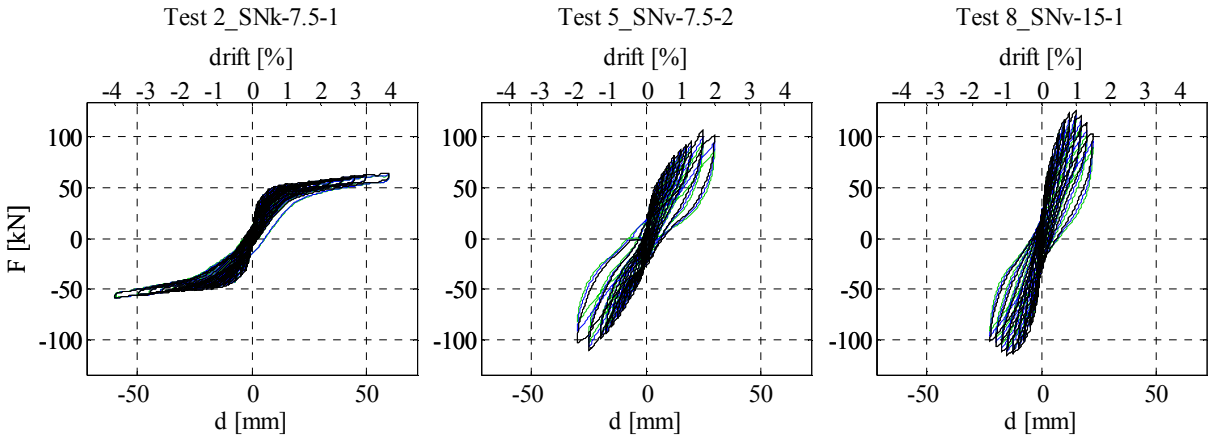

Slika 8.8: Karakteristični histerezni odziv (horizontalna sila - horizontalni pomik) za različne dobljene porušne mehanizme; upogibni (levo), mešani (na sredini) in diagonalni strižni mehanizem (desno)
Figure 8.8: Characteristic hysteretic response (lateral load - lateral displacement) for various failure mechanisms obtained; rocking (left), mixed mode (middle) and diagonal shear mechanism (right)

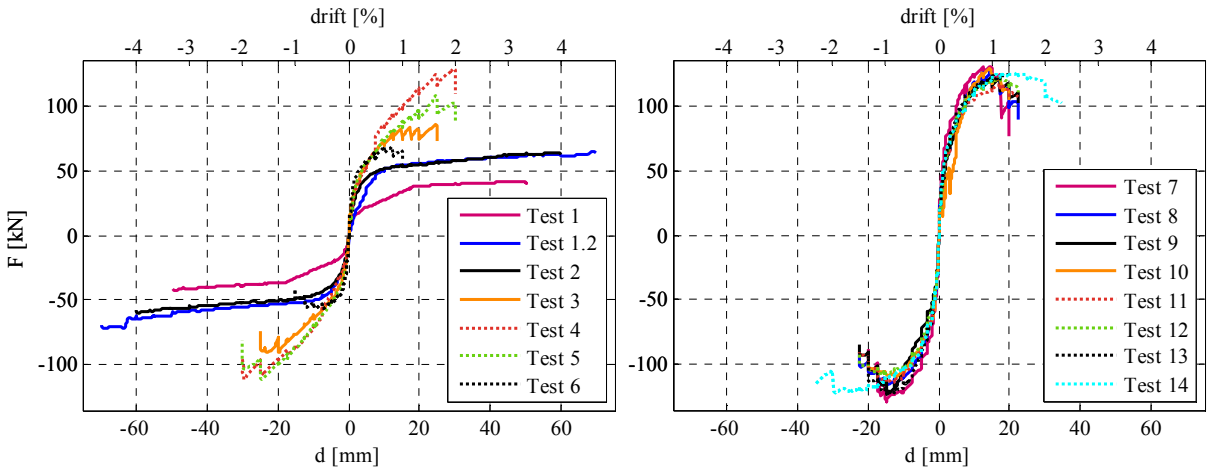

Slika 8.9: Histerezne ovojnice odziva horizontalna sila-horizontalni pomik za teste 1-6 in 7-14
Figure 8.9: Hysteretic envelopes of lateral load - lateral displacement responses for tests 1-6 and 7-14

Poleg maksimalnih strižnih sil, ki jih zidovi prenesejo, ter maksimalnih doseženih pomikov so bile iz rezultatov preiskav določene tudi druge karakteristike obnašanja, od katerih so najpomembnejše predstavljene v nadaljevanju.

Med njimi so pomiki, pri katerih so dosežena določena stanja, in sicer pomik, pri katerem pride do prve strižne razpoke d_{cr} ter pripadajoča sila F_{cr}, maksimalna dosežena nosilnost F_{max} ter pripadajoči pomik d_{Fmax} in mejni pomiki pri porušitvi d_{max} ter pripadajoča sila F_{dmax}. Njihove vrednosti (povprečja obeh smeri obremenjevanja) so za posamezne teste podane v Preglednici 8.3.

Table 8.3: Average values of characteristic points in both directions of force - displacement diagrams obtained in tests
Preglednica 8.3: Povprečne vrednosti karakterističnih točk diagramov sila - pomik obeh smeri

		Prva strižna razpoka		Maksimalna sila		Maksimalen pomik	
Št. testa	Ime	d_{cr} [mm]	F_{cr} [kN]	d_{Fmax} [mm]	F_{max} [kN]	d_{max} [mm]	F_{dmax} [mm]
1	1-SPk-5-1	0.00	0.0	49.6	42.1	49.8	41.2
1.2	1.2-SPk-7.5-1	34.70	57.7	69.5	68.5	69.7	66.1
2	2-SNk-7.5-1	17.37	51.9	58.1	61.8	59.8	60.3
3	3-SNv-7.5-1	7.44	61.2	22.3	88.2	24.9	73.0
4	4-SPv-7.5-1	7.45	60.9	29.7	119.9	29.9	101.7
5	5-SNv-7.5-2	9.93	73.0	24.7	109.0	29.9	83.3
6	6-SPv-7.5-2	7.45	60.2	9.9	61.9	14.9	50.8
7	7-SPv-15-1	2.98	81.4	14.8	129.2	19.9	81.9
8	8-SNv-15-1	4.96	85.7	14.9	121.2	22.4	90.3
9	9-SPv-15-2	1.98	52.5	16.1	122.1	22.4	93.6
10	10-SNv-15-2	2.98	60.9	13.4	119.4	19.9	100.8
11	11-SNk-15-1	2.98	68.3	15.0	114.5	22.4	98.6
12	12-SPk-15-1	2.98	65.8	15.2	114.0	22.4	100.9
13	13-SPk-15-2	2.98	72.2	16.2	122.5	19.9	104.7
14	14-SNk-15-2	4.97	84.5	26.0	123.7	34.9	108.0

Iz primerjave rezultatov je jasno viden tako vpliv nivoja tlačnih obremenitev, kot tudi robnih pogojev vpetja. Glede na različne mehanizme obnašanja, ki so se razvili, so precej različni tudi sile in pomiki za posamezna karakteristična stanja. Pri upogibnem mehanizmu so nosilnosti sicer najnižje, so pa maksimalni pomiki zelo veliki, veliko večji kot pri drugih mehanizmih. Pri mešanem odzivu se je povečala maksimalna nosilnost, vendar pa so se močno zmanjšali maksimalni pomiki. Pomiki so bili še vedno večji kot v primeru strižnega mehanizma, razlika je še nekoliko večja, če se iz primerjave izvzame test št. 6, pri katerem je zid v primerjavi z drugimi zidovi zaradi debelejših horizontalnih spojnic izkazal opazno manjšo nosilnost in mejne pomike (zaradi navedenega razloga je v nadaljevanju pri primerjavi rezultatov testov test št. 6 izvzet). Dosežene nosilnosti so bile pri strižni porušitvi najvišje.

Presenetljivo se je izkazalo, da pri čistih strižnih obremenitvah v ravnini zidov za preskušani tip zidov prisotnost povezovalnih kamnov ne doprinese ne k večjim nosilnostim, ne k izboljšanju maksimalnih pomikov zidov. Primerjava povprečnih rezultatov testov z enako morfologijo je za posamezne kombinacije vertikalnih obremenitev in robnih pogojev prikazana v Preglednici 8.4. Višja nosilnost v primeru povezovalnih kamnov je bila zaznana pri višjih tlačnih obremenitvah in vpetih robnih pogojih (za 4.4% napram nepovezanim zidovom), pri nižji vertikalni obremenitvi in vpetih robnih pogojih je

nosilnost povezanih zidov večja za 21.6%. Edino v slednjem primeru so bili v primeru povezanih zidov večji tudi maksimalni pomiki, drugače pa so bili ali enaki ali manjši.

Table 8.4: Mean values of force - displacement response characteristic values for tests with the morphology, pre-compression level and boundary conditions

Preglednica 8.4: Povprečne vrednosti karakterističnih točk diagramov sila - pomik po testih glede na morfologijo, nivo tlačnih obremenitev ter robne pogoje

Mejno stanje	Prva strižna razpoka				Maksimalna sila				Maksimalen pomik			
	d_{cr} [mm]		F_{cr} [kN]		d_{Fmax} [mm]		F_{max} [kN]		d_{max} [mm]		F_{dmax} [kN]	
Povezovalni kamni:	Da	Ne	Da	Ne	Da	Ne	Da	Ne	Da	Ne	Da	Ne
7.5% f_{Mc}, konzolno	34.7	17.4	57.7	51.9	69.5	58.1	68.5	61.8	69.7	59.8	66.1	60.3
7.5% f_{Mc}, vpeti	7.45	8.69	60.6	67.1	19.8	23.5	90.9	98.6	22.4	27.4	76.2	78.1
15% f_{Mc}, vpeti	2.48	3.97	66.9	73.3	15.5	14.1	125.7	120.3	21.1	21.1	87.7	95.6
15% f_{Mc}, konzolno	2.98	3.97	69.0	76.4	15.7	20.5	118.2	119.1	21.1	28.6	102.8	103.3

Glede na to, da pri rezultatih testov povezanih in nepovezanih zidov ni očitne razlike pri obnašanju, so v nadaljevanju vsi rezultati prikazani le v odvisnosti od kombinacije robnih pogojev in nivoja tlačnih obremenitev ali dobljenega porušnega mehanizma.

8.2.3.4 Idealizacija histereznih ovojnic in analiza rezultatov

Za primerjavo z vrednostmi v predpisih ter z rezultati testov drugih raziskovalcev so bile histerezne ovojnice idealizirane. Pri idealizaciji eksperimentalnih strižnih preiskav zidov je najbolj pogosta bi-linearna idealizacija, ki temelji na enaki količini vnesene energije (površine pod krivuljo) dejanske histerezne ovojnice ter idealizacije ter drugih predpostavkah, ki nekoliko variirajo v odvisnosti od raziskovalcev. Pri idealizaciji rezultatov testov je bil mejni pomik d_u predpostavljen kot pomik, pri katerem sila pade na 80% F_{max}, oziroma pomik d_{max}, v kolikor prejšnji kriterij ni bil dosežen, ter efektivna togost K_{ef} enaka togosti v točki, kjer je sila enaka 2/3 F_{max}. Glede na prejšnje kriterije se je potem določilo idealizirano silo F_{id} ter pomik na meji elastičnosti d_e. Pri analizi idealiziranega odziva se ponavadi analizira tudi duktilnost μ, ki je razmerje med mejnim in elastičnim pomikom d_u/d_e. Povprečne vrednosti značilnih parametrov bi-linearnih krivulj so podani v Preglednici 8.5.

Table 8.5: Average characteristic points' values of bi-linearly idealised force - displacement diagrams with c.o.v. for the same pre-compression level and boundary conditions applied

Preglednica 8.5: Povprečne vrednosti karakterističnih točk bi-linearno idealiziranih diagramov sila - pomik s k.v. glede na nivo tlačnih obremenitev ter robne pogoje

Nivo vertikalne obremenitve, robni pogoji	F_{id} [kN]	k.v. [%]	d_e [mm]	k.v. [%]	K_{ef} [kN/mm]	k.v. [%]	d_u [mm]	k.v. [%]	μ	k.v. [%]
7.5% f_{Mc}, konzolno	57.8	3.0	8.4	14.6	7.0	11.8	64.8	7.7	7.80	7.1
7.5% f_{Mc}, vpeti	100.2	11.5	13.2	15.8	7.8	7.9	28.2	8.3	2.23	11.6
15% f_{Mc}, vpeti	113.7	2.0	5.9	21.4	21.2	22.1	21.0	5.3	3.92	18.2
15% f_{Mc}, konzolno	112.6	4.0	5.6	9.7	20.4	7.1	24.9	23.5	4.46	14.8

Iz F_{id} je bila za teste po En. 8.1 izračunana natezna trdnost zidov f_{Mt}, ki izhaja iz Turnšek in Čačovićevega modela za diagonalno porušitev zidov, in je določena kot kritična vrednost glavnih napetosti v sredini zidov, pri katerih pride do diagonalne porušitve. V enačbi τ predstavlja povprečno strižno napetost na prerezu, b koeficient, ki upošteva geometrijo zidov (v našem primeru b = 1.5, ker

imajo zidovi razmerje višine in dolžine zidu h_w/l_w enako 1.5), in σ_0 povprečno vertikalno napetost zidu. Iz K_{ef} in E_M, dobljenega iz tlačnih testov, se lahko po En. 3.12 izračuna strižni modul zidov G_M, pri čemer je ψ koeficient, ki upošteva robne pogoje, in sicer $\psi = 4$ za konzolne in $\psi = 1$ za vpete robne pogoje. Povprečni rezultati f_{Mt} in G_M za teste z enakimi pogoji so predstavljeni v Preglednici 8.6.

$$f_{Mt} = -0.5 \cdot \sigma_0 + \sqrt{\left(0.5 \cdot \sigma_0\right)^2 + \left(b \cdot \tau\right)^2}\ , \qquad \textbf{8.1}$$

$$G_M = \frac{K_{ef}}{\frac{l_w \cdot h_w}{1.2 \cdot h_w} - \frac{\psi \cdot K_{ef}}{1.2 \cdot E_M}\left(\frac{h_w}{l_w}\right)^2}, \qquad \textbf{8.2}$$

$$G_M = \frac{\tau}{\gamma} = \frac{F \cdot h_w}{A_w \cdot d} \qquad \textbf{8.3}$$

Table 8.6: Average tensile strength f_{Mt} and G_M moduli obtained in various ways for tests with the same pre-compression level and boundary conditions applied

Preglednica 8.6: Natezne trdnosti f_{Mt} in G_M moduli, izračunani po različnih metodah za teste z enakimi nivoji tlačnih obremenitev ter robnimi pogoji

Nivo vert. obremenitve, robni pogoji	f_{Mt} [MPa]	k.v.	G_M [MPa]	k.v.	$K_{1.5mm}$ [kN/mm]	k.v.	$^{**}G_{1.5mm}$ [MPa]	k.v.	$^{***}G_{1.5mm}$ [MPa]	k.v.
7.5% f_{Mc}, konzolno	0.087	5.1	47.2	17.7	16.1	/	277	/	122	/
7.5% f_{Mc}, vpeti*	0.214	17.2	38.8	8.9	20.2	5.8	118	7.5	76	20.7
15% f_{Mc}, vpeti	0.165	3.4	129.9	29.3	26.8	31.3	240	26.9	122	26.0
15% f_{Mc}, konzolno	0.162	7.0	2094	64.6	33.4	4.0	-287	-8.1	125	19.1

** izračunan po En. 3.12 (z upoštevanjem efektivne togosti K_{ef} in E_M modula)

*** izračunan po En. 3.13 (razmerje strižne napetosti τ in strižne deformacije γ)

Najvišje f_{Mt} so bile izračunane za nižji nivo tlačnih obremenitev ter vpete robne pogoje, kjer je bil dobljen mešani mehanizem porušitve. Za 30.7% presežejo vrednosti f_{Mt}, dosežene v primeru strižnega mehanizma, ki so sicer zelo podobne za oboje robne pogoje; 0.165 MPa in 0.162 MPa za vpete in konzolne.

Vrednosti G_M, izračunane iz K_{ef} in E_M po En. 3.12, so v nekaterih primerih bile nerealne, čemur razlog so nizke vrednosti E_M. To je bilo zaradi izrazito anizotropnega obnašanja zgodovinske zidovine že pri začetnih nivojih obremenjevanja potrjeno že v [47]. Strižni moduli so bili zato izračunani tudi iz začetnih togosti K, dobljenih pri začetnih pomikih testov (za d=1.5 mm in 3 mm) po En. 3.13, pri čemer je F strižna sila v točki vrednotenja K določenega pomika, γ pa strižna deformacija. V tem primeru so bile sicer dobljene vrednosti modulov stabilnejše (v Preglednici 8.6 podani kot $G_{1.5\ mm}$), a še vedno veliko manjše kot tiste iz rezultatov tlačnih testov.

V predpisih so navadno podani mejni zasuki zidov, za izvedene teste pa so zasuki za karakteristična stanja prikazani na Sliki 8.1, medtem ko so v Preglednici 8.7 podane priporočene vrednosti mejnih zasukov po evropskih predpisih EN 1998-3: 2005 [49] ter ameriških FEMA 306 [95].

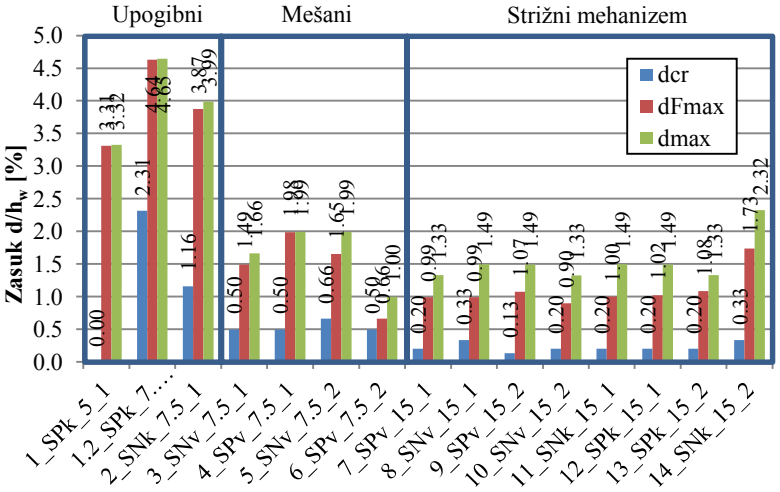

Slika 8.10: Povprečni zasuki d/h_w obeh smeri obremenjevanja za zidove v karakterističnih točkah odziva
Figure 8.10: Average drifts d/h_w of both directions for the walls in characteristic performance limit states

Table 8.7: Recommended drift limits in [%] according to code provisions considering specific slenderness of the tested walls and boundary conditions applied

Preglednica 8.7: Priporočene vrednosti zasukov v [%] po predpisih glede na vitkost testiranih zidov in robne pogoje

Predpis	Prevladujoči porušni mehanizem	Upogibni			Strižni		
EC8-3	Mejno stanje	DL	SD	NC	DL	SD	NC
	Zasuk	/*	0.8 h_0/l_w	4/3 θ_{SD}	/*	0.4	4/3 θ_{SD}
	Konzolni	/*	1.20	1.60	/*	0.4	0.53
	Vpeti	/*	0.60	0.80	/*		
FEMA	Mejno stanje	IO	LS	CP	IO	LS	CP
	Drift	0.1	0.3 h_0/l_w	0.4 h_0/l_w	/**	/**	/**
	Konzolno	0.1	0.45	0.60	/**	/**	/**
	Vpeti		0.225	0.30	/**	/**	/**

*zasuki so določeni analitično iz togosti in nosilnosti zidov

**strižni mehanizem se po FEMA priporočilih v splošnem smatra kot krhki mehanizem in se posledično kontrolira s silo

Kot vidimo so zasuki, ki so bili dobljeni pri testih, znatno višji od dovoljenih v standardih. Velja poudariti, da so v predpisih dovoljeni mejni pomiki enaki za vse vrste zidovine. V primeru upogibnega mehanizma sta vrednosti zasukov za mejno stanje "NC" (blizu porušitve) po EC8-3 oziroma "CP" (preprečitev porušitve) po FEMA priporočilih 1.60% in 0.60%; doseženi zasuki so torej za 149% večji od tistih v EC8-3 in za 564% od tistih v FEMA-i. Tudi dosežene povprečne vrednosti zasukov pri d_e, ki se lahko primerjajo z vrednostmi 0.1% v FEMA-i, so za 630% višje. Vrednosti za strižni mehanizem so podane v EC8-3 in znašajo 0.53% za "NC" mejno stanje. Ne glede na to, ali so primerjani zasuki pri d_u ali d_u^* (le do tam, kjer dejanska sila ne pade pod F_{id}), so vrednosti zasukov iz testov višje; za 188% pri d_u in za 133% pri d_u^*.

8.2.3.5 Disipacija energije in ekvivalentno viskozno dušenje

Eden od pokazateljev različnega obnašanja zidovine pri potresnih obremenitvah je tudi disipacija energije. Disipirana energija pri določenem ciklu obremenjevanju $E_{DIS,i}$ se določi iz histereznega diagrama sila-pomik, saj predstavlja površino znotraj posamezne histerezne zanke. Smiselno jo je primerjati z vneseno energijo E_{INP}, in sicer delom bata, potrebnim za deformiranje zidu do določenega

pomika. Za posamezen cikel se $E_{INP,i}$ izračuna iz diagrama prečne sila – pomik kot površina pod delom krivulje, kjer absolutna vrednost pomika narašča (glej definicije v 2.3.2.4.1).

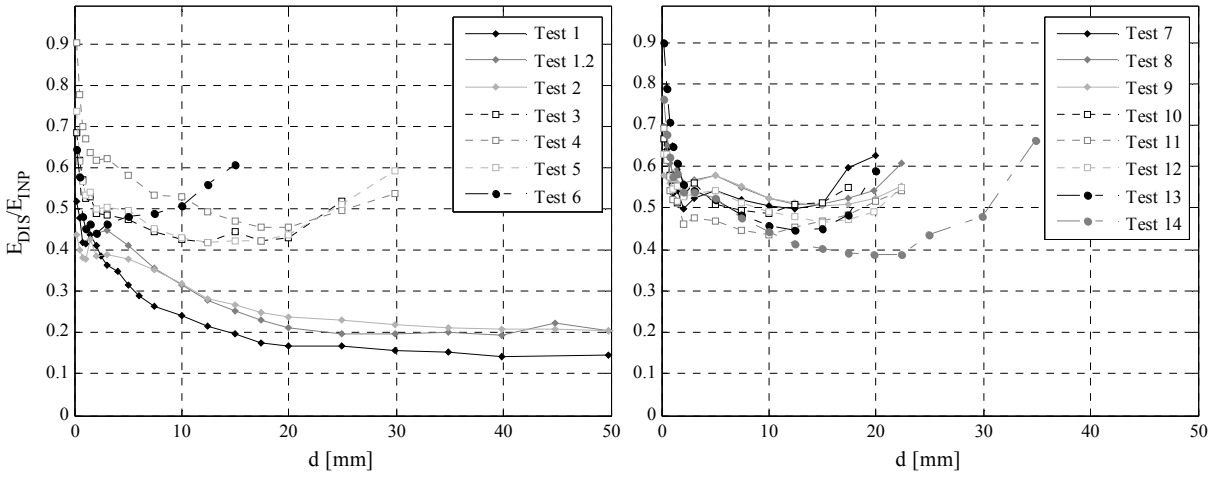

Slika 8.11: Razmerje disipirane in vnesene energije v 1. ciklih amplitudnih pomikov za teste 1-6 in 7-14
Figure 8.11: Dissipated and input energy ratio at 1st cycles of amplitude displacements for tests 1-6 and 7-14

Primerjava razmerja med disipirano in vneseno energijo E_{DIS}/E_{INP} (Slika 8.11) je znova jasno pokazala razlike odziva glede na pogoje testiranja ter dobljene mehanizme obnašanja. Relativna disipirana energija (glede na vneseno) je v primeru strižnega mehanizma veliko večja kot v primeru upogibnega mehanizma. Le pri začetnih ciklih, kjer je disipacija energije zaradi začetnih poškodb najvišja (celo višja kot potem pri nastanku večjih poškodb po dosegu maksimalne sile), so vrednosti primerljive. Po začetnih poškodbah razmerje E_{DIS}/E_{INP} pade, nato pa se začne povečevati pri dosegu F_{max} in s poškodbami zopet raste. Te rasti seveda ni zaznati pri upogibnem mehanizmu, pri katerem ne pride do drobljenja pete.

Table 8.8: Mean values of dissipated to input energy ratios with c.o.v. for the same pre-compression level and boundary conditions for the 1st cycles

Preglednica 8.8: Povprečne vrednosti razmerij disipirane in vnesene energije za 1. cikle karakterističnih pomikov s k.v. za teste z enako tlačno obremenitvijo ter robnimi pogoji

	d_{cr}		d_e		d_{Fmax}		d_{max}			
Nivo vert. obremenitve, robni pogoji	E_{DIS}/E_{INP} povpr.	k.v. [%]	E_{DIS}/E_{INP} povpr.	k.v. [%]	E_{DIS}/E_{INP} povpr.	k.v. [%]	E_{DIS}/E_{INP} povpr.	k.v. [%]	$cumE_{DIS}$ / $cum\ E_{INP}$ povpr.	k.v.[%]
7.5% f_{Mc}, konzolno	0.226	11.1	0.336	5.6	0.187	2.2	0.187	2.2	0.214	4.4
7.5% f_{Mc}, vpeti	0.471	9.8	0.446	4.7	0.524	1.9	0.551	5.8	0.471	9.8
15% f_{Mc}, vpeti	0.549	3.9	0.549	6.3	0.509	0.5	0.585	5.7	0.534	2.3
15% f_{Mc}, konzolno	0.519	4.9	0.514	5.1	0.482	15.1	0.587	8.2	0.490	2.5

Kot drugi pokazatelj disipacije energije se pogosto uporablja tudi ekvivalentni koeficient viskoznega dušenja ξ, ki predstavlja histerezno dušenje sistema in ga je, kot je zapisano v En. 2.35, definiral Jacobsen [114]. V enačbi E_{DIS}^{+} in E_{INP}^{-} predstavljata vneseno energijo v posamezni smeri obremenjevanja (pozitivni in negativni), izračunano za pozitivno smer po En. 2.32, K^{+} predstavlja togost posameznega cikla v točki njegovega maksimalnega pomika v pozitivni smeri $d_{max,i}$. Za drugo smer obremenjevanja pa so navedeni parametri v enačbi vzeti za negativni cikel.

$$\xi_{eq} = \frac{1}{2\pi}\frac{E_{DIS}}{E_{INP}} = \frac{1}{2\pi}\frac{E_{DIS}}{(E_{INP}^{+} + E_{INP}^{-})}, \quad \textbf{8.4}$$

$$E_{INP} = \frac{1}{2}K^{+} \cdot d_{\max,i}{}^{2} = \frac{1}{2}F_{d,\max,i} \cdot d_{\max,i} \quad \textbf{8.5}$$

Povprečne vrednosti ξ, izračunane za teste z enakim porušnim mehanizmom, so pri maksimalnih nosilnostih za upogibni odziv 0.035, za mešani upogibno-strižni 0.047 in za strižni 0.131.

8.2.3.6 Padanje nosilnosti

Analize so pokazale, da so kljub temu, da strižni mehanizem v splošnem velja za krhkega, zidovi pri strižnem mehanizmu izkazali postopno zmanjšanje nosilnosti z nadaljnjim povečanjem pomikov po dosegu maksimalne sile. V povprečju je znašal d_{Fmax} za strižni mehanizem 72% d_{max}, pri čemer so bile vrednosti sile F_{dmax} v povprečju 80.8% F_{max}.

8.2.4 Obnašanje ometov na zidovih

Tako pri tlačnih kot tudi pri strižnih preizkusih je bila ves čas med testi natančno spremljana poškodovanost ometov. Beležili so se pomiki, pri katerih je prišlo do prvega odstopanja ometa od zidu (DS A1), pomiki, pri katerih so nastale posamezne razpoke na ometu (DS A2), ter njihova pozicija, debelina razpok, pomiki, pri katerih je bil omet po celotni višini ločen od zidu (DS A3), ter pomiki, kjer se je porušil omet (DS A4). Pri strižnih testih je bila za pomoč pri beleženju pomikov in njihovo nadaljnjo analizo uporabljena fotogrametrija. Na omete so bili narisani krogi v rastru 10 cm x10 cm, ki so služili kot detajlne točke in katerih pomike smo dobili kot rezultat. Za preračun pa so bile postavljene tudi točke v prostoru, katerih pozicije so bile točno izmerjene s teodolitom. Fotogrametrične meritve so se izvajale v pozitivnih in negativnih amplitudah tretjih ciklov določenih amplitud, pri katerih je bilo obremenjevanje ustavljeno. Za določanje nastanka in širjenja oziroma napredovanja razpok so bili narejeni tudi orto-foto posnetki.

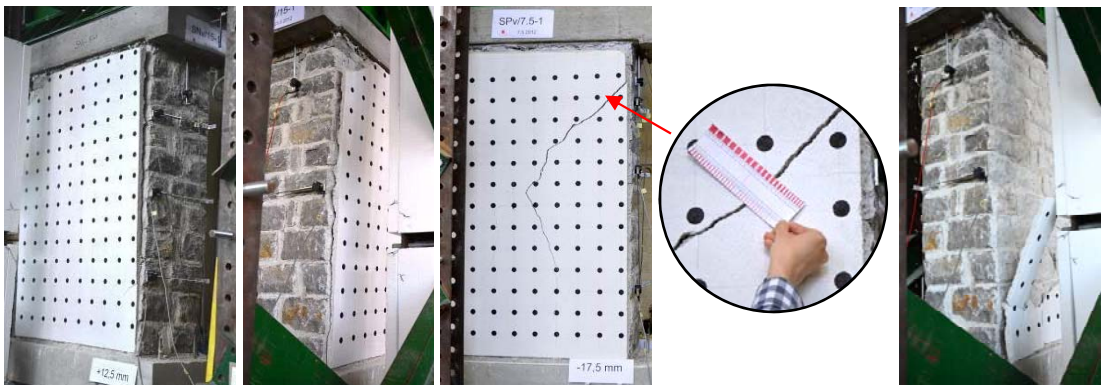

Slika 8.12: Odstopanje ometa pri testu 8 po celotni višini zidu na levi in na desni strani, strižna razpoka na ometu pri testu 4 ter bližja fotografija debeline razpoke, porušitev ometa pri testu 8 (od leve proti desni)
Figure 8.12: Detachment of the plaster at left and right side of the wall at test 8, shear crack on the plaster at test 4 and its up-close photo, collapse of the plaster at test 8 (from left to right)

Vrednosti povprečnih rotacij zidov, pri katerih je prišlo do zgoraj omenjenih karakterističnih stanj poškodb, ki so oštevilčena v skladu s PERPETUATE metodologijo [1] od DS A1 - DS A4, so za posamezne porušne mehanizme navedeni v spodnji tabeli.

V primeru upogibnega mehanizma se omet ni porušil, temveč je bil ob straneh ločen od zidov, pri čemer je bilo odstopanje ponekod pri večjih obremenitvah večje od 1 cm (Slika 8.12). Razpoke na ometu so se pojavile pri večjih pomikih zidov (povprečna rotacija 1.67%). Pri mešanem in strižnem mehanizmu je prišlo do porušitve ometa, in sicer pri mešanem pozneje (v povprečju zasuki 1.13%) kot pri strižnem (0.79%). Enako velja tudi za stanja pojava prvih razpok ter odstopanja ometa po celi višini zidov. Upogibni mehanizem je torej deloval ugodno glede na velikosti rotacij, je pa bila potem porušitev hitrejša glede na pojav razpok; razmerje pomikov pri DS A2 in DS A4 je za strižni mehanizem 0.10, za mešani pa 0.32.

Table 8.9: Average values of drifts of walls in characteristic damage states of the plaster for walls with the same wall failure mechanism

Preglednica 8.9: Povprečne vrednosti zasukov zidov v karakterističnih stanjih poškodb ometa za zidove z enakim porušnim mehanizmom zidov

Prevladujoči porušni mehanizem	Zasuki [%]							
	DS A1	k. v.	DS A2 ($d_{cr,AA}$)	k. v.	DS A3	k. v.	DS A4 ($d_{max,AA}$)	k. v.
Upogibni	0.37	0.09	1.67	0.40	3.83	0.04	/	/
Mešani	0.15	0.19	0.38	0.58	0.95	0.22	1.13	0.16
Strižni	0.07	0.23	0.08	0.27	0.42	0.45	0.79	0.14

Ker je obnašanje ometa vezano na obnašanje zidov, so v Preglednici 8.1 podana razmerja zasukov zidov mejnih stanj ometa ter mejnih stanj zidov (tako histerezne ovojnice kot idealizirane bi-linearne krivulje.)

Table 8.10: Average values of various plaster limit state wall drifts and characteristic wall drifts ratios for the same failure mechanism (with c.o.v.)

Preglednica 8.10: Povprečne vrednosti pomikov zidov za različna mejna stanja ometa in karakterističnih pomikov zidov za teste z enakim porušnim mehanizmom (s k.v.)

Prevladujoči porušni mehanizem	$d_{DS,A2}/d_{cr}$ (k.v.)	$d_{DS,A2}/d_e$ (k.v.)	$d_{DS,A2}/d_{DS,A4}$ (k.v.)	$d_{DS,A4}/d_{DS,A3}$ (k.v.)	$d_{DS,A3}/d_e$ (k.v.)	$d_{DS,A4}/d_e$ (k.v.)	$d_{DS,A4}/d_u$ (k.v.)
Upogibni	0.94	2.86	/	/	7.03	/	/
	(0.078)	(0.270)	/	/	(0.188)	/	/
Mešani	0.81	0.50	0.37	0.85	1.19	1.42	0.65
	(0.353)	(0.328)	(0.385)	(0.124)	(0.029)	(0.154)	(0.076)
Mešani (upoštevan test št. 6)	0.67	0.58	0.32	0.84	1.94	2.37	0.70
	(0.505)	(0.351)	(0.481)	(0.113)	(0.669)	(0.699)	(0.129)
Strižni	0.37	0.20	0.10	2.00	1.04	2.12	0.52
	(0.274)	(0.359)	(0.375)	(0.368)	(0.176)	(0.173)	(0.274)

8.2.5 Analiza in komentar rezultatov tlačnih in strižnih testov zidov z ometi ter primerjava z obstoječimi modeli za izračun karakteristik obnašanja

Tlačne trdnosti f_{Mc} troslojnih zidov, dobljene s tlačnimi testi, 6.00 MPa in 6.10 MPa za povezani in nepovezani zid, se dobro ujemajo z vrednostmi podanimi v italijanskih predpisih NTC08, kjer sta za obravnavano vrsto zidovine dani minimalna in maksimalna mejna vrednost f_{Mc} 6 MPa in 8 MPa. Za analitični izračun tlačne trdnosti je bil uporabljen EC6 model [37] ter modeli za troslojno zidovino avtorjev Egermann [39], Binda s sod. [40], Tassios in Chronopoulos [41,42] (za večslojno zidovino in za zidovino iz enega sloja), rezultati so podani v Preglednici 8.1.

Table 8.11: Literature reference f_{Mc} values and values calculated according to various analytical models
Preglednica 8.11: Referenčne vrednosti f_{Mc} iz literature ter po različnih analitičnih modelih izračunane vrednosti f_{Mc}

f_{Mc} [MPa]								
Vrednosti iz literature				Analitični modeli				
NTC08 (Italija)	PIET 70 (Španija in Portugalska)	Slovenija [244]	Hrvaška [242]	EC6	Egermann	Binda	Tassios	Tassios (single-leaf)
6.0 (min)	4.0	1.2 (min)	4.7 (min)	19.9	3.44 (*)	4.73 (*)	2.66 (+)	6.51 (+)
8.0 (max)		1.6 (max)	5.5 (max)		4.49 (**)	6.23 (**)	1.42 (++)	6.75 (++)

*, ** za vrednosti f_{Mc}^{e} sta pri izračunu upoštevani minimalna (*) in maksimalna (**) vrednost f_{Mc} po NTC08
+, ++ izračunano z upoštevanjem koeficientov za zidovino z obdelanim kamnom (+) in klesanci (++)

Rezultati, dobljeni z različnimi modeli, se zelo razlikujejo. Model v EC6 za oceno f_{Mc} historičnih zidov, zgrajenih z malto manjših trdnosti, ni primeren. Za testirani tip zidov vsi modeli podcenjujejo f_{Mc}, kar je verjetno posledica tega, da zaradi dobre povezanosti vseh slojev zidov ni bil dosežen najbolj tipičen mehanizem porušitve večslojnih zidov. Tako je ocena f_{Mc} Tassios-a in Chronopoulos-a za enoslojne zidove najbližja dejanskim vrednostim; za 7.6% je sicer f_{Mc} precenjen za visoke zidove, vendar je ocena glede na rezultate zidkov na varni strani.

Dobljeni vrednosti E_M in G_M sta manjši od pričakovanih in navedenih v literaturi; NTC08 [60] navaja mejni vrednosti 2400 MPa in 3200 MPa za E_M ter 780 MPa in 940 MPa za G_M , medtem ko sta bili pri testih doseženi povprečni vrednosti E_M in G_M za oba tipa zidov (povezane in nepovezane) 968 MPa in 357 MPa.

Pri strižnih testih so bili v odvisnosti od različnih nivojev tlačnih obremenitev ter robnih pogojev vpetja dobljeni različni porušni mehanizmi, pri čemer ločevanje slojev ni bilo tako izrazito, kot je bilo pričakovano, saj je bilo pri strižnem mehanizmu problematično le v območju obremenjevanja od dosega F_{max} naprej. Najnižja nosilnost in največji pomiki so bili dobljeni za upogibni porušni mehanizem (povprečni vrednosti 57.5 kN in 59.8 mm). Mešani odziv, do katerega je prišlo pri spremembi konzolnih robnih pogojev v vpete pri nižji vertikalni obremenitvi, je povečal nosilnost, a zmanjšal mejne pomike (105.7 kN in 28.2 mm). Največje nosilnosti so bile dosežene pri strižnem porušnem mehanizmu (120.8 kN pri višjem nivoju vertikalnih obremenitev ne glede na robne pogoje), ker pa je bil mehanizem diagonalni in ne zdrsni, so se doseženi pomiki dodatno zmanjšali (v povprečju 23.0 mm). Je pa treba omeniti, da tudi pri strižnem porušnem mehanizmu porušitev ni bila krhka. Po dosegu maksimalnih nosilnosti so zidovi izkazali nezanemarljive pomike, saj so bile vrednosti doseženih maksimalnih pomikov v povprečju za 40% višje od pomikov, kjer je bila dosežena

maksimalna sila (d_{Fmax} = 1.40 d_{max}). Na drugi strani je bila porušitev bolj zgodnja pri mešanem odzivu zidov (d_{Fmax} = 1.10 d_{max}). Pri strižnih testih je prišlo tudi do najvišjih padcev sile po dosegu F_{max}, v povprečju za 18.8%, vendar pa so se le-ti močno razlikovali od robnih pogojev (v povprečju 35.2% za vpete in 13.2% za konzolne). Pri upogibnih testih do padca sil ni prišlo, ali pa je bil le-ta zelo majhen.

Tudi z vidika disipacije energije strižni mehanizem ni neugoden; povprečne vrednosti kumulativno disipirane energije v primerjavi s kumulativno vneseno ($cumE_{DIS}/cumE_{INP}$) znašajo 0.214, 0.491 in 0.512 za upogibni, mešani in strižni mehanizem, povprečni ekvivalentni koeficienti viskoznega dušenja ξ pa 0.035, 0.047 in 0.131. Tudi če primerjamo ekvivalentno elastično nosilnost bi-linearne idealizacije (F_{id}·μ), je (diagonalni) strižni mehanizem ugodnejši od upogibnega, saj znaša 474 kN napram 342 kN pri upogibu.

Primerjava nosilnosti idealizirane histerezne ovojnice z rezultati najbolj razširjenih modelov za oceno strižne nosilnosti (Preglednica 8.11), in sicer po modelu za izračun upogibne nosilnosti $V_{Rd,r}$, po modelu za strižno diagonalno porušitev zidu $V_{Rd,d}$ [54], pri kateri je bila po NTC08 upoštevana f_{Mt} 0.18 MPa, za diagonalno porušitev zidu po spojnicah $V_{Rd,dj}$ ter po kamnu oziroma zidaku $V_{Rd,du}$ [119] ter z zdrsnim modelom za mejno nosilnost $V_{Rd,s}$ (Mohr - Coulomb-ov kriterij), je potrdila zadovoljivo oceno nosilnosti tako v primeru upogibnega mehanizma z uporabo modela za upogib (V_{Rd} = 0.96 F_{id}), kot tudi strižnega (diagonalnega) mehanizma po Turnšek - Čačovićevim modelu (V_{Rd} = 1.02 F_{id}). Problem pa je, da poda najbolj kritične rezultate za vse primere model za diagonalno porušitev po spojnicah ($V_{Rd,dj}$), ki očitno v primerih šibke, a duktilne malte ter ne pretirano debelih spojnicah, preveč konservativno oceni nosilnost. Se je pa kriterij izkazal bolje v primeru testa 6, ki je imel napram drugim debelejše horizontalne spojnice, kar je povzročilo tako manjšo nosilnost kot tudi mejne pomike. V modelih za oceno nosilnosti debelina spojnic pri določitvi nosilnosti ni upoštevana. V_{Rd} so bile izračunane tako z upoštevanjem celotnega prereza zidov A_w, kot tudi z upoštevanjem neto prereza $A_{w,n}$, to je samo zunanjih slojev zidu. Za zidove, kjer so sloji dobro povezani in je debelina jedra manjša oz. enaka 25% celotne debeline zidov, se za oceno nosilnosti lahko uporabi celoten prerez.

Table 8.12: Average ratios of analytically calculated shear resistances considering netto and gross creoss section for various failure mechanisms and idealized resistances obtained through tests

Preglednica 8.12: Povprečne vrednosti razmerij analitično izračunanih mejnih horizontalnih sil z upoštevanjem neto in celotnega prereza za različne porušne mehanizme z idealiziranimi maksimalnimi silami, dobljenimi po testih

Nivo vert. obremenitve, robni pogoji	$V_{Rd,r}$ / F_{id}		$V_{Rd,d}$ / F_{id}		$V_{Rd,dj}$ * / F_{id}		$V_{Rd,du}$ / F_{id}		$V_{Rd,s}$ / F_{id}	
	(A_w)	($A_{w,n}$)	(A_w)	($A_{w,n}$)	(A_w)	($A_{w,n}$)	(A_w)	($A_{w,n}$)	(A_w)	($A_{w,n}$)
7.5% f_{Mc}, konzolno	0.96	0.94	1.56	1.30	0.58	0.68	115.3	85.7	1.04	1.04
7.5% f_{Mc}, vpeti (vsi)	1.33	1.29	1.07	0.90	0.52	0.56	78.2	58.5	1.43	1.43
7.5% f_{Mc}, vpeti (brez testa 6)	1.12	1.09	0.91	0.76	0.44	0.48	66.3	49.6	1.21	1.21
Samo test št. 6	1.93	1.88	1.56	1.30	0.75	0.82	114.0	85.2	2.09	2.09
15% f_{Mc}, konzolno	1.86	1.74	1.05	0.89	0.76	0.71	57.1	43.5	2.19	2.19
15% f_{Mc}, vpeti	0.939	0.88	1.064	0.90	0.73	0.66	58.1	44.3	1.11	1.11

Kar se tiče doseženih maksimalnih pomikov, so povprečne vrednosti tako za strižni (zasuki 1.53%) kot tudi za upogibni mehanizem (zasuki 3.99%) precej večje od tistih, predpisanih v standardih. Mejni zasuki po EC8-3 za mejno stanje ”NC” (blizu porušitve) v primeru upogibnega mehanizma znašajo za testirane zidove 1.60% za konzolno vpete ter 0.80% za vpete, medtem ko po FEMA standardu 0.60% in 0.30%, za strižni mehanizem pa so vrednosti po EC8-3 0.53%. Tudi pomiki za mejno stanje ”DL”

(omejitev poškodb) ter ”SD” (večja poškodovanost) v standardih so precej manjši od dobljenih, pa najsi bodo prvi primerjani s pomiki na meji elastičnosti d_e ali s pomiki, kjer pride do prvih strižnih razpok d_{cr}. Dobljeni rezultati kažejo na to, da so morda vrednosti zasukov v standardih za historično zidovino, katere glavna karakteristika v primerjavi s sodobno zidovino je duktilna malta, prenizke.

S spremljanjem in analizo poškodovanosti ometov na zidovih so bila določena 4 karakteristična stanja poškodb, in sicer DS A1 – opaženo prvo odstopanje ometa od zidu, DS A2 - pojav prve razpoke na ometu, DS A3 – omet močno poškodovan in/ali ločen od zidu, a še vedno popravljiv ter DS A4 – porušitev ometa. Izkazalo se je, da so mejna stanja povezana z dobljenim porušnim mehanizmom zidu. V Preglednici 8.13 so za omenjena mejna stanja ometov za strižni in upogibni mehanizem priporočene vrednosti za nadaljnjo uporabo, ki temeljijo na dobljenih vrednosti pomikov za posamezna stanja ometov pri testih in so podani relativno na elastični pomik idealizirane krivulje odziva d_e, izračunane pa so kot 95% interval zaupanja (z minimalnim odstopanjem zaradi zaokroževanja).

Table 8.13: Proposal for plaster performance limit states estimation relative to elastic displacement of the bi-linear curve d_e with regard to predicted response of the wall for shear and rocking failure mechanism

Preglednica 8.13: Predlog ocene pomikov zidov za določitev mejnih stanj ometov glede na predvideni upogibni ali strižni mehanizem obnašanja zidov, podan v odvisnosti od elastičnega pomika bi-linearne krivulje d_e

	Mejno stanje obnašanja		
Porušni mehanizem	"DL"	"SD"	"NC"
Upogibni	1.3 d_e	4 d_e	/
Strižni	0.1 d_e	0.3 d_e	1.3 d_e

8.3 Sanacija in utrjevanje poškodovanih zidov s karakterizacijo uporabljenih materialov

V drugem sklopu doktorske naloge so bile, kot že rečeno, preskušane tehnike utrjevanja, pri čemer je bil velik poudarek na uporabi ukrepov in materialov, kompatibilnih s staro zidovino oziroma z materiali, ki jo sestavljajo. Določene zahteve glede materialov so pripeljale do lastnega, z izbranimi materiali še neizvedenega načina utrjevanja, in sicer s steklenimi vrvicami, vgrajenimi v horizontalne maltne spojnice. Predhodno so bili zidovi sanirani z linijskim injektiranjem.

8.3.1 Izbor sanacijskih in utrditvenih ukrepov

Ker so bili vsi zidovi po strižnih testih poškodovani, so bili vzdolž razpok linijsko injektirani z apneno-cementno malto (Slika 8.13). Ker je bilo jedro med zunanjima slojema kamnov precej zapolnjeno in ni imelo dovolj votlin, sistematično injektiranje niti ni bila ena od možnosti.

Slika 8.13: Injektiranje zidov z iztekanjem injekcijske mase in zidovi po injektiranju
Figure 8.13: Grouting of walls along the cracks with grout leakage and specimens after grouting

Da bi ohranili zunanjo teksturo zidov, je bila za utrjevanje izbrana namestitev steklenih vrvic v horizontalne maltne spojnice (Slika 8.14). Za namestitev utrditev pod površino zidov se uporablja akronim NSM (okrajšava za angleško poimenovanje utrjevanja "Near Surface Mounting"). Namestitev vrvic v horizontalni smeri je bila naravna glede na geometrijo zidov. Prednost uporabljenega sistema utrjevanja je uporaba upogljive vrvice namesto togih palic ali lamel, saj impregnacija na mestu utrjevanja omogoča njihovo oblikovanje v želeno obliko. Z njo bi torej bilo možno utrjevati tudi zidovino z manj pravilno teksturo. Steklena vlakna so bila uporabljena namesto karbonskih zato, ker so manj toga. V kolikor bi bila dobavljiva bazaltna vrvica dovolj majhnega premera, bi bila uporabljena le-ta. Z njo bi se izognili potencialni alkalno-silikatni reakciji pri uporabi steklenih vrvic. Steklena vlakna so bila impregnirana z epoksi smolo, za boljši oprijem namočena v kremenov presek in vgrajena v spojnice s podaljšano cementno malto, kljub običajni in s strani proizvajalcev priporočeni uporabi epoksidne malte. Vrvice niso bile sidrane, saj je bilo predpostavljeno, da naj bi bil stik vrvice z malto in zidom dovolj močan za prenos sil. Izpraznjene fuge so bile nato do konca zapolnjene z enako podaljšano cementno malto. Za primerjavo vpliva veziva za vgradnjo vrvic je bil NSM na enem zidu izveden po priporočilih podjetja, ki je proizvajalec vrvice ter ima na voljo tudi svoje komercialne sisteme utrjevanja zidov. Pri tem zidu je bila vrvica vgrajena z epoksidno malto, pri čemer vrvica ni bila namočena v pesek, ampak je bila spojnica predhodno premazana s temeljnim sprijemnim premazom (eng. "primer"). Fuge so bile zapolnjene z epoksidno malto. Pri tem zidu je bilo sidranje narejeno na način, da so se vrvice upognile v prečni del zidu v sami izpraznjeni fugi.

Število in premer vgrajenih vrvic sta bila optimizirana z oceno prispevka nosilnosti vrvic k nosilnosti neutrjenih zidov po priporočilih ACI [254].

Slika 8.14: Zid, pripravljen za NSM (delno izpraznjene in očiščene spojnice), vstavljanje vrvic v spojnice, zapolnitev spojnic z malto in prečno povezovanje zidov (od leve proti desni)
Figure 8.14: Wall prepared for NSM of cords (partially emptied and cleaned joints), inserting the cords into horizontal joints, repointed horizontal joints and transversal connecting of the wall with cords (from left to right)

Za omejitev izven-ravninskih deformacij in ločevanja posameznih slojev zidu ter zagotovitev monolitnega obnašanja zidov se kot utrditveni ukrep pri večslojnih zidovih uporablja prečno povezovanje slojev. Tudi pri izvedenem utrjevanju je bilo v nekaterih kombinacijah ukrepov za testiranje prečno utrjevanje na zidovih izvedeno, in sicer z enako stekleno vrvico kot za NSM, namočeno v epoksi smolo ter v kremenov pesek in vstavljeno v izvrtane prečne luknje v zidovih, ki so zaradi veliko lažje izvedbe bile narejene skozi horizontalne maltne spojnice (Slika 8.14). Pri vleki vrvic skozi zid je pri odprtinah nastal čep iz mivke (ki je vsebovala tudi smolo), kar smo na mestu predpostavili kot zadostno sidranje. Pri zidu, kjer je bil NSM izveden z epoksidno malto namesto podaljšane cementne, je bilo sidranje prečnih povezav zagotovljeno z razprostiranjem posameznih nitk vrvic na več strani v izpraznjene fuge.

Za primerjavo učinkovitosti posameznih ukrepov utrjevanja (injektiranje, NSM, prečno povezovanje) ter hkratno ugotavljanje učinkovitosti NSM utrditev z vrvico pri nekaterih variacijah aplikacije NSM, so bili posamezni ukrepi izvedeni le na določenih zidovih. Ker je testirano utrjevanje bilo primarno mišljeno za objekte kulturne dediščine, kjer zaradi zahtev konservatorjev posegi na obeh licih zidu pogosto niso možni zaradi zahtev po ohranitvi ometov, je ena izmed variant bila namenjena ugotavljanju učinkovitosti NSM, če je le-ta izveden le na eni strani (shema S3). Testiranje s shemo S6 je služilo za analizo učinkovitosti NSM v primeru, ko vrvica ni vgrajena v vsako vrsto, temveč v vsako drugo. Kombinacije utrjevanj zidov, namenjenih za strižne in tlačne preiskave, so prikazane v Preglednici 8.14.

Table 8.14: Retrofitting and strengthening combinations of the walls
Preglednica 8.14: Kombinacije utrditev zidov

Shema ukrepov Št. testa in ime		Predhodni test	Povezovalni kamni	Injektiranje	NSM	strani zidov (NSM)	Št. vrvic na posamezni strani (NSM)	NSM malta*	Prečno povezovanje
Zidovi za strižne teste									
S1	I (n)	2-SNk-7.5-1	NE	DA	NE	/	/	/	NE
S2	I (p)	13-SPk-15-2	DA	DA	NE	/	/	/	NE
S3	I.S1 (p)	1.2-SPk-5-7.5	DA	DA	DA	1	11	apn.-cem.	NE
S4	I.S2 (p)	4-SPv-7.5-1	DA	DA	DA	2	11	apn.-cem.	NE
S5	I.S2.P (p)	9-SPv-15-2	DA	DA	DA	2	11	apn.-cem.	DA
S6	I.S2-.P (n)	10-SNv-15-2	NE	DA	DA	2	6	apn.-cem.	DA
S7	I.P (n)	14-SNk-15-2	NE	DA	NE	/	/	/	DA
S8	I.S2e.P (n)	11-SNk-15-1	NE	DA	DA	2	11	epoksi	DA
Zidovi za tlačne teste									
T1	I (n)	3-SNv-7.5-1	NE	DA	NE	/	/	/	NE
T2	I.S2.P (n)	5-SNv-7.5-2	NE	DA	DA	2	11	apn.-cem.	DA
T3	(n)	8-SNv-15-1	NE	NE	NE	/	/	/	NE

* apn.-cem. je okrajšava za apneno-cementna

Razlaga imen utrditev

Prva črka in številka se nanašata na vrsto in zaporedno številko testa:

T*i* … tlačni test, kjer *i* predstavlja številko testa, S*i* … strižni test, kjer *i* predstavlja številko testa,

Naslednje oznake se nanašajo na vrsto utrditvenega ukrepa ter morfologijo zidov:

I … pove, ali je bil zid injektiran,

S … pove, ali je bil izveden NSM:

- 1 … vgradnja vrvic na eni strani zidov in
- 2 … vgradnja vrvic na obeh strani zidov,
- - … vgradnja vrvic v vsako drugo vrsto in
- e … uporaba epoksi malte namesto apneno-cementne (apn.-cem.) za vgradnjo vrvic;

P … pove, ali so zidovi prečno povezani (z vgradnjo prečnih vrvic),

(n) ali (p) … pove, ali gre za zid brez (n) ali z (p) povezovalnimi kamni

8.3.2 Karakterizacija uporabljenih materialov za utrjevanje

8.3.2.1 Injekcijska mešanica

Za linijsko injektiranje zidov je bila uporabljena komercialna apneno-cementna injekcijska mešanica z volumskim razmerjem cement : apno enako 0.75 : 0.25, vodovezivnim razmerjem 1.0 ter 2% superplastifikatorja. Glede na študijo injekcijskih mas v [252] je bila uporabljena relativno večja količina cementa. Poleg cementa so bile v predhodnih študijah za injektiranje [251] izvedeni preizkusi različnih mešanic na osnovi čistega apna (tako apnenega testa kot hidratiziranega apna) , hidravličnega apna, dodatkov tufa itd. Vendar pa v fazi pred utrjevanjem zidov lastnosti mešanic še niso bile zadovoljive s stališča začetnega kot tudi končnega krčenja, zaradi česar se je podvomilo v kakovost stika med injekcijsko mešanico in obstoječo zidovino.

Za uporabljeno mešanico so bili izvedene preiskave v svežem in strjenem stanju; gostota sveže mešanice 1378 kN/m^3 (test izveden po SIST EN 1015-6 [238]), izveden je bil test pretočnosti ter izločanja vode po SIST EN 445 [258], medtem ko so bile lastnosti strjene mešanice preizkušane na standardnih prizmah ter valjih, ki so posnemali notranjost zidov, pri starosti 22 dni. Na valjih je bila

določena tlačna trdnost 7.95 MPa, cepilna natezna trdnost 1.00 MPa (po SIST EN 12390-6:2001 [241]) ter elastični modul 12.4 MPa, medtem ko je tlačna trdnost prizem znašala 14.7 MPa (k.v. 6.27%), upogibna natezna pa 2.10 MPa (k.v. 8.02%) (po SIST EN 1015-11 [239]).

8.3.2.2 NSM steklene vrvice v horizontalne fuge

Za utrditev je bila uporabljena vrvica iz ne-impregniranih enosmernih steklenih vlaken premera 6 mm, ovitih z zaščitno mrežico. Podatki proizvajalca o vrvici so podani v Preglednici 8.15. Vrvica je bila impregnirana z dvokomponentno epoksidno smolo in v vseh primerih, razen pri zidu S8, posuta s kremenovim peskom z velikostjo zrn 1.0-2.0 mm.

Table 8.15: Technical data on the glass cord, provided by the producer
Preglednica 8.15: Tehnični podatki o vrvici s steklenimi vlakni

Vrsta vlaken	E-steklo
Gostota [g/cm^3]	2.62
Natezna trdnost [N/mm^2]	2560
Modul elastičnosti [GPa]	80.7
Deformacija pri pretrgu [%]	3–4
Ekvivalentna površina samih vlaken [mm^2] za Φ 6 mm in Φ 10 mm	15.70 26.79

Vrvice so bile, razen pri zidu za test S8, vgrajene z najbolj običajno in razširjeno podaljšano cementno malto z razmerjem cement : apno : agregat 1 : 1 : 6, pri čemer je bil uporabljen običajni cement CEM I, hidratizirano apno in agregat frakcije 0/2 mm. Za vgradnjo vrvic je bilo uporabljeno vodovezivno razmerje 0.63, za lažjo zapolnitev spojnic pa nekoliko večje, in sicer 0.77. Tlačna in upogibna natezna trdnost malte sta po 28 dneh znašali 9.29 MPa in 2.29 MPa.

Za zid 8 je bila za vgradnjo uporabljena dvokomponentna epoksidna malta, pred vgradnjo pa je bila površina kamna v spojnici, kot že omenjeno, premazana z dvokomponentnim temeljnim sprijemnim epoksidnim premazom.

V sklopu diplomske naloge Luke Božiča [255] se je preučevalo trdnost stika vrvica-malta-kamen pri uporabi različnih veziv ter tudi kamnin. V skladu z razpoložljivo opremo se je pripravil primeren način testiranja, ki je bil neke vrste izvlečni test. Priprava vzorcev in postavitev testa so vidni na Sliki 8.15. Izvedeni testi so med drugim pokazali, da sta trdnosti stika v primeru uporabe obeh malt v različnih velikostnih razredih; povprečna vrednost trdnosti stika za apneno-cementno malto 0.23 MPa in približno vsaj 10-krat višja za epoksidno malto, pri čemer pri testih s slednjo ni prišlo do porušitve stika, temveč do pretrga vrvice na mestu vpetja v PVC čep.

Slika 8.15: Priprava vzorcev za teste stika kamen-malta-vrvica: a) impregnirana in s kremenčevim peskom posuta steklena vrvica, vpeta v PVC čep, b) sušenje vrvic, c) nanos temeljno sprijemnega premaza (v primeru uporabe epoksi malte), d) vgradnja vrvice z izbrano malto, e) vertikalna namestitev vrvice v vzorcu, f) strjevanje vzorcev ter g) postavitev testa [255]

Figure 8.15: Preparation of samples for stone-mortar-cord junction tests: a) with epoxy resin impregnated cord coated with quartz sand and mounted with epoxy mortar in a PVC cap, b) hardening of the cords, c) application of the primer (in case of epoxy mortar), d) installing the cord with selected mortar, e) vertical positioning of the cord, f) hardening of the samples and g) test setup [255]

8.3.2.3 Prečno povezovanje zidov

Za povezovanje je bila uporabljena enaka vrvica kot za NSM, premera 6 mm, impregnirana ter posuta s kremenovim peskom.

8.3.3 Komentar

Utrjevanje je bilo izvedeno po načrtih z nekaj manjšimi spremembami. Potekalo je brez težav in izbrana komercialna injekcijska mešanica je bila enostavna za uporabo.

Večji zalogaj pa je predstavljajo NSM utrjevanje zidov in prečno povezovanje, posebno zato, ker tak način utrjevanja v Sloveniji ni pogost postopek. Delna izpraznitev spojnic je bila časovno precej potratna, saj uporaba krožne žage, s katero se običajno prazni fuge, v laboratoriju ni bila dovoljena. Za zelo praktično se je s stališča dela izkazala uporaba kremenovega posipa, saj je preprečevala pretirano kapljanje impregnacijske smole in s tem omogočila bolj estetski končni zgled. Slednji ni bil ravno najlepši pri utrjevanju zidu S8, kjer bi bilo potrebno sam postopek vgradnje vrvice z epoksidno malto nekoliko dodelati. Tako se je tudi s stališča vgrajevanja izkazala podaljšana cementna malta za ugodno, saj je na zidovih pustila manj madežev, ti pa so bili lažje odstranljivi. Edina šibka točka je bil razmeroma kratek razpoložljiv čas za vgrajevanje.

Pri prečnem povezovanju je bilo treba izvrtati večje luknje kot po načrtih; vrvica premera 6 mm, posuta s peskom, je bila komaj povlečena skozi odprtino premera 22 mm. V primeru, da spojnice ne bi

bile tako debele oziroma bi uporabili debelejši premer vrvice, bi bilo potrebno vrtanje skozi kamen, kar bi predstavljajo zahtevno nalogo v primeru močnega kamna in debelega zidu.

Predpostavljam, da bi z pogosto uporabo takega načina utrjevanja v praksi omenjeni problemi bili zelo hitro rešeni.

8.4 Rezultati testov utrjenih zidov in analiza učinkovitosti utrditev

8.4.1 Tlačni testi

Dva, pravzaprav trije, zidovi so bili tlačno testirani, pri čemer tretji ni bil utrjen, temveč je služil za določitev tlačne trdnosti poškodovanega, neutrjenega zidu. Preizkusi so bili narejeni z enako postavitvijo testa ter protokolom obremenjevanja kot pri preizkušanju neutrjenih zidov. Prav tako so bile deformacije merjene z 12 uporovnimi merilniki, razen pri testu neutrjenega zidu, kjer je zaradi nepredvidljivega obnašanja bilo nameščenih manj merilcev, pa še ti so bili tekom testa preventivno odstranjeni.

Slika 8.16: Poškodba zidov pri tlačnih testih: poškodovanost na licu zidu in razpoka med slojema na strani pri injektiranem zidu (levi dve) ter poškodovanost injektiranega, z NSM utrjenega ter povezanega zidu ter porušitev stika med malto in vrvico na sredini zidu (desni dve)

Figure 8.16: Damage of walls in compression tests: crack pattern and leaf separation on grouted wall (left two), damage of the grouted wall additionally strengthened by NSM of glass cords and transversally connected, failure of mortar-cord connection (right two)

Injektirani zid je dosegel tlačno trdnost f_{Mc} 6.55 MPa, z NSM dodatno utrjen in prečno povezan zid pa 7.18 MPa. Injektiranje je očitno dovolj dobro povezalo zidovje, da je bila dosežena f_{Mc} primerljiva z f_{Mc} nepoškodovanih zidov, glede na f_{Mc} poškodovanega zidu 4.66 MPa (test T3) pa kar 40% višja. Razpoke se niso pojavile le tam, kjer so že obstajale, temveč so nastale tudi nove. Ločevanje slojev je bilo bolj očitno na eni strani (Slika 8.16 levi dve). V primerjavi s samo injektiranim zidom (T1) so steklene vrvice v horizontalnih spojnicah omejile vzdolžne horizontalne deformacije zidu, hkrati pa so prečne povezave dovolile večje razpoke med sloji, kar je skupaj omogočilo doseg višje f_{Mc}. Na sredinskem delu zidu so vrvice odstopale od zidu, porušitev je večinoma potekala po stiku med malto za vgradnjo vrvice in samo vrvico. Na konceh zidu stik vrvice in zidu ni bil porušen (Slika 8.16, desni dve sliki).

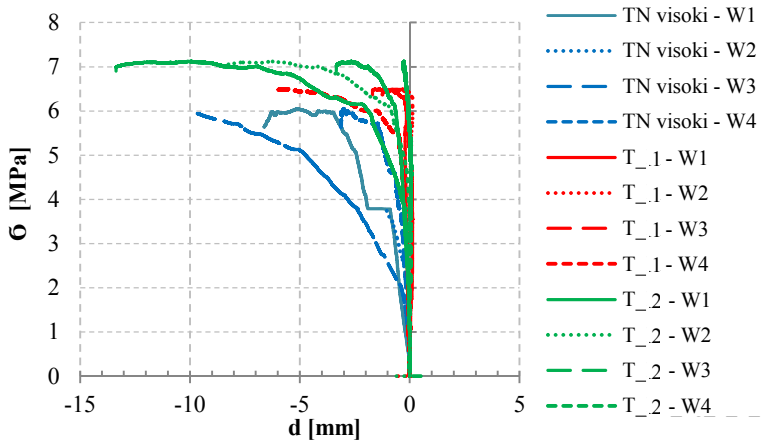

Slika 8.17: Diagram napetost - deformacije za prečne horizontalne LVDT-je (označene z W) za izvedene tlačne teste
Figure 8.17: Stress - displacement diagram for transversal horizontal LVDTs (labelled W) for performed compression tests

V Preglednici 8.16 so podani rezultati tlačnih testov ter razmerja glede na neutrjeni nepoškodovani ter poškodovani zid. Modula E_M in G_M sta izračunana po enakem postopku kot pri neutrjenih zidovih, za vrednosti G_M v Preglednici 8.16 pa so pri izračunu upoštevane tako vzdolžne kot prečne horizontalne deformacije zidov. Togostne karakteristike so se povečale tako pri utrjevanju za T1 kot tudi za T2, modula E_M in G_M sta več kot 2-krat višja za oba primera glede na neutrjeni zid. Glede na primerjavo rezultatov obeh utrjenih zidov lahko sklepamo, da gre povečanje predvsem na račun injektiranja in ne NSM utrditev.

Table 8.16: Results of compression tests
Preglednica 8.16: Rezultati tlačnih testov

	Test	σ_{max} [MPa]	Razmerje z neutrjenim (s poškodovanim)	E_M [MPa]	Razmerje z neutrjenim	G_M [MPa]	Razmerje z neutrjenim	G_M/E_M
T1	Injektirani zid	6.55	1.083 (1.40)	2254	2.33	929	2.60	0.412
T2	Injektirani, z NSM utrjeni zid	7.18	1.187 (1.54)	2219	2.29	914	2.56	0.412
T3	Neutrjeni zid (poškodovani)	4.66	0.771 (/)					

8.4.2 Strižni testi

Tudi za strižne teste je bila uporabljena enaka postavitev in protokol testiranja kot pri testih neutrjenih zidov, pri čemer so bili vsi testi narejeni pri višjem nivoju tlačnih obremenitev, robni pogoji pa so bili pri testih S1-S4 konzolni, pri testih S5-S8 pa vpeti. Tudi merilniki deformacij so bili postavljeni enako, dodan je bil horizontalni merilnik na polovici višine čez celo dolžino zidu, ki je neposredno meril velikost razpok na sredini zidu.

Z različnimi kombinacijami in variacijami utrditev smo v odvisnosti od robnih pogojev pri posameznih testih dobili različne porušne mehanizme, ki so povzeti v Preglednici 8.17. Naj omenimo, da je bil pri konzolnih robnih pogojih z aplikacijo NSM strižni porušni mehanizem spremenjen v upogibnega, pri vpetih se je v primeru testa S5 aktiviralo delovanje vrvice tako, da je prevzemala tudi obremenitve, pri aplikaciji NSM v vsako drugo spojnico se je aktiviral upogibni mehanizem z

drobljenjem pete, pri testu S8, kjer je bil NSM izveden z epoksi malto, pa je strižni mehanizem bil ponovno v celoti spremenjen v upogibnega.

Table 8.17: Summary of characteristic damage, obtained failure mechanisms and leaf separation of retrofitted/strengthened walls, tested in shear

Preglednica 8.17: Karakteristične poškodbe, prevladujoči porušni mehanizmi ter razslojitev slojev strižno testiranih utrjenih zidov

Št. testa	Ime	Robni pogoji	Opaženi mehanizmi	Prevladujoči porušni mehanizem	Razpoka med sloji oz. ločevanje slojev
1	S1 - I (n)	konzolni	Strižni, drobljenje pete	Strižni	Zmerno, po doseženi F_{max}
2	S2 - I (p)		Strižni	Strižni	Zmerno, po doseženi F_{max}
3	S3 - I.S1 (p)		Upogibni (strižni, drobljenje pete)	Mešani	Znatno, po doseženi F_{max}
4	S4 - I.S2 (p)		Upogibni, drobljenje pete	Upogibni	Majhno
5	S5 - I.S2.P (p)	vpeti	Strižni, drobljenje pete	Strižni	Znatno; zmerno pred doseženo F_{max}, progresivno po
6	S6 - I.S2-.P (n)		Strižni, drobljenje pete	Mešani	Znatno; zmerno pred doseženo F_{max}
7	S7 - I.P (n)		Strižni	Strižni	Zmerno (že pred doseženo F_{max})
8	S8 – I.S2e.P (n)		Upogibni	Upogibni	/

Dobljeni histerezni odziv je za nekatere teste prikazan na Sliki 8.18, prikazana pa je tudi primerjava histereznih ovojnic vseh testov. V Preglednici 8.17 so podane povprečne vrednosti sil in pomikov za obe smeri obremenjevanja v karakterističnih mejnih stanjih testa.

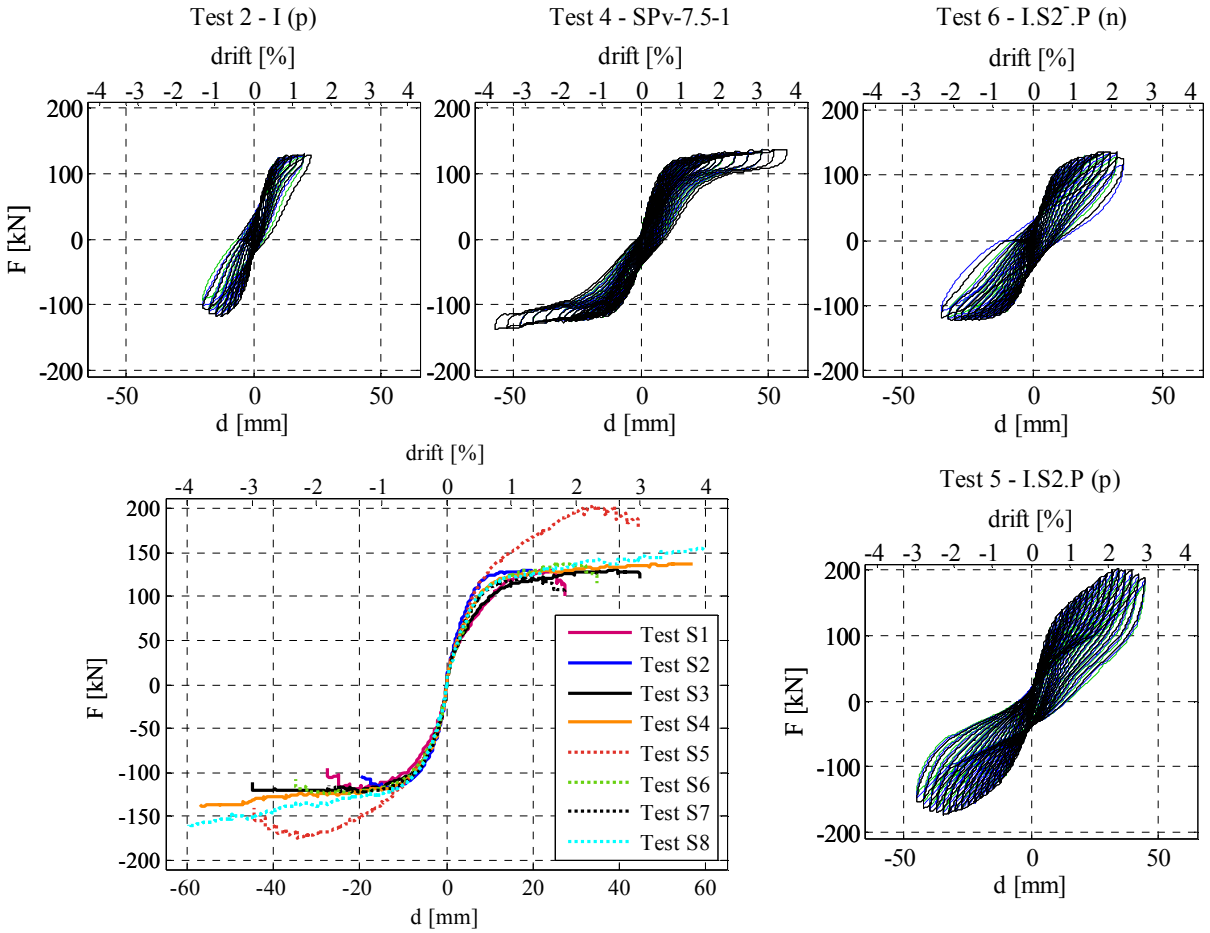

Slika 8.18: Histerezni odziv (horizontalna sila - horizontalni pomik) za teste različno utrjenih zidov, testiranih pri različnih robnih pogojih, ter primerjava histereznih ovojnic vseh strižnih testov utrjenih zidov (spodaj levo)

Figure 8.18: Hysteretic response (lateral load - lateral displacement) for tests of walls, strengthened with various measures, and comparison of hysteresis envelopes of all shear tests of strengthened walls (bottom left)

Table 8.18: Average characteristic values of force - displacement diagrams for both directions

Preglednica 8.18: Povprečne vrednosti karakterističnih točk odziva sila - pomik obeh smeri obremenjevanja utrjenih zidov

Mejno stanje	Prva strižna razpoka		Maksimalna sila		Maksimalni pomik	
Test	d_{cr} [mm]	F_{cr} [kN]	d_{Fmax} [mm]	F_{max} [kN]	d_{max} [mm]	F_{dmax} [mm]
Utrjeni						
S1 - I (n)	7.5	84.9	23.5	124.9	27.4	97.3
S2 - I (p)	3.0	65.4	17.3	124.1	21.1	115.8
S3 - I.S1 (p)	26.3	122.4	29.9	126.4	44.8	116.3
S4 - I.S2 (p)	5.0	79.4	54.7	137.5	57.1	136.3
S5 - I.S2.P (p)	14.8	142.5	34.3	188.7	44.5	158.4
S6 - I.S2-.P (n)	9.9	108.5	27.7	130.4	34.8	111.5
S7 - I.P (n)	12.4	115.4	18.8	122.9	27.3	109.5
S8 - I.S2e.P (n)	/	/	59.3	157.8	59.6	156.8
Neutrjeni (povprečje)						
11-14 konzolni	3.5	72.7	18.1	118.7	24.9	103.0
7-10 vpeti	3.2	70.1	14.8	123.0	21.1	91.7

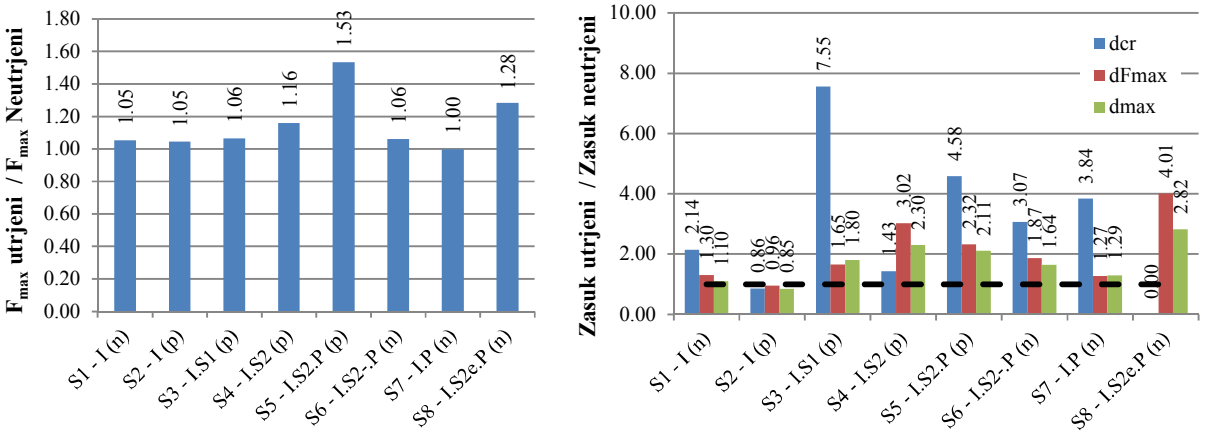

Slika 8.19: Primerjava mejnih rotacij utrjenih zidov s povprečnimi vrednostmi neutrjenih zidov
Figure 8.19: Comparison of drift limits of strengthened walls to average values of un-strengthened walls

Injektiranje z apneno-cementno malto je omogočilo doseg primerljivih strižnih nosilnosti in pomikov v primerjavi z neutrjenimi zidovi; natezna trdnost zidov se je povečala za 11%, medtem ko so bili mejni pomiki bolj poškodovanega zidu za 15% manjši kot pri neutrjenih, še vedno pa precej večji od priporočenih za strižni mehanizem v standardih (1.41% zasuka v primerjavi z 0.53% v EC8-3 in FEMA 273 predpisih).

Pri utrditvah z NSM je ponovno jasno, da so maksimalne sile in mejni zasuki odvisni od tega, kateri mehanizem se sproži. Maksimalne sile pri nobeni variaciji utrditve niso bile manjše od zidov neutrjenih. Pri testih S4 in S8, kjer je bil sprožen čisti upogibni mehanizem, so bile sile večje za 16% in 28%, so pa bili kot posledica upogibnega mehanizma doseženi maksimalni pomiki več kot 200% (230% test S4 in 282% test S8). Pri testih S3 in S6, kjer je bil NSM izveden le na eni strani zidu oziroma v vsaki drugi spojnici, NSM ni prispeval k dvigu nosilnosti (pri obeh povečanje nosilnosti za 6%) ali k spremembi mehanizma, so pa vrvice prispevale k povečanju mejnih pomikov, za 80% za test S3 ter za 64% za test S6. Pri testu S5, kjer je prišlo do strižnega mehanizma z delovanjem vrvice, je bila sila večja kar za 55% v primerjavi z neutrjenimi, mejni pomiki pa za 111%.

Ena od ugotovitev je, da je za tak tip zidov potrebna namestitev vrvic v vsako spojnico, v kolikor hočemo, da le te prenašajo del obremenitev in bistveno prispevajo k nosilnosti. Z namestitvijo v vsako drugo spojnico ali le na eno stran zidu se sicer povečajo pomiki, posebno v kolikor je spremenjen porušni mehanizem, večjega prirasta nosilnosti pa ne gre pričakovati, razen če se za refugiranje uporabi močnejša malta (kot pri testu S8)

8.4.3 Analitična ocena nosilnosti s FRP utrjenih zidov po obstoječih modelih in standardih

Narejena je bila primerjava rezultatov testov z različnimi modeli za izračun prispevka FRP utrditev V_f k nosilnosti neutrjenih zidov (URM zidovi) V_m, in sicer z uporabo predpisov (ACI 440.7R 2010 [220], CNR-DT 200/2004 [209] in CNR-DT 200 REV. 2013 [221]) ter modelov avtorjev, ki se lahko uporabijo za NSM utrjevanje (Triantafillou (1998) [212], Triantafillou et al (2000) [213,220], Nanni et al (2003) [214], Tumilian (2001) [179,213], Li (2005) [174], Wang (2006) [217]). Tumilian (2001) in

Li (2005) sta razvila modela specifično za NSM utrjevanje, medtem ko so bili ostali modeli razviti za utrjevanje zidov z lepljenjem FRP na zunanjo površino. Izračunani so bili tako prispevki FRP, kot tudi celotna strižna nosilnost V_{Rd}, saj različni modeli predpostavljajo tudi drugačen izračun V_m. Na Sliki 8.2 so prikazani rezultati, pri čemer oznaka na grafu "V_exp" predstavlja eksperimentalno dobljene rezultate (idealizirane nosilnosti F_{id}), relativna primerjava računskih rezultatov V_{Rd} z dobljenimi idealiziranimi nosilnostmi iz testov F_{id} pa je podana na Sliki 8.21.

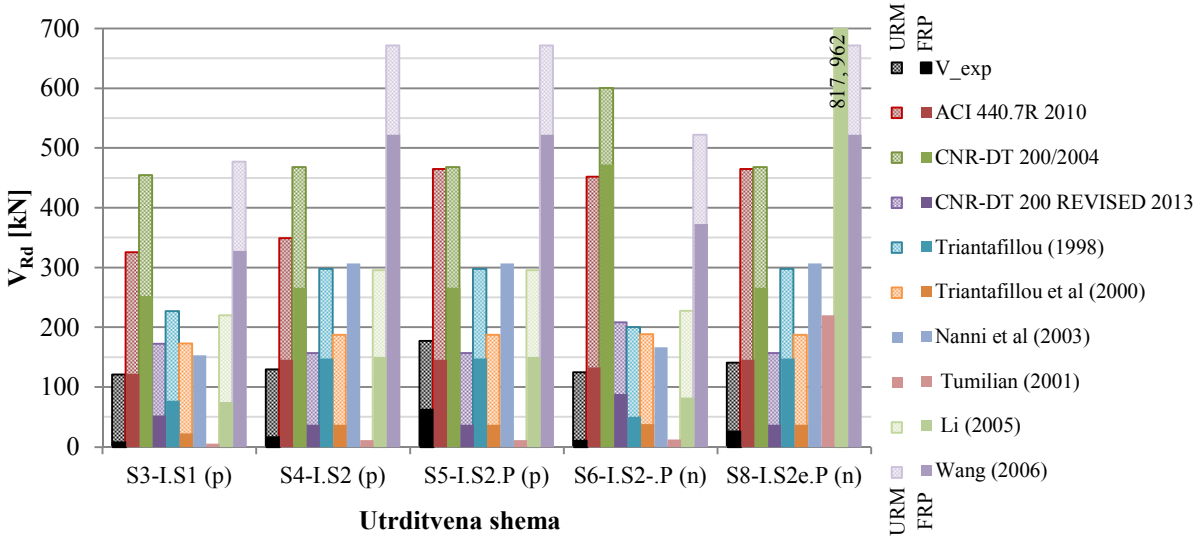

Slika 8.20: FRP prispevki in prispevki neutrjenih zidov k strižni nosilnosti zidov V_{Rd}, dobljeni iz testov in izračunani po različnih predpisih in modelih, za različne sheme utrditev

Figure 8.20: FRP and URM contributions to walls' total lateral resistance V_{Rd} obtained through tests and calculated according to various code provisions and models for various strengthening schemes

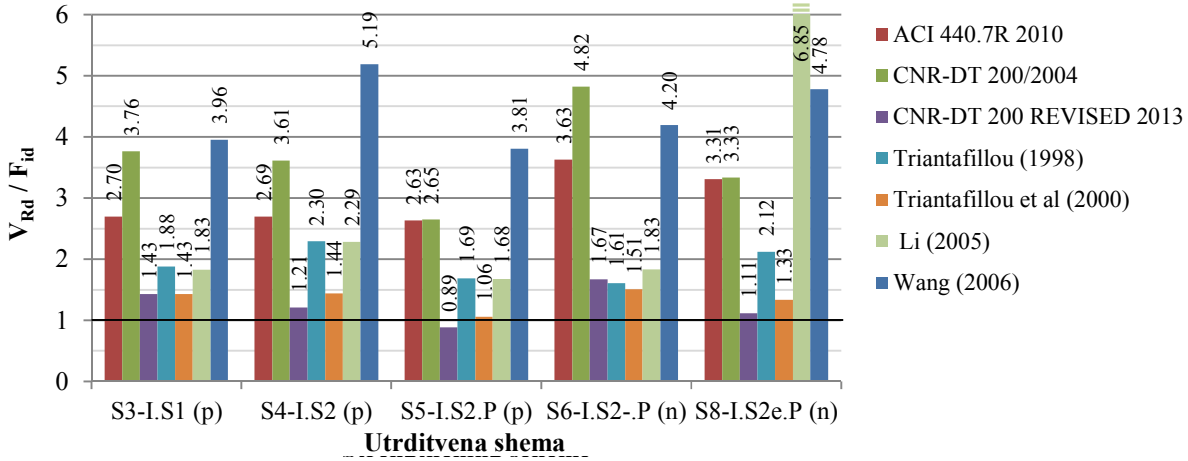

Slika 8.21: Razmerja celotnih strižnih nosilnosti zidov, izračunanih po različnih predpisih in modelih, z dobljenimi iz testov za različne sheme utrditev

Figure 8.21: Ratio of the total wall lateral resistances, calculated according to various code provisions and models, to the idealized lateral resistances obtained in the tests for various strengthening schemes

Primerjava pokaže, da za zidove, utrjene z NSM, po pričakovanju ne obstaja noben model za oceno nosilnosti, ki bi vsaj približno dobro ocenil učinkovitost v primeru različnih variacij ter robnih pogojev. Izračun V_f po modelih v CNR-DT 200 REV. 2013, Triantafillou (2000), ACI 440.7R 2010 in

Tumilian (2001) je sprejemljiv, v kolikor se dejansko sproži strižni mehanizem ter vrvice aktivirajo tako, da prevzamejo dodatne strižne sile.

Vendar pa je, kot je videti tudi iz rezultatov testov, porušni mehanizem težko z gotovostjo predpostaviti. Glede na rezultate bi bilo za zidane elemente, utrjene s FRP, pri numerični oceni prispevka FRP, namesto sile bolj varno povečati kapaciteto pomikov. To bi se lahko naredilo ali s povečanjem duktilnosti ali s povečanjem mejnih zasukov. Glede na rezultate testov je bilo v vseh primerih utrjevanja z NSM dobljeno povečanje pomikov za 64% (test S6) ali več. Glede na rezultate drugih avtorjev bi bilo smiselno povečanje mejnih zasukov zidov v primeru utrjevanja s FRP za koeficient 1.5.

8.5 Numerična analiza vpliva dobljenih eksperimentalnih rezultatov na potresno obnašanje dejanske zgodovinske stavbe

Dobljeni eksperimentalni rezultati so bili aplicirani na dejansko stavbo s čimer se je želel pokazati vpliv predpostavk mejnih pomikov na potresno obnašanje stavbe. Za analizo je bila izbrana vila Vipolže in sicer zato, ker je reprezentativna stavba z bogato zgodovino, poleg tega pa ima zelo podoben tip zidovine, kot je bil testiran v sklopu doktorske naloge. V vrhnjem nadstropju stavbe se nahajajo tudi freske (Slika 8.22 levo spodaj), tako je bilo možno aplicirati eksperimentalne rezultate mejnih stanj ometov na dejanski objekt in oceniti potresno obnašanje glede na poškodovanost fresk. Ker namen analize ni bil presojati dejansko stanje objekta, temveč predvsem pokazati vpliv mejnih pomikov ter prikazati primer analize obnašanja objekta pri potresu glede na različne zahteve, so bile nekatere lastnosti in detajli konstrukcije predpostavljeni, model pa nekoliko poenostavljen. Zato se naj tudi rezultatov ne smatra kot »točnih« oziroma nanašajočih se na dejansko stanje, temveč bolj kot ilustrativne.

8.5.1 Opis objekta

Del objekta, ki se ga danes smatra kot vilo, je bil v večjem delu zgrajen do konca 16. stoletja pod grofi Thurn, na začetku 17. stoletja pa preoblikovan v pozno renesančno oziroma manieristično vilo. En del južnega fasadnega zidu je del prvotnega gradu iz 12. stoletja. Objekt je 41 m dolg in 16.6 m širok, rahlo v obliki paralelograma. Ima 3-4 nadstropja. Glavnemu delo sta bila na vogalih severne fasade dograjena nadstropje nižja rombasta stolpa dimenzij 10 m x 11 m. Vertikalno nosilno konstrukcijo predstavljajo 82-140 cm debeli kamniti zidovi, s teksturo podobno testiranim, horizontalno nosilno konstrukcijo pa oboki nad pritličjem in leseni stropovi nad višjimi nadstropji ter leseno ostrešje.

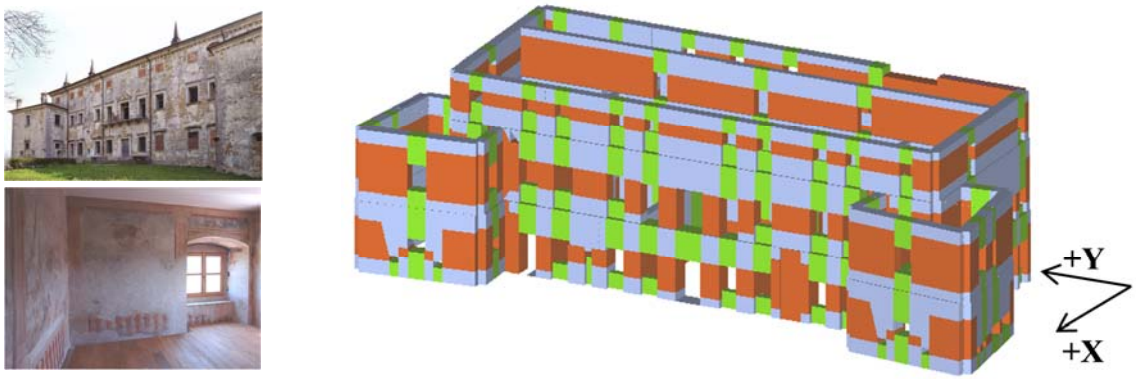

Slika 8.22: Severna fasada vile [268] (levo zgoraj) in freske v zgornjem nadstropju (levo spodaj), 3D model z ekvivalentnimi okvirji stavbe, z označenimi koordinatnimi osmi za analizo (desno)
Figure 8.22: North façade of the mansion [268] (upper left) and frescoes in the top floor (bottom left), equivalent frame 3D model of the structure with coordinate axes for the analysis (right)

8.5.2 Potresna analiza

Ocena potresnega obnašanja je bila narejena po EC predpisih z nelinearno statično ("potisno") analizo. Kot merilo za oceno je bil izbran projektni pospešek tal za tla kvalitete A, a_g. Projektni pospešek za potres s 475-letno povratno dobo za območje vile znaša 0.20 g. Spremenljiva obtežba na objektu je bila določena v skladu z EC1-1 [271], pri analizi je bilo ne glede na dejansko poznavanje objekta predpostavljeno dobro poznavanje stavbe, s čimer je bila vzeta vrednost faktorja zaupanja *CF* enaka 1.0 (za takšen faktor sicer potrebno dobro poznavanje konstrukcije, detajlov in materialov). Pri potisni analizi je bila upoštevana 5% ekscentričnost mase ter horizontalna porazdelitev sil v razmerju mas 1. nihajne oblike (na slikah označeno s "first mode") ter v razmerju dejanskih mas ("mass"), narejene pa so bile analize v vzdolžni (X) ter prečni (Y) smeri objekta s pozitivno in negativno usmerjenostjo.

3D model z ekvivalentnimi okvirji objekta je bil narejen v programu 3muri (Slika 8.22 desno), pri čemer je bilo upoštevano stanje objekta pred obnovo v zadnjih letih. V modelu so bila upoštevana nadstropja nad kletjo. Stropovi so bili modelirani nad pritličjem kot oboki, v višjih nadstropjih pa kot podajni leseni stropovi s strižno togostjo G=10 MPa. Vrednosti materialnih karakteristik zidov so bile enake povprečnim vrednostim, dobljenih pri testih. Predpostavljene pa so bile različne vrednosti mejnih zasukov zidov; pri analizi A1: EC sta bila mejna zasuka za strižni in upogibni mehanizem enaka vrednostim, določenim v EC (0.4% in 0.8%), pri A2: tests_min enaka minimalnim mejnim vrednostim, dobljenih pri eksperimentalnih testih (1.33% in 3.32%), pri A3: tests_ave pa povprečnim (1.53% in 3.99%). Kot kriterij mejnih sil je za strižni mehanizem bil upoštevan model diagonalne porušitve s predpostavljeno f_{Mt}.

Potisne krivulje so bile idealizirane v elasto-plastične krivulje po principu enake energije, pri čemer sta bila predpostavljena togost ter mejni pomik d_u (enak pomiku, kjer celotna strižna sila pade na 80% maksimalne). Iz kritičnih potisnih krivulj (glede na dosežene mejne a_g) so bila za vsako smer posameznih analiz analizirana mejna stanja pri majhni poškodovanosti (PL2), pri večji poškodovanosti objekta (PL3) ter stanje blizu porušitve objekta (PL4). Stanje PL2 je ustrezalo pomiku na meji elastičnosti d_e idealizirane krivulje, PL3 pomiku, enakemu 0.75 d_u, ter PL4 pomiku d_u.

8.5.2.1 Primerjava rezultatov za različno predpostavljene mejne zasuke zidov

Kritične potisne krivulje z označenimi točkami mejnih stanj DL2–DL4 so za posamezne analize za obe smeri prikazane na Sliki 8.23. Za bolj kritično se je izkazala prečna (Y) smer objekta. Mejni pospeški $a_{g,PLi}$, ki jih konstrukcija v Y smeri prenese za stanja PL2–PL4 za posamezne analize (A1-A3), so prikazani na Sliki 8.24.

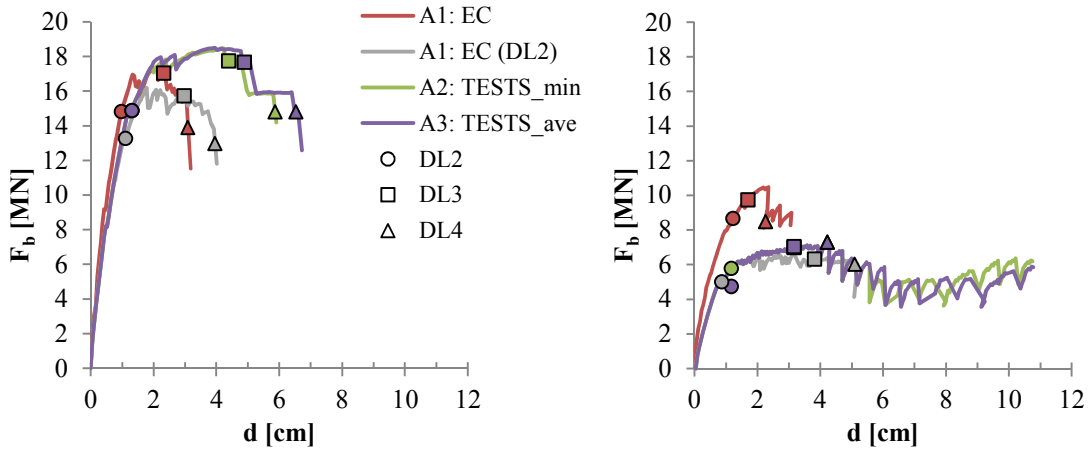

Slika 8.23: Potisne krivulje za X (levo) in Y (desno) smer analiz
Figure 8.23: Pushover curves for X (left) and Y (right) direction of analyses

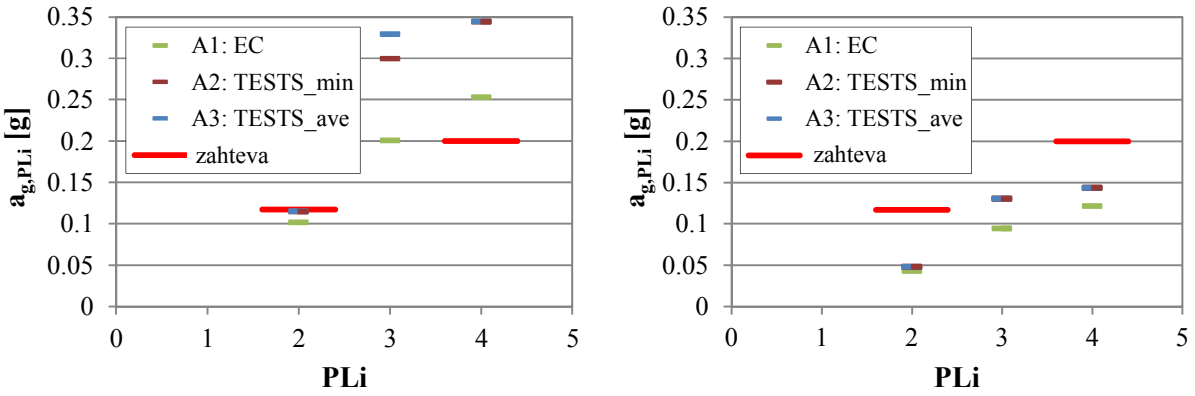

Slika 8.24: Vrednosti mejnih pospeškov tal za analizirana mejna stanja PLi, dobljena s tremi različnimi predpostavkami mejnih zasukov (A1-A3), za analize v X (levo) in Y (desno) smeri
Figure 8.24: Maximum ground accelerations the building can sustain for performance levels PLi, obtained with the three different drift capacity assumptions (A1-A3), for X (left) and Y (right) direction analyses

Vpliv predpostavk mejnih zasukov je viden. Če se pri analizi namesto mejnih zasukov po EC (A1: EC) upošteva minimalne zasuke, dobljene pri testih (A2: tests_min), se potresno obnašanje glede na $a_{g,PL4}$ izboljša za 36.4% v X in 18.1% v Y smeri. Pri povečanju zasukov na povprečne vrednosti iz testov (A2: tests_ave), se $a_{g,PL4}$ v smeri Y ne poveča. Pri določitvi rezultatov $a_{g,PL4}$ pri analizah A2 in A3 je prišla v poštev po italijanskih predpisih OPCM [245] določena omejitev ekvivalentnega faktorja obnašanja q^* na 3; v kolikor te omejitve ne bi bilo, bi se za primer A2 mejna $a_{g,PL4}$ v X in Y smeri povečala za 53.3% in 43.4%.

Poleg izboljšanja $a_{g,PL4}$ pa se je s povečanjem mejnih zasukov zidov znatno izboljšala predvsem duktilnost odziva; v X smeri se je duktilnost povečala za 41.4%, v Y smeri pa za 95.9%. Glede na rezultate bi bilo za bolj duktilno zidovino (kot je ponavadi zgodovinska) smiselno dodatno preučiti smotrnost povečanja mejnih vrednosti zasukov v predpisih.

8.5.2.2 Ocena potresnega obnašanja glede na konstrukcijske poškodbe objekta ter glede na poškodbe fresk

Glede na prej opisana mejna stanja poškodovanosti konstrukcije (PL2-PL4) ter glede na stanja poškodb fresk (zidov s freskami) so bili ocenjeni mejni pospeški $a_{g,PLi}$ ter pripadajoče povratne dobe potresov za primer A2: tests_min. Kritična mejna stanja zidov z ometi so bila: pomik, kjer pride do prve razpoke na ometu (PL1,AA), pomik, kjer je omet močno poškodovan (PL2,AA), ter pomik, kjer se omet poruši (PL3,AA). Velikost kritičnih pomikov je bila za dobljeni porušni mehanizem zidu določena glede na rezultate testov v odvisnosti od elastičnega pomika zidu d_e.

Freske se nahajajo v jugovzhodnem delu zgornje etaže na vzdolžnem notranjem zidu (P4) ter zunanjem prečnem zidu (P1). Za analizo poškodovanosti zidov z ometi so bile kontrolirane vse izvedene analize za posamezni primer, saj kritični rezultati glede na poškodovanost posameznih zidov ne sovpadajo nujno s kritičnimi rezultati glede mejnih $a_{g,PLi}$. Rezultati mejnih $a_{g,PLi}$ so za posamezna mejna stanja, določena glede na poškodovanost zidov z ometi (PL1,AA-PL3,AA) ter glede na poškodovanost konstrukcije (PL2-PL4), prikazani na Sliki 8.25.

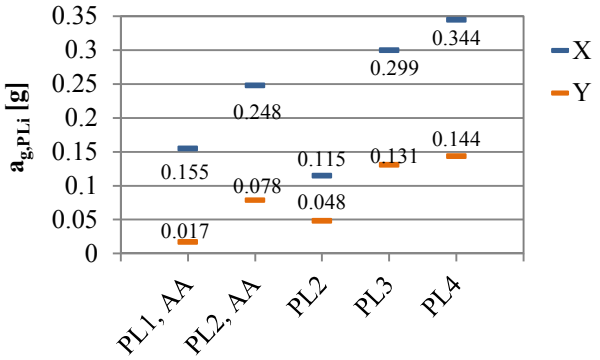

Slika 8.25: Maksimalni projektni pospeški tal, ki jih stavba prenese, za različna mejna stanja tako glede na konstrukcijske poškodbe (PLi) kot tudi na freske (PLi,AA), za A2: tests_min
Figure 8.25: Maximum design ground acceleration the building can sustain considering various performance levels with regard to structural damage (PLi) as well as to frescoes (PLi,AA) for A2: tests_min

Izkazalo se je, da do poškodb na zidovih pride relativno kasno ter da so le-te upogibne. Tako do same porušitve ometa (PL3,AA) oziroma zidu, ker je mehanizem upogibni, niti ne pride pred porušitvijo stavbe (PL4) za nobeno smer potresne analize. Bolj kritična je tudi tu smer Y; do prvih razpok na ometu (PL1,AA) pride v X smeri pri $a_{g,PL1,AA}$ 0.155 g in v Y smeri 0.017 g, medtem ko do večjih poškodb (PL3,AA) pri $a_{g,PL3,AA}$ 0.248 in 0.078 g.

8.6 Zaključki

Zaključke in izvirne prispevke znanosti raziskovalnega dela, s katerim je bilo študirano obnašanje neutrjenih troslojnih kamnitih zidov z ometi ter obnašanje utrjenih zidov in učinkovitost ukrepov, lahko strnemo v naslednjih točkah:

- Pri izvedenih štirih tlačnih in petnajstih strižnih cikličnih (v ravnini zidov) testih na zidovih za testiran tip troslojne kamnite zidovine prisotnost povezovalnih kamnov prečno preko slojev ni bistveno vplivala na obnašanje zidov ne pri tlačnih kot tudi ne pri strižnih obremenitvah v ravnini zidov.
- Za testirani tip troslojnih zidov do izven-ravninskega mehanizma pri strižnih obremenitvah v ravnini ni prišlo pred dosegom maksimalnih strižnih sil; do večjega razslojevanja je prišlo pri strižnem mehanizmu pri konzolnih robnih pogojih.
- Doseženi mejni zasuki zidov so bili za vse mehanizme poškodb oziroma porušitev veliko večji kot v predpisih; v povprečju 1.53% pri strižnem mehanizmu, 1.88% pri mešanem in 3.99% pri upogibnem. Analiza obnašanja je pokazala duktilno obnašanje zidov ne glede na porušni mehanizem. Strižni mehanizem, ki v splošnem velja za krhkega in neugodnega, je pokazal znatne pomike po dosegu nosilnosti; mejni pomik je bil v povprečju za 40 % večji od tistega, kjer je bila dosežena strižna nosilnost, pri čemer je vrednost sil pri porušitvi v povprečju znašala 80.2% nosilnosti.
- Ker izven-ravninski mehanizem za testirani tip zidov ni bil kritičen, so ocene za tlačnih trdnosti zidov po modelih za večslojno zidovino preveč konzervativne. Po drugi strani pa je zelo neprimeren tudi model v EC6, ki močno preceni trdnost. Ocena z modelom Tassios-a in Chronopoulos-a [41,42] za enoslojno zidovino je zelo dobra. Tudi ocene mejnih strižnih sil so z modeloma za mehanizma, ki sta bila izkazana (upogibni in diagonalni strižni), zelo dobre. Problem pa je, da z modeli za druge porušne mehanizme (z modelom za diagonalno strižno porušitev po spojnicah ter pri določenih pogojih tudi z modelom za zdrs) dobimo nižje nosilnosti.
- Za analitično oceno nosilnosti zidov iz več slojev, kjer so le-ti dobro povezani z malto, ne vsebujejo preveč praznin in debelina zunanjih sloje ne znaša manj kot 75% celotne debeline zidov, so rezultati boljši z upoštevanjem celotnega prereza zidov in ne le zunanjih slojev.
- Z analizo stanja poškodovanosti ometov na zidovih pri strižnih testih so bila definirana štiri karakteristična stanja poškodovanosti ter določeni mejni zasuki zidov, pri katerih je prišlo do posameznih poškodb. Kvantitativne vrednosti zasukov zidov z ometi (absolutne in relativne na dosežene elastične zasuke zidov) predstavljajo prve referenčne vrednosti, uporabne za analizo potresnega obnašanja zgodovinskih stavb z upoštevanjem kontrolnih stanj elementov s poslikavami.
- Zidovi so bili utrjeni z novim načinom utrjevanja in sicer po predhodnem linijskem injektiranju razpok z apneno-cementno injekcijsko mešanico so bile v horizontalne spojnice pod površino vstavljene steklene vrvice, impregnirane z epoksidno smolo ter za boljši oprijem posipane s kremenovim peskom. Vgrajene so bile z apneno-cementno malto. Zidovi so bili s steklenimi vrvicami tudi prečno povezani.
- Za posamezne zidove so bile variirane kombinacije in parametri utrditev. Z utrditvami so bili v nekaterih primerih spremenjeni porušni mehanizmi zidov. Pri testiranjih se je izkazalo, da se

vrvice aktivirajo tako, da prevzamejo same strižne obremenitve, le v primeru, da so vstavljene v vsako spojnico. V tem primeru se je maksimalna sila povečala za 53%, mejni zasuk pa za več kot 100%.

- V kolikor vrvice niso bile vstavljene v vsako horizontalno spojnico oziroma na obe strani zidov, do večjega povečanja sil ni prišlo, so se pa znatno povečali mejni zasuki zidov.
- Nobeden od analitičnih modelov za oceno doprinosa FRP utrditev k strižni nosilnosti zidov ne napove doprinosa zadovoljivo za vse primere. Vsi modeli predpostavljajo, da se FRP utrditve aktivirajo tako, da prevzemajo sile. Če se je slednje zgodilo, so dali zadovoljivo oceno dodatne nosilnosti modeli v CNR (popravljena verzija) [221], Triantafillou [213,220] in Tumilian [179].
- Glede na rezultate bi bilo bolj varno računsko upoštevati utrditev s FRP-ji s povečanjem mejnih zasukov oziroma duktilnosti zidov ali pa bi bilo treba podati določena priporočila, kako naj bo utrjevanje izvedeno, da se bo mehanizem res sprožil.

BLANK PAGE

»Ta stran je namenoma prazna.«

LITERATURE

[1] Lagomarsino, S., Cattari, S. 2015. PERPETUATE guidelines for seismic performance-based assessment of cultural heritage masonry structures. Bulletin of Earthquake Engineering. 13, 1: 13-47. 10.1007/s10518-014-9674-1.

[2] Kržan, M., Gostič, S., Bosiljkov, V. 2015. Application of different in-situ testing techniques and vulnerability assessment of Kolizej palace in Ljubljana. Bulletin of Earthquake Engineering. 13, 1: 389-410. 10.1007/s10518-014-9639-4.

[3] MIT. 2009. Istruzioni per l'applicazione delle nuove norme tecniche per le costruzioni di cui al Decreto Ministeriale 14 Gennaio 2008. Circ. C.S.Ll.Pp. No. 617 of 2/2/2009. Ministry of Infrastructures and Transportations.

[4] Binda, L., Saisi, A., Messina, S., Tringali, S. 2001. Mechanical damage due to long term behaviour of multiple-leaf pillars in Sicilian churches. In: P. B. Lourenço, P. Roca, (Ed.). 3rd International Seminar on Historical Constructions, Historical Constructions 2001, Possibilities of numerical and experimental techniques. Guimarães, Portugal, University of Minho: pp. 707-718.

[5] Binda, L., Cantini, L., Condoleo, P., Saisi, A. 2013. Non destructive testing techniques applied to the masonry and timber structures of the Crocifisso Church in Noto. Retrofitting of Heritage Structures: Design and Evaluation of Strengthening Techniques. S. Syngellakis, (Ed.). WIT Press: pp. 76-87.

[6] Silva, B., Dalla Benetta, M., da Porto, F., Modena, C. 2014. Experimental assessment of in-plane behaviour of three-leaf stone masonry walls. Construction and Building Materials. 53, 0: 149-161. http://dx.doi.org/10.1016/j.conbuildmat.2013.11.084.

[7] Debs, M. 2013. The Suffering of Symbols: Giotto Frescoes and the Cultural Trauma of Objects. Cultural Sociology. 7, 4: 479-494. 10.1177/1749975512454086.

[8] Priestley, M. 2000. Performance based seismic design. Bulletin of the New Zealand National Society for Earthquake Engineering. 33, 3: 325-346.

[9] US Building Seismic Safety Council. 1991. NEHRP recommended provisions for the development of seismic regulations for new buildings. Earthquake Hazard Reductions Series, US Federal Emergency Management Agency (FEMA).

[10] Calderini, C., Abbati, S. D., Cotič, P., Kržan, M., Bosiljkov, V. 2015. In-plane shear tests on masonry panels with plaster: correlation of structural damage and damage on artistic assets. Bulletin of Earthquake Engineering. 13, 1: 237-256. 10.1007/s10518-014-9632-y.

[11] ICOMOS/ISCARSAH. 2003. ICOMOS Charter–Principles for the analysis, conservation and structural restoration of architectural heritage. T. I. t. G. Assembly, (Ed.). Victoria Falls, Zimbabwe.

[12] Forsyth, M. (Ed.). 2008. Materials and Skills for Historic Building Conservation. Department of Architecture and Civil Engineering, University of Bath, Blackwell Publishing.

[13] Vitruvius, P. 1960. Vitruvius: the ten books on architecture. M. H. Morgan: translator, New York, Dover Publications p.

[14] Davies, N., Jokiniemi, E. 2008. Dictionary of architecture and building construction. Routledge p.

[15] Carbonara, G. 1996. Teoria e metodi del restauro. In: G. Carbonara, (Ed.). Trattato di restauro architettonico. Torino, Italy, Utet Scienze Tecniche. p. 107.

[16] Giuffrè, A. 1990. Letture sulla meccanica delle murature storiche (in Italian). Kappa, Rome, Italy, p.

[17] Binda, L., Penazzi, D., Saisi, A. 2003. Historic masonry buildings: necessity of a classification of structures and masonries for the adequate choice of analytical models. In. 6th International symposium on computer methods in structural masonry (STRUMAS VI). . Roma, Computers & Geotechnics Ltd,: pp. 168-173.

[18] Binda, L., Cardani, G. 2007. Linee guida per la compilazione della scheda di valutazione della qualita' muraria (in Italian). In: Proposta di una metodologia per la valutazione della qualità muraria, In: Reluis, progetto esecutivo 2005 – 2008.
[19] Lagomarsino, S., Magenes, G. 2009. Evaluation and Reduction of the Vulnerability of Masonry Buildings. In: G. Manfredi, M. Dolce, (Ed.). The state of earthquake engineering research in Italy: the ReLUIS-DPC 2005–2008 project. Doppiavoce, Naples, Italy. pp. 1-50.
[20] Borri, A. 2006. Proposta di una metodologia per la valutazione della qualità muraria. In: Reluis, progetto esecutivo 2006-2008, Progetto di ricerca n.1, Valutazione e riduzione della vulnerabilità sismica di edifici in muratura, rendicontazione scientifica 1°anno. 1.
[21] Bosiljkov, V., Maierhofer, C., Koepp, C., Wöstmann, J. 2009. Assessment of Structure Through Non-Destructive Tests (NDT) and Minor Destructive Tests (MDT) Investigation: Case Study of The Church at Carthusian Monastery at Žiče (SLOVENIA). International Journal of Architectural Heritage. 4, 1: 1-15. 10.1080/15583050902731031.
[22] Borri, A., De Maria, A. 2009. L'indice di Qualità Muraria (IQM): Evoluzione ed Applicazione nell'Ambito delle Norme Tecniche per le Costruzioni del 2008. In. 13th Italian national conference for earthquake engineering. Bologna, Italy.
[23] Lourenço, P., Hees, R., Fernandes, F., Lubelli, B. 2014. Characterization and Damage of Brick Masonry. In: A. Costa, J. M. Guedes, H. Varum, (Ed.). Structural Rehabilitation of Old Buildings, Springer Berlin Heidelberg: 4. pp. 109-130.
[24] Kržan, M., Gostič, S., Cattari, S., Bosiljkov, V. 2015. Acquiring reference parameters of masonry for the structural performance analysis of historical buildings. Bulletin of Earthquake Engineering. 13, 1: 203-236. 10.1007/s10518-014-9686-x.
[25] Moropoulou, A., Labropoulos, K., Konstanti, A., Roumpopoulos, K., Bakolas, A., Michailidis, P. 2006. Weathering. In: S. Kourkoulis, (Ed.). Fracture and Failure of Natural Building Stones, Springer Netherlands: 18. pp. 291-297.
[26] Peulić, Đ. 1976. Konstruktivni elementi zgrada. Dio 1. Zagreb, Croatia, Tehnička knjiga p.
[27] Jäger, W., Marzahn, G. 2010. Mauerwerk: Bemessung nach DIN 1053-100. Wiley-VCH Verlag GmbH & Co. KGaA: 537 p.
[28] Schubert, P. 2009. Eigenschaftswerte von Mauerwerk, Mauersteinen, Mauermörtel und Putzen. In: W. Jäger, (Ed.). Mauerwerk-Kalender 2009, Ernst & Sohn Verlag für Architektur und technische Wissenschaften GmbH, Berlin. pp. 1-27.
[29] Palomo, A., Blanco-Varela, M., Martinez-Ramirez, S., Puertas, F., Fortes, C. 2002. Historic mortars: characterization and durability. New tendencies for research. In. Advanced Research Centre for cultural heritage interdisciplinary projects. Fifth Framework Programme Workshop, Prague.
[30] Chidiac, S., Foo, S. 2000. Guidelines for the seismic assessment of stone-masonry structures. Public Works and Government Services Canada. Hull, Quebec, Canada: 111 p.
[31] Schäfer, J., Hilsdorf, H. K. 1993. Struktur und mechanische Eigenschaften von Kalkmörteln. In: F. Wenzel, (Ed.). Erhalten historisch bedeutsamer Bauwerke – Baugefüge, Konstrukionen, Werkstoffe. Berlin, Germany, Ernst & Sohn. pp. 65-76.
[32] Houben, H., Guillaud, H. 1994. Earth construction : a comprehensive guide. London, Intermediate Technology Publ. p.
[33] Müller, U., Gardei, A., Massah, S., Meng, B. 2008. Hydraulische Bindemittel (Hydraulic binders). In. Denk-mal an Beton! / Vereinigung der Landesdenkmalpfleger in der Bundesrepublik Deutschland., Petersberg, Michael Imhof Verlag: pp. 9-21.
[34] Magalhães, A., Veiga, R. 2009. Physical and mechanical characterisation of historic mortars. Application to the evaluation of the state of conservation. p.
[35] Bosiljkov, V., Kržan, M. 2012. Results of laboratory and in-situ tests on masonry properties and tables with mechanical parameters to be adopted in numerical modelling, PERPETUATE Project, Deliverable D15.
[36] Sabha, A., Neuwald-Burg, C. 1999. Assessment of the loadbearing capacity of historic masonry. In. International conference structural studies, repairs and maintenance of historical buildings: pp. 107-116.
[37] EN 1996-1-1: 2005. 2005. Eurocode 6: Design of masonry structures – Part 1-1: General rules for reinforced and unreinforced masonry structures. Brussels, Belgium, CEN.

[38] Binda, L., Fontana, A., Anti, L. 1992. Load transfer in multiple leaf masonry walls. In. International Workshop Effectiveness of injection techniques for retrofitting of stone and brick masonry walls in seismic areas,. Milan, Italy.

[39] Egermann, R. 1993. Investigation on the load bearing behaviour of multiple leaf masonry. IABSE reports = Rapports AIPC = IVBH Berichte. 70. 10.5169/seals-53311.

[40] Binda, L., Pina-Henriques, J., Anzani, A., Fontana, A., Lourenço, P. B. 2006. A contribution for the understanding of load-transfer mechanisms in multi-leaf masonry walls: Testing and modelling. Engineering Structures. 28, 8: 1132-1148. 10.1016/j.engstruct.2005.12.004.

[41] Tassios, T., Chronopoulos, M. 1986. Aseismic dimensioning of interventions on low-strength masonry buildings. In. Middle east and mediterranean regional conference on low strength masonry in seismic areas. Middle East Technical University, Ankara.

[42] Tassios, T. 2004. Recupero di murature tri-strato (Rehabilitation of three-leaf masonry). Evoluzione nella sperimentazione per le costruzioni, seminario internazionale. Bolzano, Italy: pp. 137-63.

[43] Korpič, J. 2012. Eksperimentalne tlačne preiskave večslojnih kamnitih zidov diplomska naloga. B.Sc. Thesis. Ljubljana, University of Ljubljana p.

[44] Uranjek, M. 2011. Propadanje in trajnostna obnova ovoja stavbne dediščine doktorska disertacija = Degradation and Sustainable Renovation of Heritage Buildings Envelope : doctoral thesis. PhD Thesis. Ljubljana, University of Ljubljana: 219 p.

[45] Magenes, G., Galasco, A., Penna, A., Da Paré, M. 2010. In-plane cyclic shear tests of undressed double leaf stone masonry panels (paper no. 1435). In. 14th European conference on earthquake engineering. . Ohrid, FYROM.

[46] Tomaževič, M. 1999. Earthquake-resistant design of masonry buildings. London, UK, Imperial College Press: 268 p.

[47] Bosiljkov, V., Totoev, Y. Z., Nichols, J. M. 2005. Shear modulus and stiffness of brickwork masonry: an experimental perspective. Structural engineering and mechanics. 20, 1: 21-43.

[48] Elmenshawi, A., Duchesne, D., Paquette, J., Mufti, A., Jaeger, L., Shrive, N. 2011. Elastic moduli of stone masonry based on static and dynamic tests. In. 11th NAMC. Minneapolis, USA.

[49] EN 1998-3: 2005. 2005. Eurocode 8: Design of structures for earthquake resistance – Part 3: Assessment and retrofitting of buildings. Brussels, CEN.

[50] Bosiljkov, V. 2000. Eksperimentalne in računske raziskave vpliva modificiranih malt na mehanske lastnosti opečne zidovine : doktorska disertacija št. 128. PhD Thesis. Ljubljana, Slovenia, University of Ljubljana.

[51] Bosiljkov, V., Bokan-Bosiljkov, V., Strah, B., Velkavrh, J., Cotič, P. 2010. Review of innovative techniques for the knowledge of cultural assets, PERPETUATE Project, Deliverable D6.

[52] Calderini, C., Cattari, S., Lagomarsino, S. 2010. The use of the diagonal compression test to identify the shear mechanical parameters of masonry. Construction and Building Materials. 24, 5: 677-685. http://dx.doi.org/10.1016/j.conbuildmat.2009.11.001.

[53] Lourenco, P. 2012. Non-linear numerical modelling of masonry, Part I: Masonry Behavior and Modeling (invited lecture). 15th IBMAC. Florianopolis, Brazil.

[54] Turnšek, V., Čačovič, F. 1971. Some experimental results on the strength of brick masonry walls. In: H. W. H. West, K. H. Speed, (Ed.). 2nd International Brick Masonry Conference. Stoke-on-Trent, London, England, Brick Development Association, British Ceramic Research Association: pp. 149-156.

[55] Bosiljkov, V., Page, A., Bokan-Bosiljkov, V., Žarnić, R. 2003. Performance based studies of in-plane loaded unreinforced masonry walls. Masonry International. 16: 39-50.

[56] Magenes, G. 1992. Seismic behavior of brick masonry: strength and failure mechanism. PhD, University of Pavia.

[57] Corradi, M., Borri, A., Vignoli, A. 2008. Experimental Evaluation of In–plane Shear Behaviour of Masonry Walls Retrofitted Using Conventional and Innovative Methods. Masonry International. 21, 1: 1-48.

[58] ASTM. 2002. ASTM E 519-02: Standard test method for diagonal tension (shear) in masonry assemblages. Annual Book of ASTM Standard. American Society for Testing and Materials.

[59] Brignola, A., Frumento, S., Lagomarsino, S., Podestà, S. 2008. Identification of Shear Parameters of Masonry Panels Through the In-Situ Diagonal Compression Test. International Journal of Architectural Heritage. 3, 1: 52-73. 10.1080/15583050802138634.

[60] NTC08. 2008. D.M. 14 gennaio 2008—Norme tecniche per le costruzioni (in Italian). Ministero delle Infrastrutture.

[61] Willsdon, C. A. P. 2000. Mural Painting in Britain 1840-1940: Image and Meaning. Oxford University Press p.

[62] Ignatiev, N., Chatterji, S. 1992. On the mutual compatibility of mortar and concrete in composite members. Cement and Concrete Composites. 14, 3: 179-183. http://dx.doi.org/10.1016/0958-9465(92)90011-J.

[63] Kovler, K., Frostig, Y. 1998. On the problem of cracking in plaster layers. Construction and Building Materials. 12, 5: 251-258. http://dx.doi.org/10.1016/S0950-0618(98)00013-0.

[64] Suo, Z., Hutchinson, J. 1990. Interface crack between two elastic layers. International Journal of Fracture. 43, 1: 1-18. 10.1007/BF00018123.

[65] Hutchinson, J. W., Suo, Z. 1991. Mixed mode cracking in layered materials. Advances in applied mechanics. 29: 63-191.

[66] Li, S., Wang, J., Thouless, M. D. 2004. The effects of shear on delamination in layered materials. Journal of the Mechanics and Physics of Solids. 52, 1: 193-214. http://dx.doi.org/10.1016/S0022-5096(03)00070-X.

[67] Cotterell, B., Chen, Z. 2000. Buckling and cracking of thin films on compliant substrates under compression. International Journal of Fracture. 104, 2: 169-179. 10.1023/A:1007628800620.

[68] Yu, H.-H., Hutchinson, J. 2002. Influence of substrate compliance on buckling delamination of thin films. International Journal of Fracture. 113, 1: 39-55. 10.1023/A:1013790232359.

[69] FEMA P-58-1. 2012. Seismic performance assessment of buildings, volume 1-methodology. P-58-1 Washington, DC, Applied Technology Council.

[70] ASCE/SEI 41-13. 2014. Seismic Evaluation and Retrofit of Existing Buildings. American Society of Civil Engineers.

[71] Freeman, S., Nicoletti, J., Tyrell, J. 1975. Evaluations of existing buildings for seismic risk–A case study of Puget Sound Naval Shipyard, Bremerton, Washington. In. Proceedings of the 1st US National Conference on Earthquake Engineering, Earthquake Engineering Research Institute Oakland, CA: pp. 113-122.

[72] Fajfar, P. 2000. A nonlinear analysis method for performance-based seismic design. Earthquake spectra. 16, 3: 573-592.

[73] Cattari, S., Lagomarsino, S., D'Ayala, D., Novelli, V., Bosiljkov, V. 2012. Correlation of perfomance levels and damage states for types of buildings, PERPETUATE Project, Deliverable D17.

[74] Calderini, C., Cattari, S., Lagomarsino, S., Rossi, M. 2010. Review of existing models for global response and local mechanisms, PERPETUATE Project, Deliverable D7.

[75] Lagomarsino, S., Abbas, N., Calderini, C., Cattari, S., Rossi, M., Ginanni Corradini, R., Marghella, G., Mattolin, F., Piovanello, V. 2011. Classification of cultural heritage assets and seismic damage variables for the identification of performance levels. In. 12th international conference on structural studies, repairs and maintenance of heritage architecture (STREMAH). Chianciano Terme, Italy, WIT Trans Built Environ: pp. 697–708.

[76] Magenes, G., Calvi, G. M. 1997. In-plane seismic response of brick masonry walls. Earthquake Engineering & Structural Dynamics. 26, 11: 1091-1112. 10.1002/(SICI)1096-9845(199711)26:11<1091::AID-EQE693>3.0.CO;2-6.

[77] Page, A. 1981. The biaxial compressive strength of brick masonry. ICE Proceedings: pp. 893-906.

[78] Page, A. 1983. The Strength of Brick Masonry under Biaxial CompressionTension. International Journal of Masonry Construction. 3, 1: 26-31.

[79] Tomaževič, M. 1987. Masonry buildings in seismic regions (in Slovenian). Ljubljana, Faculty of Arhitecture, Civil Engineering and Geodesy p.

[80] Yi, T. 2004. Experimental investigations and numerical simulation of an unreinforced Masonry structure with flexible diaphragms. PhD..

[81] Paulay, T., Priestley, M. J. N. 1992. Seismic design of reinforced concrete and masonry buildings. New York, USA, Wiley: 744 p.
[82] Mendes, N. 2012. Seismic assessment of ancient masonry buildings : shaking table tests and numerical analysis. PhD, University of Minho.
[83] Johnson, F. B., Thompson, J. N. 1969. Development of diametral testing procedures to provide a measure of strength characteristics of masonry assemblages. In: F. B. Johnson, (Ed.). Designing, engineering and constructing with masonry products. Houston, Texas, USA, Gulf Publishing Company. pp. 51-57.
[84] Samarasinghe, W. 1980. The In-Plane Failure of Brickwork. PhD Thesis. Edinburgh, UK, University of Edinburgh: 225 p.
[85] Samarasinghe, W., Hendry, A. 1982. The strength of brickwork under biaxial tensile and compressive stress. In. Int. Symp. on Load-Bearing Brick Work. London, UK, British Ceramic Society: pp. 129-139.
[86] Page, A. W. 1982. An Experimental Investigation of the Biaxial Strength of Brick Masonry. In. 6th International Brick Masonry Conference. Rome, Italy: pp. 3-15.
[87] Hamid, A., Drysdale, R. 1980. Behaviour of brick masonry under combined shear and compression loading. In. 2nd Canadian Masonry Symposium. Ottawa, Canada: pp. 57-64.
[88] Ganz, H. R., Thürlimann, B. 1982. Versuche über die Festigkeit von zweiachsig beanspruchtem Mauerwerk, Bericht Nr. 7502-3. 3-7643-1339-0. 61 S. Zürich, Switzerland, Institut für Baustatik und Konstruktion ETH Zürich
[89] Dhanasekar, M., Page, A., Kleeman, P. 1985. The failure of brick masonry under biaxial stresses. In. Institution of Civil Engineers (ICE). London, UK, Thomas Telford: pp. 295-313.
[90] Ganz, H. 1985. Mauerwerksscheiben Unter Normalskraft Und Schub. Bericht Nr. 148. Zürich, Switzerland, Institut Fur Baustatik Und Konstruktion ETH.
[91] Ganz, H. 1989. Failure criteria for masonry. In. 5th Canadian Masonry Symposium. Vancouver, BC, Canada, University of British Columbia: pp. 65-76.
[92] Tassios, T. P., Vachliotis, C. 1989. Failure of masonry under heterosemous biaxial stresses. In. Structural conservation of stone masonry. International technical conference. Athens, Greece, ICCROM: pp. 273-282.
[93] Andreaus, U., Ceradini, G. 1992. Failure modes of solid brick masonry under in-plane loading. Masonry International. 6, 1: 4-8.
[94] Tomaževič, M., Lutman, M., Petković, L. 1996. Seismic Behavior of Masonry Walls: Experimental Simulation. Journal of Structural Engineering. 122, 9: 1040-1047. doi:10.1061/(ASCE)0733-9445(1996)122:9(1040).
[95] FEMA 306. 1998. Evaluation of earthquake damaged concrete and masonry wall buildings. Basic procedures manual. USA, Applied Technology Council for the Federal Emergency Management Agency.
[96] Petry, S., Beyer, K. 2015. Limit states of modern unreinforced clay brick masonry walls subjected to in-plane loading. Bulletin of Earthquake Engineering. 13, 4: 1073-1095. 10.1007/s10518-014-9695-9.
[97] Abrams, D., Smith, T., Lynch, J., Franklin, S. 2007. Effectiveness of Rehabilitation on Seismic Behavior of Masonry Piers. Journal of Structural Engineering. 133, 1: 32-43. doi:10.1061/(ASCE)0733-9445(2007)133:1(32).
[98] Vasconcelos, G. d. F. M. 2005. Experimental investigations on the mechanics of stone masonry: characterization of granites and behaviour of ancient masonry shear walls. PhD Thesis. Guimarães, Portugal Universidade do Minho: 276 p.
[99] Abrams, D. P. 2001. Performance-based engineering concepts for unreinforced masonry building structures. Progress in Structural Engineering and Materials. 3, 1: 48-56. 10.1002/pse.70.
[100] Anthoine, A., Magenes, G., Magonette, G. 1994. Shear compression testing and analysis of brick masonry walls. In: G. Duma, (Ed.). 10th European Conference on Earthquake Engineering. Vienna, Austria, Balkema: pp. 1657–1662.
[101] Bosiljkov, V., Tomaževič, M. 2005. Optimization of shape of masonry units and technology of construction for earthquake resistant buildings, Research Report - part three. Slovenia, Ljubljana, ZAG Ljubljana.

[102] Gouveia, J. P., Lourenco, P. B. 2009. Masonry Shear Walls subjected to Cyclic Loading: Influence of Confinement and Horizontal Reinforcement. In. 10th North American Masonry Conference. St. Louis, Missouri, USA.

[103] Tomaževič, M. 2007. Damage as a measure for earthquake-resistant design of masonry structures: Slovenian experienceThis article is one of a selection of papers published in this Special Issue on Masonry. Canadian Journal of Civil Engineering. 34, 11: 1403-1412. 10.1139/L07-128.

[104] Vasconcelos, G., Lourenço, P. B. 2009. Experimental characterization of stone masonry in shear and compression. Construction and Building Materials. 23, 11: 3337-3345. http://dx.doi.org/10.1016/j.conbuildmat.2009.06.045.

[105] Bosiljkov, V., Page, A. W., Bokan-Bosiljkov, V., Zarnic, R. 2010. Review Paper, Progress in Structural Engineering and Material: Structural Masonry. Structural Control & Health Monitoring. 17, 1: 100-118. 10.1002/stc.299.

[106] Rota, M., Penna, A., Magenes, G. 2010. A methodology for deriving analytical fragility curves for masonry buildings based on stochastic nonlinear analyses. Engineering Structures. 32, 5: 1312-1323. http://dx.doi.org/10.1016/j.engstruct.2010.01.009.

[107] Augenti, N., Parisi, F., Acconcia, E. 2012. MADA: Online experimental database for mechanical modelling of existing masonry assemblages. In. 15th World Conference on Earthquake Engineering. Lisbon, Portugal: 10 p.

[108] Tomaževič, M., Lutman, M., Bosiljkov, V. 2006. Robustness of hollow clay masonry units and seismic behaviour of masonry walls. Construction and Building Materials. 20, 10: 1028-1039. http://dx.doi.org/10.1016/j.conbuildmat.2005.05.001.

[109] Petry, S., Beyer, K. 2014. Influence of boundary conditions and size effect on the drift capacity of URM walls. Engineering Structures. 65, 0: 76-88. http://dx.doi.org/10.1016/j.engstruct.2014.01.048.

[110] Čeru, A. 1996. HISPA-programsko orodje za analizo histereznega odziva konstrukcij (in Slovenian). undergraduate Thesis. Ljubljana, University of Ljubljana: 158 p.

[111] Abdel-Halim, M. A. H., Barakat, S. A. 2003. Cyclic Performance of Concrete-Backed Stone Masonry Walls. Journal of Structural Engineering. 129, 5: 596-605. doi:10.1061/(ASCE)0733-9445(2003)129:5(596).

[112] Shing, P., Noland, J., Klamerus, E., Spaeh, H. 1989. Inelastic Behavior of Concrete Masonry Shear Walls. Journal of Structural Engineering. 115, 9: 2204-2225. doi:10.1061/(ASCE)0733-9445(1989)115:9(2204).

[113] Chopra, A. K. 1995. Dynamics of Structures: Theory and Applications to Earthquake Engineering. Englewood Cliffs, New Jersey, Prentice Hall, Englewood Cliffs, p.

[114] Jacobsen, L. S. 1930. Steady forced vibration as influenced by damping. Transactions of ASME 52: 13.

[115] Sinha, B., Hendry, A. 1969. Racking tests on storey-height shear-wall structures with openings, subjected to pre-compression. In: F. B. Johnson, (Ed.). Designing, engineering and constructing with masonry products: Proceedings. Houston, Texas, USA, Gulf Publication Co. pp. 192-199.

[116] Yokel, F. Y., Fattal, S. G. 1976. Failure hypothesis for masonry shear walls. Journal of the Structural Division. 102, 3: 515-532.

[117] Hegemeir, G. A., Nunn, R. O., Arya, S. K. 1978. Behavior of Concrete Masonry under Biaxial Stress. In. 1st North American Masonry Conference. Boulder, Colorado, USA: pp. 1-24.

[118] Hamid, A. A., Drysdale, R. G. 1981. Proposed Failure Criteria for Concrete Block Masonry under Biaxial Stresses. ASCE J Struct Div. 107, 8: 1675-1687.

[119] Mann, W., Müller, H. 1982. Failure of shear-stressed masonry - an enlarged theory, tests and application to shear walls. In: H. W. H. West, (Ed.). Proceedings of the British Ceramic Society: Load-Bearing Brickwork, British Ceramic Society. pp. 223-235.

[120] Ganz, H., Thürlimann, B. 1984. Bruchbedingung Fur Zweiachsig Beanspruchtes Mauerwerk (Tests on masonry walls under normal and shear loading), Bericht Nr. 143. Zürich, Switzerland, Institut Fur Baustatik Und Konstruktion ETH.

[121] Drysdale, R. G., Hamid, A. A. 1984. Tension Failure Criteria for Plain Concrete Masonry. Journal of Structural Engineering. 110, 2: 228-244. doi:10.1061/(ASCE)0733-9445(1984)110:2(228).
[122] Daou, Y., Hobbs, B. 1991. Strength of brickwork loaded in different orientations. In. Brick and Block Masonry. Berlin, Germany: pp. 157-163.
[123] Dialer, C. 1991. Some remarks on the strength and deformation behaviour of shear stressed masonry panels under static monotonic loading. In. 9th IBMAC. Berlin, German: pp. 276-283.
[124] Andreaus, U. 1996. Failure Criteria for Masonry Panels under In-Plane Loading. Journal of Structural Engineering. 122, 1: 37-46. doi:10.1061/(ASCE)0733-9445(1996)122:1(37).
[125] Seim, W., Schweizerhof, K. 1997. Nichtlineare FE-Analyse eben beanspruchter Mauerwerkscheiben mit einfachen Werkstoffgesetzen (Teil 1). Beton-und Stahlbetonbau. 92, 8: 201-207.
[126] Calderini, C., Cattari, S., Lagomarsino, S. 2009. In-plane strength of unreinforced masonry piers. Earthquake Engineering & Structural Dynamics. 38, 2: 243-267. 10.1002/eqe.860.
[127] Ganz, H. R., Thürlimann, B. 1985. Plastic strength of masonry shear walls", Proc. Of the 7th International Brick Masonry Conf. In. Melbourne, Australia: pp. 837-846.
[128] Ur. list SRFJ št.31. 1981. Pravilnik o tehničnih normativih za graditev objektov visoke gradnje na seizmičnih območjih.
[129] DIN 1053-1: 1996-11. 1996. Mauerwerk - Teil 1: Berechnung und Ausführung. Berlin, Institut für Normung e.V.: Beuth Verlag.
[130] SIA 266: 2003. 2003. Structural masonry. Swiss Society of Architects and Engineers. Zürich.
[131] Lagomarsino, S., Penna, A., Galasco, A., Cattari, S. 2013. TREMURI program: An equivalent frame model for the nonlinear seismic analysis of masonry buildings. Engineering Structures. 56, 0: 1787-1799. http://dx.doi.org/10.1016/j.engstruct.2013.08.002.
[132] Kržan, M., Žarnić, R., Bosiljkov, V. 2011. Design of lateral resistance of URM blockwork through theoretical models and code provisions. 9th Australasian Mansonry Conference. J. M. Ingham, (Ed.). Queenstown, New Zealand, Australasian Masonry Conferenc: pp. 451-462.
[133] AS 3700-2001. 2001. AS 3700-2001 Masonry Structures. Standards Australia.
[134] BS. 2005. BS 5628:2005 – Code of Practice for the Use of Masonry. BSI.
[135] CSA. 2001. S304.1-04 Design of Masonry Structures. CSA.
[136] MSJC. 2008. Building Code Requirements and Specification for Masonry Structures (TMS 402/ACI 530/ASCE 5 and TMS 602/ACI 530.1/ASCE 6) The Masonry Society.
[137] NZS. 2004. NZS 4230:2004 Design of Reinforced Concrete Masonry Structures. Standards New Zealand.
[138] SIA 266. 2003. Structural masonry. Swiss Society of Architects and Engineers. Zürich.
[139] SIA D0237. 2010. Beurteilung von Mauerwerksgebäuden bezüglich Erdbeben. Zürich, Switzerland, Swiss Society of Engineers and Architects.
[140] Terčelj, S., Turnšek, V., Sheppard, P. 1981. Report on the testing of the load-carrying capacity of grouted stone-masonry walls. Ljubljana, ZRMK.
[141] Tomazevic, M., Apih, V. 1993. Ojacevanje kamnitega zidovja z zidovju prijaznim injektiranjem. Gradbeni vestnik. 42: 45-48.
[142] Vintzileou, E., Tassios, T. P. 1995. Three-Leaf Stone Masonry Strengthened by Injecting Cement Grouts. Journal of Structural Engineering. 121, 5: 848-856.
[143] Modena, C. 1999. Interpretazione dei risultati ottenuti dalle prove in sito nell'ambito delle tre convenzioni con gli istituti di ricerca di Firenze e Milano e modellazione del comportamento strutturale dei componenti rinforzati. In: Convenzione di ricerca tra la Regione Toscana e il Dipartimento di Costruzioni e Trasporti dell'Università degli Studi di Padova. Italy, University of Padua.
[144] Valluzzi, M. R. 2000. Comportamento meccanico di murature storiche consolidate con materiali e tecniche a base di calce. PhD, University of Trieste.
[145] Toumbakari, E. E. 2002. Lime-pozzolan-cement grouts and their structural effects on composite masonry walls. Thesis. Belgium, Katholieke Universiteit Leuven p.
[146] Valluzzi, M. R., da Porto, F., Modena, C. 2004. Behavior and modeling of strengthened three-leaf stone masonry walls. Materials and Structures. 37, 3: 184-192. 10.1007/bf02481618.

[147] Vintzileou, E., Miltiadou-Fezans, A. 2008. Mechanical properties of three-leaf stone masonry grouted with ternary or hydraulic lime-based grouts. Engineering Structures. 30, 8: 2265-2276. 10.1016/j.engstruct.2007.11.003.
[148] Galasco, A., Penna, A., Magenes, G. 2009. Caratterizzazione meccanica di muratura in pietra. parte prima: Prove di compressione semplice e di compressione diagonale. Technical report, Allegato 4.2-UR01-1, Università degli Studi di Pavia.
[149] Toumbakari, E. E., Van Gemert, D. 1997. Lime pozzolana cement injection grouts for the repair and strengthening of three leaf masonry structures. In. 4th Intern. Conf. on the conservation of monuments in the Mediterranean Basin. Rodhes, Greece: pp. 385-394.
[150] Oliveira, D., Silva, R., Garbin, E., Lourenço, P. 2012. Strengthening of three-leaf stone masonry walls: an experimental research. Materials and Structures: 1-18. 10.1617/s11527-012-9832-3.
[151] Galasco, A., Penna, A., Magenes, G. 2009. Caratterizzazione meccanica di muratura in pietra. parte seconda: prove cicliche di taglio-compressione su pannelli di grandi dimensioni. Technical report, Allegato 4.2-UR01-2, Università degli Studi di Pavia.
[152] Tomazevic, M., Sheppard, P. 1983. Revitalizacija kamnitih zidanih zgradb z vidika seizmicne zascite. Gradbeni vestnik, 32: 63-70.
[153] Drei, A., Fontana, A. 2001. Influence of geometrical and material properties on multiple-leaf walls behaviour. In. 7th International conference on structural studies, repairs and maintenance of heritage arhitecture (STREMAH). Bologna, Italy: pp. 681-691.
[154] Drei, A., Fontana, A. 2000. Response of multiple-leaf walls to horizontal Forces. In. 2th IBMaC. Madrid, Spain: pp. 597-609.
[155] Corradi, M., Borri, A., Vignoli, A. 2003. Experimental study on the determination of strength of masonry walls. Construction and Building Materials. 17, 5: 325-337. 10.1016/s0950-0618(03)00007-2.
[156] Uranjek, M., Bosiljkov, V., Žarnić, R., Bokan-Bosiljkov, V. 2012. In situ tests and seismic assessment of a stone-masonry building. Materials and Structures. 45, 6: 861-879. 10.1617/s11527-011-9804-z.
[157] Corradi, M., Borri, A., Vignoli, A. 2002. Strengthening techniques tested on masonry structures struck by the Umbria–Marche earthquake of 1997–1998. Construction and Building Materials. 16, 4: 229-239. http://dx.doi.org/10.1016/S0950-0618(02)00014-4.
[158] Tomaževič, M., Klemenc, I., Lutman, M. 2000. In situ tests for the assessment of seismic resistance of old stone-masonry houses. In. 12th World conference on earthquake engineering. Auckland, New Zeland, Upper Hutt, N.Z.: pp. 1975-1982.
[159] Mazzon, N., Valluzzi, M. R., Aoki, T., Garbin, E., de Canio, G., Ranieri, N., Modena, C. 2009. Shaking table tests on two multi-leaf stone masonry buildings. 11th Canadian Masonry Symposium. W. W. El-Dakhakhni, R. G. Drysdale, (Ed.). Toronto, Ontario, Canada: pp. 325-334.
[160] Mazzon, N. 2010. Influence of Grout Injection on the Dynamic Behaviour of Stone Masonry Buildings. PhD Thesis. Italy, University of Padova.
[161] 1964. International charter for the conservation and restoration of monuments and sites.
[162] Project, N. 2010. Critical review of retrofitting and reinforcement techniques related to possible failure, Deliverable 3.2. Italy.
[163] Gostič, S., Uranjek, M., Jarc Simonič, M., Štampfl, A. 2012. Results of experimental tests on strengthening techniques and guidelines for the design, PERPETUATE Project, Deliverable D34.
[164] Islam, R. 2008. Inventory of FRP strengthening methods in masonry structures. Thesis. Barcelona, Spain, Technical University of Catalonia: 131 p.
[165] Binda, L., Modena, C., Baronio, G. 1993. Strengthening of masonries by injection technique. In. 6th NAMC Philadelphia, USA: pp. 1-14.
[166] Binda, L., Modena, C., Baronio, G., Abbaneo, S. 1997. Repair and investigation techniques for stone masonry walls. Construction and Building Materials. 11, 3: 133-142. http://dx.doi.org/10.1016/S0950-0618(97)00031-7.

[167] Binda, L., Cardani, G., Saisi, A. 2009. A classification of structures and masonries for the adequate choice of repair. In: C. Groot, (Ed.). Workshop Repair Mortars for Historic Masonry, RILEM Publications SARL: pp. 20-34.

[168] Vintzileou, E. N., Toumbakari, E.-E. E. 2001. The effect of deep rejointing on the compressive strength of brick masonry. Masonry International. 15, 4: 8-12.

[169] Corradi, M., Tedeschi, C., Binda, L., Borri, A. 2008. Experimental evaluation of shear and compression strength of masonry wall before and after reinforcement: Deep repointing. Construction and Building Materials. 22, 4: 463-472. http://dx.doi.org/10.1016/j.conbuildmat.2006.11.021.

[170] Binda, L., Borri, A., Corradi, M., Tedeschi, C. 2005. Experimental evaluation of shear and compression strength of masonry wall before and after reinforcement: deep re-pointing. In. 1st Canadian Conference on Effectiveness Design of Structures. Hamilton, Ontario, Canada: pp. 293-304.

[171] Valluzzi, M. R., Binda, L., Modena, C. 2005. Mechanical behaviour of historic masonry structures strengthened by bed joints structural repointing. Construction and Building Materials. 19, 1: 63-73. http://dx.doi.org/10.1016/j.conbuildmat.2004.04.036.

[172] Binda, L., Modena, C., Valluzzi, M. R., Zago, R. 1999. Mechanical effects of bed joint steel reinforcement in historic brick masonry structures. In. 8th International Conference and Exhibition on Structural Faults and Repair. London, UK.

[173] Binda, L., Modena, C., Saisi, A., Tongini Folli, R., Valluzzi, M. 2001. Bed joints structural repointing of historic masonry structures. In. 9th Canadian Masonry Symposium 'Spanning the centuries'. Fredericton, New Brunswick, Canada: pp. 4-6.

[174] Modena, C., Valluzzi, M. R., Tongini Folli, R., Binda, L. 2002. Design choices and intervention techniques for repairing and strengthening of the Monza cathedral bell-tower. Construction and Building Materials. 16, 7: 385-395. http://dx.doi.org/10.1016/S0950-0618(02)00041-7.

[175] Hollaway, L. C. 2003. The evolution of and the way forward for advanced polymer composites in the civil infrastructure. Construction and Building Materials. 17, 6–7: 365-378. http://dx.doi.org/10.1016/S0950-0618(03)00038-2.

[176] Triantafillou, T. C. 1998. Composites: a new possibility for the shear strengthening of concrete, masonry and wood. Composites Science and Technology. 58, 8: 1285-1295. http://dx.doi.org/10.1016/S0266-3538(98)00017-7.

[177] Tinazzi, D., Modena, C., Nanni, A. 2000. Strengthening of masonry assemblages with FRP rods and laminates. In: Crivelli-Visconti, (Ed.). Int. Meeting on Composite Materials, PLAST 2000. Milan, Italy: pp. 411-418.

[178] Tinazzi, D., Nanni, A. 2000. Assessment of technologies of masonry retrofitting with FRP, Report of the Center for Infrastructure Engineering Studies, CIES 2000. University of Missouri–Rolla

[179] Tumialan, J., Huang, P., Nanni, A., Silva, P. 2001. Strengthening of masonry walls by FRP structural repointing. In. Non-Metallic Reinforcement for Concrete Structures, FRPRCS-5. Cambridge, England: pp. 1033-1042.

[180] Valluzzi, M. R., Disarò, M., Modena, C. 2003. Bed joints reinforcement of masonry panels with cfrp bars. In: D. Bruno, G. Spadea, N. Swamy, (Ed.). International Conference on Composites in Construction. Rende, Italy: pp. 427-432.

[181] Tinazzi, D., Valluzzi, M., Bianculli, N., Lucchin, F., Modena, C., Gottardo, R. 2003. FRP strengthening and repairing of masonry under compressive load. In. 10th International Conference on Structural Faults and Repair. London, UK.

[182] Saisi, A., Valluzzi, M., Binda, L., Modena, C. 2004. Creep behavior of brick masonry panels strengthened by the bed joints reinforcement technique using CFRP thin strips. In. IV Int. Seminar on Structural Analysis of Historical Constructions-possibilities of experimental and numerical techniques. Padova, Italy: pp. 837-846.

[183] Li, T., Galati, J. N., Tumialan, G., Nanni, A. 2005. Analysis of Unreinforced Masonry Concrete Walls Strengthened with Glass Fiber-Reinforced Polymer Bars. Structural Journal. 102, 4: 569-577. 10.14359/14561.

[184] Li, T., Galati, N., Tumialan, G., Nanni, A. 2005. FRP strengthening of URM walls with openings–experimental results. Mason Soc J. 23, 1: 47-58.
[185] Silva, P. F., Belarbi, A., Li, T. 2006. In-plane performance assessment of URM walls retrofitted with FRP. Masonry Soc J. 24, 1: 57-68.
[186] Turco, V., Secondin, S., Morbin, A., Valluzzi, M. R., Modena, C. 2006. Flexural and shear strengthening of un-reinforced masonry with FRP bars. Composites Science and Technology. 66, 2: 289-296. http://dx.doi.org/10.1016/j.compscitech.2005.04.042.
[187] Garbin, E., Valluzzi, M. R., Saisi, A., Binda, L., Modena, C. 2009. Compressive behaviour of brick masonry panels strengthened with CFRP bed joints reinforcement. In. 9th Canadian Masonry Symposium. Toronto, Ontario, Canada.
[188] Petersen, R., Masia, M., Seracino, R. 2010. In-Plane Shear Behavior of Masonry Panels Strengthened with NSM CFRP Strips. I: Experimental Investigation. Journal of Composites for Construction. 14, 6: 754-763. doi:10.1061/(ASCE)CC.1943-5614.0000134.
[189] Mahmood, H., Ingham, J. 2011. Diagonal Compression Testing of FRP-Retrofitted Unreinforced Clay Brick Masonry Wallettes. Journal of Composites for Construction. 15, 5: 810-820. 10.1061/(ASCE)CC.1943-5614.0000209.
[190] Konthesingha, K. M. C., Masia, M. J., Petersen, R. B., Mojsilovic, N., Simundic, G., Page, A. W. 2013. Static cyclic in-plane shear response of damaged masonry walls retrofitted with NSM FRP strips – An experimental evaluation. Engineering Structures. 50, 0: 126-136. http://dx.doi.org/10.1016/j.engstruct.2012.10.026.
[191] Dizhur, D., Griffith, M., Ingham, J. 2013. In-Plane Shear Improvement of Unreinforced Masonry Wall Panels Using NSM CFRP Strips. Journal of Composites for Construction. 17, 6: 04013010. 10.1061/(ASCE)CC.1943-5614.0000400.
[192] Shrive, N. G. 2006. The use of fibre reinforced polymers to improve seismic resistance of masonry. Construction and Building Materials. 20, 4: 269-277. http://dx.doi.org/10.1016/j.conbuildmat.2005.08.030.
[193] ElGawady, M. A., Lestuzzi, P., Badoux, M. 2005. Aseismic retrofitting of unreinforced masonry walls using FRP. Composites Part B: Engineering. 37, 2–3: 148-162. http://dx.doi.org/10.1016/j.compositesb.2005.06.003.
[194] ElGawady, M. A., Lestuzzi, P., Badoux, M. 2006. Shear strength of URM walls retrofitted using FRP. Engineering Structures. 28, 12: 1658-1670. http://dx.doi.org/10.1016/j.engstruct.2006.03.005.
[195] Prota, A., Marcari, G., Fabbrocino, G., Manfredi, G., Aldea, C. 2006. Experimental In-Plane Behavior of Tuff Masonry Strengthened with Cementitious Matrix–Grid Composites. Journal of Composites for Construction. 10, 3: 223-233. 10.1061/(ASCE)1090-0268(2006)10:3(223).
[196] Marcari, G., Manfredi, G., Prota, A., Pecce, M. 2007. In-plane shear performance of masonry panels strengthened with FRP. Composites Part B: Engineering. 38, 7–8: 887-901. http://dx.doi.org/10.1016/j.compositesb.2006.11.004.
[197] Tomaževič, M., Klemenc, I., Weiss, P. 2009. Seismic upgrading of old masonry buildings by seismic isolation and CFRP laminates: a shaking-table study of reduced scale models. Bulletin of Earthquake Engineering. 7, 1: 293-321. 10.1007/s10518-008-9086-1.
[198] Roca, P., Araiza, G. 2010. Shear response of brick masonry small assemblages strengthened with bonded FRP laminates for in-plane reinforcement. Construction and Building Materials. 24, 8: 1372-1384. http://dx.doi.org/10.1016/j.conbuildmat.2010.01.005.
[199] Santa-Maria, H., Alcaino, P. 2011. Repair of in-plane shear damaged masonry walls with external FRP. Construction and Building Materials. 25, 3: 1172-1180. http://dx.doi.org/10.1016/j.conbuildmat.2010.09.030.
[200] Luccioni, B., Rougier, V. C. 2011. In-plane retrofitting of masonry panels with fibre reinforced composite materials. Construction and Building Materials. 25, 4: 1772-1788. http://dx.doi.org/10.1016/j.conbuildmat.2010.11.088.
[201] Capozucca, R. 2011. Experimental analysis of historic masonry walls reinforced by CFRP under in-plane cyclic loading. Composite Structures. 94, 1: 277-289. http://dx.doi.org/10.1016/j.compstruct.2011.06.007.

[202] Marcari, G., Oliveira, D. V., Fabbrocino, G., Lourenço, P. B. 2011. Shear capacity assessment of tuff panels strengthened with FRP diagonal layout. Composites Part B: Engineering. 42, 7: 1956-1965. http://dx.doi.org/10.1016/j.compositesb.2011.05.031.

[203] Mosallam, A., Banerjee, S. 2011. Enhancement in in-plane shear capacity of unreinforced masonry (URM) walls strengthened with fiber reinforced polymer composites. Composites Part B: Engineering. 42, 6: 1657-1670. http://dx.doi.org/10.1016/j.compositesb.2011.03.015.

[204] Lutman, M., Bohinc, U., Gams, M., Tomaževič, M. 2012. In situ tests for the assessment of seismic strengthening historic brick masonry walls with carbon fiber fabric. In. 15th WCEE. Lisbon, Portugal.

[205] Tomaževič, M., Gams, M., Berset, T. 2014. Strengthening of stone masonry walls with composite reinforced coatings. Bulletin of Earthquake Engineering: 1-25. 10.1007/s10518-014-9697-7.

[206] Corradi, M., Borri, A., Castori, G., Sisti, R. 2014. Shear strengthening of wall panels through jacketing with cement mortar reinforced by GFRP grids. Composites Part B: Engineering. 64, 0: 33-42. http://dx.doi.org/10.1016/j.compositesb.2014.03.022.

[207] Jarc Simonič, M., Gostič, S., Bosiljkov, V., Žarnić, R. 2015. In-situ and laboratory tests of old brick masonry strengthened with FRP in innovative configurations and design considerations. Bulletin of Earthquake Engineering. 13, 1: 257-278. 10.1007/s10518-014-9644-7.

[208] Gattesco, N., Boem, I. 2015. Experimental and analytical study to evaluate the effectiveness of an in-plane reinforcement for masonry walls using GFRP meshes. Construction and Building Materials. 88, 0: 94-104. http://dx.doi.org/10.1016/j.conbuildmat.2015.04.014.

[209] CNR-DT 200/2004. 2004. Guide for the Design and Construction of Externally Bonded FRP Systems for Strengthening Existing Buildings. Rome, Italy, CNR: 152 p.

[210] Valluzzi, M. R., Tinazzi, D., Modena, C. 2002. Shear behavior of masonry panels strengthened by FRP laminates. Construction and Building Materials. 16, 7: 409-416. http://dx.doi.org/10.1016/S0950-0618(02)00043-0.

[211] Stratford, T., Pascale, G., Manfroni, O., Bonfiglioli, B. 2004. Shear Strengthening Masonry Panels with Sheet Glass-Fiber Reinforced Polymer. Journal of Composites for Construction. 8, 5: 434-443. 10.1061/(ASCE)1090-0268(2004)8:5(434).

[212] Triantafillou, T. 1998. Strengthening of Masonry Structures Using Epoxy-Bonded FRP Laminates. Journal of Composites for Construction. 2, 2: 96-104. 10.1061/(ASCE)1090-0268(1998)2:2(96).

[213] Triantafillou, T., Antonopoulos, C. 2000. Design of Concrete Flexural Members Strengthened in Shear with FRP. Journal of Composites for Construction. 4, 4: 198-205. 10.1061/(ASCE)1090-0268(2000)4:4(198).

[214] Nanni, A., Galati, N., Tumialan, J. 2003. Outline of provisional design protocols and field applications of strengthening of URM walls. In: I. Crivelli-Visconti, (Ed.). Advancing with Composites, Plast 2003. Milan, Italy: pp. 187-197.

[215] Zhao, T., Zhang, C., Xie, J. 2003. Experimental study on earthquake strengthening of brick walls with continuous carbon fibre sheet. Masonry Int. 16, 1: 21-25.

[216] Zhao, T., Zhang, C., Xie, J. 2004. Shear behaviour of UCMW using CFRP sheet: a case study. Masonry Soc J. 22, 1: 87-95.

[217] Wang, Q., Chai, Z., Huang, Y., Yang, Y., Zhang, Y. 2006. Seismic shear capacity of brick masonry wall reinforced by GFRP. Asian journal of civil engineering (building and housing). 7, 6: 563-580.

[218] ElGawady, M. A., Lestuzzi, P., Badoux, M. 2006. Analytical model for the in-plane shear behavior of URM walls retrofitted with FRP. Composites Science and Technology. 66, 3–4: 459-474. http://dx.doi.org/10.1016/j.compscitech.2005.06.015.

[219] Garbin, E., Galati, N., Nanni, A., Modena, C., Valluzzi, M. R. 2007. Provisional design guidelines for the strengthening of masonry structures subject to in-plane loading. In: U. St. Louis, (Ed.). 10th North American masonry conference: pp. 3-5.

[220] ACI 440.7R-10. 2010. Guide for Design & Constr of Externally Bonded FRP Systems for Strengthening Unreinforced Masonry Structures. American Concrete Institute: 46 p.

[221] CNR-DT 200 R1/2013. 2013. Guide for the Design and Construction of Externally Bonded FRP Systems for Strengthening Existing Buildings. Rome, Italy, CNR: 152 p.

[222] Zhuge, Y. 2010. FRP-Retrofitted URM Walls under In-Plane Shear: Review and Assessment of Available Models. Journal of Composites for Construction. 14, 6: 743-753. 10.1061/(ASCE)CC.1943-5614.0000135.
[223] Mahmood, H., Ingham, J. 2011. Proposed design guidelines for shear retrofit of in-plane loaded clay brick wall using externally-bonded FRP. In: J. Ingham, M. Dhanasekar, M. J. Masia, (Ed.). 9th Australasian Masonry Conference. Queenstown, New Zealand: pp. 97-106.
[224] Benedetti, A., Sacco, E. 2012. The new Italian guide lines for FRP strengthening of masonry and timber structures. 15th IBMAC. Florianopolis, Brazil.
[225] MSJC. 2008. Building Code Requirements for Masonry Structures (ACI 530-05 / ASCE 5-05 / TMS 402-05). American Concrete Institute, American Society of Civil Engineers, The Masonry Society.
[226] Morbin, A., Nanni, A. 2002. Strengthening of Masonry Elements with FRP Composites, Report CIES 02-23. Rolla, Missouri, USA, Center for Infrastructure Engineering Studies, University of Missouri-Rolla.
[227] Grando, S., Valluzzi, M. R., Tumialan, J. G., Nanni, A. 2003. Shear Strengthening of URM Clay Walls with FRP Systems. In: X. L. Gu, Y. Ouyang, W. P. Zhang, F. F. Ye, (Ed.). International Symposium FRPRCS-6. Singapore: pp. 1229-1238.
[228] Santa Maria, H., Duarte, G., Garib, A. 2004. Experimental Investigation of Masonry Panels Externally Strengthened with CFRP Laminates and Fabric Subjected to In-Plane Shear Load. In. 13th Word Conference on Earthquake Engineering. Vancouver, BC, Canada: Paper No. 1627.
[229] Santa Maria, H., Alcaino, P., Luders, C. 2006. Experimental Response of Masonry Walls Externally Reinforced with Carbon Fiber Fabrics. In. 8th U.S. National Conference on Earthquake Engineering. San Francisco, CA, USA: Paper No. 1402.
[230] Senescu, R., Mosalam, K. 2004. Retrofitting of Unreinforced Masonry Walls Using Fiber Reinforced Polymer Laminates, Report UCB/SEMM 2004/3. Berkeley, CA, USA, University of California.
[231] Lorenzis, L., Nanni, A. 2001. Characterization of FRP Rods as Near-Surface Mounted Reinforcement. Journal of Composites for Construction. 5, 2: 114-121. 10.1061/(ASCE)1090-0268(2001)5:2(114).
[232] Hassan, T., Rizkalla, S. 2003. Investigation of Bond in Concrete Structures Strengthened with Near Surface Mounted Carbon Fiber Reinforced Polymer Strips. Journal of Composites for Construction. 7, 3: 248-257. 10.1061/(ASCE)1090-0268(2003)7:3(248).
[233] Turco, V., Galati, N., Tumialan, G., Nanni, A. 2003. Flexural Strengthening of URM Walls with FRP Systems. In. 6th International Symposium on FRP Reinforcement for Concrete Structures (FRPRCS-6). Singapore, World Scientific Publishing Company: pp. 1219-1228.
[234] UBC. 1997. Uniform building code. In. International Conference of Building Officials. Whittier, CA.
[235] De Lorenzis, L. 2000. Strengthening of RC structures with near surface mounted FRP rods. Thesis. Rolla, Missouri, USA, University of Missouri - Rolla: 175 p.
[236] Crisafulli, F., Carr, A., Park, R. 1995. Shear strength of unreinforced masonry panels. In. Pacific Conference on Earthquake Engineering. Melbourne, Australia: pp. 77-86.
[237] SIST EN 1015-3:2001. 2001. Metode preskušanja zidarskih malt – 3 del: Določevanje konsistence sveže malte (s stresalno mizo). Slovenski inštitut za standardizacijo: 10 p.
[238] SIST EN 1015-6:1999. 1999. Metode preskušanja zidarskih malt – 6. del: Ugotavljanje prostorninske mase sveže malte. Slovenski inštitut za standardizacijo: 9 p.
[239] SIST EN 1015-11:2001 – Metode preskušanja zidarskih malt – 11. del: Določevanje upogibnein tlačne trdnosti strjene malte: 12 p.
[240] Hocevar, A., Bokan-Bosiljkov, V., Kavcic, F. 2007. Vpliv vrste cementa na sulfatno odpornost betona : diplomska naloga = The influence on types of cement on sulfate resistance of concrete : graduation thesis. Ljubljana.
[241] SIST EN 12390-6:2001 – Preskušanje strjenega betona – 6. del: Cepilna natezna trdnoststrjenega betona: 10 p.

[242] Aničić, D., Sorić, Z., Morić, D., Macan, H. 1989. Mechanical properties of stone masonry walls. In: C. A. Brebbia, (Ed.). Structural repair and maintenance of historical buildings. Basel, Computational Mechanics Publications; Birkháuser. pp. 95-102.
[243] PIET 70. 1971. Obras de fábrica. Prescripciones del Instituto Eduardo Torroja. Madrid, Spain, Consejo Superior de Investigaciones Científicas.
[244] Bosiljkov, V., Tomaževič, M., Bohinc, U., Leskovar, I. 2004. On-site investigation techniques for the structural evaluation of historic masonry buildings. Deliverable D10.2 & 10.4. Report on the evaluation at pilot sites (Report for owners of historic buildings) : pilot site: Pišece / Slovenia : revised report. In: ONSITEFORMASONRY project. Ljubljana, Zavod za gradbeništvo Slovenije.
[245] OPCM n. 3274. 2003. Primi elementi in materia di criteri generali per la classificazione sismica del territorio nazionale e di normative tecniche per le costruzioni in zona sismica Italy (in English). Ordinanza del Presidente del Consiglio dei Ministri.
[246] Kržan, M., Bosiljkov, V. 2012. Results of the cyclic shear tests on three-leaf stone masonry walls Ljubljana, UL FGG.
[247] Kurnjek, L. 2012. Ciklo - program for the analysis of the masonry wall histeresis response results (eng. Ciklo - program for the analysis of the masonry wall histeresis response results). B.Sc. Thesis. Ljubljana, University of Ljubljana: 94 p.
[248] Costa, A. A., Arêde, A., Costa, A., Oliveira, C. S. 2011. In situ cyclic tests on existing stone masonry walls and strengthening solutions. Earthquake Engineering & Structural Dynamics. 40, 4: 449-471. 10.1002/eqe.1046.
[249] Cotič, P. 2014. The synthesis of multisensor non-destructive testing of civil engineering structural elements with the use of clustering methods. PhD Thesis. Ljubljana, University of Ljubljana: 100 p.
[250] Špeglič, D. 2013. Občutljivostna analiza kamnitih zidov z uporabo georadarja (Performance based assessment of stone masonry with GPR, in Slovene). B.Sc. Thesis. Ljubljana, University of Ljubljana: 71 p.
[251] Arrigler, A. 2013. Študij ureditvenih ukrepov za kamnite zidove (eng. Studies of retrofitting measures for stone masonry walls). B.Sc. Thesis. Ljubljana, UL: 164 p.
[252] Uranjek, M. 2011. Propadanje in trajnostna obnova ovoja stavbne dediščine : doktorska disertacija = Degradation and sustainable renovation of heritage buildings envelope : doctoral thesis. Doctoral Theses, Ljubljana: 2011. p.
[253] Thomas, M. D. A., Fournier, B., Folliard, K. J. 2013. Alkali-Aggregate Reactivity (AAR) Facts Book, Report FHWA-HIF-13-019 FHWA.
[254] Institute, A. C. 2010. Guide for the design and construction of externally bonded fiber-reinforced polymer systems for strengthening unreinforced masonry structures. Farmington Hills [MI].
[255] Božič, L. 2014. Utrjevanje poškodovanih zidov s steklenimi vrvicami in epoksidnimi smolami (eng. Retrofitting damaged walls with glass chord and epoxy resins) B.Sc. Thesis. Ljubljana, UL: 57 p.
[256] TKK. "Tekamal injekcem C, Tekamal injekcem CA." http://www.tkk.si/si/files/default/tehnicni_listi/malte/24%20Tekamal%20Injekcem%20C%20CA%20slo.pdf.
[257] Uranjek, M. 2011. Degradation and sustainable renovation of heritage buildings envelope (in Slovenian). Doctoral Theses, University of Ljubljana
[258] SIST EN 445:2008. 2008. Injekcijska masa za prednapete kable - Preskusne metode. Slovenski inštitut za standardizacijo: 18 p.
[259] SIST EN 1015-10:2001/A1:2007: Metode preskušanja zidarske malte - 10. del: Določevanje suhe prostorninske mase strjene malte.
[260] 1983. JUS U. M1. 025. Beton - Određivanje statičkog modula elastičnosti pritiskom.
[261] Mapei. MapeWrap C Fiocco, MapeWrap G Fiocco.
[262] Mapei. "MapeWrap 21." http://www.mapei.com/public/COM/products/1007_mapewrap21_gb2.pdf.
[263] KEMA. 2006. "Fuga sand, Technical data sheet (in slovenian)."

file:///G:/0_WORK/DOKTORAT/Ojacevanje/Product%20information/SI_TL_FugaSand%20(2).pdf.
[264] Mapei. "MapeWrap 11, MapeWrap 12." http://www.mapei.com/public/COM/products/1006_mapewrap_11-12_gb.pdf.
[265] Mapei. "MapeWrap Primer 1. http://www.mapei.com/public/COM/products/1005_mapewrap_primer_1_gb.pdf.
[266] Bergant, M., Dolinšek, B. Utrjevanje kamnitih in opečno-kamnitih zidov z injektiranjem.
[267] Kržan, M., Bosiljkov, V. 2013. Results of the cyclic shear tests on strengthened three-leaf stone masonry walls Ljubljana, UL FGG.
[268] Stopar, I. 2011. Najlepši slovenski dvorci. Ljubljana, Cankarjeva zalozba: 336 p.
[269] Sapač, I. 2011. Grajske stavbe v zahodni Sloveniji, Četrta knjiga Brda in Zgomje Posocje. Ljubljana, Viharnik p.
[270] EN 1998-1: 2004. 2004. Eurocode 8: Design of structures for earthquake resistance – Part 1: General rules, seismic actions and rules for buildings. Brussels, Belgium, CEN.
[271] SIST EN 1998-1: 2004. 2004. Eurocode 1: Actions on structures – Part 1-1: General actions - Densities, self-weight, imposed loads for buildings. Ljubljana, Slovenia, SIST.
[272] Roca, P., Molins, C., Marí, A. 2005. Strength Capacity of Masonry Wall Structures by the Equivalent Frame Method. Journal of Structural Engineering. 131, 10: 1601-1610. doi:10.1061/(ASCE)0733-9445(2005)131:10(1601).
[273] S.T.A. Data. 2009. 3muri, General description, Version: 4.
[274] Gorica, P. d. d. N. 2007. PGD – Statična sanacija in obnova fasade Vile Vipolže v Goriških Brdih. V. Durcik, M. Skubin, (Ed.). Nova Gorica.
[275] Binda, L., Saisi, A., Benedictis, R., Tringali, S. 2003. Experimental study on the damaged pillars of the Noto Cathedral. In. 8th Int. Conf. on Structural Studies, Repairs and Maintenance of Heritage Architecture.: pp. 89-98.
[276] Bosiljkov, V., Uranjek, M., Žarnić, R., Bokan-Bosiljkov, V. 2010. An integrated diagnostic approach for the assessment of historic masonry structures. Journal of Cultural Heritage. 11, 3: 239-249. 10.1016/j.culher.2009.11.007.
[277] Tomaževič, M. 1987. Zidane zgradbe na potresnih obmocjih. Ljubljana, Fakulteta za arhitekturo, gradbenistvo in geodezijo.
[278] Tassios, T. 2004. Recupero di murature tri-strato. 22.
[279] SIST EN 1998-3: 2005. 2005. Evrokod 8: Projektiranje potresnoodpornih konstrukcij – 3. del: Ocena in prenove stavb. Ljubljana, SIST.